Remote Sensing in Shallow Lake Ecology

Peter David Hunter

Submitted to the School of Biological and Environmental Science

University of Stirling

October 2007

For the degree of Doctor of Philosophy

Supervisors: Dr A.N. Tyler, Dr. N.J. Willby and Dr. D.J. Gilvear

UNIVERSITY OF STIRLING

This research was undertaken at the School of Biological and Environmental Science,
University of Stirling Scotland, FK9 4LA

STATEMENT OF ORIGINALITY

I hereby confirm that this is an original piece of work conducted independently by the undersigned and all work contained herein has been not been submitted for any other degree. All research material has been duly acknowledged and cited.

Signature of Candidate:

Peter David Hunter

Date: 28 September 2007

for my parents, David and Sheila

ABSTRACT

Shallow lakes are an important ecological and socio-economic resource. However, the impact of human pressures, both at the lake and catchment scale, has precipitated a decline in the ecological status of many shallow lakes, both in the UK, and throughout Europe. There is now, as direct consequence, unprecedented interest in the assessment and monitoring of ecological status and trajectory in shallow lakes, not least in response to the European Union Water Framework Directive (2000/60/EC).

In this context, the spatially-resolving and panoramic data provided by remote sensing platforms may be of immense value in the construction of effective and efficient strategies for the assessment and monitoring of ecological status in shallow lakes and, moreover, in providing new, spatially-explicit, insights into the function of these ecosystems and how they respond to change. This thesis examined the use of remote sensing data for the assessment of (i) phytoplankton abundance and species composition and (ii) aquatic vegetation distribution and ecophysiological status in shallow lakes with a view to establishing the credence of such an approach and its value in limnological research and monitoring activities.

High resolution *in-situ* and airborne remote sensing data was collected during a 2-year sampling campaign in the shallow lakes of the Norfolk Broads. It was demonstrated that semi-empirical algorithms could be formulated and used to provide accurate and robust estimations of the concentration of chlorophyll-a, even in these optically-complex waters. It was further shown that it was possible to differentiate and quantify the abundance of cyanobacteria using the biomarker pigment C-phycocyanin. The subsequent calibration of the imagery obtained from the airborne reconnaissance missions permitted the construction of diurnal and seasonal regional-scale time-series of phytoplankton dynamics in the Norfolk Broads. This approach was able to deliver unique spatial insights into the migratory behaviour of a potentially-toxic cyanobacterial bloom.

It was further shown that remote sensing can be used to map the distribution of aquatic plants in shallow lakes, importantly including the extent of submerged vegetation, which is central to the assessment of ecological status. This research theme was subsequently extended in an exploration of the use of remote sensing for assessing the ecophysiological response of wetland plants to nutrient enrichment. It was shown that remote sensing metrics could be constructed for the quantification of plant vigour. The extrapolation of these techniques enabled spatial heterogeneity in the ecophysiological response of *Phragmites australis* to lake nutrient enrichment to be characterised and assisted the formulation of a mechanistic explanation for the variation in reedswamp performance in these shallow lakes.

It is therefore argued that the spatially synoptic data provided by remote sensing has much to offer the assessment, monitoring and policing of ecological status in shallow lakes and, in particular, for facilitating the development of pan-European scale lake surveillance capabilities for the Water Framework Directive (2000/60/EC). It is also suggested that remote sensing can make a valuable contribution to furthering ecological understanding and, most significantly, in enabling ecosystem processes and functions to be examined at the lake-scale.

ACKNOWLEDGMENTS

I am heavily indebted to many people, whether they are aware of it or not, for their help and support in the completion of this thesis. First, and foremost, I would like to express my gratitude to my principal supervisor, Dr. Andrew Tyler, for all his guidance, mentoring and friendship during the course of this research project. I would also like to extend my appreciation to my other supervisors, Dr. Nigel Willby and Dr. David Gilvear, for their advice, support and good humour at various times over the last four years.

This research project was jointly funded by the former Faculty of Natural Sciences, University of Stirling, and the Northumbria, Essex and Suffolk Water Group, to whom I am very grateful for their financial support. I would also like to acknowledge the support of the National Environmental Research Council's Airborne Research and Survey Facility, and their crew, who acquired so much of the data used in this thesis. This project was also supported by the Norfolk Broads Authority and the Environment Agency as part of the Upper Thurne Studentships Steering Group; in particular, I would like to convey my appreciation to Andrea Kelly and Phil Heath of the Broads Authority, and Jennifer Johnson of the Environment Agency, for assistance and forbearance when dealing with my many queries and seemingly incessant requests for yet more data.

I would also like to express my appreciation to Professor Tom Preston of the Scottish Universities Environmental Research Centre, and Dr. Mátyás Présing and Dr. Atilla Kovács of the Balaton Limnological Research Institute, for their collaboration on various parts of the project and, moreover, simply for providing an opportunity to visit Lake Balaton. I would also like to thank several members of the technical staff in the School of Biological and Environmental Science; including Helen Ewen for her help, and patience, with my own, somewhat unique, approach to lab work, Jon McArthur, Scott Jackson and Bill Jamieson, for solving my computing and cartographic dilemmas and, especially, Stuart Bradley, for being of so much help and good wit on our numerous adventures to the Broads.

I must also convey my appreciation to many of the present, and former, Ph.D. students of the School of Biological and Environmental Science, University of Stirling, who have variously assisted in the field, in the lab, or simply been a great source of friendship over the past years. Indeed, I would especially like to mention my office mates, Crona, Rich, Adel, Tory, Stuart and Joe, for all their support and encouragement. And, to all my much neglected friends, at home, or in Scotland, who have endured this Ph.D. alongside me, I must apologise for those missed weekends and nights out, I'm sure they are as glad as I am that it's now finished. Finally, and most importantly, I would like to say a special thank you to my parents, without whose continual support and encouragement, none of this would have ever been possible.

TABLE OF CONTENTS

LIST OF FIGURES

LIST OF TABLES

LIST OF ACRONYMS AND ABBREVIATIONS

AAS	Atomic Absorption Spectrometry
AISA	Airborne Hyperspectral Imaging System
ANN	Artificial Neural Network
AOP	Apparent Optical Properties
ASD	Analytical Spectral Devices
AR	Analytical Reagent
ARSF	Airborne Remote Sensing Facility
ASTER	Advanced Spaceborne Thermal Emission and Reflection Radiometer
ATM	Airborne Thematic Mapper
BA	Broads Authority
BD	Continuum-Removed Band Depth
BDR	Continuum-Removed Band Depth Ratio
BLRI	Balaton Limnological Research Institute
CASI	Compact Airbone Spectrographic Imager
CCD	Charged Coupled Device
CDOM	Coloured Dissolved Organic Matter
CRDR	Continuum-Removed Derivative Reflectance
Chl-a	Chlorophyll Alpha
C-PC	Cyanobacterial Phycocyanin
CZCS	Coastal Zone Color Scanner
DOC	Dissolved Organic Matter
d*R*/dλ	First-Derivative of Reflectance
EA	Environment Agency
EMD	Euclidean Minimum Distance
EO	Earth Observation
EO-1	Earth Observing 1 (Satellite)
ESA	European Space Agency
EU WFD	European Union Water Framework Directive
FOV	Field of View
Fuco	Fucoxanthin
FWHM	Full Width at Half Maximum
GCP	Ground Control Point
GMT	Greenwich Mean Time
GPS	Global Positioning System
HAB	Harmful Algal Bloom
IKONOS	IKONOS-1 Satellite; *ikonos* (Greek) = image
IOP	Inherent Optical Properties

LAI	Leaf Area Index
Landsat TM	Landsat Thematic Mapper
$L_w(0+,\lambda)$	Water Leaving Radiance at Wavelength λ
LC	Liquid Chromatography
LSMM	Linear Spectral Mixing Model
LST	Lake Surface Temperature
MDA	Multiple Discriminant Analysis
MDL	Minimum Detection Limit
MERIS	Medium Resolution Imaging Spectrometer
MLC	Maximum Likeihood Classification
MNF	Minimum Noise Fraction
MODIS	Moderate Resolution Imaging Spectrometer
MSR	Mulitple Subsets Regression
MTMF	Mixture Tuned Matched Filtering
NASA	National Aeronautics and Space Administration
NBDR	Continuum-Removed Band-Depth Ratio
NERC	National Environmental Research Council
NIR	Near Infrared
$_nL_w$	Normalised Water Leaving Radiance
NPP	Net Primary Productivity
OM	Organic Matter
PCA	Principal Components Analysis
PDA	Photo Diode Array
PLS	Partial Least-Squares Regression
PML	Plymouth Marine Laboratory
PPI	Pixel Purity Index
$R_{(\lambda)}$	Reflectance at Wavelength λ
$R'_{(\lambda)}$	Continuum-Removed Refectance
RMSE	Root Mean Square Error
RP-HPLC	Reversed-Phased High Performance Liquid Chromatography
RSDAS	Remote Sensing Data Analysis Service
RTE	Radiative Transfer Equation
$R_{rs}(0+,\lambda)$	Subsurface Remote Sensing Reflectance at Wavelength λ
SAM	Spectral Angle Mapper
SAV	Submerged Aquatic Vegetation
SBES	School of Biological and Environmental Science
SDD	Secchi Disc Depth
SeaWiFS	Sea-Viewing Wide Field-of-View Sensor
SFF	Spectral Feature Fitting

SMACC	Sequential Maximum Angle Convex Cone
SPM	Suspended Particulate Matter
SPIM	Suspended Particulate Inorganic Matter
SPOM	Suspended Particulate Organic Matter
SVM	Support Vector Machine
TN	Total Nitrogen
TP	Total Phosphorus
USDA	United States Department of Agriculture
VIS	Visible Spectrum
VNIR	Very Near Infrared
WD	Water Depth

1 INTRODUCTION

1.1 RESEARCH IN CONTEXT

Science is often concerned with the observation of patterns in nature and, moreover, attempts to relate patterns to processes. Patterns are, essentially, a symptom of the natural spatial and temporal heterogeneity that is inherent in all ecosystems (Levin, 1992). Our understanding of how ecosystems function, interact, and respond to change, is dependent on an ability to characterise this heterogeneity across meaningful scales, and interpret its ecological significance (Underwood *et al.,* 2000; Turner *et al.,* 2003). Shallow lakes are no exception in this context. Shallow lakes, like many ecosystems, are spatially complex and transient environments, which can respond probabilistically or stochastically to perturbations and pressures which, themselves, may occur at varying scales. Our understanding of shallow lakes, their processes, and function, will thus be conditioned by our ability to measure and monitor patterns of change in these ecosystems and at ecologically pertinent spatial and temporal scales.

Scientific interest in shallow lakes has intensified as the ecological and socio-economic value of these ecosystems has been slowly recognised. It is rather ironic, therefore, that this recognition has emerged during a period in which lakes and, indeed, other freshwater ecosystems, have been subjected to unprecedented pressures from human activity. The ecological health, or status, of many shallow lakes has been severely affected by pressures from processes like acidification, abstraction, eutrophication, hydrological modification and pollution or, in some cases, even by the invasion of alien species (Scheffer, 1998). In the future, shallow lakes will also have to respond to the pressures exerted by global climate change (Carvalho & Kirika, 2003). It is now indisputable that one of the major challenges currently facing society is how to adequately protect and conserve our freshwater resources.

The European Union's Water Framework Directive (2000/66/EC) (EU WFD) was implemented on the 22 December 2000 with the aim of establishing a new, integrated, approach to the

protection, improvement and sustainable use of Europe's rivers, lakes, estuaries, coastal and groundwaters. In the context of lakes, the EU WFD stipulates all Member States must achieve "good and non-deteriorating ecological status" in these waters by 2015. The assessment of ecological status is to be measured against a lengthy list of (i) hydromorphological, (ii) physicochemical and (ii) biological criteria and, additionally, the directive places much emphasis on the need for Member States to develop efficient and effective surveillance, operational and investigative monitoring strategies to facilitate the assessment and policing of ecological status in lakes. The implementation of the EU WFD, however, will be a serious challenge for the relevant regulatory authorities, given the sheer number and geographical distribution of lakes covered by the legislation, and the number of separate elements for which monitoring is required. It is evident that, if Member States are to achieve the successful, and long-term, implementation of the EU WFD, monitoring strategies must be constructed that (i) can provide data that are objective and quantitative, (ii) are robust, repeatable, and cost-effective and, critically, (iii) can be implemented at the pan-European scale.

The accepted methodologies for lake survey and monitoring are often highly, or totally, dependent on point-sampling approaches. Point-sampling approaches, whist they readily provide accurate data, can seldom adequately describe the heterogeneity inherent in lake ecosystems without disproportionate sampling effort or the over-reliance on spatial inferences (Rantajarvi *et al.,* 1998). This deficiency is a substantial obstacle to the elucidation of spatial variability in lake process and function. Moreover, from a monitoring perspective, point-sampling approaches are not conducive, nor cost-effective, for survey at regional-to-global scales.

The spatially-resolving panoramas afforded by remote sensing technologies (spaceborne or airborne sensors) have the capability to provide data as a continuum and can afford a much needed spatial context for point-based measurements (Rainey *et al.,* 2003; Tyler *et al.,* 2006). This is important if the spatial-dependence and spatial-heterogeneity of ecosystem processes and function is to be effectively elucidated. Remote sensing has often proved to be of value for qualitative mapping exercises (Kent *et al.,* 1997; Kent & Mast, 2005; McDermid *et al.,* 2005).

However, advancements in the spatial, spectral and radiometric capabilities of remote sensing instruments have enabled scientists to increasingly begin to extract quantitative bio-physical information from spaceborne and airborne data (Aplin, 2005). This improved capability has increased the breadth of application remote sensing has found in ecology and, importantly, has often allowed scientists to form new and unparalleled understandings of how ecosystems function, interact and respond to change (Kerr & Ostrovsky, 2003; Cohen & Goward, 2004).

It is thus not unexpected that remote sensing has found use in the study of aquatic ecology. There are numerous examples of its appliance in the study of river (e.g. Bryant & Gilvear, 1999; Mertes, 2002; Gilvear *et al.,* 2007), estuarine (e.g. Paterson *et al.,* 1998; Rainey *et al.,* 2003; Yang, 2005), and marine (e.g. Brown & Podesta, 1997; Weeks *et al.,* 2004; Miller *et al.,* 2005) environments. Remote sensing has also found application in the study of lake ecosystems. Workers have shown, for instance, that remote sensing can be used to measure various water quality parameters (e.g. transparency, seston dry weight, coloured dissolved organic matter) and estimate phytoplankton biomass (chlorophyll-a) (Dekker *et al.,* 1991; Lindell *et al*., 1999; Thiemann & Kaufmann, 2000; George & Malthus, 2001; Ammenberg *et al.,* 2002; Tyler *et al.,* 2006; Giardino *et al.,* 2007). It has also been demonstrated, albeit in a limited number of studies, that remote sensing can be used to map aquatic plant species and communities (Malthus & George, 1997; Dekker *et al.,* 2005; Nelson *et al.,* 2006; Pengra *et al.,* 2007).

The spatially-resolving data provided by remote sensing in these contexts has been shown to contribute much to the understanding of ecosystem process and function and, importantly, at the lake-scale. However, the use of remote sensing for lake research and monitoring has often been restricted by the spatial and spectral capabilities of the available technology. The vast scale of the oceans inherently lends itself to observation from spaceborne instruments. The dedicated ocean colour satellites (e.g. MERIS, MODIS, SeaWiFS), that are specially configured for the specific bio-optical properties of aquatic media, thus have coarse spatial resolutions (0.3-1.1 km) that are not harmonious with the scale of the vast majority of lakes and other inland waters. The alternative use of data from terrestrial earth-observing satellites, which do have spatial resolutions (2-30 m) conducive to the observation of lakes is, in optically-complex

lake waters, restricted by the typically limited spectral capabilities (i.e. broad channel configurations) of these instruments (Lindell *et al*., 1999; Tyler *et al.,* 2006).

The latest generation of hyperspectral imaging satellite-mounted sensors (i.e. NASA's EO-1 Hyperion) now offer the combination of high spatial and high spectral resolution data. This new class of earth observation (EO) data has, in the long-term, much to offer the study of lakes and other inland waters. The EO-1 Hyperion mission was, however, designed largely for validation/demonstration purposes and, as such, the operational lifespan of the mission is limited. In this context, airborne remote sensing, which can provide high spatial and spectral resolution data, and offers a flexible time-series surveillance capability, may be highly valuable for developing the use of remote sensing technologies for lake research and monitoring purposes until the promise of further hyperspectral EO satellites is realised. Whilst it is clear that the spatially-resolving data delivered by remote sensing platforms may have much to offer the study of lake ecology. It is also apparent that remote sensing surveillance may be able to make a substantial contribution to the monitoring of lakes for the purposes of the EU WFD, as it has the capacity to provide information on elements relevant to the assessment of ecological status in lakes (e.g. phytoplankton, aquatic vegetation). The ability of remote sensing platforms to capture this information at the regional-scale would be highly pertinent for the construction of an operational, pan-European, monitoring strategy.

Remote sensing for lake monitoring is currently not at an operational stage of development. There is a need for considerable further research to prove the accuracy and robustness of the remote sensing approach. This is particularly true for small and shallow lakes. The vast majority of studies that have examined the development of remote sensing for lake research and monitoring have, perhaps for instrumentational considerations, been conducted in large and moderately deep lakes. It is also clear few attempts have been made to use data derived from remote sensing technologies to study the spatial intricacies of shallow lake processes and function and, further, to use these insights to inform and refine ecological understanding. It is therefore clear that the examination of remote sensing technologies in shallow lake research and monitoring warrants some further detailed consideration.

1.2 THESIS AIM AND STRUCTURE

The aim of this thesis is to examine the application of high spatial and high spectral resolution remote sensing for the assessment and monitoring of ecological status in shallow lakes. Specific focus will be given to the development, refinement, and application of techniques for ecological assessment that have value in the study of lake ecology and, further, have a synergy with the monitoring requirements of the EU WFD. This will include an evaluation of techniques for the assessment of (i) phytoplankton (and other water quality parameters) and (ii) aquatic vegetation in shallow lakes (Figure 1.1).

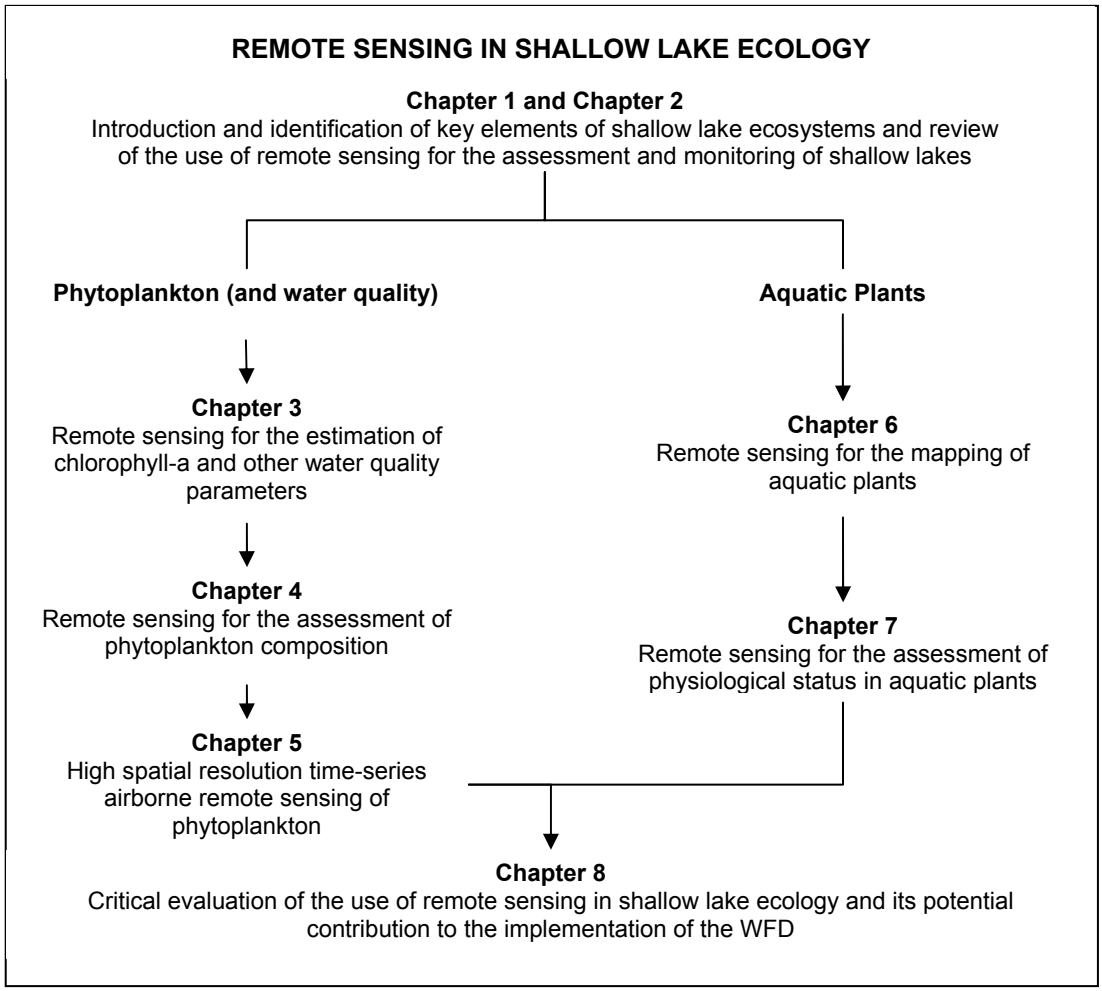

Figure 1.1 Flow diagram detailing the structure of the thesis and the approach taken to the evaluation of remote sensing in shallow lake ecology and its role in the implementation of the EU WFD (2000/66/EC).

1.3 STUDY SITE

The Norfolk Broads (52º44'17''N; 1º34'29''E) are the main study site for the research presented in this thesis (Figure 1.2). The Norfolk Broads are a series of small (< 130 ha) and shallow (< 2.5 m) mesotrophic and eutrophic shallow lakes, locally referred to as Broads, which were formed when 12th and 13th Century peat excavations flooded under rising seas.

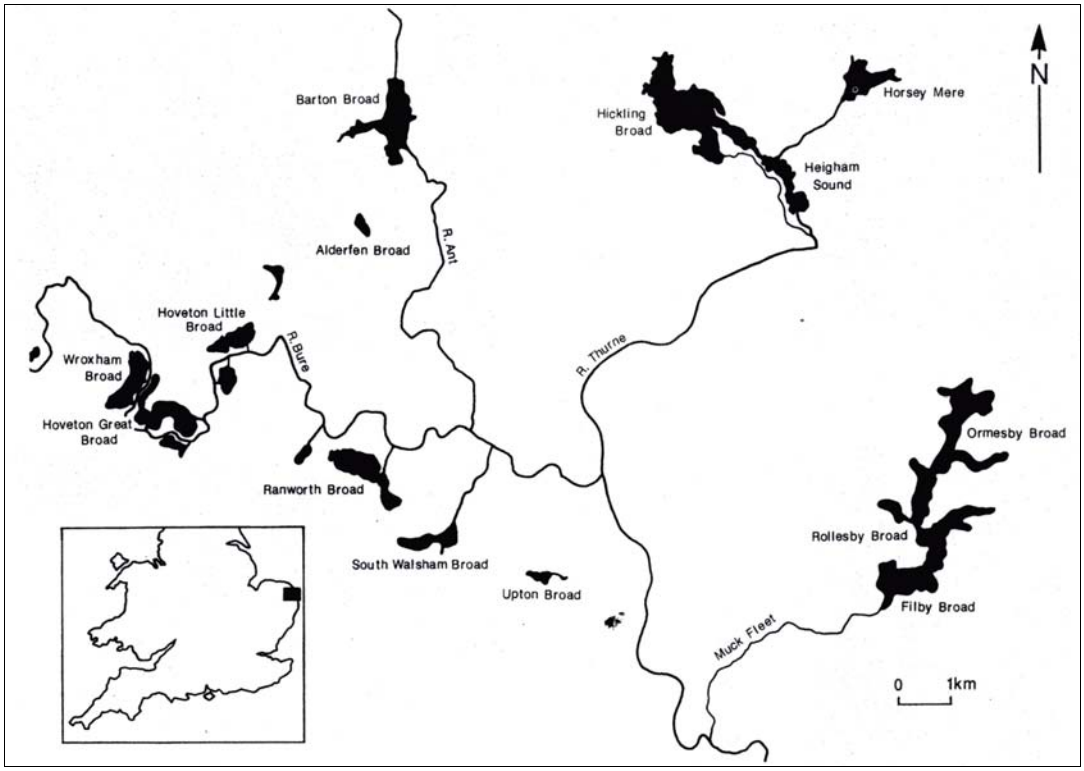

Figure 1.2 The shallow lakes of the Norfolk Broads in southeast England (map courtesy of the Broads Authority).

The Norfolk Broads (or Broadland) are the largest protected wetland in the U.K. whose ecological and socio-economic value is recognised in numerous national and international conservation designations (e.g. under the Ramsar convention). The ecological status of the Broads has declined in recent decades, largely due to pressures from eutrophication and, as a result, in many lakes the characteristically diverse aquatic flora has been replaced by nuisance blooms of pelagic phytoplankton. In this context, the Norfolk Broads would therefore seem to present a unique environment in which to explore the use of remote sensing for research and monitoring in shallow lakes.

2 SHALLOW LAKES AND REMOTE SENSING

2.1 INTRODUCTION

The following chapter reviews in relevant detail the science that underpins the research presented in this thesis. The initial focus of this chapter is to review some of the major concepts in the field of shallow lake ecology with a view to identifying the key abiotic processes and biotic elements that control the structure and function of shallow lake ecosystems. In this context, the shallow lakes of the Norfolk Broads (UK) are introduced as the dedicated study site for later investigations. The emphasis then shifts to the application of remote sensing for the assessment and monitoring of shallow lakes with particular reference to (i) phytoplankton and (ii) aquatic plants. Finally, priority areas for further research are identified from this review and these form the foundation for the research presented in this thesis.

2.2 THE ECOLOGY OF SHALLOW LAKES

2.2.1 Principle Characteristics of Shallow Lakes

Shallow lakes are an important ecological and socio-economic resource and pristine shallow lakes often support high biodiversity. However, as a result of human activities (physical modification, eutrophication, acidification) many shallow lake ecosystems, particularly in Europe, have suffered a decline in their ecological status and it can be argued that there is currently an unprecedented interest in the ecology of these systems. Lakes vary dramatically in their physical, chemical and biological characteristics and shallow lake ecosystems are no exception in this context. Shallow lakes, globally, encompass a diverse range of environments from small artificial lakes (< 1 km^2) (e.g. Norfolk Broads, UK; Loosdrecht Lakes, Netherlands) to natural and large epicontinental systems (> 1000 km^2) (e.g. Lake Chad, Africa; Lake Balaton, Hungary; Lake Peipus, Estonia/Russia) and, further, comprise both highly acidic/dystrophic systems (e.g. Lake Flosek, Poland) and highly alkaline systems (e.g. Mono Lake, USA; Lake Nakuru, African Rift Valley).

However, the term ‘shallow lake’ is somewhat ambiguous. The dissimilarity between shallow and deep lakes goes beyond the obvious difference in water depth; rather, this dissimilarity is one of a fundamental difference in processes and function (Nixdorf & Deneke, 1997; Havens *et al.,* 2001). Shallow lakes typically share one definitive characteristic that distinguishes them from deeper systems: the absence of prolonged thermal water column stratification (Burgis & Morris, 1987; Scheffer, 1998; Havens *et al.,* 2001). The absence of thermal stratification is a common attribute of lakes where the mean water depth is *c.* < 3 m (although certainly not exclusively) and this threshold is often used as an arbitrary boundary for the distinction between shallow and deep systems (Moss, 1998; Padisak & Reynolds, 2003). Deeper systems (i.e. > 3 m), however, may often behave as ‘functionally’ shallow lakes where various factors (e.g. the hydrodynamic regime, wind exposure) combine to ensure the system is regularly mixed (Burgis & Morris, 1987). Shallow lakes, as a result of their bathymetry, are also often characterised by short residence times and high rates of flushing.

The polymictic nature of shallow lakes influences many other lake-scale processes and functions and, in particular, the nutrient cycling regime. There is a common trend for shallow lakes to be typically more fertile, *per se*, than comparable deeper systems. This fertility is often a result of the efficient recycling of resources and, in particular, a nutrient cycle that, in comparison to regularly stratified systems, is governed by internal processes. Indeed, the physical, chemical, and biological regulation of nutrient fluxes between bottom sediments, the overlying water column and the atmosphere is a key ecological process in shallow lakes (Sondergaard *et al.,* 1992; Blom *et al.,* 1992; Sondergaard *et al.,* 2003).

Shallow lakes also have a disproportionately large euphotic zone which promotes the rate and influence of benthic processes (e.g. biofilm development, mineralization of organic matter) (Padisak & Reynolds, 2003). In pristine clear water shallow lakes, the colonisation of the bottom sediments by aquatic plants (macrophytes) promotes high benthic productivity. In such lakes, aquatic plants dominate the base of the limnetic food web and are critical to the function of many lake-scale processes (Jeppesen *et al.,* 1997; Madsen *et al.,* 2001; Kufel & Kufel, 2002; Takamura *et al.,* 2003). However, in turbid shallow lakes, submerged macrophyte growth may

be precluded and, under such circumstances, phytoplankton may replace aquatic plants as the dominant primary producers (Sandjensen & Borum, 1991). The often intense competition for resources between submerged aquatic plants and phytoplankton is a defining characteristic of shallow lake environments and its impact on ecosystem stability has been the recent focus of considerable scientific interest (Sandjensen & Borum, 1991; Scheffer *et al.,* 1993; Blindow *et al.,* 1993; Scheffer *et al.,* 2001; Peckham *et al.,* 2006; Van Nes *et al.,* 2007; Scheffer & Jeppesen, 2007; Dokulil *et al.,* 2007).

2.2.2 Suspended Sediment Dynamics

The sediment in suspension in shallow lake environments (suspended particulate matter (SPM) or seston) consists of variable proportions of suspended particulate inorganic matter (SPIM) and suspended particulate organic matter (SPOM). SPM can also be divided into living (plankton) and non-living (tripton) components. SPM in lakes is derived from both allocththonous (inputs of terrigenous material via river tributaries) and autochthonous (resuspension of bottom sediments) sources. In shallow lakes, bottom sediments are readily resuspended by wave action, as such the predominant source of SPM is invariantly autochthonous (Bloesch, 1995; Markensten & Pierson, 2003). High rates of sediment resuspension often result in shallow lakes often having significantly higher SPM loads than deeper systems (up to several orders of magnitude) (Scheffer, 1998).

There are two predominant mechanisms of sediment resuspension in shallow lakes: (i) suspension due to shear waves induced by wind, seiche, or boat wash action (Garrad & Hey, 1987; Bloesch, 1995; Markensten & Pierson, 2003; Cozar *et al.,* 2005), and (ii) bioturbidation of the sediment by foraging benthic fish such as bream (*Abramis brama*) and carp (*Cyprinus carpio*) (Luettich *et al.,* 1990; Havens, 1991; Breukelaar *et al.,* 1994). However, sediment resuspension may be further affected by factors such as the inherent cohesive nature of the sediment (Scheffer, 1998), sediment consolidation by microphytobenthos growth (Delgado *et al.,* 1991), and sediment consolidation and flow impedance by macrophyte colonisation (Crawford, 1979; Dieter, 1990; Scheffer, 1999; Schallenberg & Burns, 2004).

The resuspension of bottom sediments has significant implications for the ecology of shallow lakes. High sediment loads reduce water transparency and may result in the light-limitation of benthic photosynthesis (Scheffer, 1998). Moreover, the resuspension of bottom sediments is also central to the cycling of nutrients (particularly phosphorus) in shallow lake ecosystems. In deep, stratified lakes, phosphorus (P) is continuously lost from the epilimnion to the hypolimnion as particulate matter sinks through the thermocline and is mineralised in the bottom sediment. This pool of P may cycle between benthic sediments and the hypolimnion, but it is essentially unavailable to autotrophic organisms in the epilimnion (i.e. phytoplankton) until stratification is lost and the lake mixes (Moss, 1998). In contrast, in shallow lakes, continual disturbance of the sediment-water interface resulting from turbulence-induced resuspension processes, or bioturbidation, promotes the diffusion of the benthic P pool into the overlying water column, where it is immediately available to autotrophic organisms. Thus, the bottom sediments of shallow lakes often act as an autochthonous net source of P (rather than as a sink environment as in many deep lakes) particularly during summer months (Spears *et al.,* 2007). In eutrophic shallow lakes, the legacy of nutrient enrichment can result in a substantial accumulation of P in bottom sediments; this sediment-related P is typically partitioned between several pools, some of which, such as the pH and redox sensitive Fe-P and Mn-P complexes, can be highly labile. Thus, in shallow lakes it is not uncommon for the annual internal P load (i.e. that derived entirely from recycling) to be substantially larger than the external P load (i.e. that derived from the catchment) (Scheffer, 1998).

The importance of suspended sediment dynamics to shallow lake ecology has resulted in substantial research being devoted to examining the impact of sediment resuspension on nutrient loading (e.g. Sondergaard *et al.,* 1992; Reddy *et al.,* 1996; Fan *et al.,* 2001; Sondergaard *et al.,* 2003; Qin *et al.,* 2004). In addition, the remobilisation of sediment in lake systems may also have significant implications for the fate of heavy metals (Linge & Oldham, 2002; Mason *et al.,* 2003) and organic contaminants (Bogdan *et al.,* 2002) and can have radical effects on the ecology of phytoplankton and macrophyte communities (Barko *et al.,* 1991; Jensen *et al.,* 1994; Ogilvie & Mitchell, 1998; Nalewajko & Murphy, 1998; Millie *et al.,* 2002).

The distribution and flux of sediment through lake systems is largely governed by the complexities of hydraulic circulation. The varied controls on sediment dynamics in shallow lake ecosystems mean that often the concentration of suspended sediment, even in well mixed systems, can be highly variable both spatially and temporally. Efforts to characterise the dynamism of SPM resuspension and transportation in lakes have conventionally relied upon *in-situ* point-based measurements (e.g. water sampling, sediment traps). However, as Nellis *et al*. (1998) recognise, the often-pronounced spatial variability in the distribution of suspended sediment in lakes means that point-scale approaches can seldom provide an adequate spatial understanding of suspended sediment dynamics. Increasingly, in an effort to gain a spatially-explicit understanding of suspended sediment fluxes in lakes, workers are employing advanced 2-dimension and 3-dimensional hydrodynamic models (Bailey & Hamilton, 1997; Teeter *et al.,* 2001; Vanderploeg *et al.,* 2007; Jin *et al.,* 2007) and data derived from remote sensing platforms (Nellis *et al.,* 1998; Bergmann *et al.,* 2004; Budd, 2004)

2.2.3 Phytoplankton

2.2.3.1 What are Phytoplankton?

The phytoplankton (*phyton* = plant, *planktos* = wandering) are an immensely diverse group of microscopic algae that form the base of the pelagic food web and, as such, are one of the most important biotic elements of shallow lake ecosystems. The phytoplankton assemblages of shallow lakes represent a sizeable component of the biodiversity of these ecosystems and have an important functional role in several ecosystem processes, not least, in the regulation of biogeochemical cycling. The vast majority of phytoplankton species are eukaryotic algae. However, two divisions of prokaryotic photosynthetic bacteria (the prochlorophyta and cyanophyta) are also an important component of the phytoplankton assemblages found in freshwaters. The five most important phytoplankton divisions in freshwaters are the bacillariophytes (diatoms), cryptophytes (cryptomonads), chlorophytes (green algae), dinophytes (dinoflagellates) and cyanophytes (cyanobacteria) (Schmid *et al.,* 1998).

2.2.3.2 Population Dynamics in Shallow Lakes

Phytoplankton populations are arguably amongst the most dynamic biological assemblages encountered in nature and can be conspicuously subject to rapid fluctuations in both size and composition. Changes in phytoplankton populations may occur as a response to the intermittent pulsing of resources through the system or, in contrast, may result from the effect of large-scale episodic disturbances (e.g. flushing, mixing) (Jacobsen & Simonsen, 1993; Reynolds, 2006). The dynamism of phytoplankton communities is essentially a reflection of the capacity of different species, through their specific functional traits, to adapt and exploit changing environmental conditions. It is has been suggested that such environmental heterogeneity prevents phytoplankton communities from seldom realising a steady-state equilibrium (Padisak, 1993; Reynolds, 2006).

The growth of phytoplankton populations can be rapid. Laboratory steady-state experiments have recorded growth rates > 10 divisions day^{-1} (Reynolds, 2006). In natural environments, resource limitation (e.g. N, P, Si, light, temperature) inevitably results in slower *in-situ* growth rates but, under favourable conditions, phytoplankton populations can still attain growth rates > 1 division day^{-1} (Reynolds, 2006). In shallow lake ecosystems, particularly eutrophic systems, readily accessible resource pools and the efficient recycling of nutrients can foster rapid phytoplankton growth and the development of mass populations either as blooms, scums or biofilms.

In shallow lakes, changes in population size may also arise as a result of catastrophic losses incurred from mass sinking, flushing events and intense top-down predation. Losses incurred from sinking are typically low in well-mixed shallow lakes. However, during short-lived conditions of benign mixing, sinking losses can be exceptionally high in shallow lakes (Scheffer, 1998). In addition, short residence times and regular flushing can also result in large-scale phytoplankton population losses (Jacobsen & Simonsen, 1993). Moreover, in macrophyte-dominated shallow lakes, significant losses may be incurred by the grazing of zooplankton. Indeed, top-down grazing pressure can be so intense in shallow lakes that turbid,

phytoplankton-dominated, waters can be temporary replaced by clear water conditions (Townsend *et al.,* 1994; Jurgens & Stolpe, 1995).

The species composition of phytoplankton communities is often highly diverse and, as a result of both allogenic and autogenic factors, communities can often demonstrate pronounced successional patterns. Spring (or vernal) blooms are typically dominated by small *r*-selected (or C-adapted) species which are able to rapidly exploit nutrient pulses. Diatoms often dominate spring blooms as they favour the unstable hydrodynamic conditions and are well-adapted for growth in environments that may be light and/or temperature limited. In contrast, later successional stages, particularly towards late-summer, are typically dominated by more slow-growing and stress-tolerant *K*-selected (or S-adapted) species that are able to out-compete other species for limited resources (nutrients, light) (Agbeti *et al.,* 1997; Talling & Parker, 2002; Celik & Ongun, 2006; Reynolds, 2006).

In eutrophic shallow lakes, later successional stages are often dominated by cyanobacteria (blue-green algae). The phenomenon of cyanobacterial dominance in eutrophic shallow lakes has received considerable attention and numerous mechanisms explaining cyanobacterial dominance have been proposed (see for example Hysenstrand *et al.,* 1998; Dokulil & Teubner, 2000). Cyanobacterial dominance in (shallow and deep) lakes has often been linked to factors such as elevated water temperatures (Robarts & Zohary, 1987; McQueen & Lean, 1987), low TN:TP ratios (Smith, 1983; Presing *et al.,* 2001), nitrate deficiency (Blomqvist *et al.,* 1994), the capacity for intracellular nutrient storage (Eckerrot & Pettersson, 1993) and an ability to compete through toxicity (Lindholm *et al.,* 1989). However, in shallow lakes, it has been suggested that the often persistent late-summer dominance of cyanobacteria, particularly by filamentous species (e.g. *Limnothrix* spp. *Planktothrix* spp. (formerly *Oscillatoria*)), is owed to an ability to tolerate the effects of shade in turbid shallow lakes (Scheffer et al., 1997). In addition, some cyanobacteria species (e.g. *Microcystis* spp., *Anabaena* spp.) are able to evade light-starvation in turbid waters through buoyancy-regulated vertical migrations to well-illuminated near-surface waters.

2.2.3.3 Spatial Distribution in Shallow Lakes

The planktic nature of algae means their distribution, whilst in suspension, is principally determined by the patterns of hydraulic circulation (Reynolds, 2006). Complexities in the pattern of hydraulic circulation can lead to the creation of marked heterogeneity in the distribution of phytoplankton in lakes. This heterogeneity – often described as patchiness – is often evident at various scales (micro-, meso- and macro-scale) and may be observed in both horizontal and vertical dimensions (George & Edwards, 1976; George & Heaney, 1978; Frempong, 1981; George & Jones, 1987).

Heterogeneity in horizontal planes is predominantly governed by two mechanisms: (1) transportation in wind- and/or hydrothermal-induced currents (George & Edwards, 1976; George & Heaney, 1978) or (2) localised variation in phytoplankton growth and mortality (George & Jones, 1987). Patchiness at the micro-scale (< 1 m) may result from stochastic variability (i.e. presence/absence) but, arguably, such small-scale variability has little underlying ecological significance. Meso-scale patchiness (*c.* 1-100 m) is often the result of variations in hydraulic circulation – such as those created by Langmuir rotations (George & Edwards, 1976; Evans & Taylor, 1980; Leibovich, 1983; Hedger *et al.,* 2004). Langmuir rotations promote the clustering of positively buoyant phytoplankters in the region of convergence between adjacent downwelling Langmuirian cells. In contrast, negatively buoyant phytoplankters congregate in the region of convergence between adjacent upwelling Langmurian cells. Fluctuations in wind speed and direction can add additional complexity by distorting these patterns and superimposing new patterns upon existing ones. However, the transient nature of Langmurian and similar features means that these spatial patterns are generally not compounded by differences in local population growth before such patterns disintegrate and new patterns form (Reynolds, 2006).

The controls upon macro-scale patchiness (> 100 m) are more varied and complex than those that govern meso-scale features. Hydraulic circulation again can often play a pivotal role in the creation of large-scale features (Webster, 1990). Strong prevalent winds often result in the downwind accumulation of phytoplankton towards the leeward shores of lakes. In small and

enclosed basins, downwind hydraulic currents are compensated by deeper advective flows. Buoyant phytoplankton species (e.g. cyanobacteria) are particularly susceptible to downwind accumulation, but resist entrainment into the advective flows returning at depth; whereas, non-buoyant species become entrained in the deep advective current and are transported in an upwind direction. Macro-scale heterogeneity is also generally more persistent than micro- and meso-scales features and, as such, localised population growth can often compound the patterns created (George & Jones, 1987).

The mechanisms that create heterogeneity in the vertical plane include vertical migration by motile phytoplankton and the break down of mixing (perhaps leading to brief microstratification). Vertical migrations by motile phytoplankton (most notably the buoyancy-regulating cyanobacteria ecotypes, or flagellate species) enable species to maintain station in horizons of favourable insolation or evade nutrient depletion or predation (Salonen *et al.,* 1984; Salonen & Rosenberg, 2000). In particular, benign mixing can promote the accumulation of positively buoyant phytoplankters in near-surface epilimnion waters. Indeed, the near-surface accumulation of buoyant cyanobacteria during periods of benign mixing (wind speeds < 4 m s^{-1}) can result in the creation of a pronounced vertical biomass gradient (Reynolds & Walsby, 1975; Ye *et al.,* 2006). Short-lived periods of benign mixing in shallow lakes may also result in non-motile phytoplankters sinking through the temporary metalimnion where they are confined to bottom waters until mixing resumes.

2.2.4 Aquatic Vegetation

2.2.4.1 Occurrence in Shallow Lakes

Shallow lake environments of good ecological status are often characterised by extensive and floristically diverse beds of aquatic plants. In clear shallow waters, where the light climate is favourable, aquatic plants can often colonise the entire lake bed. The aquatic vegetation of lakes can be classified on the basis of three distinct growth habits: (i) *emergent* – plants which root in the sediment, but aerial parts protrude above the water surface; (ii) *floating* – plants which may or may not root in the sediment, but have leaves which float on the water surface; and (iii) *submerged* – plants which grow completely below the water surface. Submerged

plants may further categorised into those species which (i) form low-growing canopies (such as *Chara* spp. or *Nitella* spp.) and, (ii) form near-surface canopies (such as some *Potamogeton* spp. or *Myriophyllum* spp.) (Scheffer, 1998).

The distribution of macrophytes in shallow lakes typically shows a clear and systematic zonation with depth (and/or water transparency). The shallower waters of the littoral are often colonised by emergent species (e.g. *Phragmites australis*, *Typha latifolia*, *Phalaris arundinacea*). These emergent species may grade into beds of floating (e.g. *Nuphar lutea*, *Lemma* spp.) and, latterly, submerged (e.g. *Chara* spp, *Nitella* spp.) species as the water depth increases towards the lower region of the littoral (Chambers & Kalff, 1985; Canfield *et al.,* 1985; Skubinna *et al.,* 1995; Scheffer, 1998). The abundance and distribution of submerged plants is highly dependent on underwater light climate, with a shift from low-growing species, to near-surface-canopy-forming species occurring with increased turbidity. In highly turbid water the submerged community may be conspicuously absent. The distribution of aquatic plants in lakes may also be affected by factors such as sediment chemistry and exposure to wave action (Vanwijk, 1988). These various factors ensure that the distribution of aquatic vegetation in shallow lakes can be complex and often communities form heterogeneous mosaics and ecotone features with both the terrestrial and pelagic interface.

2.2.4.2 Functional Importance of Aquatic Vegetation

The abundance, distribution and composition of aquatic vegetation communities exerts a profound influence upon many processes and functions in shallow lake ecosystems (Phillips *et al.,* 1978; Carpenter & Lodge, 1986; Scheffer, 1998). Carpenter & Lodge (1986) suggest that the importance of aquatic plants (particularly submerged species) to the ecology of shallow lakes stems from the fact that they occupy a series of key ecological niches. The extent of macrophyte colonisation is thus considered a key indicator of ecological status. Indeed a growing volume of research has shown that aquatic plants are critical to the ecological stability of shallow lake ecosystems (Scheffer *et al.,* 1993; Van Nes & Scheffer, 2003; Scheffer & Carpenter, 2003; Scheffer & Van Nes, 2007; Scheffer & Jeppesen, 2007).

Aquatic plant colonisation can influence the (i) physical, (ii) chemical, and (iii) biological function of shallow lake ecosystems. Modifications to physical processes include the increased extinction of light (Titus & Adams, 1979; Pokorny *et al.,* 1984), increased temperature gradients with depth (Dale & Gillespie, 1977) and the stabilisation of bottom substrates (Scheffer, 1998). The impedance of water flow is another important function of aquatic plants, for it reduces the resuspension of bottom sediments and increases the sedimentation of fine particulates, which has been shown to substantially reduce internal nutrient loading in shallow lake ecosystems (Rooney *et al.,* 2003).

Modifications to chemical processes include the assimilation and release of macro- and micronutrients, the immobilisation of waterborne contaminants, and amendments to the chemistry of rooting sediments. Aquatic plants, for example, provide a critical sink environment for nutrients and can act as a buffer against excessive phosphorus and nitrogen loadings in shallow lakes. This capability for nutrient sequestration can help suppress the development of phytoplankton blooms which, in turn, facilitates the perseverance of favourable water quality status (Kufel & Kufel, 2002; Takamura *et al.,* 2003). Aquatic plants can also provide an important sink for heavy metals and other toxic contaminants (Ye *et al.,* 2001) and have a marked influence on sediment pH, redox and nutrient release (Carpenter & Lodge, 1986).

The biological function of shallow lakes can be drastically transformed by the presence of aquatic plants as they form an important link in many cascading trophic interactions (Jones & Sayer, 2003). In particular, aquatic plants provide critical habitat refuges for many aquatic biota – especially zooplankton communities – and thus have an important function in maintaining top-down control of phytoplankton crops (Stansfield *et al.,* 1995; Stansfield *et al.,* 1997; Lacroix *et al.,* 1999; Horppila & Nurminen, 2001; Balayla & Moss, 2003). Aquatic plant beds are also an important habitat for invertebrate, fish and bird populations (Scheffer, 1999).

2.2.5 Shallow Lakes and Eutrophication

2.2.5.1 Phytoplankton, Aquatic Plants and Alternative Stable States

Shallow lakes of good ecological status are often characterised by a natural state of macrophyte-dominance (Scheffer *et al.,* 1993; Scheffer & Jeppesen, 2007). The dominance of aquatic plants is essentially fostered by the persistence of clear water conditions. The sequestration of nutrients by aquatic plants helps create an environment of moderate nutrient stress which, in turn, suppresses the growth of phytoplankton, and helps to maintain clear water conditions. This positive feedback fosters macrophyte-dominance and promotes ecosystem stability.

However, anthropogenic nutrient enrichment has precipitated a loss of macrophyte-dominance in many shallow lakes (Scheffer *et al.,* 1993; Scheffer *et al.,* 2001; Havens *et al.,* 2001; Scheffer & Carpenter, 2003; Scheffer & Jeppesen, 2007; Scheffer & Van Nes, 2007; Scheffer & Jeppesen, 2007). The increased provision of nutrients has been shown to stimulate the undesirable growth of phytoplankton and epiphytic algae. The resulting increases in turbidity impede the growth of submerged macrophytes; the loss of macrophyte cover only serves to further promote phytoplankton growth, which instils instability in the ecosystem and, in due course, a switch to phytoplankton-dominance can transpire (Scheffer *et al.,* 1993; Scheffer *et al.,* 2001; Havens *et al.,* 2001; Scheffer & Carpenter, 2003; Scheffer & Van Nes, 2007; Scheffer & Jeppesen, 2007).

Shallow lakes are thus an example of an ecosystem which can exist in two (or more) alternative ecological states: (1) macrophyte dominance or (2) phytoplankton dominance (Scheffer *et al.,* 1993). The model of stable state behaviour proposed by Scheffer *et al*. (1993) suggests that alternative stable states can exist over a broad and common range of nutrient conditions, but only one state can exist at the extremes of this nutrient gradient (see Figure 2.1). Conceptual models of stable state behaviour indicate that switches between stable states in shallow lakes occur at a critical threshold of turbidity. The position of the critical turbidity threshold often varies between ecosystems as a result of their varying capacity to buffer nutrient loadings; this can lead to hysteretic behaviour in the response of shallow lake ecosystems to eutrophication.

It has also been suggested that, in addition to a critical turbidity threshold, various trigger mechanisms may be necessary to precipitate changes in ecosystem state (Stansfield *et al.,* 1989; Irvine *et al.,* 1993; Jak *et al.,* 1996; Jones & Sayer, 2003).

Stable state theory in shallow lakes has been recently embellished to acknowledge the existence of further possible stable states. Scheffer *et al*. (1997) and Scheffer (1998) propose a model of ecosystem behaviour involving three stable states: (i) a macrophyte dominated state; (ii) a state dominated by eukaryotic phytoplankton (green algae); and (iii) a state dominated by prokaryotic phytoplankton (blue-green algae). It is suggested that dominance by shade-tolerant cyanobacteria is fostered in highly turbid shallow lakes. Stable states dominated by charophytes, submerged angiosperms, and filamentous green algae have also been theorised (Scheffer *et al.,* 2003; Irfanullah & Moss, 2005; Scheffer & Van Nes, 2007).

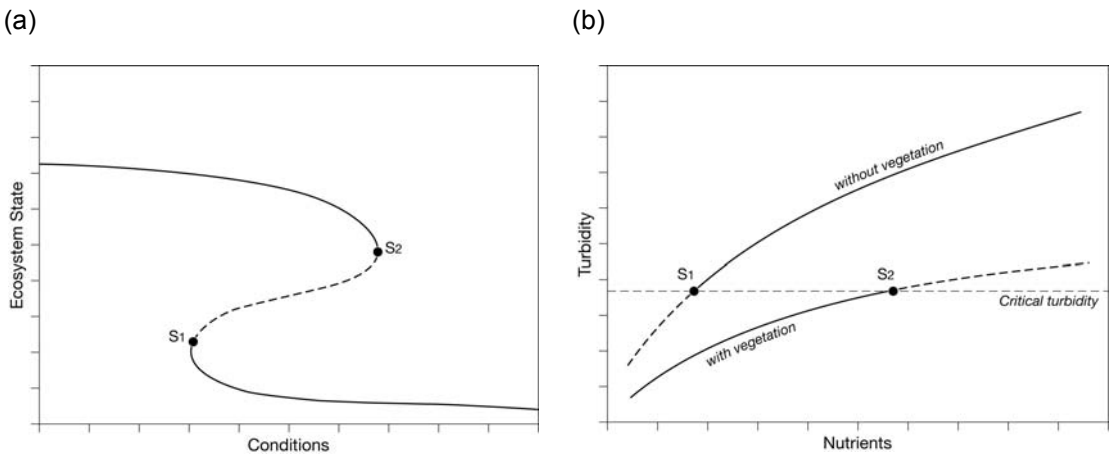

Figure 2.1 (a) An example of a ecosystem that can more than one stable state (S_1 and S_2) over a range of conditions (hysteresis), and (b) the theory of alternative stable states applied to shallow lakes, states of phytoplankton-dominance and macrophyte-dominance can exist over a common nutrient gradient, but switch to phytoplankton-dominance is hypothesised once a critical turbidity (phytoplankton density) is reached. Note at the extremes of the nutrient gradient only one state can persist. The distance between S_1 and S_2 in (a) reflects the buffering capacity of aquatic plants to nutrient enrichment (modified from Scheffer & Carpenter, 2003).

The concept of alternative ecosystem equilibria in shallow lakes underlines the complexity of the trophic linkages that exist between the various biotic elements in shallow lakes and offers an apt explanation of the dynamic behaviour (erratic or cyclic) of these ecosystems (Van Nes *et al.,* 2007). Indeed, there is now recognition that the response of shallow lake ecosystems to a

perturbation gradient (eutrophication) may be seen as a dynamic continuum in which gradual species replacements are interrupted at critical points by more dramatic shifts to contrasting alternative regimes dominated by different biotic elements (Van Nes *et al.,* 2007; Scheffer & Van Nes, 2007). This concept of dynamic regime shifts now also recognises the importance of spatial heterogeneity in controlling ecosystem responses to perturbation (Van Nes & Scheffer, 2005; Scheffer & Van Nes, 2007).

2.2.5.2 Potentially-Toxic Cyanobacterial Blooms

The development of mass populations (blooms, scums and biofilms) of cyanobacteria is common occurrence in shallow lake ecosystems subject to eutrophication. Mass populations of cyanobacteria are significant problem for the ecological integrity of shallow lakes and, further, they can present a serious hazard for both human and animal health. Cyanobacteria are not themselves microbial pathogens, but their toxins (cyanotoxins) constitute one of the most high risk categories of waterborne toxins. Many cyanobacteria genera common to shallow lakes can produce numerous potent toxins (e.g. *Anabaena, Aphanizomenon, Anabaenopsis, Cylindrospermopsis, Microcystis, Nodularia, Planktothrix, Oscillatoria, Raphidiopsis*). These species can produce a variable cocktail of cyanotoxins including hepatotoxic (e.g. microcystins) and neurotoxic (e.g. anatoxin-a, BMAA) agents. Cyanotoxins have been linked to incidents of fish and bird kills and, in humans, symptoms of exposure include skin irritation, fever, intestinal problems and allergic reactions (Chorus *et al.,* 2000; Codd *et al.,* 2005).

There is increasing national and international recognition of the need for improved risk management of cyanobacteria and cyanotoxins to protect water resources, water-based economies and human health (Codd *et al.,* 2005). Rapid assays for the presence of cyanotoxins in lakes have yet to be developed, thus the current approach to risk management is largely based upon the early identification of mass cyanobacterial population growth.

2.2.5.3 Reedswamp Dieback

Reedswamp is a functionally important component of the littoral environment of shallow lake ecosystems. In recent decades there has been a large-scale decline in the reedswamp habitat

of many European lakes and, in particular, that composed of the common reed (*Phragmites australis* (Cav.) Trin. Ex Steudel) (Boar *et al.,* 1989; Van Der Putten, 1997; Fogli *et al.,* 2002).

The decline of *Phragmites australis* reedswamp in European lakes has been strongly linked to eutrophication and the consequent development of phytotoxic compounds in nutrient-enriched littoral sediments (Armstrong & Armstrong, 2001). Cizkova *et al*. (1996) suggest that, in eutrophic lake systems, increased primary productivity can lead to the substantial accumulation of organic matter in reedswamp habitats. The copious flux of organic-C to littoral hydrosoils accelerates decompositional processes, increasing the microbial demand for oxygen, and ultimately leading to the development of oxygen-stressed anaerobic conditions. The resulting switch to anaerobic microbial metabolism can, in turn, lead to the production of numerous phytotoxic metabolites as the end-products of anaerobic decomposition (Santruckova *et al.,* 2001). The accumulation of these phytotoxic metabolites (typically organic acids), in combination with conditions of oxygen stress, is believed to be a major cause of reed decline in European lakes and their associated wetland environments (Boar *et al.,* 1989; Armstrong *et al.,* 1996; Armstrong *et al.,* 1996; Vanderputten *et al.,* 1997; Cizkova *et al.,* 1999).

2.3 THE NORFOLK BROADS (UK)

2.3.1 Location, Catchment and Limnology

The Norfolk Broads (52º44'17''N; 1º34'29''E) are a series (*c*. 63) of small shallow lakes in southeast England (East Anglia, U.K.) that formed when 12th and 13th century peat excavations were flooded by rising sea levels (Lambert & Smith, 1961). The Broads range in extent from 0.1-130 ha (0.001-1.3 km^2) and typically have a mean depth < 2.5 m. The Broads lie in the valleys of the rivers Ant, Bure, Thurne, Yare and Waveney; these slow moving rivers and a network of artificial canals and dykes provide a hydrological connection between many of the lakes and form the most extensive navigable, lock-free, waterway in the U.K. (190 km) (Mason & Bryant, 1975; Moss, 2001).

The three largest rivers, the Yare, Waveney and Bure, drain a catchment that totals an area of approximately 3,180 km^2. The catchment lies at an altitude that varies from -1 to 101 m above

sea level with a geology that is primarily composed of Cretaceous Chalks and Pleistocene calcareous sands overlain by glacial tills, sands and gravels (Gilvear & Mcinnes, 1994; Moss, 2001). The Pleistocene calcareous sands form the large Norwich Crag aquifer that underlies much of Broadland. The main land uses within the catchment are intensive arable agriculture (*c*. 49.6%) and extensive agricultural pasture (*c*. 32.6%), while just over 10% of the catchment is occupied by urban development (Moss, 2001).

The climate of the East Anglia region is more continental than that experienced elsewhere in the U.K. with minimum and maximum temperatures of 2.2-6 °C in January rising to 13.3-20 °C in August. The prevailing wind direction is from the north-east and annual precipitation is in the magnitude of 600-700 mm. The chemical composition of the Broadland water courses reflects the underlying geology being rich in Ca, Mg and HCO_3 (Table 2.1). The Broadland waters maintain a constant pH in the range 7.1-9.1 because of a strong buffering capacity provided by the calcareous water chemistry (Moss, 2001). The lakes are typically well flushed with residence times varying from a matter of days in winter to a few weeks in summer (Moss, 2001). The Thurne Broads endure a small tidal influence which equates to 40-70 cm in the lower river reaches and up to 20 cm in the upper reaches on the spring tide and the percolation of saline water into the underlying Crag aquifer means the lakes in Thurne system are more brackish in nature than those on the other river systems (Moss, 2001).

Table 2.1 The typical major ionic composition of some Broadland water courses (mg l^{-1}) compared to that typical of the English Lake District (Moss, 2001)

	Ca	**Mg**	**Na**	**K**	**HCO_3**	**Cl**
Yare	143	5.9	37.1	4.3	336	48
Ant	128	11	46	9.4	238	77
Thurne	234	306	856	31	165	544
English Lake District	2.2	0.8	3.8	0.4	3.5	7.6

2.3.2 Past and Present Ecological Status

Many natural historians writing from the 19th century to the pre-WWII period made reference to the rich and diverse fauna and flora and that characterised many of the Norfolk Broads (Davies, 1883; Patterson, 1920; Ellis, 1935). It is significant that these accounts recall a Broadland environment noted for the clarity of its waters and the richness of the aquatic plants that dominated the lake bed of many Broads. Palaeolimnological evidence substantiates these accounts and has confirmed that the Broads were previously more nutrient poor than at present (Moss, 1978; Kerrison *et al.,* 1988).

It became apparent in the 1950s and 1960s that the Broadland environment was very different from that described by the 19th century naturalists. The waters of the Broads had become turbid with the growth of phytoplankton and increased concentrations of suspended sediment, while the consequent loss of water column transparency had resulted in the loss of submerged plants from many of the lakes. These changes were inevitably linked to the increased nutrient loads the Broads had received from domestic, industrial and agricultural sources (or, in the case of the Thurne Broads, from guanotrophication). This largely cultural eutrophication had serious deleterious impacts on water quality and the diversity of the aquatic plant, invertebrate, fish and wildfowl communities in the Broads (Moss, 2001).

Considerable effort has been invested over recent years in attempting to restore the Broads back to a state comparable to that described by the late 19th and early 20th century natural historians. Central to this effort has been the establishment of measures to protect Broadland's remaining biodiversity. The Norfolk Broads was granted National Park status in 1988 through the legislation of the Norfolk and Suffolk Broads Act and the Broads Authority was thus charged with the conservation and management of the fledgling National Park. In addition to National Park status, 29 SSSIs (Sites of Special Scientific Interest), 7 NNRs (National Nature Reserves), 2 Ramsar sites, 2 SPAs (Special Protection Areas) and 2 SACs (Special Areas of Conservation) have been established. Intensive lake restorations schemes (isolation, biomanipulation, suction dredging) have been implemented in an attempt to restore good

ecological status in the Broads. However, despite these efforts, many Broads still remain in a state of poor ecological health.

2.4 REMOTE SENSING

2.4.1 Remote Sensing and Shallow Lake Ecology

Remote sensing – here taken to refer to the method of observing the earth from airborne or spaceborne sensors – is one of the most powerful analytical tools available to ecologists; yet it remains one of the most underused (Aplin, 2005). The value of remote sensing, when compared to measurements made using conventional point-based techniques, is that it can provide spatially explicit appraisals of environmental phenomena, and at a range of spatial and temporal scales that are relevant to ecological investigations. In complex systems, the spatially and temporal resolving datasets afforded by remote sensing have been shown to be invaluable in delivering information on dynamic ecological processes and functions that would be otherwise unobtainable with point-based sampling methods (Winterbottom & Gilvear, 1997; Bryant & Gilvear, 1999; Davids & Tyler, 2003; Rainey *et al.,* 2003).

Remote sensing also affords many other benefits. Spaceborne and airborne instruments, where available, can provide an immediate scientific response to episodic environmental events. This has been demonstrated pertinently in the aftermath of catastrophic natural disasters such as the Asian Tsunami (Ramakrishnan *et al.,* 2005) and Hurricane Katrina (Duda & Abrams, 2005); but it is also evident that remote sensing can provide rapid reconnaissance of more local-scale events (e.g. storm events, pollution discharges) that are of relevance to function of aquatic and terrestrial ecosystems. Moreover, the data legacy of past and present spaceborne instruments provides an extensive archive of data through which hind-cast analysis can be undertaken, offering an effective means of establishing retrospective baselines, and an invaluable resource for studies concerned with change detection (Munyati, 2000; Li & Narayanan, 2003).

In ecology, remote sensing has often been employed to simply map the distribution of species, habitats and biotopes but, increasingly, it is being used for the direct measurement of

biophysical properties (e.g. LAI, NPP) and to integrate such measurements at the ecosystem-, landscape- and global-scale. Remote sensing has found varied application in lake ecology. It has been used to compile lake inventories (Finlayson & Vandervalk, 1995), monitor patterns in water resource use (Beeri & Phillips, 2007) and in hazard and risk assessments (Quincey *et al.,* 2007; McKillop & Clague, 2007). However, remote sensing has found more common application in the quantification of water quality parameters, such as lake surface temperature (LST) (George, 1993; Kay *et al.,* 2005), Secchi disc depth (SDD) (Harrington *et al.,* 1992; Baban, 1993; Nellis *et al.,* 1998; Zhang *et al.,* 2003), coloured dissolved organic matter (CDOM) (Kutser *et al.,* 2005b; Zhang *et al.,* 2007) suspended sediments (tripton) (Lathrop *et al.,* 1991; Choubey & Subramanian, 1992; Ghezzi *et al*., 1998) and chlorophyll-a (George & Malthus, 2001; Koponen *et al.,* 2002; Ammenberg *et al.,* 2002; Tyler *et al.,* 2006). Remote sensing has also been used to map the distribution of aquatic plants in shallow lakes (Malthus & George, 1997; Dekker *et al.,* 2005; Yuan & Zhang, 2007) and assess the physiological status of emergent macrophytes (Penuelas *et al.,* 1993).

It should be noted, however, that remote sensing data, and the measurements derived there from, have been seldom integrated into studies concerned with the nature of processes and function in shallow lake ecosystems. There are some notable exceptions in this context. George (2000) used thermal imaging to track the episodic transport of phosphorus-laden water from the littoral zone of a thermally-stratified shallow lake (Esthwaite Water, UK). Hedger *et al*. (2002) combined remote sensing with a fluid-dynamics model to provide an understanding of the controls on the distribution of phytoplankton in a shallow lake (Loch Leven, UK). Peckham *et al*. (2006) developed a lake trophic state index (TSI) from data derived from satellite remote sensing to provide evidence for alternative stable state behaviour in shallow lakes in Wisconsin (USA). Budd *et al*. (2001) used archive remote sensing data to retrospectively investigate the impact of the Zebra mussel on water clarity in Lake Huron. Pengra *et al*. (2007) used remote sensing to map the invasion of *Phragmites australis* into a shallow lake ecosystem. Tilley *et al*. (2003) used remote sensing to examine the response of emergent macrophytes to a gradient in water column ammonium and Valta-Hulkkonen *et al*. (2004) used remote sensing, in combination with GIS, to assess the responses of shallow lakes to restoration measures.

It is clear, from the above examples, that remote sensing technologies can, when used, make a significant contribution to the study of lake ecology. In shallow lakes, it would seem that remote sensing surveillance has particular merit for the assessment and monitoring of both phytoplankton and aquatic vegetation. Moreover, the spatially-explicit data derived from remote sensing would seem to be capable of providing novel insights into the nature of shallow lake processes and function and lake-scale ecosystem responses to perturbation. In this context, remote sensing (and GIS) may represent an effective tool for lake management (Janauer, 1997; Baban, 1999; Dimitriou & Zacharias, 2007; Alexandridis *et al.,* 2007) and in the assessment of ecological status under the EU WFD (Chen *et al.,* 2004; Gilvear *et al.,* 2004a; Rowan *et al.,* 2006).

2.4.2 Spectral and Spatial Considerations in Shallow Lakes

Remote sensing has been used extensively in the study of ecological processes and function in terrestrial and marine environments. Indeed, optical remote sensing has become established as the principal tool for monitoring primary productivity in the oceans (ocean colour remote sensing). However, it can be argued that remote sensing, at present, does not fulfil a comparable role in study of inland and transitional waters (e.g. lakes, reservoirs, rivers and estuaries). This shortcoming can be explained largely by simple instrumentational limitations and, more specifically, by the lack of available satellite data of the apposite spatial, spectral and radiometric resolution.

The scale of many terrestrial and marine ecosystems (and processes therein) inherently lends themselves to spaceborne observation. Lake ecosystems and, in particular, shallow lakes are often, in comparison, much smaller in scale (although there are obvious exceptions). For example, the largest shallow lake in the UK, Loch Leven, has a surface area of just 13.3 km^2. Therefore, the scale of the vast majority of lakes is prohibitive to observation from spaceborne instruments with spatial resolutions > 30 m. However, those spaceborne instruments with spatial resolutions more harmonious to the scale requirements of inland waters (e.g. Landsat TM, ASTER, IKONOS, QuickBird, etc.) have been designed, in the main, for terrestrial

applications and, therefore, the spectral resolution and channel configuration (i.e. number and positioning of bands) is typically not optimised for applications in lake environments (or other inland or transitional waters). The poor radiometric capabilities (i.e. low signal-to-noise ratio) of the terrestrial satellites are a further constraint on their use for the observation of inland waters (particularly targets with low backscattering) {Lindell *et al*, 1999}.

Table 2.2 The spatial and spectral resolutions, revisit period, and typical applications of current satellite remote sensing instruments

	Spatial Resolution	Spectral Resolution	Revisit Period	Primary Application(s)
ALI	30 m	Multispectral 10 bands 0.4-2.4 µm	16 days	Designed to replace the Landsat TM instrument
ASTER	15 m	Multispectral 3 bands 0.52-0.86 µm	16 days	Vegetation mapping and thermal applications
AVHRR	1.1 km	Multispectral 5 bands 0.58-12.5 µm	1 day	Large scale vegetation mapping
Hyperion	30 m	Hyperspectral 220 bands 0.4-2.5 µm; 10 nm bandwidth	16 days	Varied applications
IKONOS	4 m	Multispectral 4 bands 0.45-0.88µm	1-2 days	Terrestrial mapping
Landsat TM 7	30 m	Multispectral 5 bands 0.5-1.1 µm	16 days	Geological and vegetation
MERIS	300 m	Multispectral 15 bands 0.39-1.04 µm	3 days	Oceanography
MODIS	0.25-1.2 km	Multispectral 36 bands 0.4-14.4 µm	2-4 days	Terrestrial, oceanography and atmospheric
QuickBird	2.5 m	Multispectral 5 bands 0.44-0.9 µm	1-3.5 days	Terrestrial mapping
SeaWiFS	1.1 km	Multispectral 8 bands 0.4-0.885 µm	1 day	Ocean colour
SPOT XS	20 m	Multispectral 3 bands 0.5-0.89 µm	26 days	Terrestrial mapping

The current generation of multispectral satellites, with spectral resolutions more congruent to application in lakes (e.g. MODIS, MERIS, SeaWiFS) have been designed primarily for observation of oceanscapes and/or landscapes and, as such, the spatial resolution of these instruments is often too crude (0.25-1.1 km) to permit the observation of all but the largest epicontinental lakes (i.e. lakes on the scale of Baikal, Michigan, Superior and Tanganyika) (Li *et al.,* 2004; Heim *et al.,* 2005; Shuchman *et al.,* 2006; Bergamino *et al.,* 2007) (see Table 2.2).

Table 2.3 The spatial and spectral resolutions, swath width and applications of current airborne remote sensing instruments

	Max. Spatial Resolution (Alt. = 1000 m)	**Spectral Resolution**	**Max. Swath Width (Alt. = 1000 m)**	**Primary Application(s)**
AISA Eagle & Hawk	1 m	Hyperspectral (dual) 488 bands 0.4-0.97 µm (Eagle) 254 bands 0.97-2.45 µm (Hawk)	0.43 (Hawk) -1 km (Eagle)	Any optical and SWIR
AVIRIS	< 5 m	Hyperspectral 224 bands 0.4-2.5 µm	535 m	Any optical to MIDIR
ATM	2.5 m	Multispectral 11 bands 0.42-13 µm	2000 m	Terrestrial and thermal
CASI-2	2.0 m	Multispectral 18 bands 0.405-0.95 µm Hyperspectral 288 0.405-0.95 µm	1030 m	Vegetation and water quality
HYDICE	< 4 m	Hyperspectral 210 bands 0.4-2.5 µm	500 m	Any optical to MIDIR SWIR
HyMap	< 5 m	Hyperspectral 0.45-12 µm; bandwidth 0.01-0.02 nm (VIS-SWIR), 0.1-0.2 µm (TIR)	1060 m	Any optical to MIDIR

The latest generation of hyperspectral satellites that fuse high spatial and high spectral capabilities (i.e. Hyperion on NASA's EO-1 satellite) are more suitable for application in studies of lake ecosystems and increasing provision of such data will afford improved opportunities to employ remote sensing more extensively in the study of lake ecology. However, the availability of hyperspectral satellite data still remains somewhat limited. The high tasking demands placed upon EO-1 Hyperion and its limited operational lifespan will ultimately restrict data availability

until further hyperspectral satellites are introduced. In this context, multispectral and hyperspectral airborne remote sensing instruments (e.g. CASI-2, HyMap, ASIA Eagle & Hawk) may be pertinent to observation of lakes (and other inland and transitional waters). Airborne sensors can be deployed at low flight altitudes providing spatially-resolving capabilities less than 5 m. Airborne systems also have the advantage of flexible deployment that can be harmonised to temporal frequency of the phenomenon under observation. However, whilst airborne remote sensing may offer an excellent option for those employed in expeditious research projects, its high operational costs would seem prohibit its use in longer-term monitoring programmes (see Table 2.3).

2.4.3 Remote Sensing of Phytoplankton and Water Quality

2.4.3.1 Bio-optical Properties and Spectral Signatures of Shallow Lakes

The application of remote sensing in aquatic environments is dependent upon a comprehensive understanding of their bio-optical properties. This section seeks to review only the essential optical properties of inland waters, but further, and more detailed, information can be found in texts such as Kirk (1994) and Lindell *et al*. (Lindell *et al*., 1999).

The optical characteristics of aquatic environments can be regarded as complex function of several optically active components (Malthus & Dekker, 1995; Lindell *et al*., 1999). Light entering the water column as downwelling irradiance (E_d) is subject to attenuation from absorption (a, m^{-1}) and scattering (b, m^{-1}) processes associated with the optically active components of the water column. In oceanic waters (CASE I), the dominant optically active constituent is phytoplankton (and associated by-products). However, in inland (and coastal) waters (CASE II), other optically active components in addition to phytoplankton, such as CDOM and tripton, may greatly affect the attenuation of the ambient light field.

The optically active components of CASE II waters typically comprise: (i) pure water (*w*); (ii) CDOM (also referred to as aquatic humus, yellow substance or Gelbstoff) (*ah*); phytoplankton (*ph*); and tripton (*t*). The a and b_b processes are wavelength-dependent (λ, nm) and subscribe

to Beer's Law which enables total absorption ($a_{total}(\lambda)$) and backscattering ($b_{b,total}(\lambda)$) to be expressed as a function of each optically active component (Equation 2.1 and Equation 2.2).

$$a_{total}(\lambda) = a_w(\lambda) + a_{ph}(\lambda) + a_t(\lambda) + a_{ah}(\lambda) \quad \textbf{Equation 2.1}$$

$$b_{b,total}(\lambda) = b_{b,w}(\lambda) + b_{b,ph}(\lambda) + b_{b,t}(\lambda) + b_{b,ah}(\lambda) \quad \textbf{Equation 2.2}$$

The combined effect of absorption and backscattering are given by the coefficient of beam attenuation ($c(\lambda)$, m^{-1}) (Equation 2.3) which describes the attenuation of light per unit depth. It is evident from Equation 2.3 that the total absorption and backscattering are inherently inversely proportional. Thus, waters with high $a(\lambda)$, typically have lower $b_b(\lambda)$ and, conversely, waters with high $b_b(\lambda)$ typically have lower $a(\lambda)$ (Bricaud *et al.,* 1983). These factors, $a(\lambda)$, $b_b(\lambda)$, and $c(\lambda)$, are collectively referred to as the inherent optical properties (IOPs). The IOPs are independent of the ambient light field in the sense that they do not vary with changes in the nature of the incident illumination (i.e. irradiance, solar zenith and azimuth) (Kirk, 1994; Malthus & Dekker, 1995; Lindell *et al*., 1999).

$$c(\lambda) = a(\lambda) + b(\lambda) \quad \textbf{Equation 2.3}$$

The IOPs can be estimated through laboratory or *in-situ* measurements (Lindell *et al*., 1999). However, remote sensing instruments cannot make direct measurements of the IOPs. Instead, remote sensing instruments provide measures of the apparent optical properties (AOPs). The AOPs measured by remote sensing instruments include water-leaving-radiance ($L_w(0+,\lambda)$) and (above-surface) remote-sensing-reflectance ($R_{rs}(0+,\lambda)$). $R_{rs}(0+,\lambda)$ – the most useful AOP for remote sensing studies – is calculated from Equation 2.4 which describes the ratio of upwelling radiance from the water surface, L_u, to the downwelling irradiance from the sun, E_d (Lindell *et al*., 1999).

$$R_{rs}(0+,\lambda) = \frac{L_u(0+,\lambda)}{E_d(0+,\lambda)} \quad \textbf{Equation 2.4}$$

The relationship between the IOPs and AOPs are described by Equation 2.5; where $R(0-,\lambda)$ is the subsurface remote-sensing-reflectance, at depth 0-, and f is an experimental constant

dependent on the light field and volume scattering function (Gordon *et al.,* 1975; Morel & Gentili, 1991).

$$R(0-,\lambda) = f\frac{b_b(\lambda)}{a(\lambda)+b_b(\lambda)} \qquad \textbf{Equation 2.5}$$

$R(0\text{-},\lambda)$ can be related to $R_{rs}(0+,\lambda)$ through the inclusion of an empirical parameter, Q, which accounts for the geometrical attenuation of light exiting the water column (Equation 2.6) (Dall'Olmo & Gitelson, 2005). $R_{rs}(0+,\lambda)$ is preferred over L_w as it is fully independent of the nature of the incident light field and the atmosphere. The computation of normalised-water-leaving-radiance ($_nL_w$) allows for the fact that L_w is dependent on the angle of solar zenith and (when measured from space) the state of the atmosphere (Gordon, 1988). In the absence of a correction to $_nL_w$, measurements of L_w must be normalised through empirical means to allow comparison.

$$R_{rs}(0+,\lambda) \propto \frac{f}{Q}\frac{b_b(\lambda)}{a(\lambda)+b_b(\lambda)} \qquad \textbf{Equation 2.6}$$

Measurements of R_{rs} and L_w can be related to the concentration optically active components in the water column through (i) empirically derived algorithms, (ii) semi-empirically derived algorithms (which employ *a priori* knowledge of the optical properties of the parameters of interest to optimise empirical models), and (iii) inversion of bio-optical models. Empirical and semi-empirical models are easily formulated through statistical analyses (i.e. regression) between the AOPs and the measured concentration of optically active components. Such models do not require information on the IOPs (measurements of which are often lacking), but it has been alleged that empirically- and semi-empirically-derived algorithms lack robustness when extrapolated to independent datasets (Malthus & Dekker, 1995; Lindell *et al*., 1999).

Numerical bio-optical models can be used to model the AOPs as a function of the IOPs (as described above) and thus generate a synthetic dataset from which algorithms can be derived semi-empirically or, as is increasingly the case, analytically. Analytical algorithms can be formulated from the inversion of the bio-optical model to permit the IOPs to be estimated from AOP measurements. The concentration of an optically active component (*i*) can subsequently

be estimated from the computed absorption coefficient ($a_i(\lambda)$) derived from model inversion by dividing by the specific absorption coefficient for that component ($a_i^*(\lambda)$, $m^2\ mg^{-1}$) (Equation 2.7).

$$[\text{Concentration}_i] = a_i(\lambda) / a_i^*(\lambda) \qquad \textbf{Equation 2.7}$$

Bio-optical model inversion techniques are advantageous in that, as they are analytical rather than empirical, they retain greater transferability when applied to independent datasets. However, the formulation and inversion of bio-optical models is reliant on extensive and accurate (often prohibitively so) IOP and AOP measurements. The extrapolation of algorithms derived from the inversion of bio-optical models to airborne and spaceborne data is also dependent on the availability and efficacy of an atmospheric correction model.

In optically shallow waters, L_w and R_{rs} are also affected by absorption ($a_{bot}(\lambda)$) and backscattering ($b_{b,bot}(\lambda)$) processes associated with the lake bottom (Zaneveld & Boss, 2003; Liu *et al.,* 2003; Islam *et al.,* 2004; Cannizzaro & Carder, 2006). Lake bottom attenuation of L_w or R_{rs} is dependent upon both water depth and transparency; attenuation is greatest in very shallow and highly transparent waters. In such waters, high bottom radiance, can lead to substantial over-estimation of optically active component concentrations. Shallow waters are also prone to high and variable concentrations of tripton (largely inorganic clays, slits, and sands and organic detritus) which can mask the other optically active components (notably chlorophyll-a) thus impeding their estimation (Tyler *et al.,* 2006).

A typical $R_{rs}(0+,\lambda)$ signature of a shallow phytoplankton-dominated lake is depicted in Figure 2.2. The reflectance minimum located at approximately 440 nm (a) is related to principally to chlorophyll-a absorption but, in this region, carotenoid pigments and CDOM also contribute significantly to absorption. The reflectance minimum at approximately 480 nm is caused primarily by the presence of carotenoid pigments. The large peak at *c*. 575 nm (the “green peak”) (b) is caused by significant decreases in pigment absorption allied to increased scattering from algal cells and tripton (Dekker *et al.,* 1991; Mittenzwey *et al.,* 1992). The

position of this peak has been suggested to sensitive to phytoplankton composition (Schalles *et al.,* 1998; Gitelson *et al.,* 1999).

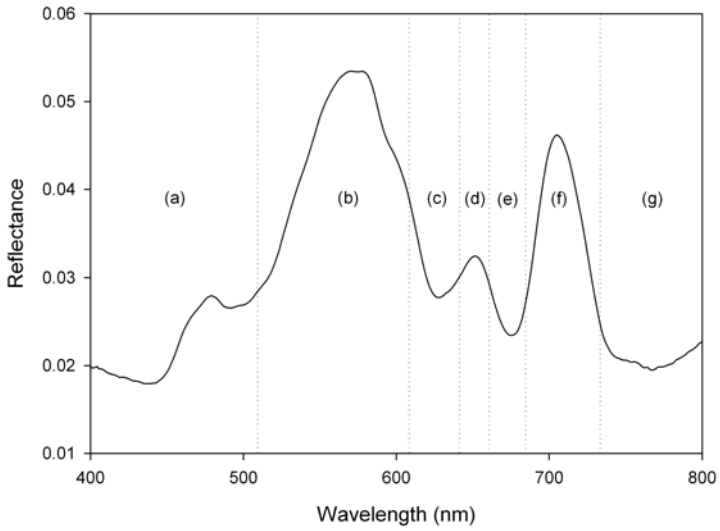

Figure 2.2 An example of a typical $R_{rs}(0+,\lambda)$ signature of a shallow phytoplankton-dominated lake (Barton Broad, UK).

The reflectance trough at approximately 620 nm (c) is the result of high absorption by the cyanobacterial pigment C-phycocyanin. The subsequent reflectance peak at *c*. 650 nm (d) has been related to both CDOM backscattering (Gitelson, 1992) and the C-phycocyanin fluorescence emission maximum (Ahn *et al.,* 1992). The prominent reflectance trough at *c*. 675-680 nm (e) is caused by the chlorophyll-a absorption maximum. Backscattering at these wavelengths is largely attributable to the inorganic component of the tripton (i.e. SPIM). The large reflectance peak at *c*. 705 nm (f) is caused by intense backscattering from algal cells and tripton and the subsequent trough > 750 nm is related to high water absorption.

2.4.3.2 Remote Sensing of Chlorophyll-a

In limnology and oceanography the concentration of chlorophyll-a is used to estimate phytoplankton biomass/biovolume, monitor ecosystem productivity and assess trophic status. The concentration of chlorophyll-a in lakes can often be highly spatially variable because of the typically patchy distribution of phytoplankton; this high spatial variability is difficult to adequately capture when using conventional *in-situ* point-sampling methods (Kutser, 2004; Svab *et al.,*

2005; Tyler *et al.,* 2006). This failing has impelled scientists to examine other means of quantifying the spatial distribution of phytoplankton in lakes and increasingly remote sensing platforms and sensors are being employed to quantify chlorophyll-a in lakes.

Platforms and Sensors—The remote-sensing-based quantification of chlorophyll-a in lakes has been achieved using data collected from both (i) satellite-mounted instruments, and (ii) airborne-mounted instruments. Satellite systems can offer regional-scale coverage of lake systems and, importantly, continuity in data acquisition; in contrast, airborne systems, while operationally expensive, afford much greater deployment flexibility and are apt for expeditious ecosystem-scale studies.

Several previous studies have shown that lake chlorophyll-a concentrations can be estimated from broad bandwidth multispectral satellite data. Allee & Johnson (1999) used Landsat TM imagery to map chlorophyll-a in Bulls Shoals Reservoir (USA) with an overall accuracy of R^2 = 0.80-0.84 and Ostlund *et al*. (2001) used Landsat TM imagery to retrieve estimates of chlorophyll-a in Lake Erkan (Sweden) with an accuracy of R^2 = 0.76-0.93. Baban (1993) assessed the trophic status of shallow lakes in the Norfolk Broads using Landsat TM imagery returning a coefficient of determination of R^2 = 0.73 for the fit against chlorophyll-a. Duan *et al*. (2007) used Landsat TM to assess the trophic status of Lake Chagan (China). Tyler *et al*. (2006) used a novel linear spectral mixture modelling algorithm in combination with Landsat TM imagery to measure the chlorophyll-a concentration in Lake Balaton (Hungary) (R^2 = 0.95).

Notwithstanding the success of these studies, several authors have suggested that, in lakes with high and variable concentrations of tripton, the remote-sensing-based estimation of chlorophyll-a concentrations is often difficult with broad-band multispectral data (Ekstrand, 1992; Dekker *et al.,* 1992; Dekker & Peters, 1993; Carrick *et al.,* 1994; Svab *et al.,* 2005). The use of multispectral satellite products with improved spectral resolution (e.g. MERIS, MODIS, SeaWIFS) has been shown to increase the efficacy of chlorophyll-a retrieval in optically complex lakes. Budd & Warrington (2004), Heim *et al*. (Heim *et al.,* 2005) and Pozdnyakov *et al*. (2005) used SeaWiFS data to characterise the chlorophyll-a concentration in Lake Superior

(R^2 = 0.87), Lake Baikal (R^2 = 0.85) and Lake Michigan (R^2 = 0.82) respectively. Giardino *et al*. (2005) used MERIS data to quantitatively map chlorophyll-a distributions in Lake Garda (Italy) and Novo *et al*. (2006) used MODIS imagery to assess seasonal changes in chlorophyll-a concentrations in Amazonian floodplain lakes.

The latest generation of hyperspectral satellites have also been shown to hold much potential for mapping chlorophyll-a concentrations in lakes. Kutser (2004) employed EO-1 Hyperion imagery to map the distribution of chlorophyll-a in a cyanobacteria bloom in the Gulf of Finland (R^2 = 0.90-0.95). Similarly, Yan *et al*. (2006) and Giardino *et al*. (2007) both used EO-1 Hyperion data to map chlorophyll-a concentrations in Lake Taihu (China) and Lake Garda (Italy) respectively.

Several studies have demonstrated that airborne remote sensing can also provide an effective platform for mapping chlorophyll-a in lakes. George (1997) used Airborne Thematic Mapper (ATM) imagery to map the distribution of chlorophyll-a in several tarns and lakes of the English Lake District (UK) (R^2 = 0.94). Härmä *et al*. (2001) used AISA imagery to map chlorophyll-a in several Finnish lakes (R^2 = 0.90). Thiemann & Kaufmann (2002) used HyMap and CASI-2 imagery to monitor chlorophyll-a concentrations in the Mecklenburg Lake District (Germany). Further, George & Malthus (2001) exploited CASI-2 imagery to map the distribution of chlorophyll *a* in a series of lakes in North Wales (UK). CASI-2 imagery has also been used to measure chlorophyll-a concentrations by Flink *et al*. (2001) and Ammenberg *et al*. (2002); whilst AVIRIS airborne imagery products have been utilised by Hamilton *et al*. (1993), Jaquet *et al*. (1994) and Melack & Gastil (2001).

Methods and Models—The retrieval of chlorophyll-a concentrations from remote sensing data has been achieved through various methods. Many initial algorithms were based upon simple empirical analyses between the measured concentration of chlorophyll-a and the value of L_w or R_{rs} in a single spectral band (Baban, 1993; George, 1997). However, single channel chlorophyll-a algorithms often break down in CASE II waters where the coincidental presence of other optically active components (such as tripton and/or CDOM) significantly influence L_w or

R_{rs}. Single band algorithms based on L_w are also sensitive to variation in illumination (E_d) intensity and geometry. Thus, most semi-empirically derived chlorophyll-a retrieval algorithms now incorporate spectral band ratios or multiple band combinations; such algorithms have been found to be more robust and less sensitive to interference from other optically active components. Band ratios often take the form of Equation 2.8, where *β(λ)* is band centred at a wavelength in which chlorophyll-a related backscatter is high (e.g. in the green and NIR) and *α(λ)* is a band centred at a wavelength in which chlorophyll-a absorbs strongly (e.g. in the blue and red).

$$[\text{chlorophyll - a}] \propto \frac{\beta(\lambda)}{\alpha(\lambda)} \qquad \textbf{Equation 2.8}$$

In ocean colour remote sensing, algorithms incorporating green/blue band-ratios have been widely employed (e.g. the current SeaWiFS and MODIS operational algorithms) and these ratios have also been used for the quantification of chlorophyll-a in lakes with some limited success (particularly those more oligotrophic in nature) (George & Malthus, 2001). However, green/blue band-ratios have not always proved effective when employed for the estimation of chlorophyll-a in turbid eutrophic lakes. More commonly, algorithms have been based upon NIR/red band-ratios (Mittenzwey *et al.,* 1991; Dekker, 1993; Han & Rundquist, 1997). Gitelson *et al*. (1986), for example, demonstrated that algorithms incorporating the [$R_{rs}(700)/R_{rs}(670)$] ratio could be used to estimate chlorophyll-a concentrations in lakes. Multiple band-ratio algorithms, such as those proposed by Mittenzwey *et al*. (Mittenzwey *et al.,* 1991) have also shown to be effective for the quantification of chlorophyll-a in lakes (see Table 2.4). Some workers have also advocated the use of near-infrared peak algorithms which exploit the increase in NIR L_w or R_{rs} that occurs with increasing chlorophyll-a concentration (Gitelson *et al.,* 1993).

The use of first and second derivative transformations of reflectance data has also been shown by some workers to be an effective method for deriving semi-empirical algorithms for the estimation of chlorophyll-a in lakes. It has been suggested that n^{th}-derivative transformations effectively normalise reflectance spectra for differences in the backscattering contribution from

tripton and are thus useful for estimating chlorophyll-a concentrations in optically complex shallow lakes (Malthus & Dekker, 1995; Rundquist *et al.,* 1996; Han & Rundquist, 1997).

Table 2.4 Examples of foregoing band ratio and band combinations algorithms used to estimate the concentration of chlorophyll-a in lakes.

Chlorophyll-a Band Ratio or Combination	Reference
[$L_w(560)/R_{rs}(440)$]	George & Malthus (2001)
[$R_{rs}(700)/R_{rs}(670)$]	Gitelson *et al*. (1986)
[$R_{rs}(706)/R_{rs}(676)$]	Dekker (1993)
[$R_{rs}(705)/R_{rs}(670)$] [$R_{rs}(705) – R_{rs}(670)]/[R_{rs}(550)$] [$R_{rs}(705) – R_{rs}(670)]/[R_{rs}(550) - R_{rs}(670)$] [$R_{rs}(705) – R_{rs}(670)]/[R_{rs}(550) - R_{rs}(760)$]	Mittenzwey *et al*. (1991)
[$R_{rs}(670\text{-}750)$] SUM[$R_{rs}(670\text{-}750)$]	Gitelson *et al*. (1993)

Simulated datasets derived from bio-optical modelling approaches have been often used to optimise the configuration of algorithms for the estimation of chlorophyll-a (see for example the method of Ammenberg *et al.,* 2002); bio-optical modelling approaches – providing the inherent and apparent optical properties can be fully characterised – also enable chlorophyll-a to be estimated from the derivation of a fully- or semi-analytical solution of the underwater ambient light field through model inversion (Pierson & Strombeck, 2001; Ma *et al.,* 2006; Dall'Olmo & Gitelson, 2006; Giardino *et al.,* 2007). Tyler *et al*. (2006) present a contrasting methodology for the estimation of chlorophyll-a in lakes based upon a multivariate algorithm derived from a linear spectral mixing model of Landsat TM data; it is suggested that such an approach has value in optically complex shallow waters (e.g. high and heterogeneous tripton) and, in particular, if the available data is of an inferior spectral resolution.

Time-Series Remote Sensing—The temporally-resolving datasets afforded by remote sensing platforms, both spaceborne and airborne, present a means of monitoring seasonal and annual changes in the chlorophyll-a concentration of lakes. Thiemann & Kaufmann (2002) examined both intra- and inter-annual changes in phytoplankton communities in the Mecklenberg Lake District (Germany). Tyler *et al*. (2006) used a retrospective approach to examine change in eutrophication driven phytoplankton blooms in Lake Balaton (Hungary). Similarly, Ritchie *et al*.

(1994) used Landsat MSS data to examine time-series changes in the chlorophyll-a concentration of three lakes over a 12-year period (1976-1988).

However, few studies conducted to date have employed remote sensing to examine diurnal patterns in the distribution of phytoplankton chlorophyll-a. Jernakoff *et al*. (Jernakoff *et al.,* 1996) used an airborne Digital Multi-Spectral Video (DMSV) to monitor the dynamic behaviour of a phytoplankton bloom in Swan River (Western Australia) and noted that remote sensing could enable near-surface migrations by buoyant cyanobacteria to be observed in lakes. However, the poor spectral capabilities of the DMSV system prevented quantitative analysis of bloom behaviour. The latest generation of high spectral resolution airborne spectral imagers have proven effective for the quantification of chlorophyll-a and, in this context, their operational flexibility could be highly useful for monitoring the diurnal dynamics of phytoplankton blooms

2.4.3.3 Remote Sensing of Phytoplankton Community Composition

Numerous studies have demonstrated the potential of airborne and satellite remote sensing for retrieving accurate estimates of chlorophyll-a concentrations in inland waters (George, 1997; Hoogenboom *et al.,* 1998; Thiemann & Kaufmann, 2000; Ostlund *et al.,* 2001; George & Malthus, 2001; Flink *et al.,* 2001; Ammenberg *et al.,* 2002; Tyler *et al.,* 2006). However, few studies have attempted to make the progression from mapping the bulk chlorophyll signal to more informative discriminative mapping of phytoplankton taxonomic groups.

Chlorophyll-a is the dominant light harvesting pigment in the majority of phytoplankton and is therefore common to all taxonomic groups (except the divinyl chlorophyll-a containing prochlorophytes). Thus, its surrogate use in mapping phytoplankton distributions in inland waters through remote sensing results in the acquisition of a bulk species signal that does not permit taxonomic differentiation. However, phytoplankton contain a range of accessory pigments (carotenoids, phycobiliproteins) as part of their photosynthetic systems in addition to chlorophyll-a, many of which are taxon-specific (Rowan, 1989; Richardson, 1996). The taxonomic-specificity of several carotenoids and the phycobiliproteins means that these pigments can be used as qualitative or quantitative biomarkers for the presence and abundance

of their respective taxa. While several other accessory pigments have less taxonomic-specificity, some nevertheless maintain high concentrations in a limited number of taxa (e.g. fucoxanthin) sufficient to enable their effective use as quantitative biomarkers for species groups (Rowan, 1989; Jeffrey & Vesk, 1997).

The accessory pigments have relevance to remote sensing studies of phytoplankton in lakes. The optical properties of the accessory pigments are varied and some are spectrally discernable to optical remote sensing systems. Foregoing research by a limited number of workers has examined the potential of remote sensing for mapping the distribution of phytoplankton taxonomic groups in lakes on the basis of accessory pigments. The majority of the studies have focused on mapping cyanobacteria blooms using the biomarker pigment C-phycocyanin (Dekker, 1993; Schalles & Yacobi, 2000; Vincent *et al.,* 2004; Simis *et al.,* 2005; Yang & Pan, 2006; Sridhar & Vincent, 2007; Simis *et al.,* 2007). C-phycocyanin absorbs strongly at *c*. 620 nm, the effect of which often can be observed as a prominent minimum (trough) in L_w or R_{rs} spectra, and several workers have exploited this spectral feature as a route to pigment quantification.

Dekker (1993) developed a baseline algorithm for the estimation of C-phycocyanin in several Dutch lakes. Similarly, Schalles & Yacobi (2000) developed a semi-empirical band ratio for the quantification of C-phycocyanin in Carter Lake (USA) (R^2 = 0.61). Simis *et al*. (2005) used a bio-optical model to derive a semi-analytical algorithm for the retrieval of C-phycocyanin concentrations in turbid, cyanobacteria dominated, waters yielding R^2 = 0.77 for the fit against measured C-phycocyanin concentrations. The algorithm derived by Simis *et al*. (2005) has been subsequently validated in other cyanobacterial-dominated waters, but it has been observed that the quantification of C-phycocyanin can be greatly affected by the coincidental presence of other optical active pigments (chlorophyll-a, chlorophyll-b), high intra- and inter-species variability in C-phycocyanin content, and influence of cyanobacterial physiology on the specific absorption coefficient of C-phycocyanin (Simis *et al.,* 2007). Examples of remote sensing algorithms used to quantify C-phycocyanin are shown in Table 2.5.

Table 2.5 Examples of foregoing algorithms used to estimate the concentration of C-phycocyanin in lakes

C-phycocyanin Algorithm	Reference
$[[0.5[R_{rs}(600)+R_{rs}(648)]]-R_{rs}(624)]$	Dekker (1993)
$[R_{rs}(650)/R_{rs}(625)]$	Schalles & Yacobi (2000)
$[R_{rs}(709)/R_{rs}(620)]$	Simis *et al*. (2005)[†]

[†]See Simis *et al*. (2005) for full explanation of the semi-analytical algorithm

The potential to retrieve estimates of the concentration of other biomarker pigments, such as fucoxanthin, using remote sensing has received little consideration. Sathyendranath *et al.* (2004) derived an algorithm for the optical discrimination of diatoms in marine waters. Similar work has yet to be undertaken in lakes. However, Richardson (1996), Gitelson *et al*. (1999) and Millie *et al*. (2002) have demonstrated that diatoms have unique spectral characteristics because of, in part, the presence of the fucoxanthin pigment, which intimates that it may offer a means to their quantification through remote sensing in lakes.

2.4.3.4 Remote Sensing of SPM (seston)

The concentration of SPM in shallow lakes is an important metric of ecosystem function as it is recognised to have important linkages to nutrient and contaminant cycling and can have a substantial influence upon the underwater ambient light climate. Many workers have used remote sensing to map the quantitative distribution of SPM, SPIM and, to a somewhat lesser extent, SPOM in inland waters. The presence of SPM can significantly increase the intensity of backscattering processes within the water column, leading to subsequent increases in L_w or R_{rs} that are proportional to the concentration of the material in suspension. The greatest increase in L_w or R_{rs} has been found to occur at short wavelengths (400-600 nm) when the concentration of SPM is low (*c*. < 20 mg l^{-1}). However, it has been noted that the wavelength position of maximum L_w or R_{rs} shifts towards longer wavelengths as the concentration of SPM increases (*c*. > 20 mg l^{-1}) (Curran & Novo, 1988; Lindell *et al*., 1999). Therefore, the optimal wavelength(s) for incorporation into SPM retrieval algorithms is, to an extent, dependent on the concentration of SPM in suspension.

Several different types of algorithms have been used to retrieve SPM estimates in inland waters; the vast majority of the published studies have been based upon empirical or semi-empirical analysis, but some semi-analytical and analytical algorithms have also been derived from bio-optical models (Dekker *et al.,* 2001; Dekker *et al.,* 2002). Choubrey & Subramanian (1992) used a linear algorithm to derive estimates of SPM in a central Indian reservoir using IRS LISS-I data. Lathrop *et al*. (1991) used an exponential empirical model to derive SPM estimates from Landsat TM data (R^2 = 0.88) and, in similarity, Ghezzi *et al*., (1998) used an empirical power model to derive SPM estimates in Lake Garda (Italy) (R^2 = 0.70).

Few workers have attempted to estimate the inorganic and organic fractions of the (total) SPM in lakes. Ammenberg *et al*. (2002) used a bio-optical model to estimate the SPIM fraction in Lake Malaren (Sweden) and Pierson & Strombeck (2001) used a bio-optical model to derived semi-analytical algorithms for the estimation of SPIM and SPOM in Lake Malaren (Sweden). However, in the case of Pierson & Strombeck (2001), whilst the concentration of SPIM could be accurately estimated from remote sensing data, the estimation of SPOM was more problematic. This difficulty was largely due to the optical properties of SPOM (i.e. low backscatter)

2.4.3.5 Remote Sensing of CDOM

Lakes can provide an important sink environment for carbon and thus the concentration and flux dynamics of dissolved organic carbon is an important measure of ecosystem function (Kullberg *et al.,* 1993; Blomqvist *et al.,* 2001). However, the concentration of CDOM in inland waters is perhaps the most difficult of water quality parameters to retrieve using remote sensing and few published studies have been able to derive accurate estimates {Lindell *et al*., 1999}. CDOM absorbs light intensely between 350 and 550 nm. However, at these wavelengths, absorption by phytoplankton pigments and SPOM, combined with high SPIM scattering, often complicates the retrieval of CDOM concentrations from remote sensing data.

Notwithstanding these issues, some limited success has been achieved; Dekker (1993) used a bio-optical modelling approach to retrieve estimates of the CDOM concentration in the Loosedrect Lakes (The Netherlands). Furthermore, Kutser *et al*. (2005b) used a band ratio

power algorithm to successfully retrieve CDOM estimates from ALI imagery in several lakes across Finland and Sweden (R^2 = 0.82). Brezonik *et al*. (Brezonik *et al.,* 2005) were able to map the concentration of CDOM in several lakes in Minnesota (USA) using Landsat TM data (R^2 > 0.70). However, in a later study, Menken & Brezonik (2006) could not derive an effective algorithm for the estimation of CDOM in other Minnesotan Lakes. It has been suggested that the estimation of CDOM in lakes is dependent on the existence of a large concentration gradient to aid algorithm development (Giardino *et al.,* 2007).

2.4.4 Remote Sensing of Aquatic Vegetation

2.4.4.1 The Spectral Signature of Vegetation

The spectral signature of vegetation is a complex interaction of many factors operating at various scales from that of individual leaves to the canopy. The remote sensing of vegetation communities is reliant on a clear mechanistic understanding of the spectral response of vegetation communities under a variety of conditions. The spectral signature of individual leaves is largely determined by a combination of foliar biochemistry and the internal cell structure (Campbell, 2002). Figure 2.3 shows a typical spectral response from a single leaf measured under controlled conditions. The spectral response between 400-500 nm (a) is largely a function of absorption by leaf pigments (chlorophylls, xanthophylls and carotenoids). Chlorophyll-a, in particular, absorbs strongly at *c*. 436 nm. The local reflectance maximum at *c*. 550 nm (b) known as the "green peak" is largely the result of decreased pigment absorption and increase in chlorophyll-a related backscattering.

The reflectance minimum located 600-700 nm (c) is caused by high absorption by chlorophyll pigments; the pronounced feature located at *c*. 680 nm reflects the absorption maximum of chlorophyll-a. The rapid increase in reflectance >700 nm (d), referred to as the "red-edge", and the NIR plateaux feature (>750 nm) (e), are a function of negligible pigment absorption allied to high backscattering from the interaction of incident light with spongy mesophyll tissue and palisade cells (Danson & Plummer, 1995). The spectral response of leaves beyond the NIR region (i.e. 1400-2500 nm) is governed by absorption due to the presence of structural compounds such as lignin, tannin and cellulose and absorption by water.

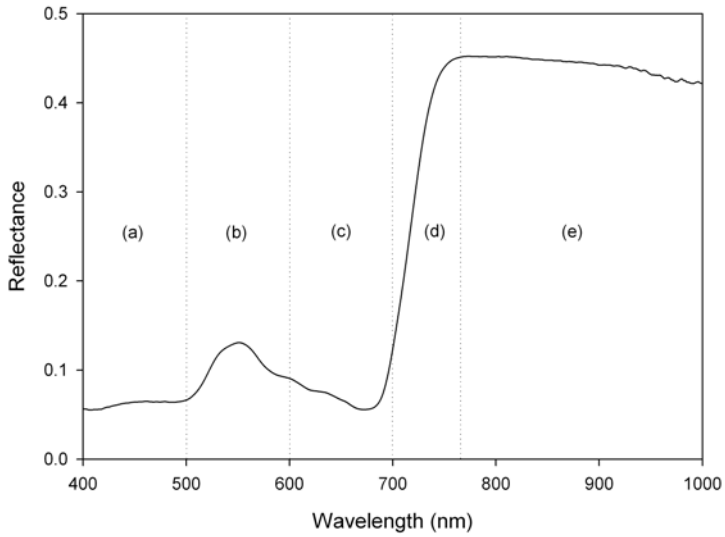

Figure 2.3 The spectral response of a *Phragmites australis* leaf measured under laboratory darkroom conditions using an artificial source of illumination.

Many of the factors that affect the spectral response of vegetation at the leaf-scale also operate at the canopy-scale. However, the spectral signatures of vegetation at the canopy-scale are also influenced by other factors and, in particular, the bio-physical structure of plants. Vegetative canopies are composed of many individual leaves that may vary in their size, shape, orientation and ground coverage. Variations in plant morphology can dramatically affect the interaction with incident light and therefore canopy architecture can have a profound effect upon the spectral response of vegetation. Spanglet *et al*. (1998) noted that canopies that have an orientation that tends towards the vertical (erectophile) display a much smaller vegetative surface than canopies that have a more horizontal orientation (planophile) which results in a significantly different spectral response. Spanglet *et al*. (1998) also showed that canopies with a spherical architecture can demonstrate pronounced variability in spectral reflectance signatures due to complex internal scattering processes. Variability in canopy geometry also influences the amount of canopy shadow and the extent to which reflectance from non-vegetative background surfaces occurs; both these factors have been shown to further moderate the spectral response of vegetation (Spanglet *et al.,* 1998).

The varied biochemical and biophysical properties of natural vegetation communities can thus result in significantly different spectral responses being observed both between, and within, communities. This provides a basis upon which remote sensing can be used to (i) map different vegetation communities and (ii) quantitatively assess differences in the biochemical and biophysical (e.g. chlorophyll-a, LAI, biomass) properties of vegetation communities.

2.4.4.2 Mapping the Distribution of Aquatic Vegetation

The abundance, distribution and composition of aquatic vegetation is a key measure of shallow lake ecological status. Field-based aquatic plant surveys are time-consuming. Moreover, field-based aquatic plant surveys are ineffective for mapping vegetation over large spatial areas and the discontinuous nature of point-based survey data may seldom adequately describe the true distribution of aquatic plant communities, particularly where complex mosaics, transitional assemblages and ecotones occur (Janauer, 1997; O'Shea, 2005).

The spatially-resolving data afforded by remote sensing would seem to have much to offer with respect to the mapping of vegetation communities in shallow lakes (and their peripheral wetlands). In this context, several workers have previously employed various forms of remote sensing for the mapping of aquatic vegetation communities. Aerial photography has been used on numerous occasions. Boorman & Fuller (1981) used historical aerial photography to map changes in the extent of reedswamp in the Norfolk Broads. Similarly, Windham & Lathrop (1999) used aerial photography to map the invasion of *Phragmites australis* in brackish tidal marshes in eastern USA. Aerial photography has also been used to map the distribution of submerged aquatic vegetation; for example, Stankelis *et al*. (2003) retrospectively analysed historical aerial photographs to determine the former extent of SAV in the Patuxent estuary (USA). Comparable studies utilising aerial photography to map aquatic vegetation have also been conducted by, amongst others, Kelly *et al*. (2001), Lathrop *et al*. (2001), Frederiksen *et al*. (2004) and Valta-Hulkkonen *et al*. (2005).

Multi- and hyperspectral remote sensing has been recently examined by several authors for aquatic vegetation mapping. Malthus & George (1997) used ATM imagery to map the

distribution of macrophytes in the Cefni Reservoir (UK) using a simple minimum distance classification algorithm. A classification accuracy of 79% was achieved against conventional field-based survey despite the limited radiometric capabilities of the ATM sensor. Williams *et al*. (2003) used continuum removal analysis of hyperspectral airborne imagery (HyMap) to demonstrate that two submerged macrophyte species (*Myriophyllum spicatum* and *Vallisneria americana*) are sufficiently spectrally dissimilar to enable them to be mapped independently using remote sensing imagery. Nelson *et al*. (2006) used Landsat TM to conduct a region-scale assessment of the aquatic vegetation cover in several shallow lakes in Michigan (USA). Similarly, Albright *et al.* (Albright *et al.,* 2004) used satellite data to map the extent of *Eichhornia crassipes* (Water Hyacinth) invasion in lakes across the African continent. Stcyr et *al*. (Stcyr *et al.,* 1994) used remote sensing imagery to estimate the seasonal storage of heavy metals in the aquatic vegetation of Lake St. Pierre (Quebec). These and several other published studies demonstrate the capability of remote sensing as a tool for mapping the distribution of aquatic vegetation in shallow lakes and wetlands (Jakubauskas *et al.,* 2000; Arzandeh & Wang, 2003).

2.4.4.3 Remote Sensing of Vegetation Physiological Status

It has been shown that remote sensing offers a means of mapping aquatic vegetation in shallow lakes. However, emerging research from studies of terrestrial vegetation now suggests that remote sensing can also be used to quantitatively assess the physiological status (i.e. vigour) of plant communities. Remote sensing based studies of vegetation physiological parameters (i.e. chlorophyll-a, LAI, biomass) were initially pioneered in agricultural and agri-forestry contexts. Nevertheless, increasingly remote sensing approaches to characterising plant physiology have now started to find application in the examination of natural vegetation communities (Davids & Tyler, 2003).

The physiological status of plants is principally conditioned by the nature of the immediate environment (e.g. nutrition, light, exposure to stressors). Common plant responses to differences in the quality of the growth habitat include changes in photosynthetic activity, photosynthetic pigmentation, tissue biochemistry and plant morphology (Lichtenthaler, 1996). It has been shown that remote sensing can be used to quantify such phytophysiological

parameters in natural vegetation communities through the derivation of various spectral vegetation indices. Examples of such indices include the NDVI (which has been extensively use to estimate biomass in various plant communities) (Equation 2.9), more novel hyperspectral-based derivative indices such as the chlorophyll red-edge index and continuum removed indices (Penuelas *et al.,* 1993; Kokaly & Clark, 1999; Davids & Tyler, 2003).

$$\mathrm{NDVI} = \frac{[\mathrm{red} - \mathrm{NIR}]}{[\mathrm{red} + \mathrm{NIR}]} \qquad \textbf{Equation 2.9}$$

Numerous authors have exemplified that remote sensing can be used to retrieve accurate estimates of foliar chlorophyll-a concentrations at both the leaf- and the canopy-scale (Gitelson & Merzlyak, 1997; Jago *et al.,* 1999; Gitelson *et al.,* 1999; Datt, 1999; Raychaudhuri, 2004; Blackburn, 2007). Blackburn (1999) used several different spectral vegetation indices to quantify the chlorophyll-a concentration in broadleaved plants (max. R^2 = 0.88). Similarly, Blackburn & Steele (1999) used narrow band ratio and first-derivative reflectance indices to estimate the chlorophyll-a content of matorral vegetation at both the leaf- and canopy-scale.

The use of spectral reflectance indices for the quantification of plant vigour has been developed further in more applied contexts. Smith *et al*. (2004) used first-derivative indices obtained from hyperspectral data to identify stress effects in plants exposed to experimental gas leaks in several grass and cropland species. Similarly, Davids & Tyler (2003) used a variety of vegetation indices to examine the radionuclide-induced tree stress in the Chernobyl exclusion zone (Ukraine). In a context more relevant to shallow lakes, Kooistra *et al*. (2003), Clevers *et al*. (2004) and Kooistra *et al*. (2004) successfully demonstrated that plant stress resulting from heavy metal contamination (Cd, Cu, Ni, Pb, and Zn) in a wetland floodplain environment could be identified through spectral reflectance measurements made at the canopy-scale.

However, few workers have used remote sensing to quantify changes in the physiological status of aquatic plants. There are some notable exceptions. Penuelas *et al*. (1993) used spectral reflectance measurements to estimate the chlorophyll-a content, photosynthetic efficiency and biomass in emergent aquatic plants in Searsville Lake (USA). Yuan & Zhang

(2007) used an NDVI transformation of spectral reflectance measurements to quantify the biomass of the submerged aquatic plant *Vallisneria spiralis*.

2.5 SUMMARY AND FUTURE RESEARCH PRIORITIES

2.5.1 Shallow Lakes as Complex Ecosystems

Shallow lakes are complex ecosystems. The dynamic interaction of numerous physical, chemical and biological processes serves to ensure that shallow lake ecosystems (or elements therein) are often in a state of flux. This dynamism can be seen both in the abiotic processes (e.g. in the interrelated processes of mixing, sediment resuspension, and nutrient cycling) that regulate ecosystem function and the biotic elements (e.g. aquatic plants and phytoplankton communities) that respond to, and consequently modify, such processes.

Shallow lakes can exist in various states of either, (i) aquatic plant-dominance, or (ii) phytoplankton dominance, and the ecological status and trajectory of shallow lakes is largely conditioned by competition between these biotic elements. Aquatic plant dominance in shallow lakes is typically equated as being indicative of good ecological status, whilst phytoplankton dominance is, conversely, considered to be symptomatic of an ecosystem in poor ecological health. It can be argued therefore that ecological status in shallow lakes could be elucidated, albeit at a basic level, from the broad-scale assessment of these two major biotic elements.

The EU WFD (2000/66/EC) now requires the assessment of ecological status in all fresh and saline waters, including shallow lake ecotypes, across all EU Member States (Moss *et al.,* 2003; Dworak *et al.,* 2005). The sheer extent and number of waters to be assessed, monitored and policed will be the greatest obstacle to the successful implementation of the EU WFD. In addition, methodologies for the assessment of ecological status across respective EU Member States need to be objective and harmonious in their approach, independent of expert opinion, and free from political interference. In this context, remote sensing technologies would seem to be highly relevant to the objectives of the EU WFD (Chen *et al.,* 2004).

2.5.2 Remote Sensing and Shallow Lake Ecology

It has been shown, albeit from a number of limited studies, that remote sensing can be used to assessment various elements of shallow lake ecosystems at regional-to-global scales. The advantage of remote sensing reconnaissance in comparison to *in-situ* survey and monitoring approaches is that it can provide data (i) as a spatial continuum, (ii) at contrasting spatial and temporal scales, (iii) where an immediate scientific response is desired, and (iv) for the construction of retrospective baselines.

In the context of shallow lakes, whilst there are many important elements that cannot be observed through remote sensing, it can nevertheless be used to obtain information concerning several important ecosystem components (see Figure 2.4). In particular, previous work suggests that information relevant to the assessment of ecological status in shallow lakes could be obtained from remote sensing for both (i) phytoplankton (chlorophyll-a, composition and cyanobacterial abundance) and (ii) aquatic plant (distribution, composition and physiological status) elements. This information, when equated against appropriate reference conditions, would go some way towards providing an assessment of ecological status (and trajectory) for shallow lake ecosystems and, it can also be argued that, it could be achieved at a scale (spatial and temporal) that could not be realised cost-effectively through sole reliance on *in-situ* survey and monitoring approaches.

The integration of remote sensing reconnaissance into shallow lake ecology and, ultimately, its use in the implementation of the EU WFD, will depend on the development of robust methodologies for ecosystem assessment and monitoring. This can only be achieved through the creation of a sizeable evidence base derived from the continued application of remote sensing technologies in studies of shallow lake ecosystem process and function.

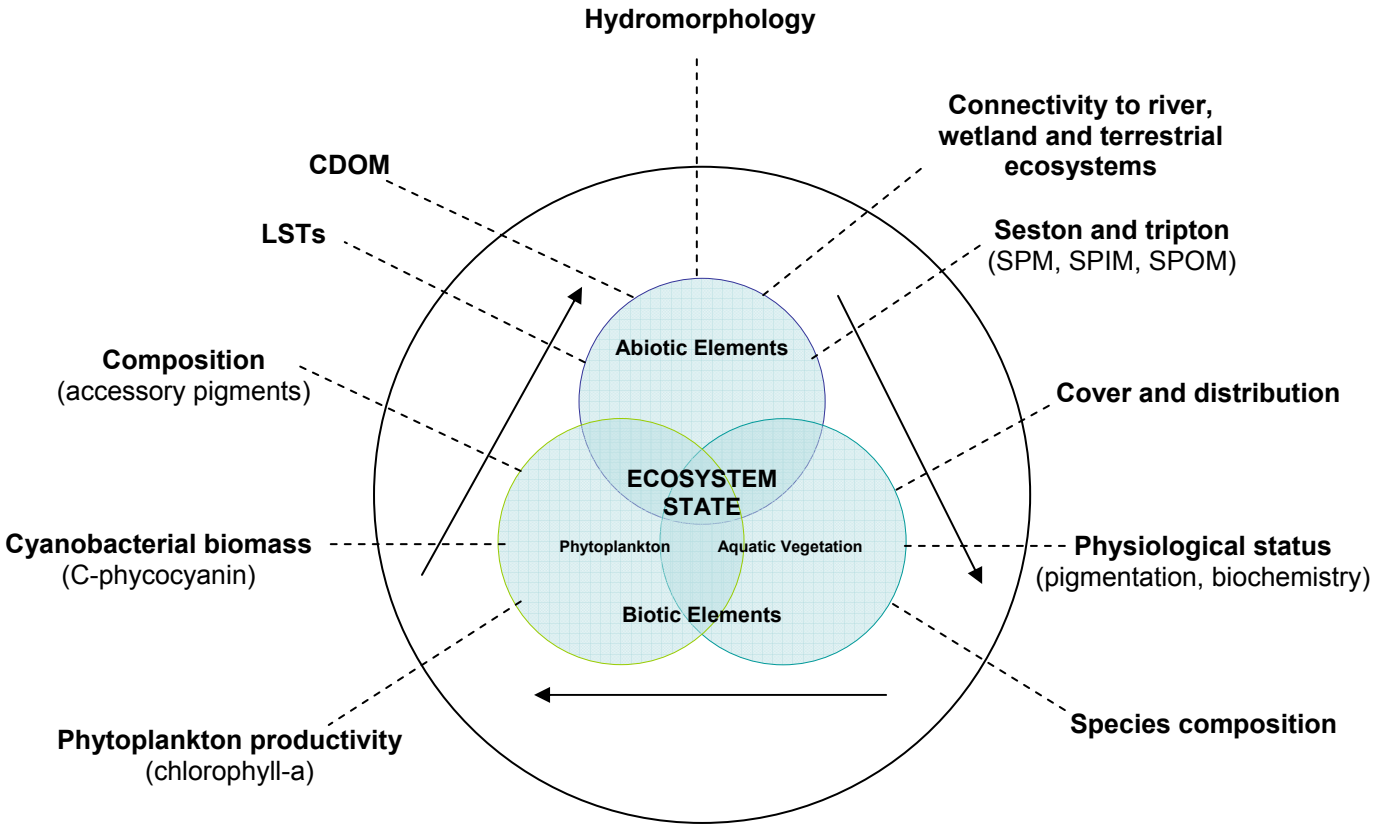

Figure 2.4 A conceptual Venn diagram illustrating key areas in which remote sensing could contribute to monitoring of ecological status in shallow lakes.

2.5.3 Thesis in Context

This thesis addresses the use of remote sensing in shallow lake ecology. Through a series of linked proof-of-concept-type studies it aims to make a significant contribution to the growing evidence base that supports the expeditious use of remote sensing for the assessment of ecological status in shallow lakes. In particular, this thesis aspires to develop and refine remote sensing methodologies for the assessment of (i) phytoplankton and (ii) aquatic plant elements in shallow lakes. Specific objectives for this thesis can be outlined as follows.

(i) Phytoplankton

Objective 1—To examine the use of multispectral and hyperspectral remote sensing data for the quantification of chlorophyll-a concentrations and other important water quality parameters (e.g. suspended particulate matter and CDOM) in shallow lakes of varying optical properties.

Objective 2—To examine the extent to which taxonomic information can be derived from hyperspectral remotely sensed data, with particular reference to the development of techniques for the quantification of cyanobacterial abundance in shallow lakes.

Objective 3—To examine the use of high spatial resolution remote sensing reconnaissance to map spatial and temporal (diurnal and seasonal) change in the distribution of phytoplankton in shallow lakes and to provide a mechanistic insight into the behaviour of phytoplankton blooms in shallow lakes.

(ii) Aquatic plants

Objective 4—To examine the use of high spatial remote sensing reconnaissance to map the distribution and composition of aquatic plants in shallow lakes.

Objective 5—To examine the use of hyperspectral remote sensing to assess the physiological status of emergent aquatic plants in shallow lakes in relation to pressures induced by eutrophication-related processes.

The collation of the results obtained from the aforementioned proof-of-concept-type studies will be used to critically evaluate (i) the use of remote sensing survelliance for providing spatially-explicit insights into shallow lake procesess and function and thus the furthering of ecological understanding and (ii) the merit of integrating such technologies for the assessment, monitoring and policing of ecological status in shallow lakes to aid the implementation of the EU WFD.

3 HYPERSPECTRAL REMOTE SENSING OF WATER QUALITY IN SHALLOW LAKES

3.1 INTRODUCTION

The preceding chapter (Chapter 2) discussed the application of remote sensing in shallow lake ecology. It was identified that the optical-complexity of shallow lakes may present an obstacle to the accurate estimation of certain water parameters (e.g. chlorophyll-a) from remotely sensed data. This chapter seeks to examine the efficacy of hyperspectral data for the estimation of various water quality parameters in shallow lakes (chlorophyll-a, SPM, CDOM) through a thorough evaluation of different semi-empirical approaches to algorithm development.

3.2 RATIONALE

The assessment of water quality is central to lake research and monitoring and is now a legislative requirement for EU Member States under the WFD (2000/60/EC). In this context, remote sensing technologies could make a significant contribution to limnological monitoring as they have the ability to provide quantitative regional-scale panoramas of water quality conditions in lakes. Many workers have demonstrated that several water quality parameters can be estimated using remote sensing data, including the concentrations of chlorophyll-a, SPM (seston dry weight), CDOM, and measures of water transparency (i.e. Secchi disc depth or nephelometric turbidity) (George, 1997; Hoogenboom *et al.,* 1998; Thiemann & Kaufmann, 2000; Flink *et al.,* 2001; George & Malthus, 2001; Ostlund *et al.,* 2001; Ammenberg *et al.,* 2002; Tyler *et al.,* 2006).

The estimation of SPM has proven achievable in most lakes using simple empirical algorithms formulated using single VNIR bands, or more complex analytical solutions derived from bio-optical modelling simulations (Han & Rundquist, 1997; Dekker *et al.,* 2002). However, the retrieval of chlorophyll-a and CDOM concentrations using data derived from broadband remote sensing instruments (e.g. Landsat TM, SPOT) has often proved problematic in lakes,

particularly those characterised by high and non-co-varying concentrations of tripton (Lindell *et al*., 1999; Tyler *et al.,* 2006). This is exemplified by Sváb *et al*. (2005) who demonstrated that the retrieval of chlorophyll-a from simulated Landsat TM data in Lake Balaton (Hungary) was prohibited by the presence of high and heterogeneous concentrations of SPIM. Similar observations are echoed in Dekker *et al*. (1991) Quibell (1991), Goodin *et al*. (1993) and Han & Rundquist (1997).

In very shallow lakes, such as the Norfolk Broads (< 2.5 m), the wind-driven resuspension of bottom sediments can promote very high concentrations of tripton in the water column. In these waters, high and heterogeneous tripton loads may be a significant obstacle to the estimation of chlorophyll-a. Furthermore, in shallow waters, the signal from the lake bottom can provide an additional source of spectral confusion and may influence the accuracy of remote sensing algorithms for the retrieval of water quality parameters (Liu *et al.,* 2003).

There is now considerable effort being directed towards the development and refinement of algorithms for chlorophyll-a retrieval in CASE II waters (Thiemann & Kaufmann, 2000; Kallio *et al.,* 2001; Flink *et al.,* 2001; Ammenberg *et al.,* 2002; Dall'Olmo *et al.,* 2005; Tyler *et al.,* 2006). In this context, high spectral resolution data seems to offer increased flexibility for algorithm formulation and has been shown to improve the accuracy of water quality estimation using remote sensing (Han & Rundquist, 1997). Workers have shown that the effect of high and non-co-varying concentrations of tripton on the retrieval of chlorophyll-a concentrations may be circumvented by deriving algorithms incorporating NIR/red narrow band-ratios (as opposed to the green/blue band-ratios often used in CASE I algorithms), or through the employment of first- or second-derivative transformations of hyperspectral reflectance data (Malthus & Dekker, 1995; Han & Rundquist, 1997; Han, 2005). In addition, recent research has also showed that statistically more complex 'soft-classification' approaches to algorithm development, such as linear spectral mixture modelling (LSMM), can yield superior estimates of chlorophyll-a concentrations in comparison to more convention semi-empirical band-ratio or band-combination approaches (Thiemann & Kaufmann, 2000; Tyler *et al.,* 2006; Oyama *et al.,* 2007).

The fact that a plethora of different algorithms for the retrieval of chlorophyll-a concentrations in CASE II waters have been proposed in the literature suggests that any single formulation may not be appropriate for application in all lake types. This has been noted by Kallio *et al*. (Kallio *et al.,* 2001) who examined the effect of lake type and seasonality on the accuracy of chlorophyll-a retrieval in variety of lakes in Southern Finland using airborne AISA data. Interestingly, it was found that the accuracy of the chlorophyll-a estimation diminished when the derived algorithms were applied across contrasting lake types.

It is therefore vital that, in order to maximise the effectiveness of remote sensing for lake monitoring, efforts are made to identify the optimum algorithm formulation(s) for the estimation of water quality parameters in the lakes, or lake types, of interest (Lindell *et al*., 1999). There has been little consideration given to the optimum formulation of remote-sensing-based chlorophyll-a algorithms for application in optically-complex and very shallow lakes. Thus, it would seem pertinent to further examine the efficacy of different approaches to the formulation of hyperspectral remote-sensing-based algorithms for the estimation of water quality parameters in shallow lakes.

3.3 AIMS AND OBJECTIVES

The aim of the research presented in this chapter was thus to attempt to identify candidate spectral algorithm formulations for the estimation of water quality (chlorophyll-a, SPM, SPIM, SPOM, CDOM and SDD) using multi-temporal shipboard hyperspectral remote-sensing-reflectance measurements acquired from sampling stations in the shallow lakes of the Norfolk Broads (UK). This chapter also intends to explore the effect of variable tripton, CDOM and bottom reflectance on the estimation of chlorophyll-a in shallow lakes through theoretical bio-optical simulations using the Hydrolight v.4.2 model.

The objectives for the chapter can be thus summarised as:

a) To identify optimum hyperspectral single-band, band-ratio and band-combination algorithms for the estimation of chlorophyll-a, SPM, SPIM, SPOM, CDOM and SDD in the shallow lakes of the Norfolk Broads in terms of (i) accuracy and (ii) robustness.

b) To examine the efficacy of novel first-derivative, continuum-removed and multivariate hyperspectral algorithms for the estimation of chlorophyll-a in the shallow lakes of the Norfolk Broads in terms of (i) accuracy and (ii) robustness.

c) To examine the effect of shallow lake type (i.e. variable optical conditions) on the accuracy of chlorophyll-a retrieval through a sensitivity analysis using the Hydrolight v.4.2 bio-optical radiative transfer model.

3.4 METHODS

3.4.1 Shipboard Spectrometry and Water Sampling

Shipboard spectrometry surveys and contemporaneous water sampling was conducted in the Norfolk Broads in southeast England (UK) (52º 44' 17'' N; 1º 34' 29'' E) during three lake cruises on 18 May 2004, 22 June 2005 and 29 August 2005. The various lakes sampled during each campaign are listed in Table 3.1. The three lake sampling cruises were conducted concomitant to airborne remote sensing campaigns by the National Environmental Research Council's Airborne Research and Survey Facility (NERC ARSF) in the Norfolk Broads (data presented in Chapter 5). Lake sampling was conducted in a strategic manner in an attempt to sample across the maximum possible water quality gradient. No effort was made to avoid very shallow regions, or lakes where submerged aquatic plants may be present. Where possible, however, an effort was made to encompass common sampling stations within each cruise but, for logistical reasons, this was not always possible.

Table 3.1 The various lakes sampled during the three shipboard spectrometry and lake sampling cruises in 2004 and 2005.

Lake Cruise		
18 May 2004	22 June 2005	29 August 2005
Hickling Broad	Hickling Broad	Hickling Broad
Heigham Sound	Heigham Sound	Heigham Sound
Horsey Mere	Horsey Mere	Horsey Mere
	Martham North Broad	Martham North Broad
	Ormesby Broad	

Measurements of above-surface radiance reflectance, $R_{rs}(\lambda,0+)$, were acquired at each sampling station using a portable ASD (Analytical Spectral Devices) FieldSpec® HandHeld Spectroradiometer (Figure 1). The specifications of the ASD FieldSpec® instrument are detailed in Table 3.2. $R_{rs}(\lambda,0+)$ was calculated according to Equation 3.1 (after Lindell *et al*., 1999); where L_u is the upwelling radiance just above the water surface and E_d is the downwelling irradiance from the sun. The ASD FieldSpec® instrument cannot directly measure the value of E_d. This measurement was thus obtained from spectral scans taken from a white Spectralon® calibration panel (~100% reflectivity).

$$R_{rs}(\lambda,0+) = \frac{L_u(\lambda,0+)}{E_d(\lambda,0+)} \qquad \textbf{Equation 3.1}$$

The acquisition of $R_{rs}(\lambda,0+)$ measurements was restricted to between 10.00-15.00 h GMT to minimise the possible influence of solar zenith variations. The spectrometer was mounted on a telescopic pole which enabled the instrument to be positioned away from the proximity of the boat. A constant geometry between the sun and the spectrometer was maintained and the instrument was held, at nadir, at a height of 0.5 m above the surface of the water. The shipboard $R_{rs}(\lambda,0+)$ measurements were acquired as a mean of 10 instantaneous scans automatically averaged by the instruments dedicated software; $R_{rs}(\lambda,0+)$ was subsequently calculated from the mean of 25 replicate measurements obtained at each station. Spectralon® panel calibration measurements for the estimation of E_d were acquired prior to the acquisition of the spectral measurements at each station. A preliminary visual inspection of the data allowed

any measurements believed to be adversely affected by glint (i.e. Fresnel reflectance) from the water's surface to be discarded prior to further analysis.

Figure 3.1 Photograph showing an example of the technique used to acquire shipboard $R_{rs}(\lambda,0+)$ measurements (Esthwaite Water, English Lake District).

Surface water samples for the analysis for chlorophyll-a, SPM, SPIM, SPOM and CDOM were collected at each sampling station contemporaneous to the acquisition of the spectral measurements using a pre-washed wide-necked bottle; in addition, the SDD was measured according to standard procedures. Water samples were, where possible, kept in the dark in a cool box until further processing (i.e. filtration) could be undertaken.

Table 3.2 Instrument specifications for the ASD FieldSpec® HandHeld spectrometer.

Spectral range	325-1075 nm
Spectral resolution	3.5 nm @ 700 nm
Sampling interval	1.6 nm @ 325-1075 nm
Typical data collection rate (solar illumination)	0.7 spectra s^{-1}
Detector	512 element Si photodiode array 325-1075 nm
Input	Fixed 25º field of view. Optional fibre optics and foreoptics.
Calibration	Wavelength, reflectance, radiance, irradiance. All calibrations are NIST traceable.
Noise Equivalent Radiance	UV/VNIR 5.0 x 10^{-9} W/cm/nm/sr @700 nm

3.4.2 Chlorophyll-a, SPM and CDOM Analysis

The collected water samples were stored in the dark until filtration; this was always performed within 2-12 h of sample collection. Sample aliquots for chlorophyll-a analysis were vacuum filtered onto pre-washed 47 mm diameter Whatman GF/C filters (the filtrate was retained for CDOM analysis), wrapped in aluminium foil, and immediately quick-frozen in liquid-N for transportation back to the laboratories at the School of Biological and Environmental Science (University of Stirling) where the samples were stored at -40-80°C upon receipt until further analysis could occur. Filter papers were stored for no longer than 14 d to prevent pigment degradation. Chlorophyll-a was extracted from the GF/C filter papers in 90% (HPLC grade) acetone (90% acetone: 10% water v/v) in the dark for 20 h at 4ºC and clarified in a refrigerated centrifuge (4ºC) for 10 min at > 5 000 *g*. The concentration of chlorophyll-a in the supernatant was determined spectrophotometrically on a Cecil 1021 series spectrophotometer using the equations of Lorenzen & Jeffrey (1980).

Total SPM (seston dry weight) and the SPIM and SPOM fractions were measured gravimetrically according to the method of Strickland and Parsons (1972). A known volume of water was filtered onto a pre-washed and pre-weighed 47 mm diameter Whatman GF/C and the total concentration of SPM was determined by re-weighing the filter after drying at 75ºC for 12 h. The concentrations of SPIM and SPOM were obtained by subsequently ashing the filter at 500ºC for 24 h. The resulting weight loss on ignition provided the concentration of SPOM. The concentration of SPIM was calculated as the difference between the weight of SPM and the weight of SPOM.

The concentration of CDOM was measured spectrophotometrically on a Cecil 1021 series spectrophotometer following filtration of the water samples through a pre-washed 47 mm diameter Whatman GF/C filter and secondary filtration through a pre-washed Millipore 0.22 µm filter. The apparent absorption coefficient (χ_λ) was calculated using Equation 3.2 where D_λ is the measured absorbance at a given wavelength λ and r is the curvette length in metres.

$$\chi_\lambda = 2.303\, D_\lambda / r \qquad \textbf{Equation 3.2}$$

The true absorption coefficient (g_λ), corrected for scattering, was calculated according to Equation 3.3 where χ_L is the apparent absorption coefficient at a long wavelength (in this instance 740 nm) and χ_λ is the apparent absorption coefficient at a given wavelength (λ) (in this instance 440 nm). Results were expressed as true absorption coefficients g_{440} (m^{-1}) (after Lindell *et al*., 1999).

$$g_\lambda = \chi_\lambda - \chi_L^{(L/\chi)} \qquad \textbf{Equation 3.3}$$

3.4.3 Processing and Analysis of R_{rs}(λ,0+) Measurements

3.4.3.1 Spectral Pre-processing

The raw hyperspectral data were interpolated to a final spectral resolution of 0.5 nm and truncated between 400 and 800 nm to remove noisy data incurred at the extremes of the spectrometer's sampling range. The resulting data were then smoothed to further reduce the influence of noise prior to analysis by passing a 5 nm running mean filter over the entire spectrum (after Dall'Olmo *et al.,* 2005).

3.4.3.2 Algorithms for the Estimation of SPM, CDOM and SDD

Indices for the estimation of SPM fractions, CDOM and SDD were derived in a purely empirical fashion. The datasets were checked for normality in MINTAB v.14 using the Anderson-Darling method (95% significance level). Pearson's Product-Moment correlation analysis was initially used to identify the optimum wavelength(s) for the estimation of SPM fractions, CDOM and

SDD and, subsequently, algorithms for the estimation of the various water quality parameters were derived using linear and non-linear least-squares regression models.

3.4.3.3 Band-Ratio and Band Combination Indices for Chlorophyll-a

Candidate band-ratio and band-combination indices for the estimation of the chlorophyll-a concentration were identified from the literature (see Table 3.3). These spectral indices were subsequently calculated from the $R_{rs}(\lambda,0+)$ datasets obtained during the sampling campaigns in the Norfolk Broads. This included the medium-independent pigment index model proposed in Dall'Olmo *et al*. (2003); where $R_{\lambda 1}$, is a spectral region maximally sensitive to the absorption of the pigment of interest; $R_{\lambda 2}$, is a spectral region minimally sensitive to the absorption of the pigment of interest, but for which absorption by other components is approximately equal to that at $R_{\lambda 1}$; and $R_{\lambda 3}$, is a spectral region minimally affected by the absorption of any pigments and thus can be used to correct for variability in backscatter between measurements (Equation 3.5).

$$\text{Pigment Concentration} \propto \left(R_{\lambda 1}{}^{-1} - R_{\lambda 2}{}^{-1}\right) \times R_{\lambda 3} \qquad \textbf{Equation 3.5}$$

Dall'Olmo *et al*., (2003) defined $R_{\lambda 1}$, $R_{\lambda 2}$ and $R_{\lambda 3}$ empirically, essentially allowing the algorithm to be spectrally-tuned to optimise chlorophyll-a estimation. The parameterisation of $R_{\lambda 1}$, $R_{\lambda 2}$ and $R_{\lambda 3}$ in the index as suggested in Dall'Olmo *et al*. (2003) was found to be generally appropriate and thus no further efforts were made to refine the index empirically.

3.4.3.4 First-Derivative and Continuum-Removed Indices for Chlorophyll-a Estimation

Novel chlorophyll-a indices based upon the first-derivative transformation of the $R_{rs}(\lambda,0+)$ spectra (hereafter denoted by $dR/d\lambda$) and continuum-removed spectra (hereafter denoted by $R'(\lambda)$) were also formulated in addition to the more conventional band-ratio and band-combination approaches. First- and second-derivative transformations have been shown to be effective for suppressing the effect of variable SPM (or, more specifically, tripton) backscattering on $R_{rs}(\lambda,0+)$ spectra acquired over inland waters, and have thus been shown to

improve the accuracy of chlorophyll-a estimation in lakes (Malthus & Dekker, 1995; Han & Rundquist, 1997; Han, 2005).

The first-derivative transformation of the $R_{rs}(\lambda,0+)$ data was achieved using Equation 3.4; where $dR/d\lambda_i$ is the first-derivative reflectance at the midpoint, *i*, between wavelengths *j* and *j*+1. $R_{\lambda(j)}$ is the reflectance at wavelength *j*, $R_{\lambda(j+1)}$ is the reflectance at wavelength *j*+1, and Δ_λ is the wavelength difference between *j* and *j*+1. Candidate $dR/d\lambda$ indices were identified from the literature and subsequently calculated from the $R_{rs}(\lambda,0+)$ measurements obtained from the Norfolk Broads (Table 3.3).

$$dR / d\lambda_i = \left(R_{\lambda(j+1)} - R_{\lambda(j)}\right) / \Delta_\lambda \qquad \textbf{Equation 3.4}$$

The efficacy of continuum removal analysis for estimating the concentration of chlorophyll-a was examined, to the best of the author's knowledge, for the first time in the context of inland waters. Continuum removal can be used to isolate and normalise target absorption features in $R_{rs}(\lambda,0+)$ spectra in order to permit comparisons from a common baseline. The continuum is a convex hull fitted over the top of the spectral curve, thus connecting local $R_{rs}(\lambda,0+)$ maxima. Linear continua were fitted between the start (650 nm) and end-point (700 nm) of the main chlorophyll-a absorption-related feature in the $R_{rs}(\lambda,0+)$ spectra. The continuum removed reflectance $R'_{(\lambda)}$ was obtained by dividing $R_{rs}(\lambda,0+)$ for each wavelength, *i*, in the absorption feature by the $R_{rs}(\lambda,0+)$ of the continuum line (convex hull) $R_{c(\lambda)}$ at the corresponding wavelength (*i*) (Equation 3.6) (Mutanga *et al.,* 2004).

$$R'_{(\lambda i)} = \frac{R_{(\lambda i)}}{R_{c(\lambda i)}} \qquad \textbf{Equation 3.6}$$

The indices for the retrieval of chlorophyll-a concentrations derived from the $R'(\lambda)$ spectra included (for further details see Mutanga *et al.,* 2004):

a) The value of continuum-removed reflectance (or band-depth (BD)) for the target absorption feature (and thus the precise location of chlorophyll-a absorption maxima) calculated by dividing subtracting $R'_{(\lambda)}$ from 1:

$$BD_{(\lambda i)} = 1 - R'(\lambda_i)$$

b) The normalised band-depth ratio (BDR) was calculated by dividing the $BD_{(\lambda i)}$ by the band centre (Dc) (which equates to the maximum band-depth):

$$BDR_{(\lambda i)} = \frac{BD_{(\lambda i)}}{Dc}$$

c) The normalised band depth index (NBDI) was calculated by subtracting the maximum band depth (Dc) from the band depth (BD) at wavelength *i* and dividing by their sum:

$$NBDI_{(\lambda i)} = \frac{BD_{(\lambda i)} - Dc}{BD_{(\lambda i)} + Dc}$$

d) Continuum-removed derivative reflectance (CRDR) was calculated by applying the first-derivative transformation described in Equation 3.4 to the continuum-removed spectra, $R'_{(\lambda)}$.

e) The full width at half maximum (FWHM) of the continuum-removed absorption feature was calculated according to Figure 3.2.

f) The area of the continuum-removed absorption feature (AREA) was estimated using the trapezium rule:

$$\int_{x_0}^{x_n} f(x)\,dx = 0.5h\left[\left(y_0 + y_n\right) + 2\left(y_1 + y_2 + \ldots y_{n-1}\right)\right]$$

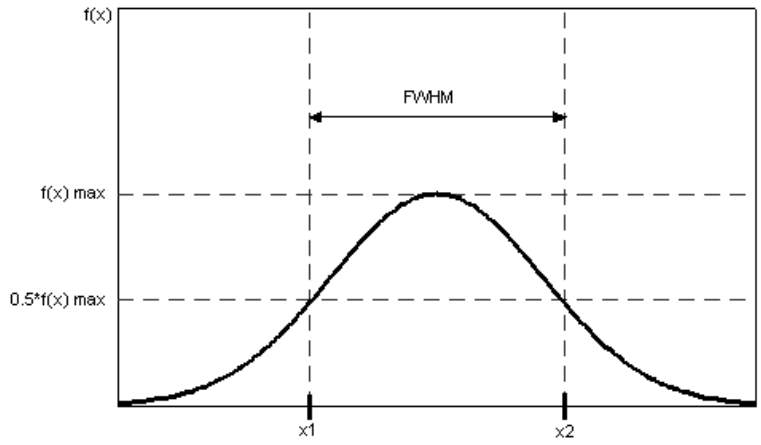

Figure 3.2 A graphical illustration of the calculation of the FWHM from f(x), where the distance x1 to x2 represents the value of the FWHM for the function f(x).

3.4.3.5 Statistical Analyses and Chlorophyll-a Algorithm Development

The datasets were checked for normality in MINTAB v.14 using the Anderson-Darling method (95% significance level). The spectral datasets from the three sampling cruises were examined individually and as an amalgamated multi-temporal dataset. Pearson's Product-Moment correlation analysis was then performed between the spectral indices ($R_{rs}(\lambda,0+)$, $dR/d\lambda$ and $R'(\lambda)$) and the measured concentrations of chlorophyll-a.

Where significant associations were observed (at the 95% significance level), linear and non-linear least-squares regression models were used to derive best-fit algorithms for the retrieval of chlorophyll-a concentrations. In an attempt to ensure some generic value, and to avoid possible over-fitting using non-linear regression models, consistency was sought in the nature of the best-fit model used. Thus, linear or exponential regression models were generally favoured, as these are used extensively in existing ocean colour algorithms (O'Reilly *et al.,* 1998). The temporal robustness of the chlorophyll-a algorithms was assessed by validating against the remaining independent multi-temporal datasets.

Table 3.3 The previously published chlorophyll-a indices that were examined in this study.

	Index	Description	Reference
Band-difference and band-ratio Indices	$[R_{rs}(433)/R_{rs}(555)]$	Blue/green ratio for CASE I waters	O'Reilly *et al*. (1998)
	$[R_{rs}(490)/R_{rs}(555)]$	Blue/green ratio for CASE I waters	O'Reilly *et al*. (1998)
	$[R_{rs}(510)/R_{rs}(555)]$	Blue/green ratio for CASE I waters	O'Reilly *et al*. (1998)
	$[R_{rs}(705)/R_{rs}(670)]$	NIR/red ratio for CASE II waters	Han & Rundquist (1997)
	$[R_{rs}(765)/R_{rs}(670)]$	NIR/red ratio for CASE II waters	Dall'Olmo *et al*. (2005)
	$[R_{rs}(705)/R_{rs}(664)]$	NIR/red ratio for CASE II waters	Ammenberg *et al*. (2002)
	$[R_{rs}(704)/R_{rs}(672)]$	NIR/red ratio for CASE II waters	Ruddick *et al*. (2001)
	$[(R_{rs}^{-1}(675)-R_{rs}^{-1}(720))xR_{rs}(750)]$	Medium-independent NIR/red difference index	Dall'Olmo *et al*. (2003)
First-derivative indices	$[dR/d\lambda_{620}]$	First derivative at 620 nm for CASE II waters	Malthus & Dekker (1995)
	$[dR/d\lambda_{638}]$	First derivative at 638 nm for CASE II waters	Malthus & Dekker (1995)
	$[dR/d\lambda_{661}]$	First derivative at 661 nm for CASE II waters	Malthus & Dekker (1995)
	$[dR/d\lambda_{690.5}]$	First derivative at 690.5 nm for CASE II waters	Han & Rundquist (1997)

3.4.3.6 Multivariate Chlorophyll-a Retrieval Algorithms

In addition to the derivation of algorithms formulated using single bands or band-ratios, multivariate models – multivariate stepwise regression (MSR) and partial least-squares regression (PLS) – were also formulated for the estimation of chlorophyll-a. MSR and PLS models enabled the efficacy of multivariate algorithms (containing greater wavelength information) to be compared against more conventional band-ratio approaches to algorithm formulation. It was hypothesised that increased wavelength information may improve the predictive power of the algorithms. Moreover, PLS regression is particularly powerful in instances, as here, when the number of predictor variables (i.e. wavelengths) is substantially greater than the number of observations (i.e. chlorophyll-a measurements). In addition, PLS regression models, because of the inherent "PCA-type" component transformation, are comparable, although not analogous, to the linear spectral mixture models that have proved to be effective for deriving water quality information from remote sensing imagery. Thus, in this context, it was considered that PLS regression may provide insights into the potential efficacy of spectral unmixing approaches (Thiemann & Kaufmann, 2002; Tyler *et al.,* 2006). The MSR and

PLS models were formulated in MINITAB v.14 using the hyperspectral $R_{rs}(\lambda,0+)$ measurements from the Norfolk Broads as predictor variables and the contemporaneous chlorophyll-a measurements as the single response variable.

3.4.4 Hydrolight Modelling of Shallow Lake Types

3.4.4.1 Bio-optical Model Development and Custom Parameterisation

Hydrolight is a one dimensional numerical radiative transfer model (Mobley & Sundman, 2001) that can compute radiance distributions and derived quantities for natural CASE I and CASE II waters. Hydrolight uses a time-independent radiative transfer equation (RTE) to obtain the radiance distribution within and leaving any plane-parallel water body as a function of wavelength (λ), depth (z) and viewing direction (θ, φ). The upwelling radiance just above the water surface (L_u) includes both the water-leaving radiance (L_w) and the radiance reflected from the waters surface (L_r). Hydrolight calculates L_w and L_r separately to isolate L_w. To enable Hydrolight to solve the RTE the IOPs (absorption (a), backscatter (b_b) and the scattering phase function (b_b/b)) for each optical component in the water column, the nature of the wind-blown water surface, the bottom boundary conditions and the sky radiance incident of the water surface must be specified.

The radiance distribution of different water types can be simulated through the custom parameterisation of the Hydrolight model. Previous workers have used Hydrolight to simulate the radiance distribution of a range of aquatic environments including deep ocean waters (e.g. "Van Luijn *et al.,* 1999), shallow coastal waters (Brando & Dekker, 2003; Chang *et al.,* 2003), lakes (Albert & Mobley, 2003; Bergmann *et al.,* 2004; Belzile *et al.,* 2004) and rivers (Legleiter & Roberts, 2005). In an experiment somewhat similar in concept to that presented here, Legileiter & Roberts (Legleiter & Roberts, 2005) were able to accurately simulate the effects of different river channel morphologies on remote sensing reflectance using various parameterisation scenarios in the Hydrolight model and, in the most part, using the various default IOP subroutines provided with the Hydrolight model.

In this study, the Hydrolight model was used to simulate $R_{rs}(\lambda,0+)$ distributions for different (hypothetical) shallow lakes types using variations on the default parameterisation of Hydrolight for CASE II waters. These model simulations were used to perform simple sensitivity analyses for the effect of varying concentrations of tripton and CDOM and bottom boundary conditions (i.e. benthic substrate) on the remote-sensing-based estimation of chlorophyll-a. The simulated lake types are listed in Table 3.4. The Hydrolight model was parameterised using default IOP measurements provided with the Hydrolight software and/or numerically modelled IOP measurements using standard equations. The parameterisation of the model was based approximately on the Norfolk Broads (but included a shallow humic lake type). However, as no specific IOP data were available, the objective was not to accurately simulate the radiance distributions of the Norfolk Broads, but merely to explore the effect of optical heterogeneity in shallow lake types.

The radiance distributions of the various shallow lake typologies were modelled using a standard four component optical model for CASE II waters (abcase2). The modelled optical components comprised: (1) pure water (*w*), (2) chlorophyllous particles (phytoplankton) (*ph*), (3) CDOM (not co-varying with chlorophyll) (*CDOM*) and (4) mineral particles (*tripton*). The contribution of each component to total absorption (a_{total}) and backscatter ($b_{b,total}$) was modelled using Equations 3.7 and 3.8.

$$a_{total}(\lambda) = a_w(\lambda) + a_{ph}(z, \lambda) + a_{CDOM}(z, \lambda) + a_{tripton}(z, \lambda) \qquad \textbf{Equation 3.7}$$

$$b_{b,total}(\lambda) = b_{b,w}(\lambda) + b_{b,ph}(z, \lambda) + b_{b,CDOM}(z, \lambda) + b_{b,tripton}(z, \lambda) \qquad \textbf{Equation 3.8}$$

The IOPs (a_w and b_b/b) for the pure water component were defined using the pure water absorption spectrum described by Pope & Fry (1997) and the default pure water phase function provided with Hydrolight v.4.2.

Table 3.4 The shallow lake typologies simulated using the Hydrolight bio-optical model.

	Lake Type	Max. Depth (m)	Bottom Substrate	Tripton Mineralogy	Chl-a (mg m^{-3})	CDOM (a_{440} m^{-1})	Tripton (mg L^{-1})
I	Very shallow clear water mesotrophic lake	3	Clean Seagrass	Brown Soil	2-25	1.5	0.5-5
II	Very shallow clear water mesotrophic lake with submerged vegetation	3	Green Algae	Brown Soil	2-10	1.5	0.5-5
III	Very shallow, turbid, eutrophic lake	3	Clean Seagrass	Brown Soil	10-75	1.5	5-30
IV	Very shallow humic lake	3	Clean Seagrass	Brown Soil	2-10	1-12.5	5

The IOPs for chlorophyllous particles (a_{ph}, $b_{b,ph}$ and b_b/b) were modelled to be constant with depth. The phytoplankton specific absorption coefficient ($a_{ph}(\lambda)$) was specified using the equation detailed in Morel (1991) and Mobley (1994) based on the original model of Prieur & Sathyendranath (1981) (Equation 3.9); where a_C is the specific absorption coefficient for chlorophyll-a (chlororphyll-a + pheophytin-a) and C is the concentration of chlorophyll-a in mg m^{-3}.

$$a_{\mathrm{ph}}(\lambda) = 0.06 a_{\mathrm{C}}(\lambda) C^{0.65} \qquad \textbf{Equation 3.9}$$

The equation of Morel (1991) assumes that chlorophyll-a is the only bio-optically active pigment in the water column. This is an obvious simplification, but in the absence of phytoplankton absorption and backscattering profiles, it was a necessary compromise. This prohibited the effect of variable community structure being investigated.

Phytoplankton scattering was modelled using the linear function presented in Gould *et al*. (Gould *et al.,* 1999) which Mobley & Sundman (2001) used to simulate the radiance distribution of CASE II waters (Equation 3.10) where b_0 = 0.3, λ_0 = 550 nm, n = 0.62, m = -0.00112, i = 1.62517 and X is the chlorophyll-a concentration.

$$b(\lambda) \quad = \quad b_0 X^n \frac{(m\lambda + i)}{(m\lambda_0 + i)} \qquad \textbf{Equation 3.10}$$

The scattering phase function for phytoplankton ($b_{b\text{ph}}$) was modelled using a Fornier-Forand phase function; $b_{b,\text{ph}}$ was specified to be 0.5% of total phytoplankton-derived scattering ($b_{b,\text{ph}}$ = 0.005) as suggested by Sathyendranath *et al*. (1989) and adopted by Mobley & Sundman (2001) and Ammenberg *et al*. (2002).

CDOM absorption (a_{CDOM}), in similarity to the vertical profile of chlorophyll-a, was modelled to be constant with depth for all shallow lake types (Mobley & Sundman, 2001). CDOM was assumed to be non-scattering. Specific absorption coefficients for CDOM were derived using the equation of Bricaud *et al*. (1981) (Equation 3.11) where λ_0 = 440 nm and γ = 0.014.

$$a_{\text{CDOM}}(\lambda) = a(\lambda_0)^{[-\gamma(\lambda-\lambda_0)]} \qquad \textbf{Equation 3.11}$$

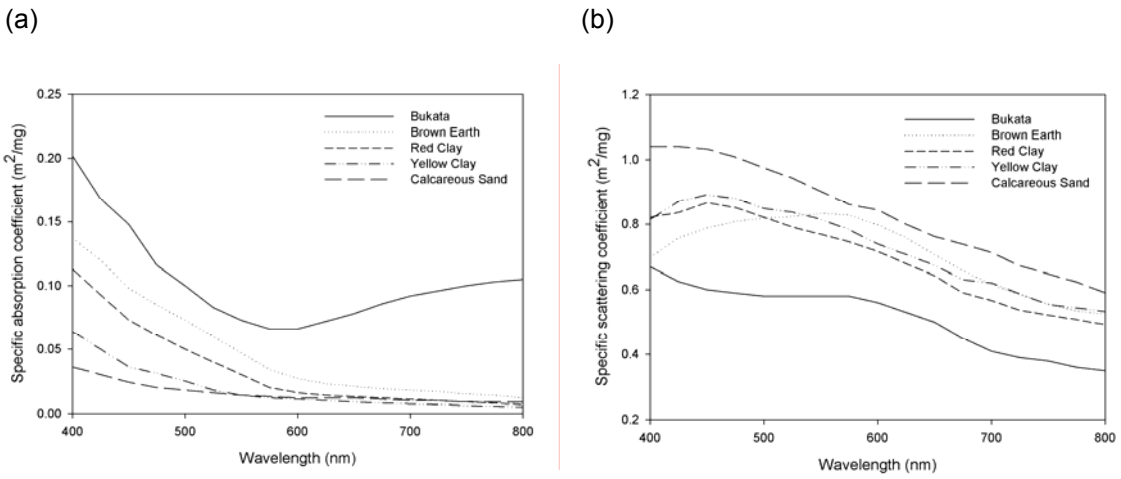

Figure 3.3 The (a) specific absorption and (b) specific scattering coefficients for the various mineral types provided by the Hydrolight model. In this study the *brown earth* type was used.

The IOPs for the mineral component (tripton) were again modelled to be constant with depth. The specific absorption and scattering coefficients were specified using the default data subroutines provided with the Hydrolight v.4.2; the model allows the IOPs of several different minerogenic and organic sediment particles with contrasting values of a_{tripton} and $b_{b,\text{tripton}}$ to be specified (see Figure 3.3). The mineral component for shallow lake types was defined using the absorption and backscatter coefficients of the default *brown soil* spectra provided with

Hydrolight; this was assumed to be representative of a tripton component with a high organic content, as is often found in fertile shallow lakes (e.g. the Norfolk Broads).

The bottom boundary conditions for the shallow lake types were specified using a finite depth (z_{max}) of 3 m. However, the optical depth may have, at times, been shallower than the geometric lake depth, particularly in simulations of turbid waters. The irradiance reflectance of bottom substrate (R_b) was modelled as a function of wavelength using the default bottom reflectance measurements provided with the Hydrolight model. Two bottom reflectance models were used: (1) the default *clean seagrass* irradiance reflectance spectrum to simulate an organic bottom substrate with some benthic microalgae growth (i.e. biofilm) and (2) the default *green algae* irradiance reflectance spectrum to simulate a bottom substrate with submerged macroalgae/aquatic plant cover (Figure 3.4).

The Hydrolight model scenarios also accounted for the contributions of Raman scattering and chlorophyll-a and CDOM fluorescence to total inelastic scattering (Mobley & Sundman, 2001). Bioluminescence was assumed to be negligible and thus excluded from the model. The air-water surface boundary conditions were specified for a constant wind speed of 5 ms^{-1} for all simulations.

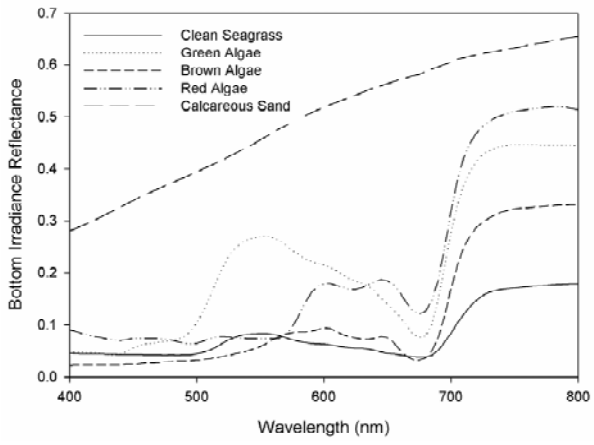

Figure 3.4 The bottom irradiance reflectance (R_b) spectra provided by the Hydrolight model. The *clean seagrass* and *green alage* spectra were used in this study to parameterise the bottom boundary conditions for the Hydrolight simulations.

The sky radiance, direct and diffuse irradiance, was modelled using the semi-empirical RADTRAN model (run as a subroutine within Hydrolight). RADTRAN was parameterised to compute the sky radiance for all simulations using the Norfolk Broads locale (52º44'17''N; 1º34'29''E) on Julian Day 180 (28 June 2006) at 12.00 h GMT under a clear sky (the atmospheric parameters used by RADTRAN are detailed in Table 3.5). The RADTRAN parameterisation was constant regardless of lake type to exclude the effect of the solar zenith and atmosphere boundary conditions on the results. The angular pattern of sky radiance was modelled using the semi-empirical sky model of Harrison & Coombes (1988).

Table 3.5 The atmospheric parameters used as inputs into RADTRAN

Sea-Level Pressure	29.92 inches Hg
24-hr Average Wind Speed	5 m s^{-1}
Average Horizontal Visibility	15 km
Relative Humidity	80%
Precipitable Content	2.5 cm
Airmass Type	Marine

Hydrolight uses Equations 3.7 and 3.8 to estimate the irradiance reflectance field $E_u(\lambda,0-)/E_d(\lambda,0-)$ just below the water surface using the equation of Kirk (1994) (Equation 3.12); where μ_0 is the cosine of the solar zenith under the water surface.

$$\frac{E_u(\lambda,0-)}{E_d(\lambda,0-)} = (0.975 - 0.629\mu_0)\frac{b_b(\lambda)}{a(\lambda)} \qquad \textbf{Equation 3.12}$$

Using the calculated irradiance reflectance values Hydrolight then solves the radiative transfer function to derive estimates of radiance reflectance ($R_{rs}(\lambda,0+)$) by dividing $E_u(\lambda,0-)/E_d(\lambda,0-)$ by the so-called Q factor (Equation 3.13) which accounts the transfer and focussing of the radiance flux through the water surface (Mobley, 1994). Kirk (1994) suggests that Q ranges between 3.14 and 5 for natural waters.

$$R_{rs}(\lambda,0+) = \frac{L_u(\lambda,0-)}{E_{\mathrm{d}}(\lambda,0-)} = \frac{E_{\mathrm{u}}(\lambda,0-)}{E_{\mathrm{d}}(\lambda,0-)}/Q \qquad \textbf{Equation 3.13}$$

The output of the Hydrolight model was set to provide modelled $R_{rs}(\lambda,0+)$ measurements with a 5 nm resolution between 400 and 800 nm.

3.4.4.2 Analysis of Hydrolight Data

The simulated $R_{rs}(\lambda,0+)$ data from the Hydrolight model was compared graphically by lake type. Furthermore the data were used to compute two spectral indices commonly used in remote-sensing-based algorithms for the estimation of chlorophyll-a: (1) the NIR/red band-ratio [$R_{rs}(670)/R_{rs}(705)$] and, (2) the value of first-derivative of $R_{rs}(\lambda,0+)$ at 667.5 nm, [$dR/d\lambda_{667.5}$]. These two indices were selected as they have been both demonstrated to be sensitive to variations in the chlorophyll-a concentration in lakes in foregoing studies (the $dR/d\lambda$ index was centred on 667.5 nm, rather than 665 nm, as described in the literature, due to the spectral resolution of the Hydrolight dataset) (Malthus & Dekker, 1995; Han & Rundquist, 1997; Han, 2005). This allowed the efficacy of NIR/red band-ratios and first-derivative indices to be compared for the estimation of chlorophyll-a across shallow lake types. Pearson's Product-Moment correlation and least-squares regression analysis was used to assess the effect of variable tripton, CDOM and benthic substrate on the estimation of chlorophyll-a using the two different approaches to algorithm formulation.

3.5 RESULTS AND DISCUSSION

3.5.1 Water Quality Measurements

The water quality conditions at the stations sampled during the three cruises was highly variable both within and between the various lakes. The water quality data for each lake cruise are summarised in Table 3.6 and the degree of correlation between the various water quality components is detailed in Table 3.7. In general, the concentration of chlorophyll-a was relatively low in the macrophyte-dominated mesotrophic waters of Martham North Broad and Ormesby Broad (*c*. < 5 mg chlorophyll-a m^{-3}) but, not surprisingly, significantly higher in the more eutrophic waters of Hickling Broad and Horsey Mere (*c*. > 25 mg chlorophyll-a m^{-3}). It is

also notable that the Norfolk Broads can carry very high concentrations of SPM (seston) (max. = 95.7 mg L^{-1}). SPM concentrations were also far higher on the larger and more eutrophic lakes (Hickling Broad, Heigham Sound, Horsey Mere) – likely to due increased phytoplankton biomass and bottom sediment resuspension. SPM concentrations were much lower in the smaller and more mesotrophic, macrophyte-dominated lakes (the Martham Broads, Ormesby Broad).

The stations sampled on the 18 May 2004 cruise were all located on eutrophic lakes (Hickling Broad, Heigham Sound and Horsey Mere). Thus it is not unexpected that the highest mean chlorophyll-a concentration measured over the three lake sampling cruises was encountered on the 18 May 2004 cruise (42.33 mg m^{-3}). The range in the chlorophyll-a concentration was also relatively small (23.80-49.47 mg m^{-3}) on the 18 May 2004 cruise. The mean concentration of SPM was 32.60 mg L^{-1}. This was largely composed of organic material (mean SPOM = 23.61 mg L^{-1}); the inorganic component (mean SPIM = 9.03 mg l^{-1}) made a relatively small contribution to total SPM. The correlations between chlorophyll-a and the various SPM fractions were atypically low on the 18 May 2004 (Table 3.7). The seston dry weight is often highly correlated with phytoplankton biomass (i.e. chlorophyll-a) in lakes but, in very shallow waters such as the Norfolk Broads, this relationship can be severely affected by the resuspension of bottom sediments.

The low correlation coefficients observed between chlorophyll-a and SPOM (r = 0.30) on 18 May 2004 may thus suggest that the organic matter in the water column was largely composed of detritus (rather than phytoplankton cells), either from the *in-situ* decay of plankton, or the resuspension of bottom sediments. The concentration of chlorophyll-a and SPIM were more highly correlated (r = 0.72). This may be due to the nature of the mineralogy of the material being resuspended from the lake bed (i.e. fine organics, rather than larger inorganic particulates), or perhaps the prevalence of siliceous phytoplankton (i.e. late-spring diatom bloom).

Table 3.6 Summary of the water quality datasets collected during the three lake cruises in the Norfolk Broads during 2004 and 2005. The concentration of CDOM was not determined on the 18 May 2004 or the 29 August 2005.

	Chlorophyll-a (mg m^{-3})			**SPM (mg L^{-1})**			**SPIM (mg L^{-1})**			**SPOM (mg L^{-1})**			**CDOM (g_{440} m^{-1})**		
	Min	Max	Mean	Min	Max	Mean	Min	Max	Mean	Min	Max	Mean	Min	Max	Mean
18 May 2004	23.80	49.47	42.33	25.70	40.30	32.60	5.50	13.95	9.03	18.20	29.57	23.61	-	-	-
22 June 2005	1.40	48.89	14.89	3.11	95.69	39.93	0.58	50.86	14.85	2.33	50.00	25.08	1.15	6.91	3.00
29 August 2005	4.01	24.53	12.14	7.40	62.22	27.09	3.20	24.44	8.97	3.00	43.33	18.11	-	-	-
Combined	1.40	49.47	23.12	3.11	95.69	33.21	0.58	50.86	10.95	2.33	50.00	22.27	-	-	-

Table 3.7 The correlation coefficients (*r*) for the association between the measured concentrations of chlorophyll-a (chl-a), SPM, SPIM and SPOM for the individual and combined cruises.

		chl-a	SPM	SPIM	SPOM
18 May 2004	chl-a	-	0.64	0.72	0.30
	SPM	0.64	-	0.66	0.82
	SPIM	0.72	0.66	-	0.12
	SPOM	0.30	0.82	0.12	-
22 June 2005	chl-a	-	0.79	0.67	0.78
	SPM	0.79	-	0.91	0.94
	SPIM	0.67	0.91	-	0.73
	SPOM	0.78	0.94	0.73	-
29 August 2005	chl-a	-	0.91	0.98	0.85
	SPM	0.91	-	0.92	0.99
	SPIM	0.98	0.92	-	0.85
	SPOM	0.85	0.99	0.85	-
Combined	chl-a	-	0.48	0.37	0.50
	SPM	0.48	-	0.90	0.94
	SPIM	0.37	0.90	-	0.72
	SPOM	0.50	0.94	0.72	-

The chlorophyll-a concentrations measured on 22 June 2005 exhibited the greatest range (1.40-48.89 mg m^{-3}), but had a lower mean concentration (14.89 mg m^{-3}); predominantly, this was the result of extending sampling to encompass stations situated on the mesotrophic, clear water, Martham North and Ormesby Broads. The mean concentration of SPM on the 22 June 2005 was the highest observed during the three lake sampling cruises (39.93 mg L^{-1}) and, further, the inorganic fraction of the total SPM load was far greater than that encountered during previous or preceding cruises (SPIM = 14.85 mg L^{-1}). This may suggest the wind-driven resuspension of a more minerogenic bottom sediment. The concentration of SPOM on the 22 June 2005 was also the highest observed during the three lake sampling cruises (25.08 mg L^{-1}). The concentration of chlorophyll-a and SPOM were more highly correlated on this occasion (r = 0.78). This correlation was found only to be significant between lakes, chlorophyll-a and SPOM did not necessarily co-vary within individual lakes. This again suggests wind-driven resuspension of detritus was contributing significantly to the SPOM load.

Mean chlorophyll-a concentrations were significantly lower during the 29 August 2005 cruise (12.14 mg m^{-3}) and the chlorophyll-a concentration range was the smallest encountered (4.01-24.53 mg m^{-3}). The low mean concentration of chlorophyll-a was largely due to the occurrence of the late-summer minimum on Hickling Broad (the chlorophyll-a maximum on Hickling Broad

occurs during winter) on which most sampling stations were located. In similarity, the concentrations of SPM, SPIM and SPOM were also relatively low on the 29 August 2005 cruise – which may be indicative of more benign conditions on the lakes (i.e. an absence of wind-driven resuspension of bottom sediments). The suggested lack of wind-driven resuspension may mean, in this instance, that the seston in the water column may have been largely composed of phytoplankton. This would explain the higher correlation coefficients between chlorophyll-a and SPM detailed in Table 3.7.

3.5.2 $R_{rs}(\lambda,0+)$ Measurements

The $R_{rs}(\lambda,0+)$ measurements made at the sampling stations located across the Norfolk Broads on 18 May 2004, 22 June 2005 and 29 August 2005 are depicted in Figure 3.5. The spectra measured during the three lake cruises show characteristic features typical of CASE II waters. These features include: (i) low $R_{rs}(\lambda,0+)$ between 400 and 500 nm due to absorption by phytoplankton pigments (chlorophylls, carotenes and xanthophylls) and CDOM; (ii) a $R_{rs}(\lambda,0+)$ maximum at *c*. 570 nm due to backscattering from phytoplankton cells and SPM (tripton); (iii) a local $R_{rs}(\lambda,0+)$ minimum at *c*. 630 nm due to strong absorption by the cyanobacterial pigment C-phycocyanin; (iv) a further $R_{rs}(\lambda,0+)$ minimum at *c*. 680 nm caused by high chlorophyll-a absorption; and (v) a local $R_{rs}(\lambda,0+)$ maximum at *c*. 705 nm due to minimal absorption by phytoplankton pigments and intense scattering by phytoplankton cells and SPM (tripton).

The spectra from the eutrophic waters of Hickling Broad, Heigham Sound and Horsey Mere also exhibit a pronounced local $R_{rs}(\lambda,0+)$ peak at *c*. 480 nm. This feature is not apparent in the $R_{rs}(\lambda,0+)$ spectra of many CASE II shallow lakes previously published in the literature (see for example Svab *et al.,* 2005) and, indeed, it is not entirely clear what is the underlying cause(s) of this $R_{rs}(\lambda,0+)$ peak. It may be a function of backscattering from algal cells or tripton. However, given the very shallow nature of the Norfolk Broads it may also be, in part, related to the optical properties of the bottom substrate(s).

The subsequent $R_{rs}(\lambda,0+)$ minimum at *c*. 500 nm most likely is an artefact of absorption by carotenoid pigments. It is also notable that the position of the chlorophyll-a absorption related feature at *c*. 680 nm varies in the $R_{rs}(\lambda,0+)$ spectra. Other authors have commented on this behaviour and have suggested that the position of this feature changes in response to the concentration of chlorophyll-a, with a shift towards the VNIR region occurring at high concentrations of chlorophyll-a (Dekker *et al.,* 1991; Mittenzwey *et al.,* 1992; Han & Rundquist, 1997).

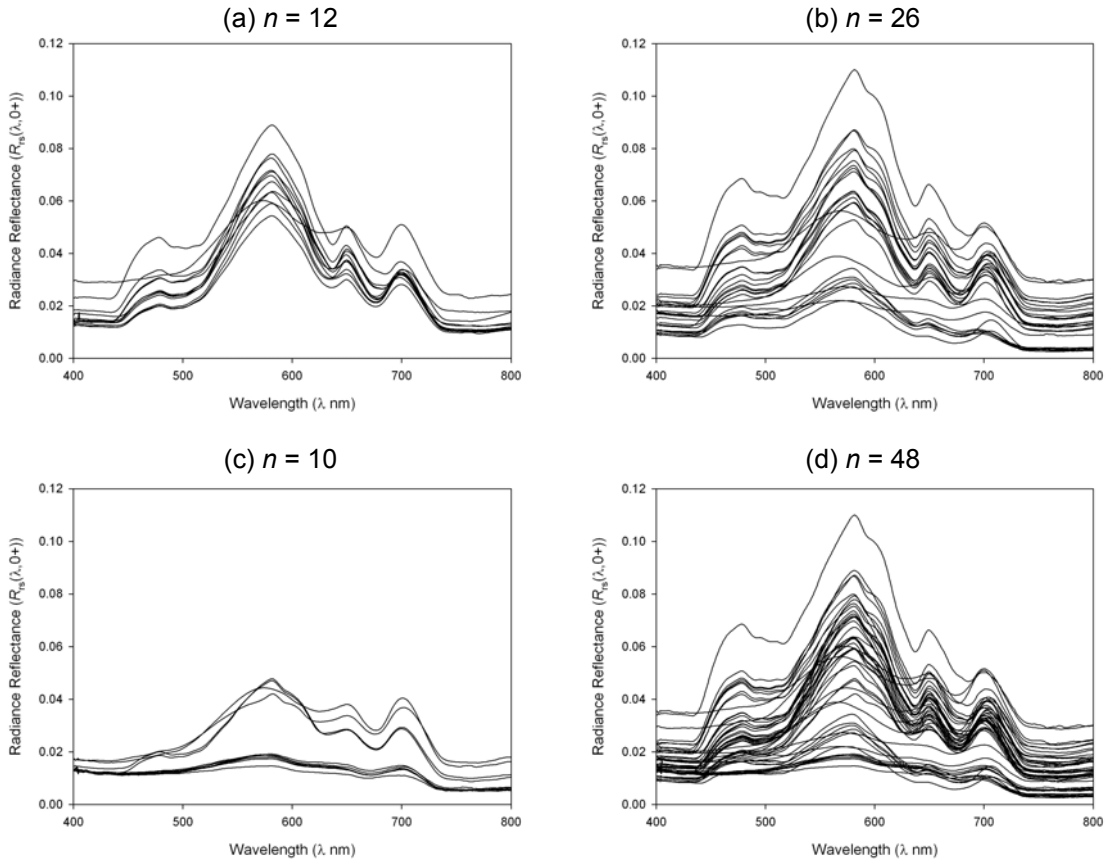

Figure 3.5 The $R_{rs}(\lambda,0+)$ measurements made at sampling stations on the (a) 18 May 2004; (b) 22 June 2005; (c) 29 August 2005; and (d) the combined datasets.

3.5.3 Suspended Particulate Matter (Seston)

The correlation coefficients observed between the spectral data (400-800 nm) and the concentration of SPM, SPIM and SPOM for the four multi-temporal datasets are detailed in Figure 3.6. It is notable that, with the exception of the 18 May 2004 dataset, the concentrations of SPM, SPIM and SPOM demonstrated positive correlations with $R_{rs}(\lambda,0+)$. $R_{rs}(\lambda,0+)$ is

generally positively related to the concentration of SPM and SPIM due to the high backscattering by these particulates (although negative relationships may occur with SPOM in some circumstances) (Lindell *et al*., 1999). It is not entirely clear why the correlations observed on 18 May 2004 should be negative for all three SPM fractions. It may be that the negative correlations observed were simply spurious (i.e. statistical noise). However, the stations sampled on the 18 May 2004 cruise were all located on eutrophic Broads with highly organic bottom sediments. The low backscattering, but high absorption, properties of this largely detrital material may explain the negative correlations observed in this instance. The spectral region that displayed the strongest correlation with SPM in the 18 May 2004 dataset was dependent upon the specific fraction targeted. The strongest correlations with total SPM were observed at *c*. 570 nm; the strongest correlations with the SPIM fraction were observed at *c*. 580 nm (although the correlation was not statistically significant); and the strongest correlations with SPOM were observed at *c*. 555 nm.

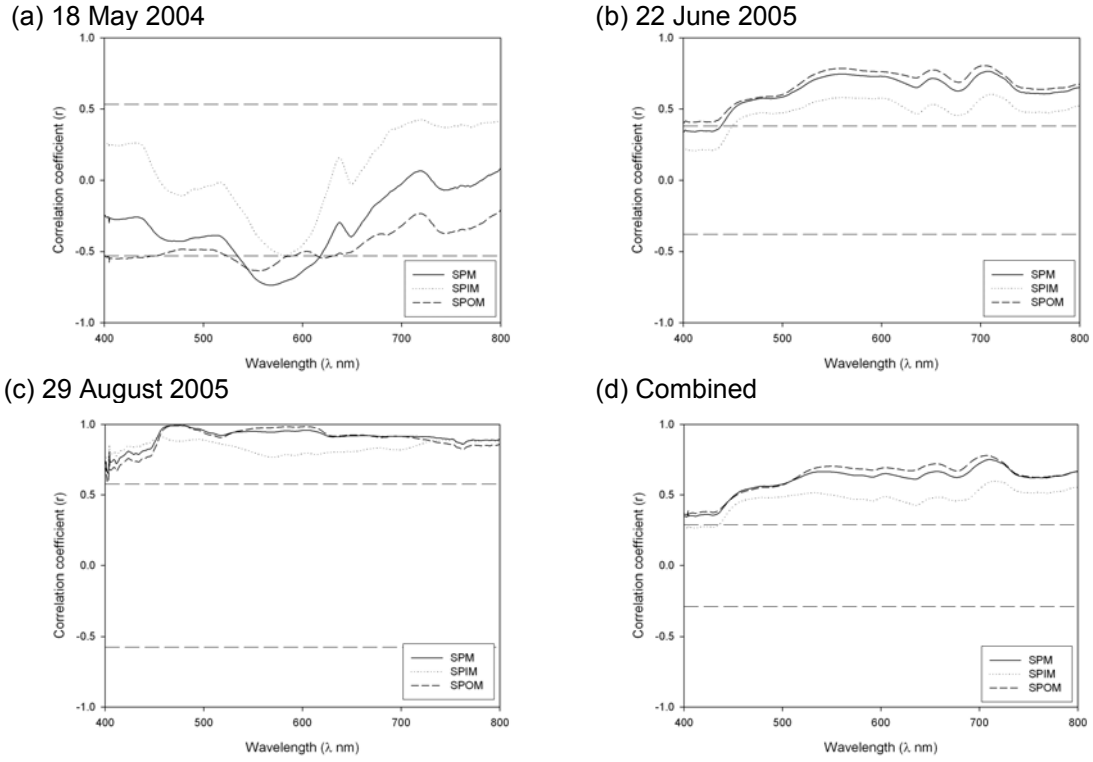

Figure 3.6 The correlation coefficients (*r*) between the $R_{rs}(\lambda,0+)$ data and the concentration of SPM, SPIM and SPOM for the four datasets. Dashed constant lines indicate the critical values of *r* (95% confidence level; two-tailed).

In contrast, for the 22 June 2005 dataset, strong and positive correlations between $R_{rs}(\lambda,0+)$ and SPM, SPIM and SPOM were observed to occur uniformly at 705 nm; although high correlation coefficients were also observed at all wavelengths > 550 nm. This probably reflects that fact the SPM in the lakes on 22 June 2005 was largely inorganic (i.e. high VNIR backscattering). The correlations derived from the 29 August 2005 dataset were the highest observed from the three sampling cruises and the SPM, SPIM and SPOM fractions demonstrated excellent correlations (r > 0.80) with $R_{rs}(\lambda,0+)$ between 450 and 750 nm. The highest correlations between $R_{rs}(\lambda,0+)$ and the SPM and SPIM fractions occurred in the 475 nm region; whereas, the highest correlation between $R_{rs}(\lambda,0+)$ and SPOM was observed at *c*. 455 nm. These regions relate to the position of the $R_{rs}(\lambda,0+)$ peak feature at *c* 480 nm; this suggests this may indeed be related to the backscattering by phytoplankton and/or tripton. In the combined dataset, the observed relationships were again positive, with the best correlations between SPM, SPIM and SPOM and $R_{rs}(\lambda,0+)$ occurring in the VNIR (705-720 nm) region.

The optimum correlation coefficients, coefficients of determination and least-squares regression models for the relationship between $R_{rs}(\lambda,0+)$ and the concentration of SPM, SPIM and SPOM for the three individual cruises and the combined dataset are shown in Table 3.8. The poorest relationships between the spectral data and the measured concentrations of SPM, SPIM and SPOM were derived from the 18 May 2004 dataset. The concentration of SPM and SPOM could be only estimated with an accuracy of R^2 = 0.54 and R^2 = 0.40 using the respective values of $R_{rs}(\lambda,0+)$ at 570 nm and 540 nm. No statistically significant relationships were observed with SPIM.

Improved relationships between $R_{rs}(\lambda,0+)$ and SPM, SPIM and SPOM were derived from the 22 June 2005 data with respective R^2 values = 0.78, 0.79 and 0.64 observed for the relationship with the value of $R_{rs}(\lambda,0+)$ at 705 nm. Other authors have shown in foregoing studies that the value of $R_{rs}(\lambda,0+)$ at *c*. 705-710 nm is sensitive to changes in SPM (e.g. Malthus & Dekker, 1995) and these previous findings would seem to go some way towards substantiating the results observed here.

Table 3.8 The correlation coefficients, regression coefficients and best-fit models for the optimum empirical relationships between the spectral data and the concentration of SPM, SPIM and SPOM. (N/S = not significant at the 95% confidence level).

	SPM				SPIM				SPOM			
	λ (nm)	*r*	Best-Fit Model	R^2	λ (nm)	*r*	Best-Fit Model	R^2	λ (nm)	*r*	Best-Fit Model	R^2
18 May 2004	570	-0.74*	$-0.0013[R_{rs}(\lambda)] + 0.1089$	0.54	580	N/S	N/S	N/S	555	-0.64*	$-0.0013R_{rs}[(\lambda)] + 0.0869$	0.40
22 June 2005	705	0.76*	$1.9856e^{85.462[Rrs(\lambda)]}$	0.78	705	0.80*	$1.5445e^{80.598[Rrs(\lambda)]}$	0.79	705	0.59*	$0.4945e^{91.305[Rrs(\lambda)]}$	0.64
29 August 2005	475	0.99**	$6048.9[R_{rs}(\lambda)] - 63.294$	0.99	475	0.99**	$4444.4[R_{rs}(\lambda)] - 48.295$	0.99	455	0.91**	$0.5723e^{169.33[Rrs(\lambda)]}$	0.89
Combined	710	0.75*	$3.2252e^{77.021[Rrs(\lambda)]}$	0.72	708	0.78*	$2.061e^{75.49[Rrs(\lambda)]}$	0.74	717	0.60*	$1.1703e^{81.953[Rrs(\lambda)]}$	0.53

*($p < 0.05$) **($p < 0.01$)

The strongest relationships between $R_{rs}(\lambda,0+)$ and SPM , SPIM and SPOM were observed during the 29 August 2005 cruise. In this instance, the relationships between SPM and SPIM and $R_{rs}(\lambda,0+)$ at 475 nm both yielded R^2 values = 0.99 using a linear best-fit model and the relationship between $R_{rs}(\lambda,0+)$ at 455 nm and SPOM produced an R^2 value = 0.89 using an exponential best-fit model. Notwithstanding the fact that the highest coefficients of determination were observed with wavelengths in the blue and green spectral regions, in the 29 August 2005 dataset, wavelengths in the VNIR also retuned R^2 values > 0.90 for the relationship with SPM and SPIM (not shown). The relationship between $R_{rs}(\lambda,0+)$ and SPM, SPIM and SPOM in the combined dataset was best modelled using exponential functions and reasonable coefficients of determination for the relationships between [$R_{rs}(710)$] and SPM (R^2 = 0.72) and, [$R_{rs}(708)$] and SPIM (R^2 = 0.74), were obtained. The relationship between the spectral data and the concentration of SPOM was more tenuous, yielding an R^2 value of 0.53 for the relationship with [$R_{rs}(717)$].

It is notable that marked differences in the strength and linearity of the relationship between $R_{rs}(\lambda,0+)$ and the SPM fractions was observed during the three lake sampling cruises. The cause of this inconsistency is not entirely clear. However, the results seem to imply that the relative concentrations of the SPIM and SPOM may influence relationships with $R_{rs}(\lambda,0+)$. SPIM and SPOM have very divergent optical characteristics and, in shallow lakes, they do not necessarily co-vary. This may greatly influence the $R_{rs}(\lambda,0+)$ signal. The linearity of the relationship between $R_{rs}(\lambda,0+)$ and SPM would seem to be influenced by the concentration gradient used in the formulation of the algorithm, with non-linear algorithms seemingly more appropriate when the SPM gradient is large. Non-linear relationships between $R_{rs}(\lambda,0+)$ and SPM have been documented in the past and, in particular, when the SPM concentration gradient is high (e.g. Lathrop *et al.,* 1991).

The results obtained here would suggest that remote sensing data can be used to estimate SPM (seston) loads in shallow lakes. The seston, or more specifically, the tripton load is important to the function of shallow lakes, particularly in relation to nutrient and contaminant

cycling and, moreover, the ambient light climate. The development of remote-sensing-based techniques for mapping SPM loads (and potentially fluxes) in shallow lakes is thus a pertinent finding. The estimation of SPM and/or SPIM would seem to be readily achievable, particularly where the concentration of inorganic tripton is high (i.e. high backscattering signal). The estimation of SPOM would seem more problematic. Organic particulates often do not have a strong backscattering signal (Lindell *et al*., 1999). Thus, the accuracy of SPOM estimation from remotely sensed data, as shown here, may be dependent on the degree of co-variance with other, more optically-active, components in the water column (e.g. SPIM or chlorophyll-a).

Many previous studies that have sought to retrieve SPM concentrations in lakes from remotely sensed data, either empirically or analytically, have not differentiated between the SPIM and SPOM fractions, despite their divergent optical properties. In this context, further consideration should be given to the effect of variable SPM mineralogy on $R_{rs}(\lambda,0+)$ in shallow lakes. In this context, bio-optical modelling may be highly pertinent (as shown by Ammenberg *et al.,* 2002).

3.5.4 Secchi Disc Depth

Measurements of the SDD (m) were made concurrent to the acquisition of $R_{rs}(\lambda,0+)$ spectra on the 29 August 2005. Table 3.9 details the SDD measurements made at the 10 stations during the 29 August 2005 lake sampling cruise. The results show a clear gradient in water transparency between stations located on the eutrophic and turbid waters of Hickling Broad, Heigham Sound, and Horsey Mere (SSD = 0.35-0.75 m) (H1-H4) and those located on the mesotrophic and clear waters of Martham North Broad (SDD > 1.2 m) (H5-H10).

Table 3.9 SDD (m) measurements made at the various sampling stations on 29 August 2005 and the associated mean, standard deviation (Std Dev) and standard error (Std Err).

	H1	H2	H3	H4	H5	H6	H7	H8	H9	H10
SDD (m)	0.75	0.35	0.4	0.35	1.2	1.25	1.2	1.25	1.3	1.25
	Mean = 0.93			Std Dev. = 0.42		Std Err = 0.13				

The correlations between the $R_{rs}(\lambda,0+)$ data and the first-derivative transformed $R_{rs}(\lambda,0+)$ data ($dR/d\lambda$) and the measured SDD are depicted in Figure 3.7. The $R_{rs}(\lambda,0+)$ data demonstrated strong negative correlative relationships with the SDD between 450 nm to 700 nm with the

resulting correlation coefficients ranging from r = -0.85 to -0.96. The strongest correlation with the SDD was observed at 620 nm (r = -0.962).

The dR/dλ data also demonstrated strong negative correlations with the measured SDD in the 500-570 nm, 580-610 nm, 625-650 nm, 650-675 nm and 700-740 nm regions. The highest correlation coefficient in this instance was observed with the value of dR/dλ at 640 nm (r = -0.981).

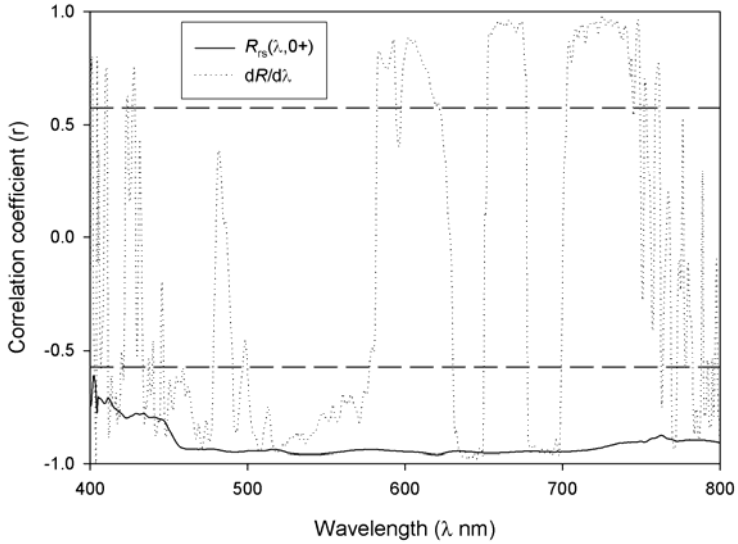

Figure 3.7 The correlation coefficients between the spectral reflectance and spectral derivative reflectance data and the measured SDD. The dashed constant lines indicate the critical values of r (±0.576) for n = 10 (95% confidence level).

Table 3.10 The best-fit models for the relationship between R and dR/dλ and the measured Secchi Disk Depth (m) on the 29 August.

Index (x)	r	Best-Fit Model	R^2	RMSE (m)
[R_{rs}(620.5)]	-0.962**	-44.338(x) + 1.8797	0.925	0.108
[dR/dλ_{640}]	-0.981**	-3969.2(x) + 1.0075	0.962	0.077

*(p < 0.05) **(p < 0.01)

The best-fit models for the optimum wavelengths for both the R_{rs}(λ,0+) and dR/dλ spectra are detailed in Table 3.10. The relationship between the R_{rs}(λ,0+) or dR/dλ and SDD were best modelled in both cases using a linear least-squares regression model. The regression models yielded a RMSE for estimation of SDD of 0.11 m [R_{rs}620.5] and 0.08 m [dR/dλ_{640}] respectively. The best-fit linear regression models for SDD estimation for both R_{rs}(λ,0+) and dR/dλ are

depicted in Figure 3.8. The least-squares regression models demonstrate a reasonable fit against the measured SDD. It is noticeable that the data are clustered at the extremes of the SDD gradient. However, such an effect is inevitable when, as in this case, sampling is conducted across lakes of highly contrasting turbidity. The scatter observed within the clusters is likely to be due, at least in part, to the inherent inaccuracies of the SDD technique as a measurement of water transparency.

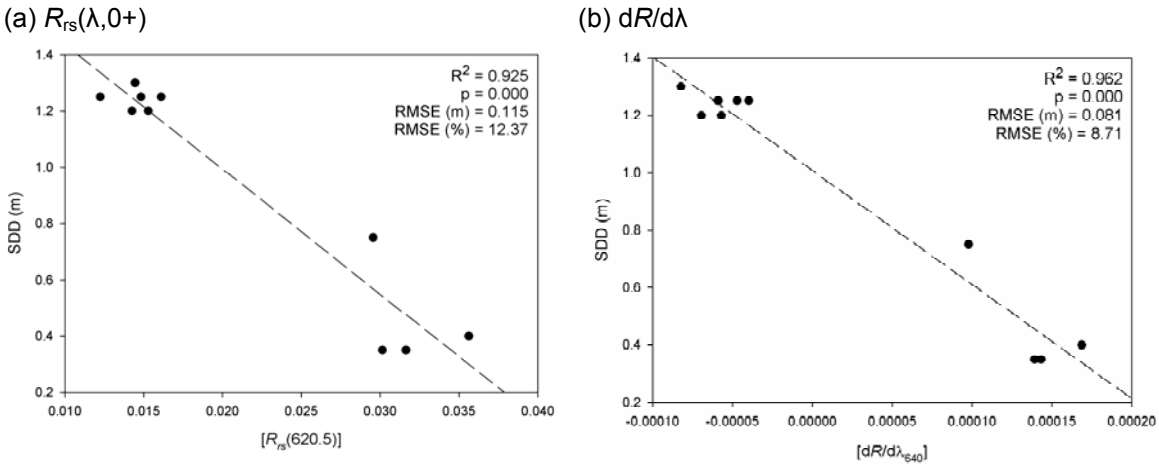

Figure 3.8 The best-fit linear regression models for the relationship between (a) $R_{rs}(\lambda,0+)$ at 620.5 nm and the SDD and (b) dR/dλ at 640 nm and SDD. Dashed lines correspond to 95% confidence intervals for the best-fit models.

The SDD, despite being prone to inaccuracies, is favoured by limnologists as a simple measurement of water transparency. The results observed here, albeit from a single sampling occasion, clearly demonstrate that remote sensing data can be used to provide estimates of the SDD in shallow lakes and, in this context, remote sensing could therefore be used to monitor changes in the ambient underwater light field of shallow lakes.

3.5.5 Coloured Dissolved Organic Matter

Measurements of CDOM (g_{440} m^{-1}) were made during the lake sampling conducted on 22 June 2005. No measurements of CDOM are available that coincide with the datasets acquired on 18 May 2004 or 29 August 2005. Figure 3.9 shows the correlation coefficients between the measured concentration of CDOM ($g440$ m^{-1}) and the $R_{rs}(\lambda,0+)$ and dR/dλ data. The correlations between the measured concentration of CDOM and the spectral data ($R_{rs}(\lambda,0+)$ and

d*R*/dλ) were poor. No significant correlations were observed between the measurements of CDOM absorption and $R_{rs}(\lambda,0+)$. The only significant correlations were observed between the measurements of CDOM absorption and d*R*/dλ in the 520-580 nm and > 750 nm region ($r \sim \pm 0.50$).

The strongest correlation was observed to occur with the value of d*R*/dλ at 764 nm. However, as CDOM absorption, backscattering and fluorescence is essentially negligible in the VNIR region, this correlation lacks a mechanistic explanation and, thus, seems somewhat spurious. Indeed, it may be an artefact of covariance between CDOM and another component that is optically active in the VNIR. Kallio *et al*., (Kallio *et al.,* 2001) also report similar findings.

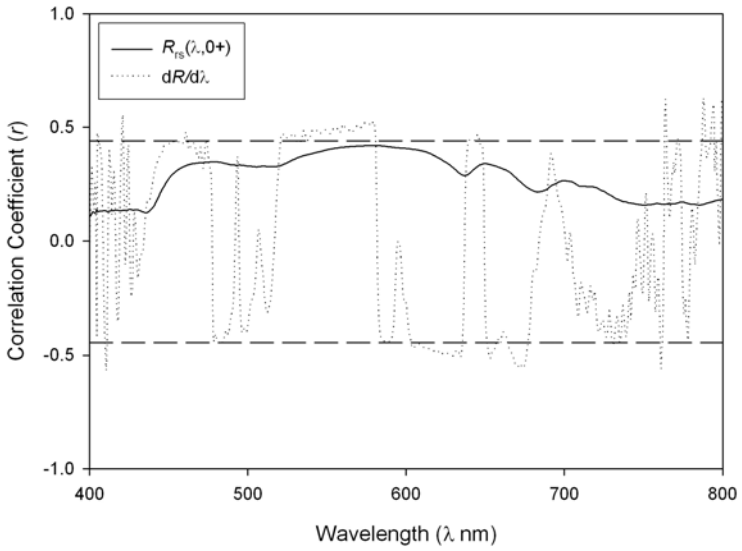

Figure 3.9 The correlation coefficients between the $R_{rs}(\lambda,0+)$ and d*R*/dλ data and the measured concentration of CDOM. The dashed constant lines indicate the critical values of *r* (±0.444) for *n* = 20 (95% significance level).

In addition to simple empirical analysis using single bands, the CDOM band-ratio index [$R_{rs}(565)/R_{rs}(660)$] derived by Kutser *et al*. (2005a) was also calculated from the $R_{rs}(\lambda,0+)$ data and correlated against the CDOM measurements. However, the index proposed by Kutser *et al*. (Kutser *et al.,* 2005b) also did not demonstrate a significant correlation with the measurements of CDOM in the Broads ($r = 0.352$; critical $r = \pm 0.444$).

The lack of strong significant correlations between the $R_{rs}(\lambda,0+)$ data and CDOM in the Broads may have been the result of spectral masking effects caused by other optical components (e.g. phytoplankton pigments). In addition, the poor results may also be related to the fact that concentration of CDOM was uniformly low in the three Broads sampled on 22 June 2005. In contrast, the band-ratio algorithm derived by Kutser *et al*., (Kutser *et al.,* 2005b) was formulated using CDOM measurements from 18 Finish and Swedish lakes over the range a_{CDOM} = 0.5-12 m^{-1} (R^2 = 0.84). Giardino *et al*., (2007) suggests the estimation of CDOM from remotely sensed data is largely dependent on the existence of a pronounced concentration gradient for algorithm formulation. Thus, extending the lake sampling campaigns to include lakes more humic in nature would, almost certainly, have improved the derived correlations. Unfortunately, it was not possible to sample such water types in the Upper Thurne system of the Norfolk Broads.

The cycling of dissolved organic matter (DOM) is an important processes in lake ecosystems and has significance for both lake biota (e.g. heterotrophic bacteria) and for wider carbon cycle dynamics. The concentrations of DOM and CDOM are usually very well correlated (Tranvik, 1990) and thus the development of remote-sensing-based techniques for the quantification of CDOM in lakes would represent a significant advancement for studies of carbon cycling between terrestrial and freshwater ecosystems. However, the results obtained here (and elsewhere (e.g. Giardino *et al.,* 2007) indicate the formulation of algorithms for the estimation of CDOM concentrations from remote sensing data can be problematic (particularly in non-dystrophic lakes). Nonetheless, the encouraging results achieved by Arenz *et al*. (1996), Kallio *et al*. (2001), Hirtle & Rencz (2003) and Kutser *et al*. (2005b) suggest that this is an area where valuable further work can be pursued.

3.5.6 Chlorophyll-a

3.5.6.1 $R_{rs}(\lambda,0+)$ and $dR/d\lambda$ Based Algorithms

The correlation coefficients between the $R_{rs}(\lambda,0+)$ and $dR/d\lambda$ spectra and the measured concentration of chlorophyll-a for the various cruises are depicted in Figure 3.10. It is again noticeable that, in similarity to the correlations observed with SPM, $R_{rs}(\lambda,0+)$ was also negatively associated with the concentration of chlorophyll-a on 18 May 2004.

(a) 18 May 2004

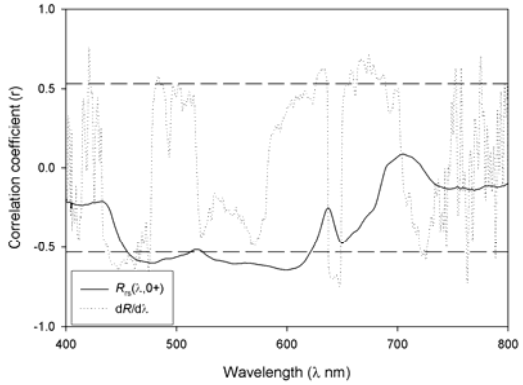

(b) 22 June 2005

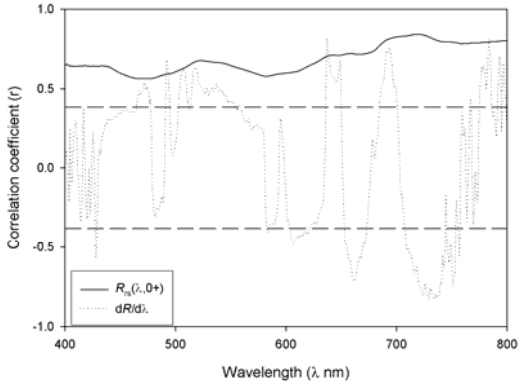

(c) 29 August 2005

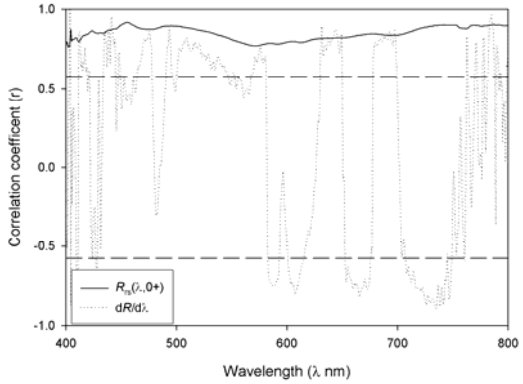

(d) Combined dataset

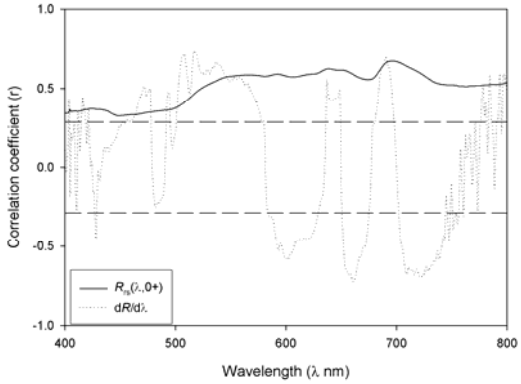

Figure 3.10 The correlation coefficients between the $R_{rs}(\lambda,0+)$ and $dR/d\lambda$ data and the concentration of chlorophyll-a for the four datasets. The dashed lines indicate the critical values of *r* (95% confidence level).

The existence of negative relations between chlorophyll-a and $R_{rs}(\lambda,0+)$ is again difficult to explain. It may be due to the fact the background concentration of SPIM (tripton) was relatively invariable on 18 May 2004 (5.50-13.95 mg L^{-1}). It can be argued that increases in the concentration of chlorophyll-a against a constant SPIM background (i.e. constant backscattering) would promote increased absorption at specific wavelengths and thus yield negative relationships between $R_{rs}(\lambda,0+)$. This effect would not be expected if, as in the case of the latter datasets, sampling is conducted across lakes with a more pronounced gradient in SPIM (i.e. variable backscattering). Interestingly, Han (2005) also noted negative relationships between $R_{rs}(\lambda,0+)$ and the concentration of chlorophyll-a in the coastal waters of Pensacola Bay

(USA). In this context it may be significant that the strongest negative correlations occurred in regions of high pigment absorption (Figure 3.10a).

In contrast, $R_{rs}(\lambda,0+)$ demonstrated positive correlations with chlorophyll-a in the 22 June 2005, 29 August 2005 and the combined dataset; the highest correlations occurred in the 690-710 nm region (22 June 2005 and combined dataset) and *c*. 450 nm and > *c*. 720 nm (29 August 2005 dataset). The correlations observed between the $dR/d\lambda$ spectra and the concentration of chlorophyll-a demonstrated both positive and negative coefficients dependent upon the gradient (slope) of the $dR/d\lambda$ spectra at specific wavelengths. Significant correlations were noted at *c*. 630 nm, 660 nm and 690 nm in the four $dR/d\lambda$ datasets and, in most cases, the correlation coefficients were comparable or greater than those achieved with the untransformed $R_{rs}(\lambda,0+)$ data.

The correlation coefficients, coefficients of determination and best-fit least-squares regression models for the relationship between the chlorophyll-a retrieval indices and the measured concentration of chlorophyll-a for the 18 May 2004 dataset are detailed in Table 3.11. The best estimates of chlorophyll-a for the dataset derived from the 18 May 2004 cruise were provided by the NIR/red band-ratio index $[R_{rs}(705)/R_{rs}(670)]$ (R^2 = 0.69) and the $[(R_{rs}^{-1}(675)-R_{rs}^{-1}(720))xR_{rs}(750)]$ index proposed by Dall'Olmo *et al*. (2003) (R^2 = 0.64) using exponential least-squares regression models.

The correlation coefficients, coefficients of determination and best-fit least-squares regression models for the relationships between the chlorophyll-a retrieval indices and the measured concentration of chlorophyll-a for the 22 June 2005 dataset are detailed in Table 3.12. The highest coefficients of determination observed for the relationship with the chlorophyll-a concentration were provided by the value of $dR/d\lambda$ at 638 nm and 631 nm (R^2 = 0.653-0.656); the NIR/red and green/blue band-ratio indices did not demonstrate strong relationships with chlorophyll-a (max. R^2 = 0.460, but typically not significant).

Reasonable coefficients of determination (R^2 > 0.50) were also obtained for the other NIR/red band-ratios and for the value of dR/dλ at 638 nm (R^2 = 0.41). No significant relationships between $R_{rs}(\lambda,0+)$ and the concentration of chlorophyll-a could be derived using the CASE I-type green/blue band-ratio indices.

Table 3.11 The results for the chlorophyll-a retrieval indices from the 18 May 2004 dataset (n = 12) (N/S = not significant at the 95% confidence level).

Index (x)	***r***	**Best-Fit Least-Squares Regression Model**	***R*²**
$[R_{rs}(433)/R_{rs}(555)]$	0.119	N/S	N/S
$[R_{rs}(490)/R_{rs}(555)]$	0.432	N/S	N/S
$[R_{rs}(510)/R_{rs}(555)]$	0.315	N/S	N/S
$[R_{rs}(705)/R_{rs}(670)]$	0.726**	67.324x - 39.663	0.528
$[R_{rs}(765)/R_{rs}(670)]$	0.217	N/S	N/S
$[R_{rs}(705)/R_{rs}(664)]$	0.779**	$5.5324e^{1.8685x}$	0.690
$[R_{rs}(704)/R_{rs}(672)]$	0.699*	$6.7345e^{1.4185x}$	0.562
$[(R_{rs}^{-1}(675)-R_{rs}^{-1}(720))xR_{rs}(750)]$	0.732**	$58.857e^{4.0687x}$	0.642
$[dR/d\lambda_{620}]$	-0.438	N/S	N/S
$[dR/d\lambda_{638}]$	0.639*	-90440x + 59.2	0.408
$[dR/d\lambda_{661}]$	-0.480	N/S	N/S
$[dR/d\lambda_{690.5}]$	0.448	N/S	N/S

*(p < 0.05) **(p < 0.01)

Table 3.12 The results for the chlorophyll-a retrieval indices from the 22 June 2005 dataset (n = 26) (N/S = not significant at the 95% confidence level).

Index (x)	*r*	*Best-Fit Least-Squares Regression Model*	*R²*
$[R_{rs}(433)/R_{rs}(555)]$	0.077	N/S	N/S
$[R_{rs}(490)/R_{rs}(555)]$	0.149	N/S	N/S
$[R_{rs}(510)/R_{rs}(555)]$	0.053	N/S	N/S
$[R_{rs}(705)/R_{rs}(670)]$	0.089	N/S	N/S
$[R_{rs}(765)/R_{rs}(670)]$	0.672**	$0.9642e^{5.3646}$	0.460
$[R_{rs}(705)/R_{rs}(664)]$	0.065	N/S	N/S
$[R_{rs}(704)/R_{rs}(672)]$	0.094	N/S	N/S
$[(R_{rs}^{-1}(675)-R_{rs}^{-1}(720))xR_{rs}(750)]$	0.400*	N/S	N/S
$[dR/d\lambda_{620}]$	--0.410*	$6.6669e^{-1245.8x}$	0.260
$[dR/d\lambda_{638}]$	0.733**	$5.9662e^{5211.6x}$	0.652
$[dR/d\lambda_{661}]$	-0.714**	$2.9683e^{-3690.8x}$	0.656
$[dR/d\lambda_{690.5}]$	0.722**	$3.9182e^{2665.5x}$	0.623

*(p < 0.05) **(p < 0.01)

The correlation coefficients, coefficients of determination and best-fit least-squares regression models for the relationships between the chlorophyll-a retrieval indices and the measured concentration of chlorophyll-a for the 29 August 2005 dataset are detailed in Table 3.13. The data derived from the 29 August 2005 cruise produced the strongest relationship between the $R_{rs}(\lambda,0+)$ and $dR/d\lambda$ indices and the measured concentration of chlorophyll-a that was obtained over the 2-year sampling period. The best estimate of the chlorophyll-a concentration was provided by the medium-independent pigment index $[(R_{rs}^{-1}(675)-R_{rs}^{-1}(720))xR_{rs}(750)]$ developed by Dall'Olmo (2003) (R^2 = 0.93) using a linear least-squares regression model (see Figure 3.11).

Table 3.13 The results for the chlorophyll-a retrieval indices from the 29 August 2005 dataset (n = 10) (N/S = not significant at the 95% confidence level).

Index (x)	r	Best-Fit Least-Squares Regression Model	R^2
$[R_{rs}(433)/R_{rs}(555)]$	0.700*	$50.532e^{-2.8326x}$	0.600
$[R_{rs}(490)/R_{rs}(555)]$	0.690*	$103.58e_{-3.612x}$	0.594
$[R_{rs}(510)/R_{rs}(555)]$	0.631	N/S	N/S
$[R_{rs}(705)/R_{rs}(670)]$	0.825**	$0.0081e^{5.8669x}$	0.800
$[R_{rs}(765)/R_{rs}(670)]$	0.368	N/S	N/S
$[R_{rs}(705)/R_{rs}(664)]$	0.820**	$0.0001e^{9.9387x}$	0.772
$[R_{rs}(704)/R_{rs}(672)]$	0.366	N/S	N/S
$[(R_{rs}^{-1}(675)-R_{rs}^{-1}(720))xR_{rs}(750)]$	0.962**	172.03x + 23.021	0.925
$[[dR/d\lambda_{620}]$	-0.415	N/S	N/S
$[dR/d\lambda_{638}]$	0.819**	90071x + 8.7686	0.671
$[dR/d\lambda_{661}]$	-0.733*	$4.8925e^{-2590.3x}$	0.646
$[dR/d\lambda_{690.5}]$	0.813**	$6.2203e^{1694.8x}$	0.716

*(p < 0.05) **(p < 0.01)

The NIR/red band-ratios, $[R_{rs}(705)/R_{rs}(670)]$ and $[R_{rs}(705)/R_{rs}(664)]$, and $[dR/d\lambda_{638}]$, $[dR/d\lambda_{661}]$, and $[dR/d\lambda_{690.5}]$ also demonstrated good relationships with the measured concentration of chlorophyll-a. Interestingly, reasonable coefficients of determination were also derived for the CASE I-type green/blue band-ratios, $[R_{rs}(433)/R_{rs}(555)]$ and $[R_{rs}(490)/R_{rs}(555)]$, despite their alleged unsuitability for chlorophyll-a estimation in CASE II waters. The excellent relationships between the $R_{rs}(\lambda,0+)$ indices and the measured concentration of chlorophyll-a in the 29 August 2005 dataset may be associated with the lower coincidental concentrations of SPM (both SPIM

and SPOM) in the water column, particularly given the strong relationships observed with the CASE I green/blue band-ratios

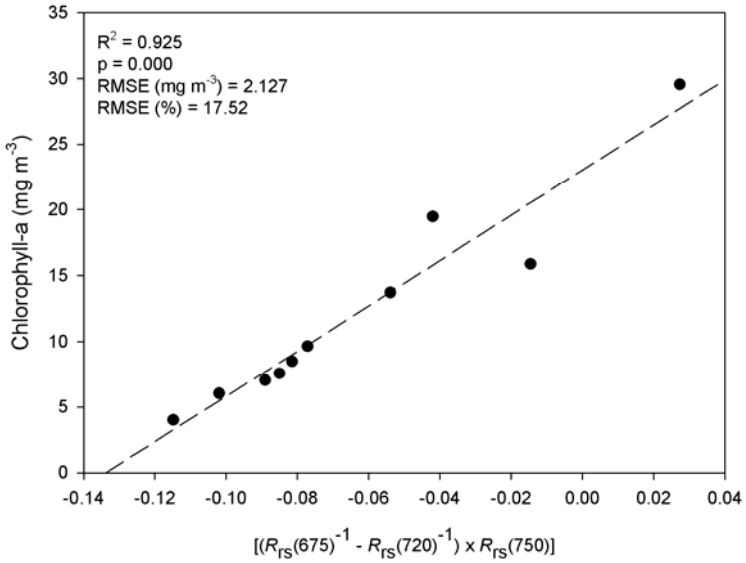

Figure 3.11 The linear regression relationship between the medium independent pigment index proposed by Dall'Olmo *et al*. (2003) and the measured concentration of chlorophyll-a during the 29 August 2005 cruise.

The correlation coefficients, coefficients of determination and best-fit least-squares regression models for the relationships between the $R_{rs}(\lambda,0+)$ and $dR/d\lambda$ indices and the measured concentration of chlorophyll-a for the combined dataset are detailed in Table 3.14. In contrast to the results obtained from the independent datasets, the best estimate of the measured concentration of chlorophyll-a in the combined dataset was provided by the $[dR/d\lambda_{661}]$ index (R^2 = 0.69). It is notable that no statistically significant relationships were observed between the NIR/red band-ratios and the concentration of chlorophyll-a.

These results intimate that NIR/red band-ratios may provide a less robust estimation of chlorophyll-a, when applied to multi-season data, than the $dR/d\lambda$ indices. The $[dR/d\lambda_{661}]$ index exploits a wavelength that is positioned in close proximity to the chlorophyll-a absorption feature at *c*. 670-680 nm in $R_{rs}(\lambda,0+)$ spectra which provides a mechanistic rationalisation for its sensitivity to chlorophyll-a variations. The superior performance of the $dR/d\lambda$ indices in the combined multi-season dataset could be due to the fact that first-derivative transformations of $R_{rs}(\lambda,0+)$ data are known to be effective at normalising spectra for latent differences in

backscattering derived from non-chlorophyllous particles (i.e. variable tripton backscatter) (Malthus & Dekker, 1995; Han & Rundquist, 1997). In contrast, NIR/red band-ratios are believed to be more sensitive to variability in backscatter from non-chlorophyllous particles, particularly if the absorption and backscatter coefficients for the tripton component(s) (SPIM and SPOM) are wavelength-dependent. Han & Rundquist (1997) demonstrated that, while NIR/red band-ratios could be used to retrieve accurate estimates of the chlorophyll-a concentration on a single sampling occasion, d*R*/dλ indices (in this instance, [d*R*/d$\lambda_{690.5}$]) provided an improved estimation of the chlorophyll-a concentration from multi-season $R_{rs}(\lambda,0+)$ data. Han (2005) also suggests that first-derivative transformations are effective for the removal of specular reflectance caused by wave effects. This may also explain the efficacy of the d*R*/dλ indices for the estimation of chlorophyll-a, as the nadir measurements of $R_{rs}(\lambda,0+)$ in the Norfolk Broads appeared to somewhat prone to the effects of sun glint on occasion.

Table 3.14 The results for the chlorophyll-a retrieval indices from the combined datasets (*n* = 48) (N/S = not significant at the 95% confidence level).

Index (x)	*r*	Best-Fit Least-Squares Regression Model	R^2
$[R_{rs}(433)/R_{rs}(555)]$	-0.471**	-67.861x + 56.747	0.298
$[R_{rs}(490)/R_{rs}(555)]$	-0.572**	-66.461x + 60.039	0.278
$[R_{rs}(510)/R_{rs}(555)]$	-0.532**	-60.774x + 62.538	0.193
$[R_{rs}(705)/R_{rs}(670)]$	0.172	N/S	N/S
$[R_{rs}(765)/R_{rs}(670)]$	0.258	N/S	N/S
$[R_{rs}(705)/R_{rs}(664)]$	0.050	N/S	N/S
$[R_{rs}(704)/R_{rs}(672)]$	0.112	N/S	N/S
$[(R_{rs}^{-1}(675)-R_{rs}^{-1}(720))xR_{rs}(750)]$	0.238	N/S	N/S
$[[dR/d\lambda_{620}]$	-0.456**	$8.6573e^{-1224.5x}$	0.380
$[dR/d\lambda_{638}]$	0.469**	$9.0445e^{4369.6x}$	0.428
$[dR/d\lambda_{661}]$	-0.724**	$3.777e^{-3293.9x}$	0.689
$[dR/d\lambda_{690.5}]$	0.463**	$4.8543e^{2605.2x}$	0.639

*(p < 0.05) **(p < 0.01)

The temporal robustness of the optimum chlorophyll-a retrieval algorithms derived from the three independent sampling cruises in the Norfolk Broads (18 May 2004, 22 June 2005, 29 August 2005) was assessed by validating each algorithm against the remaining, independent, datasets. The performance of the optimum algorithm derived from the amalgamated multi-

season dataset was also examined for each individual sampling occasion. The validation accuracy (RMSE) of the optimum chlorophyll-a retrieval algorithms is detailed in Table 3.15.

The validation results show that the performance of the chlorophyll-a algorithms varied enormously between the multi-season datasets. The optimum algorithm developed from the 18 May 2004 dataset produced reasonable estimates of chlorophyll-a when applied to the 22 June 2005 dataset (RMSE = 10.52 mg chlorophyll-a m^{-3} (24.85%)). However, the optimum 18 May 2004 algorithm did not perform well when validated against the 29 August 2005 dataset. This lack of multi-temporal transferability may be due to fact the optimum 18 May 2004 algorithm was formulated from a dataset derived from measurements made at stations located on turbid lakes and did not contain measurements from the clear waters of Martham North Broad or Ormesby Broad.

Table 3.15 Multi-temporal validation of the optimum chlorophyll-a (Chl-a) retrieval algorithms extrapolated to independent datasets (N/S = not significant). Grey text details the performance of the algorithm against the original calibration dataset.

	Optimum Least-Squares Regression Algorithm	**Validation Dataset**	***n***	R^2	**RMSE (mg m^{-3})**	**RMSE (%)**
18 May 2004	Chl-a (mg m^{-3}) = $5.5324e^{1.8685x}$ Where, x = [$R_{rs}(705)/R_{rs}(664)$]	18 May 2004	12	0.67	7.24	17.01
		22 June 2005	26	N/S	10.52	24.85
		29 August 2005	10	0.69	34.85	82.33
22 June 2005	Chl-a (mg m^{-3}) = $2.9683e^{-3690.8x}$ Where, x = [$dR/d\lambda_{661}$]	18 May 2004	12	0.26	19.81	133.04
		22 June 2005	26	0.53	10.52	70.65
		29 August 2005	10	0.50	6.86	46.07
29 August 2005	Chl-a (mg m^{-3}) = 172.03x + 23.021 Where, x = [($R_{rs}^{-1}(675)$-$R_{rs}^{-1}(720)$)x$R_{rs}(750)$]	18 May 2004	12	0.54	35.86	295.39
		22 June 2005	26	0.16	18.91	64.20
		29 August 2005	10	0.93	2.02	16.64
Combined*	Chl-a (mg m^{-3}) = $3.777e^{-3293.9x}$ Where x = [$dR/d\lambda 661$]	18 May 2004	12	N/S	18.94	81.92
		22 June 2005	26	0.66	10.13	43.81
		29 August 2005	10	0.65	3.18	13.75
		Combined	48	0.69	12.41	53.68

* Algorithm validation not based upon independent data

The optimum algorithm derived from the 22 June 2005 dataset, based upon the [$dR/d\lambda_{661}$] index, provided reasonable estimates of chlorophyll-a when validated against the 29 August 2005 dataset (RMSE = 6.86 mg chlorophyll-a m^{-3} (46.07%)). The same algorithm, however, yielded poorer estimates of the chlorophyll-a concentration when validated against the 18 May 2004 dataset (RMSE = 19.81 mg chlorophyll-a m^{-3} (133.04%)). Similarly, notwithstanding the

fact that the optimum algorithm derived from the 29 August 2005 dataset using the medium-independent index proposed by Dall'Olmo *et al*. (2003) was the single best algorithm (R^2 = 0.93) derived from the any of the calibration datasets, it did not perform well when validated against the 18 May 2004 and 22 June 2005 datasets, yielding RMSEs of 35.86 and 18.91 mg chlorophyll-a m^{-3}. The reasoning behind poor performance this index is not entirely clear, particularly as the calibration dataset was drawn from both clear and turbid lakes. However, the concentration of SPM (both SPIM and SPOM) was somewhat lower in the Broads sampled on 29 August 2005; thus the index may not be appropriate from waters with high concentrations of tripton.

The optimum algorithm derived from the combined multi-season dataset using the [$dR/d\lambda_{661}$] index, not unexpectedly, demonstrate the greatest degree of transferability when applied to the 18 May 2004, 22 June 2005 and 29 August 2005 datasets; the RMSEs for the estimated chlorophyll-a concentration were 18.94, 10.13 and 3.18 mg chlorophyll-a m^{-3}. This does not constitute a full independent validation of the algorithm (having been calibrated and validated using some common data points), however, it does serve to emphasise the fact that the derivation of chlorophyll-a algorithms should be performed on large and, where possible, multi-season datasets that encompass measurements derived from lakes covering a range of water quality conditions. This demonstrates, moreover, why many workers advocate the use of bio-optical models for the development of semi-empirical or analytical algorithms as such an approach permits the full water quality conditions for any particular lake(s) to be simulated and, thus, the derived algorithm(s) should, in theory, be more robust and retain greater transferability.

The concentration of chlorophyll-a is an important measure of the ecological status of lakes. The results obtained here clearly demonstrated that $R_{rs}(\lambda,0+)$ NIR/red band-ratios and $dR/d\lambda$ indices can be used to quantify the concentration of chlorophyll-a, even in shallow waters characterised by high, and often non-co-varying, concentrations of SPM. The formulation of algorithms based upon $dR/d\lambda$ indices would seem especially apt for the estimation of chlorophyll-a in shallow lakes with high SPM (tripton) loads. Indices based upon the first-

derivative transformation of $R_{rs}(\lambda,0+)$ data also seem to retain greater transferability between datasets collected from lakes of contrasting water quality status. However, based upon the results obtained here, it is evident that the algorithms lack the robustness that would be required if remote sensing were to be employed to estimate chlorophyll-a concentrations in shallow lakes on a routine basis. The formulation of semi-empirical or analytical algorithms from comprehensive bio-optically modelled datasets may provide a means of improving algorithm reliability and, in addition, would yield a more mechanistic understanding of algorithm behaviour in response to changes in lake water quality.

However, it is also likely that to enable the multi-season estimation of chlorophyll-a in lakes of varying water quality status, multiple algorithms may be required. Similar problems have been encountered in ocean colour remote sensing which has promoted the development of season- or province-specific chlorophyll-a algorithms or, as in the case of the current operational empirical SeaWiFS OC4v4 and the MODIS OC3M chlorophyll-a algorithms, compound maximum-band-ratios (MBR) models have been developed. MBR models can be automatically spectrally-optimised to suit the specific optical properties of the ocean province under scrutiny. The formulation of similar algorithms may be beneficial for the remotely sensed determination of chlorophyll-a in lakes; it would important that the correct algorithm formulation is identified for the specific lake, or lake type, of interest.

3.5.6.2 Continuum-Removed Based Algorithms

Continuum removal has been used extensively for the analysis of hyperspectral remote sensing data and, in particular, in contexts concerned with geological exploration or vegetation mapping (Sunshine *et al.,* 1990; Kokaly & Clark, 1999; Schmidt & Skidmore, 2003; Kokaly *et al.,* 2003; Mutanga *et al.,* 2004; Mutanga *et al.,* 2004; Boyd *et al.,* 2006). In these contexts, continuum removal has proved effective in targeting and standardising absorption-related $R_{rs}(\lambda,0+)$ features allowing analysis to be performed from a common and normalised baseline. Continuum removal was explored in this study as a means of removing spectral interference on the estimation of chlorophyll-a from high and variable concentrations of SPM (tripton).

Continuum removal was applied to the $R_{rs}(\lambda,0+)$ feature related to the chlorophyll-a absorption maximum centred at *c*. 670 nm. The derived continuum-removed spectra ($R'_{(\lambda)}$) are depicted in Figure 3.12. Linear and non-linear least-squares regression analysis was performed in order to examine the relations between $R'_{(\lambda)}$ indices and the measured concentrations of chlorophyll-a in the Norfolk Broads datasets. Table 3.16 details the coefficients of determination and best-fit least-squares regression algorithms for the relationship between the $R'_{(\lambda)}$ indices and the measured concentration of chlorophyll-a.

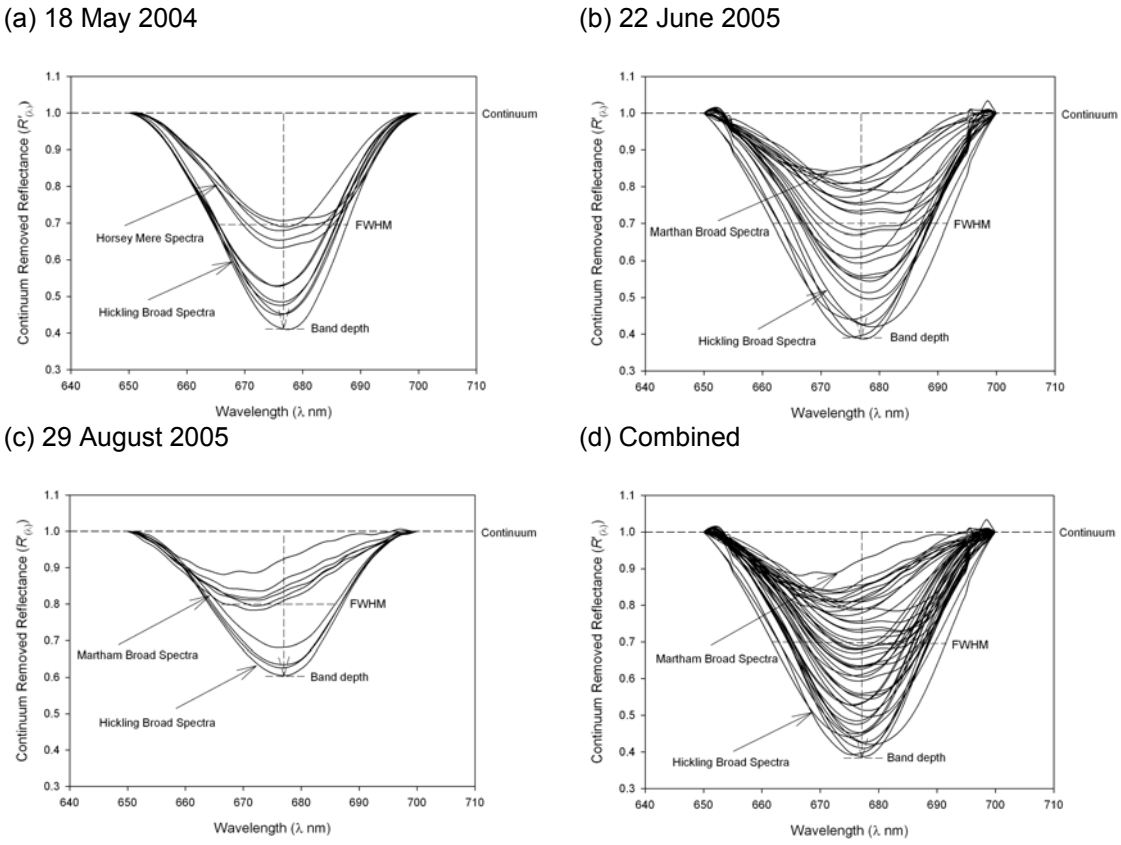

Figure 3.12 Continuum removed spectra ($R'_{(\lambda)}$) of the $R_{rs}(\lambda,0+)$ feature related to chlorophyll-a absorption for the 18 May 2004, 22 June 2005, 29 August 2005 and combined data.

The relationships between the $R'_{(\lambda)}$ indices and the measured concentration were, in general, poorer than those observed using the $R_{rs}(\lambda,0+)$ NIR/red band-ratio and d*R*/dλ indices. The coefficients of determination derived for the 18 May 2004, 22 June 2005 and combined datasets were $R^2 < 0.60$. The best results were again observed for the dataset acquired on 29 August 2005 lake sampling cruise; the single best index, [BDR_{683}], yielded $R^2 = 0.81$ for the

relationship with the measured concentration of chlorophyll-a using a linear best-fit least-squares regression algorithm (see Figure 3.13).

Table 3.16 The optimum relationships between the $R'_{(\lambda)}$ indices and the measured concentration of chlorophyll-a for the datasets derived from the individual lake cruises and the amalgamated datasets (N/S = not significant at the 95% confidence interval).

	Index (x)	*n*	R^2	Best-fit Least-Squares Regression Model
18 May 2004	$[BD_{650.5}]$	12	0.527	$37.575e^{-187.06x}$
	$[BDR_{684}]$		N/S	N/S
	$[NDBI_{650.5}]$		0.443	377.87x + 400.6
	$[CRDR_{650}]$		0.527	$37.575e^{93.53}$
	[FWHM]		N/S	N/S
	[AREA]		N/S	N/S
22 June 2005	$[BD_{652.5}]$	26	0.544	$17.991e^{43.903x}$
	$[BDR_{657.5}]$		N/S	N/S
	$[NDBI_{652.5}]$		0.573	$10^{15}e^{31.788x}$
	$[CRDR_{651}]$		0.447	$17.345e^{-96.664x}$
	[FWHM]		N/S	N/S
	[AREA]		N/S	N/S
29 August 2005	$[BD_{684}]$	10	0.706	$4.3655e^{-5.253x}$
	$[BDR_{683}]$		0.810	754.81x – 697.62
	$[NDBI_{687}]$		0.596	53.415x – 52.269
	$[CRDR_{677}]$		0.759	$22.352e^{147.93}$
	[FWHM]		N/S	N/S
	[AREA]		0.655	2.3957x – 122.49
Combined	$[BD_{676.5}]$	48	0.181	45.275x + 7.9354
	$[BDR_{657.5}]$		0.269	119.43x + 119.52
	$[NDBI_{676.5}]$		0.186	22.925x – 15.085
	$[CRDR_{667.5}]$		0.293	817.01x + 8.6773
	[FWHM]		N/S	N/S
	[AREA]		0.128	1.5605x – 68.3

Notwithstanding the fact that continuum-removed indices have been used to successfully related to the bio-physical composition of various vegetation communities (inc. chlorophyll-a), in comparison to conventional $R_{rs}(\lambda,0+)$ NIR/red band-ratios and $dR/d\lambda$ indices, the results obtained here using the $R'_{(\lambda)}$ indices were somewhat disappointing for the estimation of the chlorophyll-a concentration in shallow lakes. Nevertheless, clear discrepancies in the size and shape of the $R'_{(\lambda)}$ feature associated with chlorophyll-a absorption can be observed in Figure 3.13. These variations in the $R'_{(\lambda)}$ spectra are without doubt, in part, related to changes in the concentration of chlorophyll-a, which suggests that continuum-removal analysis may have potential for the estimation of chlorophyll-a in lakes. The poor performance of the $R'_{(\lambda)}$ indices may have been the result of other optically active components, independent of chlorophyll-a, influencing the size and/or shape of the $R'_{(\lambda)}$ feature related to chlorophyll-a absorption. In this

context, further examination of continuum removal for the estimation of pigment concentrations in shallow lakes is warranted.

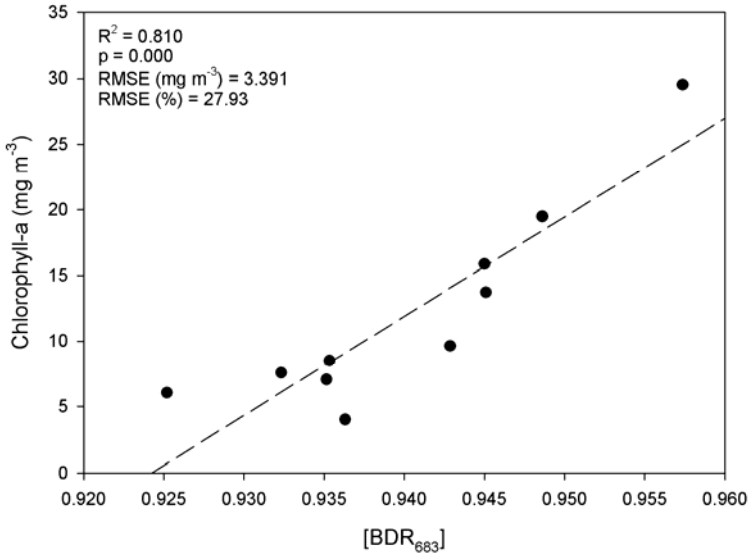

Figure 3.13 The linear least-squares regression relationship between the $R'_{(\lambda)}$ index [BDR_{686}] and the measured concentration of chlorophyll-a on 29 August 2005.

3.5.6.3 Multivariate Chlorophyll-a Retrieval Algorithms

In addition to the (univariate) $R_{rs}(\lambda,0+)$, $dR/d\lambda$ and $R'_{(\lambda)}$ based algorithms for the estimation of chlorophyll-a, the efficacy of multivariate algorithms (i.e. multiple wavelengths) for the estimation of chlorophyll-a in the Norfolk Broads was also examined. Few previous studies have examined multiple-wavelength models for the retrieval of chlorophyll-a from remote sensing data, perhaps due to concerns of over-complexity, or the fact that some multivariate models (e.g. neural networks, partial least squares regression) are, to an extent, 'black-boxes' and thus lack the desired mechanistic clarity. However, if it is possible to establish a valid theoretical basis for the inclusion of wavelength variables in model development, either through the pre-screening of wavelengths used in algorithm formulation, or through the retrospective analysis of the derived model, then multiple wavelength algorithms may prove to have greater power for chlorophyll-a estimation, particularly in optically-complex lakes than, for instance, more conventional band-ratios algorithms. Rationalisation for such an approach can, in part, be taken from studies employing multivariate soft-classification image analysis procedures (e.g. linear spectral mixture models) which utilise information from many wavelengths and have been

shown to outperform more conventional band-ratio algorithms for chlorophyll-a estimation in CASE II waters (Thiemann & Kaufmann, 2000; Tyler *et al.,* 2006).

Two multivariate techniques, multivariate stepwise regression (MSR) (using forward and backward propagation) and partial-least-squares-regression (PLS), were examined using the $R_{rs}(\lambda,0+)$, $dR/d\lambda$, $R_{(\lambda)}$-ratios and $R'_{(\lambda)}$ data and the accuracy of the chlorophyll-a estimation was compared to the univariate models. Cross-validation procedures were used to provide a more conservative estimate of the potential predictive power of the multivariate algorithms. It can be a common tendency for multivariate regression models to over-fit observational data (i.e. too many free predictors); in respect, the PLS and MSR models were evaluated on the basis the R^2 (predicted) value; the PLS cross-validation procedure, however, should account for possibility of over-fitting in model formulation.

The results for the multivariate models are detailed in Table 3.17. In general, the multivariate models (MSR and PLS) demonstrated equal or better relationships with the measured concentration of chlorophyll-a than the univariate models employing $R_{rs}(\lambda,0+)$ NIR/red band-ratios, $dR/d\lambda$ indices and $R'_{(\lambda)}$ indices. In particular, the MSR models formulated with the $dR/d\lambda$ data provided better estimates of the chlorophyll-a concentration for the 18 May 2004 and 22 June 2005 datasets – where the previous univariate models had been somewhat disappointing. Excellent relationships were also observed for the 29 August 2005 dataset; although the conventional NIR/red band-ratio and $dR/d\lambda$ indices also performed well here. Significant PLS cross-validation models could not be derived from the 18 May 2004 and 29 August 2005 datasets due to the limited number of observations.

Table 3.17 The accuracy of the chlorophyll-a retrieval models derived using MSR and PLS regression for the 18 May 2004, 22 June 2005, 29 August 2005 and combined datasets.

	Spectral Variables	Model	No. Free Predictors	R^2 (adj.)	R^2 (pred.)	Selected Wavelengths (nm) /Indices for MSR
18 May 2004	$R_{rs}(\lambda,0+)$	MSR	1	0.357	0.109	599.5
		PLS	2	0.469	*	N/A
	$R_{rs}(\lambda,0+)$ band-ratio(s)	MSR	1	0.628	0.431	[$R_{rs}(710)/R_{rs}(490)$]
		PLS	9	0.984	0.250	N/A
	dR/dλ	MSR	5	0.996	0.986	409.5, 421, 648, 771, 787
		PLS	2	0.993	0.014*	N/A
	$R'_{(\lambda)}$ BD	MSR	1	0.400	0.207	650.5
		PLS	5	0.709	*	N/A
22 June 2005	$R_{rs}(\lambda,0+)$	MSR	4	0.830	0.790	450.5, 518.5, 720, 721.5
		PLS	3	0.813	0.737	N/A
	$R_{rs}(\lambda,0+)$ band-ratio(s)	MSR	3	0.797	0.748	[$R_{rs}(443)/R_{rs}(555)$] [$R_{rs}(710)/R_{rs}(490)$] [$R_{rs}(748)/R_{rs}(670)$]
		PLS	7	0.864	0.646	N/A
	dR/dλ	MSR	5	0.847	0.799	427.5, 492, 729, 753, 776
		PLS	2	0.733	0.512	N/A
	$R'_{(\lambda)}$	MSR	5	0.632	0.527	652.5, 655.5, 665.0, 674, 697
		PLS	5	0.730	0.320	N/A
29 August 2005	$R_{rs}(\lambda,0+)$	MSR	5	0.996	0.996	512, 525, 533, 632, 662
		PLS	5	0.997	*	N/A
	$R_{rs}(\lambda,0+)$ band-ratio(s)	MSR	1	0.916	0.858	[($R_{rs}(670)^{-1}$-$R_{rs}(720)^{-1}$) x$R_{rs}(750)$]
		PLS	5	0.990	*	N/A
	dR/dλ	MSR	5	1.000	1.000	412.5, 427.5, 429.5, 782.5, 785
		PLS	5	0.999	*	N/A
	$R'_{(\lambda)}$ BD	MSR	2	0.900	0.734	675.5, 684
		PLS	5	0.967	*	N/A
Combined	$R_{rs}(\lambda,0+)$	MSR	2	0.566	0.520	444, 696.5
		PLS	6	0.742	0.607	N/A
	$R_{rs}(\lambda,0+)$ band-ratio(s)	MSR	3	0.617	0.580	[$R_{rs}(490)/R_{rs}(555)$] [$R_{rs}(705)/R_{rs}(670)$] [$R_{rs}(765)/R_{rs}(670)$]
		PLS	3	0.592	0.483	N/A
	dR/dλ	MSR	4	0.728	0.684	598.5, 776, 778.5, 797.5
		PLS	2	0.631	0.531	N/A
	$R'_{(\lambda)}$ BD	MSR	7	0.637	0.526	652, 657.5, 664.5, 666.5, 668.5, 677, 679.5, 680
		PLS	3	0.431	0.254	N/A

*denotes too few observations for meaningful cross-validation analysis

The MSR models formulated with dR/dλ data also demonstrated improved relations with the concentration of chlorophyll-a in the combined multi-season dataset. In this respect, it could be argued that the improved results obtained using the multivariate models, suggests that the incorporation of information from multiple wavelengths (particularly first-derivative data) into algorithms can provide a more effective estimation of the chlorophyll-a concentration and, in particular, if the data is drawn from multi-season measurements from lakes of varying water

quality. The relationship between the PLS-modelled and measured concentration of chlorophyll-a for the combined datasets are depicted in Figure 3.14.

It is notable that the multivariate models formulated using the $R_{rs}(\lambda,0+)$ and $R_{rs}(\lambda,0+)$ band-ratios consistently selected wavelength variables centred in the blue and green regions (i.e. *c*. 400-600 nm). These wavelengths are rarely incorporated into algorithms for the estimation of chlorophyll-a in CASE II waters. However, the results obtained here suggest the spectral information at these wavelengths may be relevant to the estimation of chlorophyll-a in shallow lakes. Chlorophyll-a absorbs strongly in the blue region – which might explain the consistent selection of these wavelengths in the multivariate algorithms. However, it is difficult to derive a full mechanistic explanation for this observation based solely on the data presented here. In this context, bio-optical modelling of the shallow lakes of the Norfolk Broads, or similar shallow lake ecosystems, may provide a more appropriate base from which to explore the use of multivariate algorithms and assess their underlying mechanistic validity.

(a) PLS modelled chlorophyll-a (b) PLS cross-validated chlorophyll-a

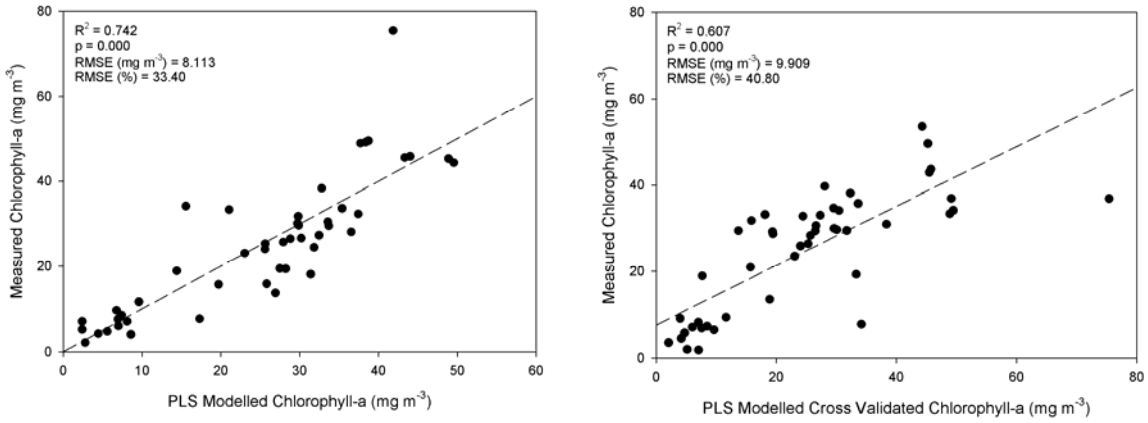

Figure 3.14 Scatter plots for the (a) PLS model (R^2) and (b) the cross validated PLS model (R^2 (pred.)) for chlorophyll-a estimation derived from the combined multi-season dataset.

3.5.7 Hydrolight Bio-Optical Model Simulations

The results obtained from the various lake sampling cruises in the Norfolk Broads seems to suggest that the estimation of chlorophyll-a using remote-sensing-based algorithms formulated with $R_{rs}(\lambda,0+)$ band-ratios, $dR/d\lambda$ indices and $R'_{(\lambda)}$ indices may be affected to varying degrees

by the non-phytoplankton-related bio-optical properties of shallow lakes (e.g. tripton, CDOM, bottom substrate conditions). This implies that use of any single algorithm formulation may thus not be appropriate for the estimation of the chlorophyll-a concentration in all lake types and under all water quality conditions. The effect of non-chlorophyllous bio-optical component variability on the estimation of chlorophyll-a in shallow lakes was investigated expeditiously using simple sensitivity analyses performed using the Hydrolight radiative transfer model. The simulated $R_{rs}(\lambda,0+)$ signals for each shallow lake type are depicted in Figure 3.15.

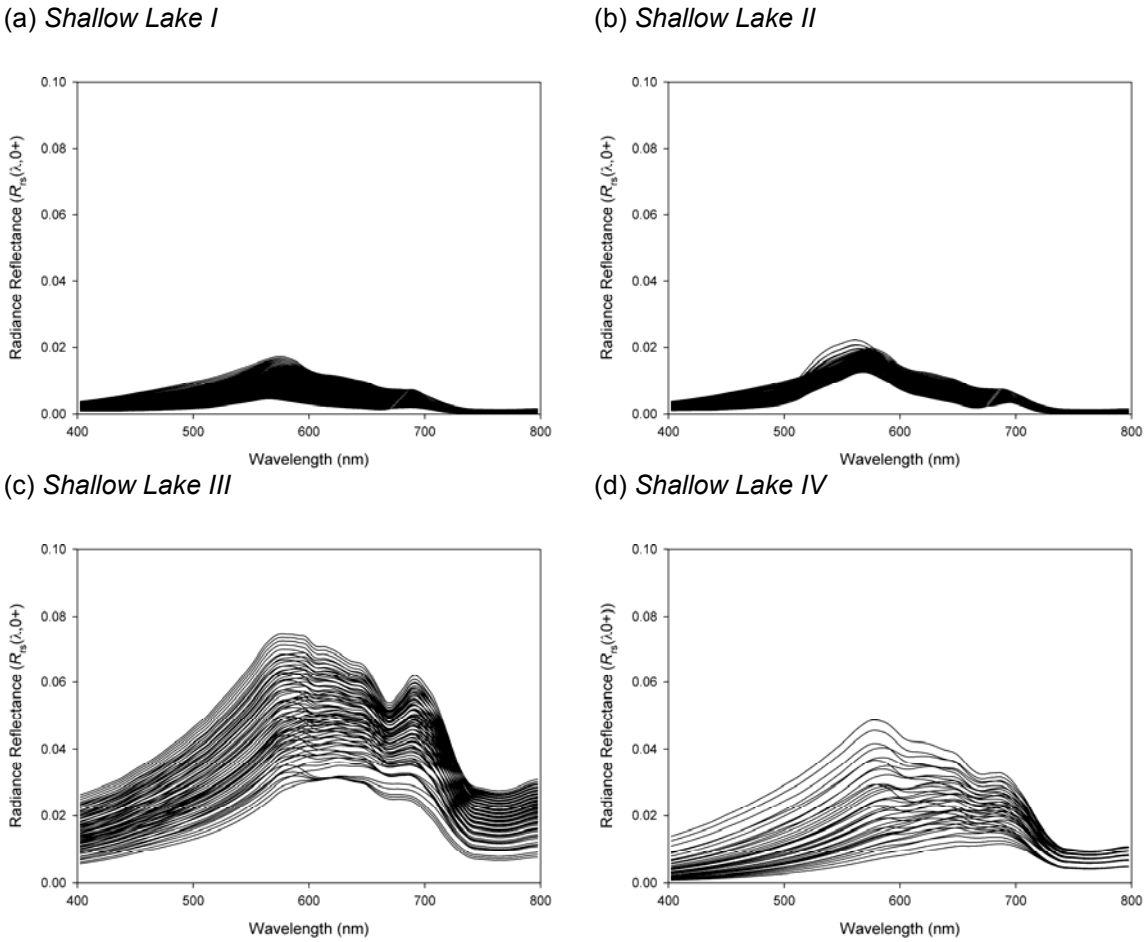

Figure 3.15 The $R_{rs}(\lambda,0+)$ spectra for the four shallow lake types simulated using the Hydrolight v.4.2 bio-optical model. (a) *Shallow Lake 1*: chlorophyll-a 2-15 mg m^{-3}, CDOM 1.5 (a_{440} m^{-1}), tripton 0.5-5 mg L^{-1}, no submerged plants; (b) *Shallow Lake 2*: chlorophyll-a 2-10 mg m^{-3}, CDOM 1.5 (a_{440} m^{-1}), tripton 0.5-5 mg L^{-1}, submerged plants; (c) *Shallow Lake 3*: chlorophyll-a 10-75 mg m^{-3}, CDOM 1.5 (a_{440} m^{-1}), tripton 5-30 mg L^{-1}, no submerged plants; (d) *Shallow Lake 4*: chlorophyll-a 2-10 mg m^{-3}, CDOM 1-12.5 (a_{440} m^{-1}), tripton 5 mg L^{-1}, humic/no submerged plants. Axes standardised for comparability.

It can be seen that the variable bio-optical conditions simulated for each shallow lake type had a significant influence on the $R_{rs}(\lambda,0+)$ signature. The simulated clear water lake, with no submerged aquatic vegetation (*Shallow Lake I*), exhibited the weakest $R_{rs}(\lambda,0+)$ signal. This was no doubt a function of strong absorption by water (and, although to a lesser extent, chlorophyll-a) allied to the lower concentrations of tripton (0.5 mg L^{-1}) used in the simulation (i.e. low backscattering). It should also be noted that the $R_{rs}(\lambda,0+)$ signature of *Shallow Lake I* is not that dissimilar from the spectral profiles measured in Martham North and Ormesby Broad. The $R_{rs}(\lambda,0+)$ signature of *Shallow Lake II* (clear water lake, but with submerged aquatic plant growth) was broadly similar to that of *Shallow Lake I*, but the $R_{rs}(\lambda,0+)$-maxima at *c*. 570, 650 and 690 nm can be seen to increase in prominence. The chlorophyll-a concentration for the *Shallow Lake II* scenario was lower (2-10 mg m^{-3}) than that used with the non-vegetation *Shallow Lake I* (2-25 mg m^{-3}) and the tripton component was kept constant. The increased prominence of the $R_{rs}(\lambda,0+)$-maxima at *c*. 570, 650 and 690 nm was probably associated with the chlorophyll-a signal from the simulated submerged vegetation. Thus, not entirely unexpectedly, the model scenario would suggest that benthic vegetation can have a pronounced effect on the $R_{rs}(\lambda,0+)$ signature of the shallow lakes. This raises some interesting questions with regards to the potential efficacy of remote sensing for the estimation of water quality parameters in clear, macrophyte-dominated, lakes where the bottom radiance signal is strong.

The $R_{rs}(\lambda,0+)$ signature for the turbid, phytoplankton-dominated, shallow lake type (*Shallow Lake III*) was, again not unexpectedly, markedly different from those of the other lakes. The high $R_{rs}(\lambda,0+)$ signal observed from the *Shallow Lake III* is a function of the high concentrations of chlorophyll-a (10-75 mg m^{-3}) and tripton (5-30 mg L^{-1}) used in the simulation. The bottom boundary conditions probably had little effect on the $R_{rs}(\lambda,0+)$ signal in this instance, as the optical depth is likely to have been much shallower that the actual geometric lake depth for many of the Hydrolight simulations for this lake type. The effect of high chlorophyll-a concentrations on the $R_{rs}(\lambda,0+)$ signal can be seen in the increased prominence of the chlorophyll-a absorption-related $R_{rs}(\lambda,0+)$-minimum at *c*. 670 nm, and the chlorophyll-a scattering–related green and NIR peaks at *c*. 580 nm and *c*. 705 nm respectively. It is notable

that increased concentrations of tripton resulted in the the chlorophyll-a absorption-related feature at *c*. 670 nm increasing further in prominence. This observation suggests that algorithms formulated using baseline (e.g. Dekker, 1993) or continuum-removed approaches to chlorophyll-a estimation may not be appropriate in waters with high and non-co-varying tripton.

The $R_{rs}(\lambda,0+)$ signature of *Shallow Lake III* is again not too dissimilar from the profiles measure in the turbid, phytoplankton-dominated, waters of Hickling Broad, Heigham Sound and Horsey Mere. The most notable differences occur between the modelled and measured spectral in the < 550 nm region; this is largely due to the fact the Hydrolight model assumed that chlorophyll-a was the only bio-optically active pigment in the water column and, therefore, there is an absence of carotenoid-related spectral features in this region.

The *Shallow Lake IV* simulation was used to model the $R_{rs}(\lambda,0+)$ signal that might be typical of a humic or dystrophic shallow lake (a_{440} 1-12.5 m^{-1}). It is again notable that the $R_{rs}(\lambda,0+)$ signature of this lake scenario is significantly dissimilar from the modelled signatures of the other three lake types. The most marked effect of CDOM was the decreasing $R_{rs}(\lambda,0+)$ signal and the "flattening" of the signature at high CDOM concentrations (e.g. a_{440} > 5 m^{-1}). In particular, it is apparent that the chlorophyll-a absorption-related $R_{rs}(\lambda,0+)$-minimum at *c*. 670 is readily masked when the CDOM concentration is high. This would seem to suggest that the remote-sensing-based estimation of chlorophyll-a in humic and dystrophic shallow lakes may be problematic.

The influence of lake type and, therefore, (non-chlorophyll-related) variability in the bio-optical conditions of shallow lakes, on the relationship between the NIR/red band-ratio [$R_{rs}(705)/R_{rs}(670)$], and the first-derivative index [$dR/d\lambda_{667.5}$], and the parameterised concentration of chlorophyll-a is depicted in Figure 3.16(a-h).

(a) *Shallow Lake I* – [$R_{rs}(705)/R_{rs}(670)$]

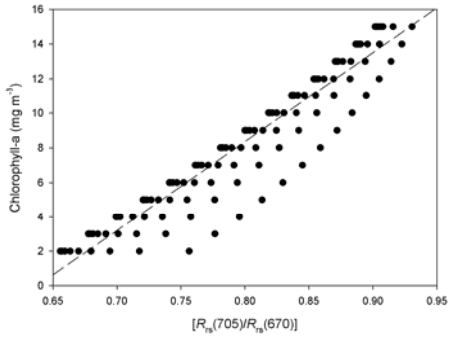

(b) *Shallow Lake I* – [$dR/d\lambda_{667.5}$]

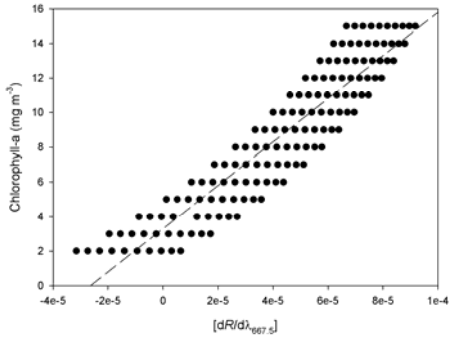

(c) *Shallow Lake II* – [$R_{rs}(705)/R_{rs}(670)$]

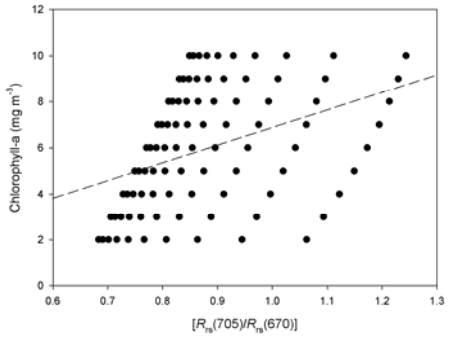

(d) *Shallow Lake II* – [$dR/d\lambda_{667.5}$]

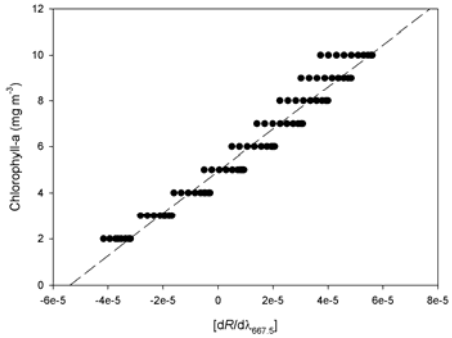

(e) *Shallow Lake III* – [$R_{rs}(705)/R_{rs}(670)$]

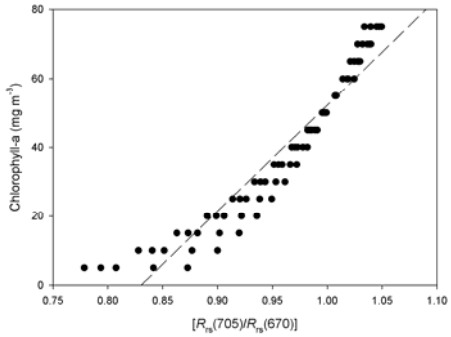

(f) *Shallow Lake III* – [$dR/d\lambda_{667.5}$]

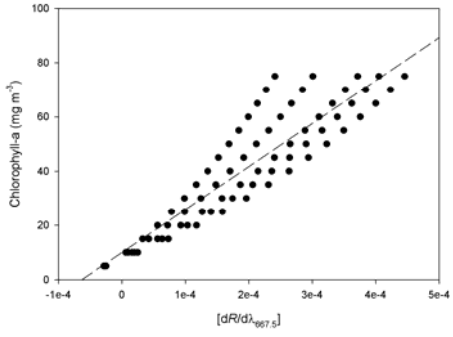

(g) *Shallow Lake IV* – [$R_{rs}(705)/R_{rs}(670)$]

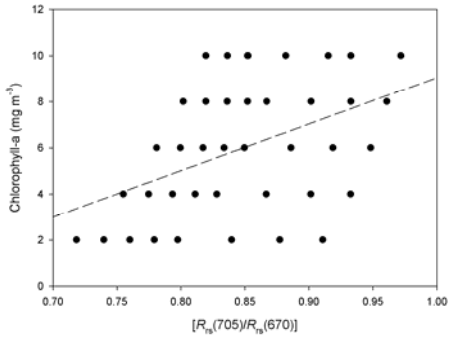

(h) *Shallow Lake IV* – [$dR/d\lambda_{667.5}$]

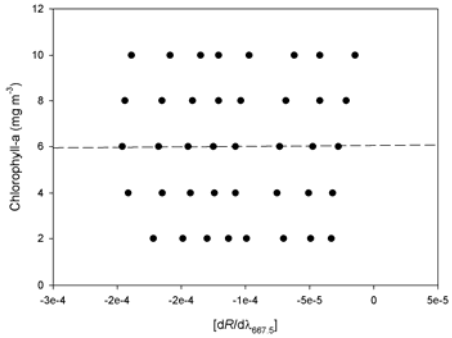

Figure 3.16 The effect of shallow lake type on the relationship between chlorophyll-a and the NIR/red band-ratio [$R_{rs}(705)/R_{rs}(670)$] and the first-derivative index [$dR/d\lambda_{667.5}$]. Linear least-square regression models were used for all lake type scenarios.

It is even more evident from Figure 3.16 that variability in the non-chlorophyllous bio-optical conditions, within and between different shallow lake types, can have a profound effect on the relationship between $R_{rs}(\lambda,0+)$-derived indices and the chlorophyll-a concentration. This effect is evaluated in quantitative terms (coefficients of determination (R^2)) in Table 3.18. The estimation of chlorophyll-a (using a standard linear least-squares regression approach) was severely affected by the specific bio-optical condition simulated in each shallow lake type. The estimation of chlorophyll-a in *Shallow Lake I* was achievable (to a good degree of accuracy – R^2 > 0.86) using algorithms formulated with both the [$R_{rs}(705)/R_{rs}(670)$] and the [$dR/d\lambda_{667.5}$] indices. In this instance, the [$R_{rs}(705)/R_{rs}(670)$] index was marginally more sensitive to changes in the parameterised chlorophyll-a concentration than the [$dR/d\lambda_{667.5}$] index.

The simulation of vegetated bottom boundary conditions (*Shallow Lake II*), however, severely reduced the efficacy of the [$R_{rs}(705)/R_{rs}(670)$] index for the estimation of chlorophyll-a (R^2 = 0.16). In contrast, the first-derivative index was seemingly not influenced by the presence of benthic vegetation and provided a good fit against the parameterised chlorophyll-a concentration (R^2 = 0.95). This would suggest that algorithms formulated using first-derivative indices may be more appropriate than those based upon NIR/red band-ratios for the estimation of chlorophyll-a in clear water shallow lakes where the bottom substrate (particularly if vegetated) may greatly influence the $R_{rs}(\lambda,0+)$ signal.

Table 3.18 The coefficients of determination (R^2) for the linear least-squares regression relationship between the chlorophyll-a concentrations and the [$R_{rs}(705)/R_{rs}(670)$] and [$dR/d\lambda_{667.5}$] spectral indices for each shallow lake type simulated using Hydrolight v.4.2.

		R^2	
	n	**[$R_{rs}(705)/R_{rs}(670)$]**	**[$dR/d\lambda_{667.5}$]**
Shallow Lake I	140	0.897	0.863
Shallow Lake II	90	0.158	0.952
Shallow Lake III	75	0.904	0.909
Shallow Lake IV	40	0.200	0.067
All Lake Simulations	345	0.347	0.772

The two contrasting spectral indices both demonstrated a good relationship with the parameterised concentration of chlorophyll-a for the *Shallow Lake III* simulations. The high coefficients of determination observed (R^2 = 0.90-0.91) arguably reflect that fact that a large

gradient in chlorophyll-a (10-75 mg m^{-3}) was used in the *Shallow Lake III* scenario. However, in this scenario high, and non-co-varying, concentrations of tripton were also modelled using Hydrolight. The good relationships observed between the spectral indices and the parameterised chlorophyll-a concentration would seem to suggest that both index formulations are effective at reducing the attenuating influence of tripton on the remotely sensed retrieval of chlorophyll-a.

The scatter plots do, however, reveal that the [$dR/d\lambda_{667.5}$] index was more effective for parameterised chlorophyll-a concentrations < 25 mg m^{-3}; whereas, the [$R_{rs}(705)/R_{rs}(670)$] index was more effective for chlorophyll-a concentrations > 25 mg m^{-3}. This suggests that first-derivative indices may be more suitable for enhancing the latent chlorophyll-a signal in waters with high and variable tripton. This confirms the previous observations made by Dekker & Malthus (1995), Han & Rundquist (1997) and Han (2005) and, importantly, also provides some substantiation for the results obtained here for the Norfolk Broads.

The estimation of the chlorophyll-a concentration in the humic lake scenario (*Shallow Lake IV*) proved problematic. Neither index formulation returned a strong coefficient of determination for the relationship with parameterised chlorophyll-a concentration (R^2 = 0.07-0.20). Spectral attenuation by high CDOM absorption would therefore seem to be a barrier to the estimation of chlorophyll-a in heavily coloured waters. However, it was noted that $R_{rs}(\lambda,0+)$ and $dR/d\lambda$ demonstrated significant relationships with chlorophyll-a at wavelengths closer towards 800 nm (where CDOM absorption is absent) (not shown here); reflectance of first-derivative reflectance in the VNIR might therefore be more provide a route to the estimation of chlorophyll-a in more humic waters.

It is again noteworthy that the first-derivative index was more highly correlated with the parameterised concentration of chlorophyll-a for all combined shallow lake types (R^2 = 0.77), than the NIR/red band ratio index (R^2 = 0.35). This is an important finding, as it suggests that first-derivative indices may be more suitable for the estimation of chlorophyll-a across shallow, or indeed, any lakes where there is a pronounced inter-lake variation in the bio-optical

properties. This observation may also explain the improved performance of the first-derivative indices in the Norfolk Broads, particularly in respect to the multi-lake and/or multi-temporal datasets. This also emphasises the value of hyperspectral data (which permits the formulation of derivative indices) for the estimation of chlorophyll-a in lakes.

The results of the Hydrolight modelling, and indeed those from the lake sampling cruises in the Norfolk Broads, have demonstrated that the accuracy to which remote-sensing-based approaches can be used to estimate the concentration of chlorophyll-a in lakes is largely dependent upon the non-phytoplankton-related, and phytoplankton-related, bio-optical properties of the water and the bottom boundary conditions. It has been shown that the capacity of different spectral index and algorithm formulations for the estimation of chlorophyll-a is also largely dependent on lake (or water) type. It would appear that some index formulations, such as derivative approaches, may retain greater transferability over a wider range of bio-optical conditions. However, even these indices are not appropriate in all circumstances. The SALMON project (SAtellite remote sensing for Lake MONitoring) also found that the performance of different chlorophyll-a algoirhtms varied considerably between different lakes types (Lindell *et al*., 1999).

It is therefore clear that to further the use of remote sensing for inland water quality monitoring a far greater understanding of the efficacy of different algorithm formulations under varying water quality situations needs to be sought. This would allow the optimum algorithm formulation to be selected for each lake/water type (see Figure 3.17). Another approach, may be to simultaneously use multiple algorithms to calculate a mean predicted concentration of chlorophyll-a, this mean predicted value could then be used to further refine algorithm selection through the calculation of a second weighted-average chlorophyll-a concentration based upon a knowledge of the performance of different algorithm formulations at varying concentrations of chlorophyll-a. The maximum-band-ratio approach used in CASE 1 ocean colour algorithms should also be examined in the context of inland waters.

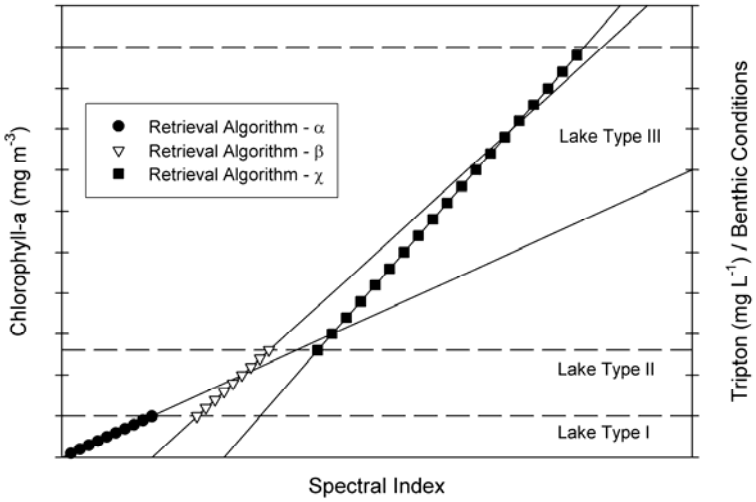

Figure 3.17 A theoretical illustration of the possible effect of lake type on the accuracy of chlorophyll-a retrieval from remote sensing data and the potential efficacy of deriving algorithms (α, β, χ) spectrally tuned to specific lake types (as a function of trophic status for example).

3.6 CONCLUSIONS

The efficacy of various remote sensing indices for the retrieval of water quality parameters (SPM (seston), SDD, CDOM and chlorophyll-a) in shallow lakes was investigated using shipboard hyperspectral $R_{rs}(\lambda,0+)$ data gathered from expeditious multi-temporal cruises conducted in the shallow lakes of the Norfolk Broads. The estimation of SPM fractions from the $R_{rs}(\lambda,0+)$ proved viable using algorithms empirically formulated with $R_{rs}(\lambda,0+)$ indices. However, the accuracy of these algorithms varied significantly between the multi-temporal datasets (R^2 = 0.40-0.99). This variability was suggested to be a function of the mineralogy of the SPM in suspension, its concentration and the degree of co-variance between the various inorganic and organic components.

The retrieval of the SDD from the $R_{rs}(\lambda,0+)$ data proved more straightforward (albeit the results were derived from a single sampling occasion) (max. R^2 = 0.98). However, the retrieval of CDOM was more problematic. No significant relationships could be derived between the $R_{rs}(\lambda,0+)$ data and the measured concentrations of CDOM. It was reasoned that the low concentrations of dissolved organic carbon, allied to spectral masking effects incurred from other optically active pigments, were responsible for the absence of a relationship with CDOM

in this instance. It is suggested that further work should focus on the derivation of algorithms for the estimation of CDOM.

Numerous different approaches to the formulation of algorithms for the estimation of the chlorophyll-a concentration were trialled in the Norfolk Broads. These included conventional green/blue and NIR/red band-ratios and more innovative first-derivative, continuum-removed and multiple-wavelength formulations. In similarity to the relationships observed with SPM, the performance of the different algorithm formulations varied considerably. This variability was largely attributed to the high and variable concentrations of SPM (or more specifically tripton) that occur in the shallow waters of the Norfolk Broads (largely due to resuspension processes). The influence of the bottom boundary conditions may also have affected the remotely sensed estimation of chlorophyll-a. Importantly, the effect of variable tripton and bottom boundary conditions on the accuracy of chlorophyll-a retrieval was again confirmed theoretically using bio-optical modelling.

The NIR/red band-ratios and, in particular, the first-derivative indices, often provide the most accurate and robust estimation of chlorophyll-a. The multiple-wavelength algorithms were seen to increase the accuracy of chlorophyll-a estimation, but these algorithms suffer from a lack of mechanistic clarity. Significantly, the first-derivative indices seemed to retain greater transferability, across water types or, indeed, when applied to multi-temporal data. This finding was later substantiated using a novel bio-optical modelling approach.

The results obtained from the shipboard hyperspectral $R_{rs}(\lambda,0+)$ data and the Hydrolight bio-optical modelling emphasise the fact that caution that must be taken to ensure that algorithms formulate for the estimation of water quality parameters, particularly chlorophyll-a, are appropriate for the water quality conditions in the lake(s) of interest. The performance of remote-sensing-based algorithms for the estimation of chlorophyll-a would seem to be particularly sensitive to variations in the bio-optical conditions. On this basis, it is suggested that further work should be concentrated on refining algorithms for specific lake types. An improved understanding of the performance of different algorithm formulations in specific water

types will be fundamental to the construction of an effective remote-sensing-based strategy for lake monitoring and, in particular, for implementation at a pan-European scale (i.e. in the context of the EU WFD).

4 REMOTE SENSING OF PHYTOPLANKTON COMPOSITION IN SHALLOW LAKES

4.1 INTRODUCTION

The previous chapter (Chapter 3) demonstrated how the remote-sensing-based estimation of chlorophyll-a concentrations could be used to monitor the dynamics of phytoplankton communities in shallow lakes. However, increasing evidence is emerging that remote sensing may also be capable of providing information on the taxonomic composition of phytoplankton communities. This chapter uses data from experimental mesocosm experiments and *in-situ* measurements from the Norfolk Broads in order to further investigate the remote-sensing-based assessment of phytoplankton community composition in shallow lakes. Work extracted from this chapter has been accepted for publication in *Remote Sensing of Environment* (Hunter, P.D., Tyler, A.N., Presing, M., Kovacs, A.W., Preston, T. (in press.) Spectral discrimination of phytoplankton colour groups: the effect of suspended particulate matter and sensor spectral resolution, *Remote Sensing of Environment*).

4.2 RATIONALE

Numerous workers have shown that satellite and airborne remote sensing data products can be used to quantitatively map the distribution of phytoplankton in inland waters using the concentration of chlorophyll-a as a surrogate measure of biomass or biovolume (George, 1997; George & Malthus, 2001; Ammenberg *et al.,* 2002; Pozdnyakov *et al.,* 2005). However, as chlorophyll-a is a pigment common to almost all species of phytoplankton, such an approach is incapable of providing information on the species composition of the target environment. The development of remote sensing techniques for the discriminative mapping of phytoplankton taxonomic groups has long been an objective for both limnological and oceanographical remote sensing (Dekker, 1993; Richardson, 1996; Vincent *et al.,* 2004). Foregoing research has suggested that certain groups of phytoplankton may be spectrally discernable as a result of inherent differences in their cell size and structure and/or their photosynthetic pigment complexes (Ahn *et al.,* 1992; Richardson, 1996; Aguirre-Gomez *et al.,* 2001a; Aguirre-Gomez *et*

al., 2001b) with the most prominent spectral dissimilarities occurring at the broad class (i.e. bacillariophyte, chlorophyte, cyanophyte) or colour group level (i.e. brown, green, blue-green, red) (Richardson, 1996). Moreover, in a few limited instances, it has been shown that the concentration of specific biomarker pigments (i.e. the cyanobacterial pigment C-phycocyanin) can be retrieved using remote sensing data (Dekker, 1993; Simis *et al.,* 2005; Kutser *et al.,* 2006). However, there is a clear need to extend this research to, (i) further understand the extent to which variations in cell morphology and photopigment composition mediate the spectral signature of phytoplankton taxa and thus of lakes and other inland waters, (ii) for a greater variety of taxonomic groups and, in particular, those of ecological significance in freshwaters and, (iii) to examine the extent to which other (non-photopigment-related) optically active components (e.g. tripton and CDOM) may influence the remotely sensed resolution and detection-limits of phytoplankton taxa in natural waters.

The eventual realisation of a remote-sensing-based technique for phytoplankton taxonomic group mapping would provide the end-user community (e.g. aquatic scientists, regulatory authorities and conservation agencies) with an invaluable tool for expeditious research and monitoring of intra- or inter-annual phytoplankton community succession and, in particular, in relation to studies concerned with harmful algal bloom (HAB) monitoring (Codd *et al.,* 2005). Progress has made in this context in the marine environment where near-real-time remote sensing imagery products are being used to monitor the development and dispersal of HABs (Ramos *et al.,* 2005; Miller *et al.,* 2006) but few comparable studies in inland waters have been undertaken.

4.3 AIMS AND OBJECTIVES

The aim of the research presented in this chapter was to assess the spectral dissimilarities of several common freshwater phytoplankton taxa and evaluate the extent to which qualitative or quantitative information concerning the floristic composition of natural phytoplankton populations in shallow lakes could be retrieved from remote sensing data. This generic aim was examined through an experimental proof-of-concept mesocosm investigation combined with *in-situ* shipboard spectrometry of natural phytoplankton communities in the shallow lakes of

the Norfolk Broads (UK). This explorative approach was adopted with a view to establishing a theoretical basis for mapping phytoplankton taxa using high spatial and spectral resolution remote sensing imagery products.

The specific research objectives can be outlined as follows:

a) To characterise the spectral signatures of various phytoplankton species and broader colour group associations.

b) To assess the potential of remote sensing for the qualitative discrimination between broad colour groups in simulated communities composed of single (bloom-like) and mixed species using simple qualitative techniques.

c) To examine the potential to retrieve quantitative estimates of biomarker pigment concentrations for taxonomic groups independent of chlorophyll-a.

d) To examine the effect of sensor spectral resolution and the co-incidental presence of SPIM, SPOM and CDOM on the dissimilarity of colour groups.

e) To examine the potential retrieval of specific biomarker pigment concentrations in the natural inland waters of the Norfolk Broads (UK).

4.4 METHODS

4.4.1 Phytoplankton Cultures

The pseudo phytoplankton communities simulated in the laboratory mesocosm experiments were created using artificially cultured species. The colour group species selected for use in the mesocosm experiments included diatoms (brown algae), chlorophytes (green algae) and cyanophytes (blue-green algae). These species were specifically selected due to their prevalence (and ecological significance) in mesotrophic and eutrophic shallow lakes. The phytoplankton cultures were grown at the Balaton Limnological Research Institute (BLRI) of the

Hungarian Academy of Sciences situated on the shore of Lake Balaton in Tihany, Hungary. The species of phytoplankton cultivated included the green chlorophytes *Scenedesmus armatus* (ACT 9710) and *Selenastrum capricornutum* (ACT 97100) and the blue-green cyanophytes *Cylindrospermopsis raciborskii* (ACT 9502) and *Synechococcus* sp. (ACT 9802). Limited volumes of a red (C-phycoerythrin rich) cyanobacterium (*Synechococcus* sp. (ACT 9807) were also cultured for comparative purposes (although it is recognised that red algae are not a common component of freshwater phytoplankton assemblages).

It proved problematic to grow a sufficient crop of diatoms in the mass culture system; thus a compound diatom culture was created from scrapings of epilithic diatoms from the shores of Lake Balaton. The scraped epilithic diatoms were clarified by filtration through a 25 µm mesh using pre-filtered water from Lake Balaton. Microscopic cell counts confirmed that diatoms represented > 95% of the species biomass of these scrapings. The dominant epilithic diatom species were *Cymbella* spp*., Gomphonema* spp*., Fragilaria* spp*.,* and *Diatoma vulgare*. The pigment signatures and spectral characteristics of these epilithic species were assumed to be representative of planktonic diatoms. Mass cultivation of the various phytoplankton species was performed in 16 L glass cylinders operated as part of a semi-continuous system; approximately 70% of the culture volume was refreshed every 5-8 days. The chlorophyte and *Synechococcus* strains were cultured in BG11 medium (Rippka *et al.,* 1979). *Cylindrospermopsis raciborskii* was also cultured in BG11 medium but with no addition of $NaNO_3$. Illumination was provided by cool white fluorescent tubes (Tungsram F33; 40 W) with an approximate irradiance of 70-500 µmol m^{-2} s^{-1} (depending on the species under cultivation). The irradiance was measured by US-SQS/L Spherical Micro Quantum Sensor (Walz) in the centre of culturing tubes. A constant temperature of 24±1 °C was maintained and the cultures were aerated with sterile air to aid aggregation and increase the supply of CO_2. The chlorophyte and cyanophyte cultures were grown on a continuous light cycle. It is acknowledged that the phytoplankton were cultivated under optimum conditions. However, it was assumed for the purposes of this research that the pigment composition of the cultivated species was not radically different from that which would be typically observed in natural waters with favourable nutrition (e.g. light, nutrients). To limit the effect of photoacclimation on the

pigment composition of the phytoplankton species, the time which elapsed between the introduction of the cultured species into the tank mesocosm and the acquisition of spectral reflectance measurements was minimised as far as was practical.

Figure 4.1 The epilithic diatoms used to create a mock culture for the mesocosm experiments growing on the shore of Lake Balaton.

Figure 4.2 The semi-continuous mass cultivation system used to grow the phytoplankton species for use in the mesocosm experiments.

4.4.2 Mesocosm Experiments

4.4.2.1 Spectral Reflectance Measurements

The phytoplankton cultures were used to simulate various pseudo phytoplankton communities in a controlled tank mesocosm environment as a series of individual treatments consisting of different combinations of single and multiple species at varying concentrations (after Gitelson *et al.,* 1999; Svab *et al.,* 2005). The tank mesocosm (max Ø = 0.4 m; z = 0.4 m) was composed of black plastic and had been sprayed prior to the experiments with matt black paint to ensure that reflectance ($R_{(\lambda)}$) from the tank itself was < 1% (400-1000 nm). A constant water volume of 10 L was maintained during all the mesocosm experiments. Spectral reflectance measurements ($R_{(\lambda)}$) from the various treatments were obtained under controlled laboratory darkroom conditions using a portable ASD (Analytical Spectral Devices) FieldSpec® HandHeld Spectroradiometer. The specifications of the ASD FieldSpec® instrument are detailed in Table 3.2. Two 300 W Kaiser® video lamps provided an artificial source of illumination and a 3.5º FOV (field of view) limiter was attached to the sensor to exclude non-target reflectance. The spectrometer was tripod mounted at a constant height of 0.5 m above the water level within the tank (see Figure 4.3 and Figure 4.4).

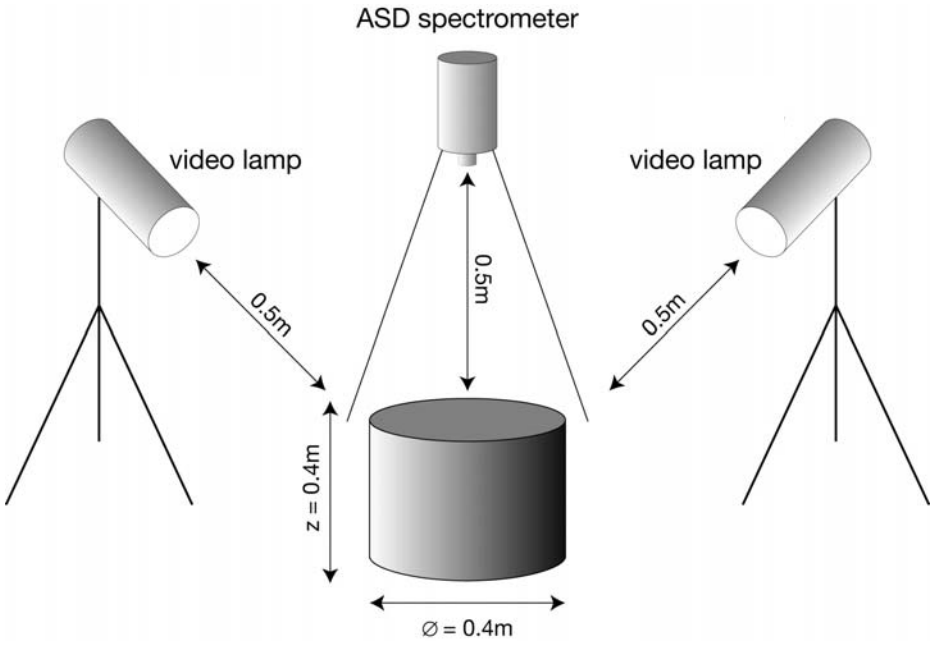

Figure 4.3 Schematic diagram showing the configuration of the laboratory mesocosm and the arrangement of the ASD FieldSpec instrument in relation to the two illumination sources.

The instrument was calibrated to reflectance using a white Spectralon® reference panel (≈ 100% reflectivity). Given illumination was artificially provided, it was considered inappropriate to adopt the terminology of remote-sensing-reflectance ($R_{rs}(0+,\lambda)$) and, instead, the measurements are simply referred to here as reflectance ($R_{(\lambda)}$). To exclude ambient noise, the spectral measurements were acquired against a background consisting of black cloth ($R_{(\lambda)}$ < 5% (400-1000 nm)) that was laid beneath the tank and over adjacent surfaces. Reference panel calibrations and dark-current measurements were performed after every sequence of 10 $R_{(\lambda)}$ measurements. The spectrometer was configured to acquire measurements as a mean of 25 successive scans which were automatically averaged by the dedicated ASD FieldSpec software and 10 sets of replicate scans were acquired from each individual mesocosm treatment.

Figure 4.4 The tank mesocosm configuration detailing the tripod mounted ASD FieldSpec® HH spectrometer and the two 300 W video lamps.

Two contrasting sediments where used to provide background concentrations of SPM (tripton) for specific mesocosm treatments: (1) a largely inorganic (dolerite limestone) sediment (organic matter < 5%) obtained from the bed of Lake Balaton (Hungary) (Herodek, 1988) and (2) a more organic dominated sediment (organic matter > 30-65%) obtained from the bed of Hickling Broad (UK). It was intended that the Lake Balaton sediment would replicate the effects of a largely

inorganic SPM component (i.e. high backscatter, low absorption) on the spectral response of the pseudo-communities, while the Hickling Broad sediment would replicate the effects of a largely organic SPM component (i.e. low backscatter, high absorption) on the spectral response of the pseudo-communities. Background concentrations of CDOM were achieved by introducing the phytoplankton cultures into humic water obtained from the western basin of Lake Balaton where inputs of water rich in dissolved organic carbon (DOC) (humic and fluvic acids) are received from the River Zala (after Svab *et al.,* 2005).

It was intended that the concentrations of optically active components used in the mesocsom experiments would be similar to those encountered in natural shallow lakes. However, preliminary measurements indicated that it was necessary to use higher concentrations than those commonly encountered to improve the signal-to-noise ratio.

4.4.2.2 The Phytoplankton Community Treatments

The phytoplankton pseudo-communities replicated in the mesocosm treatments included communities comprised of single and mixed species with variable background concentrations of SPIM, SPOM and CDOM. Spectral measurements were acquired from the six species at a range of concentrations (treatments 1-6). The concentration of a single green (*Selenastrum capricornutum*), blue-green (*Cylindrospermopsis raciborskii*) and brown (diatom) species was then increased incrementally against various backgrounds of high SPOM (Hickling Broad sediment), high SPIM (Lake Balaton sediment) and CDOM (humic water) (treatments 7-16). However, it was not possible to increase the concentrations of the diatom or the red *Synechococcus* sp. phytoplankton against a background of humic water due to a shortage of culture material. The single species treatments are outlined in Table 4.1.

The mixed pseudo-communities treatments were designed to replicate various successional stages between (1) an initial diatom-dominated community and a succeeding chlorophyte-dominated community and (2) an initial chlorophyte-dominated community and a succeeding cyanophyte-dominated community. These various communities were achieved by creating an initial monospecific pseudo-community composed of a single phytoplankton species and then

progressively diluting the composition of this initial pseudo-community with increasing concentrations of a second phytoplankton species (treatments 33-47). It was ensured that the total chlorophyll-a concentration of the each pseudo-community was maintained at approximately 200 mg chlorophyll-a m^{-3}. Subsequently, SPOM and SPIM concentrations were increased incrementally in two mixed pseudo-communities (*c*. 1:1 diatom/chlorophyte and 1:1 chlorophyte/cyanophyte v/v) to assess the potential spectral masking effects of SPOM and SPIM (treatments 48-51). The various mixed species pseudo-community treatments are outlined in Table 4.2.

Table 4.1 The single species pseudo-communities replicated in the mesocosm experiment (B = blue-green species; R = red species).

Treatment No.	Phytoplankton Species	Chl-a Range (mg m^{-3})	SPOM Range† (mg L^{-1})	SPIM Range‡ (mg L^{-1})	CDOM Background (Y/N)
1	Diatom	0-200	0	0	N
2	*Selenastrum*	0-200	0	0	N
3	*Scendesmus*	0-200	0	0	N
4	*Cylindrospermopsis*	0-200	0	0	N
5	*Synechococcus* (B)	0-200	0	0	N
6	*Synechococcus* (R)	0-200	0	0	N
7	Diatom	0-200	300	0	N
8	*Selenastrum*	0-200	300	0	N
10	*Cylindrospermopsis*	0-200	300	0	N
12	*Synechococcus* (R)	0-200	300	0	N
13	Diatom	0-200	0	300	N
14	*Selenastrum*	0-200	0	300	N
16	*Cylindrospermopsis*	0-200	0	300	N
18	*Synechococcus* (R)	0-200	0	300	N
19	Diatom	200	0-300	0	N
20	*Selenastrum*	200	0-300	0	N
21	*Cylindrospermopsis*	200	0-300	0	N
22	*Synechococcus* (R)	200	0-300	0	N
23	Diatom	200	0	0-300	N
24	*Selenastrum*	200	0	0-300	N
25	*Cylindrospermopsis*	200	0	0-300	N
26	*Synechococcus* (R)	200	0	0-300	N
27	*Cylindrospermopsis*	0-200	0	0	Y
28	*Synechococcus* (B)	0-200	0	0	Y
29	*Selenastrum*	200	0-300	0	Y
30	*Cylindrospermopsis*	200	0-300	0	Y
31	*Selenastrum*	200	0	0-300	Y
32	*Cylindrospermopsis*	200	0	0-300	Y

†Hickling Broad sediment
‡Lake Balaton sediment

Table 4.2 The various mixed phytoplankton pseudo-communities used in the mesocosm experiments (brown = diatom; green = chlorophyte; blue-green = cyanophyte).

Treatment No.	Species Composition (%)			SPM Background (mg L^{-1})	
	Brown	Green	Blue-Green	SPOM	SPIM
33	100	0	0	0	100
34	80	20	0	0	100
35	60	40	0	0	100
36	55	45	0	0	100
37	45	55	0	0	100
38	40	60	0	0	100
39	20	80	0	0	100
40	0	100	0	0	100
41	0	80	20	0	100
42	0	60	40	0	100
43	0	55	45	0	100
44	0	45	55	0	100
45	0	40	60	0	100
46	0	20	80	0	100
47	0	0	100	0	100
48	50	50	0	0-300	100
49	50	50	0	0	100-400
50	0	50	50	0-300	100
51	0	50	50	0	100-400

4.4.3 Shipboard Spectrometry

Shipboard reflectance spectrometry was conducted at a number of stations located on several of the Norfolk Broads in southeast England (UK) (52º 44' 17" N 1º 34' 29" E) during two lake cruises conducted on 22 June 2005 and 31 August 2005. The two cruises were conducted synchronous with NERC ARSF campaigns during which CASI-2 imagery of the Norfolk Broads was acquired (see Chapter 5). The individual Broads sampled during each cruise are listed in Table 3.1. Remote-sensing-reflectance (radiance reflectance) measurements ($R_{rs}(0+,\lambda)$) were acquired from each station in accordance with the methods described in Section 3.3.1 and a surface water sample for subsequent chemo-taxonomic pigment analysis was collected using a pre-washed wide necked bottle.

4.4.4 Analysis of Water Samples

4.4.4.1 RP-HPLC Photopigment Signatures

The water samples removed from the mesocosm experiments were filtered onto 25 mm diameter Whatman GF/F filter papers, wrapped in aluminium foil, and immediately frozen at -

75ºC prior to transportation on dry ice to the reverse-phase high performance liquid chromatography (RP-HPLC) laboratory (SBES, University of Stirling) where chemotaxonomic pigment analysis was performed. The water samples collected from the lake sampling cruises in the Norfolk Broads were filtered onto 47 mm diameter GF/C filter papers, wrapped in aluminium foil, and immediately quick-frozen in liquid-N prior to transportation back to the RP-HPLC laboratory (SBES, University of Stirling).

The configuration of the RP-HPLC system included a Dionex quaternary gradient pump connected to a Spherisorb^{TM} OSD2 reverse-phase C-18 column (25 cm x 4.6 mm, 5 µm particles, 90-100 000 plates m^{-1}) and a Lab Alliance UV6000LP photo diode array detector (PDA). An oven was used to maintain the Spherisorb^{TM} OSD2 reverse-phase C-18 column at 30°C during analysis. Pigments for RP-HPLC analysis were extracted from filter papers in 100% methanol for 20 h in the dark at 4ºC following sonication in an ice slurry for 1 min in 15 s bursts) (Mantoura & Llewellyn, 1983). Methanol extracts were clarified by centrifugation (10 000 *g* for 10 min) and an ion-pairing agent (1 M ammonium acetate v/v) was added to the extract to improve peak resolution. 250 µl of the extract was manually injected into the RP-HPLC system for analysis (the injection value was interfaced with a 100 µl Dionex stainless steel LC sample loop).

The chromatic conditions for pigment separation followed the protocol of Wright *et al*. (1991) which employs three mobile-phase solvents in a linear gradient programme (Table 4.3): *Solvent A*, 80:20 methanol: 0.5 M ammonium acetate (v/v); *Solvent B*, 90:10 acetronitrile: water (v/v); and *Solvent C*, 100% ethyl acetate. A constant flow rate of 1 ml min^{-1} was used. Pigment peaks were quantified using absorbance (mAU) at 436 nm. The pigment peaks were identified through comparisons to standard reference pigments obtained from the Water Quality Institute (VKI), Hørsholm, Denmark and via comparisons to published pigment PDA absorption spectra, elution sequences and retention times (RTs). The solvents used were HPLC grade and distilled water was purified using a Millipore Milli-Q system. Ammonium acetate was A.R. grade.

Table 4.3 The RP-HPLC solvent system used in the (a) start-up, (b) analytical and (c) shut-down protocols employed in the analysis of phytoplankton pigment signatures in samples from the mesocosm experiments and from the Norfolk Broads (after Wright *et al.,* 1991).

Time (min)	Flow rate (ml min^{-1})	Solvent A (%)	Solvent B (%)	Solvent C (%)	Conditions
(a) Start-up protocol					
0	1.0	0	0	100	Start-up
3	1.0	0	0	100	Washing
6	1.0	0	0	100	Linear gradient
16	1.0	0	100	0	Linear gradient
17	1.0	100	0	0	Ready for analysis
(b) Analytical gradient protocol					
0	1.0	100	0	0	Injection
4	1.0	0	100	0	Linear gradient
18	1.0	0	20	80	Linear gradient
21	1.0	0	100	0	Linear gradient
24	1.0	100	0	0	Linear gradient
29	1.0	100	0	0	Equilibrium
(c) Shut-down protocol					
0	1.0	100	0	0	Analysis complete
3	1.0	0	100	0	Linear gradient
6	1.0	0	0	100	Linear gradient
16	1.0	0	0	100	Washing
17	1.0	0	0	100	Shut down

4.4.4.2 Chlorophyll-a, C-phycocyanin and DOC

The concentration of chlorophyll-a in the water samples removed from the mesocosm experiments was determined by spectrophotometry in the BLRI laboratory. Pigments were extracted from the frozen filter papers using 100% hot methanol (spectrophotometric grade)

and clarified by centrifugation (10 000 *g* for 10 min). Chlorophyll-a was quantified using the equations of Iwamura *et al*. (1970). Chlorophyll-a in the samples from the Norfolk Broads was determined according to the method of Lorenzen & Jeffrey (1980) as detailed in Section 3.3.2. C-phycocyanin in the samples from the mesocosm experiments and the Norfolk Broads was extracted from frozen filter papers using an adaptation of the freeze-thaw method described in Sarada *et al*. (1999). Filter papers were immersed in 50mM sodium phosphate buffer (pH 6.8) and subjected to 8 consecutive freeze-thaw cycles. Following the completion of the freeze-thaw cycles, the efficiency of the extraction was improved by subjecting the samples to 1 min probe sonication in an ice slurry (15 s bursts). C-phycocyanin in the extracts was quantified using the equations of Bennett & Bogorad (1973) (Equation 4.1).

$$C - Phycocyanin \ \ (mg\ ml^{-1}) = \frac{A_{615} - 0.474(A_{652})}{5.34} \qquad \textbf{Equation 4.1}$$

The concentration of dissolved organic carbon (DOC) in the mesocosm samples was determined in the BLRI laboratories via thermal catalysis at 950ºC in an Elementar High TOC instrument (Elementar Analysensysteme GmbH, Germany); the instrument was equipped with a platinum cartridge and used synthetic air as a carrier gas (Svab *et al.,* 2005).

4.4.5 Spectral Data Analysis

4.4.5.1 Mesocosm Reflectance Measurements

The raw hyperspectral data were interpolated to a spectral resolution of 0.5 nm and truncated between 400-1000 nm to exclude noisy data at the extremes of the ASD FieldSpec® instrument's sampling range. The resulting data were smoothed by passing a 5 nm running mean filter over the entire spectrum (after Dall'Olmo *et al.,* 2005). The spectral dissimilarity of the various phytoplankton species and the pseudo-communities was explored qualitatively through comparison of their hyperspectral $R_{(\lambda)}$ signatures using principal components analysis (PCA) and multivariate discriminant analysis (MDA).

PCA is often used to reduce the dimensionality of large multivariate datasets through the derivation of a limited number of new component variables that seek to encapsulate the maximum amount of variance from the original dataset as possible. In this study, PCA was used to reduce the dimensionality of the large hyper- and multi-spectral datasets to enable the spectral dissimilarities of the individual species and pseudo-communities to be assessed in a visually-interpretive fashion through projection in 2-dimensional PCA-component feature space (after Svab *et al.,* 2005). The selected PCA-components strictly adhered to Kasier criterion (eigenvalues ≥ 1) and typically explained (cumulatively) ≥ 95% of the original dataset variance. MDA (also referred to as Canonical discriminant analysis) can be used to classify observation data into discrete categorical groups with common attributes using numerous predictor variables. In this study, MDA was used to classify the $R_{(\lambda)}$ spectra obtained from the mesocosm experiments based upon their dominant species composition. In essence, the MDA was used to examine the potential efficacy of a remote-sensing-based classification scheme for the determination of dominant taxa within single bloom-like and mixed phytoplankton communities.

In order to perform the PCA and MDA analyses, and to gauge the effect of variable sensor spectral resolution on the spectral dissimilarities of the pseudo-communities (after Dekker *et al.,* 1992; Svab *et al.,* 2005), it was necessary to reduce the dimensionality of the original 0.5 nm resolution hyperspectral dataset. Thus the original hyperspectral dataset (hereafter deemed HYPER-1) was devolved to four coarser resolution datasets: (1) with a spectral resolution of 5 nm (400-1000 nm) (hereafter deemed HYPER-2); (2) with a spectral resolution of 10 nm (400-1000 nm) (hereafter deemed HYPER-3); (3) with a spectral resolution of 15 nm (400-1000 nm) (hereafter deemed HYPER-4); and (5) with a spectral resolution of 20 nm (400-1000 nm) (hereafter deemed HYPER-5). The original hyperspectral dataset was also used to simulate the spectral response of the SeaWiFS, Landsat TM7, IKONOS and ASTER satellites. First-derivative analysis was applied to the HYPER-2, HYPER-3, HYPER-4, HYPER-5, SeaWiFS, Landsat, IKONOS and ASTER datasets in an effort to enhance latent information in the spectra and accentuate any dissimilarities that may be due to the presence of $R_{(\lambda)}$ features related to accessory pigment absorption (derivative datasets are hereafter denoted by the subscript suffix $dR/d\lambda$ – e.g. HYPER-$2_{dR/d\lambda}$) (Malthus & Dekker, 1995; Aguirre-Gomez *et al.,* 2001b). The first-

derivative transformation was achieved following the method described in Section 3.4.3. The first-derivative transformed datasets were subsequently subjected to the same PCA and MDA analyses used with the untransformed $R_{(\lambda)}$ data.

In order to examine the potential retrieval of biomarker pigment concentrations for brown (fucoxanthin) and blue-green (C-phycocyanin) taxa from hyperspectral remote sensing data, indices were derived from the HYPER-1 datasets using the method described in Dall'Olmo *et al*. (Dall'Olmo *et al.,* 2003) (see Section 3.3.3). In addition, simple single-band first-derivative indices were developed empirically from the HYPER-$1_{dR/d\lambda}$ dataset. Data was check for normality in Mintab v.14 using the Anderson-Darling method (95% confidence level). Correlation and least-squares regression analysis was then used to examine the relationship between $R_{(\lambda)}$ and $dR/d\lambda$ within the various simulated multispectral and hyperspectral datasets and the measured concentrations of selected biomarker pigments in the mesocosm pseudo-communities.

4.4.5.2 Norfolk Broads $R_{rs}(0+,\lambda)$ Data

The raw $R_{rs}(0+,\lambda)$ data were interpolated, truncated and smoothed prior to analysis according to the methods described in Section 4.3.5. Indices and algorithms for the retrieval of biomarker pigment concentrations were developed using band-ratio, normalised-difference band-ratio and single-band first-derivative templates. These indices were derived empirically using correlation analysis to spectrally tune and thus optimise index formulation. Indices were also derived using the methods described in Dall'Olmo (2003) (see Section 3.3.3) and following continuum-removal analysis ($R'_{(\lambda)}$) of the original $R_{rs}(0+,\lambda)$ data (after Kokaly & Clark, 1999; Schmidt & Skidmore, 2003; Mutanga *et al.,* 2004). Data was checked for normality in Minitab v.14 using the Anderson-Darling method (95% confidence level). Linear and non-linear least-squares regression analysis was then used to examine the relationship between the $R_{rs}(0+,\lambda)$, $dR/d\lambda$ and $R'_{(\lambda)}$ spectral indices derived from the various simulated hyper- and multi-spectral datasets and the measured concentrations of biomarker pigments in the water samples obtained from the shallow lakes of the Norfolk Broads.

4.5 RESULTS AND DISCUSSION

4.5.1 Pigment Signatures of Phytoplankton Colour Groups

The RP-HPLC pigment signatures chromatograms of the various phytoplankton colour group taxa are depicted in the in Figure 4.5. The chromatograms illustrate the marked variation that occurs in the photopigment composition of freshwater phytoplankton colour groups. The photosynthetic pigment composition of the brown diatom species was comprised of chlorophyll-a and chlorophyll-c_{1+2} (chlorophyll c_1 and c_2 co-eluted and could not be resolved in isolation); the xanthophylls fucoxanthin and diadinoxanthin; and the β-carotene pigment. The photosynthetic pigment composition of the green chlorophyte species (*Scendesmus armatus*) was comprised of chlorophyll-a and chlorophyll-b; the xanthophylls neoxanthin, violaxanthin and lutein (which often co-eluted with chlorophyll-b); and the co-eluting group of α-, β-, and γ-carotene pigments.

The photosynthetic pigment composition of the blue-green cyanophyte (*Cylindrospermopsis raciborskii*) was comprised of chlorophyll-a; the xanthophyll echinenone; and the β-carotene pigment. The photosynthetic pigment composition of the red cyanophyte (*Synechococcus* sp.) was comprised of chlorophyll-a; the xanthophyll zeaxanthin; and the β-carotene pigment. The diverse pigment signatures of the four colour groups are consistent with the pigment signatures described by several previous workers including Rowan (1989), Wright *et al*. (1991), Jeffrey & Vesk (1997) and Barlow *et al*. (1997) (see Table 4.4).

The blue-green cyanophytes species (*Cylindrospermopsis raciborski* and *Synechococcus* sp.) were also found to contain significant concentrations of the phycobiliprotein C-phycocyanin, while the red cyanophyte (*Synechococcus* sp.) was found to contain significant concentrations of the phycobiliprotein C-phycoerythrin. These observations concur with the findings of Siegelman & Kycia (1978) who also noted significant concentrations of phycobiliprotein pigments in various species of cyanobacteria. Example PDA absorbance spectra for chlorophyll-a, chlorophyll-b, chlorophyll-c_{1+2}, fucoxanthin, lutein and zeaxanthin are detailed in Figure 4.6.

(a) Brown (diatom)

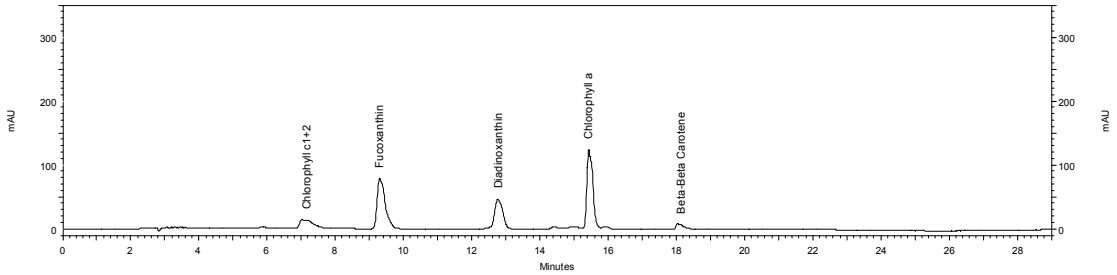

(b) Green (chlorophyte) – *Scenedesmus armatus* (ACT 9710)

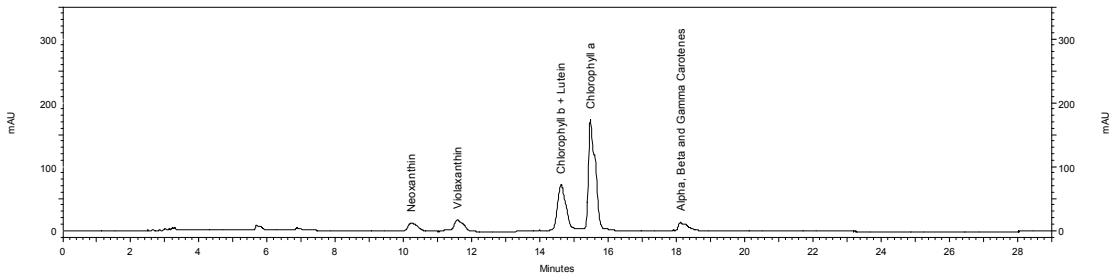

(c) Blue-green (cyanophyte) – *Cylindrospermopsis raciborskii* (ACT 9502)

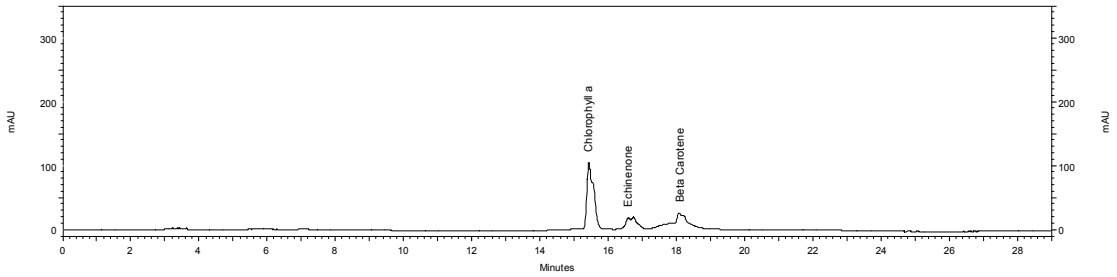

(d) Red (cyanophyte) – *Synechococcus* (ACT 9807)

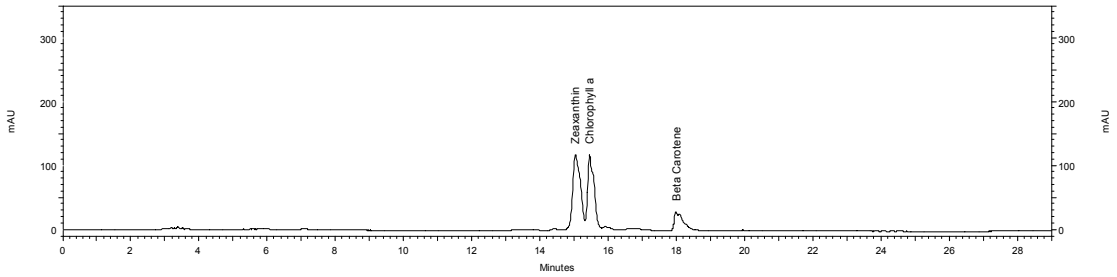

Figure 4.5 Example chromatograms (Retention Time [min] vs. Absoprtion @ 436 nm [mAU]) detailing the complete photosynthetic chlorophyll-and carotenoid pigment signatures of the four colour group representatives (a-d).

Table 4.4 The class distribution of various phytoplankton photosynthetic pigments in several important freshwater taxa (adapted from Jeffrey & Vesk, 1997). Species not examined in the mesocosm experiments are also detailed for the purpose of comparison but are shown in grey text.

		Bacillariophytes (brown)	Chlorophytes (green)	Cryptophytes	Cyanophytes (blue-green)	Dinophytes
Chlorophylls	*a*	●	●	●	●	●
	b		●			
	c_1	●				
	c_2	●		●		●
Carotenes	β,ε		•	•		
	β, β	•	●		●	•
Xanthophylls	Alloxanthin			●		
	Diadinoxanthin	●				●
	Diatoxanthin	•				•
	Dinoxanthin					●
	Fucoxanthin	●				
	Lutein		●			
	Neoxanthin		●	•		
	Peridinin					●
	Violaxanthin		●			
	Zeaxanthin		•		●	
Phycobiliproteins	Allophycocyanins				●	
	Phycocyanins			●	●	
	Phycoerythrins			●	●	

● = major pigment (>10%) ● = minor pigment (1-10%) • = trace pigment (<1%) of total chlorophylls and carotenoids

(a) Chlorophyll-a

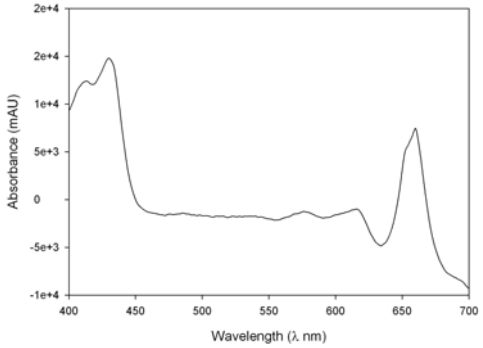

(b) Chlorophyll-b

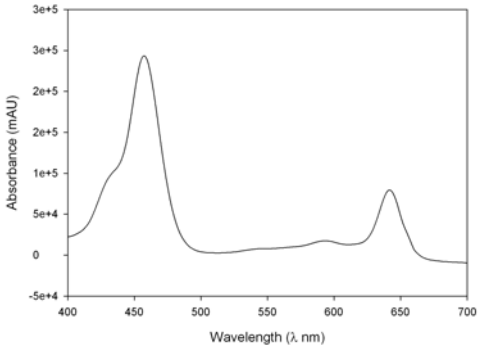

(c) Chlorophyll-c_{1+2}

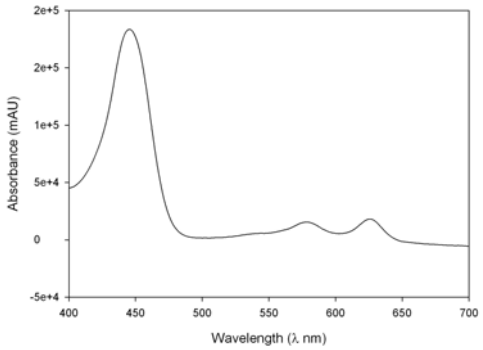

(d) Fucoxanthin

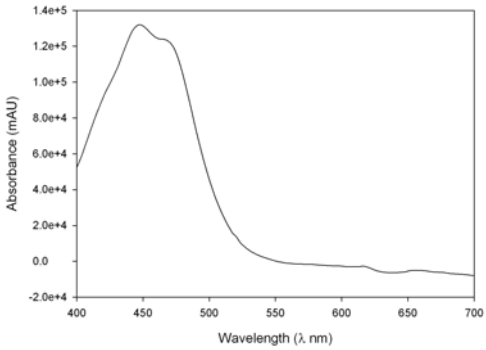

(e) Lutein

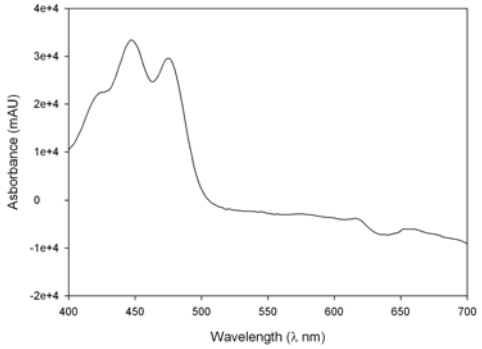

(f) Zeaxanthin

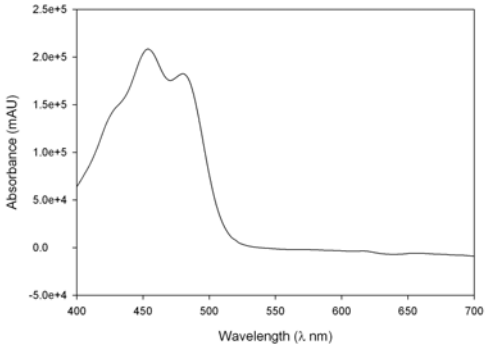

Figure 4.6 Example PDA absorbance spectra of six major chlorophyll-and xanthophyll pigments identified in the various phytoplankton species used in the mesocosm experiments.

4.5.2 Single Species Pseudo-Communities

4.5.2.1 HYPER-1 Spectral Signatures at "Bloom-like" Concentrations

The hyperspectral (HYPER-1) signatures of the six phytoplankton species examined in the mesocosm experiments at high and near-equivocal chlorophyll-a concentrations are shown in Figure 4.7. It is evident that the phytoplankton colour groups examined demonstrate significant differences in their respective spectral characteristics in terms of both (i) the magnitude of $R_{(\lambda)}$ across optical and VNIR wavelengths and, (ii) the composite shape of the spectral signature

and the wavelength-position and magnitude of localised $R_{(\lambda)}$ peaks and troughs. The spectra of all six species exhibit low $R_{(\lambda)}$ in the blue region (<500 nm) due to strong absorption by chlorophyll-a and carotenoid pigments. It is notable that there is no distinct $R_{(\lambda)}$-minimum in the brown diatom spectra in the *c.* 450-470 nm region where fucoxanthin absorption is maximal (fucoxanthin is a major photosynthetic pigment used as a chemotaxonomic biomarker for bacillariophyte species (amongst others)). The absence of this feature is likely to be the result of the masking effects of the other chlorophyll and carotenoid pigments which also have prominent absorption maxima in this region.

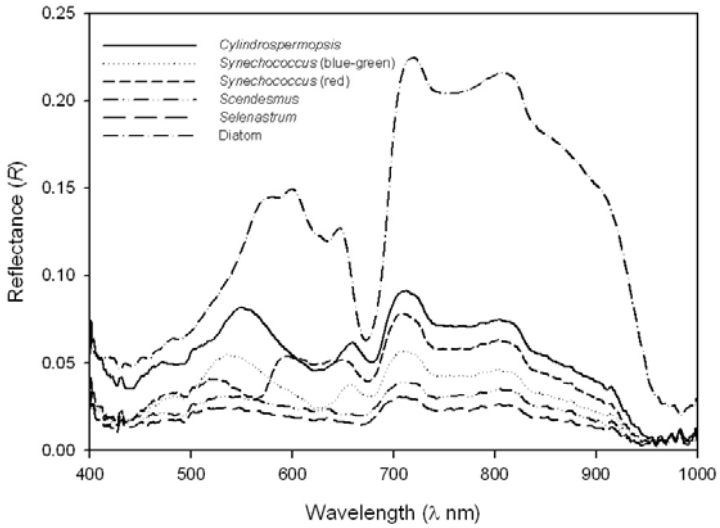

Figure 4.7 The HYPER-1 signatures of the six species of phytoplankton examined in the mesocosm experiments at broadly equilavent concentrations of chlorophyll-a. Chlorophyll-a concentrations: *Cylindrospermopsis* = 301 mg m^{-3}; *Synechococcus* (blue-green) = 211 mg m^{-3}; *Synechococcus* (red) = 222 mg m^{-3}; *Scendesmus* = 232 mg m^{-3}; *Selenastrum* = 212 mg m^{-3}; diatom = 462 mg m^{-3}.

The six species demonstrate increased $R_{(\lambda)}$ in the green region of the spectrum forming a local $R_{(\lambda)}$-maximum at *c*. 530-570 nm (the "green peak"). It is noticeable that the position of this local $R_{(\lambda)}$-maximum in the brown diatom spectra is significantly red-shifted relative to the positions of the equivalent maxima in the spectra of the chlorophyte and cyanophyte species. Previous workers have suggested changes in the position of the green peak may be related to changes in the floristic composition of phytoplankton communities (Schalles *et al.,* 1998; Gitelson *et al.,* 1999).

The red cyanophyte spectrum has a unique local $R_{(\lambda)}$-minimum located at *c*. 570 nm that is not evident in the spectra of any of the other species; the position of this feature would suggest that it is related to absorption by C-phycoerythrin. Unique local $R_{(\lambda)}$-minima can also be identified in the spectra of the two blue-green cyanophyte species located at *c*. 630 nm; these features are without doubt associated with the absorption maximum of C-phycocyanin. The *in-vivo* absorption maximum of C-phycocyanin occurs at 620 nm; the shift in the position of the resulting C-phycocyanin-related feature in the $R_{(\lambda)}$ spectra is caused by the overlap with chlorophyll-a absorption. The diatom spectrum also exhibits a unique $R_{(\lambda)}$-minimum at *c*. 640 nm; this may be related to the high concentrations of chlorophyll-c_{1+2} found in bacillariophytes – a similar feature was observed in the spectra of benthic diatoms by Meleder *et al*. (2003).

The HYPER-1 spectra of all species exhibit local $R_{(\lambda)}$-maxima in the red region at *c*. 630-660 nm immediately prior to the $R_{(\lambda)}$-minimum related to chlorophyll-a absorption (*c*. 670-690 nm). The chlorophyll-a $R_{(\lambda)}$-minimum is common to the HYPER-1 spectra of all six phytoplankton species – although the exact position of the chlorophyll-a absorption feature varies – which may be a function of differences in the concentration of the pigment between the various species (Dekker *et al.,* 1991; Dekker, 1993; Han & Rundquist, 1997). The six phytoplankton species exhibit increased $R_{(\lambda)}$ at the red-edge and into the VNIR region (*c*. > 700 nm) (the VNIR plateaux). $R_{(\lambda)}$ decreases after *c*. 815 nm in the spectra due to intense absorption by water.

The marked variations in the magnitude of $R_{(\lambda)}$ between the various species can be attributed to disparities in the backscattering properties of the phytoplankton cells which is, at least in part, a function of cell morphology (Ahn *et al.,* 1992; Sathyendranath *et al.,* 2005). The variations observable in the composite shape of the $R_{(\lambda)}$ signatures would seem to be a function of absorption by species-specific accessory pigments (e.g. C-phycocyanin and C-phycoerythrin). It is notable that the $R_{(\lambda)}$ spectra of species from mutual colour groups (i.e. the two blue-green cyanophytes and the two green chlorophytes) are near identical in terms of the composite shape of the spectrum but exhibit significant differences in the magnitude of $R_{(\lambda)}$.

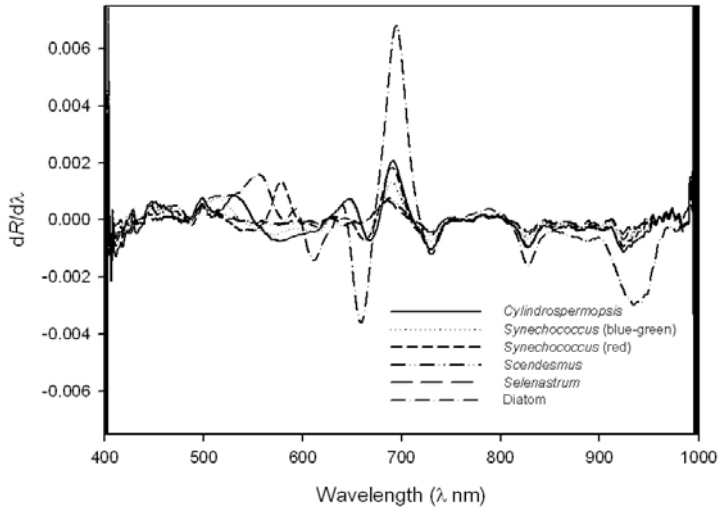

Figure 4.8 The HYPER-$1_{dR/d\lambda}$ signatures of the six species of phytoplankton examined in the mesocosm experiments at broadly equivalent concentrations of chlorophyll-a. Chlorophyll-a concentrations: *Cylindrospermopsis* = 301 mg m^{-3}; *Synechococcus* (blue-green) = 211 mg m^{-3}; *Synechococcus* (red) = 222 mg m^{-3}; *Scendesmus* = 232 mg m^{-3}; *Selenastrum* = 212 mg m^{-3}; diatom = 462 mg m^{-3}.

The first-derivative spectra (d*R*/dλ) of the six phytoplankton species are depicted in Figure 4.8. The d*R*/dλ spectra of the six phytoplankton species further emphasise the main spectral regions in which the greatest dissimilarity occurs. Peaks and troughs in the d*R*/dλ spectra represent prominent inflection points: peaks relate to negative gradients in the $R_{(\lambda)}$ spectrum (e.g. prior to absorption-related $R_{(\lambda)}$ features) and troughs relate to positive gradients in the $R_{(\lambda)}$ spectrum (e.g. due to increased backscattering). It is notable that, in the d*R*/dλ spectra of both the cyanophyte and diatom species, peaks and troughs can be identified that are absent in the chlorophyte d*R*/dλ spectra. The d*R*/dλ spectra suggests that significant spectral dissimilarities between the species occur in the 500-600 nm region, particularly at the colour group level, as both the diatom and cyanophyte spectra have prominent d*R*/dλ features in this region that are not evident in the chlorophyte d*R*/dλ spectrum. In the case of the cyanophyte spectrum these d*R*/dλ features indicate the approximate position of the absorption maxima of C-phycocyanin and C-phycoerythrin. It is also significant that in the d*R*/dλ spectra the phytoplankton species from the mutual colour groups (i.e. the two blue-green cyanophyte species and the two green chlorophyte species) have near identical d*R*/dλ signatures. Thus, in this instance, the first-derivative analysis would seem to be have been effective in normalising differences in $R_{(\lambda)}$

between species from common colour groups. The first-derivative signatures show improved resolution of pigment-induced changes in the spectral response of the various phytoplankton species; as such, first-derivative, or even n^{th}-derivative, analysis may be a pertinent technique for enhancing and extracting taxonomic information from remote sensing data.

4.5.2.2 HYPER-1 Spectral Signatures at Varying Concentrations of Chlorophyll-a

The spectral response of each colour group (brown, green, blue-green and red) at incrementing concentrations of chlorophyll-a (*c*. 0-200 mg m^{-3}) is depicted in Figure 4.9. In this instance, a single species was examined from each colour group (*Scendesmus armatus* – green and *Cylindrospermopsis raciborskii* – blue-green). It is notable that increases in the concentration of the colour group species had variable effects upon the resulting $R_{(\lambda)}$ signatures. Increases in the concentration of the (brown) diatom species resulted in proportional increases in $R_{(\lambda)}$ across the entire VIS and VNIR spectrum. It is notable that the increase in $R_{(\lambda)}$ in the diatom spectra was, with the exception of wavelengths in the vicinity of the chlorophyll-a absorption maximum, almost wavelength-independent and, in particular, in the region between 400 and 800 nm. In contrast, increases in the concentration of the (green) chlorophyte did not result in significant increases in $R_{(\lambda)}$; rather, incremental increases in the concentration of the chlorophyte seemed to precipitate decreases in $R_{(\lambda)}$ in the blue and green regions (probably due to increased carotenoid and chlorophyll absorption) and also in the red region (in proximity to the chlorophyll-a absorption maximum).

In the blue-green cyanophyte spectra, $R_{(\lambda)}$ increased in proportion with the concentration of chlorophyll-a, but it is evident, that as the concentration of blue-green cyanophyte was increased, the $R_{(\lambda)}$-minima associated with C-phycocyanin and chlorophyll-a absorption increased in prominence. Similar effects can be observed in the spectra of the red cyanophyte, but in this instance $R_{(\lambda)}$ decreased with increasing algal concentration < 600 nm and, in particular, in the proximity of the C-phycoerythrin absorption feature, but increased with higher algal concentrations > 600 nm (but with increased prominence of the chlorophyll-a related $R_{(\lambda)}$-minimum).

(a) Brown (diatom)

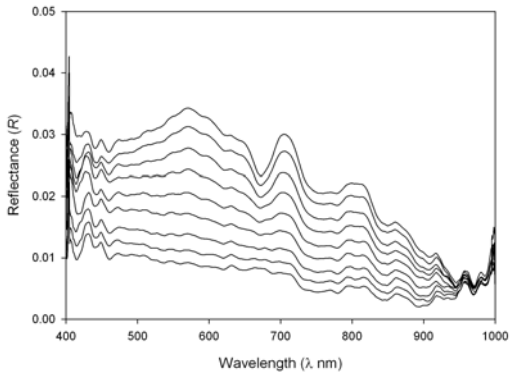

(b) Green (chlorophyte)

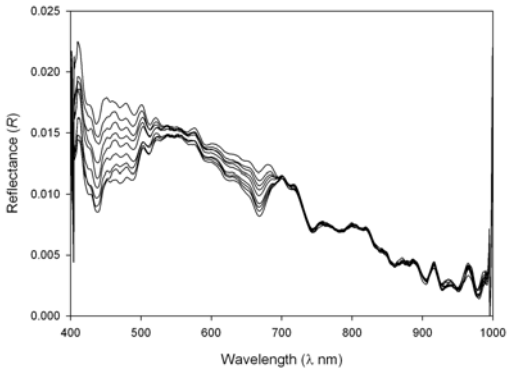

(c) Blue-Green (cyanophyte)

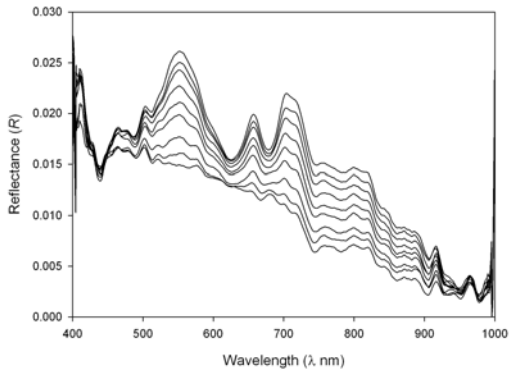

(d) Red (cyanophyte)

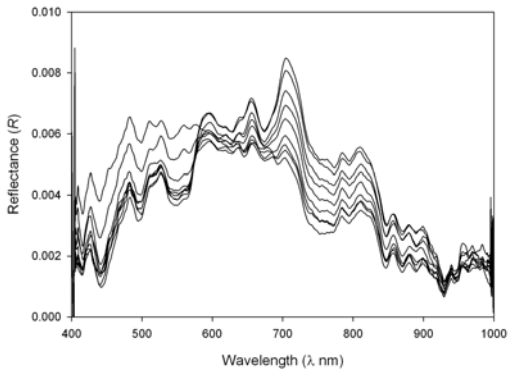

Figure 4.9 The HYPER-1 $R_{(\lambda)}$ signatures of the various colour groups at incrementing concentrations (c. 0, 25, 50, 75, 100, 125, 150, 200 mg chlorophyll-a m^{-3}).

The PCA transformation of the various colour groups at incremental concentrations of chlorophyll-a (*c*. 0-200 mg m^{-3}) is depicted in Figure 4.10. The PCA transformation enables the spectral dissimilarities of the various colour groups to be expressed in a qualitative, but visually-interpretative, format. The $R_{(\lambda)}$ spectra of the brown diatom exhibited the greatest response to increasing concentrations of chlorophyll-a from the initial clear-water state. The blue-green and red cyanophytes also demonstrated significant change in their spectral response with increasing chlorophyll-a. In contrast, the green chlorophyte demonstrated the weakest spectral response with incremental increases in the concentration of chlorophyll-a.

The extent to which incrementally-increasingly the concentration of chlorophyll-a for each colour group specimen moderated the resulting spectral signature would appear to be largely a function of the absorption and, more prominently, backscattering efficiency of each colour group

species. Different species of phytoplankton are recognised to have different scattering efficiencies (Ahn *et al.,* 1992). Kirk (1994) noted that the backscattering coefficients of freshwater phytoplankton can vary between 0.044 and 0.535 m^2 mg chlorophyll-a^{-1} (550 or 590 nm). Kirk (1994) also noted that diatoms and some cyanobacteria species can often exhibit higher backscattering due to siliceous cell walls (diatoms) or the presence of refractive intracellular gas vacuoles (cyanophytes). This would explain the significant variations noted here and, in particular, in the case of the diatom spectra where $R_{(\lambda)}$ was up to four times greater than that observed from pseudo-communities composed of the other colour group species.

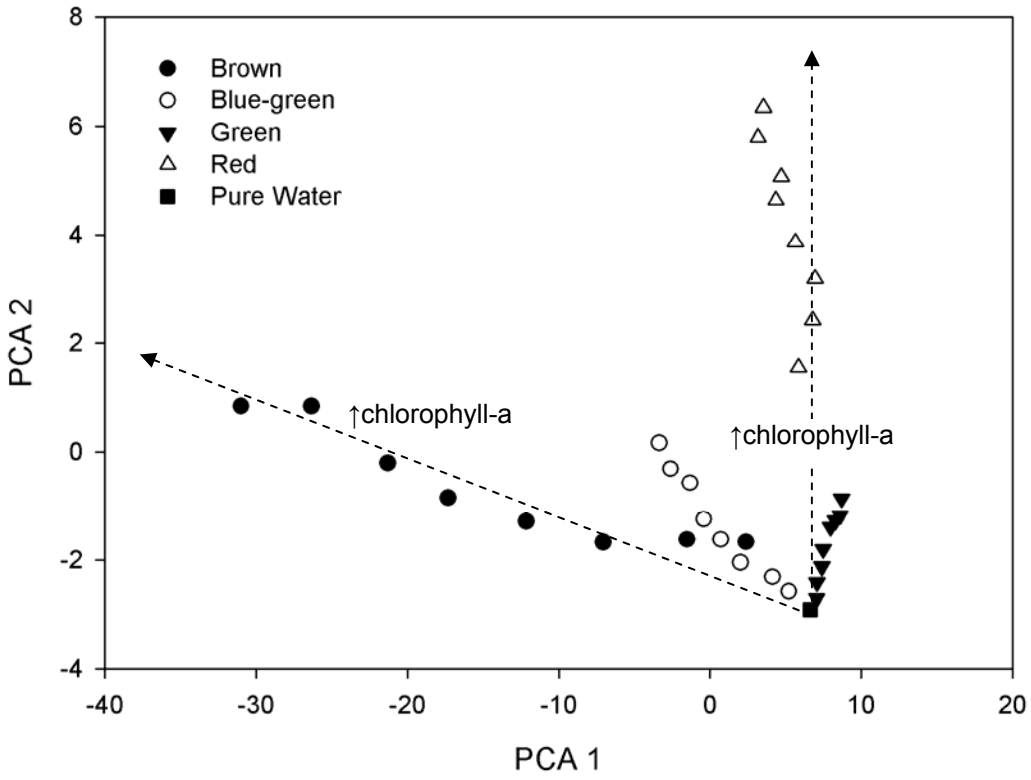

Figure 4.10 PCA transformation of the HYPER-2 dataset illustrating the degree of spectral dissimilarity between the four phytoplankton colour groups in response to incremental increases in the concentration of chlorophyll-a (0-200 mg m^{-3})

It is also notable that dissimilarities between the colour group species are more subtle at low concentrations of chlorophyll-a but become more prominent as the concentration of chlorophyll-a increases until very distinct spectral end-members are formed. This observation suggests that the discrimination of different bloom-forming colour group species, not unexpectedly, may be more easily achieved at high concentrations of chlorophyll-a. Kutser *et al*. (2006) noted that

the low concentration of C-phycocyanin in marine waters made the detection of blue-green species problematic unless concentrated blooms occurred; this suggests that resolution of phytoplankton species composition information from remotely sensed data may be dependent on the exceedance of a minimum detection limit (MDL) for specific diagnostic pigments. Kutser (2006) suggests that in CASE II coastal waters the MDL for C-phycocyanin may be in the order of 10-30 mg m^{-3}. The biomarker pigment MDL capabilities of remote sensing instruments would have implications for the potential use of such technologies in early-warning systems for HAB development and, thus, the results obtained here would seem to be of relevance in this context.

4.5.3 Mixed Species Pseudo-Communities

The HYPER-1 signatures of the mixed pseudo-communities are shown in Figure 4.11; the mixed species $R_{(\lambda)}$ spectra further illustrate the extent to which changes in the species composition of a phytoplankton community can be resolved through changes in spectral response and, importantly in this instance, largely independent of the chlorophyll-a concentration. It is notable, for example, that increases in diatom concentration in the brown/green pseudo-community precipitated consequent increases in $R_{(\lambda)}$ despite a near constant chlorophyll-a concentration being maintained. The other notable effects of increased diatom abundance include the red-shift of the $R_{(\lambda)}$-maximum between 500 and 600 nm and the greater prominence of the local $R_{(\lambda)}$-maximum located at *c*. 635 nm.

In CASE II waters and, in particularly shallow lakes, backscattering associated with tripton, or the lake bottom, may potentially mask increases in $R_{(\lambda)}$ arising from floristic changes within the phytoplankton community. Therefore, increased backscattering, and thus $R_{(\lambda)}$, attributable to increasing diatom abundance may not be an effective means of detecting such compositional changes in natural waters. In this context, the observed red-shift of the green-peak feature may be more useful within natural phytoplankton communities. However, the cause(s) of the shift in the position of the green peak and, potentially, in relation to changes in the floristic composition of the phytoplankton community, has not been examined for natural waters and, as such, it would seem pertinent to examine this effect further in future studies.

In similarity, increased blue-green cyanophyte abundance also resulted in increases in $R_{(\lambda)}$ being observed from the green/blue-green pseudo-community. However, the major effect of increasing blue-green composition was the progressive deepening of the $R_{(\lambda)}$-minimum related to C-phycocyanin absorption at *c*. 630 nm and the emerging prominence of the $R_{(\lambda)}$-maximum at *c*. 650 nm subjugating the $R_{(\lambda)}$-minima associated with C-phycocyanin and chlorophyll-a absorption. In this context, the proportional response in the depth of the C-phycocyanin absorption feature observed with increased blue-green composition would seem to provide an obvious means to the identification and quantification of blue-green cyanobacteria in lakes and, indeed, other inland waters. Similar conclusions have been reached by other workers (Dekker, 1993; Schalles & Yacobi, 2000; Simis *et al.,* 2005; Simis *et al.,* 2007).

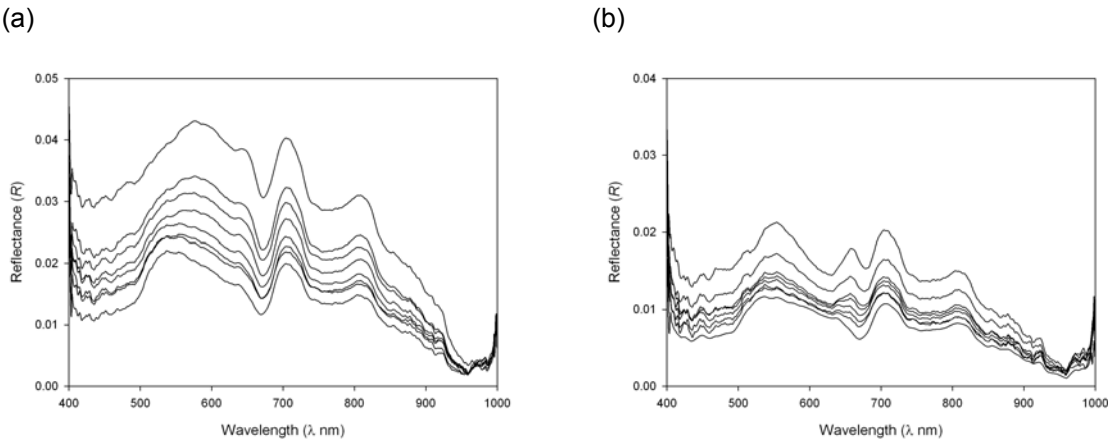

Figure 4.11 The HYPER-1 spectral signatures of (a) the transition from a brown (diatom) dominated pseudo-community to green (chlorophyte) dominated pseudo-community and (b) the transition from a green (chlorophyte) dominated pseudo- community to blue-green (cyanophyte) dominated pseudo-community. Total chlorophyll-a = *c*. 200 mg m^{-3}.

The score plot derived from the PCA transformation of the HYPER-2 signatures of the mixed pseudo-communities is shown in Figure 4.12. The PCA score plot shows the monospecific pseudo-communities (i.e. 100 B, 100 G, 100 BG) forming well defined polar end-members in PCA-component feature space with the intermediate mixed pseudo-communities distributed in a near linear fashion between these polar end-members. Significantly, the PCA score plot illustrates that the spectral dissimilarity between the various pseudo-communities was greatest when the floristic assemblage was dominated by a single phytoplankton species (i.e. 80-100%

total abundance). The spectral dissimilarity was not as pronounced when the pseudo-community contained two near co-dominant species.

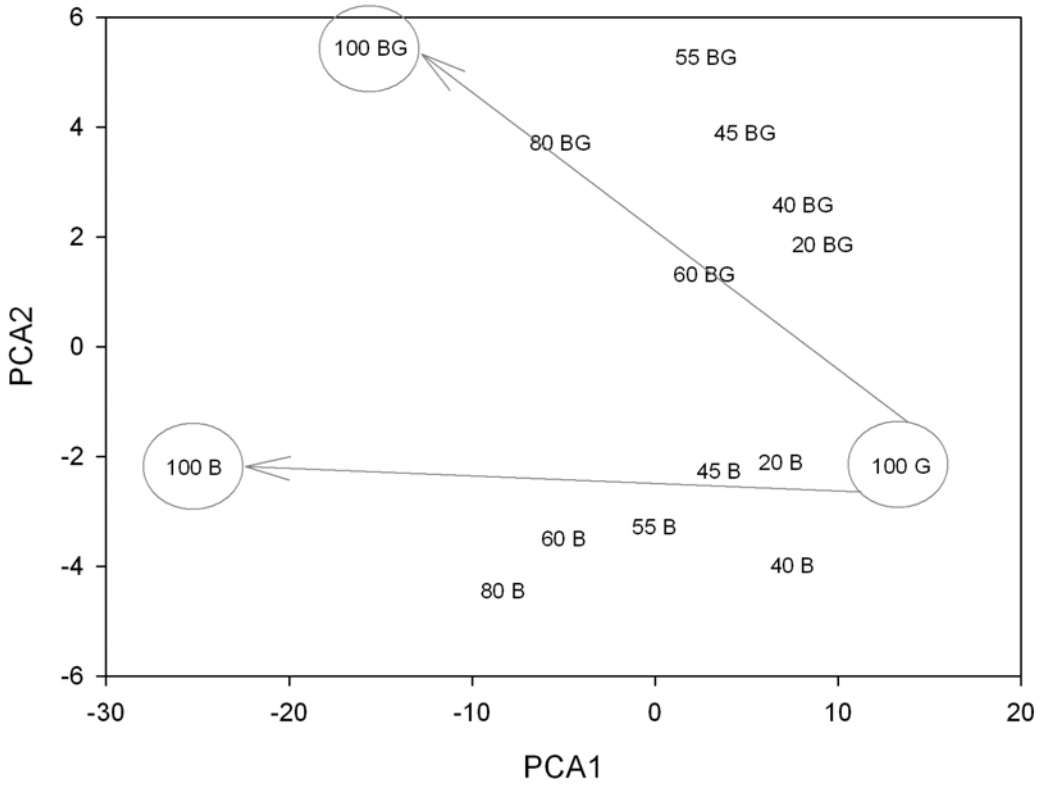

Figure 4.12 PCA score plots for the HYPER-2 dataset showing the spectral transition from a brown (diatom) (B) dominated pseudo-community through a green (chlorophyte) (G) dominated pseudo-community to a blue-green (cyanophyte) (BG) dominated pseudo-community. Symbol numbers relate to the approximate percentage abundance (%) of each colour group. Total chlorophyll-a *c*. 200 mg m^{-3}. PCA1 explained 88.2% and PCA2 10.5% of the total statistical variance of the original HYPER-1 dataset.

The score plot from the PCA transformation of the HYPER-$2_{dR/d\lambda}$ dataset is shown in Figure 4.13. The objective of utilising first-derivative analysis was normalise the variance in $R_{(\lambda)}$ between the various mixed pseudo-communities in an attempt to enhance latent spectral information associated with the presence of diagnostic biomarker pigments. Thus, it is noteworthy that the pseudo-communities remain spectrally distinct and, in fact, it could be argued that the feature space separation of the pseudo-communities was improved following the first-derivative transformation. The first-derivative transformation also improved the linearity of the distribution of the intermediate pseudo-communities of mixed composition between the pure end-member pseudo-communities.

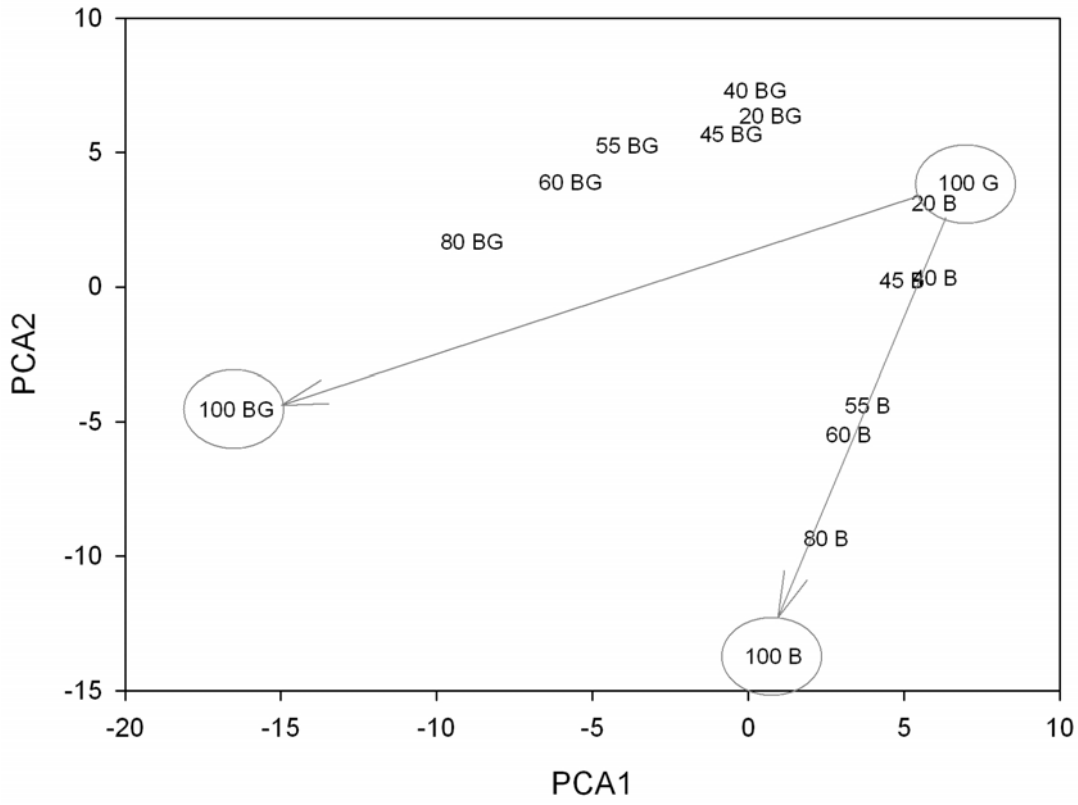

Figure 4.13 PCA score plot for the first two extracted components from the HYPER-$2_{dR/d\lambda}$ dataset for the transition from a brown (diatom) (B) dominated pseudo-community through a green (chlorophyte) (G) dominated pseudo-community to a blue-green (cyanophyte) (BG) dominated pseudo-community. Symbol numbers relate to the approximate percentage abundance (%) of each colour group. Total chlorophyll-a *c*. 200 mg m^{-3}. PCA1 explained 68.0% and PCA2 33.1% of the total statistical variance of the original HYPER-1 dataset.

The PCA transformation of the HYPER-$2_{dR/d\lambda}$ dataset suggests that subtle changes in the shape of $R_{rs}(0,\lambda)$ measurements from lakes, such as those resulting from the presence of diagnostic absorption features, could be potentially related to underlying change in the floristic composition of phytoplankton communities. In shallow lakes, where $R_{rs}(0,\lambda)$ is strongly influenced by the other optically active components (particularly tripton backscattering), the capability to derive taxonomic information from what may be subtle, but diagnostic, changes in the shape of $R_{rs}(0,\lambda)$ signatures, would be highly advantageous. In this context, the use of first-derivative and, indeed, n^{th}-derivative, analysis should be further explored in future studies concerned with the assessment of phytoplankton composition in lakes.

4.5.4 The Effect of Other Optically Active Components

The coincidental presence of other optically active components (e.g. SPIM, SPOM, CDOM) can significantly attenuate the $R_{rs}(0,\lambda)$ signatures of shallow lakes to the extent that attempts to retrieve underlying pigment concentrations from remote sensing data products have often proved problematic (Svab *et al.,* 2005; Tyler *et al.,* 2006). The coincidental presence of other optically active components is likely to have a similar detrimental effect on the extraction of taxonomic information from remotely sensed data. In this study, this was examined through the controlled addition of SPM and water rich in DOC to the pseudo-communities simulated in the mesocosm environment.

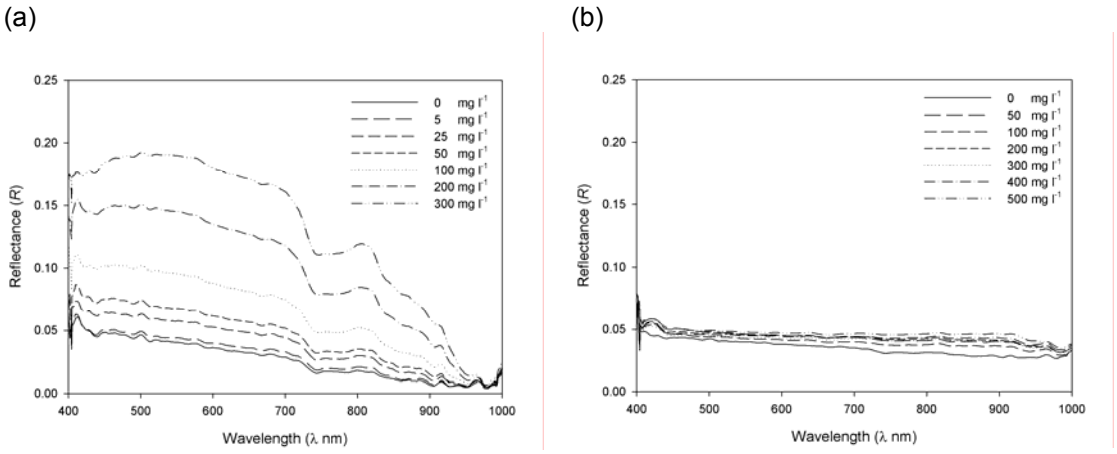

Figure 4.14 The spectral characteristics of (a) SPIM (Lake Balaton) and (b) SPOM (Norfolk Broads) type sediments used in the mesocosm experiments at concentrations of 0-300 mg l^{-1} and 0-500 mg L^{-1} respectively (the axes have been standardised to aid comparability).

The effect of coincidental concentrations of SPM was examined using two sediments of contrasting mineralogy. The spectral characteristics of the inorganic (SPIM-like) and organic (SPOM-like) sediment types used in the mesocosm experiments are depicted in Figure 4.14 at various concentration increments. It is clear that the two sediment types have very different spectral properties. Increases in the concentration of the predominantly inorganic sediment obtained from Lake Balaton resulted in significant increases in $R_{(\lambda)}$ from the mesocosm water column between 400-800 nm. In complete contrast, the more organic sediment from the Norfolk Broads demonstrated almost negligible increases in $R_{(\lambda)}$ relative to the sediment from Lake Balaton. The observed differences in the spectral characteristics of the two sediment

types is likely to be due to the fact the inorganic type sediment from Lake Balaton will invariantly have a far greater backscattering efficiency than the more organic sediment from the Norfolk Broads which, in contrast, promotes strong absorption of the downwelling ambient light field.

The effect of coincidental concentrations of SPIM and SPOM on the spectral response of the brown, green and blue-green colour groups is shown in Figure 4.15. Similarly, the effect of coincidental concentrations of SPIM and SPOM on the spectral response of the mixed pseudo-communities is shown in Figure 4.16. It is notable that the two sediment types have very different effects upon the $R_{(\lambda)}$ measured from the various single and mixed pseudo-communities. The incremental additions of SPIM into the pseudo-communities resulted in large increases in $R_{(\lambda)}$ across the VIS/VNIR spectrum, but interestingly prompted little change in the shape of the spectral signatures. Moreover, and arguably more significantly, the introduction of SPIM into the pseudo-communities can be seen to increase the prominence of the $R_{(\lambda)}$-minima associated with the absorption maxima of chlorophyll-a and C-phycocyanin.

In the literature, it has often been suggested that high and variable concentrations of SPIM can mask pigment-related features in $R_{rs}(0,\lambda)$ spectra and, as such, SPIM is considered to be a major obstacle to the remote-sensing-based estimation of pigment concentrations in lakes (Quibell, 1991; Svab *et al.,* 2005). Indeed, the results presented here demonstrate that SPIM can strongly attenuate the spectral response of lake waters. However, it is notable that the effect of increased SPIM concentration on the $R_{(\lambda)}$ measured from the mesocosm pseudo-communities was largely wavelength-independent and, even at very high concentrations of SPIM, the $R_{(\lambda)}$-minima associated with pigment absorption maxima were preserved. This suggest that, even in lakes with high and variable concentrations of SPIM, it should be possible to resolve the diagnostic $R_{rs}(0,\lambda)$ features associated with phytoplankton pigments and, further, provided the effects of SPIM can be satisfactorily removed, it should remain possible to quantify pigment concentrations under such conditions.

(a) Brown with increasing SPIM

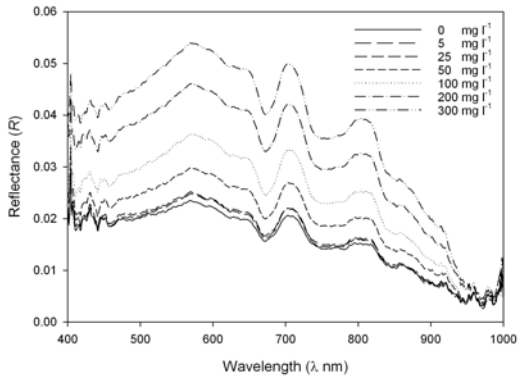

(b) Brown with increasing SPOM

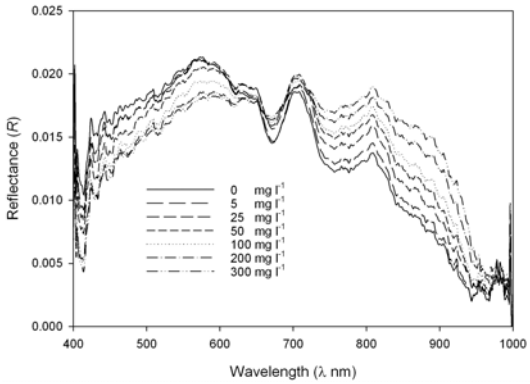

(c) Green with increasing SPIM

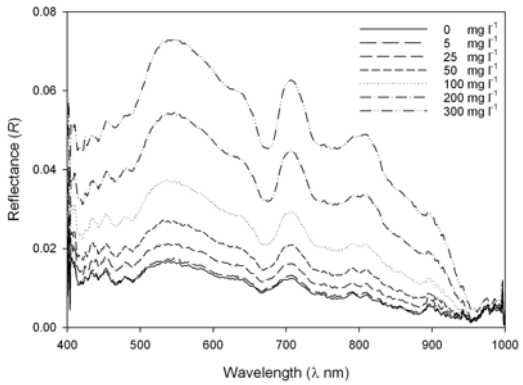

(d) Green with increasing SPOM

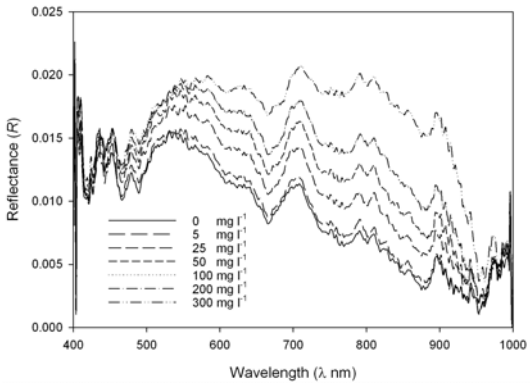

(e) Blue-green with increasing SPIM

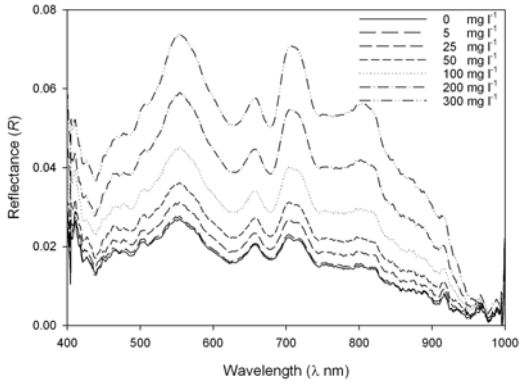

(f) Blue-green with increasing SPOM

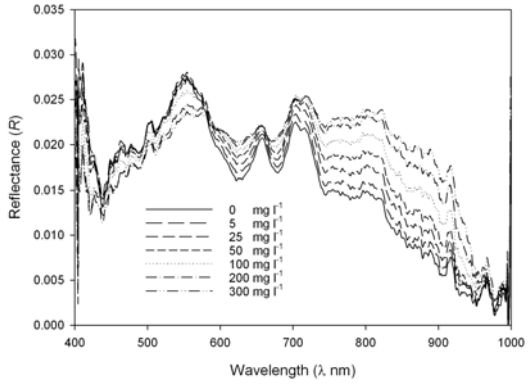

Figure 4.15 The effect of SPIM and SPOM concentrations (0-300 mg L^{-1}) on the spectral response of the brown, green and blue-green colour group taxa.

(a) Brown/Green with increasing SPIM

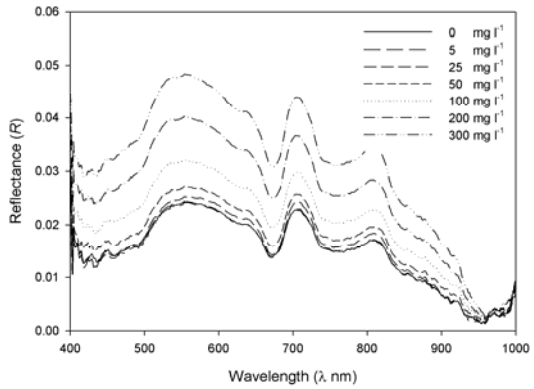

(b) Brown/Green with increasing SPOM

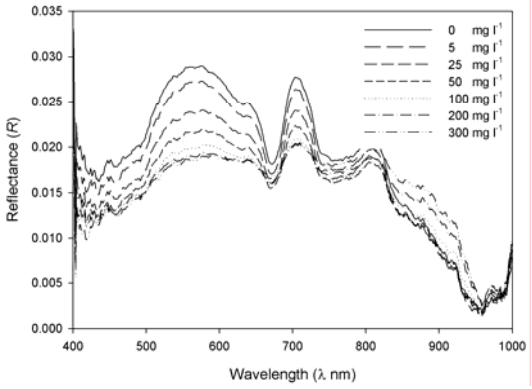

(c) Green/Blue-green with increasing SPIM

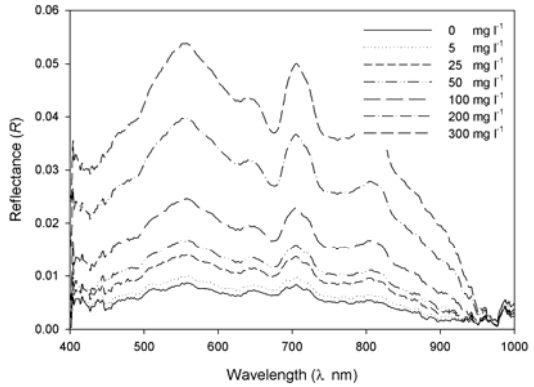

(d) Green/Blue-green with increasing SPOM

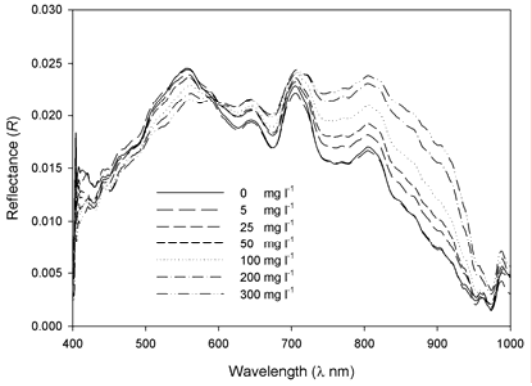

Figure 4.16 The effect of coincidental concentrations of SPIM and SPOM (0-300 mg L^{-1}) on the spectral characteristics of mixed phytoplankton pseudo-communities.

In comparison, the effects of SPOM on the pseudo-communities were somewhat varied. Whilst, the SPIM precipitated almost uniform increases in $R_{(\lambda)}$ across the VIS/VNIR spectrum, the introduction of SPOM into the mesocosm resulted in wavelength-dependent decreases in $R_{(\lambda)}$ < 600 nm (i.e. due to increased absorption). These effects were most evident in the pseudo-community treatments composed of diatoms, where the high $R_{(\lambda)}$ derived from the siliceous cell walls of the algae was increasingly attenuated through the introduction of SPOM. Conversely, at wavelengths > 700 nm, SPOM appeared to promote small increases in $R_{(\lambda)}$ (probably due to the limited inorganic material in the Norfolk Broad sediment). More significantly, in contrast to the effects observed with SPIM, it is evident that coincidental concentrations of SPOM, resulted in radical modifications to the shape of the $R_{(\lambda)}$ signatures. This observation suggests that high and variable concentrations of (non-algal) SPOM may

present a significant barrier to the retrieval of taxonomic information from remote sensing data and, in particular where spectral features in the VIS < 600 nm are vital to the differentiation of taxonomic groups. In fertile shallow lakes, such as the Norfolk Broads, where there is often substantial concentrations of (non-algal) SPOM in the system (often in the form of detritus), the results suggest that it may prove difficult to adequately resolve some taxonomically-significant $R_{rs}(0,\lambda)$ features.

The effect of CDOM on the spectral response of the phytoplankton colour group species (green and blue-green species only) was assessed by suspending the cultured species in humic water from the Western basin of Lake Balaton (Figure 4.17). The concentration of DOC in the water obtained from the Western basin of Lake Balaton was approximately 12.5 mg L^{-1}. The effect of CDOM on the spectral response of the various phytoplankton species is shown in Figure 4.17. It is notable, but not unexpected, that the introduction of CDOM into the pseudo-communities resulted in the strong attenuation of $R_{(\lambda)}$ in the short-wavelength VIS regions of the spectrum. It can be clearly seen that the $R_{(\lambda)}$ spectra of the phytoplankton species are 'flatter' than the comparable signatures measured in the absence of CDOM, particularly at wavelengths < 600 nm where CDOM absorption is most intense (Lindell *et al*., 1999). CDOM also caused severe attenuation of the green peak feature (*c*. 550 nm).

CDOM absorption also had a perceivable impact on the $R_{(\lambda)}$-minimum related to C-phycocyanin absorption and resulted in the feature decreasing in prominence relative to that observed in the absence of CDOM. However, it is notable that the C-phycocyanin related $R_{(\lambda)}$-minimum feature could still be clearly resolved in the humic water. The $R_{(\lambda)}$-minimum related to chlorophyll-a absorption is not affected by the presence of CDOM as it occurs at longer wavelengths (*c*. 680 nm) where CDOM absorption is not intense. Thus, the results suggest that in shallow lakes with high concentrations of CDOM (i.e. dystrophic systems), the resolution of taxonomically significant features < 600 nm may be problematic.

(a) Green with increasing SPIM

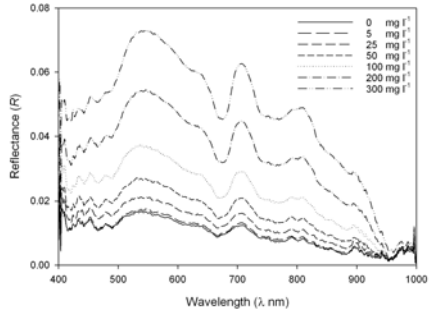

(b) Green with increasing SPIM in humic water

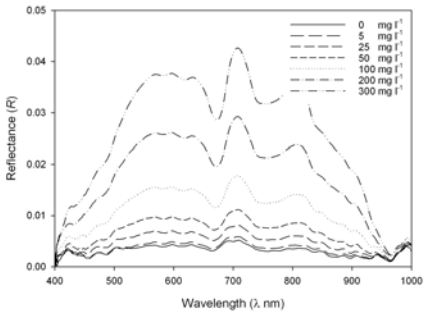

(c) Green with increasing SPOM

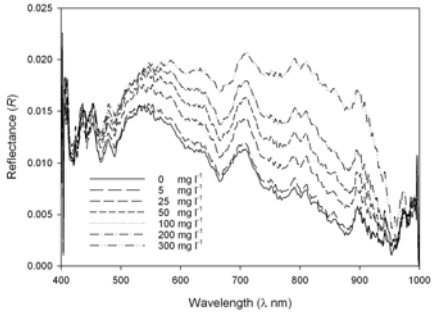

(d) Green with increasing SPOM in humic water

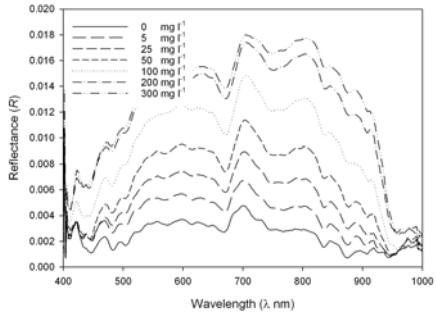

(e) Blue-green with increasing SPIM

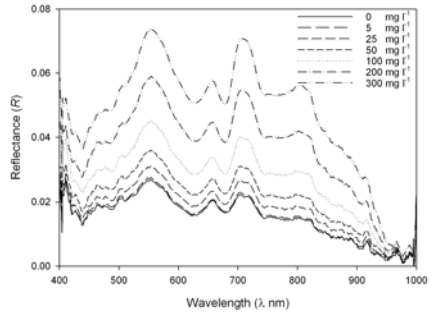

(f) Blue-green with increasing SPIM in humic water

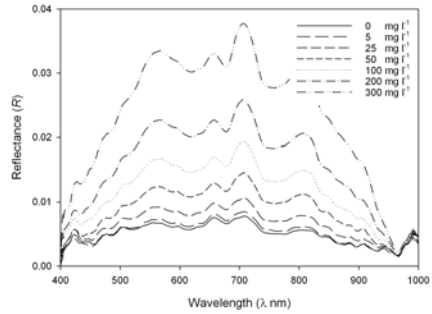

(g) Blue-green with increasing SPOM

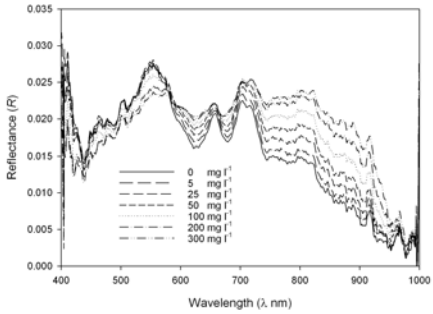

(h) Blue-green with increasing SPOM in humic water

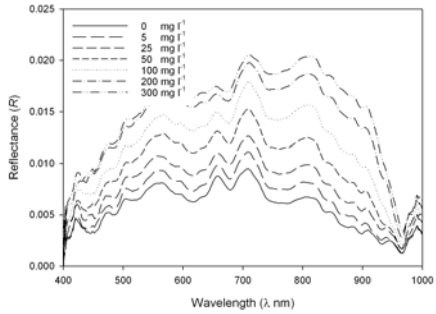

Figure 4.17 The effect of coincidental CDOM (DOC = 12.5 mg L^{-1}) on the spectral signatures of green and blue-green pseudo-communities with varying concentrations of SPIM and SPOM.

4.5.5 The Effect of Variable Sensor Spectral Resolution

The effect of variable sensor resolution on the $R_{(\lambda)}$ signatures of the four 'pure' colour group end-member pseudo-communities is depicted in Figure 4.18. It is evident that sensor spectral resolution is pivotal to the extent to which the various colour group taxa can be differentiated. Sufficient spectral detail is encapsulated within the hyperspectral datasets (HYPER-2, -3, -4, -5) to suggest that the various colour groups are certainly resolvable with data comprised of numerous high resolution (*c*. 5-20 nm) spectral bands. The various colour group taxa would also appear to be spectrally dissimilar in the multispectral SeaWiFS dataset; given that the channel configuration of the SeaWiFS sensor is optimised for ocean colour monitoring, this is perhaps not unexpected. It would appear however that the coarser spectral resolutions of the Landsat TM, IKONOS and ASTER sensors would be prohibitive to the differentiation of the various colour groups given the lack of spectral detail encapsulated in these datasets.

The effect of variable sensor resolution on the hyper- and multi-spectral dR/dλ signatures of the four 'pure' colour group end-member pseudo-communities is shown in Figure 4.19. In similarity to the effects observed on the $R_{(\lambda)}$ signatures of the colour group taxa, the dissimilarity of the dR/dλ signatures was also highly dependent upon the spectral capabilities of the simulated sensors. The hyperspectral dR/dλ datasets appear to retain sufficient spectral information to enable the discrimination of the various colour group taxa. However, as the spectral resolution of the simulated datasets declines, the loss of information would seem to greatly impair the degree to which the various colour groups can be discerned using the first-derivative analysis approach, to the extent that in the datasets of low spectral resolution (i.e. Landsat TM, IKONOS and ASTER) the dR/dλ signatures demonstrate little variation.

The influence of variable sensor spectral resolution on the spectral signatures of the various mixed phytoplankton pseudo-communities for the hyper- and multi-spectral $R_{(\lambda)}$ and dR/dλ datasets are shown in Figure 4.20 and Figure 4.21 respectively. These effects are further examined through the comparison of the score plots and eigenvalues derived from PCA analysis in Figure 4.22 and Figure 4.23; Table 4.5 contains the corresponding component

eigenvalues derived from the PCA analysis. It is even more evident from Figures 4.22 and 4.23 that sensor spectral resolution has a significant effect upon the spectral dissimilarity of the mixed phytoplankton pseudo-communities. The hyperspectral datasets demonstrate the greatest spectral separation between the various pseudo-communities with the end-member pseudo-communities (i.e. 100 B, 100 G, 100 BG) clearly defined. Moreover, the pseudo-communities of intermediate composition can be seen to be distributed in a near linear fashion between these polar end-members.

However, the spectral distinction between the pseudo-communities progressively declines with decreasing spectral resolution to the extent that the various pseudo-communities are no longer discernable in the simulated multispectral Landsat TM, IKONOS and ASTER datasets. At these poorer spectral resolutions, the polar distribution of the 'pure' end-member pseudo-communities in component space is lost and the remaining variability would appear to be merely an artefact of residual differences in $R_{(\lambda)}$ across the spectrum. The clear horseshoe effects apparent in the distribution of the pseudo-communities in component space in the $R_{(\lambda)}$ datasets is further evidence of the loss of spectral separation.

In the same manner, the distribution of pseudo-communities in component space in the $dR/d\lambda$ datasets shows excellent separation between the 'pure' end-members and with improved linearity in the distribution of the intermediate pseudo-communities in the hyperspectral and SeaWIFS $dR/d\lambda$ datasets. However, once the spectral resolution of the simulated sensors declines beyond that of the SeaWiFS satellite, the pseudo-communities are again no longer spectrally distinct.

(a) HYPER-2

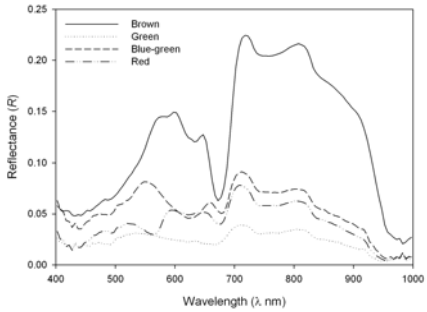

(b) HYPER-3

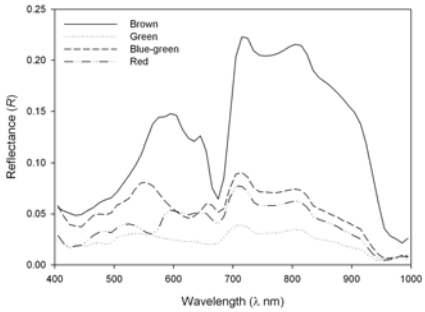

(c) HYPER-4

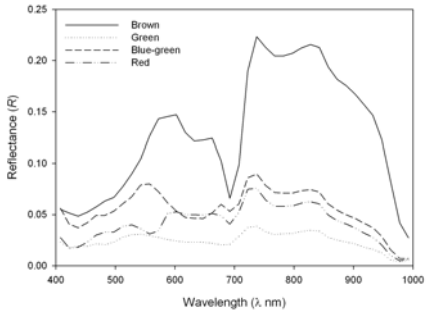

(d) HYPER-5

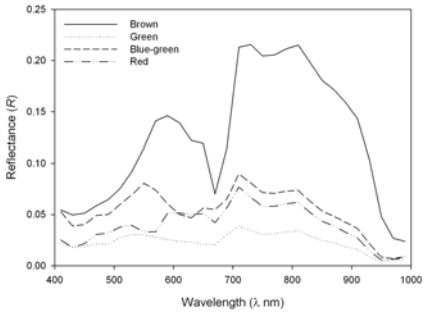

(e) SeaWiFS

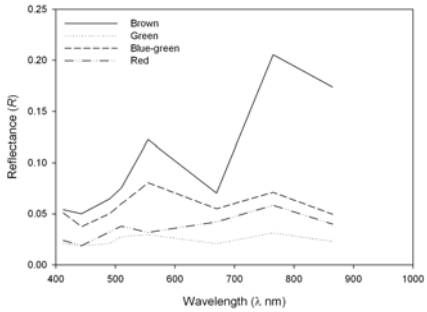

(f) Landsat TM

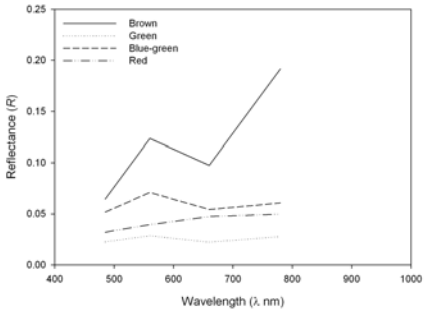

(g) IKONOS

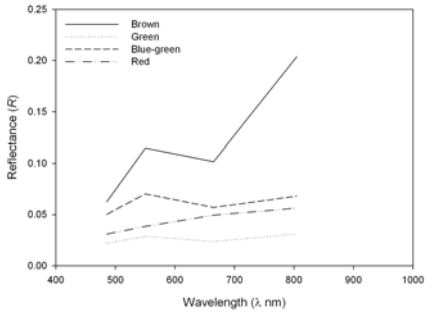

(h) ASTER

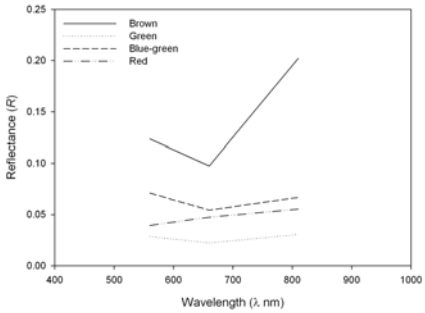

Figure 4.18 The effect of variable sensor spectral resolution: the $R_{(\lambda)}$ hyperspectral and multispectral signatures of the 'pure' colour group end-member pseudo-communities.

(a) HYPER-2$_{dR/d\lambda}$

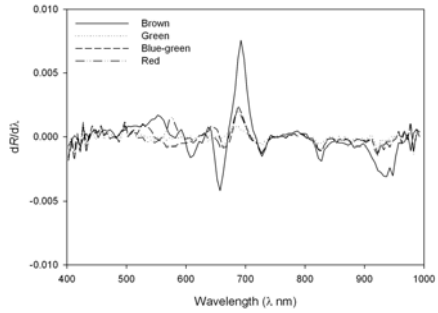

(b) HYPER-3$_{dR/d\lambda}$

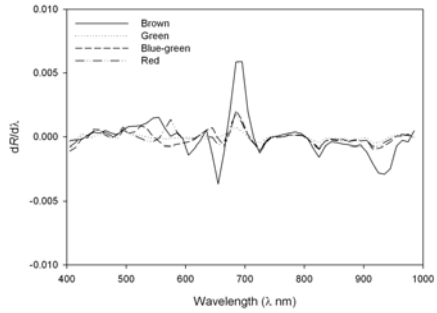

(c) HYPER-4$_{dR/d\lambda}$

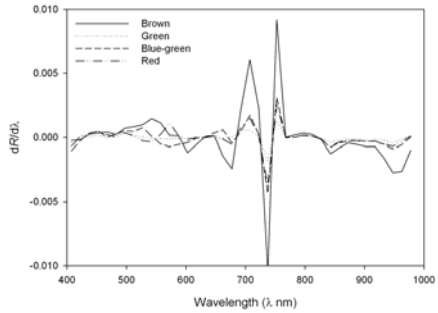

(d) HYPER-5$_{dR/d\lambda}$

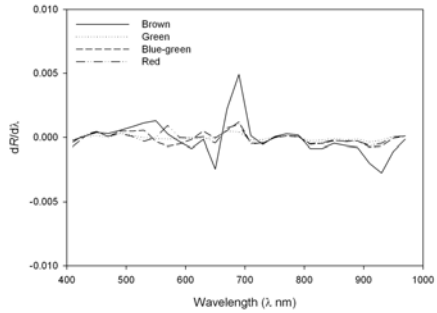

(e) SeaWiFS$_{dR/d\lambda}$

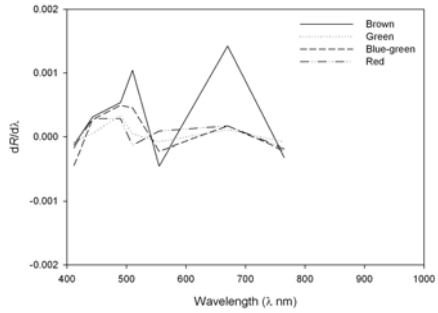

(f) Landsat TM$_{dR/d\lambda}$

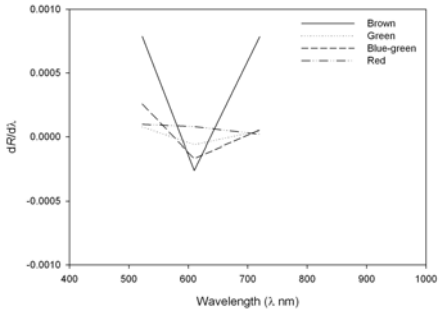

(g) IKONOS$_{dR/d\lambda}$

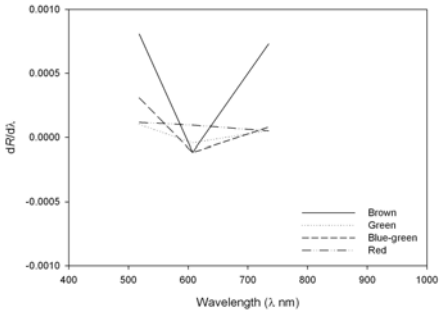

(h) ASTER$_{dR/d\lambda}$

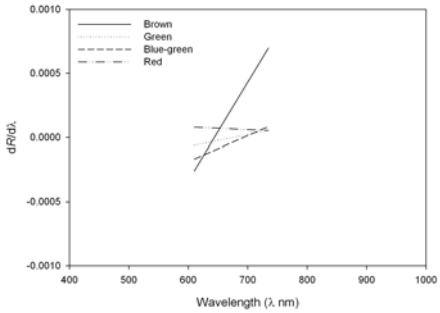

Figure 4.19 The effect of variable sensor spectral resolution: the d*R*/dλ hyperspectral and multispectral signatures of the 'pure' colour group end-member pseudo-communities.

(a) HYPER-2

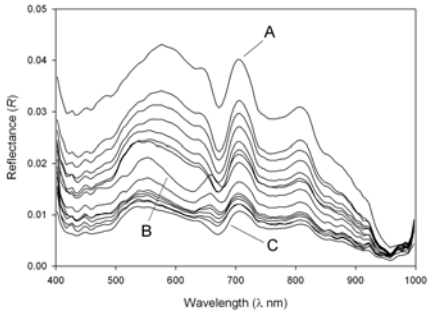

(b) HYPER-3

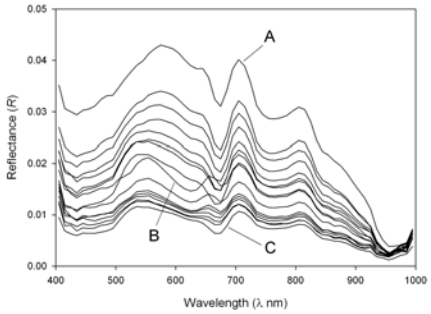

(c) HYPER-4

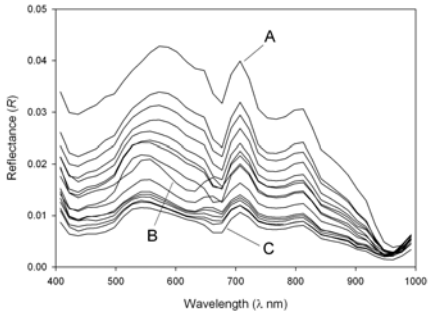

(d) HYPER-5

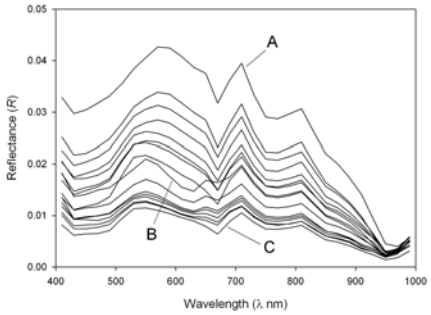

(e) SeaWiFS

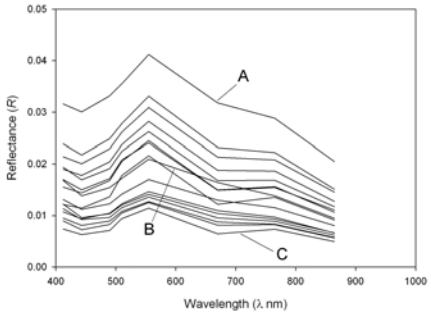

(f) Landsat TM

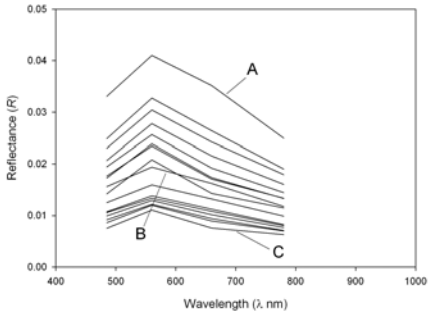

(g) IKONOS

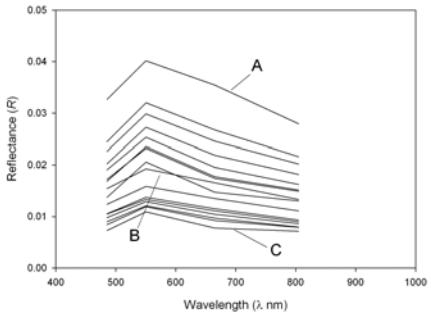

(h) ASTER

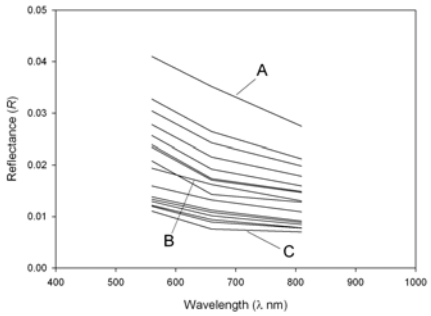

Figure 4.20 The effect of variable sensor spectral resolution: hyperspectral and multi-spectral $R_{(\lambda)}$ signatures of the mixed pseudo-communities (A – 'pure' brown community; B – 'pure' blue-green community; C – 'pure' green community).

(a) HYPER-2$_{dR/d\lambda}$

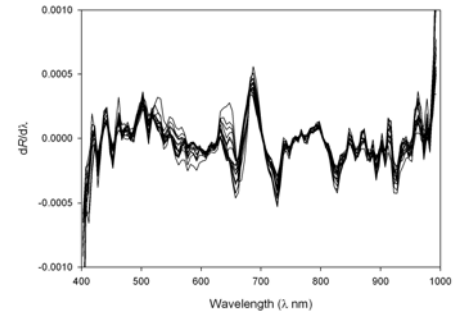

(b) HYPER-3$_{dR/d\lambda}$

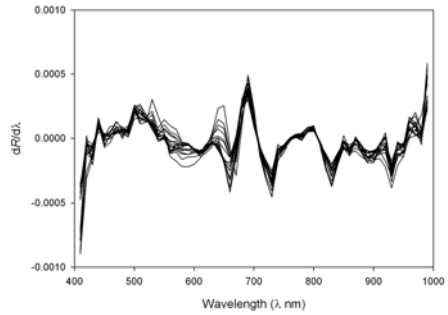

(c) HYPER-4$_{dR/d\lambda}$

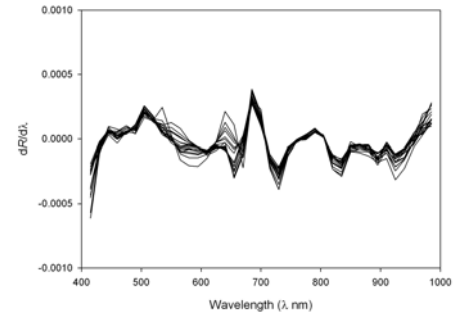

(d) HYPER-5$_{dR/d\lambda}$

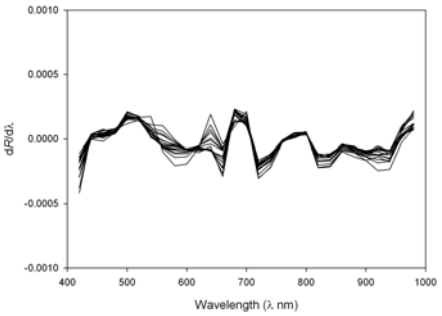

(e) SeaWiFS$_{dR/d\lambda}$

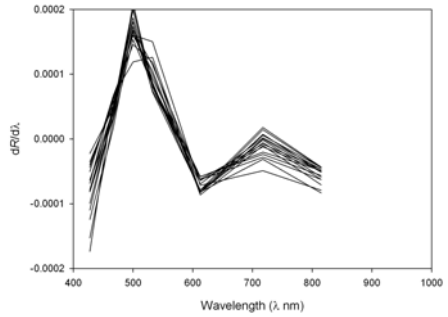

(f) Landsat TM$_{dR/d\lambda}$

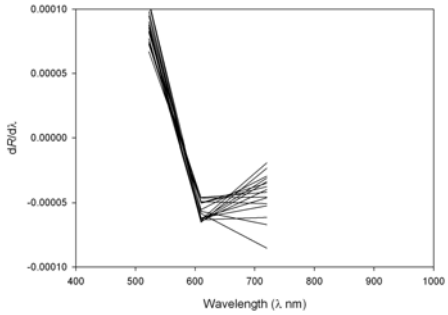

(g) IKONOS$_{dR/d\lambda}$

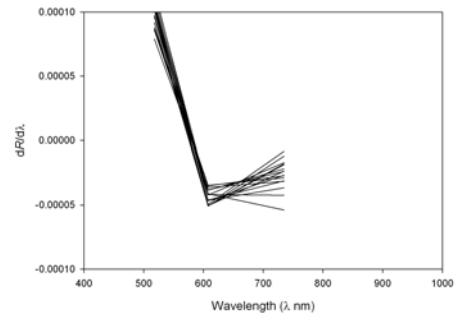

(h) ASTER$_{dR/d\lambda}$

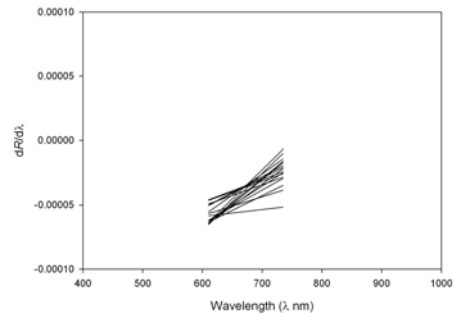

Figure 4.21 The effect of variable sensor spectral resolution: hyperspectral and multispectral d*R*/dλ signatures of the mixed pseudo-communities.

(a) HYPER-2

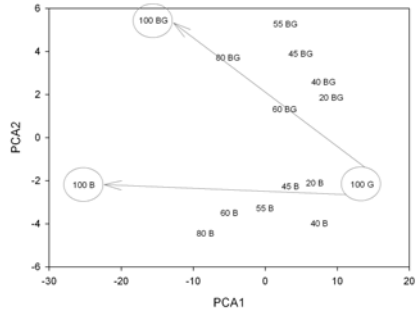

(b) HYPER-3

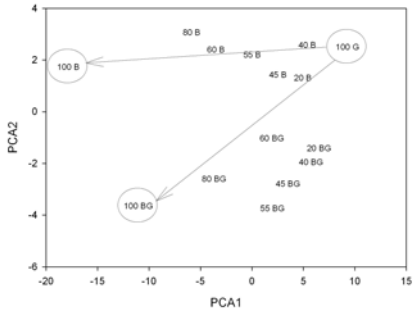

(c) HYPER-4

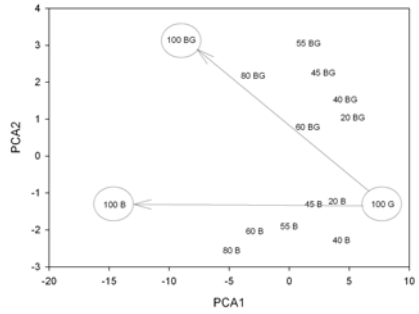

(d) HYPER-5

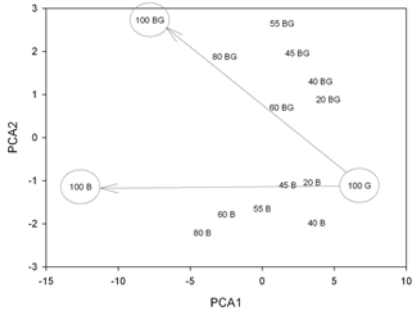

(e) SeaWiFS

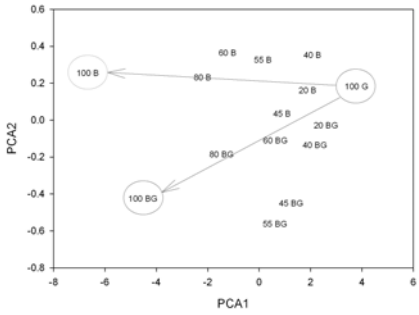

(f) Landsat TM

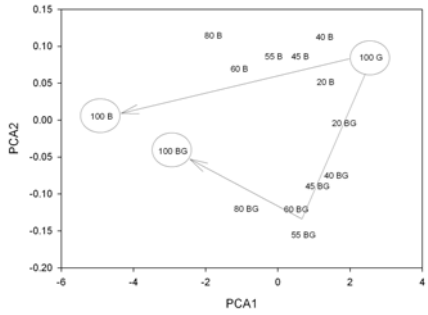

(g) IKONOS

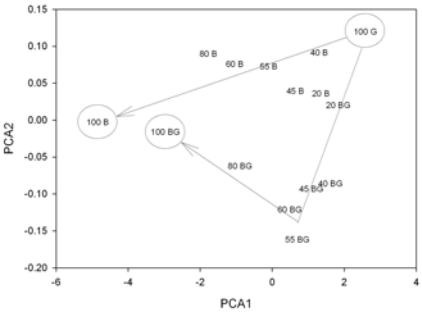

(h) ASTER

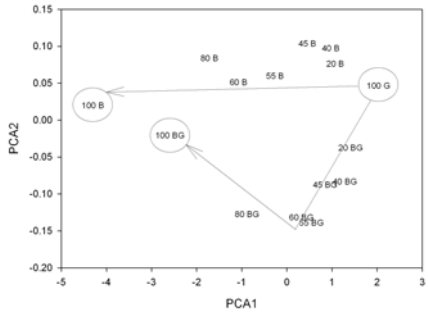

Figure 4.22 PCA score plots for the various simulated hyperspectral and multispectral $R_{(\lambda)}$ datasets derived from the mixed species pseudo-communities. Open circles and vectors indicate spectral trends between end-member pseudo-communities.

(a) HYPER-2$_{dR/d\lambda}$

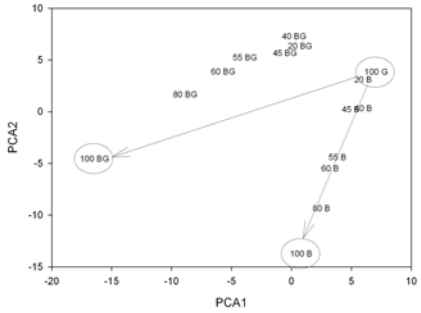

(b) HYPER-3$_{dR/d\lambda}$

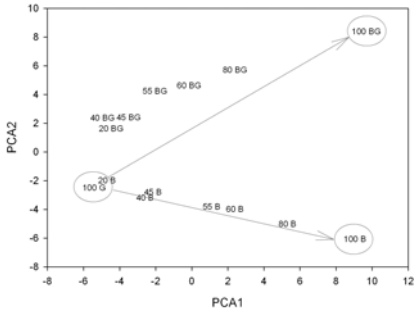

(c) HYPER-4$_{dR/d\lambda}$

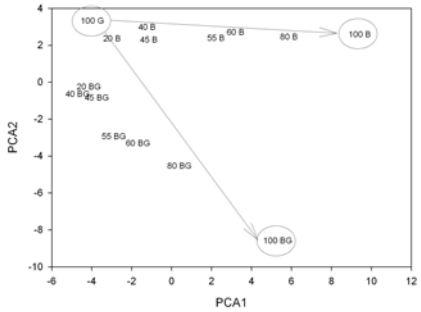

(d) HYPER-5$_{dR/d\lambda}$

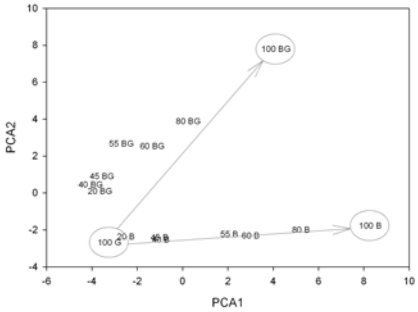

(e) SeaWiFS$_{dR/d\lambda}$

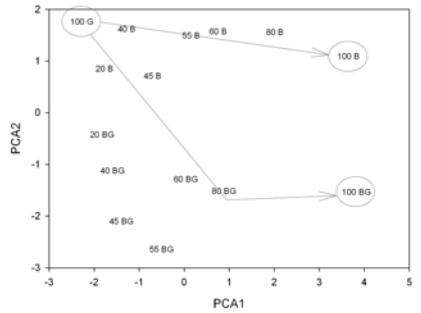

(f) Landsat TM$_{dR/d\lambda}$

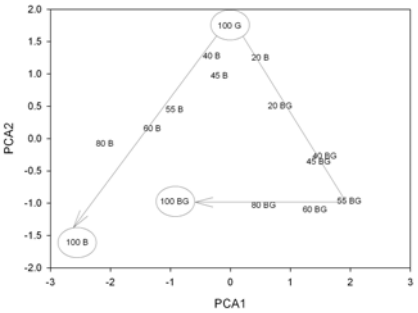

(g) IKONOS$_{dR/d\lambda}$

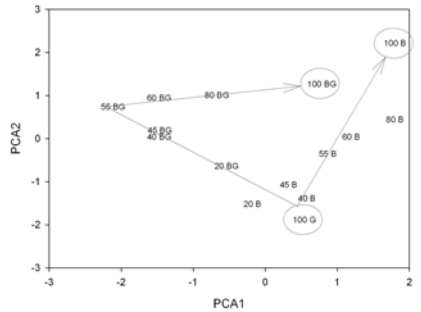

(h) ASTER$_{dR/d\lambda}$

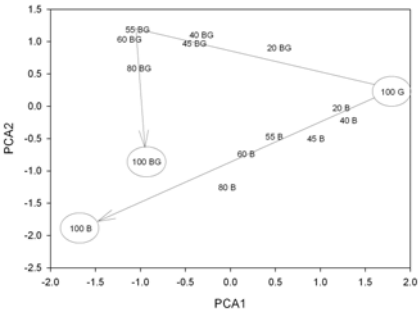

Figure 4.23 PCA score plots for the various simulated hyperspectral and multispectral d*R*/dλ datasets from the mixed species pseudo-communities. Open circles and vectors indicate spectral trends between end-member pseudo-communities.

Table 4.5 Eigenvalues of the first two extracted components derived from the PCA of the simulated $R_{(\lambda)}$ and dR/dλ datasets obtained from the mixed species pseudo-communities and the proportion and cumulative variance explained (%).

	PCA1						PCA2					
	Eigenvalue		Proportion		Cumulative		Eigenvalue		Proportion		Cumulative	
	$R_{(\lambda)}$	dR/dλ	$R_{(\lambda)}$	dR/dλ	$R_{(\lambda)}$	dR/dλ	$R_{(\lambda)}$	dR/dλ	$R_{(\lambda)}$	dR/dλ	$R_{(\lambda)}$	dR/dλ
HYPER-2	105.9	41.6	0.88	0.35	0.88	0.35	12.6	38.7	0.11	0.33	0.99	0.68
HYPER-3	53.0	24.3	0.88	0.41	0.88	0.41	6.3	19.8	0.11	0.34	0.99	0.75
HYPER-4	35.4	18.5	0.88	0.47	0.88	0.47	4.2	12.2	0.11	0.31	0.99	0.79
HYPER-5	26.5	14.0	0.89	0.48	0.89	0.48	3.2	9.5	0.11	0.33	0.99	0.81
SeaWiFS	7.9	3.7	0.98	0.53	0.98	0.53	0.99	2.5	0.01	0.35	0.99	0.88
Landsat	4.0	1.9	0.99	0.63	0.99	0.63	0.01	1.0	0.00	0.35	0.99	0.97
IKONOS	4.0	1.6	0.99	0.52	0.99	0.52	0.01	1.3	0.00	0.44	0.99	0.96
ASTER	3.0	1.1	0.99	0.54	0.99	0.54	0.01	0.91	0.00	0.46	0.99	1.00

It is evident that the spectral differentiation of the various single and mixed pseudo-communities is highly dependent upon the spectral resolution of the dataset. These experimental findings support the work of Kutser *et al*. (2006) who evidenced that the detection of C-phycocyanin in cyanobacterial blooms was not possible with broadband multispectral satellites because the bandset configuration does not permit the resolution of the diagnostic $R_{(\lambda)}$-minimum at *c*. 620-630 nm that is associated with C-phycocyanin. The results obtained here would seem to suggest that, in terms of the necessary sensor specifications, the minimum spectral resolution required to permit any form of taxonomic differentiation would be comparable to that of the SeaWiFS ocean colour satellite. Moreover, it is apparent that the ability to resolve the various colour group species is improved with the utilisation of hyperspectral data. In this context, of the current operational satellite systems, the NASA Hyperion instrument on the EO-1 satellite would seem the most appropriate spaceborne platform from which to pursue this research. Alternatively, the new generation of hyperspectral airborne instruments (e.g. AISA Eagle, HyMap) may also hold potential for the remote sensing of phytoplankton composition in shallow lakes.

4.5.6 MDA-based Classification of Algal Bloom Composition

MDA was used to classify the $R_{(\lambda)}$ and dR/dλ spectra on the basis of dominant phytoplankton composition. The rationale for this approach is that, in the event that quantitative measures of phytoplankton composition cannot be derived from remotely sensed data, it may be possible to

pursue more qualitative, but still informative, methods of assessing phytoplankton community structure in lakes. Similar schemes are currently being pioneered using spectral library classification schemes for the early-detection of HAB in marine and coastal waters (Miller *et al.,* 2006).

Linear MDA, with and without cross-validation analysis, was performed on the multispectral $R_{(\lambda)}$ (SeaWiFS, Landsat TM, IKONOS and ASTER) and mutli- and hyperspectral dR/dλ datasets (HYPER-$3_{dR/d\lambda,}$ HYPER-$4_{dR/d\lambda}$, HYPER-$5_{dR/d\lambda}$ SeaWiFS$_{dR/d\lambda}$, Landsat TM$_{dR/d\lambda}$, IKONOS$_{dR/d\lambda}$ and ASTER$_{dR/d\lambda}$) and the resulting classification accuracies for each sensor were compared (covariance matrices were assumed to be equal). MDA could not be performed on the HYPER-2, HYPER-3, HYPER-4, HYPER-5 and HYPER-$2_{dR/d\lambda}$ datasets because the datasets were too highly correlated following the the subtraction of group means to be included in the MDA model. Cross-validation was used to provide a conservative estimate of the classification accuracy and account for optimistic-apparent-errors incurred when the data to be classified are also used to train the classification model. Six discrete output classes, based upon the dominant species composition of the pseudo-community, were designated arbitrarily prior to analysis and are detailed in Table 4.6.

Table 4.6 The output classes designated for the MDA analysis based upon dominant species composition

Output Class	Class Description
B	Brown taxa dominant
G	Green taxa dominant
BG	Blue-green taxa dominant
R	Red taxa dominant
B-G	Brown and green taxa co-dominant
G-BG	Green and blue-green taxa co-dominant

Non-cross-validated and cross-validated classification accuracies for the $R_{(\lambda)}$ and dR/dλ datasets used in the MDA analysis are shown in Figure 4.24. It is notable that the classification accuracies achieved show significant variations between the respective datasets. The highest classification accuracies were achieved with the hyperspectral dR/dλ datasets (proportion of correct classifications (cross-validated) > 0.9). Notably, the highest classification accuracy was

achieved with the highest spectral resolution first-derivative dataset, HYPER-$3_{dR/d\lambda}$, for which the proportion of correct classifications = 1.00 and 0.92 (no cross validation and cross-validation respectively).

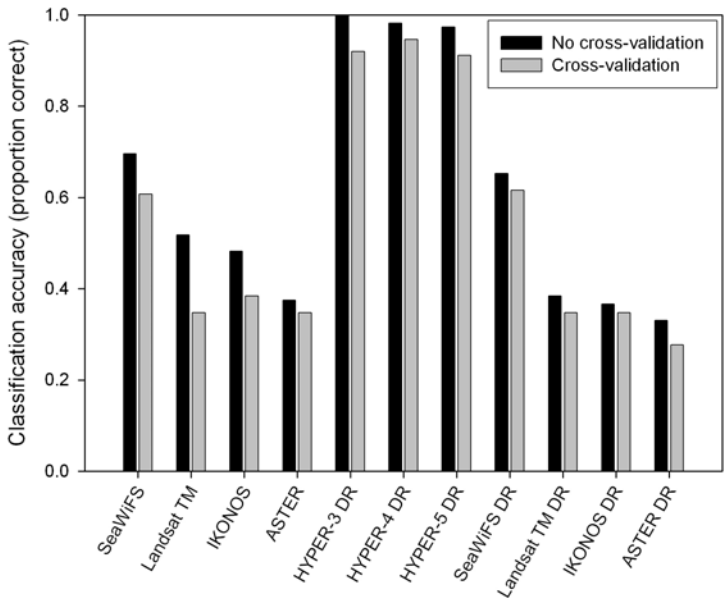

Figure 4.24 Algal bloom species composition MDA classification accuracies for the $R_{(\lambda)}$ and dR/dλ datasets (dR/dλ datasets are denoted by DR) with and without cross-validation.

It is notable that the classification accuracies, for both the $R_{(\lambda)}$ and dR/dλ datasets, decreased with corresponding decreases in the spectral resolution of the sensor to the extent that the proportion of correct classifications for the $ASTER_{dR/d\lambda}$ dataset were as low as 0.33 and 0.28 (no cross-validation and cross-validation respectively). This observation again stresses the importance of utilising high spectral resolution imagery products when attempting to discriminate between phytoplankton communities of varied species composition. Comments to the same effect have been made by previous authors and it would now seem clear that the increased provision of hyperspectral data products will be key to the advancement of techniques to detect phytoplankton community structure using remote sensing data (Kutser *et al.,* 2006).

Classification matrices for selected datasets (SeaWiFS and ASTER) are shown in Table 4.7. Closer examination of the classification matrices derived from the MDA analyses reveals some

clear trends in model performance. The model misclassifications and, in particular, in the case of the multispectral $R_{(\lambda)}$ and dR/dλ datasets, were often associated with pseudo-communities dominated by green chlorophytes. The higher misclassification rate observed for the chlorophyte-dominated pseudo-communities was probably due to the fact that the chlorophyte spectral signature lacks diagnostic $R_{(\lambda)}$-minima associated with biomarker pigment absorption features. This contrasts to the classification results for the pseudo-communities dominated by red cyanophytes, which have a prominent $R_{(\lambda)}$-minimum related to C-phycoerythrin, where no misclassifications were observed.

Table 4.7 Example MDA with cross-validation classification matrices for the SeaWiFS and ASTER datasets.

SeaWiFS		Actual Colour Group						
		B	**G**	**BG**	**R**	**B-G**	**G-BG**	**Total**
Designated Colour Group	**B**	6	2	0	0	0	0	
	G	2	14	10	0	1	0	
	BG	4	10	19	0	1	4	
	R	0	0	0	8	0	1	
	B-G	0	8	1	0	12	0	
	G-BG	0	0	0	0	0	9	
n		12	34	30	8	14	14	**112**
***n* correct**		6	14	19	8	9	9	**78**
Proportion		0.500	0.412	0.633	1.000	0.643	0.643	**0.696**
ASTER								
		B	**G**	**BG**	**R**	**B-G**	**G-BG**	**Total**
Designated Colour Group	**B**	7	8	9	0	0	0	
	G	0	0	4	0	0	2	
	BG	1	6	5	0	0	4	
	R	1	6	9	8	0	0	
	B-G	3	11	3	0	12	1	
	G-BG	0	3	0	0	2	7	
n		12	34	30	8	14	14	**112**
***n* correct**		7	0	5	8	12	7	**39**
Proportion		0.583	0.000	0.167	1.000	0.857	0.500	**0.348**

The MDA classification accuracies were also good for those pseudo-communities dominated, or co-dominated, by blue-green cyanophyte species. This is an important observation as it suggests that an image classification approach could be used to identify the development of cyanobacterial HABs in lakes. The development of such a tool would be pertinent for the rapid and expeditious assessment of HAB development in lakes and other inland waters. The work of Miller *et al*. (2006), whereby a classification model has been developed for algal blooms in coastal waters, indicates that such an approach can enable the rapid diagnosis of algal bloom composition and thus enable the prompt dissemination of information to those charged with the

management of coastal resources and the mitigation of risks associated with HABs. The development of similar approaches for lakes would now seem timely and, with the improved provision of near-real-time hyperspectral data products, increasingly achievable.

4.5.7 Estimating Biomarker Pigment Concentrations

The potential of remote sensing for retrieving concentration estimates of the biomarker pigments fucoxanthin and C-phycocyanin was examined using the data derived from the mesocosm experiments. The HYPER-1 and HYPER-$1_{dR.d\lambda}$ mixed species pseudo-community datasets were amalgamated into four further datasets: (1) mixed species with no SPM, (2) mixed species with SPIM, (3) mixed species with SPOM, and (4) mixed species with SPIM and SPOM. $R_{(\lambda)}$-based indices for the estimation of chlorophyll-a, fucoxathin and C-phycocyanin were derived following the methodology outlined in Dall'Olmo *et al*. (2003) (see Equation 4.2) from the dataset with no SPM background. In order to assess the effect of other bio-optically active components on pigment estimation the derived indices were subsequently validated against the datasets with varying SPM background concentrations.

$$\text{Pigment Content} \propto [(R_{\lambda 1}^{-1} - R_{\lambda 2}^{-1}) \times R_{\lambda 3}] \qquad \textbf{Equation 4.2}$$

Initially, for all pigment indices, the values of $R_{\lambda 2}$ and $R_{\lambda 3}$ were adopted from the chlorophyll-a index proposed by Dall'Olmo *et al*. (2003) ($R_{\lambda 2}$ = 710; $R_{\lambda 3}$ = 750); the optimum value of $R_{\lambda 1}$ for each index was then derived empirically. The values of $R_{\lambda 2}$ and $R_{\lambda 3}$ were then further refined, again in an empirical manner. The initial values of $R_{\lambda 2}$ and $R_{\lambda 3}$ were retained for the fucoxanthin index. The optimum value of $R_{\lambda 2}$ for the C-phycocyanin index was found to be closer to 660 nm (i.e. centred on the peak trailing the C-phycocyanin absorption feature).

The optimum values of $R_{\lambda 1}$ for the chlorophyll-a and C-phycocyanin indices were found to be 670 nm and 630 nm respectively; these wavelengths reflect the position of the $R_{(\lambda)}$-minima associated with the chlorophyll-a and C-phycocyanin absorption maxima and, as such, the selection of these wavelengths intimates towards the existence of an underlying mechanistic basis for the derived indices despite their largely empirical formulation. Indeed, the chlorophyll-a index derived in this instance was identical to the one formulated by Dall'Olmo *et al*. (2003)

using data from CASE II waters which would seem to suggest that the mesocosm experiments were providing a relatively accurate replication of the spectral characteristics of natural shallow lake waters.

In the instance of fucoxanthin, because no distinct $R_{(\lambda)}$–minima related to pigment absorption could be identified, $R_{\lambda 1}$ was instead centred on the green peak $R_{(\lambda)}$-maximum (575 nm) that was previously noted to respond to variations in diatom abundance; centring $R_{\lambda 1}$ in the region of the *in vivo* fucoxanthin absorption maximum (450-470 nm) did not result in the derivation of an effective index for pigment quantification.

The dR/dλ indices were also derived using a semi-empirical approach. In similarity to the $R_{(\lambda)}$ indices, the dR/dλ indices exploited wavelengths closely associated with the *in-vivo* pigment-specific absorption maxima of chlorophyll-a (670 nm) and C-phycocyanin (645 nm) and, for the dR/dλ fucoxanthin index, the green peak $R_{(\lambda)}$-maximum (565 nm). dR/dλ indices have been shown to be effective in reducing the attenuating effects of (non-algal) SPM on the retrieval of pigment concentrations from remotely sensed data (Malthus & Dekker, 1995; Han & Rundquist, 1997; Han, 2005).

In this instance, dR/dλ indices were examined as a means of minimising the effect of SPIM and SPOM on the estimation of pigment concentrations. The chlorophyll-a dR/dλ index used here is similar to those described by Malthus & Dekker (1995) which again suggests the mesocosm experiments were emulating the optical characteristics of natural shallow lakes.

Table 4.8 Correlation coefficients (*r*) for the relationships between the spectral reflectance and derivative reflectance indices and pigment concentrations in the mesocosm pseudo-communities (chlorophyll-a = Chl-a; fucoxanthin = Fuco; C-phycocyanin = C-PC; N/S = not significant).

			SPM Background											
			NONE			**SPIM**			**SPOM**			**SPIM and SPOM**		
	Target Pigment	**Optimum Index**	**Chl-a**	**Fuco**	**C-PC**	**Chl-a**	**Fuco**	**C-PC**	**Chl-a**	**Fuco**	**C-PC**	**Chl-a**	**Fuco**	**C-PC**
$R_{(\lambda)}$	Chl-a	$[(R_{675}^{-1} - R_{720}^{-1}) \times R_{750}]$	0.93			0.71			0.85			0.68		
	Fuco	$[(R_{575}^{-1} - R_{720}^{-1}) \times R_{750}]$		0.96			0.87			0.42			0.58	
	C-PC	$[(R_{630}^{-1} - R_{660}^{-1}) \times R_{750}]$			0.89			N/S			N/S			N/S
$dR/d\lambda$	Chl-a	$[dR/d\lambda_{670}]$	0.95			0.58			0.70			0.50		
	Fuco	$[dR/d\lambda_{565}]$		0.95			0.92			0.88			0.67	
	C-PC	$[dR/d\lambda_{645}]$			0.97			N/S			N/S			N/S

The correlation coefficients for the association between the derived spectral indices and the measured pigment concentrations for the various datasets are detailed in Table 4.8. The $R_{(\lambda)}$ and dR/dλ indices demonstrated strong correlations with the measured pigment concentrations in the dataset derived from treatments with no SPIM or SPOM. The correlation coefficients for the $R_{(\lambda)}$ and dR/dλ indices derived for chlorophyll-a and fucoxanthin were very similar (r = 0.93-0.96). However, in the case of C-phycocyanin, a marginally stronger correlation was observed for the dR/dλ index (r = 0.97) than the $R_{(\lambda)}$-based index (r = 0.89). The least-squares regression relationships between the dR/dλ indices and the measured pigment concentrations are shown in Figure 4.25.

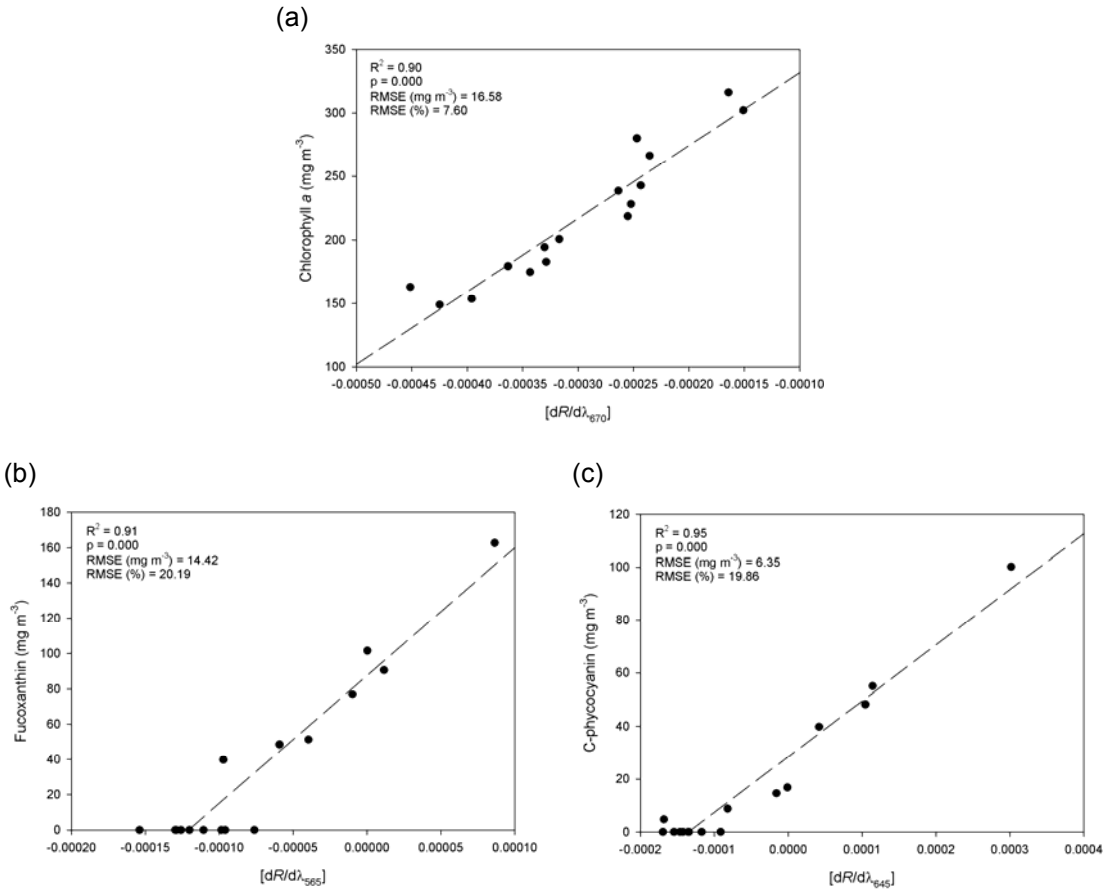

Figure 4.25 The regression relationships between the optimum first-derivative indices and the measured concentrations of the (a) chlorophyll *a*, (b) fucoxanthin and (c) C-phycocyanin.

The effect of SPM on the relationship between the derived spectral indices and the measured pigment concentrations was examined by validating the indices against the measurements obtained from mesocosm experiments involving variable concentrations of SPIM and SPOM.

The results demonstrate that the co-incidental presence of SPM, in the form of SPIM or SPOM, can have significant effects upon the relationships between both $R_{(\lambda)}$ and dR/dλ indices and measured pigment concentrations. The most marked effect was observed for the correlations between the $R_{(\lambda)}$ and dR/dλ indices and the concentration of C-phycocyanin; no significant relationships were observed with either index for measurements made from treatments with background concentrations of SPM. SPOM also had a marked negative effect on the correlation between the $R_{(\lambda)}$-based index and fucoxanthin; this is perhaps understandable given that SPOM absorption is high at the wavelengths used in the fucoxanthin index. In contrast, the fucoxanthin dR/dλ index still demonstrated a reasonable correlation with the measured fucoxanthin concentration with a coincidental background of either SPIM or SPOM. However, when both SPIM and SPOM were present, none of the indices ($R_{(\lambda)}$ or dR/dλ) demonstrated significant correlations with the measured concentrations of chlorophyll-a, fucoxanthin or C-phycocyanin.

The effect of the SPM on correlations between the spectral and pigment data was probably accentuated in the mesocosm experiments given the magnitude of the SPM concentration gradient used (0-300 mg L^{-1}). Nevertheless, these results provide further evidence that high and variable concentrations of SPM can significantly affect the potential retrieval of pigment concentrations using remote sensing data in CASE II waters (Svab *et al.,* 2005; Tyler *et al.,* 2006). In those treatments where a single sediment type was present, the $R_{(\lambda)}$ and dR/dλ indices did demonstrate reasonable correlations with the measured pigment concentrations sufficient to suggest that the remote-sensing-based detection of phytoplankton community structure would not be preclude in such waters. However, on the evidence of the mesocosm experiments, the attenuating effects of (non-algal) SPM would seem to greatest in waters with variable concentrations of both SPIM and SPOM; this was likely due to strong, wavelength-independent, absorption and backscattering effects. This may preclude the detection of community composition in some shallow lakes and other inland waters. It is acknowledged that the empirically-based indices derived from the mesocosm experiments may not be appropriate for the retrieval of accessory pigment concentrations in natural waters. However, more importantly, these experimental results clearly demonstrate that the remote sensing based

determination of phytoplankton community composition, albeit at a broad colour-group level, is possible with hyperspectral data products. In this context, further research in natural lake systems is now needed and, indeed, timely with respect to EU WFD requirements.

4.5.8 Norfolk Broads Validation

4.5.8.1 $R_{rs}(0+,\lambda)$ and $dR/d\lambda$ Algorithms

The logical progression of the mesocosm experiments was to examine if algorithms for biomarker pigment estimation could be developed using data from shallow lakes. This was pursued through two shipboard hyperspectral spectrometry cruises conducted on the 22 June 2005 and 29 August 2005 in the Norfolk Broads (UK). Relations between the measured concentrations of fucoxanthin (29 August 2005) and C-phycocyanin (22 June 2005; 29 August 2005) and $R_{rs}(0+,\lambda)$ measurements were examined using empirically and semi-empirically optimised $R_{rs}(0+,\lambda)$ and $dR/d\lambda$ indices for the estimation of the various pigment concentrations. The correlations observed between the measured concentrations of chlorophyll-a, fucoxanthin and C-phycocyanin in the various Broads sampled during the two sampling cruises are detailed in Tables 4.9 and 4.10.

Table 4.9 Correlation matrix (*r*) for the association between pigment concentrations in the various Broads sampled during the two cruises; <*n* – no correlation due to limited number of observations; * denotes missing data. Chlorophyll-a = Chl-a, fucoxanthin = Fuco, C-phycocyanin = C-PC (significant correlations are depicted in bold font; 95% confidence level).

		Hickling, Horsey and Heigham Sound			**Martham**			**Barton**		
		Chl-a	**Fuco**	**C-PC**	**Chl-a**	**Fuco**	**C-PC**	**Chl-a**	**Fuco**	**C-PC**
22 June 2005	**Chl-a**	-	*	0.206	-	*	<*n*	-	*	0.267
	Fuco	*	-	*	*	-	*	*	-	*
	C-PC	0.206	*	-	<*n*	*	-	0.267	*	-
29 August 2005	**Chl-a**	-	**0.908**	0.730	-	**0.955**	0.661	-	0.210	0.421[†]
	Fuco	**0.908**	-	0.711	**0.955**	-	0.688	0.210	-	-0.10
	C-PC	0.730	0.711	-	0.66	0.688	-	0.421[†]	-0.1	-

[†]If samples from Barton Turf (cyanobacterial scum) are removed from the analysis *r* = **0.927**

Table 4.10 Correlation matrix (*r*) for the association between pigment concentrations for all stations during the two lake sampling cruises. (Significant correlations are depicted in bold font; $p \leq 0.05$ at the 95% significance level).

		Chl-a	Fuco	C-PC
22 June 2005 *n* = 40	**Chl-a**	-	*	0.077
	Fuco	*	-	*
	C-PC	0.077	*	-
29 August 2005 *n* = 23	**Chl-a**	-	**0.678**	**0.726**
	Fuco	**0.678**	-	**0.572**
	C-PC	**0.726**	**0.572**	-

The best-fit least-squares regression algorithms for the estimation for fucoxanthin and C-phycocyanin for each lake sampling cruise are detailed in Table 4.11. It was again notable that the optimum algorithm formulation for the retrieval of biomarker pigment concentrations varied between sampling occasions. The relationship between the optimum retrieval index for C-phycocyanin, $[R_{rs}(400)/R_{rs}(637.5)]$, and the measured concentration of C-phycocyanin on 22 June 2005 provided encouraging results ($R^2 = 0.682$). However, this relationship was only valid for C-phycocyanin concentrations < 100 mg m^{-3}. The optimum $dR/d\lambda$ index, $[dR/d\lambda_{518}]$, demonstrated a weaker relationship with the measured concentration of C-phycocyanin ($R^2 = 0.612$). Moreover, it is not clear why the optimum $dR/d\lambda$ relationship occurred at 518 nm as C-phycocyanin absorption is low at this wavelength. The lack of a mechanistic underpinning suggests the correlation may have been somewhat spurious and thus the derived index may lack robustness when applied to other datasets.

Table 4.11 The optimum empirical and semi-empirical $R_{rs}(0+,\lambda)$ and $dR/d\lambda$ retrieval indices for the estimation of the biomarker pigments fucoxanthin (Fuco) and C-phycocyanin (C-PC) (NS = not significant at the 95% probability level).

	Pigment	Index (x)	*n*	R^2	Least-Squares Best-fit Regression Model
22 June 2005	C-PC	$[R_{rs}(400)/R_{rs}(637.5)]$	17*	0.682	-82.375x + 99.613
		$[dR/d\lambda_{518}]$		0.612	135935x + 6.5304
29 August 2005	Fuco	$[R_{rs}(710)/R_{rs}(470)]$	11	NS†	NS
		$[dR/d\lambda_{703.5}]$		0.903	18583x + 7.29
	C-PC	$[R_{rs}(705)/R_{rs}(638.5)]$	11	0.959	185.22x -168.88
		$[dR/d\lambda_{650}]$		0.885	790392x + 43.125

*Three sampling stations removed where C-PC > 100 mg m^{-3}
†The removal of the Hickling stations resulted in $R^2 = 0.938$ (n = 7)

The least-squares regression relationships were much improved for the 29 August 2005 dataset. The $[R_{rs}(705)/R_{rs}(638.5)]$ index demonstrated a strong relationship with the measured

concentration of C-phycocyanin (R^2 = 0.959). This relationship is depicted in Figure 4.26. It must be noted that the coefficient of determination was biased somewhat by the high C-phycocyanin concentration encountered at one sampling station (*c*. 138.76 mg m^{-3}) located on Barton Broad where a dense bloom of *Microcystis aeruginosa* had developed. Nonetheless, even with this extreme value removed, the coefficient of determination derived for the remaining data points was still R^2 = 0.856.

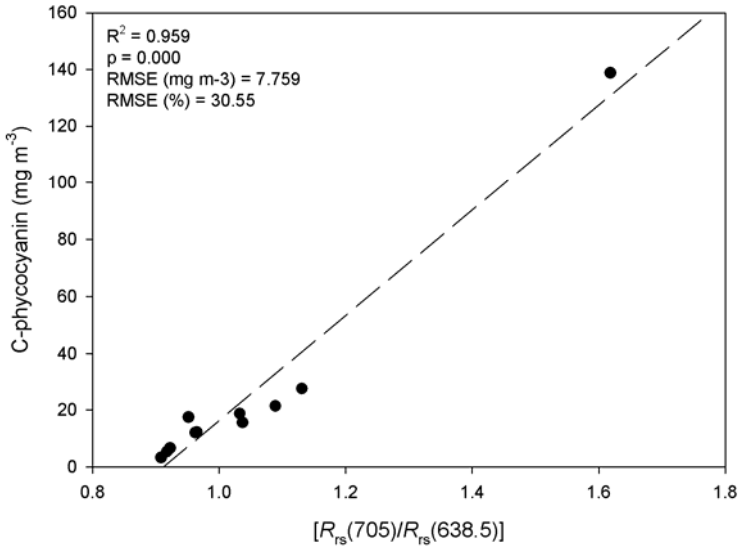

Figure 4.26 The linear regression relationship between [$R_{rs}(705)/R_{rs}(638.5)$] and the measured concentration of C-phycocyanin in the Norfolk Broads on 29 August 2005 (dashed lines represent 95% confidence intervals for the regression equation).

The fact that the [$R_{rs}(705)/R_{rs}(638.5)$] index exploits the local $R_{rs}(0+,\lambda)$ minimum associated with the *in vivo* C-phycocyanin absorption maximum (638.5 nm) suggests that there is an important mechanistic justification to the efficacy of this particular index for the estimation of C-phycocyanin. Limited cell counts (courtesy of the Environmental Agency) performed adjacent to some of the stations sampled in Barton Broad provide some support for the use of C-phycocyanin as a quantitative biomarker for cyanobacteria in this instance (Table 4.12).

The optimum $dR/d\lambda$ index, [$dR/d\lambda_{650}$], also demonstrated a good relationship with the measured concentration of C-phycocyanin (R^2 = 0.885) and the fact that the index also exploited changes in the $dR/d\lambda$ spectra adjacent to the C-phycocyanin absorption maximum again implies there is a sound mechanistic basis to the construction of this index.

Table 4.12 C-phycocyanin concentrations (29 August 2005) and *Microcystis aeruginosa* cell counts (29 August 2005) for geographically equivalent sampling stations on Barton Broad (Cell count data courtesy of the Environment Agency).

	Location of sampling stations		
	B1 – Barton Turf	**B3 – Barton Broad**	**B7 – Gay's Staithe**
C-phycocyanin (mg m^{-3})	138.76	86.61	46.55
***M. aeruginosa* (colonies ml^{-1})**	1000	600	130

The robustness of the optimum C-phycocyanin algorithm derived from the 29 August 2005 lake sampling cruise was validated against the dataset obtained from the 22 June 2005 lake sampling cruise. The calculated RMSE for the estimation of C-phycocyanin concentrations on the 22 June 2005 using the optimum 29 August 2005 algorithm was 35.81 mg m^{-3} (R^2 = 0.001). Thus, it would appear that the 29 August 2005 C-phycocyanin algorithm was, to an extent, season specific. Variations in the bio-optical properties of the various lakes sampled during the 22 June 2005 and 29 August 2005 cruises (e.g. pigment concentrations SPM, benthic vegetation) may account for the lack of algorithm transferability in this instance and, in particular, the masking effect incurred by other bio-optically-active pigments (chlorophyll-a, chlorophyll-b) at low C-phycocyanin concentrations (Simis *et al.,* 2007).

Table 4.13 Biomarker pigment to total chlorophyll-a concentration ratios measured at stations across the various Broads during the two sampling cruises. Hickling Broad data also includes samples from Heigham Sound and Horsey Mere (C-PC = C-phycocyanin; Fuco = Fucoxanthin).

		Chlorophyll-a					
		Hickling		Martham		Barton	
		Mean	Range	Mean	Range	Mean	Range
22 June 2005	**C-PC**	2.49	1.42-3.31	2.39	1.3-3.5	0.55	0.21-1.15
31 August 2005	**Fuco**	0.16	0.09-0.20	0.87	0.58-1.54	0.26	0.14-0.49
	C-PC	1.11	0.80-1.36	2.10	1.01-4.2	1.31	0.54-2.05

The estimation of fucoxanthin concentrations using the $R_{rs}(0+,\lambda)$ spectral data was more problematic and, for the 29 August 2005 cruise, no significant relations were identified using the complete dataset. However, further analysis revealed that if the data from sampling stations located on Hickling Broad were removed from the analysis then the [$R_{rs}(710)/R_{rs}(470)$] index demonstrated an excellent relationship with the measured concentration of fucoxanthin (R^2

=0.938) (Figure 4.27). The rationalisation for removing the Hickling Broad data is based upon the fact that the fucoxanthin to chlorophyll-a ratio (fuco:chl-a) was significantly lower on Hickling Broad relative to that observed in Heigham Sound, Horsey Mere, Martham North Broad and Barton Broad (mean fuco:chl-a measured at Hickling stations = 0.16; mean fuco:chl-a measured on remaining stations = 0.44) (Table 4.14). This may imply that the relative concentration of the biomarker pigments to the total chlorophyll-a concentration may affect the potential detection and retrieval of pigment concentrations from remotely sensed data. In similarity, Simis *et al*. (2007) noted that the relative concentrations of chlorophyll-a and chlorophyll-b effect the accuracy of estimation of C-phycocyanin.

The fucoxanthin index [$R_{rs}(710)/R_{rs}(470)$] was also strongly correlated with the concentration of chlorophyll-a (R^2 = 0.903) (although marginally less so than fucoxanthin) which makes it difficult to establish whether the index was actually sensitive to the presence of fucoxanthin, or that the derived relationship was simply due to high co-variance between chlorophyll-a and fucoxanthin during the 29 August 2005 cruise. Given that both pigments have prominent absorption maxima in the *c*. 470 nm region, it is difficult to establish the validity of this index.

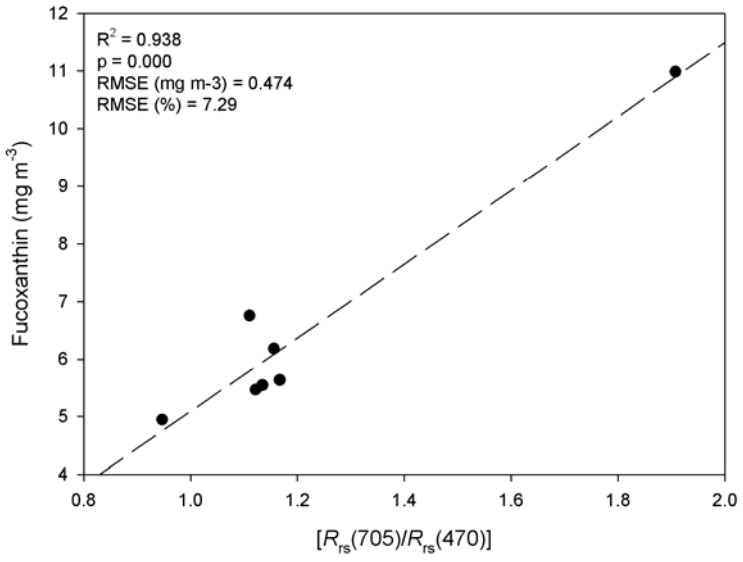

Figure 4.27 The linear regression relationship between [$R_{rs}(710)/R_{rs}(470)$] and the measured concentration of fucoxanthin in the Norfolk Broads (except Hickling Broad stations) on 29 August 2005 (dashed lines represent 95% confidence intervals for the regression equation).

The results obtained here, although somewhat tenuous, indicate that the retrieval of fucoxanthin concentrations may be possible from remotely sensed data. Similar evidence is emerging from ocean colour remote sensing. Hoepffner & Sathyendranath (1992) and Hoepffner & Sathyendranath (1993) noted that changes in the fucoxanthin:chlorophyll-a ratio can precipitate changes in blue/green $R_{rs}(0+,\lambda)$ band-ratios by a factor of 6 in oceanic waters. Comparable observations are also reported in Sathyendranath *et al*. (2001; 2004; 2005). However, further work will be needed to fully establish if the estimation of fucoxanthin is possible in lakes using $R_{rs}(0+,\lambda)$ and $dR/d\lambda$ spectra.

4.5.8.2 Continuum-Removed Algorithms

The efficacy of algorithms based on indices derived from continuum-removed ($R'_{(\lambda)}$) spectra were also evaluated for estimating C-phycocyanin and fucoxanthin pigment concentrations. The $R'_{(\lambda)}$ spectra of the $R_{rs}(0+,\lambda)$-minimum associated with C-phycocyanin absorption from the spectral datasets acquired during the cruises conducted on 22 June 2005 and 29 August 2005 are shown in Figure 4.28. The continua were fitted using start and end points of 580 nm and 650 nm respectively. It is evident from Figure 4.26 that the nature of the $R_{rs}(0+,\lambda)$-minimum demonstrated marked changes, in terms of its general form and dimensions, in relation to the variance in the concentration of C-phycocyanin encountered at the various sampling stations.

(a) 22nd June 2005 (b) 29 August 2005

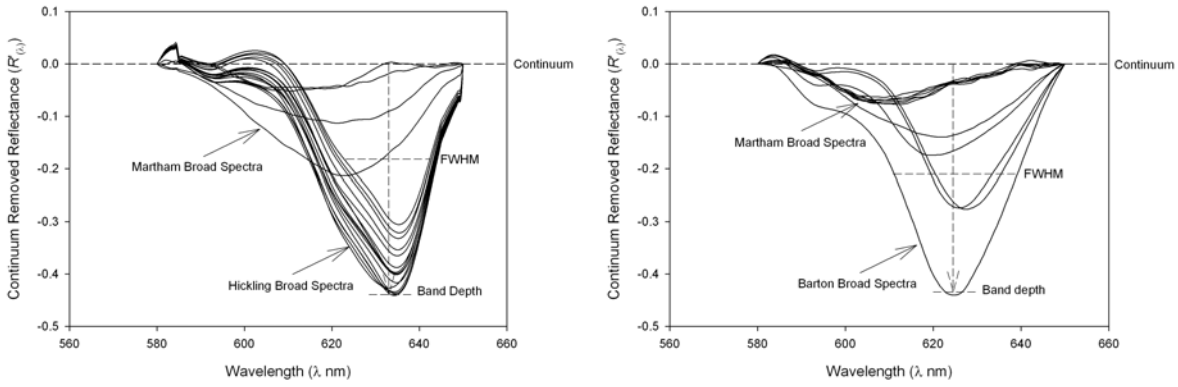

Figure 4.28 Continuum-removed spectra ($R'_{(\lambda)}$) of the C-phycocyanin absorption feature from (a) the 22 June 2005 and (b) the 29 August 2005 cruises.

It is apparent that as the concentration of C-phycocyanin increased from the lower concentrations encountered in Martham North Broad to the higher concentrations found in Hickling Broad and Barton Broad, the depth, width and area of the C-phycocyanin absorption feature also increased correspondingly. $R'_{(\lambda)}$ indices ([$R'_{(\lambda,\ MAX)}$]; [$R'_{(650)}/R'_{(\lambda,\ MAX)}$]; [$R'_{(\lambda,\ FWHM)}$]; [$CRDR_{(\lambda)}$]) (see Chapter 3, Section 3.4.3 for more detailed information) designed to exploit the changes in the dimensions of the C-phycocyanin absorption feature were derived from the spectral datasets and least-squares regression analyses were used to investigate their ability to retrieve estimates of C-phycocyanin concentrations.

Table 4.14 The regression relationships between the continuum-removed indices and the measured concentration of C-phycocyanin for the cruises conducted on 22 June 2005 and 29 August 2005 and for the combined datasets. (Significant relationships are depicted in bold; 95% confidence level; N/S = not significant).

	Index (x)	*n*	R^2	Best-fit Least-Squares Regression Model
22 June 2005	$R'_{(\lambda,\ MAX)}$	17	0.417	$3.0734e^{1.9447x}$
	$R'_{(650)}/R'_{(\lambda,\ MAX)}$		0.400	$70.647e^{-0.024x}$
	$R'_{(\lambda,\ FWHM)}$		0.507	$24.066e^{-2.0994x}$
	$R'_{(\lambda,\ AREA)}$		N/S	N/S
	$CRDR_{623}$		0.301	$29.24e^{55.156x}$
31 August 2005	$R'_{(\lambda,\ MAX)}$	11	0.660	251.69x - 265.97
	$R'_{(650)}/R'_{(\lambda,\ MAX)}$		0.621	$7.1197e^{-6.0421x}$
	$R'_{(\lambda,\ FWHM)}$		N/S	N/S
	$R'_{(\lambda,\ AREA)}$		0.782	9.6289x - 692.5
	$CRDR_{583.5}$		0.874	22834x + 9.3096

The optimum least-squares regression relationships between the continuum-removed indices and the measured concentration of C-phycocyanin for the 22 June 2005 and 29 August 2005 cruises are detailed in Table 4.14. In general, the observed relationships between the $R'_{(\lambda)}$ based indices and the measured concentration of C-phycocyanin were poorer than those observed with the $R_{rs}(0+,\lambda)$ and $dR/d\lambda$ based indices and algorithms. The [$R'_{(\lambda,\ FWHM)}$] exhibited the best relationship with the concentration of C-phycocyanin on the 22 June 2005 (R^2 = 0.507). However, the [$R'_{(\lambda,\ FWHM)}$] did not demonstrate a significant association with concentration of C-phycocyanin on 29 August 2005; instead, here, the strongest relationship was noted to occur with [$CRDR_{(583.5)}$] (R^2 = 0.874). Notwithstanding the fact the [$CRDR_{(583.5)}$] index demonstrated the single strongest empirical relationship with C-phycocyanin over the two lake sampling cruises, it was not significantly correlated with the measured concentration of C-phycocyanin on 22 June 2005, which again suggests that the derived algorithm may not be temporally robust.

The optimum least-squares regression relationships between the [$CRDR_{(583.5)}$] index and the measured concentration of C-phycocyanin derived from the 29 August 2005 data is depicted in Figure 4.29. The least-squares regression model was again influenced by the extreme data point from the solitary station located on Barton Broad, but, even with this data point removed, a reasonable coefficient of determination was still achieved (R^2 = 0.693). The use of a non-linear model improved the coefficient of determination for the regression relationship. However, a non-linear model was considered inappropriate in this instance because of the absence of data points for C-phycocyanin concentrations between 40 and 135 mg m^{-3}.

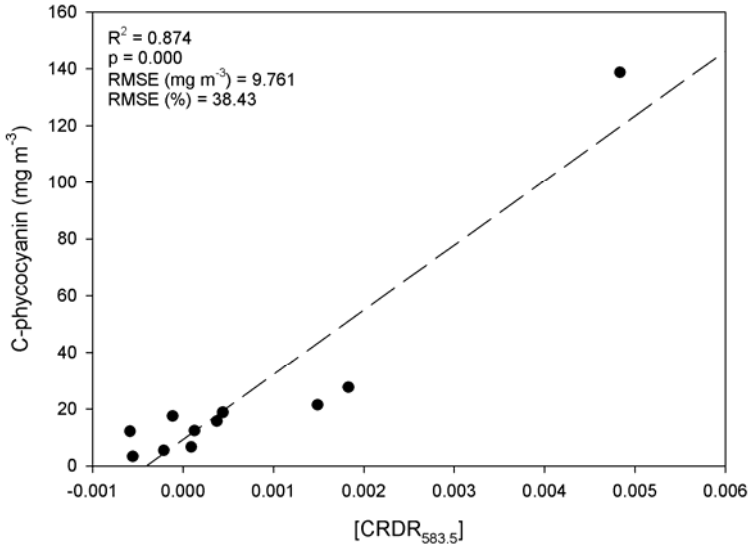

Figure 4.29 The linear regression relationship between: (a) $CRDR_{583.5}$ and the measured concentration of C-phycocyanin for the 29 August 2005 cruise (dashed lines represent 95% confidence intervals).

The retrieval of fucoxanthin concentrations using $R'_{(\lambda)}$ based indices was complicated by the lack of a diagnostic absorption feature related to the presence of fucoxanthin in the spectra. Thus, as the *in vivo* fucoxanthin absorption maximum occurs in the 445-470 nm region (Rowan, 1989), the large $R_{rs}(0+,\lambda)$-minimum (*c*. 400-480 nm) known to be associated with a variety of chlorophyll-and xanthophyll pigments had to be adopted for continuum-removal analysis (using start and end points for the continua of 400 nm and 480 nm respectively). The $R'_{(\lambda)}$ spectra of the region of fucoxanthin absorption for the 29 August 2005 dataset are shown in Figure 4.30.

Notable variations in the size and the shape of the $R_{rs}(0+,\lambda)$-minimum related (in part) to fucoxanthin can be seen in Figure 4.29 between the various sampling stations. However, correlation analyses revealed no significant relationships between the $R'_{(\lambda)}$ indices and the measured fucoxanthin concentration. Given that the $R_{rs}(0+,\lambda)$-minimum selected for continuum-removal analysis is also influenced, in addition to fucoxanthin, by chlorophyll and other carotenoid pigments, and also CDOM, the lack of significant correlative relationships is perhaps not unexpected. In this context, the use of continuum-removed reflectance as a basis for retrieving fucoxanthin concentrations would be better assessed under circumstances when the concentrations of fucoxanthin are high and, as a result, the $R_{rs}(0+,\lambda)$-minimum between 400 and 480 nm is more responsive to fucoxanthin variation (e.g. during blooms of bacillariophytes or dinophytes). This observation also applies to the derivation of both $R_{rs}(0+,\lambda)$ and $dR/d\lambda$ indices for fucoxanthin estimation.

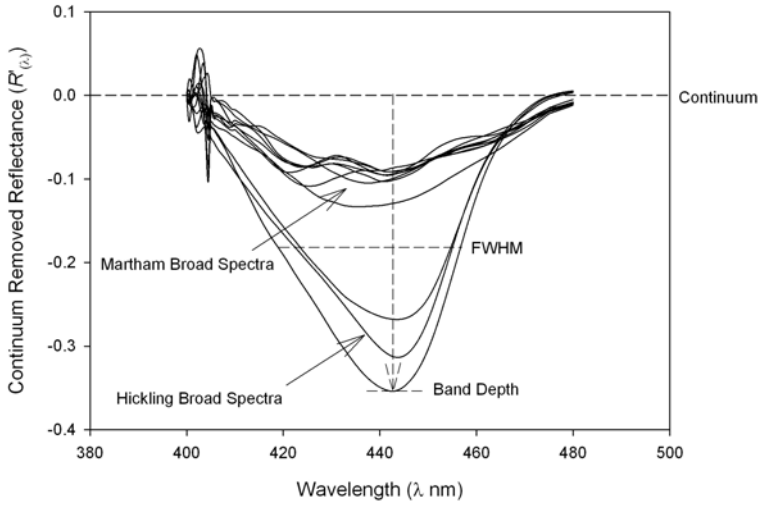

Figure 4.30 Continuum removed spectra ($R'_{(\lambda)}$) in the region of the *in vivo* fucoxanthin absorption maximum on 29 August 2005.

The expeditious results obtained from the lake sampling cruises in the Norfolk Broads provide some promising evidence to suggest that the biomarker pigments concentrations may be estimated in natural mixed communities using remote sensing data. In particular, the quantification of cyanobacterial biomass using the biomarker pigment C-phycocyanin would certainly seem achievable. The realisation of techniques to quantify cyanobacteria from remote sensing data would provide limnologists with an invaluable tool for research and monitoring and

would enabling broad-scale changes in the floristic composition of phytoplankton communities to be monitored in lakes.

The capability to discriminate cyanobacteria from other species of phytoplankton would also present a means of monitoring the development of potentially-toxic cyanobacterial blooms in inland waters which would be a significant advancement for water resource management, particularly in respect to public health concerns (Codd *et al.,* 2005), and would seem a timely development given the expected increase in blooms of cyanobacteria under future climate change scenarios (Elliott *et al.,* 2005; Mooij *et al.,* 2005).

4.6 CONCLUSIONS

The experimental mesocosm experiments and the explorative *in-situ* spectrometry cruises in the Norfolk Broads have demonstrated that it is possible to obtain information concerning the composition of phytoplankton communities from remote sensing data. The experimental mesocosm experiments demonstrated that different phytoplankton taxonomic groups can be distinguished based on their respective spectral characteristics. Spectral dissimalarity would seem to be most pronounced at the colour group level, occurring as a function of taxonomic variations in cell size and morphology and, importantly, photosynthetic pigment composition. Spectral differences were most pronounced at high chlorophyll-a concentrations and in pseudo-communities dominated by a single colour group species. First-derivative transformations of the hyperspectral data improved the extent to which pseudo-communities of differing species composition could be differentiated.

It was shown that sensor spectral resolution has a significant effect upon the degree to which the various colour group species could be distinguished. PCA revealed that dissimilarities were most pronounced in the high resolution hyperspectral datasets and the simulated SeaWiFS multispectral dataset. However, in other datasets, with reduced spectral resolution, the potential to discriminate between colour group taxa was lost. Coincidental concentrations of SPIM and, in particular, SPOM and CDOM had marked effects upon the spectral signatures of the mesocosm pseudo-communities and represent potential obstacles to the retrieval of

taxonomic information from remote sensing data. Nevertheless, in the hyperspectral datasets prominent spectral dissimilarities between pseudo-communities could still be observed regardless of the presence of SPIM, SPOM or CDOM.

MDA was used to demonstrate that a simple classification approach could be developed to diagnose the dominant species composition of rogue algal blooms and thus potentially provide a rapid risk assessment for HAB threats. It was further demonstrated using the datasets generated from the mesocosm experiments that simple $R_{(\lambda)}$ and $dR/d\lambda$ based indices could be constructed to provide quantitative estimates of the concentration of fucoxanthin and C-phycocyanin, thus enabling the biomass of specific phytoplankton colour groups to be estimated.

The extrapolation of the work pioneered within the context of the mesocosm study to the shallow lakes of the Norfolk Broads (UK) demonstrated that it was further possible to quantify the species-specific biomass of phytoplankton taxa by retrieving estimates of biomarker pigment concentrations. In particular, it was shown that the quantification of C-phycocyanin is achievable using remotely sensed data. This suggests that remote sensing could be used to monitor the development of potentially-toxic cyanobacterial blooms in lakes. In the context of shallow lakes (and indeed other inland waters), the ability to quantify cyanobacterial biomass using remotely sensed data is of direct relevance to the assessment of ecological status, and the potential ability to implement such techniques at local, regional and, indeed, global scales would seem to represent a timely development with respect to the implementation of the EU WFD.

Notwithstanding the promising results obtained here, substantial further research on the retrieval C-phycocyanin and other biomarker pigments, such as fucoxanthin, is urgently required. The semi-empirical approaches adopted here, whilst useful for expeditious investigation, suffer from a lack of mechanistic clarity. The derivation of analytical algorithms for the assessment of phytoplankton community composition using bio-optical modelling approaches may be valuable in this context (e.g. Simis *et al.,* 2005; Simis *et al.,* 2007). In

addition, the development of long-term remote sensing datasets for lakes, which can be readily paired with phytoplankton pigment and cell count data, should be made an immediate priority if the use of remote sensing for the assessment of phytoplankton community structure is to be progressed.

5 TIME SERIES AIRBORNE REMOTE SENSING OF PHYTOPLANKTON IN SHALLOW LAKES

5.1 INTRODUCTION

The two preceding chapters (Chapter 3 and Chapter 4) have shown that remote sensing data can be used to estimate the concentration of bio-optically active pigments in shallow lakes using high resolution remote-sensing-reflectance measurements acquired from *in-situ* spectrometry measurements. The following chapter seeks to extrapolate the developed methodologies and examine the efficacy of airborne remote sensing reconnaissance of phytoplankton blooms in shallow lakes. Work extracted from this chapter has been submitted for publication in *Limnology & Oceanography* (Hunter, P.D., Tyler, A.N., Gilvear, D.J. & Willby, N.J. (submitted). The spatial dynamics of vertical migration by *Microcytis aeruginosa* in a eutrophic shallow lake: A case-study using high spatial resolution time-series airborne remote sensing, *Limnology and Oceanography*).

5.2 RATIONALE

Optical remote sensing of the oceans was pioneered in the 1970s and 1980s following the launch of the Coastal Zone Color Scanner (CZCS) on board NASA's Nimbus-7 satellite. The CZCS has now been superseded by more advanced platforms such as the NASA's SeaStar SeaWIFS (Sea-viewing Wide Field-of-View Sensor), ESA's EnviSat MERIS (Medium Resolution Imaging Spectrometer), and NASA's Terra/Aqua MODIS (Moderate Resolution Imaging Spectrometer) which, collectively, offer data of an enhanced spectral resolution for ocean colour monitoring purposes. The provision of accurate, near-real-time, ocean colour products (e.g. the concentration of chlorophyll-a) from these platforms has led to remote sensing becoming established as the principal tool for monitoring primary productivity in the oceans and, as such, remote sensing data products make a significant contribution to the study of global biogeochemical cycling (e.g. Karl, 2002; Behrenfeld *et al.,* 2005; Dickey *et al.,* 2006).

The application of remote sensing for lake monitoring has developed in tandem with ocean colour research. Indeed, remote sensing has proven capable of delivering quantitative estimates of several water quality parameters (including the concentrations of chlorophyll-a, SPM and CDOM and LSTs) in lake environments (George, 1997; Hoogenboom *et al.,* 1998; Thiemann & Kaufmann, 2000; Ostlund *et al.,* 2001; George & Malthus, 2001; Flink *et al.,* 2001; Ammenberg *et al.,* 2002; Tyler *et al.,* 2006; Giardino *et al.,* 2007). The spatially-resolving and panoptic surveillance capabilities afforded by satellite remote sensing platforms enable regional-scale panoramas of lake water quality to be developed (e.g. Novo *et al.,* 2006). This permits the rapid assessment of both inter- and intra-lake variations. In contrast, conventional point-based lake sampling strategies can seldom satisfactorily describe pronounced spatial gradients in the quality of surface waters and, in particular, at the regional-scale.

However, while dedicated systems for the remote sensing of ocean colour have been in operation for decades, the remote sensing of inland waters has, in comparison, somewhat lagged behind that of ocean colour monitoring and, at present, no operational remote sensing systems have been developed for the routine monitoring of lakes and other inland waters. The reasons behind this relative lack of progress are primarily twofold: (i) the optical properties of inland waters (predominantly CASE II type waters) are more complex than those encountered in oceanic waters which often results in decreased retrieval accuracies and, (ii) there has been an absence of an apposite satellite platform (until the launch of Hyperion on NASA's EOS-1 satellite) that has both the spatial and spectral resolution required for lake monitoring purposes. However, the EU WFD (2000/60/EC) has heightened the need for effective, regional-scale, inland water quality monitoring strategies. In the context of the EU WFD, an operational remote-sensing-based system for the assessment of water quality in lakes, operating at the European level, would be hugely advantageous. However, at present, an operational system remains someway from realisation. Significant further research will be required to prove the accuracy and robustness of the remote sensing approach to lake monitoring before an effective European-wide remote-sensing-based strategy could be implemented.

Very shallow lakes (i.e. < 3 m mean depth) represent a particularly challenging environment for application of remote sensing in lake monitoring and, in particular, for the estimation of phytoplankton-related pigment parameters (e.g. chlorophyll-a). Previous studies have achieved varying degrees of success (Liu *et al.,* 2003). Numerous authors have noted that the estimation of chlorophyll-*a* concentrations in CASE II inland waters is complicated by the variable presence of other optically active components and, in particular, high and non-co-varying SPM (tripton) and CDOM (Dekker *et al.,* 1991; Lindell *et al*., 1999; Svab *et al.,* 2005; Tyler *et al.,* 2006). Shallow lakes often experience very high tripton loadings due to resuspension processes. The resulting spectral attenuation from high tripton loads may thus present a significant barrier to the accurate estimation of pigment concentrations in shallow lakes (Liu *et al.,* 2003). Moreover, in shallow lakes, the bottom substrate itself can make a significant contribution to the upwelling radiance signal, such, that it can cause gross inaccuracies in the estimation of pigment concentrations in overlying pelagic waters.

The often problematic nature of obtaining accurate estimations of phytoplankton pigment concentrations in CASE II inland waters has necessitated the development of several different approaches to the derivation of remote-sensing-based algorithms for the estimation of pigment concentrations. Many workers have employed NIR/red band-ratios in algorithms formulated either semi-empirically or analytically (i.e. through bio-optical modelling). Recent research indicates that algorithms derived from complex solutions to spectral mixing models can provide improved accuracies for the estimation of chlorophyll-a concentrations in lakes (Thiemann & Kaufmann, 2002; Tyler *et al.,* 2006; Oyama *et al.,* 2007).

The majority of foregoing studies, either because of technological constraints, or otherwise, have often focussed on large and often moderately, or very, deep lakes (e.g. Lake Baikal, Lake Balaton, Lake Carter, Lake Erie, Lake Garda, Lake Mälaren, Lake Mono, Lake Okeechobee, Lake Superior, etc.) (Schalles *et al.,* 1998; Yang *et al.,* 2000; Strombeck & Pierson, 2001; Melack & Gastil, 2001; Brivio *et al.,* 2001; Ammenberg *et al.,* 2002; Vincent *et al.,* 2004; Budd & Warrington, 2004; Auer & Bub, 2004; Heim *et al.,* 2005; Tyler *et al.,* 2006; Sridhar & Vincent, 2007; Giardino *et al.,* 2007). However, the majority of waterbodies covered by the EU WFD are

actually relatively small and often much shallower in nature. There is thus an urgent need for further evaluation of remote-sensing-based approaches for the estimation of phytoplankton pigments in shallow, and highly optically-complex, lakes. Moreover, there is also a need to validate the capacity of remote sensing for time-series monitoring of phytoplankton populations (as would be required under an operational monitoring strategy).

5.3 AIMS AND OBJECTIVES

The aim of the research presented in this chapter was (i) to derive and validate different approaches to the formulation of algorithms for the estimation of phytoplankton pigments (chlorophyll-a and C-phycocyanin) in shallow lakes using high spatial-spectral airborne remote sensing and, (ii) in a more applied context, to use the airborne remote sensing to examine the diurnal and seasonal dynamics of phytoplankton populations in shallow lakes.

The specific objectives for this chapter can be defined as:

a) To evaluate the efficacy of airborne remote sensing for the estimation of chlorophyll-a and C-phycocyanin concentrations in shallow lakes through multi-temporal validation in the Upper Thurne and Barton Broads, Norfolk, UK.

b) To compare the efficacy of algorithms for pigment estimation formulated using NIR/red band-ratio to that of algorithms formulated using more complex spectral mixing, angle mapping and continuum-removed models.

c) To use high resolution time-series imagery to examine the diurnal dynamism of cyanobacteria in shallows lakes and potentially provide new insights into the spatial ecology of potentially-toxic algal blooms.

5.4 METHODS

5.4.1 Study Site

The Norfolk Broads (UK) (52º 44' 17'' N 1 º 34' 29'' E) are a series of small (0.1-130 ha) shallow lakes (mean depth < 2.5 m) and marginal wetlands of national and international importance (for further discussion, see Chapter 2). The shallow lakes of the Norfolk Broads were chosen for this research as they provided an ideal environment in which to showcase the use of airborne remote sensing for shallow lake monitoring purposes.

5.4.2 Remote Sensing Data Capture

Image data for this project was acquired by the National Environmental Research Council's Airborne Research and Survey Facility (NERC ARSF). The NERC ARSF crew flew several data acquisition campaigns over the Upper Thurne and Barton Broads during 2004 and 2005. The NERC ARSF aircraft – a Dornier 228-101 twin turbo-prop, non-pressurised, shoulder-wing monoplane – carried two multispectral sensors as part of its payload: (1) the Airborne Thematic Mapper (ATM) instrument and (2) the Compact Airborne Spectrographic Imager (CASI-2), plus an additional Rolleiflex 6008 single-lens reflex (SLR) auto-focus (AF) digital aerial camera (see Figure 5.1).

The CASI-2 instrument is a two-dimensional CCD array-based pushbroom imaging spectrograph capable of operating in two modes: (1) *spectral* (or *enhanced spectral*) mode providing the full hyperspectral data cube (288 channels) for a maximum of 39 look-directions spread across a swath of 4, 8, 12 or 16 spatial pixels (enhanced spectral mode provides 101 adjacent spatial pixels) and (2) *spatial* mode providing a 512 pixel swath for a maximum of 18 programmable channels. The technical specifications of the CASI-2 instrument are detailed in Table 5.1. The programmable spectral channels of the CASI-2 instrument, when operated in *spatial* mode, facilitate instrument configurations to be adjusted to suit the specific application.

Figure 5.1 The NERC ARSF's Dornier 228-101 aircraft carrying the ATM and CASI-2 sensors.

Table 5.1 The technical specifications of the Compact Airborne Spectrographic Imager.

Instrument Parameter	**Description**
IFOV – Across Track	54.4º
IFOV – Along Track	0.1151º
Aperture	f/2.8-f/11 (automated iris control)
Spectral Range	405-950 nm
Spatial Samples	512 spatial pixels
Spectral Samples	288 at 1.8 nm intervals (2.2 nm FWHM @ 650 nm)
Dynamic Range	12-bits (4096 levels)
Recording	1 removable 9 GByte hard disk
Operating Modes	
Spatial Mode	512 pixels across swath, up to 18 spectra channels (fully programmable)
Spectral Mode	Full spectrum (288 channels) for up to 39 look directions spread across swath (4, 8, 12 or 16 pixel spacing between look directions)
Enhanced Spectral Mode	Full spectrum (288 channels) in a block of 101 adjacent spatial pixels
Full Frame	512 pixels across swath x 288 spectral pixels (~1-2 sec. intergration time limits use to laboratory calibration or ground based field use)
Additional Features	
Downwelling incident light sensor (ILS)	
Lumogen coating for enhancement of blue response below 450 nm	

The CASI-2 instrument was operated using the default simulated SeaWiFS bandset configuration designed to optimise the CASI-2 sensor for the observation of CASE I and CASE II waters (see Table 5.2). The data acquired by the ATM instrument is not considered further here.

The NERC ARSF campaigns were scheduled to provide data epochs covering seasonal variation in the water quality conditions of the Norfolk Broads. In addition, each NERC ARSF campaign was further sub-composed of three individual data acquisition sorties which were staggered throughout the day to provide high-resolution time-series surveillance of phytoplankton populations in the Broads. The NERC ARSF scheduled four data acquisition campaigns for 2004 and a further eight campaigns for 2005. However, as a result of poor weather in 2004 and the high demands for NERC ARSF flying time, the full flight schedule could not be completed; the completed NERC ARSF campaigns are detailed in Table 5.3.

Table 5.2 The CASI-2 default SeaWiFS channel/bandset configuration.

Channel	Centre/Width (nm)	Start (nm)	End (nm)	Equivalent SeaWiFS Channel	Purpose
1	412/20	402.81	422.15	1	CDOM + Chl
2	443/20	432.72	453.87	2	Chl + CDOM
3	490/20	480.37	499.84	3	Chl + CDOM + Access.
4	510/20	501.61	519.33	4	Access.
5	555/20	545.97	565.53	5	Access + Chl
6	620/20	610.10	629.76		MERIS + Access.
7	670/20	660.19	679.92	6	Chl + SPM + ChlF
8	682.5/5	681.72	685.31		ChlF
9	710/10	705.07	715.86		ChlF
10	752/15	744.76	759.10	7a	SPM + Aeros.
11	762/5	760.90	764.51		Oxygen Abs.
12	775/20	766.31	784.37	7b	SPM + Aeros.
13	820/10	815.13	824.18		Water Vapour Abs.
14	865/40	845.94	884.08	8	SPM Aeros.

CDOM – coloured dissolved organic matter; Chl – chlorophyll; Access. – accessory pigments; MERIS – MERIS compatible band; SPM – suspended particular matter; ChlF – chlorophyll fluorescence; Aeros. – aerosols.

To provide full, high-spatial resolution, coverage of the target lakes, several adjacent CASI-2 [SeaWiFS] flightlines had to be flown over the Upper Thurne and Barton Broads (with *c*. 30-50% overlap); these individual flights lines were subsequently appended together to form a

multi-scene mosaic encompassing the entire system of lakes. The resulting flight plans are detailed in Figure 5.2 and Figure 5.3. The flight plan used during 2004 was amended for the 2005 campaigns to provide greater overlap between individual flightlines and to incorporate an auxiliary perpendicular CASI-2 flightline – flown with the instrument configured in '*spectral*' mode – which was used as a 'tie-line' to assist with the image-to-image normalisation procedures employed during processing.

Table 5.3 The ATM and CASI-2 imagery acquired during the NERC ARSF campaigns in the Norfolk Broads during 2004 and 2005.

	Imagery Collected	**Sorties*** **(GMT)**	**Data Quality/ Cloud Cover**	**Ground Truth Data**
18 May 2004	ATM and CASI-2 [SeaWiFS]	10.00 13.00 16.00	Poor/High	Yes
02 September 2004	ATM and CASI-2 [SeaWiFS]	10.00 13.00 16.00	Poor/Moderate	No
28 February 2005	ATM and CASI-2 [SeaWiFS]	10.00 13.00 16.00	Good/Low	No
21 April 2005	ATM and CASI-2 [SeaWiFS]	10.00 13.00 16.00	Good/Low	Yes
22 June 2005	ATM and CASI-2 [SeaWiFS]	10.00 13.00 16.00	Good/Low	Yes
29 August 2005	ATM and CASI-2 [SeaWiFS]	10.00 13.00 16.00	Good/Low	Yes

*The timing of the time-series sorties varied depending on aircraft availability, atmospheric conditions and ground-truth sampling coordination (± 1 h).

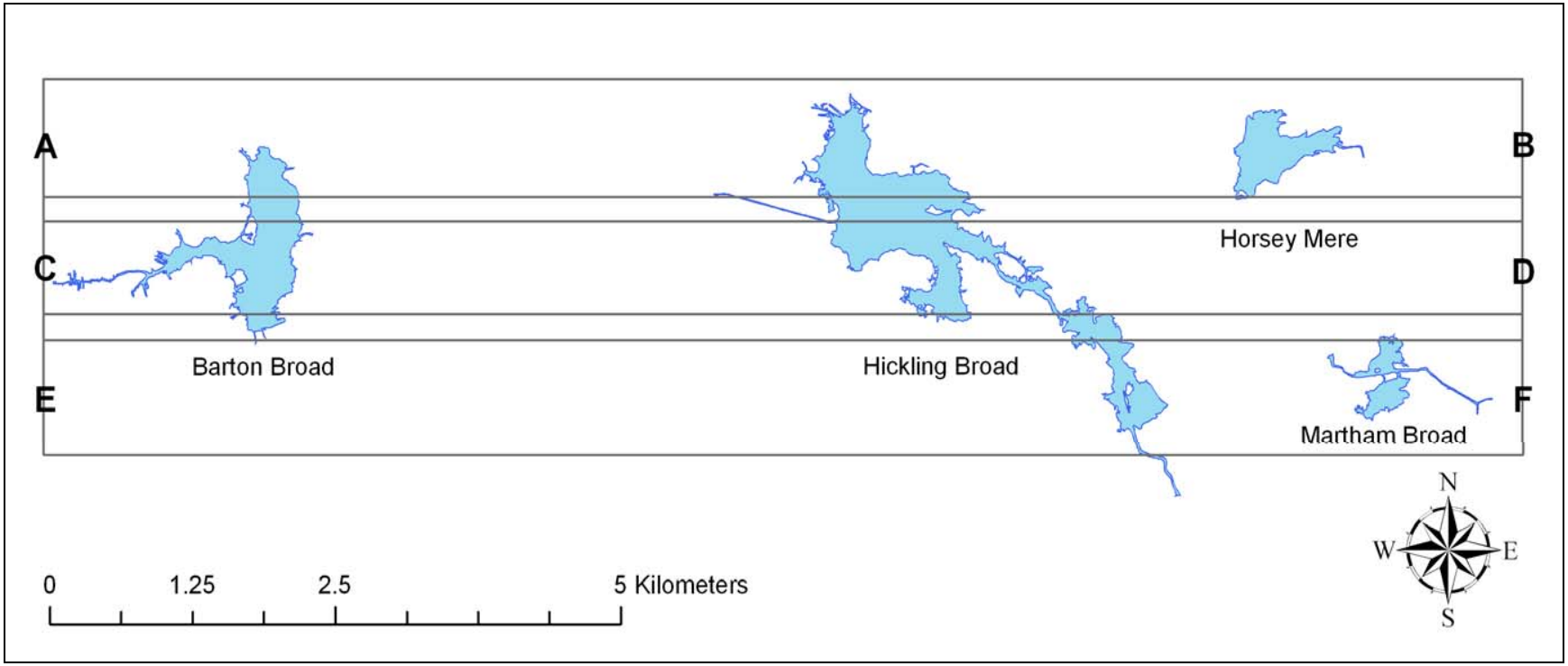

Figure 5.2 The NERC ARSF flight plan for the 2004 campaigns over the Upper Thurne and Barton Broads, Norfolk, UK. The three flightlines (A-B:E-F) formed a single data sortie; three time-series sorties (*c*. 10.00, 13.00 and 16.00 GMT) were flown during each campaign.

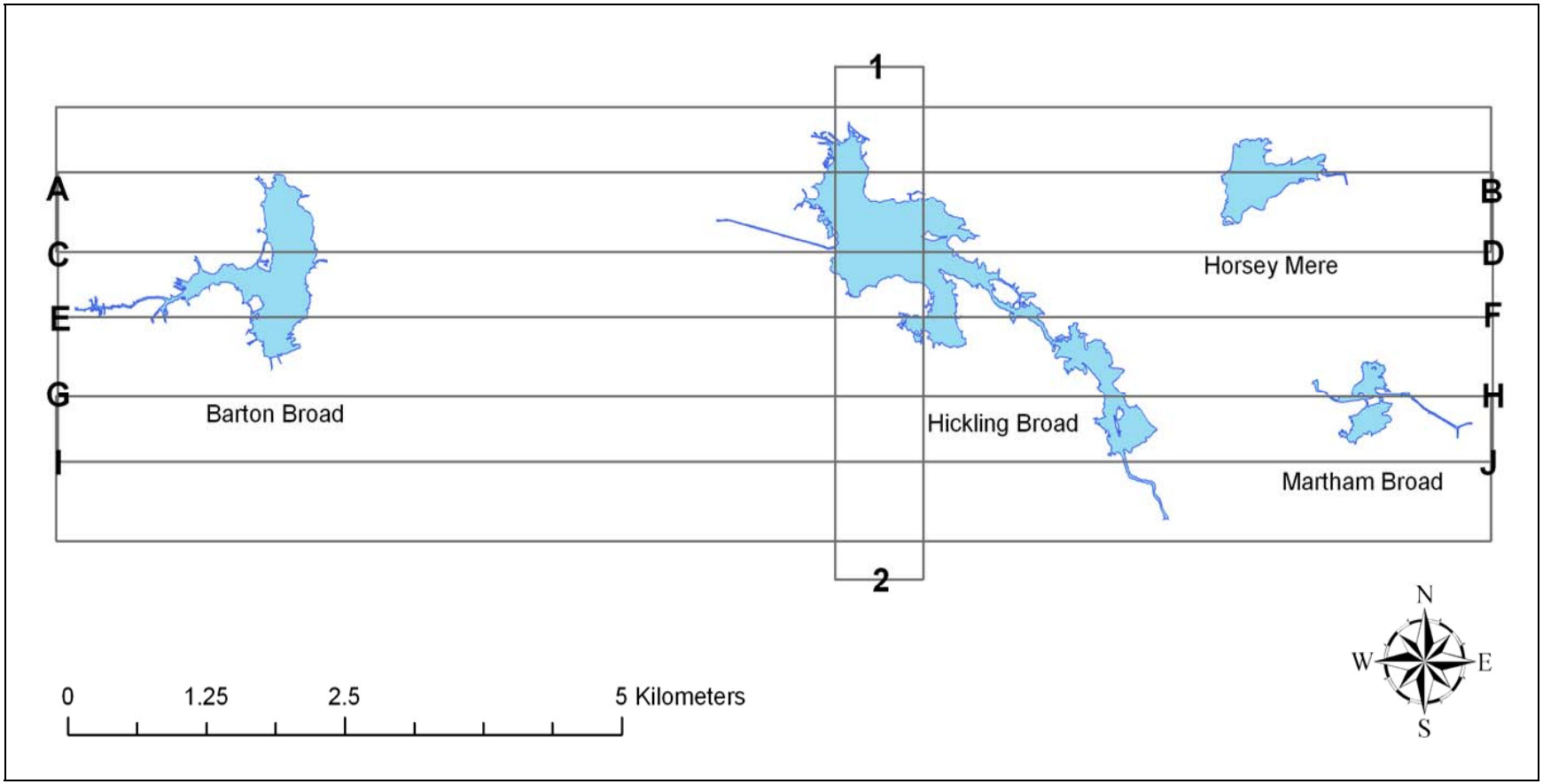

Figure 5.3 The NERC ARSF flight plan for the 2005 campaigns over the Upper Thurne and Barton Broads, Norfolk, UK. The five flightlines (A-B:I-J) and lone 'tie-line' (1-2) formed a single data sortie; three time-series sorties (*c*. 10.00, 13.00 and 16.00 GMT) were flown during each campaign.

5.4.3 Lake Sampling Cruises and Pigment Analysis

Water quality sampling was conducted contemporaneous to the NERC ARSF data acquisition campaigns to provide ground truth data for the calibration and validation of the remote sensing algorithms (with the exception of the 02 September 2004 and 28 February 2005 NERC ARSF campaigns). Lake sampling teams were deployed for the duration of the NERC ARSF flights (i.e. stations were sampled during all three data capture sorties). Sampling was conducted in a systematic manner with stations, when feasible, located on all major Broads of the River Thune and River Ant. This enabled samples to be collected across a known gradient in water quality.

Surface water samples for chlorophyll-a and C-phycocyanin analysis were collected from sampling stations using a pre-washed wide-necked bottle. The water samples were stored (on ice when possible) in the dark until filtration could occur. Filtration was always performed within 2-12 h of sample collection. Sample aliquots for chlorophyll-a and C-phycocyanin analysis were vacuum filtered onto pre-washed 47 mm diameter Whatman GF/C filters. The filter papers and filtrand were wrapped in aluminium foil and immediately quick-frozen in liquid N (-196°C) for transportation back to the laboratories at the School of Biological and Environmental Science (University of Stirling). Upon receipt at the University of Stirling, samples were stored at -40°C or -80°C upon receipt until analysis.

Filter papers were stored for no longer than 14 d to prevent pigment degradation. Filter papers for chlorophyll-and C-phycocyanin analysis can be stored at ≤ -40°C for a period up to 3 months without the significant pigment degradation occurring (Mantoura *et al*., 1997; Sarada *et al*., 2003). The concentration of chlorophyll-a and C-phycocyanin were determined according to the methods of Lorenzen & Jeffrey (1980) and Sarada *et al*. (1999) respectively (see Section 3.3.2 and 4.3.4). The concentrations of accessory carotenoid pigments (e.g fucoxanthin) were determined by RP-HPLC (see Section 4.3.1). The concentration of SPM, SPIM and SPOM were determined gravimetrically (see Section 3.3.2).

5.4.4 CASI-2 [SeaWiFS] Image Pre-processing

5.4.4.1 Image Geo-Correction and Geospatial Registration

The CASI-2 [SeaWiFS] imagery was delivered by the NERC ARSF data processing team as a level 1b product (see Table 5.4 for explanation). The level 1b imagery was geo-corrected for the effects of aircraft position, altitude and ground surface separation (roll, pitch and yaw effects) using the dedicated AZGCORR software program supplied by NERC ARSF. The AZGCORR program uses the image and post-processed navigation data to produce a map-projection-referenced rectilinear output image computed from aircraft spheroid height, digital elevation data and geodic-spheroid separation estimates (Azimuth Systems, 2005) (level 2 product). Atmospheric correction was not applied at this point. The geo-correction of these level 2 image products was then refined via further geospatial registration to known ground-control-points (GCPs) identified from an Ordnance Survey© 1:25 000 map (Outdoor Leisure No. 40) using the RSI ENVI v4.3 software package (level 3b product).

Table 5.4 Descriptions of the various image product processing levels in standard use by the NERC ARSF.

	Description
Level 0	Raw uncalibrated format at the original resolution of the sensor
Level 1a	Level 0 data reformatted to image files with appended information
Level 1b	Level 1a data to which radiometric calibration algorithms have been applied, to produce radiance or irradiance, and to which location and navigational information has been appended.
Level 2	Geophysical or environmental parameters derived from Level 1a or 1b data, may include atmospheric correction.
Level 3a	Level 1b or 2 data mapped to a geographic co-ordinate system using on-board attitude and positional information only.
Level 3b	Level 1b or 2 data mapped to a geographic co-ordinate system using on-board attitude and positional information with additional ground control points.
Level 4	Multi-temporal/multi-sensor grid data products.

5.4.4.2 Atmospheric Correction and Image-to-Image Normalisation and Mosaicing

The attenuating effects of the atmosphere (Raman scattering, aerosol absorption and refraction) can often contribute > 90% of the radiance or reflectance measured by satellite sensors over CASE I and CASE II waters (Hadjimitsis *et al.,* 2004). Atmospheric attenuation has less impact on airborne imagery, but the removal of atmospheric noise is still necessary if

derived algorithms are to retain any transferability. This project initially trialled an atmospheric correction model developed by the RSDAS (Remote Sensing Data Analysis Service) team at the Plymouth Marine Laboratory (PML) designed for the correction of CASI-2 data over CASE I waters. However, as the RSDAS model was developed for use over CASE I waters, it produced erroneous results when applied to the CASI-2 imagery of the Norfolk Broads.

Thus, an alternative approach to the atmospheric correction of the imagery had to be sought. Several models have been used for the atmospheric correction of airborne imagery products. Ammenberg *et al*. (2002), for example, used the 6S radiative transfer code (RTC) to atmospherically correct CASI-2 imagery; while Melack & Gastil (2001) used the MODTRAN model to atmospherically correct AVIRIS imagery. However, such models are primarily designed for the correction of satellite imagery products and also require extensive atmospheric measurements for parameterisation. The dedicated commercially available models for the atmospheric correction of airborne imagery (e.g. ATCOR-4 and RSI ENVI FLAASH) were unfortunately not available for this use in this project.

Interestingly, Hadjimitsis *et al*. (2004), found that simple, image-based, dark-pixel subtraction methods (also referred to as the histogram minimum method) can often offer the most accurate and practical approach to atmospheric correction over CASE II waters. The dark-pixel method uses the minimum radiance value measured in each spectral band as an approximate measure of atmospheric scattering; its subtraction from remaining image pixels thus provides a simple image-based correction for atmospheric effects. Given that no synchronous atmospheric measurements were readily available, and the intention was not to attempt to extrapolate the derived algorithms for pigment estimation to waters outwith the Norfolk Broads, the image-based dark-pixel subtraction method was considered the most practical solution to atmospheric correction in this instance.

There are a few issues concerning the use of the dark-pixel method for the correction of remote sensing imagery over CASE II waters that need to be acknowledged: (i) the dark-pixel method only corrects for atmospheric scattering and cannot correct for atmospheric absorption and, (ii)

the dark-pixel subtraction method yields image products calibrated to water-leaving-radiance (L_w) (not normalised-water-leaving-radiance (nL_w) or remote-sensing-reflectance (R_{rs})). The dark pixel method thus does not completely remove the effects of variable illumination, solar zenith and viewing geometries between individual scenes. It should also be acknowledged that remote sensing imagery acquired over CASE II waters may not often have a suitably "dark pixel", this was resolved in this instance by extending the NERC ARSF flightlines to include comparatively "darker" pixels in the waters off the Norfolk coast. Justification of the methodology used can be taken from the fact that many previous workers have also derived water quality retrieval algorithms from remote sensing imagery without full atmospheric correction to nL_w or R_{rs} products in instances where the formulated algorithms were not intended to be extrapolated to other waters (e.g. George, 1997; George & Malthus, 2001; Vincent *et al.,* 2004; Tyler *et al.,* 2006; Koponen *et al.,* 2007).

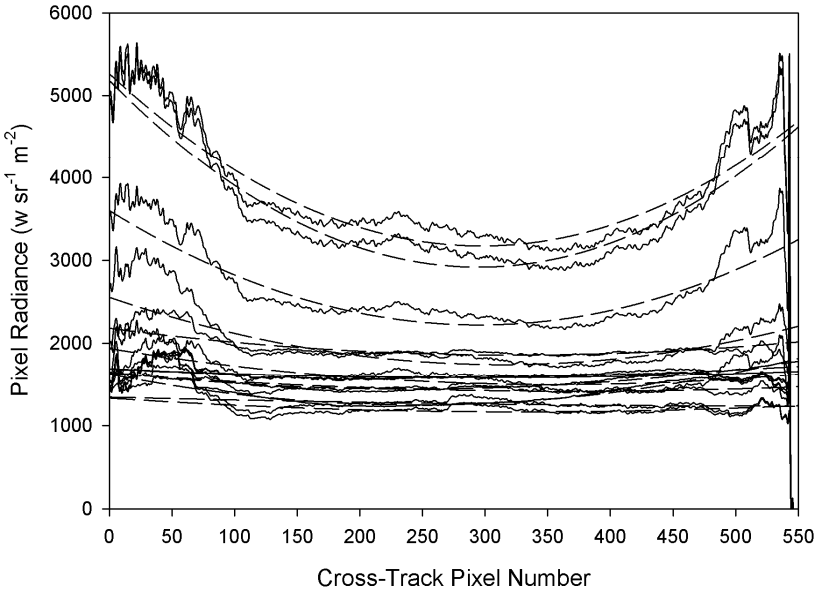

Figure 5.4 An example of the cross-track algorithms applied to the CASI-2 SeaWiFS imagery to correct for differences in the atmospheric path length across the image swath (solid lines – original band radiance; dash lines – 2nd order polynomial correction).

The CASI-2 imagery was atmospherically corrected to L_w using the dark-pixel correction model (*dark subtract* function) in ENVI v.4.3 (a detailed description of the dark pixel methodology is provided in Vincent *et al*. (2004)). The dark-pixels used for atmospheric correction were typically located, as intended, in the coastal waters off the Norfolk coast. The dark-pixel

correction was supplemented with an additional cross-track illumination correction to correct for changes in the atmospheric path length across the image swath; the cross-track illumination correction was performed using the dedicated multiplicative *cross-track illumination correction* function in ENVI v.4.3 (see Figure 5.4).

In addition to the dark-pixel atmospheric correction, an image-to-image normalisation procedure was also employed to correct for residual inter-scene variations in L_w caused variations in illumination, solar zenith and viewing geometry. Common ground-control-pixels were identified in each CASI-2 [SeaWiFS] image. The radiance values were extracted from these pixels and used to derive linear least-squares regression for the image-to-image normalisation procedure. Image-to-image normalisation was applied to each CASI-2 [SeaWiFS] flightline prior to the creation of the mosaic image. The flightline captured first (chronologically) during each NERC ARSF sortie was used as the base image and the remaining CASI-2 [SeaWiFS] images were subsequently normalised to this reference image.

The separate CASI-2 [SeaWiFS] flightlines were subsequently appended together using the *image mosaicing* function in RSI ENVI v.4.3; colour balancing algorithms were also applied during the image mosaicing process to facilitate the image-to-image normalisation procedure. Further image-to-image normalisation algorithms were then applied to each image mosaic to correct for differences between the CASI-2 [SeaWiFS] datasets from different NERC ARSF campaigns. The 16:00 h GMT 29 August 2005 CASI-2 [SeaWiFS] image was selected as the base image for these image-to-image corrections (clearest atmospheric conditions at point of image acquisition) and the remaining CASI-2 [SeaWiFS] images were normalised to this reference image (see Figure 5.5).

(a) Band 6

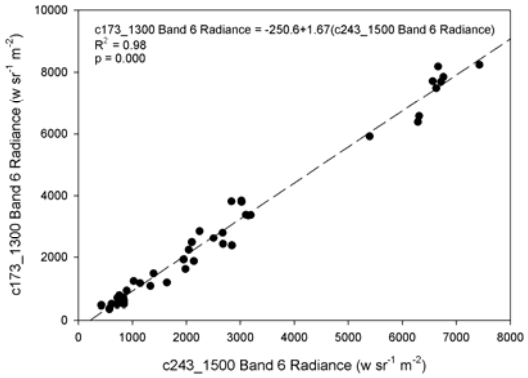

(b) Band 7

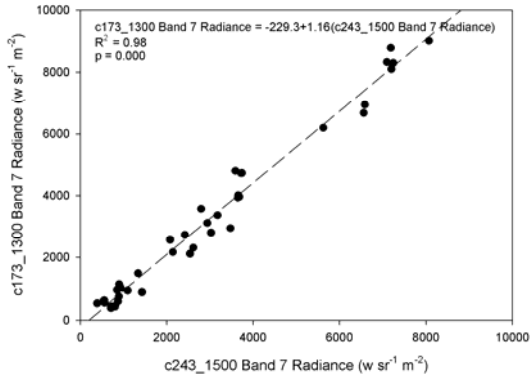

(c) Band 8

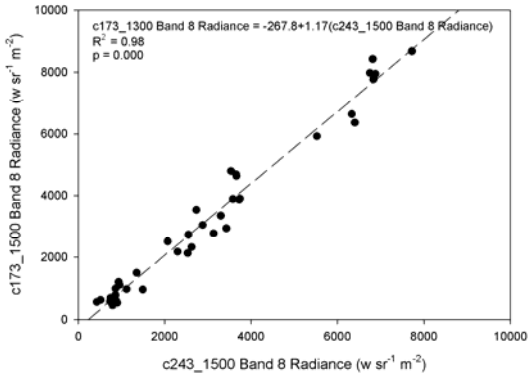

(d) Band 9

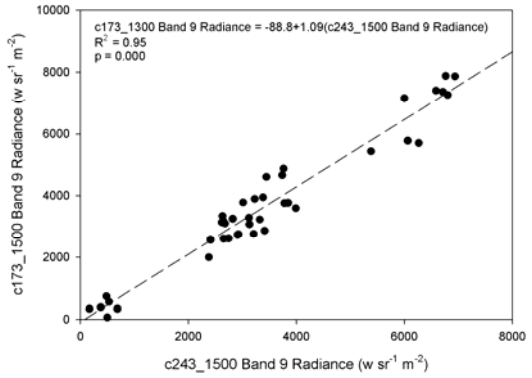

Figure 5.5 Examples of the linear least-squares regression algorithms derived for the image-to-image normalisation of the time-series CASI-2 [SeaWiFS] data from the Nofolk Broads. The graphs above show the corrections applied to the 22 June 2005 CASI-2 [SeaWiFS] image (c173_1300) Bands 6-9 (a-d) in order to normalise the image to the 29 August 2005 CASI-2 [SeaWiFS] (c243_1500) image.

5.4.5 CASI-2 [SeaWiFS] Image Analysis

5.4.5.1 Algorithm Development and Validation: Seasonal Time-Series Data

Remote sensing algorithms for the retrieval of chlorophyll-*a* and C-phycocyanin concentrations from the CASI-2 [SeaWiFS] seasonal time-series imagery of the Upper Thurne and Barton Broads were derived through three methods: (1) NIR/red L_w band-ratios; (2) spectral mixing and mapping models and (3) continuum-removal analysis (see below). In all instances, algorithm calibration was performed using the CASI-2 [SeaWiFS] imagery and contemporaneous water quality data acquired at 16:00 h GMT on 29 August 2005. The 29 August 2005 imagery was selected for algorithm development because the contemporaneous water quality data demonstrated the largest range in phytoplankton pigment concentrations measured over the 2-

year period of the NERC ARSF campaigns in the Norfolk Broads. The algorithms were developed and validated using water quality measurements collected ± 2 h (maximum) from the time of image acquisition. The optimum algorithm derived through each method (identified on the basis of the coefficient of determination and the RMSE) were subsequently validated against the remaining CASI-2 [SeaWiFS] datasets acquired on the 28 February 2005, 21 April 2005 and 22 June 2005 (the CASI-2 imagery acquired on 18 May 2004 and 2 September 2004 was excluded from the analysis because of data quality issues).

(1) NIR/red Band-Ratios

Four NIR/red band-ratios were calculated from the CASI-2 [SeaWiFS] data for the estimation of chlorophyll-a: (i) [$L_w(710)/L_w(670)$], (ii) [$L_w(710)/L_w(682.5)$], (iii) [$L_w(752)/L_w(670)$] and, (iv) [$L_w(752)/L_w(682.5)$]. These were based upon those previously used by Ostlund *et al*. (2001) on a comparable dataset. Four NIR/red band-ratios were also derived for the estimation of C-phycocyanin: (i) [$L_w(710)/L_w(620)$], (ii) [$L_w(710)/L_w(555)$], (iii) [$L_w(752)/L_w(620)$] and, (iv) [$L_w(752)/L_w(555)$]. In this instance, the selection of the CASI-2 [SeaWiFS] bands used in the indices was informed by Simis *et al*. (2005).

(2) Spectral Mixing and Spectral Angle Mapping Models

Hard-boundary approaches to remote sensing image classification (e.g. Euclidean distance classifications) assign feature vectors (pixels) to single and mutually exclusive endmember classes based upon their spectral properties. In this sense, hard-boundary classifications assume no overlap occurs in the condition densities (inter-class-boundaries) that define endmember classes in feature space. However, in reality, there is often a high degree of spectral confusion between feature vectors caused by sub-pixel variations in class composition. Soft-boundary spectral mixing models attempt to resolve sub-pixel variations in composition by estimating the primitive class mixing proportions within each feature vector. Essentially, this enables a single feature vector (pixel) to have multiple class membership. Recent research has shown that the sub-pixel class mixing proportions produced by spectral mixing models can be recombined using regression models to provide quantitative estimates of sub-pixel class abundances. In the context of water quality remote sensing, spectral mixing models can thus

be used to differentiate the spectral contributions of various optically-active components. The derived sub-pixel mixing proportions for each optical component can be subsequently recombined through regression models to provide quantitative estimates of specific optical components (e.g. chlorophyll-*a*) (Thiemann & Kaufmann, 2002; Tyler *et al.,* 2006; Oyama *et al.,* 2007).

In an extension of the methods described in Tyler *et al*. (2006), algorithms for the estimation of chlorophyll-a and C-phycocyanin were derived using three contrasting spectral mixing and mapping models: (i) mixture-tuned matched-filtering (MTMF), (ii) linear spectral mixture modelling (LSMM), and (iii) spectral angle mapping (SAM). Spectral mixing and mapping models use endmember spectra to define the mixing margins for model solutions (in the case of MTMF and LSMM) or as reference for geometric similarity analysis (in the case of SAM). The endmember spectra used to parameterise the MTMF and LSMM models were extracted from the CASI-2 [SeaWiFS] L_w data and, in addition from the CASI-2 [SeaWiFS] L_w data following a minimum-noise-fraction (MNF) transformation (see below) (Rainey *et al.,* 2003; Tyler *et al.,* 2006). The endmember spectra for the parameterisation of the SAM model were extracted from the CASI-2 [SeaWiFS] L_w data only.

Minimum Noise Fraction Transformation—The MNF transformation provides an estimate of the inherent dimensionality of remote sensing data through the segregation and equalisation of spectral noise (Galat & Verdin, 1988; Tyler *et al.,* 2006). MNF transformations can substantially improve the noise-to-signal ratio of image data, thus improving image quality whilst reducing computational requirements. The MNF transformation is essentially an improved PCA-type transformation, consisting of two successive cascading PCA transformations. MNF transformations of the CASI-2 [SeaWiFS] L_w imagery produced MNF eigenimages composed of 13 MNF bands of decreasing spectral information. Coherent MNF bands were identified from eigenvalue scree plots; the MNF eigenimage was then subset to remove superfluous MNF bands prior to endmember extraction.

Spectral Endmember Extraction—The extraction of endmember reference spectra is critical to efficacy of spectral mixing models. Endmember spectra for use in the spectral mixing models were extracted through two contrasting approaches: (1) manual extraction using *a priori* knowledge of potential endmember pixels; and (2) automated endmember extraction using the *pixel purity index* (PPI) or *sequential maximum angle convex cone* (SMACC) functions in ENVI v.4.3. The selected endmembers for inclusion in the spectral mixing models comprised (1) c-phycocyanin; (2) chlorophyll-a; (3) tripton; (4) bottom substrate; and (5) aquatic vegetation. These endmembers were chosen as it was assumed that these components have the greatest influence on the bio-optical properties (and thus L_w) of the waters in the Upper Thurne and Barton Broads (endmember spectra for CDOM could not be resolved). Examples of extracted endmember spectra are shown in Figure 5.6.

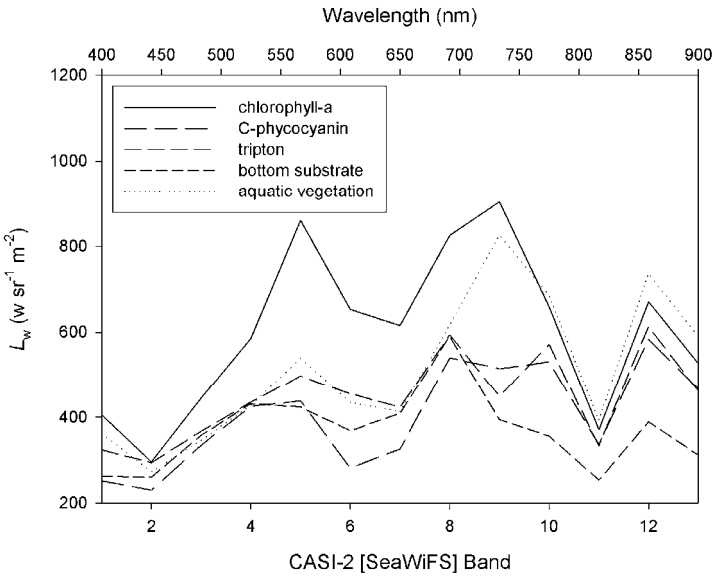

Figure 5.6 The extracted endmember spectra used for the parameterisation of the spectral mixing and SAM models

The manual extraction of endmember spectra from CASI-2 [SeaWiFS] L_w images (i.e. non-MNF transformed) was facilitated by information from the contemporaneous water quality data to enable image pixels to be identified which were considered to be "spectrally pure" representatives of the various endmember components. Briefly, sampling stations were identified where high concentrations of chlorophyll-a, C-phycocyanin or tripton (SPM) had been measured; the corresponding image pixels (5 x 5 kernal) were identified and the CASI-2

[SeaWiFS] L_w spectra from these pixels were extracted and used as endmember parameterisation. Endmember spectra for the bottom substrate were obtained from regions of clear water (biomanipulation enclosures in Barton Broad); while endmember spectra for aquatic vegetation were derived from the dense *Chara* spp. lawns in Martham Broad.

The manual extraction of endmember spectra from MNF-transformed CASI-2 [SeaWiFS] images was achieved through the identification of endmember pixel clusters from 2-D projections of the image data. Extreme pixel clusters were identified in 2-D feature space and evaluated against the various endmember classes using the *Dancing Pixels*™ function in RSI ENVI v.4.3. Pixel clusters found to relate to the desire endmember components were extracted for subsequent model parameterisation (Figure 5.7).

(a) (b)

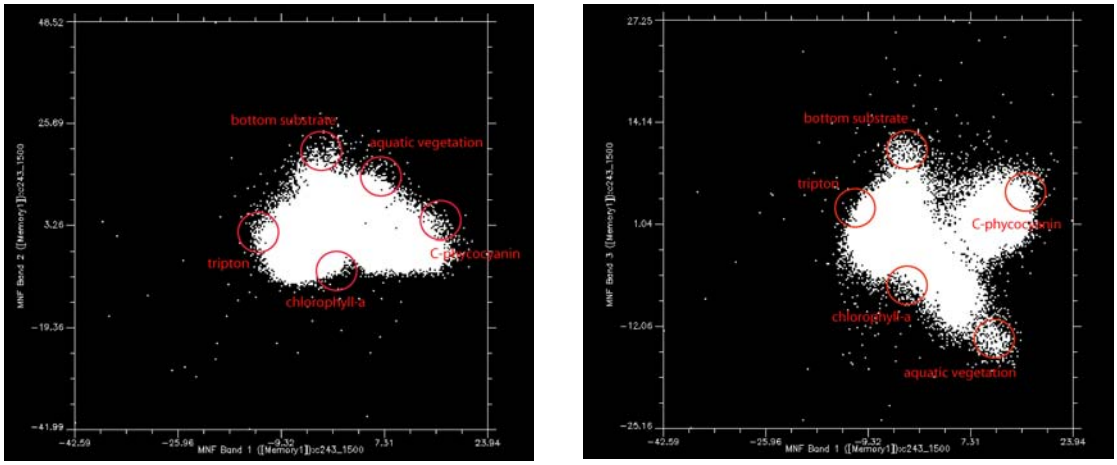

Figure 5.7 2-D scatter plots of coherent MNF-transformed bands from the 16.00 h GMT 29 August 2005 CASI-2 [SeaWiFS] image showing the extreme pixel clusters used for the identification and extraction of endmember component spectra for parameterisation of the spectral mixing models: (a) MNF band 1 vs. MNF band 2 and (b) MNF band 1 vs. MNF band 3.

In contrast to manual extraction procedures, the PPI extraction of endmember spectra used repeated projections of *n*-dimensional scatter plots on a random unit vector to identify extreme pixels; the spectra from those pixels frequently flagged as extreme were then extracted and used for endmember parameterisation. Similarly, the SMACC endmember extraction method used a convex cone model (residual minimisation) to identify an extreme pixel (first endmember); a constrained oblique projection is then applied to the existing cone to derive the

next endmember pixel. Further endmembers are derived in an iterative manner until a previously discovered pixel is located. The PPI and SMACC endmember extraction methods were applied to both the L_w and the MNF-transformed images. Image pixels relating to the endmember spectra automatically extracted using PPI and SMACC were identified and compared to the ground truth water quality datasets to enable coherent endmembers to be selected for parameterisation of the spectral mixing models.

Mixture-Tuned Matched Filtering Models—MTMF finds the relative abundances (mixing proportions) of user-defined endmember components using a partial spectral unmixing analysis. The technique maximises the response of the known endmember and suppresses the response of the composite unknown background in an attempt to match image pixel spectra to endmember reference spectra (Williams & Hunt, 2002; Williams & Hunt, 2004). The output from the MTMF model is a multi-layer greyscale image depicting the relative degree of similarity between the pixel spectrum and the endmember reference spectrum; these values represent sub-pixel endmember abundances and are scaled between 0.0 and 1.0 (where 1.0 is absolute similarity). The inclusion of the infeasibility image in the MTMF computation assists in reducing the number of false-positives (incorrect spectrum matches). MTMF models were examined here because it is suggested that they offer an improved mixing solution in situations where endmember spectra are incomplete or poorly defined. MTMF models were parameterised with the CASI-2 [SeaWiFS] L_w and MNF-transformed endmember spectra and the model solution was obtained. The sub-pixel abundance values for each endmember derived from the MTMF model solutions were then extracted from the CASI-2 [SeaWiFS] image at the location of each lake sampling station. The sub-pixel abundances were subsequently collated for use in the formulation of remote-sensing-based algorithms for pigment estimation.

Linear Spectral Mixing Models—LSMMs determine the relative abundance of user-specified endmember components on a pixel by pixel basis based upon the assumption that the radiance (or reflectance) measured at each image pixel can be modelled as a linear combination of the radiance (or reflectance) of each user-specified endmember component (Galat & Verdin, 1988; Tyler *et al.,* 2006). The number of user-specified endmembers in LSMMs must be equal to, or

less than, the spectral dimensionality of the dataset (approximated by the number of coherent spectral bands).

In this instance, the LSMM was run using two model constraint options: (1) unconstrained modelling (sub-pixel abundances may assume negative values and are not constrained by a sum-to-unity function in the linear-mixing algorithm) and (2) partially-constrained variable-weight modelling (sub-pixel abundances are forced to adhere to a sum-to-unity constraint in the linear-mixing algorithm). The partially-constrained models are more appropriate for MNF-transformed data. High variable weights (5-10) were used for partially-constrained LSMMs to force the linear-mixing algorithm to strictly adhere to the sum-to-unity constraint. The LSMMs were parameterised with the CASI-2 [SeaWiFS] L_w and MNF-transformed endmember spectra. The sub-pixel abundance values for each endmember derived from the LSMM model solutions were then extracted from the CASI-2 [SeaWiFS] image at the location of each lake sampling station. The sub-pixel abundances were subsequently collated for use in the formulation of remote-sensing-based algorithms for pigment estimation.

Spectral Angle Mapping—SAM is a physically-based classification method that uses an *n*-dimensional angle to match image pixels to endmember reference spectra. The SAM algorithm determines the similarity between spectra by calculating the angle when the spectra are simultaneously projected in *n*-dimensional feature space (Kruse *et al.,* 1993). Acute angles indicate close matches between image pixel spectra and endmember reference spectra. SAM is generally designed for use with image data calibrated to reflectance. However, SAM can also be used on radiance datasets if, as here, appropriate efforts are made to normalise the spectra.

SAM provides a hard-boundary classification image (where image pixels that match endmember reference spectra within a predefined tolerance limit are assigned to a single class) and a series of greyscale SAM rule images (which depict the probability of a match between the image pixel spectra and the endmember reference spectra). The SAM rule image probabilities are comparable, although not analogous to, the MTMF and LSMM relative abundance values.

The SAM models were parameterised with the CASI-2 [SeaWiFS] L_w endmember spectra. The SAM probability values for each endmember derived from the model solutions were then extracted from the CASI-2 [SeaWiFS] image at the location of each lake sampling station. The probability values were subsequently collated for use in the formulation of remote-sensing-based algorithms for pigment estimation. SAM has been previously been use for estimation of chlorophyll-a in coastal waters (Kutser, 2004) using a bio-optical model parameterisation approach.

(3) Continuum-Removal

Continuum-removal is a method that can be used to normalise reflectance spectra (or, in this instance, radiance spectra) allowing individual absorption features to be compared from a common baseline. The continuum is a convex hull fitted across the spectrum using straight line segments to connect local spectral maxima. The continuum is removed by dividing it into the actual spectrum for each image pixel (Equation 5.1):

$$S_{cr} = (S / C) \qquad \textbf{Equation 5.1}$$

where S_{cr} is the continuum-removed spectrum, S is the original spectrum and C is the continuum curve (for further explanation see Section 3.3.3). Continuum-removal was applied to the CASI-2 [SeaWiFS] L_w imagery and the derived continuum-removed images were used to: (i) calculate the continuum removed band-depth and, (ii) used to parameterise spectral feature fitting models (see below).

Continuum-Removed Band Depth Analysis—The continuum-removed band-depths (CRBD) obtained from the continuum-removal analysis were extracted from the CASI-2 [SeaWiFS] image at the location of each lake sampling station. The CRBDs were subsequently collated for use in the formulation of remote-sensing-based algorithms for pigment estimation.

Continuum-Removed Spectral Feature Fitting—Spectral Feature Fitting (SFF) is an absorption-feature-based methodology which compares the fit of continuum-removed image spectra to continuum-removed endmember spectra using a least-squares technique (Kokaly *et al.,* 2003).

The output derived is a scale image for each user-specified endmember depicting the relative fit between the SFF image spectrum and the endmember reference spectrum. SFF was applied to the continuum-removed image transformations of the CASI-2 [SeaWiFS] imagery and the resulting scale values were extracted from the CASI-2 [SeaWiFS] image at the location of each lake sampling station. The SFF scale values were subsequently collated for use in the formulation of remote-sensing-based algorithms for pigment estimation.

Statistical analysis—Least-squares linear and non-linear regression models for the estimation of chlorophyll-a and C-phycocyanin were developed in Minitab v.14. The NIR/red band-ratio values were non-normal (Anderson-Darling test); thus the datasets were Log_{10}-transformed prior to further statistical analysis. Algorithms for pigment retrieval based upon the NIR/red band-ratios were formulated using simple linear least-squares regression models. Algorithms for pigment retrieval using the endmember relative abundances (MTMF and LSMM), probability values (SAM), CRBD and continuum-removed scale values (SFF) were formulated using multivariate best-subsets regression. In order to preserve a degree of mechanistic clarity, the derived chlorophyll-a and C-phycocyanin endmember variables were included as fixed predictors in all models where the associated pigment was also the response variable. CRBD and SFF scale values for all endmember variables were allowed to be free predictors. The optimum best-subsets regression models were identified on the basis of the C-p Mallow's statistic, the coefficient of determination (R^2 and R^2 [adjusted]) and the RMSE.

5.4.5.2 Diurnal Time-Series Surveillance of a Potentially-Toxic Cyanobacterial Bloom

The NERC ARSF aircraft was deployed on the 29 August 2005 in a specific response to the development of a bloom of the potentially-toxic cyanobacterium *Microcystis aeruginosa* on Barton Broad. Time-series CASI-2 [SeaWiFS] imagery of the bloom was captured at 09:30, 12:00 and 16.00 h GMT. The optimum NIR/red band-ratio algorithms for the estimation of chlorophyll-a and C-phycocyanin concentrations (derived in Section 5.4.5.1) were then applied to the 29 August 2005 CASI-2 [SeaWiFS] time-series dataset to provide calibrated maps of the concentration of chlorophyll-a and C-phycocyanin in Barton Broad. These spatially-resolving images allowed diurnal change in the distribution of *M. aeruginosa* colonies in the lake to be

examined. The calibrated CASI-2 [SeaWiFS] chlorophyll-a and C-phycocyanin images were also used to produce images depicting the C-phycocyanin:chlorophyll-a ratio (C-PC:chl-a) using a simple band-math approach.

The CASI-2 [SeaWiFS] time-series imagery of the cyanobacteria bloom was supplemented with water chemistry data collected on 22 August 2005 by the Environment Agency. Hourly meteorological observations (MIDAS Land Surface Observation Station Data) from the nearest weather station (Coltishall ~ 8 km) were provided upon request courtesy of the NERC British Atmospheric Data Centre. The water chemistry and meteorological data were subsequently used to aid the interpretation of the development and diurnal spatial dynamics of the *M. aeruginosa* bloom in Barton Broad.

5.5 RESULTS AND DISCUSSION

5.5.1 Development and Validation of Algorithms

5.5.1.1 Algorithm Calibration

Water Quality Trends—The water quality in the Upper Thurne and Barton Broads over the course of the 2-year NERC ARSF data acquisition campaign was highly variable, both spatially (inter- and intra-lake) and temporally (seasonally). The water quality data obtained from the lake sampling cruises in the Upper Thurne and Barton Broads contemporaneous to the NERC ARSF data acquisition campaigns are summarised in Table 5.5. The highest mean concentration of chlororphyll-a measured in the Upper Thurne and Barton Broads over the 2-year lake sampling period was observed on 28 February 2005 (Environmental Agency data). This was largely due to the winter chlorophyll-a maximum on Hickling Broad (chlorophyll-a = 55.7 (22.1-104.0) mg m^{-3}). No measurements of C-phycocyanin are available for the 28 February 2005.

Table 5.5 Summary of the water quality data collected during the 2-year lake sampling cruises contemporaneous to the NERC ARSF campaigns.

	Chlorophyll-a (mg m^{-3})			C-phycocyanin (mg m^{-3})			SPM (mg L^{-1})			SPIM (mg L^{-1})			SPOM (mg L^{-1})		
	Min	Max	Mean	Min	Max	Mean	Min	Max	Mean	Min	Max	Mean	Min	Max	Mean
28 February 2005[†]	22.1	104.0	55.7	—	—	—	7.9	24.7	32.6	—	—	—	—	—	—
21 April 2005	17.4	31.8	23.5	0.0[‡]	44.9	14.8	4.6	20.2	9.6	1.5	8.2	3.8	3.2	12.0	5.9
22 June 2005	5.2	30.1	19.8	13.5	44.5	27.9	5.6	74.2	34.1	1.4	34.7	15.6	4.2	39.5	18.6
29 August 2005	4.0	70.9	38.6	6.6	138.8	59.8	9.6	69.0	45.5	4.4	43.5	23.2	5.2	43.3	22.2

[†]Indicative measurements provided by the Environment Agency from routine sampling in the Upper and Thurne and Barton Broads conducted on 18 February 2005.
[‡] < Minimum limit of detection

The mean concentration of chlorophyll-a was much lower on 21 April 2005 (23.5 (17.4-31.8) mg m^{-3}) and, further, the mean concentration of C-phycocyanin was the lowest measured over the 2-year sampling period (14.8 (0.0-44.9) mg m^{-3}) (i.e. low spring cyanobacterial abundance). The mean concentration of chlorophyll-a was lower again on 22 June 2005 (this was partly due to the extension of the lake sampling into the clear water Martham North Broad) (19.8 (5.2-30.1) mg m^{-3}); however, the mean concentration of C-phycocyanin was higher than that measured on 21 April 2005 (27.9 (13.5-44.5) mg m^{-3}) (i.e. increasing summer cyanobacterial abundance). The mean concentration of chlorophyll-a was significantly higher on 29 August 2005 (calibration dataset) (38.6 (4.0-70.9) mg m^{-3}); this was largely due to the *M. aeruginosa* bloom on Barton Broad. Thus, it was not unexpected that the highest mean concentration of C-phycocyanin measured over the 2-year lake sampling period was also observed on 29 August 2005 (59.8 (6.6-138.8) mg m^{-3}) concurrent to the *M. aeruginosa* bloom on Barton Broad (the SPM, SPIM and SPOM data is provided for informational purposes, but is not considered in this chapter).

Water quality measurements from several sampling stations had to be excluded from the algorithm calibration and validation process because they were taken > ±2 h from the time of the NERC ARSF data acquisition. No water quality data could be obtained contemporaneous to the 28 February 2005 NERC ARSF campaign; therefore indicative values were provided by the Environment Agency from a routine survey of water quality in the Upper Thurne and Barton Broads conducted on 18 February 2005.

NIR/red Band-Ratios—CASI-2 [SeaWiFS] L_w-signatures for Hickling and Barton Broad captured on 29 August 2005 are shown in Figure 5.8. Local L_w-minima related to absorption by bio-optically active pigments can be clearly seen in the L_w profiles. The L_w feature observable in proximity to CASI-2 [SeaWiFS] band 7 (670 nm) is related to absorption by chlorophyll-a and, in similarity, the L_w feature observable in proximity to CASI-2 [SeaWiFS] band 6 (620 nm) is associated with absorption by C-phycocyanin. The C-phycocyanin absorption feature is particularly prominent in the L_w spectra from Barton Broad due to the dense bloom of the potentially-toxic cyanobacterium *M. aeruginosa*.

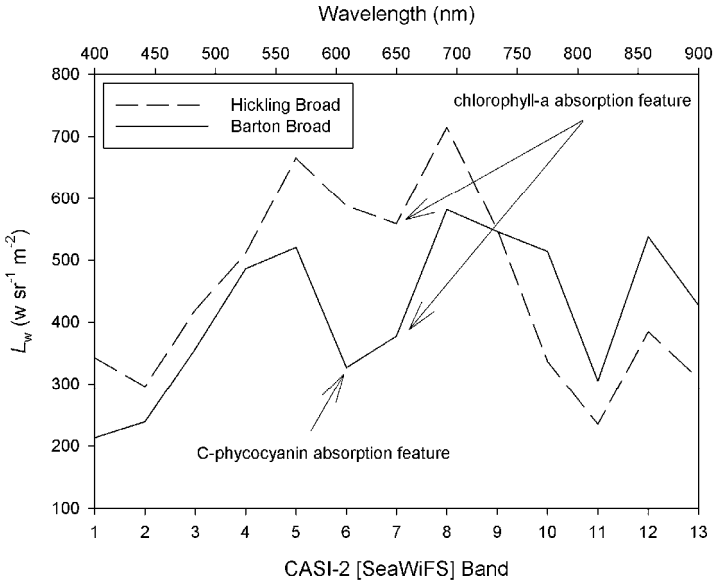

Figure 5.8 CASI-2 [SeaWiFS] water-leaving-radiance spectra from two lakes: (a) Hickling Broad and (b) the cyanobacterial-dominated Barton Broad. Note the presence of absorption features associated with chlorophyll-a at 670 nm in both spectra and the prominence of the C-phycocyanin related feature at 620 nm in the Barton Broad spectra.

The water-leaving-radiance profiles also show that the L_w signal was typically higher from Hickling Broad than that measured on Barton Broad (despite Barton Broad having a higher mean concentration of chlorophyll-a). This was largely due to increased backscattering caused by relatively higher concentrations of tripton in Hickling Broad. The lower values of L_w measured over Barton Broad were probably also the result of increased absorption by phytoplankton pigments during the bloom of *M. aeruginosa*.

The contribution of tripton scattering (and perhaps bottom radiance) to the upwelling water-leaving-radiance signal prevented strong correlations being observed between the measured concentration of chlorophyll-a or C-phycocyanin and L_w in any single CASI-2 [SeaWiFS] band (results not shown here). It was noted that strong relationships between pigment concentrations and the CASI-2 [SeaWiFS] could only be obtained following NIR/red band-ratio transformation. However, significant variation was observed in the efficacy of the various NIR/red band-ratios for the estimation of the chlorophyll-a concentration (Table 5.6). The optimum NIR/red index for the estimation of chlorophyll-a from the 29 August 2005 CASI-2 [SeaWiFS] data on the basis of the coefficient of determination and the RMSE was the

[L_w(710)/L_w(670)] band-ratio (n = 19; F = 309.0; R^2 = 0.960; p < 0.001; RMSE = 7.07 mg chlorophyll-a m^{-3}; RMSE% = 18.3).

Table 5.6 Coefficients of determination (R^2) and RMSE for the NIR/red band-ratio algorithms for the estimation of chlorophyll-a using the 29 August 2005 CASI-2 [SeaWiFS] data.

	n	**F**	***R*²**	**p**	**RMSE (mg m^{-3})**	**RMSE (%)**
[L_w(710)/L_w(682.5)]	19	154.50	0.901	0.000	9.53	24.7
[L_w(710)/L_w(670)]		309.00	0.960	0.000	7.07	18.3
[L_w(752)/L_w(682.5)]		0.00	0.000	0.981	19.74	51.2
[L_w(752)/L_w(670)]		1.27	0.069	0.276	18.24	47.3

The relationship between the [L_w(710)/L_w(670)] band-ratio and the measured concentration of chlorophyll-a was non-linear prior to Log_{10}-transformation; Log_{10}-transformation of the data substantially increased the linearity of the relationship (see Figure 5.9). The semi-empirical algorithm derived for the estimation of chlorophyll-a using the L_w(710)/L_w(670) ratio is shown in Equation 5.2.

$$\text{Chlorophyll-a (mg m}^{-3}) = 21.38 \cdot [L_w(710)/L_w(670)]^{2.44} \qquad \textbf{Equation 5.2}$$

It can be argued that the [L_w(710)/L_w(670)] band-ratio provided the best estimation of the concentration of chlorophyll-a because the index targeted the specific CASI-2 [SeaWiFS] band in which the *in vivo* chlorophyll-a absorption maximum occurs (Band 7; 670 nm). It can therefore be assumed that the index would retain maximum sensitivity to variance in the concentration of chlorophyll-a. Strong regression models were also derived between the measured chlorophyll-a concentration and the [L_w(710)/L_w(682.5)] ratio. However, statistically valid regression models could not be derived using the NIR/red band-ratios that employed L_w(752) as the numerator CASI-2 [SeaWiFS] band.

(a) (b)

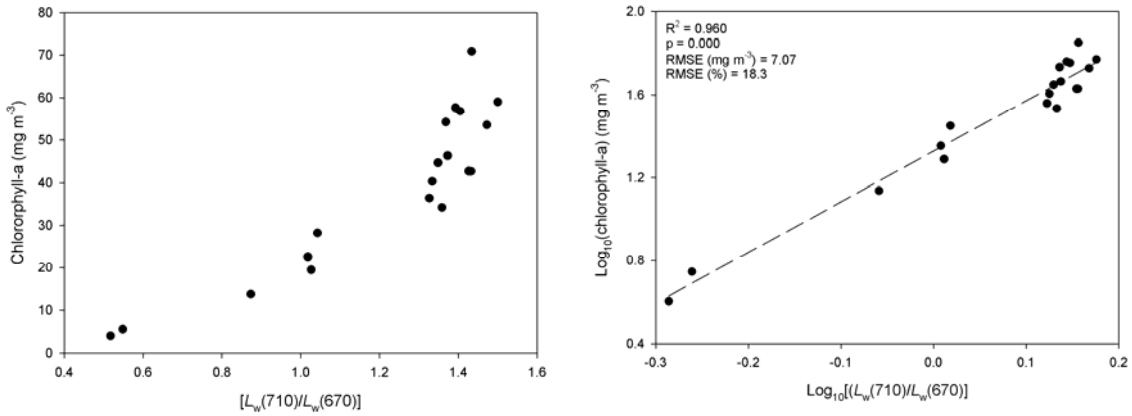

Figure 5.9 Scatter plots showing (a) the untransformed non-linear relationship between CASI-2 [SeaWiFS] [$L_w(710)/L_w(670)$] band-ratio and the measured concentration of chlorophyll-a and (b) the Log_{10}-transformed linear regression relationship between the CASI-2 [SeaWiFS] $L_w(710)/L_w(670)$ ratio and the measured concentration of chlorophyll-a in the Upper Thurne and Barton Broads.

Several previous authors have also found that the [$L_w(710)/L_w(670)$] band-ratio (or [$R_{rs}(710)/R_{rs}(670)$]) to be effective for the estimation of chlorophyll-a in CASE II waters (Dekker, 1993; Han *et al.,* 1994; Rundquist *et al.,* 1996; Han & Rundquist, 1997) including those working with CASI-2 data (Ostlund *et al.,* 2001; Ammenberg *et al.,* 2002). These previous findings provide some degree of substantiation for the results presented here. The optimum NIR/red band-ratio for the estimation of C-phycocyanin from the 29 August 2005 CASI-2 [SeaWiFS] data on the basis of the coefficient of determination and the RMSE was the [$L_w(710)/L_w(620)$] band-ratio (n = 19; F = 304.6; R^2 = 0.947; p < 0.001; RMSE = 11.9 mg chlorophyll-a m^{-3}; RMSE% = 19.9) (see Table 5.7).

Table 5.7 Coefficients of determination (R^2) and RMSE for the NIR/red band-ratio algorithms for the estimation of C-phycocyanin using the 29 August 2005 CASI-2 [SeaWiFS] data.

	n	**F**	***R*²**	**p**	**RMSE (mg m⁻³)**	**RMSE (%)**
[$L_w(710)/L_w(620)$]	19	304.62	0.947	0.000	11.90	19.9
[$L_w(710)/L_w(555)$]		45.24	0.727	0.000	26.11	46.6
[$L_w(752)/L_w(620)$]		9.70	0.363	0.006	32.99	55.1
[$L_w(752)/L_w(555)$]		3.18	0.158	0.092	37.25	62.2

The relationship between the [$L_w(710)/L_w(620)$] band-ratio and the measured concentration of C-phycocyanin was non-linear prior to Log_{10}-transformation; Log_{10}-transformation resulted in a significantly increased the linearity of the relationship (Figure 5.10). The resulting semi-empirical algorithm for the estimation of C-phycocyanin using the $L_w(710)/L_w(620)$ ratio is shown in Equation 5.3.

$$\text{C-phycocyanin (mg m}^{-3}) = 19.50 \cdot [L_w(710)/L_w(620)]^{4.12} \qquad \textbf{Equation 5.3}$$

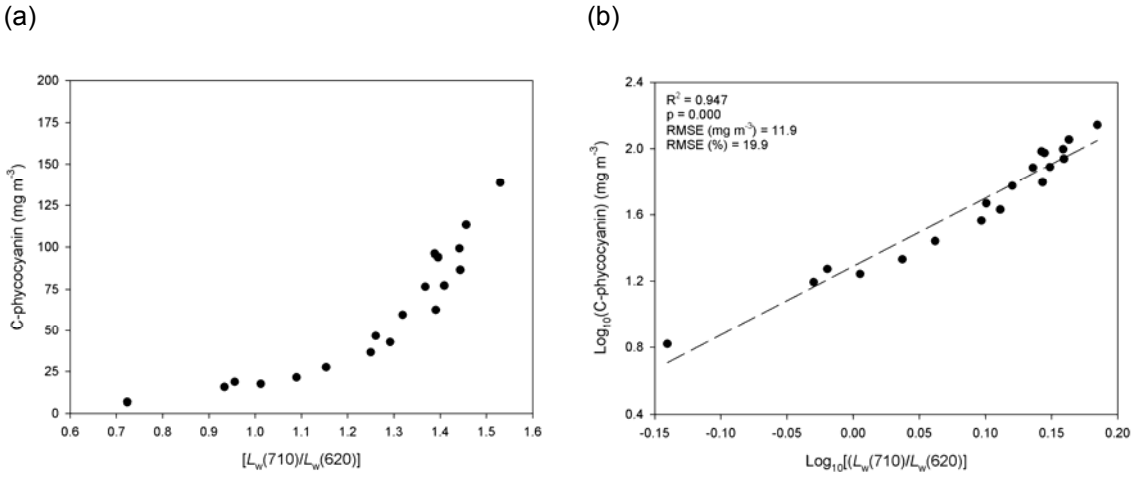

Figure 5.10 Scatter plots showing (a) the untransformed non-linear relationship between CASI-2 [SeaWiFS] [$L_w(710)/L_w(620)$] band-ratio and the measured concentration of C-phycocyanin and (b) the Log_{10}-transformed linear regression relationship between the CASI-2 [SeaWiFS] [$L_w(710)/L_w(620)$] ratio and the measured concentration of C-phycocyanin in the Upper Thurne and Barton Broads.

High coefficients of determination were also observed between the measured concentration of C-phycocyanin and the [$L_w(710)/L_w(555)$] band-ratio (n =19; F = 45.24; R^2 = 0.727; p = 0.000) – probably due to high (but not maximal) absorption by C-phycocyanin at 555 nm. In similarity to results derived from the chlorophyll-a NIR/red band-ratios, no statistically valid models could be derived with C-phycocyanin using NIR/red ratios employing $L_w(752)$ as the numerator NIR CASI-2 [SeaWiFS] band This may have been due to a low signal-to-noise ratio in CASI-2 [SeaWiFS] band 10 and strong attenuation by water absorption.

In similarity to the optimum NIR/red band-ratio for the estimation of chlorophyll-a, it can be suggested that the [$L_w(710)/L_w(620)$] band-ratio provided the best estimation of the

concentration of C-phycocyanin because it targets the specific CASI-2 [SeaWiFS] band in which the *in vivo* C-phycocyanin absorption maximum occurs (Band 6; 620 nm). It can therefore be assumed that the index would retain maximum sensitivity to variance in the concentration of chlorophyll-a. However, it must be noted that the measured concentrations chlorophyll-a and C-phycocyanin in the Upper Thurne and Barton Broads, as would be expected, demonstrated a significant degree of correlation (n = 19; r = 0.82; p = 0.000). It has been shown that, if chlorophyll-a and C-phycocyanin co-vary, strong correlations can be derived between image data and the concentration of C-phycocyanin simply because of covariance with chlorophyll-a (see for example Vincent *et al.,* 2004). However, in this instance, the coefficient of determination between the [$L_w(710)/L_w(620)$] band-ratio and the measured concentration of chlorophyll-a (n =19; F = 52.99; R^2 = 0.757; p = 0.000) was lower than that observed with the measured concentration of C-phycocyanin. This intimates that the [$L_w(710)/L_w(620)$] band-ratio held greater specificity to C-phycocyanin than chlorophyll-a. Similarly, the optimum band-ratio for chlorophyll-a, [$L_w(710)/L_w(670)$], demonstrated less specificity when correlated against the measured concentration of C-phycocyanin (n = 19; F = 48.19; R^2 = 0.739; p = 0.000). Further confidence in the C-phycocyanin specificity of the [$L_w(710)/L_w(620)$] band-ratio can be inferred from the fact that Simis *et al*. (2005) and Simis *et al*. (2007) used a similar band-ratio formulation for the estimation of C-phycocyanin in turbid cyanobacterial-dominated waters.

Spectral Mixing and SAM Models—The various multivariate regression algorithms derived from the MTMF, LSMM and SAM models for the estimation of chlorophyll-a are detailed in Table 5.8. In similarity to the results achieved with the NIR/red band-ratios, the multivariate algorithms derived from the endmember-based spectral mixing and SAM models also provided good estimations of the chlorophyll-a concentration in the Upper Thurne and Barton Broads on 29 August 2005 (R^2 = 0.699-0.815). The SAM model provided the best estimation of the chlorophyll-a (n = 19; F = 21.03; R^2 = 0.815; p = 0.000; RMSE = 8.12 mg chlorophyll-a m^{-3}; RMSE% = 21.0) when the rule image probabilities for chlorophyll-a, C-phycocyanin, tripton and the bottom substrate were recombined in the multivariate regression analysis. Whereas, of the spectral mixing models examined, the unconstrained LSMM, using endmembers derived from the MNF-transformed data, marginally demonstrated the strongest relationship with chlorophyll-

a (n = 19; F = 24.12; R^2 = 0.794; p = 0.000; RMSE = 8.57 mg chlorophyll-a m^{-3}; RMSE% = 22.2) using the recombined relative abundances for chlorophyll-a, C-phycocyanin, and tripton in the multivariate regression analysis. However, neither the LSMM or SAM multivariate regression algorithms demonstrated a better relationship with the chlorophyll-a concentration than that achieved with the [$L_w(710)/L_w(670)$] NIR/red band-ratio. The best-subsets multivariate algorithms for the estimation of chlorophyll-a are detailed in Equation 5.4 (SAM model) and Equation 5.5 (LSMM model):

$$\text{Chlorophyll-a (mg m}^{-3}) = 48.2 - 118 \cdot IRP_{chl} - 696 \cdot IRP_{C\text{-}PC} + 1009 \cdot IRP_{trip} - 300 \cdot IRP_{sub} \quad \textbf{Equation 5.4}$$

$$\text{Chlorophyll-a (mg m}^{-3}) = 23.1 - 2.28 \cdot EA_{chl} - 14.9 \cdot EA_{C\text{-}PC} - 22.2 \cdot EA_{trip} \quad \textbf{Equation 5.5}$$

where, IRP_{chl}, $IRP_{C\text{-}PC}$, IRP_{trip} and IRP_{sub} are the SAM-derived image rule probabilities for chlorophyll-a, C-phycocyanin, tripton and bottom substrate respectively; and EA_{ch}, $EA_{C\text{-}PC}$ and EA_{trip} are the LSMM-derived endmember abundances for chlorophyll-a, C-phycocyanin and tripton respectively.

Table 5.8 Comparison of the various multivariate regression models derived from the MF, MTMF, LSMM spectral mixing techniques and SAM for the estimation of chlorophyll-a.

		Data	Endmembers inc. in Model	*n*	F	R^2 (adj.)	p	RMSE (mg m^{-3})	RMSE (%)
MTMF		L_w	1,2,3,5		15.89	0.768	0.000	9.10	23.6
		MNF	1,2,3,4		11.47	0.699	0.000	10.35	26.8
LSMM	*Con.*	L_w	1,2,3		22.07	0.778	0.000	8.89	23.0
		MNF	1,3,4,5		15.86	0.768	0.000	9.10	23.6
	Uncon	L_w	1,2,3		22.07	0.778	0.000	8.89	23.0
	.	MNF	1,2,3		24.12	0.794	0.000	8.57	22.2
SAM		L_w	1,2,3,4		21.03	0.815	0.000	8.12	21.0

Con. – constrained model; *Uncon*. – unconstrained model.
L_w – endmembers extracted from untransformed CASI-2 [SeaWiFS] water-leaving-radiance data.
MNF – endmembers extracted from MNF-transformed CASI-2 [SeaWiFS] data.
Model endmembers: 1 – chlorophyll-a; 2 – C-phycocyanin; 3 – tripton; 4 – bottom substrate; 5 – aquatic vegetation.

The comparison between the fitted chlorophyll-a concentrations derived from the optimum SAM and LSMM models and the measured concentration of chlorophyll-a in the Norfolk Broads is shown in Figure 5.11. It is evident that both the SAM and LSMM derived algorithms provided a good fit against the measured chlorophyll-a values at low concentrations (i.e. stations from

Hickling Broad and the Martham Broads), but considerable scatter is observed in both models for comparisons against the high concentrations of chlorophyll-a measured during the cyanobacterial bloom in Barton Broad. This may suggest that the endmember components used in both the SAM and LSMM models were ill-defined for the specific bio-optical conditions encountered on Barton Broad.

(a) (b)

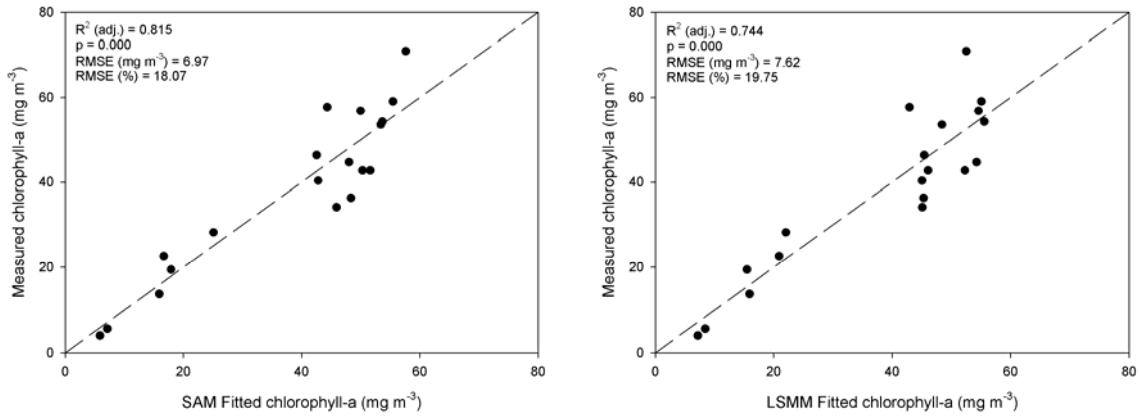

Figure 5.11 Comparison of the (a) the SAM fitted chlorophyll-a concentrations and (b) the LSMM unconstrained MNF-transformed fitted chlorophyll-a concentrations against the measured concentration of chlorophyll-a in the Upper Thurne and Barton Broads on 29 August 2005.

The various multivariate regression models derived from the MTMF, LSMM and SAM methods for the estimation of C-phycocyanin are detailed in Table 5.9. In similarity to the results observed for chlorophyll-a, the multivariate algorithms derived from the endmember-based spectral mixing and SAM models demonstrated good relationships with the concentration of C-phycocyanin concentration (R^2 = 0.680-0.801) in the Upper Thurne and Barton Broads on 29 August 2005. The SAM model again provided the best estimation of pigment concentration (n = 19; F = 21.03; R^2 = 0.815; p = 0.000; RMSE = 8.12 mg C-phycocyanin m^{-3}; RMSE% = 21.0) but, in contrast to the SAM model for chlorophyll-a, the optimum model used the recombined rule image probabilities for C-phycocyanin, tripton, bottom substrate and aquatic vegetation in the multivariate regression analysis. The results obtained from the MTMF and LSMM algorithms were very similar. However in this instance the constrained LSMM derived from the non-MNF-transformed data provided a better fit against the measured concentration of C-

phycocyanin than that obtained with the unconstrained MNF-transformed LSMM model. Nonetheless, in similarity to the results observed for chlorophyll-a, the spectral mixing and SAM models could not provide a better estimation of the C-phycocyanin concentration than that achieved with the [$L_w(710)/L_w(620)$] NIR/red band-ratio.

Table 5.9 Comparison of the various multivariate regression models derived from the MF, MTMF, LSMM spectral mixing techniques and SAM for the estimation of C-phycocyanin.

		Data	Endmembers inc. in Model	*n*	F	R^2 (adj.)	p	RMSE (mg m^{-3})	RMSE (%)
MF		L_w	1,2,4,5	19	18.47	0.744	0.000	19.30	32.3
		MNF	1,2,3,4		10.58	0.680	0.000	21.58	36.1
MTMF		L_w	1,2,4,5		18.47	0.744	0.000	19.30	32.3
		MNF	1,2,3,4		10.58	0.680	0.000	21.58	36.1
LSMM	*Con.*	L_w	1,2,3,5		14.05	0.744	0.000	19.33	32.3
		MNF	1,2,3,5		13.81	0.740	0.000	19.46	32.58
	Uncon.	L_w	1,2,3,5		14.05	0.744	0.000	19.33	32.3
		MNF	1,2,3,4		12.68	0.722	0.000	20.13	33.6
SAM		L_w	2,3,4,5		19.17	0.801	0.000	17.00	28.4

Con. – constrained model; *Uncon*. – unconstrained model.
L_w – endmembers extracted from untransformed CASI-2 [SeaWiFS] water-leaving-radiance data.
MNF – endmembers extracted from MNF-transformed CASI-2 [SeaWiFS] data.
Model endmembers: 1 – chlorophyll-a; 2 – C-phycocyanin; 3 – tripton; 4 – bottom substrate; 5 – aquatic vegetation.

The best-subsets multivariate algorithms for the estimation of C-phycocyanin are detailed in Equation 5.6 (SAM model) and Equation 5.7 (LSMM model):

$$\text{C-phycocyanin (mg m}^{-3}) = 57.8 - 3233 \cdot IRP_{\text{C-PC}} + 2857 \cdot IRP_{\text{trip}} + 1013 \cdot IRP_{\text{sub}} - 701 \cdot IRP_{\text{veg}} \quad \textbf{Equation 5.6}$$

$$\text{C-phycocyanin (mg m}^{-3}) = 74.5 - 36.1 \cdot EA_{\text{chl}} - 126 \cdot EA_{\text{C-PC}} - 112 \cdot EA_{\text{trip}} - 52.8 \cdot EA_{\text{veg}} \quad \textbf{Equation 5.7}$$

where $IRP_{\text{C-PC}}$, IRP_{trip}, IRP_{sub} and IRP_{veg} are the SAM-derived image rule probabilities for C-phycocyanin, tripton, bottom substrate and aquatic vegetation respectively; and EA_{ch}, $EA_{\text{C-PC}}$ and EA_{trip} are the LSMM-derived endmember abundances for chlorophyll-a, C-phycocyanin and tripton respectively. The comparison between the fitted C-phycocyanin concentrations derived from the optimum SAM and LSMM models and the measured concentration of C-phycocyanin in the Norfolk Broads is depicted in Figure 5.12.

(a) (b)

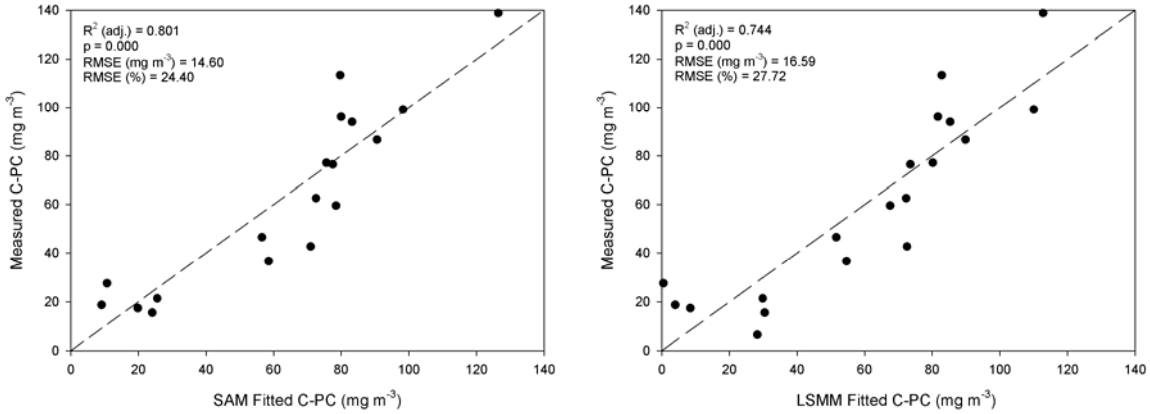

Figure 5.12 Comparison of the (a) the SAM fitted C-phycocyanin concentrations and (b) the LSMM unconstrained MNF-transformed fitted C-phycocyanin concentrations against the measured concentration of C-phycocyanin in the Upper Thurne and Barton Broads on 29 August 2005.

Continuum-Removed Band Depths and Spectra Feature Fitting—The multivariate regression algorithms for the estimation of chlorophyll-a derived from the CRBD and SFF models are detailed in Table 5.10. The optimum multivariate regression algorithm was obtained from the recombination of the CRBDs for CASI-2 [SeaWiFS] bands 4 (510 nm), 6 (620 nm), 7 (670 nm), 8 (682.5 nm) and 11 (762 nm) (n = 19; F = 18.43; R^2 = 0.828; p = 0.000; RMSE = 7.83 mg chlorophyll-a m^{-3}; RMSE% = 20.3). The continuum-removed absorption-related features occurring in CASI-2 [SeaWiFS] bands 6, 7 and 8 are predominantly related to the presence of C-phycocyanin and chlorophyll-a. The continuum-removed absorption feature occurring in CASI-2 [SeaWiFS] band 4 may be related to the overlapping absorption spectra of chlorophyll-a and carotenoids pigments allied to the presence of dissolved and particulate organics. The inclusion of these continuum-removed bands in the multivariate model for the estimation of chlorophyll-a therefore seems to be mechanistically justifiable. The inclusion of the continuum-removed absorption feature occurring in CASI-2 [SeaWiFS] band 11 (related to the oxygen absorption feature at 762 nm) is more difficult to understand; although the depth of the absorption feature in band 11 may be influenced by tripton scattering which may, in part, explain its inclusion in the multivariate model.

Table 5.10 Comparison of the various multivariate regression models derived from the CRBD and SFF analysis for the estimation of chlorophyll-a.

	Bands/Endmembers inc. in Model	*n*	F	R^2 (adj.)	p	RMSE (mg m^{-3})	RMSE (%)
CRBD	B4, B6, B7, B8, B11	19	18.33	0.828	0.000	7.83	20.3
SFF	1,2,4		10.61	0.681	0.000	10.67	27.6

Model endmembers: 1 – chlorophyll-a; 2 – C-phycocyanin; 3 – tripton; 4 – bottom substrate; 5 – aquatic vegetation.

The SFF model also provided a reasonable estimation of the concentration of chlorophyll-a; this was, however, somewhat poorer than that obtained from the CRBD model. The CRBD model provided an improvement on the estimation of chlorophyll-a in comparison to that obtained from the spectral mixing and SAM models. Nonetheless, the optimum CRBD model was again not as effective for the estimation of chlorophyll-a as the [$L_w(710)/L_w(670)$] NIR/red band-ratio. The optimum algorithm for the estimation of chlorophyll-a from the CRBD multivariate regression model is detailed in Equation 5.8:

$$\text{Chlorophyll-a (mg m}^{-3}) = 155 + 272 \cdot CRBD_{B4} - 262 \cdot CRBD_{B6} + 247 \cdot CRBD_{B7} - 250 \cdot CRBD_{B8} - 222 \cdot CRBD_{B11}$$

Equation 5.8

where $CRBD_{B4}$, $CRBD_{B6}$, $CRBD_{B7}$, $CRBD_{B8}$ and $CRBD_{B11}$ are the continuum-removed band-depths for CASI-2 [SeaWiFS] bands 4, 6, 7, 8 and 11 respectively. The comparison between the CRBD model fitted chlorophyll-a concentrations and the measured concentration of chlorophyll-a is shown in Figure 5.13. The CRBD model provided a reasonably good fit against the measured concentration of chlorophyll-a; however, it is again evident that scatter occurs in the relationship for high concentrations of chlorophyll-a.

The multivariate regression algorithms for the estimation of C-phycocyanin derived from the continuum-removed band depth and SFF models are detailed in Table 5.11. The optimum multivariate regression algorithm was obtained from the recombination of the CRBDs for CASI-2 [SeaWiFS] bands 4 (510 nm), 6 (620 nm) and 11 (762 nm) (n = 19; F= 29.17; R^2 = 0.824; p = 0.000; RMSE = 15.99 mg chlorophyll-a m^{-3}; RMSE% = 26.7).

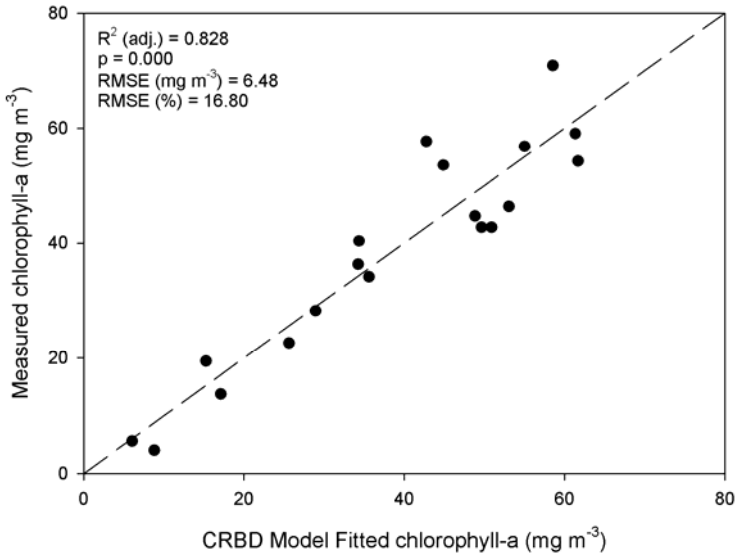

Figure 5.13 Comparison of the CRBD model fitted chlorophyll-a concentrations against the measured concentration of chlorophyll-a in the Upper Thurne and Barton Broads on 29 August 2005.

Table 5.11 Comparison of the various multivariate regression models derived from the CRBD and SFF analysis for the estimation of C-phycocyanin.

	Bands/Endmembers inc. in Model	*n*	F	R^2 (adj.)	p	RMSE (mg m^{-3})	RMSE (%)
CRBD	B4, B6, B11	19	29.17	0.824	0.000	15.99	26.7
SFF	2,3,4,5		15.96	0.769	0.000	18.36	30.7

Model endmembers: 1 – chlorophyll-a; 2 – C-phycocyanin; 3 – tripton; 4 – bottom substrate; 5 – aquatic vegetation.

In similarity to the CRBD model for chlorophyll-a, inclusion of the continuum-removed absorption features occurring in CASI-2 [SeaWiFS] bands 4 (555 nm) and 6 (620 nm) in the CRBD model for C-phycocyanin probably reflects the influence of C-phycocyanin absorption at these wavelengths. Again, CASI-2 [SeaWiFS] band 11 was also included in the model, which further suggests that its inclusion may provide some degree of correction in the regression model for the effects of tripton scattering, although the semi-empirical nature of this approach makes it difficult to obtain a complete and mechanistic understanding of algorithm construction.

The SFF model also provided a reasonable estimation of the concentration of C-phycocyanin; this was, however, somewhat poorer that that obtained from the CRBD model. The CRBD

model provided an improvement on the estimation of chlorophyll-a in comparison to that obtained from the spectral mixing and SAM models. Nonetheless, the CRBD model was again not as effective for the estimation of C-phycocyanin as the [$L_w(710)/L_w(620)$] NIR/red band-ratio. The algorithm for the estimation of chlorophyll-a from the CRBD multivariate regression model is detailed in Equation 5.9:

$$\text{C-phycocyanin (mg m}^{-3}) = 113 + 447 \cdot CRBD_{B4} - 461 \cdot CRBD_{B6} - 274 \cdot CRBD_{B11} \qquad \textbf{Equation 5.9}$$

where $CRBD_{B4}$, $CRBD_{B6}$, and $CRBD_{B11}$ are the continuum-removed band depths for CASI-2 [SeaWiFS] bands 4, 6 and 11 respectively. The comparison between the CRBD model fitted chlorophyll-a concentrations and the measured concentration of chlorophyll-a is shown in Figure 5.14.

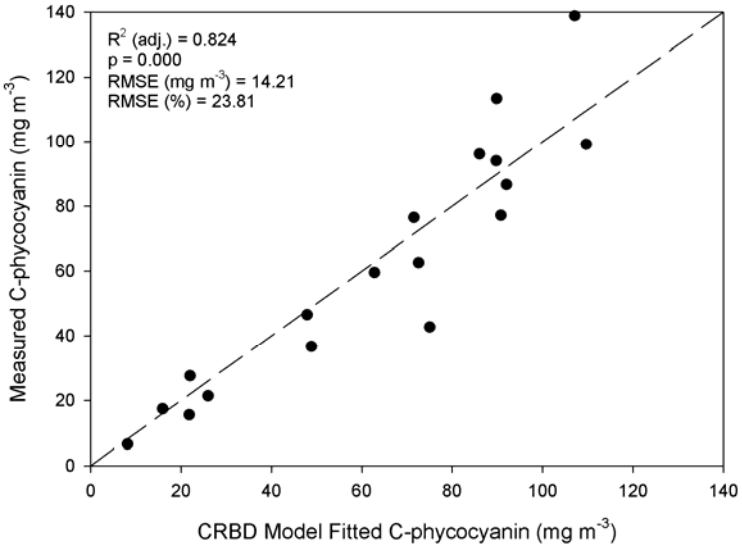

Figure 5.14 Comparison of the CRBD model fitted C-phycocyanin concentrations against the measured concentration of C-phycocyanin in the Upper Thurne and Barton Broads on 29 August 2005.

5.5.1.2 Algorithm Validation

NIR/red Band-Ratios—The optimum NIR/red band-ratio algorithm for the estimation of chlorophyll-a was applied to the CASI-2 [SeaWiFS] images acquired over the Upper Thurne and Barton Broads at 13.00 h GMT on 28 February 2005, 21 April 2005 and 22 June 2005; the derived coefficients of determination and RMSE for the validation analysis are detailed in Table

5.12. The validation analysis demonstrated that the CASI-2 [SeaWiFS] [$L_w(710)/L_w(670)$] band-ratio algorithm provided an excellent estimation of the chlorophyll-a concentration in the Upper Thurne and Barton Broads when compared to the concentration of chlorophyll-a measured at stations in the Upper Thurne and Barton Broads on the 28 February 2005, 21 April 2005 and 22 June 2005. RMSEs (mg m^{-3}) for the estimation of chlorophyll-a ranged from 3.38 mg m^{-3} on 21 April 2005 to 11.08 mg m^{-3} on 28 February 2005 and, for all CASI-2 [SeaWIFS] validation datasets; this equates to a RMSE < ±20% over the range 5.2-104.0 mg chlorophyll-a m^{-3}. This degree of predictive accuracy for NIR/red band-ratio-based chlorophyll-a retrieval algorithms compares favourably to the target of < ±35% over the range 0.05-50 mg chlorophyll-a m^{-3} adopted for the SeaWiFS ocean colour monitoring programme (Hooker & McClain, 2000).

Table 5.12 Coefficients of determination and RMSEs for the validation of chlorophyll-a concentrations derived from the CASI-2 [SeaWiFS] [$L_w(710)/L_w(670)$] NIR/red band-ratio algorithm against the measured concentration of chlorophyll-a in the Upper Thurne and Barton Broads on 28 February 2005, 21 April 2005 and 22 June 2005.

	n	***R^2***	**RMSE (mg m^{-3})**	**RMSE (%)**
28 February 2005	3	0.997	11.08	19.9
21 April 2005	7	0.687	3.38	15.7
22 June 2005	11	0.785	3.53	17.8

The largest validation errors were derived from CASI-2 [SeaWiFS] imagery acquired on 28 February 2005. However, given that the measured chlorophyll-a concentrations used to validate the algorithm were obtained on 18 February 2005 – 10 d prior to image acquisition – some degree of error would have no doubt been incurred from the lack of synchronicity between image acquisition and ground-truth sampling. The comparison between the image-predicted chlorophyll-a concentrations from the [$L_w(710)/L_w(670)$] NIR/red band-ratio algorithm and the measured concentration of chlorophyll-a in the Upper Thurne and Barton Broads for all validation datasets is shown in Figure 5.15.

The minimum detection limit for the remotely sensed estimation of phytoplankton pigment concentrations is an important consideration and, in particular, in the context of the potential implementation of a remote-sensing-based monitoring strategy for the EU WFD. It is difficult to ascertain the CASI-2 [SeaWiFS] minimum detection limit (MDL) for chlorophyll-a based solely

on data obtained here. However, based upon the results outlined above, a conservative MDL estimate for chlorophyll-a in shallow CASE II waters (comparable to those of the Upper Thurne and Barton Broads) might be placed at approximately 5 mg chlorophyll-a m^{-3}; this MDL for chlorophyll-a would certainly seem conducive to the use of remote sensing for routine lake monitoring purposes.

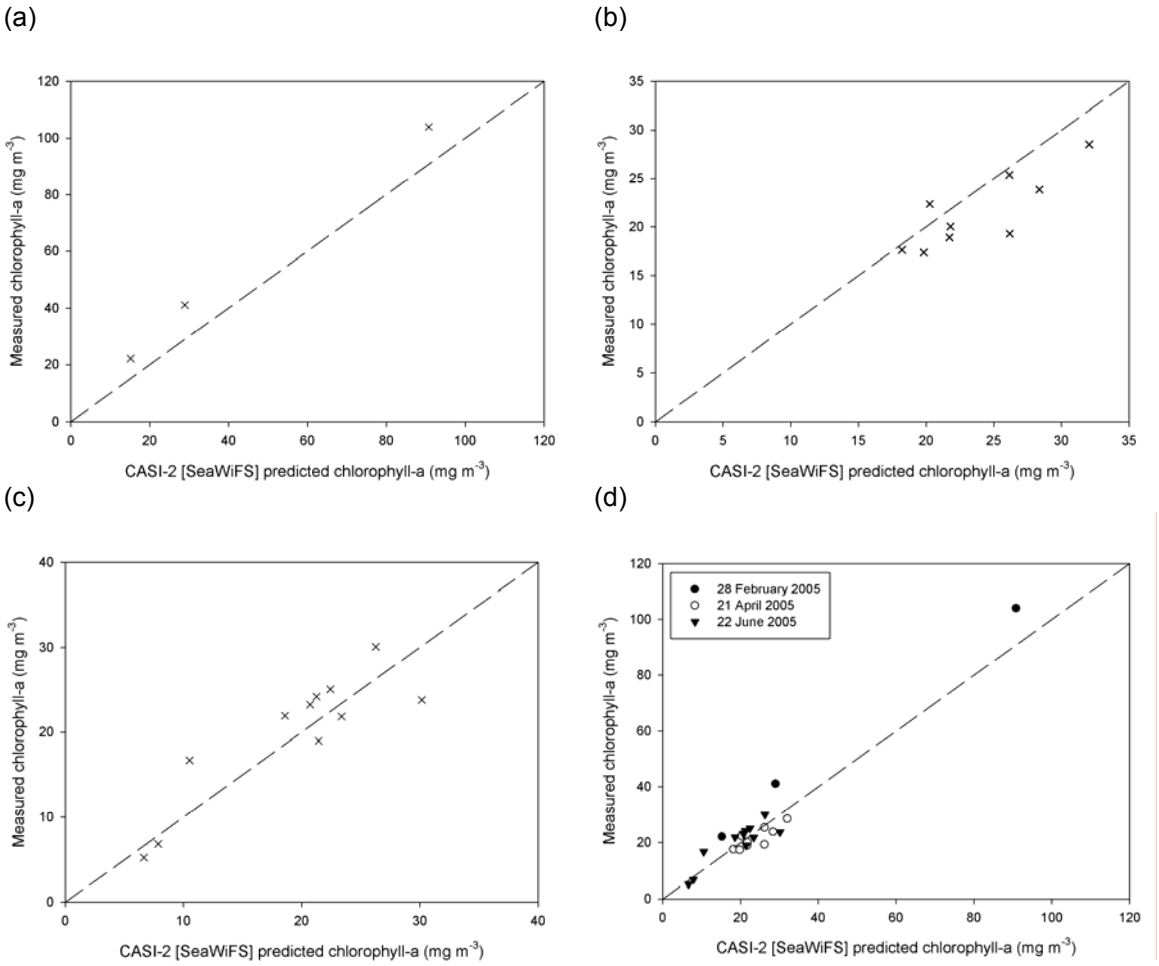

Figure 5.15 Comparison of optimum NIR/red band-ratio [$L_w(710)/L_w(670)$] algorithm predicted chlorophyll-a concentrations derived from the CASI-2 [SeaWiFS] imagery against the measured concentration of chlorophyll-a in the Upper Thurne and Barton Broads on (a) 28 February 2005, (b) 21 April 2005, (c) 22 June 2005 and (d) during all NERC ARSF campaigns.

The optimum NIR/red band-ratio algorithm for the estimation of C-phycocyanin was validated using the CASI-2 [SeaWiFS] images acquired over the Upper Thurne and Barton Broads at 13.00 h GMT on 21 April 2005 and 22 June 2005 (no measurements of the C-phycocyanin concentration were available to validate the algorithm for the 28 February CASI-2 [SeaWiFS]

image). The derived coefficients of determination and RMSEs for the validation analysis are detailed in Table 5.13.

Table 5.13 Coefficients of determination and RMSEs for the validation of C-phycocyanin concentrations derived from the CASI-2 [SeaWiFS] $L_w(710)/L_w(620)$ NIR/red band ratio algorithm against the measured concentration of C-phycocyanin in the Upper Thurne and Barton Broads on 21 April 2005, 22 June 2005 and for all sampling dates combined.

	n	R^2	**RMSE (mg m^{-3})**	**RMSE (%)**
21 April 2005	7	0.031	6.63	52.7
22 June 2005	11	0.800	9.03	33.4

The CASI-2 [SeaWiFS] [$L_w(710)/L_w(620)$] NIR/red band-ratio algorithm generally provided a good estimation of the C-phycocyanin concentration in the Upper Thurne and Barton Broads when compared to the concentration of C-phycocyanin measured at stations in the Upper Thurne and Barton Broads on 21 April 2005 and 22 June 2005. The RMSEs (mg m^{-3}) for the estimation of chlorophyll-a ranged from 6.63 mg m^{-3} on 21 April 2005 to 9.03 mg m^{-3} on 22 June 2005; these errors represent a RMSE(%) of ±33.4-52.7% over the range 8.1-54.9 mg C-phycocyanin m^{-3}.

The accuracy of the NIR/red band-ratio algorithm for the estimation of C-phycocyanin would thus seem to be slightly poorer compared to that achieved for chlorophyll-a. The incurred errors in the estimation of C-phycocyanin are probably due to interference from other bio-optically active pigments when the concentration of C-phycocyanin is low. Simis *et al*. (2007) have shown that the accuracy of the remote-sensing-based estimation of C-phycocyanin is dependent on the C-phycocyanin:chlorophyll-a and C-phycocyanin:chlorophyll-b ratios. This would seem to explain the high RMSE observed for the estimation of C-phycocyanin on the 22 April 2005 CASI-2 [SeaWiFS] image (the C-phycocyanin:chlorophyll-a ratio was lowest in April 2005). Nonetheless, the results indicate the estimation of C-phycocyanin (and hence cyanobacterial biomass) using NIR/red band-ratios algorithms is achievable in optically-complex shallow lakes.

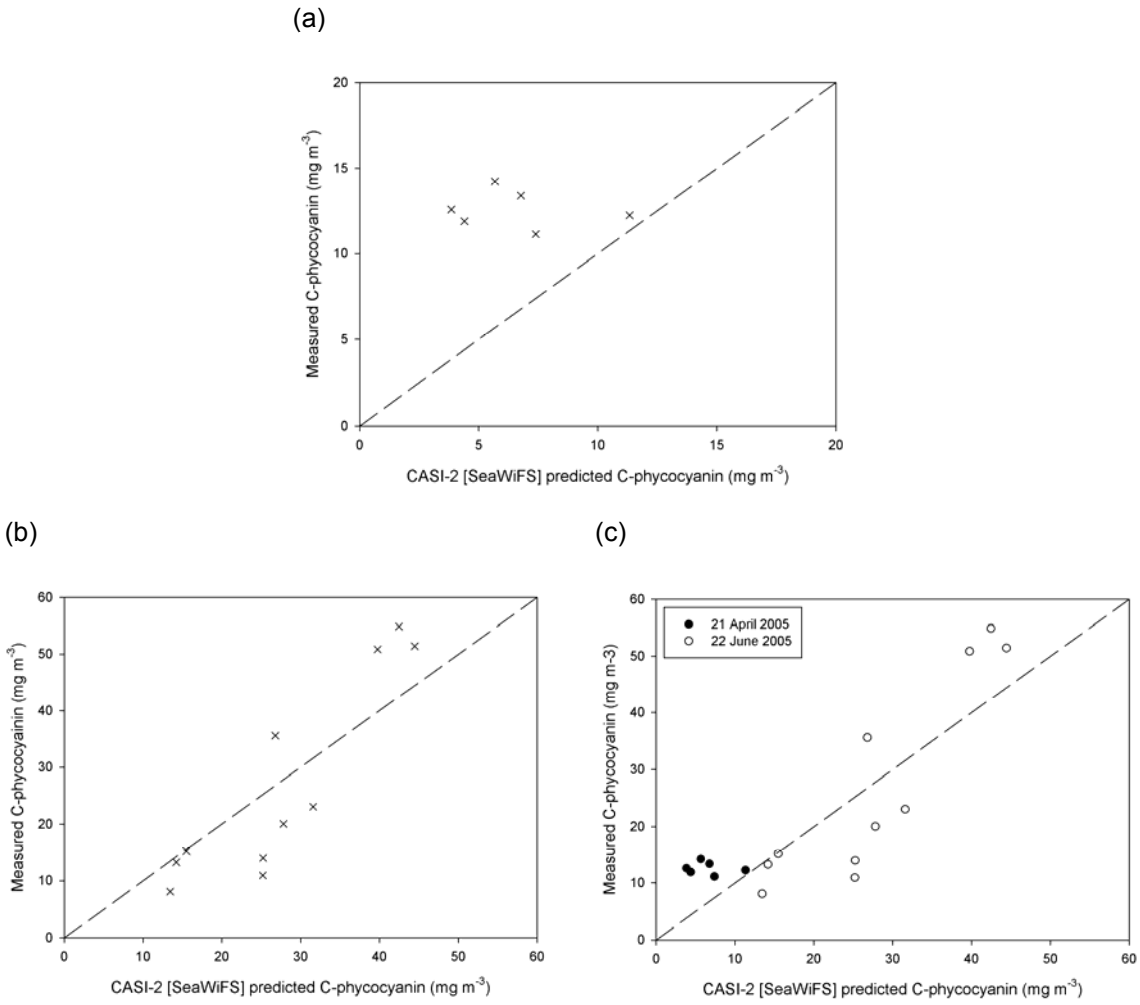

Figure 5.16 Comparison of optimum NIR/red band-ratio [$L_w(710)/L_w(620)$] algorithm predicted C-phycocyanin concentrations derived from the CASI-2 [SeaWiFS] imagery against the measured concentration of C-phycocyanin in the Upper Thurne and Barton Broads on (a) 21 April 2005 and (b) 22 June 2005 and (c) during all NERC ARSF campaigns.

The greater uncertainty apparent in the estimation of C-phycocyanin from CASI-2 [SeaWiFS] data would seem to suggest the MDL for C-phycocyanin is likely to be somewhat higher than that for chlorophyll-a. Again, it is difficult to accurately establish a MDL based solely on the data presented here. However, in Figure 5.16(c) a lower asymptote can be perceived at concentrations equivalent to ~ 10 mg C-phycocyanin m^{-3}; thus 10 mg m^{-3} may represent an approximate MDL for C-phycocyanin in the waters of the Upper Thurne and Barton Broads. Kutser *et al*. (2006) suggest a MDL for C-phycocyanin in the Baltic Sea equivalent to a chlorophyll-a concentration of ~ 10-30 mg m^{-3}; Metsamaa *et al*. (2006) also suggest that the concentration of chlorophyll-a in the Baltic Sea has to reach 8-10 mg m^{-3} before the C-phycocyanin absorption related feature is detectable from remote sensing instruments

(assuming a minimum 1000:1 signal-to-noise ratio). Thus, the 10 mg C-phycocyanin m^{-3} MDL suggested here would seem to be comparable to that proposed in previous studies.

LSMM, SAM and Continuum-Removed Models—The algorithms for the estimation of chlorophyll-a and C-phycocyanin derived from the LSMM, SAM and CRBD modelling were applied to the CASI-2 [SeaWiFS] images acquired over the Upper Thurne and Barton Broads on the 28 February 2005, 21 April 2005 and 22 June 2005 and validated against the measured concentrations of chlorophyll-a and C-phycocyanin. The unconstrained LSMM model formulated from the non-MNF-transformed L_w data was used in the validation analysis as (i) there were only marginal differences between the performance of the various LSMM models and (ii) it was perceived that the endmember spectra used in the MNF-transformed LSMM models would not be applicable to other MNF-transformed CASI-2 [SeaWiFS] datasets due to the somewhat scene-dependent nature of the MNF-transform.

The endmember spectra derived from the initial 29 August 2005 CASI-2 [SeaWiFS] image were used to parameterise LSMM and SAM models for the CASI-2 [SeaWiFS] validation datasets. The models were run and the resulting model solutions (LSMM endmember relative abundances and SAM image-rule probabilities) were recombined into the pre-derived 29 August 2005 algorithms for chlorophyll-a and C-phycocyanin. However, this validation analysis resulted in large residual errors between the model-estimated and measured pigment concentrations. Thus, it was apparent that the algorithms derived from the 29 August 2005 CASI-2 [SeaWIFS] imagery were essentially scene-dependent and could not be effectively extrapolated to the remaining multi-temporal CASI-2 [SeaWiFS] datasets. Semi-empirically derived water-leaving-radiance based algorithms often suffer from lack of transferability as they are generally only valid for application under the precise atmospheric conditions, and solar and viewing geometries, prevalent at the time of algorithm calibration. However, here, an effective image-to-image normalisation procedure was employed to enable the extrapolation of algorithms for pigment estimation between different CASI-2 [SeaWiFS] images of the Upper Thurne and Barton Broads.

The lack of algorithm transferability encountered here probably reflects, therefore, the scene-dependent nature of the LSMM, SAM and CRBD model solutions. Moreover, because of the significant variation in the water quality conditions between the various CASI-2 [SeaWiFS] images, the endmember spectra derived from the 29 August 2005 CASI-2 [SeaWiFS] image may not have been representative of the actual endmember components in the 28 February 2005, 21 April 2005 and 22 June 2005 CASI-2 [SeaWiFS] images. Indeed, 2-D projections of image pixels in component space demonstrated that endmember pixels in the CASI-2 [SeaWiFS] imagery from the 28 February 2005, 21 April 2005 and 22 June 2005 were different to those originally extracted in the 29 August 2005 CASI-2 [SeaWiFS] datasets. Most notable, was the absence of pronounced endmembers for C-phycocyanin (i.e. low cyanobacterial abundance) and aquatic vegetation (early growing season) in the 28 February 2005 and 21 April CASI-2 [SeaWiFS] images. It was also not possible to identify a pronounced C-phycocyanin endmember in the 22 June 2005 CASI-2 [SeaWiFS] image (lower C-phycocyanin:chlorophyll-a)

The definition of endmembers used to parameterise spectral mixing and angle mapping models can have a significant effect upon the model solutions and, as shown here, variability in the endmembers present within an image would seem to invalidate algorithms formulated using model solutions from other images. Similarly, in the case of the CRBD algorithms for pigment estimation the L_w-minima, associated with pigment absorption, were not consistent with the original CASI-2 [SeaWiFS] calibration dataset (i.e. the C-phycocyanin absorption feature was not present in images captured on 28 February 2005 and 21 April 2005). The CRBD algorithms derived from the 29 August 2005 CASI-2 [SeaWiFS] image were also therefore not appropriate for extrapolation to other CASI-2 [SeaWiFS] datasets.

The limited transferability of the LSMM, SAM and CRDB algorithms for pigment estimation required that either (1) new endmember spectra were extracted for each CASI-2 [SeaWiFS] image and used to derive new algorithms for pigment estimation, or (2) the original endmember spectra were preserved but new, image-specific, algorithms were derived for pigment estimation. The extraction of new image-specific endmembers would have precluded the

estimation of C-phycocyanin in the 21 April 2005 and 22 June 2005 CASI-2 [SeaWiFS] imagery (as no C-phycocyanin endmember could be adequately defined); thus the original endmember spectra were retained and used for LSMM and SAM model parameterisation, but new image-specific algorithms for pigment estimation were derived using the multivariate best-subsets regression for each CASI-2 [SeaWiFS] image.

The accuracy of the original (i.e. not recalibrated) LSMM, SAM and CRBD algorithms is compared to that of the corresponding image-specific algorithms for both chlorophyll-a and C-phycocyanin in Table 5.14. The results obtained from the derivation of image-specific LSMM, SAM and CRBD algorithms for the estimation of chlorophyll-a and C-phycocyanin demonstrate that, in the case of chlorophyll-a, the LSMM, SAM and CRBD models provide a better, although image-specific estimation, than was achieved with the NIR/red band-ratio algorithms. Coefficients of determination for the estimation of chlorophyll-a derived from the image-specific LSMM, SAM and CRBD models varied between R^2 = 0.808-0.930 for the CASI-2 [SeaWiFS] 21 April 2005 and 22 June 2005 datasets (RMSE 0.72-2.66 mg chlorophyll-a m^{-3}; RMSE% = 3.4-13.4).

In contrast to the results obtained for chlorophyll-a, the recalibration of the LSMM and SAM algorithms could not provide a statistically significant model for the estimation of C-phycocyanin and, further, an image-specific CRBD algorithm for the estimation of C-phycocyanin could only be derived for the 22 June 2005 CASI-2 [SeaWiFS] dataset. In the case of the LSMM and SAM model, this was probably largely due to the absence a C-phycocyanin endmember in the CASI-2 [SeaWiFS] images captured on 21 April 2005 and 22 June 2005. Similarly, in the case of the CRBD algorithm, the lack of a statistically valid model was likely due to the absence of a prominent C-phycocyanin absorption-related feature in the continuum-removed spectra of the 21 April 2005 CASI-2 [SeaWiFS] image.

Table 5.14 Comparison of the algorithms derived from the 29 August 2005 CASI-2 [SeaWiFS] image and the image-specific algorithms for the estimation of chlorophyll-a and C-phycocyanin concentrations.

	CASI-2 dataset	Model	Algorithm	Bands/Endmembers inc. in Model	*n*	F	R^2 (adj.)	p	RMSE (mg m^{-3})	RMSE (%)
Chlorophyll-a	February	LSMM	29 August 2005 Image-specific†		3		0.388		48.82	87.6
		SAM	29 August 2005 Image-specific†				0.019		52.13	93.5
		CRBD	29 August 2005 Image-specific†				0.100		49.38	88.62
	April	LSMM	29 August 2005		9		0.635‡		24.73	93.7
			Image-specific	1, 3, 4, 5		24.00	0.920	0.005	0.72	3.4
		SAM	29 August 2005				0.004		14.51	67.5
			Image-specific	1, 2, 3		32.75	0.923	0.001	0.79	3.69
		CRBD	29 August 2005				0.652‡		50.91	237.0
			Image-specific	B4, B6, B8		25.79	0.903	0.002	0.89	4.1
	June	LSMM	29 August 2005		11		0.466‡		17.25	84.11
			Image-specific	1, 2, 3, 5		34.25	0.930	0.000	1.49	7.5
		SAM	29 August 2005				0.024		44.85	226.5
			Image-specific	1, 3, 4		17.02	0.828	0.001	2.51	12.7
		CRBD	29 August 2005				0.003		23.59	119.1
			Image-specific	B4, B6, B8		15.07	0.808	0.002	2.66	13.4
C-phycocyanin	April	LSMM	29 August 2005 Image-specific		6		0.000		85.73	681.8
		SAM	29 August 2005 Image-specific#				0.327‡		49.50	393.7
		CRBD	29 August 2005 Image-specific#				0.030		20.39	162.2
	June	LSMM	29 August 2005 Image-specific#		11		0.321‡		331.9	1228.0
		SAM	29 August 2005 Image-specific#				0.125		233.1	1177.0
		CRBD	29 August 2005				0.074		127.1	470.5
			Image-specific	B5, B6, B7, B8, B10		6.32	0.727	0.032	6.29	23.3

†Too few ground truth measurements for image-specific algorithm to be derived.
‡Regression relationship was negative.
#Statistically significant image-specific algorithm could not be derived.
Model endmembers: 1 – chlorophyll-a; 2 – C-phycocyanin; 3 – tripton; 4 – bottom substrate; 5 – aquatic vegetation.

The obvious limitation with the use of LSMM, SAM and CRBD algorithms for pigment estimation is that, under most circumstances, the algorithms cannot be extrapolated to other image datasets without recalibration using the new model solutions. These findings contrast to those presented in Tyler *et al*. (2006) who were able to hindcast an algorithm for the estimation of chlorophyll-a in Lake Balaton (Hungary) derived from LSMM of a Landsat TM 7 acquired in 2000 scene to another Landsat TM 7 scene acquired in 1994. This improved transferability may have been due to the fact that the limited spectral capabilities of the Landsat TM 7 platform only enabled the use of 4 simple endmembers (no endmembers for C-phycocyanin, bottom reflectance, or aquatic vegetation were defined). In addition, in both Landsat TM 7 scenes analysed by Tyler *et al*. (2006) there was a large algal bloom on Lake Balaton and, as a result, there was arguably less variation in water quality condition between individual scenes as encountered in the Norfolk Broads.

Implications for the Remote Sensing of Shallow Lakes—The results presented here indicate that remote sensing can provide accurate estimations of phytoplankton pigment concentrations in very shallow and optically complex lakes. It would appear that the NIR/red band-ratios are most appropriate for pigment estimation in shallow lakes where the derived algorithms are to be extrapolated beyond the dataset used for calibration. The NIR/red band-ratio algorithms were shown capable of estimating pigment concentrations with an accuracy and, importantly, robustness, which would suggest that remote sensing platforms could be used for the routine monitoring of water quality in shallow lakes. Unfortunately, it would not be possible to extrapolate the algorithms formulated here to other shallow waters because they were derived semi-empirically using water-leaving-radiance data. In this context, the derivation of analytical (or semi-analytical) algorithms from bio-optical modelling studies using remote-sensing-reflectance (R_{rs}) (as opposed to water-leaving-radiance) measurements would provide more robust algorithms for extrapolation across time and space. This should be considered in future studies.

In instances where the optical complexity of specific lakes hinders the retrieval of accurate pigment concentrations through NIR/red band-ratio algorithms, the use of LSMM, SAM and

CRBB models would seem to offer a route forward providing that the derived algorithms are not to be extrapolated across multi-temporal images or transferred to other water bodies. The limited transferability of the algorithms derived from the spectral mixing, spectral angle mapping and continuum removed models would preclude their use for the routine monitoring of water quality in lakes, but they may be of value for expeditious, one-off, investigations. The robustness of the algorithms may be improved if the endmembers were derived using bio-optical modelling approaches and this should perhaps be considered further. In addition, the increasing availability of hyperspectral remote sensing data offers an opportunity to examine the use of spectral n^{th}-derivative indices for the estimation of pigment concentrations in shallow lakes. n^{th}-Derivative based indices may provide a more robust alternative to the use of NIR/red band-ratios for pigment estimation in shallow lakes (see Chapter 3) – but as yet no consideration has been given to their use with hyperspectral satellite data.

5.5.2 Calibrated CASI-2 [SeaWiFS] Imagery

The optimum NIR/red band-ratios for the estimation of chlorophyll-a and C-phycocyanin were used to calibrate the CASI-2 [SeaWiFS] imagery to produce spatially-resolving maps depicting seasonal change in the water quality of the Upper Thurne and Barton Broads during 2005 (Figure 5.17 and Figure 5.18). The Upper Thurne (and Barton Broad) is a hydrologically complex system and nutrient enrichment processes have affected the water quality status of several of the shallow fluvial lakes. There is thus a typically pronounced gradient (spatially and temporally) in water quality across the Upper Thurne and Barton Broads.

This pronounced water quality gradient can be see in Figure 5.17. The chlorophyll-a concentration was lowest (with the notable exception of Hickling Broad) in the CASI-2 [SeaWiFS] captured on 28 February 2005 – concentrations were typically < 25 mg m^{-3} throughout the system. The high concentrations of chlorophyll-a in Hickling Broad on 28 February 2005 (~ 100 mg m^{-3}) reflect the occurrence of the winter chlorophyll-a maximum. This atypical winter chlorophyll-a maximum in Hickling Broad is believed to be to its brackish nature and the fact that the hydrodyanmics of the lake system prevent flushing occurring during winter months (Moss, 2001). The chlorophyll-a concentration in Hickling Broad can be seen to have

decreased on 21 April 2005 to < 25 mg m^{-3}, this brief clear-water-phase is the result, at least in part, of intense grazing by zooplankton. The concentration of chlorophyll-a can be seen to have increased following the clear-water-phase to > 30 mg m^{-3} in the June 2005 CASI-2 [SeaWiFS] image.

In contrast to Hickling Broad, concentrations of chlorophyll-a in Barton Broad increased throughout the year, with the peak occurring on 29 August 2005 as a result of a bloom of *M. aeruginosa*. It is also notable that the cyanobacterial bloom caused high spatial variability in the concentration of chlorophyll-a within Barton Broad; this visibly patchy distribution is characteristic of cyanobacterial blooms composed of buoyancy-regulating species (Kutser, 2004; Reynolds, 2006). The 22 June 2005 and 29 August 2005 CASI-2 [SeaWiFS] images also show extremely high concentrations of chlorophyll-a (> 1000 mg m^{-3}) in the small pond adjacent to Horsey Mere. This hypertrophic pond is subject to high phosphorus loading due to inputs of guano derived from large populations of wading birds and wildfowl (guanotrophication); measurements of the chlorophyll-a concentration in this pond on 23 June 2005 indicated that the chlorophyll-a concentration was in excess of 1500 mg m^{-3} – which importantly substantiates the extremely high estimated chlorophyll-a concentration derived from the CASI-2 [SeaWiFS] imagery. High concentrations of chlorophyll-a are also evident in the Martham Broads in the 22 June 2005 and 29 August 2005 CASI-2 [SeaWiFS] imagery. However, the Martham Broads are clear water lakes, with summer chlorophyll-a concentrations typically < 15 mg m^{-3}, thus the high concentrations of chlorophyll-a evident in the CASI-2 [SeaWiFS] images are almost certainly associated with the submerged aquatic plant cover in these lakes (predominantly *Chara* spp.). In this context, it is apparent that the use of NIR/red band-ratios for the estimation of chlorophyll-a are likely to produce serious errors in the estimation of chlorophyll-a in lakes with substantial submerged aquatic plant cover. Interestingly, examination of the CASI-2 [SeaWiFS] imagery calibrated using the algorithms formulated using LSMM demonstrated that this approach was more successful at separating the benthic and pelagic chlorophyll-a signal; LSMM may therefore provide improved estimation of the pelagic chlorophyll-a concentration in macrophyte-dominated shallow lakes.

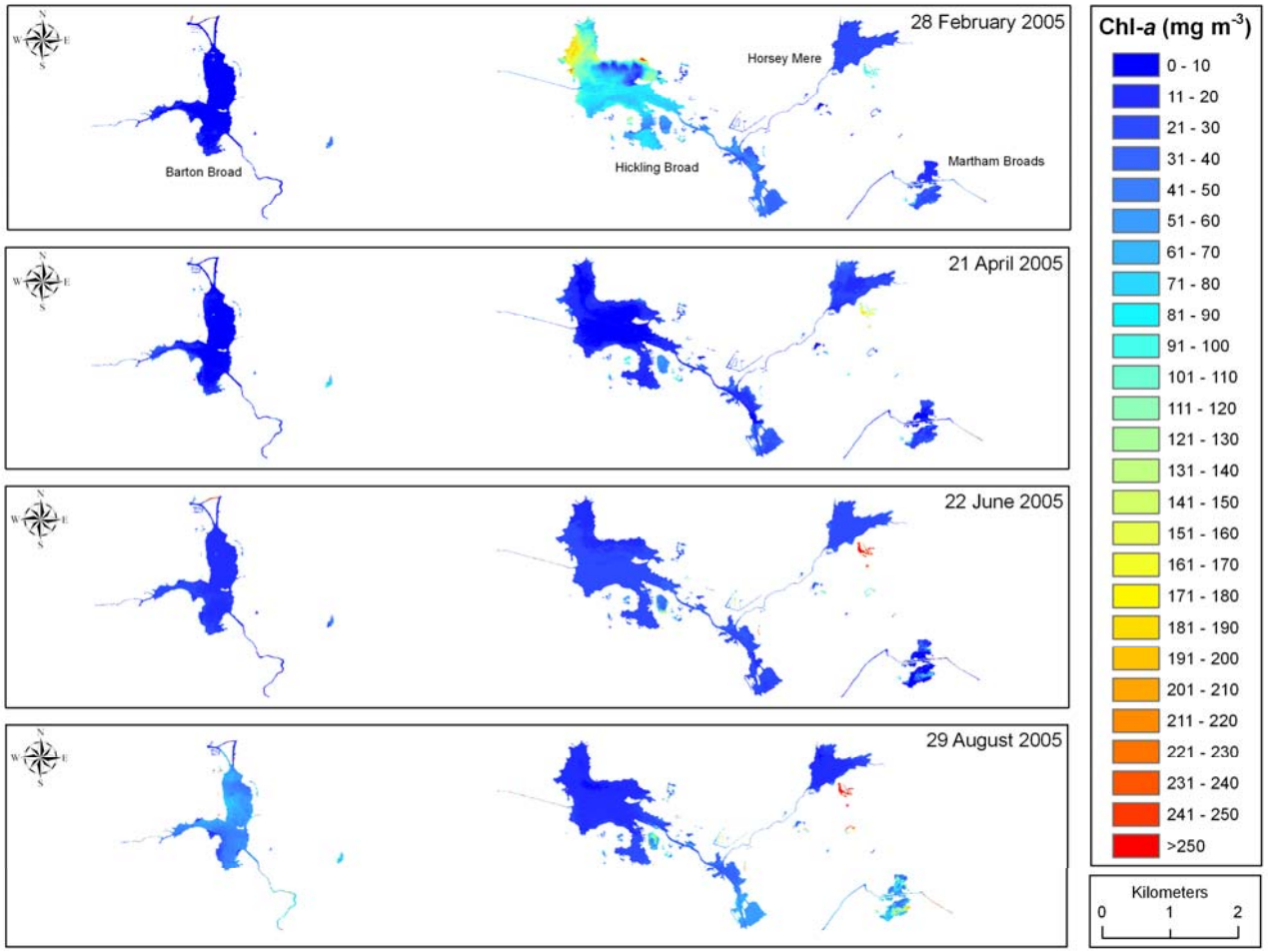

Figure 5.17 Calibrated CASI-2 [SeaWiFS] images showing spatial and temporal variability in chlorophyll-a concentrations in the Upper Thurne and Barton Broads during 2005

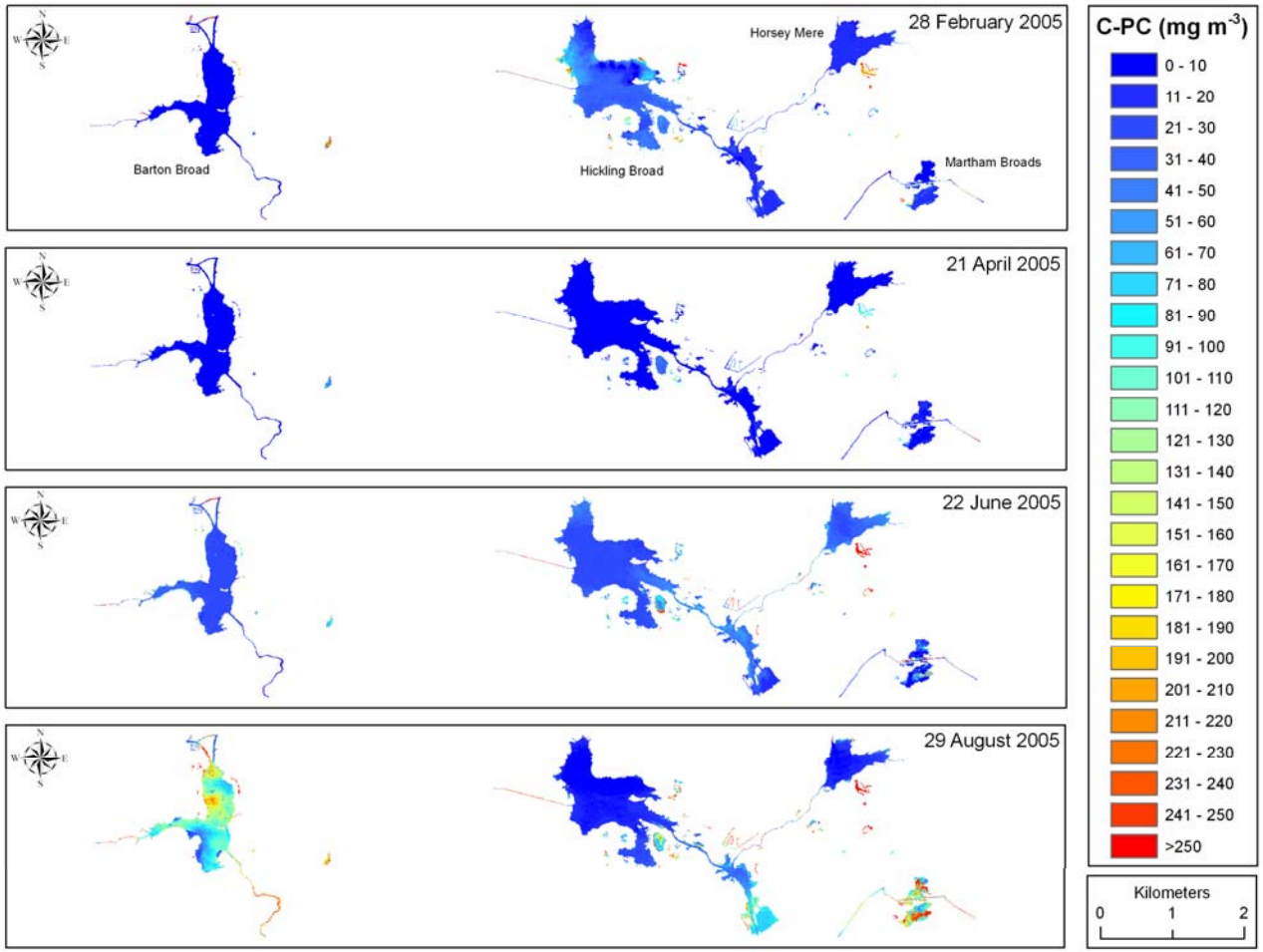

Figure 5.18 Calibrated CASI-2 [SeaWiFS] images showing spatial and temporal variability in C-phycocyanin concentrations in the Upper Thurne and Barton Broads during 2005

Spatial and temporal variation can also be seen in the calibrated CASI-2 [SeaWiFS] images depicting the concentration of C-phycocyanin in the Upper Thurne and Barton Broads. C-phycocyanin concentrations in Hickling Broad were highest on 28 February 2005 concurrent to the chlorophyll-a maximum. However, at this time, the C-phycocyanin concentration was low relative to the concentration of chlorophyll-a, which suggests that cyanobacteria were not dominant component of the Hickling Broad winter phytoplankton assemblage. It is possible that the C-phycocyanin NIR/red band-ratio algorithm may overestimate the C-phycocyanin concentration in the presence of high concentrations of chlorophyll-a because of overlap that occurs in the absorption spectra of the two pigments (Simis *et al.,* 2007). However, unfortunately, no measurements of the C-phycocyanin concentration are available to validate the estimated concentrations of C-phycocyanin on 28 February 2005.

The concentration of C-phycocyanin was low in Barton Broad until the occurrence of a bloom of cyanobacteria in the late-summer of 2005; the effects of this bloom can be clearly seen in the calibrated CASI-2 [SeaWiFS] imagery on 29 August 2005. In comparison, C-phycocyanin concentrations in Hickling Broad were substantially lower on 29 August 2005, but high concentrations of C-phycocyanin are evident towards the southern shore in Heigham Sound (near the outlet into the River Thurne). These high concentrations of C-phycocyanin may have resulted from the entrainment and transportation of buoyant cyanobacteria in the flow of water that travels southwards through Hickling Broad and out into the River Thurne. High concentrations of C-phycocyanin (> 2000 mg m^{-3}) are also evident in the hypertrophic pond south of Horsey Mere in the 22 June 2005 and 29 August 2005 CASI-2 [SeaWiFS] imagery; the measured concentration of C-phycocyanin in this pond on 23 June 2005 was in excess of ~ 2200 mg m^{-3} – which again importantly substantiates the extremely high estimated C-phycocyanin concentration derived from the CASI-2 [SeaWiFS] imagery

The calibrated CASI-2 [SeaWiFS] images of chlorophyll-a and C-phycocyanin show the potential value of using remote sensing to retrieve spatially resolving estimates of chlorophyll-a and C-phycocyanin in shallow lakes. The spatial and spatio-temporal variance in chlorophyll-a

and C-phycocyanin captured in the CASI-2 [SeaWiFS] seasonal time-series imagery could not have been revealed using conventional lake sampling approaches.

The results presented here also emphasise that the remote-sensing-based approach to the monitoring of pigment concentrations in lakes is robust (providing suitable algorithms are formulated for the waters of interest). In this context, it would seem that remote sensing surveillance capabilities could significantly enhance current lake monitoring strategies particularly, as shown here, at the regional-scale. These findings suggest that remote-sensing-based lake monitoring strategies may have direct relevance to the EU WFD (2000/60/EC).

5.5.3 Diurnal Time-Series Surveillance of a Microcystis aeruginosa Bloom

5.5.3.1 Environmental Drivers of Bloom Development and Vertical Migration Patterns

Blooms of cyanobacteria have been a common occurrence in Barton Broad since the lake became eutrophic in the mid-20th Century. These blooms, historically, have often been dominated by the filamentous oscillatorians *Planktothrix agardhii* and *Limnothrix redekei* (functional group **S1** (c.f. Reynolds *et al.,* 2002), largely because these species are well-adapted to existence in turbid but well-mixed lakes. Blooms of heterocystous dinitrogen-fixing nostocaleans (*Anabaena* spp. and *Aphanizonmenon flos-aquae* (functional group **H1**)) have also occurred intermittently – most likely in response to periods of acute nitrogen limitation. The occurrence of cyanobacteria blooms in the lake has declined following the implementation of a lake restoration scheme (Phillips *et al.,* 2005). However, in July and August 2005, a previously unprecedented bloom of the potentially-toxic cyanobacterium *Microcystis aeruginosa* (functional group $\mathbf{L_M}$) occurred in Barton Broad.

M. aeruginosa is a stress-tolerant cyanobacterial ecotype well-adapted for existence in environments subject to periodic resource depletion. However, *M. aeruginosa* is not tolerant of light starved conditions. In turbid waters, *M. aeruginosa* can alleviate light starvation through (passive) buoyancy-regulation, which enables colonies to migrate and maintain a favourable station in well illuminated near-surface waters. Buoyancy-regulation in *M. aeruginosa* is facilitated by the adjustment of gas-vesicle buoyancy using cell ballast provided by the

photosynthetic production or metabolic utilisation of carbohydrates (Oliver & Walsby, 1984; Kromkamp *et al.,* 1988). This mechanism can enable *M. aeruginosa* to undertake rapid vertical migrations; floatation velocities in natural populations can reach 2.6-10.8 m h^{-1} (Reynolds *et al.,* 1987; Humphries & Lyne, 1988; Visser, 1995).

Hunter *et al*. (submitted) have suggested that the *M. aeruginosa* bloom in Barton Broad during July and August 2005 was, in part, driven by the autogenic depletion of bioavailable nutrient (nitrate and soluble-reactive-phosphorus) pools. The poor light climate in Barton Broad prior to the development of the bloom (SDD < 0.75 m) would, however, seem to be unfavourable for the development and, moreover, persistence of a *M. aeruginosa* bloom. This would suggest that, in order for *M. aeruginosa* to become dominant under such conditions, colonies must have been able to migrate and maintain station in more favourable near-surface waters.

5.5.3.2 Spatial Patterns in Diurnal Migration by M. aeruginosa

The diurnal time-series airborne CASI-2 [SeaWiFS] reconnaissance of Barton Broad on 29 August 2005 was used to examine changes in the spatial structuring of the *M. aeruginosa* bloom. The presupposition that *M. aeruginosa* colonies were undertaking passive migrations to illuminated near-surface waters is supported in the calibrated time-series CASI-2 [SeaWiFS] images of C-phycocyanin (see Figures 5.19-5.21). The images reveal dramatic changes in the near-surface concentrations of C-phycocyanin in Barton Broad occurred between 09.30 h GMT and 16.00 h GMT. These observations are also supported in the calibrated CASI-2 [SeaWiFS] images of chlorophyll-a and the derived C-phycocyanin:chlorophyll-a ratio images (Figure 5.22). The near-surface accumulations of *M. aeruginosa* colonies evident in the 09.30 h GMT images are consistent with previous observations and models that suggest buoyant colonies perform such nocturnal migrations and amass in near-surface waters during the night (Reynolds & Rogers, 1976; Takamura & Yasuno, 1984; Visser *et al.,* 1996). The 09.30 h GMT CASI-2 [SeaWiFS] image may therefore depict the remnants of nocturnal near-surface accumulations. *In-situ* depth profiles of the C-phycocyanin concentrations measured in the lake provide an image-independent verification that near-surface accumulations of *M. aeruginosa* colonies were initially present at 09.30 h GMT (Figure 5.23).

It is notable then that these near-surface accumulations appear to have dispersed in the 12.00 h GMT CASI-2 [SeaWiFS] C-phycocyanin image. This is again coherent with previous observations which suggest that the high insolation incurred by colonies stationed in near-surface waters drives the photosynthetic production of high molecular-weight polymers (e.g. glycogen) thus increasing colony density sufficient to induce sinking to deeper horizons. However, several workers have also observed that the formation of near-surface accumulations of cyanobacteria is dependent on the degree of wind-induced mixing.

George and Edwards (1976) suggest that wind speeds in excess of ~ 4 m s^{-1} are sufficient to induce turbulent mixing in shallow lakes and suppress diurnal near-surface migrations by buoyant cyanobacteria. Weather station records for the 29 August 2005 indicate the wind speeds between 00:00 h and 06:00 h GMT were ~ 4 m s^{-1}; the wind speed then increased to > 6 m s^{-1} by 09:30 h GMT. Therefore, the dispersion of the early-morning near-surface scums was probably facilitated appreciably by the onset of wind-induced mixing.

This observation is consistent with the findings of Cao *et al*. (2006) who noted that near-surface aggregations of *M. aeruginosa* in Lake Taihu (P.R. China) were only observed during periods when the wind speed was < 4 m s^{-1}. The 16:00 h GMT CASI-2 C-phycocyanin images again show patent evidence of near-surface accumulations of *M. aeruginosa* colonies; in this instance, the image-derived near-surface C-phycocyanin concentrations were even higher than those observed at 09:30 h GMT.

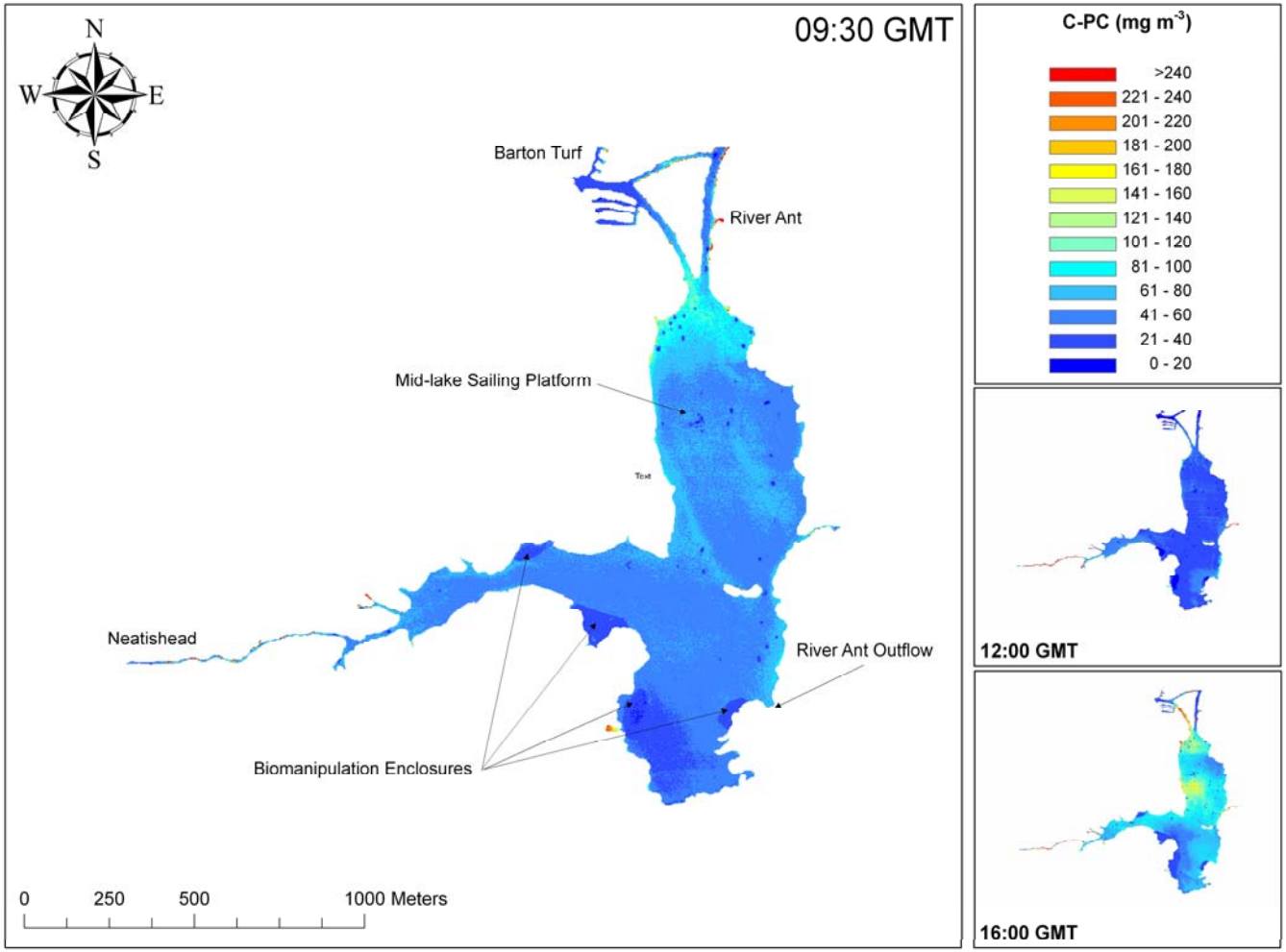

Figure 5.19 The spatial distribution of *M. aeruginosa* in Barton Broad at 09:30 h (main) and 12:00 h and 16:00 h (inset) GMT on 29 August 2005.

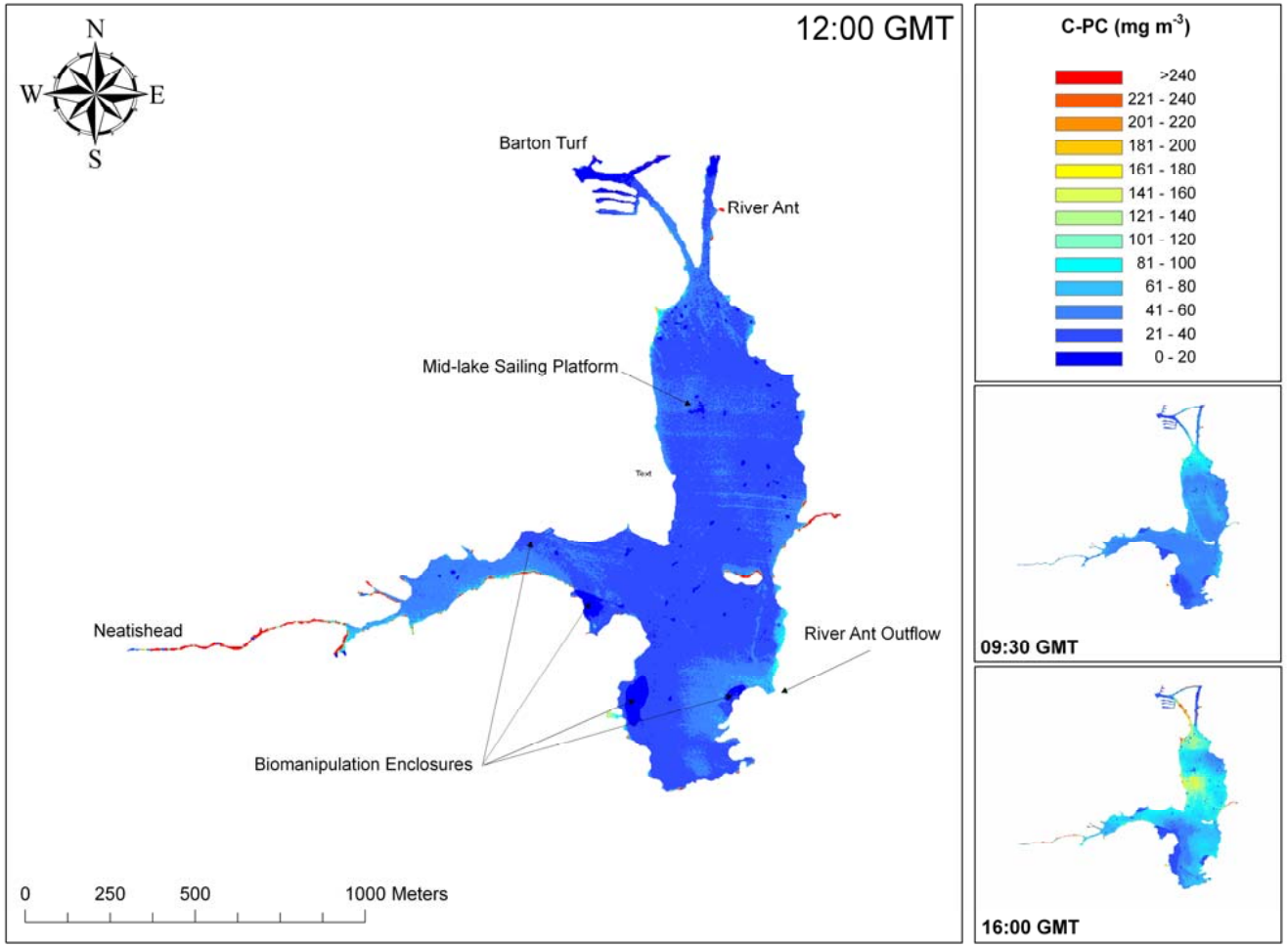

Figure 5.20 The spatial distribution of *M. aeruginosa* in Barton Broad at 12:00 h (main) and 09:30 h and 16:00 h (inset) GMT on 29 August 2005.

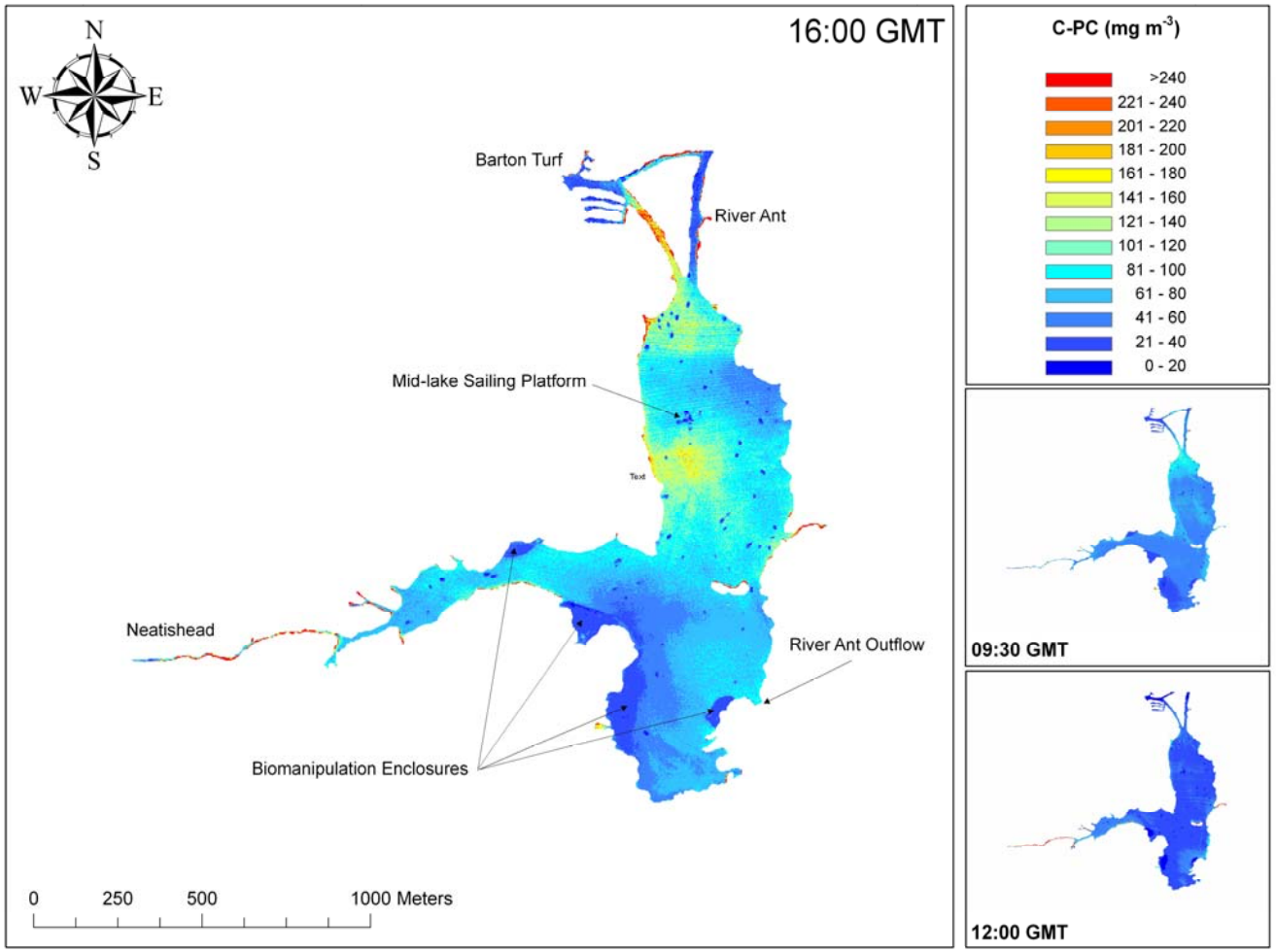

Figure 5.21 The spatial distribution of *M. aeruginosa* in Barton Broad at 16:00 h (main) and 09:30 h and 12:00 h (inset) GMT on 29 August 2005.

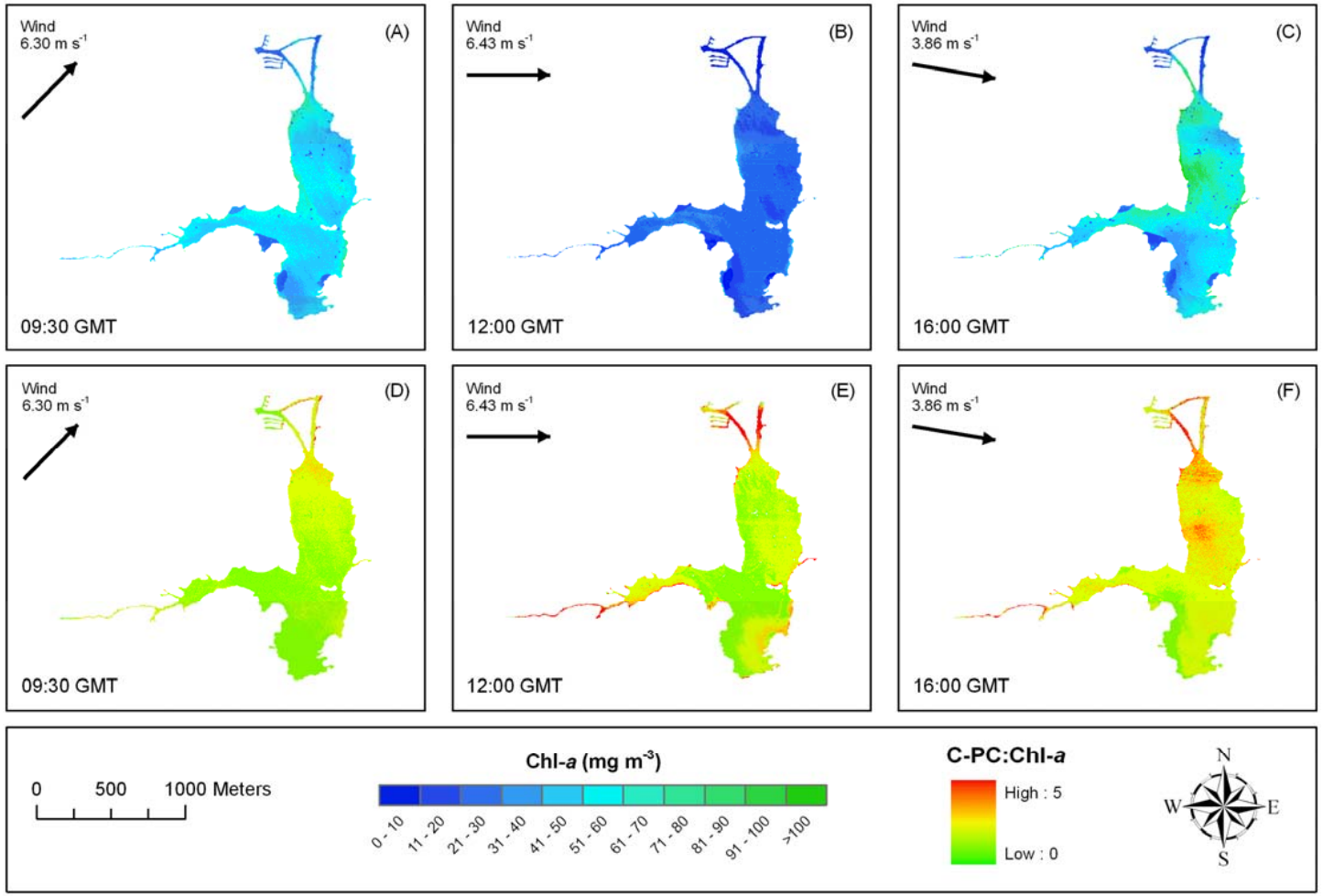

Figure 5.22 Changes in the spatial distribution of chlorophyll-a (top; A-C) and the C-phycocyanin:chlorophyll-a ratio (bottom; D-F) in Barton Broad between 09:30 h and 16:00 h GMT on 29 August 2005.

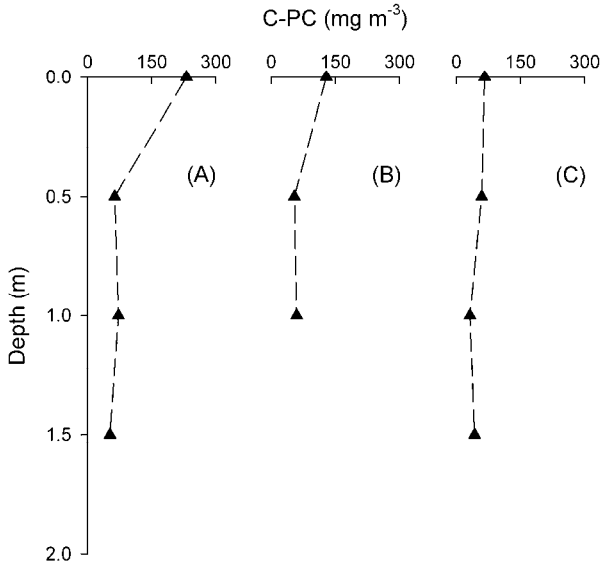

Figure 5.23 Depth-profiles of the concentration of C-phycocyanin at three stations (A-C) in Barton Broad on 29 August 2005. Near-surface accumulations of *M. aeruginosa* can be clearly observed in the depth profile obtained from station A and, although to a lesser extent, Station B.

It appears that the *M. aeruginosa* colonies recovered sufficient buoyancy from the morning to migrate and maintain station in near-surface waters; it can be suggested that these migrations, at least in-part, may have been facilitated by the depletion of intracellular photosynthate reserves whilst the colonies were temporarily immersed in deeper horizons earlier in the day. However, it must also be noted that the mean wind speed at 16:00 h GMT had fallen to > 4 m s^{-1}, which suggests an absence of turbulent mixing. The increased stability in the water column would have been important to enable the vertical migration of colonies. Indeed, it is difficult to differentiate whether the near-surface accumulations (observed at 09:30 h GMT and 16:00 h GMT) were predominantly the result of passive buoyancy-regulation (due to the production/utilisation of carbohydrate) or the response of continuously buoyant colonies to changes in water column turbulence. If conditions permit, *M. aeruginosa* can remain positively-buoyant for several days (Reynolds, 1973; Humphries & Lyne, 1988); this is advantageous as it enables colonies in shallow waters to rapidly recover an optimum station following episodic disturbance events (e.g. wind/storm induced mixing) (Reynolds, 2006).

Thus, it is possible given the shallow environment and the rate at which colonies appear to have returned to near-surface waters in the late-afternoon, that the vast majority of *M.*

aeruginosa colonies were continuously buoyant with near-surface accumulations forming during periods without significant wind-induced mixing (i.e. prior to 09:30 h GMT and 16:00 h GMT). The near-surface accumulations of *M. aeruginosa* visible in the western arm of the lake throughout the day provide some evidence to support the view that colonies remained positively-buoyant. The model scenarios of Visser *et al*. (1997) show that rapid diel migrations between deep and near-surface waters driven entirely by changes in cell ballast can occur when large colonial *M. aeruginosa* aggregations are formed (> 400 µm); the diurnal patterns of migration predicted by the model scenarios of Visser *et al*. (1997) show good agreement with those observed in Barton Broad. It can therefore be suggested that the pronounced changes observed in the diurnal distribution of *M. aeruginosa* were the result of passive-modifications to the buoyancy of colonial aggregations allied to the changes in the extent of wind-induced mixing across the lake.

The importance of the wind speed and direction in determining the spatial distribution of the *M. aeruginosa* bloom (and eukaryotic phytoplankton) is also emphasised in the CASI-2 [SeaWiFS] derived C-phycocyanin:chlorophyll-a ratio images (Figure 5.22) and the chlorophyll-b:chlorophyll-a and fucoxanthin:chlorophyll-a ratios measured at the *in-situ* sampling stations (Figure 5.24). The spatial patterns in the relative abundance of cyanobacteria show good agreement with the prevalent wind direction; accumulations of *M. aeruginosa* colonies can be observed towards the lee shore of Barton Broad at both 09:30 h GMT and 12:00 h GMT. The images indicate that the re-distribution and downwind accumulation of colonies from the northern to the northern and eastern shores between 09:30 h GMT and 12:00 h GMT in response to the prevalent wind was rapid even for a small lake. Furthermore, the prevalence of SSW winds prior to the 09:30 h GMT image appears to have prompted the accretion of non-buoyant eukaryotic phytoplankters towards the southern windward shore; the higher chlorophyll-b:chlorophyll-a and fucoxanthin:chlorophyll-a ratios encountered at the southern sampling stations can be taken to indicate a higher relative abundance of negatively-buoyant bacillariophyte and chlorophyte species. During periods of advective circulation, negatively-buoyant phytoplankton tend to aggregate towards the windward shore, as cells become entrained within sub-surface return-flows and accumulate in regions where upwelling water

occurs (George & Edwards, 1976; Hedger *et al.,* 2004; Reynolds, 2006). This provides a mechanism whereby substantial spatial variation in species composition can occur in the phytoplankton communities, even in small and shallow lakes.

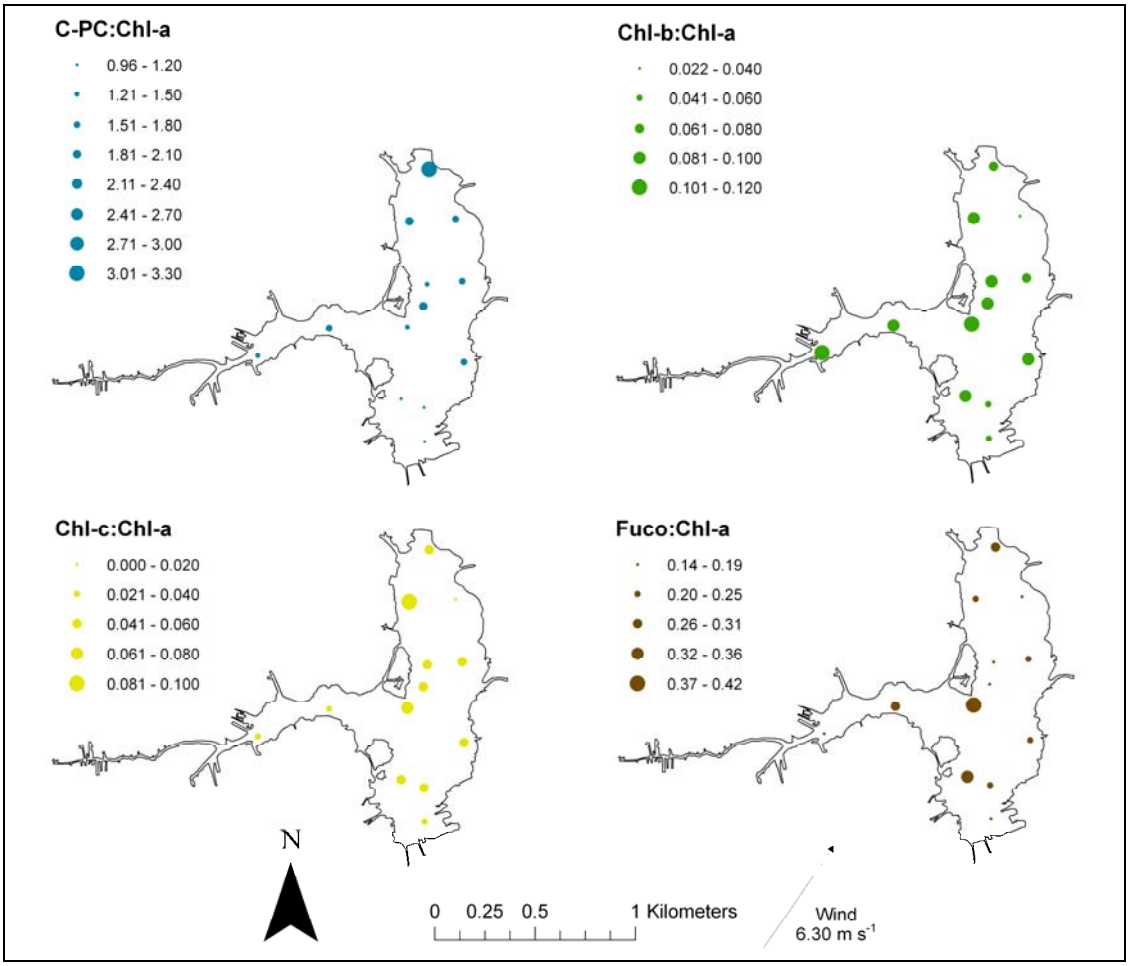

Figure 5.24 Spatial variations in accessory pigment ratios measured at sampling stations on Barton Broad on 29 August 2005 at 09:30 h GMT.

The effect of wind-induced circulation patterns on the vertical and horizontal distribution of phytoplankton has been well documented (e.g. George & Edwards, 1976; Webster, 1990; Ye *et al.,* 2006). It would seem that this process was important in structuring the spatial distribution of phytoplankton in Barton Broad. The CASI-2 [SeaWiFS] images also illustrate the extent to which the formation of near-surface accumulations of buoyant *M. aeruginosa* colonies is spatially variable within lakes; in this context, time-series airborne remote sensing can clearly provide insights that would not be achievable through conventional in-situ measurements.

The absence of turbulent mixing is essential for the development of *M. aeruginosa* blooms (Reynolds & Walsby, 1975), but in wind-exposed and very shallow lakes such as Barton Broad, it is unusual for there to be a prolonged absence of wind-induced mixing. However, the near-shore morphometry of Barton Broad creates several areas where wind-induced (or fluvial) mixing is less pronounced; the time-series CASI-2 [SeaWiFS] imagery reveals that the formation of near-surface accumulations in Barton Broad was most marked in these regions of poorly-mixed or near-stagnant water. Near-surface accumulations were persistent throughout the day in lateral arm of Barton Broad that extends westward towards Neatishead; in this region it would appear that the extent of turbulent mixing is not sufficient to entrain buoyant colonies. Moreover, it is significant that the most pronounced near-surface accumulations observed in the 16:00 h GMT CASI-2 [SeaWiFS] C-phycocyanin images occurred in proximity to the mid-lake sailing platform and in the waters adjacent to Barton Turf. It can be argued that the presence of the mid-lake sailing platform serves to suppress turbulent mixing in the immediately adjacent waters – this resulting stability would then seem to foster dense near-surface accumulations of buoyant *M. aeruginosa* colonies. The structure may also provide some protection from turbulent mixing caused by the input from the River Ant. Pronounced near-surface accumulations of *M. aeruginosa* also formed in the near-stagnant waters that extend southwards from the harbour at Barton Turf.

It can be suggested that the existence of these non-turbulent areas may have been crucial in fostering the development of the *M. aeruginosa* bloom in Barton Broad. It is notable that surface scums of *M. aeruginosa* were observed in the waters near Neatishead prior to the development of the bloom in the open waters. This may indicate that it was in these regions of poorly mixed or near-stagnant water where the initial growth of *M. aeruginosa* colonies occurred; the absence of turbulent mixing in these areas would have enabled *M. aeruginosa* colonies to migrate and maintain a favourable station in near-surface waters irrespective of turbulent conditions in the open water. Zohary & Breen (1989) showed that the formation of cyanobacterial hyperscums in a hypertrophic lake was strongly reliant on shore-mophormetry. Thus, it can be further argued that near-shore morphometry is also important in the creation of

refuges where conditions are favourable to cyanobacterial growth and persistence. The importance of spatial heterogeneity in lake habitat for phytoplankton assemblages has been also been previously documented (Padisak, 1993).

5.6 CONCLUSIONS

Time-series airborne CASI-2 [SeaWiFS] imagery was used to examine the potential of remote sensing for the estimation of pigment concentrations in shallow lakes and to subsequently examine spatiotemporal variability in the phytoplankton dynamics of the Upper Thurne and Barton Broads. CASI-2 [SeaWIFS] algorithms formulated using NIR/red band-ratios were shown to be capable of providing accurate (RMSE < ±20-35%) multi-season estimations of the chlorophyll-a and C-phycocyanin concentration in these shallow lakes. The validation of the derived algorithms demonstrated a robustness in the approach that would seem to suggest remote sensing could be used on a routine basis for lake monitoring purposes.

Algorithms formulated using spectral mixing, spectral angle mapping and continuum-removal models were also able to provide accurate estimations of the concentration of chlorophyll-a and C-phycocyanin concentrations. However, such algorithms would seem to be somewhat scene-dependent and the consequent lack of multi-temporal transferability would ultimately preclude their use for routine monitoring purposes .

High resolution time-series airborne remote sensing was also used to examine the spatial dynamics of a cyanobacterial bloom in Barton Broad. Diurnal time-series CASI-2 [SeaWiFS] images acquired over Barton Broad at 09:30 h, 12:00 h and 16:00 h GMT on 29 August 2005 demonstrated that buoyant *M. aeruginosa* colonies were passively evading the light-starved conditions encountered in the turbid waters through the formation of near-surface accumulations. The formation of these near-surface accumulations by buoyant colonies was dependent on the wind speed; wind speeds > ~ 4 m s^{-1} appeared to be sufficient to induce turbulent mixing and thus cause the dispersal of near-surface aggregations and entrain colonies within convective currents. However, in areas where complexities of the near-shore morphometry created regions of more stagnant water, persistent near-surface accumulations

were observed. It is suggested that these regions of near-stagnant water may have been important for fostering the initial development and, moreover, persistence of the *M. aeruginosa* bloom. In this context, time-series airborne remote sensing was able to provide spatial insights into the distribution and dynamism of the *M. aeruginosa* bloom that would not have been possible through conventional in-situ sampling methods and, as such, the further use of remote sensing technologies in studies concerned with the ecology of phytoplankton in shallow lakes should be encouraged.

The spatial and temporal variability observed in the water quality status of the lakes within the Upper Thurne and Barton Broad region serves to emphasise the benefits that an operational remote sensing system for the routine lake monitoring would offer. In this instance, largely due to the scale of the lakes examined, airborne remote sensing data was used. The expense of airborne remote sensing surveillance would prohibit its use for routine lake monitoring purposes. However, there is no reason to presume that the results achieved could not be repeated using data derived from high spatial and spectral resolution satellite imagery. The results suggest that the realisation of an operational remote-sensing-based strategy for water quality monitoring in lakes would be of immense value in the context of the EU WFD (2000/60/EC).

6 AIRBORNE MAPPING OF AQUATIC VEGETATION IN SHALLOW LAKES

6.1 INTRODUCTION

The preceding chapters have examined the use of remote sensing for the assessment and monitoring of water quality and phytoplankton in shallow lakes. However, in addition to the quality of surface water, the ecological status of shallow lakes is often inherently linked to the nature and extent of aquatic plant colonisation. The research presented in this chapter therefore seeks to examine the capacity of remote sensing for use in the broad-scale survey of aquatic vegetation in shallow lakes

6.2 RATIONALE

The abundance, distribution and composition of aquatic vegetation communities is inextricably linked to the ecological status of shallow lakes. In shallow lakes, aquatic plants fulfil important functions in the regulation of hydraulic circulation, sediment consolidation (Scheffer, 1998; Rooney *et al.,* 2003), the provision of a sink environment for nutrients and other waterborne pollutants (Zhou *et al.,* 2000; Kufel & Kufel, 2002), and the creation of habitat niches and refuges (e.g. Stansfield *et al.,* 1997), such that it has been shown that aquatic plants are critical to the wider stability of shallow lake ecosystems (Scheffer *et al.,* 1993; Scheffer *et al.,* 2001; Van Nes & Scheffer, 2003; Scheffer & Carpenter, 2003; Scheffer & Carpenter, 2003). However, in many nutrient enriched shallow lakes, increased turbidity from the excessive growth of phytoplankton has precipitated large scale losses of submerged aquatic flora. This decline has, in many instances, resulted in catastrophic ecosystem shifts and has often led to the development of an unfavourable state of phytoplankton dominance. The reestablishment of submerged aquatic vegetation (SAV) is therefore considered to be a key objective in the restoration of shallow lakes subject to eutrophication.

The evident linkages between the abundance and diversity of aquatic flora and the ecological status of shallow lake systems means that there is now considerable interest in the

development of effective and efficient approaches to the survey of aquatic plants in lakes. The conventional field-based approach to the survey of aquatic vegetation in lakes can often be somewhat laborious, boat access can be an issue in remote areas, extensive surveys are often disproportionately expensive (in terms of both time and finance), and often the observer error can be high (e.g. for cover estimates, species identification). Lakes (and their associated wetland areas) can be difficult to traverse and obtaining sufficient access for survey purposes, particularly in regards to submerged communities, may often be difficult. Moreover, the spatially-discontinuous data derived from conventional field-based survey techniques can seldom adequately describe the heterogeneous distribution of aquatic plants and, in particular, ecologically important, but spatially complex mosaics, ecoclines and ecotones (Janauer, 1997; Legleiter, 2003; Gilvear *et al.,* 2004b).

The implementation of the EU WFD (2000/60/EC) has placed increased emphasis on the need for regional-scale monitoring of lake ecosystems, including the abundance and distribution of aquatic plants. In some instances, aerial photography has proved to be useful for the large-scale mapping of aquatic vegetation in lakes (Windham & Lathrop, 1999). However, the interpretation of aerial photography remains somewhat subjective and the limited spectral information contained within aerial photographs prohibits the extraction of floristic or bio-physical information. In this context, satellite and/or airborne remote sensing could provide a more effective tool for the survey of aquatic vegetation in lakes.

Remote sensing has been used widely to map terrestrial vegetation communities and, indeed, some success has also been achieved in surveying the vegetation of wetlands (Schmidt & Skidmore, 2003; Rosso *et al.,* 2005; Artigas & Yang, 2005; Shanmugam *et al.,* 2006; Wright & Gallant, 2007). The remote-sensing-based mapping of aquatic vegetation communities in lakes has received less consideration; however, there are some notable exceptions. Malthus & George (1997), for example, used ATM imagery to map the distribution of aquatic plant species and growth-habit associations in the Cefni Reservoir (UK). Similarly, Williams *et al*. (2003) used hyperspectral airborne data (HyMap) to map the distribution of *Myriophyllum spicatum* and *Vallisneria americana* in the Potomac River (USA) and, further, Pengra *et al* (2007) used

hyperspectral satellite data (Hyperion) to map the distribution of the non-native common reed, *Phragmites australis*, in the coastal region of Green Bay (USA).

In addition to largely qualitative mapping exercises, further authors have also shown that it is possible to derive quantitative estimates of macrophyte cover from remote sensing data. Jakubauskas *et al*. (2000) showed that *in-situ* spectrometry data could be used to quantify *Nuphar polysepalum* cover in Swan Lake in Wyoming, USA and, similarly, Yuan & Zhang (2007) have also recently demonstrated that it was possible to retrieve quantitative estimates of *Vallisneria spiralis* biomass using high-resolution spectrometry data of experimental plots in a shallow lake in China. The success of these preceding studies intimates that remote sensing could be used on a routine basis to map aquatic vegetation in lakes. This would have enormous benefits for those concerned with the implementation of the EU WFD. However, substantial further research will be required before the effectiveness and efficiency of the remote sensing approach to the survey of aquatic vegetation in lakes is conclusively proven.

6.3 AIMS AND OBJECTIVES

The aim of the research presented here was to investigate the spectral characteristics of aquatic plants, particularly at the broad growth-habit level (i.e. emergent, floating, submerged), using high spectral resolution *in-situ* spectrometry and to evaluate the efficacy of airborne remote sensing for the mapping of aquatic plant growth-habits, and broad species assemblages, in shallow lakes.

The specific objectives for this chapter can be defined as:

a) To explore the spectral characteristics of macrophyte species common to shallow lakes in the UK at the growth-habit level (emergent, floating-leaved and submerged specimens).

b) To evaluate the discriminative capability of remote sensing reconnaissance for mapping macrophyte growth-habit assemblages in shallow lakes.

c) To examine, in more detail, the use of remote sensing reconnaissance for mapping the distribution of SAV associations in turbid and clear water shallow lakes.

6.4 METHODS

6.4.1 Study Site

The Norfolk Broads (UK) (52º 44' 17'' N 1 º 34' 29'' E) are a series of small (< 130 ha) and shallow lakes (< 2.5 m deep) with numerous conservation designations due, in part, to their botanically diverse aquatic plant communities. The vegetation of the Norfolk Broads is a complex mosaic of submerged benthic vegetation, fringing littoral reedswamp communities, fenland and carr woodland. The aquatic plant communities common to the Norfolk Broads include submerged *Chara* spp and *Najas marina* lawns, beds of floating and emergent species such as *Nuphar* spp., *Potamogeton* spp., *Myriophyllum spicatum* and *Hippuris vulgaris*, while the littoral is dominated by tall-emergents such as *Phragmites australis*, *Typha latifolia* and *Carex* spp.. The national and international importance of the aquatic vegetation found in the Broads is borne out in the fact that it includes include several species found nowhere else in the U.K., such as the Intermediate Stonewort (*Chara intermedia*) and the Holly-leaved Naiad (*Najas marina*); in addition >95% of the native UK population of the Starry Stonewort (*Nitellopsis obtusa*) and >80% of the UK population of the Water Soldier (*Stratiotes aloides*) can be found in the waters of Broadland (for more detailed information consult Kennison *et al*. (1998)).

The abundance and diversity of aquatic plants in the Norfolk Broads has been dramatically impacted by pressures from eutrophication. In particular, the deteriorating water quality status of the Broads has resulted in the extensive loss of SAV in these shallow lakes. The reestablishment and stability of the SAV cover is considered a key restoration target if the Norfolk Broads are to be returned to good ecological status as defined by the EU WFD (Broads Authority, 2004).

6.4.2 Aquatic Vegetation Surveys

Two independent vegetation surveys were conducted in the Upper Thurne region of the Norfolk Broads during 2005: (i) a boat-based, broad-scale, survey of aquatic plants was conducted

between 21-24 June 2005 and 30-31 August 2005 and, (ii) a more detailed floristic survey of the SAV in the Martham Broads was conducted by the Broads Authority using grapnel transects during 01-07 August 2005.

The initial broad-scale survey of the aquatic vegetation focused on recording the distribution of aquatic plant growth-habit assemblages in the Upper Thurne (after Malthus & George, 1997). The position and extent of macrophyte beds were identified from a boat-based survey and recorded using a Global Positioning System (GPS). Only beds large enough to be detectable from remote sensing imagery (i.e. > 5 m) were recorded. It was not considered necessary to collect detailed floristic information; instead, the dominant species (by cover) present in each bed were recorded (to genus or species level) and this information was used to pre-classify each surveyed bed into one of four growth-habit categories. The four different growth-habit assemblages comprised:

1) **Emergent** – rooted aquatic vegetation with substantial aerial biomass above the water surface (e.g. *Phragmites australis*, *Typha latifola*).
2) **Partially-emergent** – rooted or floating plants with some emergent foliage, or a substantial biomass allocation occurring at, or near, the water surface (e.g. *Hippuris vulgaris*, some *Potamogeton* spp., *Myriophyllum spicatum*).
3) **Floating** – plants with broad floating planophile leaves (e.g. *Nuphar* spp.) or plants that form dense floating mats (e.g. *Lemna* spp.).
4) **Submerged** – plants with their entire biomass located beneath the water surface often forming dense benthic lawns (e.g. *Chara* spp., *Najas marina*, *Nitellopsis obtusa*).

The inclusion of the "partially-emergent" class was considered a necessary deviation from convention to reflect the marked difference in morphology between tall-emergents, such as *Phragmites australis*, and other species, such as *Hippuris vulgaris*, which have comparatively little aerial growth. It was perceived that these phytomorphological differences would have important implications for remote sensing mapping purposes. Following the boat-based survey

of the aquatic plants, spectral reflectance measurements were acquired from each bed as detailed in Section 6.4.3.

The detailed floristic survey of SAV in the Martham Broads was conducted by the Norfolk Broads Authority and followed the methods described in Kennison *et al*. (1998). Samples of SAV were collected using a doubled-headed grapnel which was trawled behind a boat. The sampling was conducted along pre-defined and permanent transects. The abundance of each species harvested using the grapnel was estimated every 20-60 m along the transects. Macrophyte abundance was estimated on a five-point scale: 1, present but < 5% cover; 2, > 5-25% cover; 3, > 25-50% cover; 4, 50-75%; 5, 75-100% cover. The cover of floating species (e.g. *Lemna minor*, *Nuphar lutea* and *Nymphaea alba*) not sampled by the grapnel transects was estimated separately.

6.4.3 *In-situ* Spectrometry

6.4.3.1 Spectral Reflectance Measurements

In-situ spectral measurements were acquired from beds of 4 different aquatic plant species encountered during the initial broad-scale aquatic vegetation survey in the Upper Thurne. The species examined included the tall-emergent *Phragmites australis* (Common Reed), the partially-emergent plant *Hippuris vulgaris* (Mare's-Tail), the floating plant *Nuphar lutea* (Yellow Water-Lily) and the submerged plant *Chara baltica* (Baltic stonewort) (see Figure 6.1).

These four species were selected as they were considered to be representative of the four different growth-habits (emergent, partially-emergent, floating-leaved, and submerged) considered here. In addition, these species commonly formed large (> 5 m^2) and relatively monospecific beds in the Upper Thurne, such that they could, in theory, be distinguished using high spatial resolution remote sensing imagery. The survey of the Upper Thurne revealed a greater diversity of aquatic plant species than detailed above. However, often the cover of many species (e.g. *Potamogeton* spp.) was too small to allow the beds to be mapped effectively.

(a) *Chara* spp.

(b) *Nuphar lutea*

(c) *Hippuris vulgaris*

(d) *Phragmites australis*

Figure 6.1 The four aquatic plant species examined using *in-situ* spectrometry: (a) *Chara* spp. (photo: Jane Harris); (b) *Nuphar lutea* (photo: USDA); (c) *Hippuris vulgaris*; and (d) *Phragmites australis*.

Spectral reflectance ($R_{(\lambda)}$) measurements of the aquatic plant beds were acquired using a portable ASD (Analytical Spectral Devices) FieldSpec® HandHeld Spectroradiometer (the specifications of the ASD FieldSpec® instrument are detailed in Table 3.2). The instrument was calibrated to reflectance using a white Spectralon® reference panel (~ 100% reflectivity). The spectrometer was mounted on a telescopic pole which enabled the instrument to be positioned away from any potential effects incurred from the proximity of the boat. The telescopic pole also enabled measurements to be acquired at nadir over the taller plant canopies. A consistent solar geometry was maintained and the instrument was held, at nadir, at a constant height of 0.5 m above the plant canopy (emergent and floating-leaved plants) or the water's surface (submerged plants). The spectral reflectance of each macrophyte stand was measured as the instantaneous mean of 25 replicate scans; each replicate scan was itself derived from the mean of a further 15 instantaneous scans internally averaged by the instrument's dedicated software. The acquisition of spectral reflectance measurements was restricted to between the hours of 10.00 and 14.00 h GMT to minimise the effect of variable solar zenith.

Spectral reflectance measurements were also obtained from non-vegetation areas of clear (chlorophyll-a < 10 mg m^{-3}; SPM < 10 mg l^{-1}) and turbid (chlorophyll-a > 20 mg m^{-3}; SPM > 25 mg l^{-1}) water. These measurements were primarily made for comparative purposes.

6.4.3.2 Data Processing and Analysis

The raw hyperspectral reflectance data were interpolated to a spectral resolution of 0.5 nm and truncated between 400 and 800 nm to remove spectral noise at the extremes of the instrument's sampling range. The resultant data were then smoothed to further reduce the influence of noise prior to analysis by passing a 5 nm running mean filter over the entire spectrum (after Dall'Olmo *et al.,* 2005). The spectral dissimilarities of the various macrophyte species was then explored using Principle Components Analysis (PCA) and Multivariate Discriminant Analysis (MDA) (cross-validated) (for further details see Section 4.4.5). In order to perform the PCA and MDA analyses, the original 0.5 nm hyperspectral dataset had to be devolved to from a new dataset, with a spectral resolution of 5 nm, to prevent the predictor variables from being too highly correlated.

6.4.4 Airborne Remote Sensing

6.4.4.1 NERC ARSF Data Capture Campaigns

CASI-2 airborne remote sensing imagery of aquatic vegetation in the Upper Thurne region of the Norfolk Broads was captured by the NERC ARSF at approximately 13:00 h GMT on 22 June 2005 and 29 August 2005. Details of the NERC ARSF data capture campaigns in the Upper Thurne are provided in Section 5.3.2. The CASI-2 instrument was operated using the default [Vegetation] bandset configuration designed to optimise the CASI-2 instrument for the vegetation-based applications (see Table 6.1).

Table 6.1 The default CASI-2 [Vegetation] bandset configuration used for aquatic vegetation mapping in the Norfolk Broads.

Channel	Centre/Width (nm)	Band Width (from centre)	Purpose
1	449.96	10.41	Blue veg. response
2	490.13	11.41	Veg. response
3	552.23	5.82	Green veg. max
4	608.12	6.80	Acces. absorp
5	651.9	6.82	Acces. absorp
6	671.93	3.96	Veg. absorp. max (1)
7	700.59	5.88	Red-edge (1)
8	711.11	4.93	Red-edge (2)
9	739.83	6.85	Red-edge (3)
10	750.37	3.97	Red-edge (4)
11	762.83	3.02	Oxygen absorp.
12	780.09	6.85	Veg. reflec. Max
13	819.42	5.90	Water absorp.
14	865.48	5.90	NIR plateaux
15	942.16	5.89	NIR plateaux

6.4.4.2 Image Pre-processing and Classification

The capability of remote sensing as a tool for aquatic vegetation mapping in shallow lakes was examined through the application of various classification models to the CASI-2 [Vegetation] imagery. Prior to classification, the CASI-2 [Vegetation] data was geo-corrected, geo-registered atmospherically corrected (to absolute radiance [w sr^{-1} m^{-2}]) according to the methods outlined in Section 5.3.4. Image classification was performed using RSI ENVI v.4.3.

The classification procedures examined included the hard-boundary Euclidean Minimum Distance (EMD) and Gaussian Maximum Likelihood (MLC) models and, in addition, the soft-boundary support vector machine (SVM) model. The EMD and MLC classification models were chosen because they have been used widely for the classification of vegetation communities in a range of environments (e.g. Louchard *et al.,* 2003; Shanmugam *et al.,* 2006). The state-of-the-art SVM classification model was chosen as recent research has shown it to be superior to conventional hard-boundary classification algorithms, particularly when the inter-class-mixing-boundaries are complex (Brown *et al.,* 1999; Melgani & Bruzzone, 2004; Pal & Mather, 2004).

Minimum distance classification—EMD classification uses the mean vectors of user-specified endmember training pixels (classes) and calculates the Euclidean distance from each unknown pixel to the mean vector for each class. Pixels are classified to the nearest class in Euclidean space unless a distance threshold is user-specified (in which case pixels that do not meet this threshold remain unclassified) (Richards, 1999; ENVI, 2003). The Euclidean distance between two points was calculated according to Equation 6.1:

$$\sqrt{\sum_{i=1}^{n}(p_i - q_i)^2} \qquad \textbf{Equation 6.1}$$

where, p and q define the mean vectors for two points in Euclidean space.

Maximum likelihood classification—Gaussian MLC assumes that the statistics for each endmember class are normally distributed and the model calculates the probability that an unknown pixel belongs to a particular class. Pixels are assigned to the class with the highest probability (unless a probability threshold is specified, in which case pixels that do not meet this threshold remain unclassified). ENVI v.4.3 implements the maximum likelihood classification using Equation 6.2:

$$g_i(x) - \ln p(\omega_i) - 0.5\ln\left|\sum_i\right| - 0.5(x - m_i)\sum_i^{-1}(x - m_i) \qquad \textbf{Equation 6.2}$$

where *i* is the endmember class, *x* is the *n*-dimension (i.e. number of bands), $p(\omega_i)$ is the probability that class (ω_i) occurs in the image, $|\sum_i|$ is the determinant of the covariance matrix of the data class (ω_i) and $\sum_i^{-1}$ is its inverse and m_i is the mean vector.

Support vector machines—SVM are kernel-based learning classifiers based upon statistical learning theory (Cortes & Vapnik, 1995; Liu *et al.,* 2006). The SVM training algorithm attempts to find the optimal separation (or hyperplane) between classes by minimising the upper bound of the generalising error (Duan *et al.,* 2006; Su *et al.,* 2007b). The training pixels closest to the hyperplane form the support vectors in the model and are the elements critical to the effectiveness of the classification. Unlike the EMD and MLC models, SVM can be used as a non-linear classfier through the incorporation of a non-linear kernel in the training algorithm. As detailed in Su *et al*. (2007b), for two example vectors, (x_i, y_i), *i*,…*l* where $x_i \in R^N$ and $y_i \in$ [-1, +1], the SVM seeks the solution to the optimisation problem described in Equation 6.3:

$$\min_{w,b,\xi}\left(\frac{1}{2}w^T \cdot w + C\sum_{i=1}^{l}\xi_i\right) \qquad \textbf{Equation 6.3}$$

subject to $y_i(w^T \cdot \phi(x_i)+b) \geq 1-\xi_i, \xi_i \geq 0$. Where, ξ_i are positive slack variables and *C*>0 is a preset penalty parameter that allows definition of a certain degree of misclassification in the definition of the hyperplane (which is important where classes are not mutually exclusive in feature space) (ENVI, 2003); x_i is a training vector mapped into higher dimensional space (possibly infinite) by the function ϕ; $w^T \cdot \phi(x_i)+b$ is the optimised hyperplane. The kernel function is described by $k(x_i, x_j)=\phi(x_i)^T\phi(x_j)$. The classification of aquatic vegetation in the Upper Thurne was achieved using a radial basis function as the kernel in the SVM classification algorithm. The radial basis function was selected over linear, polynomial and sigmoid kernels as it enables non-linear class separation, is computationally efficient and has been used to good effect elsewhere (Su *et al.,* 2007a). The radial basis function is described in Equation 6.4:

$$k(x_i, x_j) = \exp(-\gamma \cdot \left\| x_i - x_j \right\|^2), \gamma > 0 \qquad \textbf{Equation 6.4}$$

where γ is the gamma term in the kernel function. The SVM classifier was preferred over other soft-boundary classifiers, such as artificial neural networks (ANN) and linear spectral mixture models (LSMM), because SVM, unlike ANNs, have been shown to perform well when the training dataset is small and, in comparison to LSMM, they provide a more accurate classification (also sub-pixel if desired) when the mixing regions between classes are complex and ill-defined.

The classification models were applied at two different levels of (aquatic vegetation) community organisation: (i) growth-habit associations and, (ii) SAV associations. The growth-habit classification used the aquatic plant survey data obtained from the boat-based survey; whereas, the SAV classification used the detailed floristic data obtained from the grapnel transect survey. The broad growth-habit classification was performed on the CASI-2 [Vegetation] imagery from 22 June 2005 as this image was acquired concurrent to the boat-based aquatic plant survey. The SAV classification was performed on the CASI-2 [Vegetation] imagery from 29 August 2005, because this image was acquired concurrent to the grapnel survey of SAV in the Martham Broads.

The growth-habit classification sought to classify macrophyte beds into the 4 categories recorded in the field: (1) emergent species (example species: *Phragmites australis, Typha latifolia*), (2) partially-emergent species (example species: *Hippuris vulgaris*); (3) floating species; and (4) submerged species (example species: *Chara* spp., *Nitellopsis obtusa, Najas marina*). The classification models were parameterised with endmember radiance spectra for each growth-habit class. Endmember radiance spectra for use as training data were manually extracted from the CASI-2 [Vegetation] imagery using the ground-truth macrophyte survey data to inform and identify aquatic pixels relating to the various endmember growth-habit classes. The size of the training datasets varied between the individual growth-habit classes, but in general, the training datasets consisted of a minimum of 150 pixels extracted from at least 5

discrete aquatic plant beds for each growth-habit assemblage. The exception was the floating macrophyte class, where only 25 pixels were used in the training dataset. This was largely due to problems in resolving the floating plant beds, particularly where they occurred in association with tall-emergent plants. The classification models were also parameterised with endmember spectra for an open water (i.e. no aquatic vegetation) class. This again was primarily for comparative purposes and, in this instance, no distinction between clear and more turbid water was made.

The classification models were then run using the extracted training datasets and extrapolated across the CASI-2 [Vegetation] imagery of the entire Upper Thurne system (Hickling Broad, Heigham Sound, Horsey Mere and the Martham Broads) acquired on 22 June 2005. To determine the accuracy of the classification, a large validation dataset, independent of the training datasets, was extracted from the CASI-2 [Vegetation] imagery based again on the ground-truth survey data and, in this instance, also supplemented by the interpretation of high resolution digital aerial photographs (captured by the Rollei medium format digital camera carried as part of the payload on the NERC ARSF aircraft). The validation dataset was composed of a minimum of 500 pixels per class (with the exception of the floating macrophyte class where only 150 pixels could used for validation). The classification accuracy was interpreted via the derived confusion matrices, the percentage of pixels correctly classified and the Kappa coefficient (κ).

The SAV community level classification sought to categorise the submerged aquatic plant beds according to their dominant species composition. The classification was applied at the dominant species level because it was perceived that more a detailed floristic classification would be infeasible. This was largely because the species composition of the SAV communities varied at a scale finer than the resolution of the CASI-2 [Vegetation] imagery (i.e. < 2.5 m) and, further, because it was assumed that the most dominant species would, in effect, control the spectral response. Moreover, it can be argued that more fine-scale floristic information is probably of less relevance for the assessment of ecosystem function. The poor water clarity in Hickling Broad, Heigham Sound and Horsey Mere, was perceived to be

prohibitive to classifying SAV in these lakes and thus the classification was only applied to SAV in the Martham Broads.

Training data for the classification models was obtained from the SAV surveys conducted by the Norfolk Broads Authority. The SAV transect data provided by the Broads Authority was collected as part of their routine annual macrophyte survey in the Norfolk Broads, as a consequence, the data was not collected specifically for the training and validation of the remote sensing classification models. The grapnel transect data was therefore interpreted cautiously with assistance from digital aerial photographs to inform the identification of SAV beds for which the dominant species composition could be satisfactorily identified. As a result, the SAV data was used to identify four SAV "species assemblages" to be used to train the classification models. The SAV classes defined were:

1) ***Chara hispida*** – Major species (> 50% cover): *Chara hispida*, *Chara baltica*; Minor species (< 25% cover) *Nitellopsis obtusa*, *Najas marina*, *Potamogeton pusillus, Potamogeton pectinatus*, *Chara intermedia*, *Lemna trisulca*, filamentous algae.
2) ***Chara aspera*** – Major species (> 50% cover): *Chara aspera*; Minor species (< 25% cover) *Chara intermedia, Chara hispida, Najas marina, Potamogeton pectinatus*.
3) ***Nitellopsis obtusa*** – Major species (> 50% cover): *Nitellopsis obtusa, Najas marina*; Minor species (< 25% cover) *Chara* spp. *Potamogeton* spp.
4) ***Hippuris vulgaris –*** Major species (> 50% cover): *Hippuris vulgaris*; Minor species (< 25% cover) *Myriophyllum spicatum, Callitriche* spp.

The "partially-emergent" *Hippuris vulgaris* is a prominent member of the flora of the Martham Broads; therefore, for the purposes of this classification, it was decide to include this species as a separate SAV class. Moreover, two further classes, (i) clear water and, (ii) lake bed, were also defined in an effort to ensure the classification algorithms could account for the unique spectral characteristics of these components (i.e. to avoid unnecessary and spurious misclassifications).

The position of the SAV transects were identified in the CASI-2 [Vegetation] imagery and endmember radiance spectra for use as training data in the classification models were manually extracted from the aquatic plant beds of known species composition. The size of the training dataset varied between 50-500 pixels depending on the class concerned. The SAV transect data and digital aerial photographs were also used to create an independent ground-truth dataset for the validation of the classification output; the validation dataset consisted of between 200-1250 pixels depending on the class concerned. The position of the SAV grapnel transects in the Martham Broads is detailed in Figure 6.2. The classification accuracy was interpreted via the derived confusion matrices, the percentage of pixels correctly classified and the Kappa coefficient (κ).

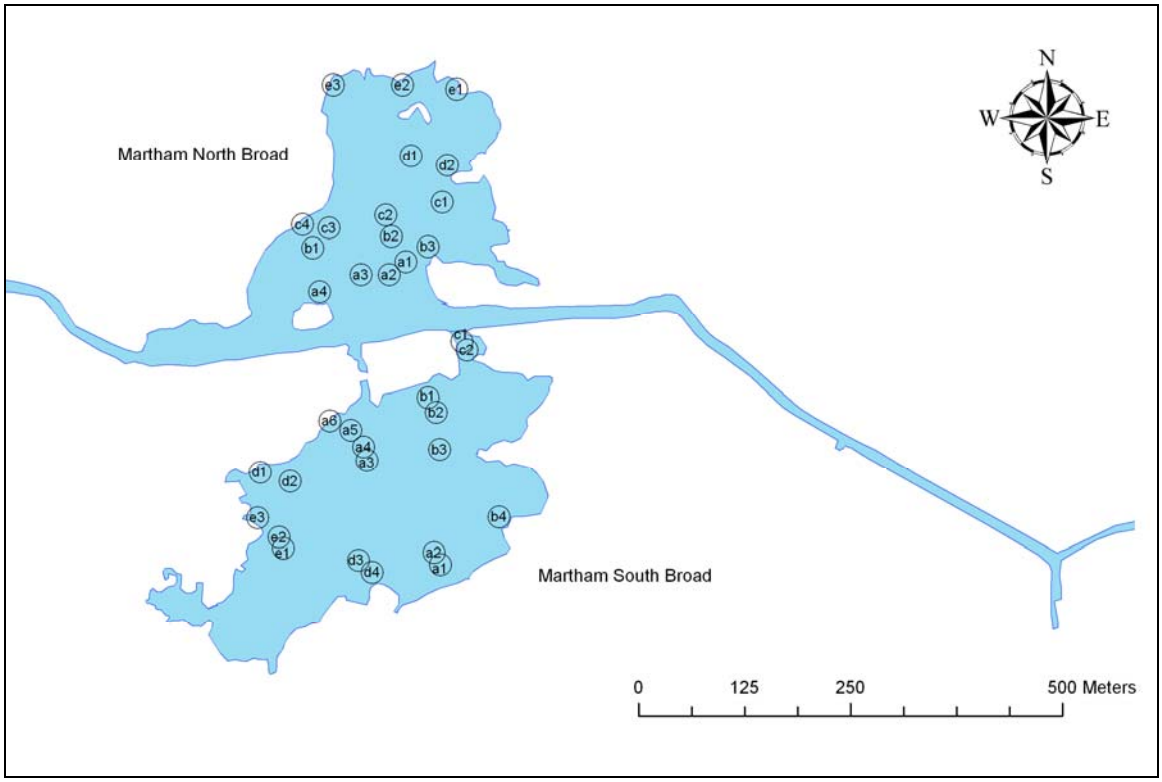

Figure 6.2 The grapnel transects used to assess the abundance and distribution of SAV in the Martham Broads, Norfolk, UK. Transect were surveyed Martham North Broad: a1→a4, b1→b2, c1→c4, d1→d2, e1→e3; Martham South Broad: a1→a5, b1→b4, c1→c2, d1→d4, e1→e3.

6.5 RESULTS AND DISCUSSION

6.5.1 Spectral Signatures of Aquatic Plants

The spectral reflectance signatures of the aquatic plant species (representatives of the four growth-habit classes) obtained from the *in-situ* spectrometry are depicted individually in Figure 6.3 and, further, the mean spectral signatures of these species are shown collectively in Figure 6.4. The spectral signatures of clear (chlorophyll-a < 10 mg m^{-3}; SPM < 5 mg l^{-1}; SDD > 1.5 m) and turbid (chlorophyll-a > 20 mg m^{-3}; SPM > 20 mg l^{-1}; SDD < 0.5 m) water are also shown for comparison.

It is evident that the $R_{(\lambda)}$ signatures of the four macrophyte species are, although to varying extents, relatively dissimilar, both in the magnitude of $R_{(\lambda)}$ and the composite shape of the spectrum. Some broad similarities can, however, be observed between the species. These characteristics include a broad $R_{(\lambda)}$-minimum at *c*. 400-500 nm, largely due to the effect of absorption by plant pigments (chlorophylls and carotenoids) and, to a variable extent, by the surrounding water column. The aquatic plant species also demonstrate a common $R_{(\lambda)}$-maxima at *c*. 550 nm (the 'green peak') (although the exact position and prominence of this feature can be seen to vary between the different species); the pronounced nature of the green peak feature is a function of the intense backscattering of green light from chlorophyllous plant tissues (and the fact that it is straddled by two prominent $R_{(\lambda)}$-minima related to pigment absorption). This green peak is, however, also apparent in the spectra of both clear and, in particular, turbid water as a result of intense backscattering from planktonic algae.

The macrophyte species also demonstrate a broad $R_{(\lambda)}$-minimum between the green peak and the VNIR shoulder (550-700 nm). This feature is largely the result of absorption by chlorophyll pigments (chlorophyll-a, chlorophyll-b) (allied to increasing water absorption). The $R_{(\lambda)}$ signatures also exhibit increased reflectance > 700 nm; this is due to the backscattering of VNIR light from plant tissues (largely due to the palisade cells within spongy mesophyll tissue) (Campbell, 2002). This VNIR shoulder is, however, notably absent in the $R_{(\lambda)}$ signature of the submerged aquatic plant (*Chara baltica*); instead, here, there is only a narrow $R_{(\lambda)}$-peak. The

absence of this feature is almost certainly due to intense absorption by the overlying water column.

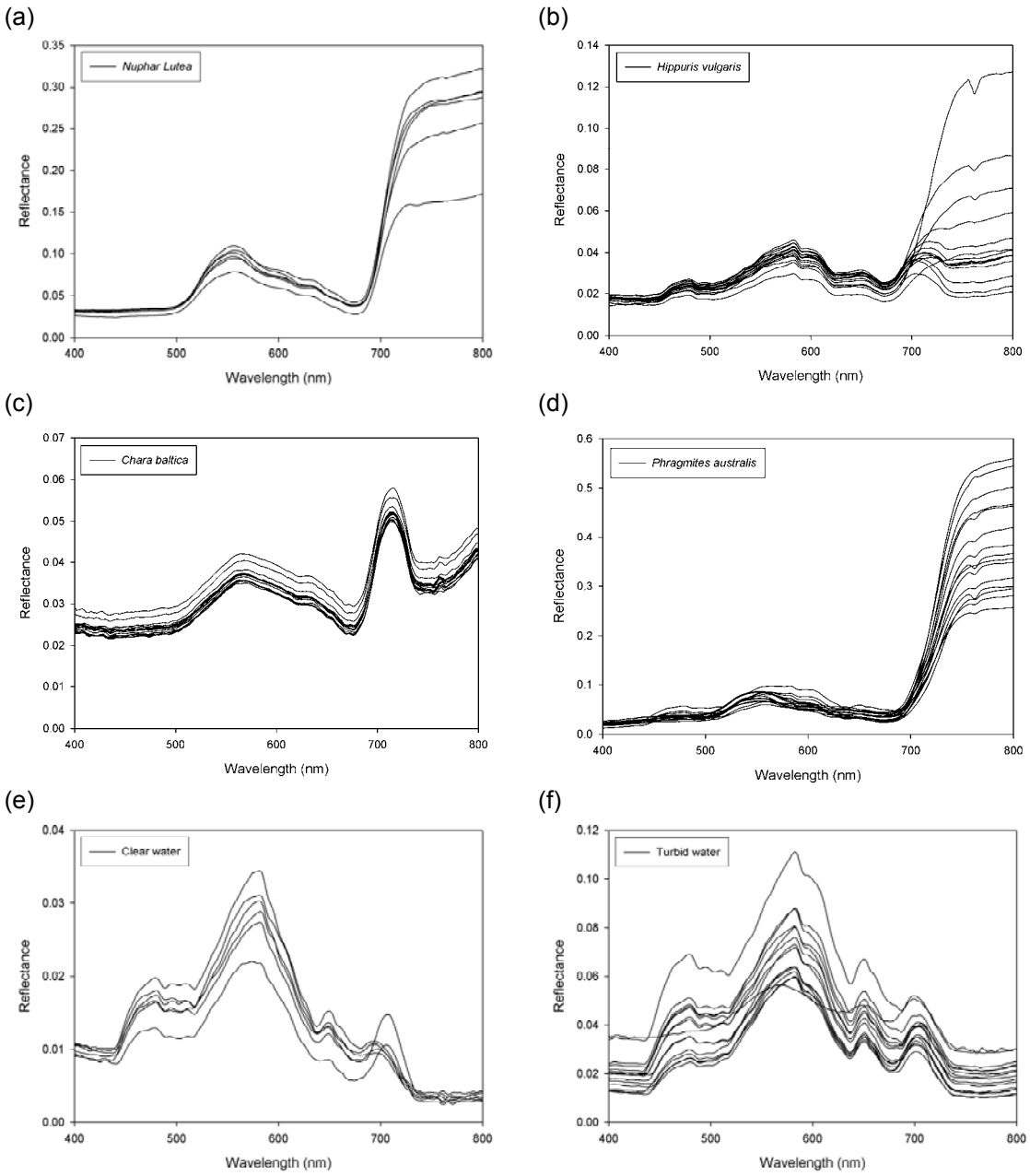

Figure 6.3 The $R_{(\lambda)}$ signatures of the four macrophyte species (a) *Nuphar lutea*, (b) *Hippuris vulgaris*, (c) *Chara baltica* and (d) *Phragmites australis* compared to the reflectance signatures of (e) clear water (chlorophyll-a < 10 mg m^{-3}; SPM < 5 mg l^{-1}; SDD > 1.5 m) and (f) turbid water (chlorophyll-a > 20 mg m^{-3}; SPM > 20 mg l^{-1}; SDD < 0.5 m).

The spectral signatures of *Phragmites australis* and *Nuphar lutea* were arguably the most distinct, both from the other aquatic plant species, and the spectra of open water. These species both demonstrated significantly higher $R_{(\lambda)}$ (400-800 nm) in comparison to the other

macrophyte species examined (e.g. 30-60% in the VNIR). The high $R_{(\lambda)}$ observed from the *Phragmites australis* stands was no doubt related to the fact that this tall monocotyledon typically forms dense, closed, canopies with substantial aerial biomass. In similarity, the high $R_{(\lambda)}$ measured from the beds of *Nuphar lutea* was probably a function of its large planophile floating-leaves, which present a large reflective surface, and obscure the surrounding water column. The spectral reflectance signatures of *Phragmites australis* and *Nuphar lutea* measured here are comparable to the *Phragmites australis* and *Polygonum amphibium* (a floating-leaved species) reflectance signatures depicted in Malthus & George (Malthus & George, 1997), which suggests a consistency in spectral response, both from identical plants in different lake systems, and from different plant species with common growth-habit characteristics.

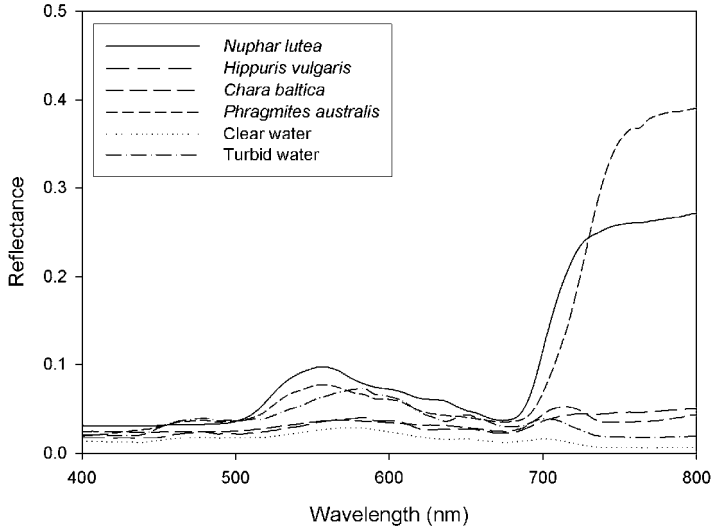

Figure 6.4 The mean $R_{(\lambda)}$ signatures of the four macrophyte species: *Nuphar lutea*, *Hippuris vulgaris*, *Chara baltica* and *Phragmites australis* compared to the reflectance signatures of clear water (chlorophyll-a < 10 mg m^{-3}; SPM < 5 mg l^{-1}; SDD > 1.5 m) and turbid water (chlorophyll-a > 20 mg m^{-3}; SPM > 20 mg l^{-1}; SDD < 0.5 m).

In comparison to *Phragmites australis* and *Nuphar lutea*, the spectral response measured over the *Hippuris vulgaris* and the *Chara baltica* beds was significantly weaker. This discrepancy was most apparent at VNIR wavelengths (> 700 nm). Indeed, the spectral responses of both of these species were broadly similar to that observed over open water. This is likely due to the fact that both species proportion the vast majority or, in the case of *Chara baltica*, all of their biomass beneath the water surface. The strong absorption of light by the water column would

therefore seem to greatly influence the spectral response of these aquatic plants. This may intimate that these species (and their respective growth-habit associations) may not be spectrally differentiable from areas of open, particularly turbid, water. The strong attenuation of VNIR light by the water column did, however, seemed to produce a characteristic and pronounced peak at *c*. 700 nm in the *Chara baltica* reflectance signature (Figure 6.3), which may be useful for delineating the extent of SAV in lakes. The *Chara baltica* $R_{(\lambda)}$ signature observed here is similar to that shown in Yuan & Zhang (2007) for the submerged plant *Vallisneria spiralis* which, again, suggests a consistency in the spectral response of aquatic plant species at the growth-habit level.

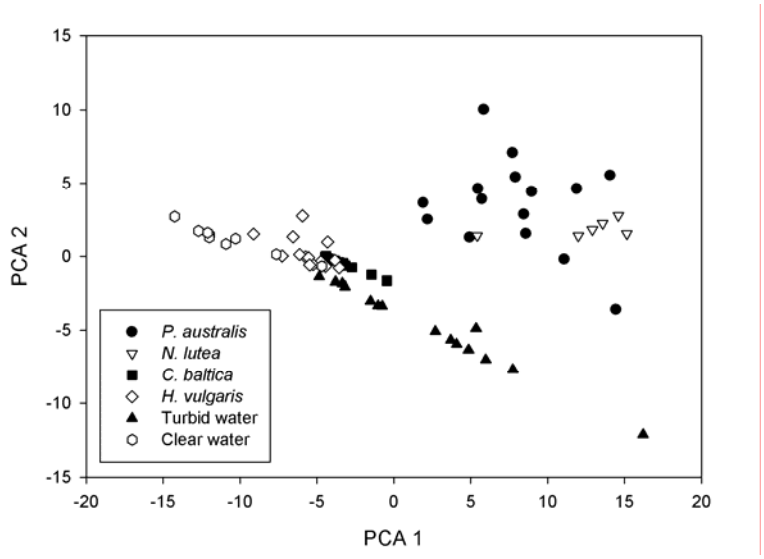

Figure 6.5 PCA score plot of the spectra reflectance signatures of the various macrophyte species examined relative to the signatures of clear and turbid water. PCA1: eigenvalue = 59.921, proportion variance explained = 0.740, cumulative variance explained = 0.740; PCA2: eigenvalue = 11.73; proportion variance explained = 0.145, cumulative variance explained = 0.885.

The spectral characteristics of the four macrophyte species (relative to clear and turbid water) were further explored using PCA and MDA analyses. The PCA score plot for the $R_{(\lambda)}$ signatures of the macrophyte species is depicted in Figure 6.5 using the first two extracted PCA components. Examination of the eigenvalue scree plot suggested that the first two PCA components contained that vast majority of the systematic variance present in the original untransformed dataset (~ 90%). The spectral reflectance measurements of the various aquatic plant species can be seen to demonstrate a reasonable degree of clustering in factorial space.

It is notable, however, that some degree of overlap occurs between some clusters. The PCA component scores for *Phragmites australis* $R_{(\lambda)}$ signatures were, as previously suggested, very distinct from the signatures of the other macrophyte species. However, interestingly, it can be seen that the variation within the *Phragmites australis* spectral response was almost as great as the variation observed between the spectral responses of the remaining aquatic plant species. This suggests that variable canopy architecture and, possibly, even the physiological status of the *Phragmites australis* plants, had a pronounced influence on the spectral response of this species.

The PCA score plot also shows that the $R_{(\lambda)}$ signature of *Nuphar lutea* was distinct from the other macrophyte species and, in particular, from the submerged and partially-emergent species. The clusters relating to the spectral signatures of the submerged *Chara baltica* and partially-emergent *Hippuris vulgaris* were, not unexpectedly, grouped closest together in PCA component space. It can be further seen that the PCA clusters for these species also demonstrate some overlap in PCA component space with the spectra of both clear and highly turbid water. Interestingly, a near-linear gradient can be perceived from the clear water PCA cluster, through the clusters associated with *Hippuris vulgaris* and *Chara baltica*, to the cluster created by the turbid water spectra. This gradient probably relates to the strength of the chlorophyll-a signal measured from these various classes. The spectral overlap in the signatures of the submerged *Hippuris vulgaris* and partially-emergent species *Chara baltica* (and indeed with that of open water) would seem to suggest that the discriminant mapping of these growth-habit associations using remote-sensing-based approaches may be problematic. The mixing boundaries between these classes, particularly for the submerged and partially-emergent species would, based on the PCA score plot, appear to be non-linear in nature. This observation may have implications for the performance of different remote-sensing-based classification algorithms.

First-derivative analysis was also explored in an effort to improve the spectral separation of the aquatic plant species (not shown). However, the first-derivative transformation drastically reduced the degree of spectral dissimilarity between the various macrophyte species. First-

derivative transformations effectively normalise $R_{(\lambda)}$ spectra for inherent differences in albedo. This suggests, importantly, in this instance, that variations in the magnitude of $R_{(\lambda)}$ observed between aquatic plants species are important for facilitating their discrimination using remote-sensing-based approaches.

The confusion matrix derived from the cross-validated MDA classification analysis of the spectral reflectance signatures of the four aquatic plant species (and the clear and turbid water spectra) are detailed in Table 6.2. It was surprising, given the degree of confusion between the spectral signatures of the aquatic plant species identified in the PCA score plot, that the MDA model achieved an exceptionally high classification accuracy (overall proportion correct = 0.959; proportion plant species correct (excluding open water spectra) = 1.000). Indeed, no misclassifications were observed for any of the macrophyte spectra. This would seem to indicate that the aquatic plant species, or perhaps more appropriately, the growth-habit classes they represent, are sufficiently spectrally differentiable to permit the discriminative mapping of aquatic vegetation in lakes. As these species exhibit pronounced morphological differences, such a level of classification accuracy should be expected, particularly if remote sensing is to be used in an operational manner for the survey of aquatic plants.

Table 6.2 The confusion matrix derived from the cross-validated MDA classification of the spectral signatures of the four aquatic plant species.

		Plant Species						
		P. aus	***N. lut***	***H. vul***	***C. bal***	**Turbid**	**Clear**	**Total**
Classified Plant Species	***P. aus***	15	0	0	0	0	0	
	N. lut	0	6	0	0	0	0	
	H. vul	0	0	14	0	0	0	
	C. bal	0	0	0	15	0	0	
	Turbid	0	0	0	0	13	1	
	Clear	0	0	0	0	2	8	
N		15	6	14	15	15	9	**74**
***n* correct**		15	6	14	15	13	8	**71**
Proportion		1.00	1.00	1.00	1.00	0.867	0.889	**0.959**

P. aus = Phragmites australis; *N. lut = Nuphar lutea*; *H. vul = Hippuris vulgaris*; *C. bal = Chara baltica*.

6.5.2 Supervised Classification of Aquatic Vegetation

6.5.2.1 Macrophyte Growth-Habit Associations in the Upper Thurne

The remote-sensing-based mapping of aquatic plant growth-habit associations was further explored by applying contrasting classification models to the airborne CASI-2 [Vegetation] imagery of the Upper Thurne Broads. The classification accuracies for the macrophyte growth-habit assemblages in the Upper Thurne system of the Norfolk Broads are compared in Table 6.3. It is notable that there were large discrepancies in the performance of some of the classification algorithms. More specifically, the EMD classifier performed poorly, providing an overall classification accuracy of just 41.7% and $\kappa = 0.09$. Further examination of the confusion matrix derived from the EMD classification (not shown) revealed that the algorithm frequently confused the water class with the submerged and, in particular, the partially-emergent macrophyte classes. The existence of spectral overlap between these classes was also identified from the PCA transformation of the *in-situ* $R_{(\lambda)}$ spectra; it would therefore seem that these growth-habit species demonstrate significant inter-class mixing. The poor performance of the EMD classifier probably reflects the fact that the Euclidean-distance between the mean centroids does not attain optimal inter-class separation in this instance.

Table 6.3 The classification accuracy and κ coefficients derived from the EMD, MLC and SVM classifications of the macrophyte growth-habit assemblages in the Upper Thurne system.

	Min. class accuracy	Max. class accuracy	Overall class accuracy	κ coefficient
EMD	9.12	57.30	41.68	0.09
MLC	22.74	99.83	97.15	0.73
SVM	22.54	99.91	97.40	0.75

In comparison, the MLC and SVM algorithms provided a highly accurate level of overall classification (97.2% and 97.4% and $\kappa = 0.73$ and 0.75 respectively). It should be noted that the overall classification accuracies attain here are distorted, to an extent, by the fact that both the MLC and SVM algorithms were highly effective at classifying open water pixels (for which large training and validation datasets were defined). Whilst, the delineation of the extent of open water is not of primary concern here, the extent of open water is, in itself, a useful metric of change in shallow lake ecosystems and, therefore, this finding should not be overlooked.

Table 6.4 Confusion matrix for the SVM classification of macrophyte growth-habit assemblages in the Upper Thurne system of the Norfolk Broads

CASI-2 Classification	Field Survey Classification					
	Emergent	Partially-emergent	Floating	Submerged	Water	User's Accuracy
Emergent	89.71	0.04	0.00	0.06	0.04	89.71
Partially-emergent	3.91	22.54	32.58	0.15	0.05	22.54
Floating	5.97	0.04	52.27	0.06	0.00	52.27
Submerged	0.00	18.37	0.76	90.04	0.00	90.04
Water	0.41	59.01	14.39	9.69	99.91	97.98
Unclassified	0.00	0.00	0.00	0.00	0.00	
Producer's Accuracy	89.71	22.54	52.27	90.04	99.91	
Class Commission	15.99	11.74	34.29	17.42	0.02	Kappa coefficient = 0.75
Class Omission	10.29	77.46	47.73	9.96	0.09	Overall accuracy = 97.40

Table 6.5 Confusion matrix for the SVM classification of macrophyte growth-habit assemblages in the Upper Thurne system of the Norfolk Broads using a 0.95 probability threshold in the classification algorithm.

CASI-2 Classification	Field Survey Classification					
	Emergent	Partially-emergent	Floating	Submerged	Water	User's Accuracy
Emergent	81.07	0.00	0.00	0.02	0.03	86.21
Partially-emergent	1.44	15.84	12.12	0.08	0.01	95.67
Floating	1.44	0.00	18.18	0.02	0.00	75.00
Submerged	0.00	0.72	0.00	81.54	0.00	99.10
Water	0.41	32.74	10.61	2.45	99.47	98.94
Unclassified	15.64	50.70	59.09	15.89	0.49	
Producer's Accuracy	81.07	15.84	18.18	81.54	99.74	
Class Commission	13.79	4.33	25.00	0.90	1.05	Kappa coefficient = 0.70
Class Omission	18.93	84.16	81.82	18.46	0.53	Overall accuracy = 96.54

The SVM classification algorithm provided a marginally better classification than the MLC algorithm; the confusion matrices derived from the SVM classification are shown in Table 6.5 and Table 6.5. The classification matrix shown in Table 6.4 was achieved without the use of a probability threshold for the SVM algorithm; the classification matrix shown in Table 6.4 was achieved using a 0.95 probability threshold for the SVM algorithm. The inclusion of the 0.95 probability threshold in the SVM algorithm provides a more conservative classification – this is important in situations (as incurred here) when the image to be classified contains ground-truth classes not defined in the algorithm training process (i.e. marshland, alder carr). The corresponding classified CASI-2 [Vegetation] images are depicted in Figure 6.6 and Figure 6.7.

It is notable that, despite the high overall classification accuracy, the classification accuracies derived for specific classes varied from 22.5% (partially-emergent macrophytes) to 99.9% (water). The lowest classification accuracies (for both SVM models) were associated with the partially-emergent and floating growth-habit classes. In the case of the partially-emergent class, 59.0% of the ground-truth validation pixels were incorrectly classified as water; the PCA ordination analysis of the *in-situ* spectrometry data identified that the spectral signatures of partially-emergent species such as *Hippuris vulgaris* are not too dissimilar from those observed from turbid, algal dominated, waters and thus these misclassifications are perhaps not to be unexpected. The cover and density of partially-emergent species (mainly *Hippuris vulgaris*, but with *Myriophyllum spicatum* and *Potamogeton* spp. also present in some areas) used as training data for the SVM classification algorithms varied considerably. These partially-emergent beds were, in places, relatively sparse and were, in effect, a mosaic of vegetation and small areas of open water. This may explain the spectral confusion between the partially-emergent class and the water class; indeed, the low user's accuracy obtained suggests that the training data for the partially-emergent class were poorly defined. The inclusion of the 0.95 probability threshold did, however, improve the user's accuracy for the partially-emergent class.

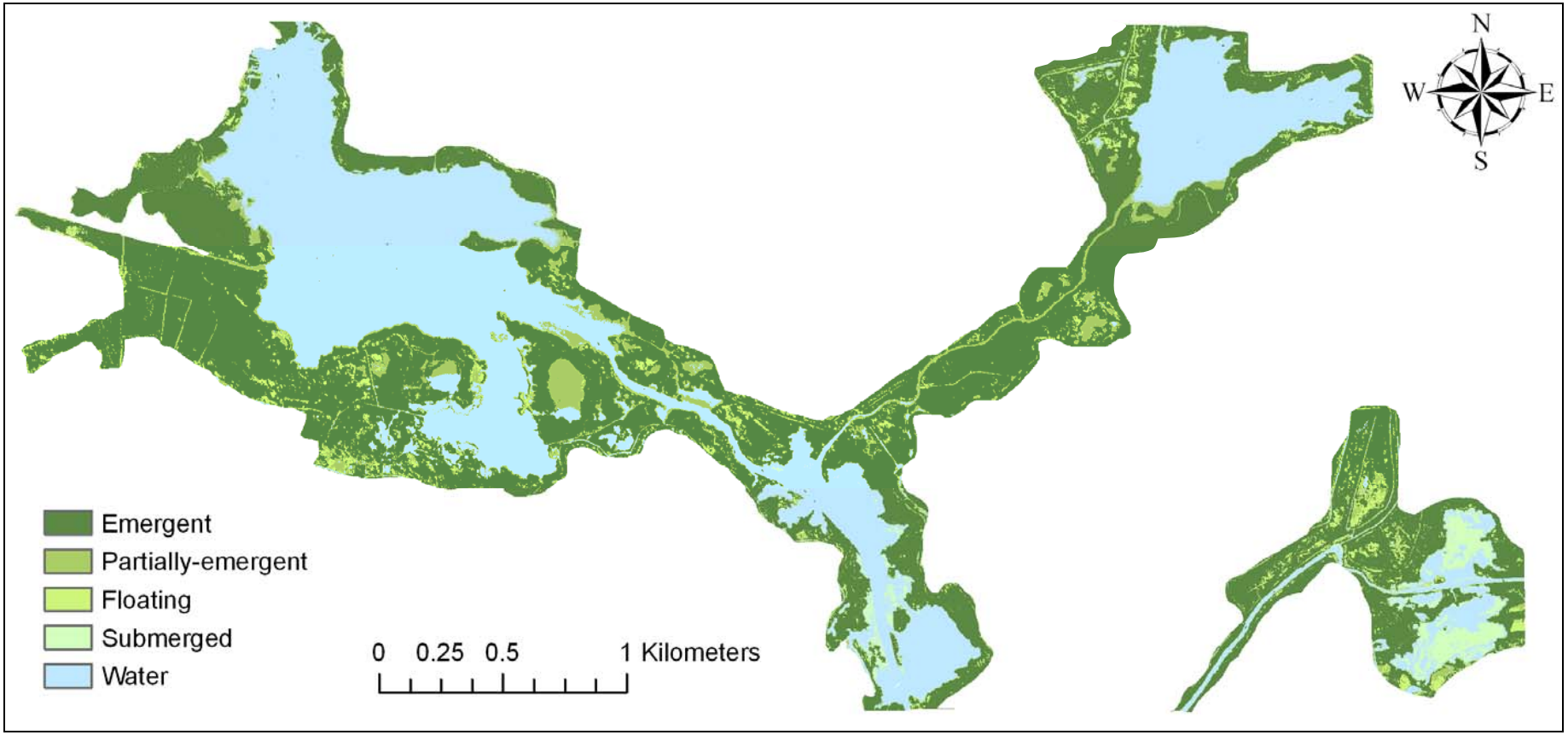

Figure 6.6 Classified CASI-2 [Vegetation] images of macrophyte growth-habit assemblages in the Upper Thurne region of the Norfolk Broads (UK) on 22 June 2005 using a SVM algorithm.

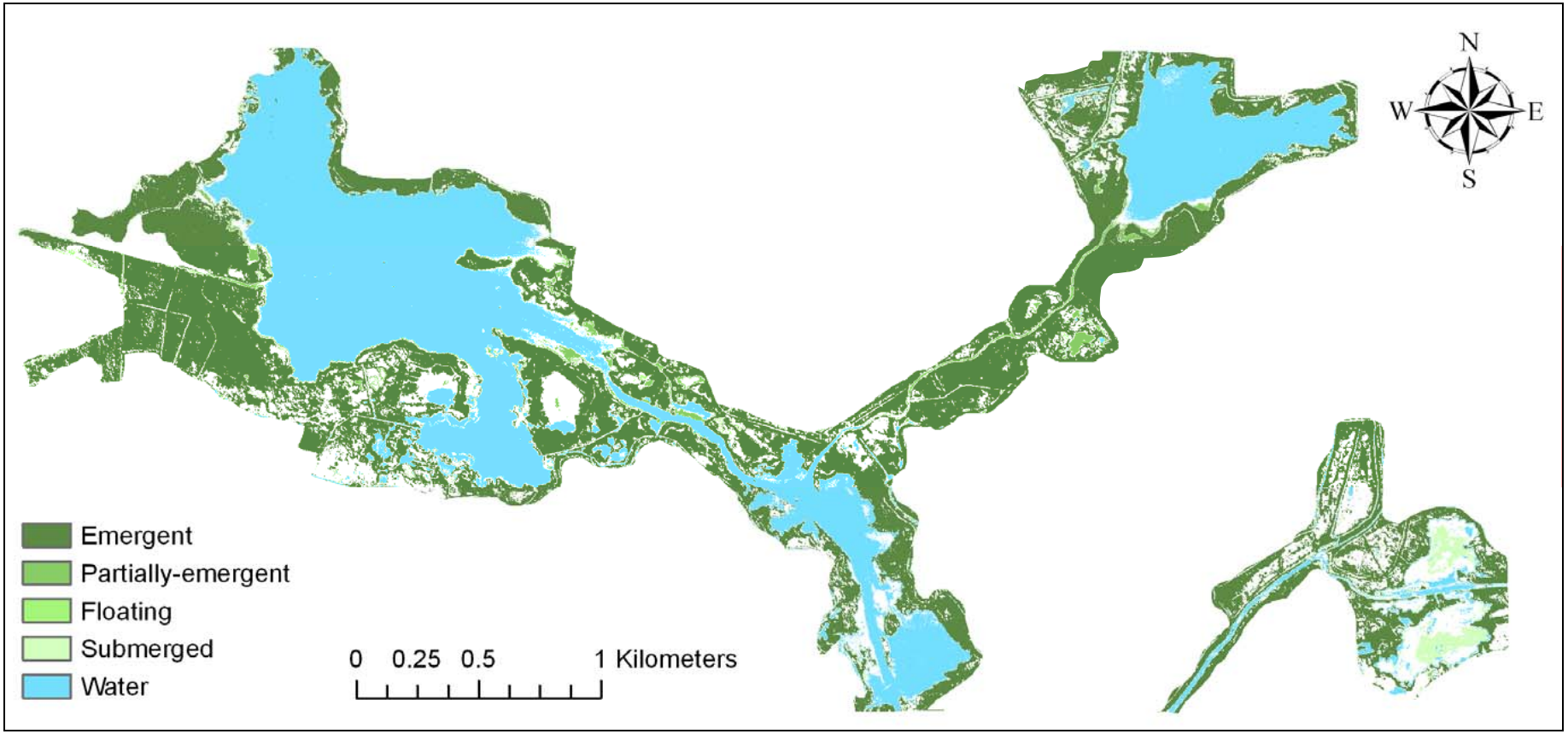

Figure 6.7 Classified CASI-2 [Vegetation] images of macrophyte growth-habit assemblages in the Upper Thurne region of the Norfolk Broads (UK) on 22 June 2005 using a SVM model with a 0.95 probability threshold included in the classification algorithm.

In the case of the floating macrophyte class, 32.6% of the ground-truth pixels were misclassified as belonging to the partially-emergent class. These errors were probably the result of confusion between areas of sparser floating macrophyte cover (largely *Nuphar lutea*) and the few very dense beds of partially-emergent species. It is also notable that the classified CASI-2 [Vegetation] images show some misclassified areas of floating macrophyte cover in the terrestrial areas surrounding Hickling Broad (Figure 6.6). This area is dominated by fenland vegetation, obviously with no floating macrophyte coverage. The introduction of the 0.95 probability threshold in the classification algorithm was, however, successful in preventing these areas from being misclassified (this is not reflected in the classification accuracies because the training and validation datasets were not extracted from the fenland areas). This demonstrates the importance of employing a conservative approach to remote sensing classification, particularly, as here, when the ground-truth available is somewhat limited.

In contrast to the partially-emergent and floating classes, classification accuracies for the emergent and submerged classes were 89.7% and 90.0% respectively. The high classification accuracy achieved for the emergent growth-habit assemblage reflects the fact that the dominant species in this class (*Phragmites australis*, *Typha latifolia*) have appreciably different spectral signatures from the other macrophyte growth-habits, largely due to their characteristic canopy architecture. The classified CASI-2 [Vegetation] images (22 June 2005) show that the vast majority of the reedswamp habitat that surrounds Hickling Broad, Horsey Mere and the Martham Broads has been correctly classified into the emergent class (Figure 6.6 and Figure 6.7). However, it is evident that some of the small areas of Alder carr that fringe Hickling Broad were also classed as emergent aquatic plants. The introduction of the 0.95 probability threshold into the algorithm, again, prevented these areas from being misclassified.

The accurate classification of the *Phragmites australis*-dominated reedswamp achieved here echoes the results described in Arzandeh & Wang (2003), Maheu-Giroux & De Blois (2005) and Pengra *et al*. (2007) who have previously demonstrated that *Phragmites australis* vegetation can be accurately mapped from remotely sensed data. Reedswamp is a key functional

component of many shallow lake ecosystems, thus the ability to monitor the extent of this habitat through remote sensing reconnaissance is a pertinent development, particularly for the assessment of ecological status in shallow lakes. Moreover, in some freshwater wetlands, *Phragmites australis* is considered to be an invasive and aggressive alien species and its rapid colonisation is a serious concern for the ecological integrity of these systems. In this context remote sensing would seem to be a useful tool for mapping the invasion of *Phragmites australis* and, indeed, other invasive macrophytes in aquatic ecosystems (Maheu-Giroux & De Blois, 2005; Pengra *et al.,* 2007).

It is of note that the submerged growth-habit class could also be mapped accurately using the CASI-2 [Vegetation] imagery despite the fact that these species (*Chara* spp., *Najas marina*, *Nitellopsis obtusa*) grow at a substantial depth (0.5-1.5 m) beneath the water surface. The PCA ordination analysis of the *in-situ* R_λ spectra suggested that some confusion may occur between the spectral signatures of SAV species and turbid water. Nonetheless, the SVM algorithm seems to have been effective for achieving sufficient class separation in this instance. It should be noted however that the SAV pixels used to define the submerged macrophyte class (and for classification validation) were extracted from the dense *Chara* spp. lawns in the Martham Broads. Some extensive areas of *Chara* spp. lawn (largely *Chara intermedia*) also occur in Hickling Broad. These lawns were not used for classification training or validation purposes, largely as it was perceived that the turbid water column of Hickling Broad (SDD < 0.4 m) would not permit these species to be mapped. This presumption was vindicated by the SVM classification, as the algorithm failed to identify the presence of the submerged *Chara* spp. lawns in Hickling Broad.

It would thus seem that, while SAV can be readily mapped in clear water shallow lakes, such as the Martham Broads, poor water transparency may prohibit the detection and mapping of SAV in turbid shallow lakes. The recolonisation of turbid, phytoplankton-dominated, lakes by SAV is often a key objective for those concerned with restoring the ecological status of these systems. The capability of remote sensing to provide information on the extent of aquatic plant colonisation would therefore be hugely beneficial to the assessment of ecological status and

trajectory in such lakes. In this context, further work should be focussed on improving the detection capabilities of remote sensing instruments (i.e. signal processing and enhancement) for benthic vegetation in turbid lakes. However, in turbid lakes, where SAV cannot be detected using remote sensing, this lack of detectability could, in itself, be interpreted as a consequence of reduced SAV canopy height (or biomass) and, therefore, may be a useful indicator of the ecological status of the system in question.

6.5.2.2 Submerged Aquatic Vegetation in the Martham Broads

The confusion matrices derived from the classification of SAV assemblages in the clear water Martham Broads using the EMD, MLC and SVM algorithms are detailed in Tables 6.6-6.8. The EMD classification algorithm was again the poorest performing classifier, although the 72.1% classification accuracy achieved at the SAV assemblage level, interestingly, represented an improvement on the classification accuracy previously achieved at the growth-habit level. This is somewhat surprising as the spectral distinction between classes should, in theory, be greater at the growth-habit assemblage level than at the species assemblage.

This presupposition is supported in the classification accuracies achieved through the MLC and SVM algorithms which, at 78.0% and 87.1% respectively, were lower than that achieved at the growth-habit level. Nevertheless, the classification accuracies achieved, particularly using the SVM algorithm, were still encouraging; for example, a classification accuracy of 80% has often been suggested to be the benchmark for the remote-sensing-based mapping of terrestrial vegetation communities (May *et al.,* 1997; Liu *et al.,* 2002) and, as such, the classification accuracy achieved here with submerged aquatic vegetation would seem to compare favourably.

The confusion matrices derived from the EMD, MLC and SVM classification again reveal that the performance of the algorithms varied significantly between classes. The EMD and MLC algorithms did not provide a good classification of the clear water pixels in the image; classification accuracies for these classes were just 45.5% and 32.4% respectively. The EMD and MLC algorithms frequently misclassified these clear water pixels as *Hippuris vulgaris* or *Nitellopsis obtusa*.

Table 6.6 Confusion matrix for the EMD classification of SAV in the Martham Broads, Norfolk, UK.

CASI-2 Classification	Field Survey Classification						
	C. hispida	C. aspera	N. obtusa	H. vulgaris	Lake bed	Clear water	User's Accuracy
C. hispida	81.36	0.93	0.00	12.22	0.68	0.00	97.32
C. aspera	0.00	93.79	2.30	8.33	5.47	0.57	80.97
N. obtusa	0.00	0.94	74.24	0.00	13.85	35.37	60.79
H. vulgaris	12.53	1.86	0.00	74.44	1.54	15.76	29.78
Lake bed	0.31	0.00	8.59	0.00	76.58	0.00	85.66
Clear water	0.00	0.00	14.63	4.44	0.00	45.46	75.66
Unclassified	5.80	2.48	0.24	0.57	1.88	2.84	
Producer's Accuracy	81.36	93.79	74.24	74.44	76.58	45.46	
Class Commission	2.68	19.03	39.21	70.22	14.34	24.34	Kappa coefficient = 0.66
Class Omission	18.64	6.21	25.76	25.56	23.42	54.54	Overall accuracy = 72.17

Table 6.7 Confusion matrix for the MLC classification of SAV in the Martham Broads, Norfolk, UK.

CASI-2 Classification	Field Survey Classification						
	C. hispida	C. aspera	N. obtusa	H. vulgaris	Lake bed	Clear water	User's Accuracy
C. hispida	96.97	3.42	0.12	17.22	4.79	1.25	93.84
C. aspera	0.00	89.44	0.85	0.00	1.37	0.00	95.05
N. obtusa	0.15	0.62	86.70	1.67	7.35	10.88	83.08
H. vulgaris	3.17	6.52	0.48	80.56	0.00	55.44	20.71
Lake bed	0.00	0.00	2.90	0.00	86.50	0.00	95.47
Clear water	0.00	0.00	8.95	0.56	0.00	32.43	79.22
Unclassified	0.00	0.00	0.00	0.00	0.00	0.00	
Producer's Accuracy	96.97	89.44	86.70	80.56	86.50	32.43	
Class Commission	6.16	4.95	16.92	79.29	4.53	20.78	Kappa coefficient = 0.73
Class Omission	3.33	10.56	13.30	19.44	13.50	67.57	Overall accuracy = 78.06

Table 6.8 Confusion matrix for the SVM classification of SAV in the Martham Broads, Norfolk, UK.

CASI-2 Classification	Field Survey Classification						
	C. hispida	C. aspera	N. obtusa	H. vulgaris	Lake bed	Clear water	User's Accuracy
C. hispida	99.30	3.42	0.12	31.11	4.27	3.97	90.93
C. aspera	0.00	96.58	1.09	0.00	3.42	0.11	91.20
N. obtusa	0.15	0.00	89.12	0.56	11.11	13.61	79.68
H. vulgaris	0.46	0.00	0.00	65.00	0.00	9.18	57.35
Lake bed	0.08	0.00	2.18	0.00	81.20	0.79	94.81
Clear water	0.00	0.00	7.50	3.33	0.00	72.34	90.37
Unclassified	0.00	0.00	0.00	0.00	0.00	0.00	
Producer's Accuracy	99.30	96.58	89.12	65.00	81.20	72.34	
Class Commission	9.07	8.80	20.32	42.65	5.19	9.63	Kappa coefficient = 0.84
Class Omission	0.70	3.42	10.88	35.00	18.80	27.66	Overall accuracy = 87.11

These misclassifications are again probably the result of the typically sparse canopy of *Hippuris vulgaris*. Similarly, the cover of *Nitellopsis obtusa* in the Martham Broads was not as dense as that of *Chara* spp. for example, thus spectral confusion with clear water areas may be somewhat expected. Furthermore, in the Martham Broads, *Nitellopsis obtusa* frequently occurred in association with several other aquatic plants (predominately *Najas marina*, but also *Chara* spp. and *Potamogeton*) which would have influence the "purity" of the spectral response and may, in part, explain the spectral confusion observed.

The EMD, MLC and, in particular, the SVM algorithm, returned good producer's accuracies for the classification of the *Chara hispida*, *Chara* aspera and *Nitellopsis obtusa* classes. However, the SVM was somewhat poorer at classifying areas of *Hippuris vulgaris*, achieving a producer's accuracy of just 65.0%, in comparison to the other algorithms (these pixels were typically misclassified as *Chara hispida*). This misclassification may have been due to the use of inappropriate training data. Indeed, the low user's accuracies for the *Hippuris vulgaris* class achieved by all three classification algorithms (20.7-57.3%) would seem to suggest that the training data for *Hippuris vulgaris* was, spectrally, ill-defined. The use of more, and better defined, training data would likely increase the producer's accuracy for this class. Further, while *Hippuris vulgaris* is a visually prominent species, from an aerial vista it is likely to have little influence upon the spectral signature of the water column unless it occurs at high densities.

The SVM provided a higher producer's accuracy for the *Chara hispida* and *Chara aspera* classes than was achieved using the EMD or MLC algorithms. Indeed, the degree of spectral differentiability between these two *Chara* spp. classes was unforeseen. The classification was probably aided, to an extent, by the fact training and validation data for these classes were readily defined as these species occurred as large, relatively monospecific, and geographically isolated lawns. The other species of *Chara* found in the Martham Broads (*Chara baltica* and *Chara intermedia*) typically grew in association with other SAV species and thus it was problematic to develop specific training and validation data for these species. Nevertheless, the classification accuracies achieved allude to the fact that remote sensing technologies may be

highly effective and efficient for the mapping of SAV lawns in clear water shallow lakes. This is a highly relevant finding in the context of the foreseen use of remote sensing for monitoring the ecological status and stability of shallow lakes.

The CASI-2 [Vegetation] image acquired on 29 August 2005 classified using the SVM algorithm is depicted in Figure 6.8. The classified CASI-2 [Vegetation] shows good agreement to the distribution of SAV inferred from the transect survey data and, in particular, the *Chara hispida* and *Chara aspera* lawns appeared to have been accurate delineated. The SVM algorithm has also accurately classified the deep areas of clear water associated with the River Thurne which flows between Martham North Broad and Martham South Broad; the pixels classified as *Nitellopsis obtusa* in the River Thurne (eastern part of channel) are misclassifications, but this river channel is heavily vegetated by a broad mix of aquatic plants, so some misclassification of the River Thurne channel is not unexpected.

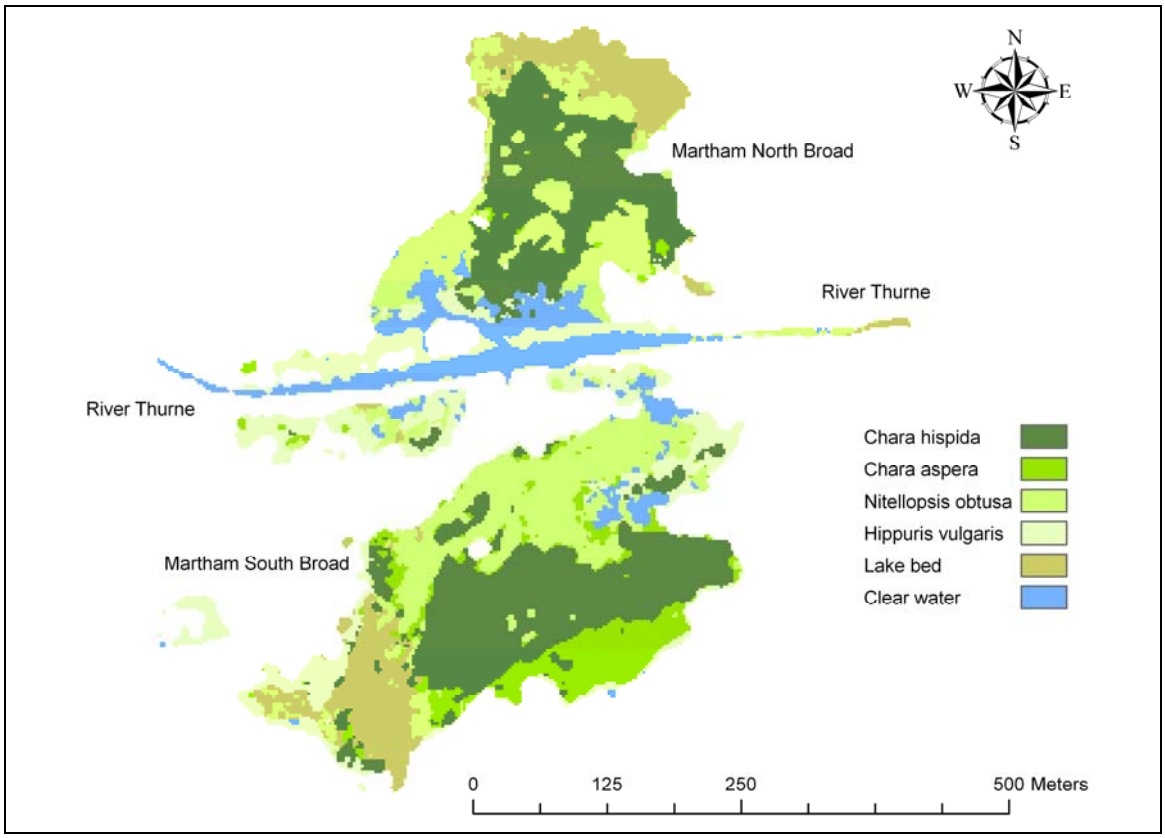

Figure 6.8 Classified CASI-2 [Vegetation] image of SAV in the Martham Broads on 29 August 2005 using a SVM algorithm.

The largest misclassification apparent in the CASI-2 [Vegetation] image would seem to occur between areas of uncolonised clear water and the *Nitellopsis obtusa* class. Significant parts of Martham South Broad – particularly towards the northern shoreline adjacent to the River Thurne – are predominantly clear water, but the corresponding image pixels have been misclassified as beds of *Nitellopsis obtusa*. These misclassifications are probably due to the fact that the mixing boundaries between these classes were poorly defined. The sparse cover of *Nitellopsis obtusa* in places made the definition of "spectrally pure" training data often problematic. Further, the stem density of *Nitellopsis obtusa* is typically low (say compared to *Chara* spp.) and, thus, at least spectrally, it is likely to be often similar in appearance to open water. Some degree of confusion with clear waters areas is therefore not to be unexpected. Larger training datasets would have no doubt improved the classification accuracies for these somewhat ill-defined, and spectrally similar, classes. However, it must be stated that the grapnel survey data did not ideally lend itself to the construction of good quality training and validation datasets. Often it was difficult to determine the SAV composition on a pixel-by-pixel basis. This emphasises the need to ensure there is a natural synergy between the ground-truth data and the data requirements for remote-sensing-based classification procedures. Sub-aqua quadrat-based survey data may have proved more effective for the construction of the ground-truth training and validation datasets; unfortunately, such data was not available for the Martham Broads in this instance.

The remote-sensing-based mapping of aquatic vegetation communities is always likely to be most effective in shallow lakes where large monospecific stands, beds, or lawns occur (e.g. *Phragmites australis*). The spatial resolution of remote sensing imagery products can dramatically influence the accuracy of classification procedures. High-spatial resolution (2.5 m) airborne imagery was used in this instance. However, even this high resolution data is probably not sufficient for aquatic vegetation mapping in shallow lakes on the scale of the Martham Broads where often the composition of the aquatic flora varied at scales < 2.5 m. Significant improvements in classification may be expected if very high resolution imagery (i.e. ≤ 1 m) were to be used. In larger lake systems, with more extensive and uniform macrophyte coverage, coarser spatial resolutions would no doubt prove equally effective. Sub-pixel variations in

floristic composition may be resolved by the use of linear spectral mixing models and, indeed SVM classifiers (when used to determine the relative abundancies of endmembers), and this may afford an alternative way forward in the absence of high-spatial resolution imagery.

6.6 CONCLUSIONS

Aquatic vegetation is an important functional component of shallow lakes and is key measure of shallow lake ecological status. Monitoring the extent of macrophyte colonisation through field-based surveys is problematic, particularly if the abundance and distribution of aquatic vegetation is to be assessed at the lake- or, indeed, the regional-scale. This study examined the use of airborne remote sensing (CASI-2) for the classification of aquatic vegetation communities in the Upper Thurne system of the Norfolk Broads. *In-situ* spectrometry was used to explore the spectral reflectance signatures of four aquatic plants species of contrasting growth-habit. The spectral reflectance signatures of these species exhibited some notable dissimilarities, particularly for species of the emergent and floating-leaved growth-habit association. These observations were further confirmed using PCA and MDA analyses.

The capability of airborne remote sensing for mapping aquatic vegetation in shallow lakes was examined using two CASI-2 vegetation images of the Upper Thurne system. Ground-truth aquatic plant survey data was used to train and validate three contrasting classification models for mapping aquatic plant based on (i) growth-habit associations, and (ii) dominant species. The use of a state-of-the-art, non-linear, radial-basis-function, support vector machine learning algorithm provided a more accurate classification of growth-habit associations (97.4%) and SAV species (87.1%) than could be achieved with either a Euclidean Minimum Distance or a Gaussian Maximum Likelihood classification algorithm. Some confusion, however, was observed between classes. In particular, classes that were comprised of aquatic plants species that often form sparse canopies or small beds (e.g. *Hippuris vulgaris*, *Nitellopsis obtusa*) were often misclassified as a result of the spectral confusion incurred from the surrounding water column.

Remote sensing, nevertheless, would seem to be a potentially effective and efficient tool for the survey of aquatic plants in shallow lakes. It would seem, importantly, that remote sensing is readily capable of resolving the distribution of submerged aquatic plant communities in clear water lakes. The abundance and distribution of SAV is a key measure of shallow lake ecological status. The spatially-resolving information afforded by remote sensing reconnaissance may therefore prove useful in furthering the understanding of SAV dynamics in shallow lakes and the response of these communities to pressures and management. Moreover, the potential to acquire such information at the regional-scale suggests that remote sensing technologies may be able to make an important contribution to the survey of vegetation in lakes as required under the EU WFD.

7 REMOTE SENSING OF AQUATIC PLANT ECOPHYSIOLOGY IN SHALLOW LAKES

7.1 INTRODUCTION

The preceding chapter examined the use of remote sensing for the classification and mapping of aquatic vegetation in shallow lakes. The research presented in this chapter seeks to build upon the use of remote sensing for the mapping of aquatic vegetation, and therefore species turnover, in shallow lakes through the development of novel quantitative techniques for the assessment of the physiological status of aquatic plants. The chapter focuses on the exploration of lake-scale spatial variation in the physiological performance of an individual dominant, *Phragmites australis*, in relation to nutrient enrichment.

7.2 RATIONALE

Shallow lake ecosystems often include an extensive littoral zone dominated by large emergent aquatic plant species such as *Typha latifolia*, *Phalaris arundinacea* and *Phragmites australis*. Littoral reedswamps are recognised to fulfil important functions in the regulation of hydraulic circulation, the suppression of bottom sediment resuspension, biogeochemical cycling and in the provision of habitat niches and refuges for other aquatic biota. Reedswamp vegetation is therefore critical to the wider status and stability of shallow lake ecosystems. However, since the 1950s, there has been a large-scale decline in the reedswamp habitat of many European lakes and, in particular, that composed of the common reed *Phragmites australis* (Cav.) Trin. Ex Steudel) (Boar *et al.,* 1989; Vanderputten *et al.,* 1997; Fogli *et al.,* 2002).

The decline of *Phragmites australis* reedswamp in European lakes has been strongly linked to nutrient enrichment (Armstrong & Armstrong, 2001). Cizkova *et al*. (Cizkova *et al.,* 1996) have suggested that, in eutrophic lake systems, increased primary productivity can lead to the substantial accumulation of organic matter in reedswamp habitats. This copious flux of organic-C to the littoral hydrosoil can accelerate decompositional processes, increasing the microbial demand for oxygen, and ultimately leading to the development of oxygen-stressed anaerobic

conditions. The resulting switch to anaerobic microbial metabolism can, in turn, lead to the production of numerous phytotoxic metabolites as the end-product of anaerobic decomposition (Santruckova *et al.,* 2001). The accumulation of these phytotoxic metabolites (typically organic acids), in combination with conditions of oxygen stress, is believed to be a major cause of reed decline in European lakes and their associated wetland environments (Armstrong *et al.,* 1996; Armstrong *et al.,* 1996; Vanderputten *et al.,* 1997; Cizkova *et al.,* 1999).

The extent of reedswamp vegetation in the Norfolk Broads has declined substantially over recent decades (examination of 18 lakes showed a collective loss > 75% of the reedswamp cover between 1880 and 1977) (Boorman & Fuller, 1981). Substantial initial losses of reedswamp vegetation were attributed to intensive grazing from introductions of Coypu (*Myocastor coypus*) (Boorman & Fuller, 1981). However, reedswamp decline was observed to continue after the extermination of *Myocastor coypus* in the Norfolk Broads. Boar *et al*. (1989) linked this further decline to increased nitrate loadings, suggesting that this can lead to disproportionate shoot-to-rhizome growth, thus rendering the plants, particularly those of the floating rhizome growth-habit, susceptible to physical damage from wave action. In the shallow lakes of the Upper Thurne region of the Norfolk Broads, *Phragmites australis* reedswamp of the floating rhizome growth-habit has all but disappeared. However, in recent years, obvious signs of further decline have been observed in the remaining areas of rooting littoral reedswamp. This suggests that the decline of reedswamp in the Norfolk Broads may be more complex than previous work has suggested and, indeed, it is clear that further consideration of the decline in *Phragmites australis* reedswamp in these lakes is needed.

The early identification of plant physiological responses to stressors in natural communities is problematic. Phytophysiological responses to stress may include change in photosynthetic rate and photosynthetic pigment composition (carotenoids and chlorophylls), changes in tissue biochemistry (micro- and macro-nutrients, cellulose, lignin and water content) and changes in plant morphology (biomass, LAI, stem length and diameter) (Lichtenthaler, 1996). However, such phytophysiological responses are typically difficult to diagnose and, moreover, quantify in the field. Indeed, it is near-impossible to adequately characterise the physiological status of

plants across extensive spatial areas using conventional point based sampling. In lakes, this represents a significant obstacle to the effective and efficient diagnosis of aquatic plant physiological responses to pressures at the ecosystem-scale.

In this context, the spatially-resolving and synoptic data provided by remote sensing platforms may provide a novel means of quantifying variations in the physiological status of aquatic plant communities in lakes. Numerous authors have demonstrated that remote sensing can be used to quantify plant stress in precision agriculture and agriforestry contexts (Liu *et al.,* 2004; Ayala-Silva & Beyl, 2005; Fitzgerald *et al.,* 2006; Shrivastava & Gebelein, 2007; Campbell *et al.,* 2007), but recent research has also shown that such techniques can be effectively transferred for the assessment of plant physiology in natural plant communities (Smith *et al.,* 2005; Artigas & Yang, 2006). Davids & Tyler (2003), for example, employed a variety of spectral-reflectance-based vegetation indices as means of quantifying radionuclide-contamination-induced tree stress in the Chernobyl exclusion zone (Ukraine). In a context more akin to shallow lake ecosystems, plant spectral reflectance characteristics have been used to examine the effects of heavy metal deposition on plants growing in floodplain wetlands (Kooistra *et al.,* 2004; Clevers *et al.,* 2004) and, significantly, Tilley *et al*. (2003) demonstrated that the spectral reflectance characteristics of two emergent macrophytes (*Typha latifolia* and *Borrichia frutescens*) could be related to nitrogen loadings in a lake system.

It would therefore seem that remote sensing could provide a potentially novel, yet highly valuable, tool for the assessment of the physiological response of aquatic plants to environmental changes and pressures in lakes that would be otherwise unachievable through conventional field-based survey.

7.3 AIMS AND OBJECTIVES

The aim of the research presented in this chapter was to explore the use of remote sensing technologies for the assessment of aquatic plant physiological responses to nutrient loading in shallow lakes. More specifically, the chapter aims to use *in-situ* and airborne remote sensing

surveys to investigate lake-scale variation in the performance of *Phragmites australis* reedswamp in relation to pressures from nutrient enrichment in Hickling Broad, Norfolk (UK).

The specific objectives for this chapter can be defined as:

a) To characterise the spectral reflectance characteristics of the emergent plant *Phragmites australis* under varying states of stress using expeditious *in-situ* spectrometry surveys and to subsequently identify a number of candidate spectral indices that are sensitive to changes in physiological status of this aquatic plant.

b) To extrapolate the candidate vegetation indices derived using *in-situ* spectrometry to CASI-2 airborne remote sensing imagery of the Norfolk Broads thus allowing the physiological status of *Phragmites australis* reedswamp to be evaluated at an unprecedented lake-scale.

c) To relate spatial variations in plant physiology, as identified by the reflectance-based spectral indices, to the underlying sediment chemistry and, in particular, the degree of nutrient enrichment with a view to providing new insights into the decline of reedswamp vegetation in the Norfolk Broads.

7.4 METHODS

7.4.1 Study Sites

The capability of remote sensing for assessing the physiological status of aquatic plants was explored in two shallow lakes. Initially, method development was performed in Lake Balaton (Hungary). Lake Balaton is Europe's largest shallow lake (mean depth *c*. 3 m; area *c*. 595 km^2). The littoral of Lake Balaton is dominated by extensive stands of *Phragmites australis* reedswamp. However, over recent decades, the extent of reedswamp in Lake Balaton has declined dramatically in response to pressures incurred from eutrophication and the artificial regulation of the water level (Cizkova *et al.,* 1999). The methods pioneered in Lake Balaton were used to assess variations in the physiological status of *Phragmites australis* plants growing in Hickling Broad (UK) (52º44'17''N; 1º34'29''E). Hickling Broad is a small shallow lake

(mean depth < 2.5 m; area *c*. 1.3 km^2) which, in similarity to Lake Balaton, is fringed by dense *Phragmites australis* reedswamp. The extent of *Phragmites australis* reedswamp in Hickling Broad has also declined dramatically over recent decades in response to a variety of pressures, including eutrophication. Further information on the decline of reedswamp in the Norfolk Broads can be found in Boorman & Fuller (1981) and Boar *et al*. (Boar *et al.,* 1989).

7.4.2 Field Sampling

7.4.2.1 Lake Balaton (Hungary)

The remote-sensing-based assessment of plant physiological status requires that responses to stressors can be identified through resulting variations in the spectral response; changes in the pigmentation of plant leaves (i.e. chlorophyll-a) are a common phytophysiological response to environmental stimuli, including variations in nutrition (Lichtenthaler, 1996). This is significant, as there is a substantial volume of work to suggest that spectral reflectance based metrics can be constructed to quantify variation in the pigment content of plant leaves, at both the leaf- and canopy-scale (Penuelas *et al.,* 1994; Gitelson & Merzlyak, 1994; Penuelas *et al.,* 1995; Blackburn, 1998; Sims & Gamon, 2002). This approach was examined here for the assessment of physiological status in *Phragmites australis* reedswamp.

It was, therefore, important to initially examine if spectral reflectance based indices could be used to diagnose and, further, quantify changes in the physiological status of *Phragmites australis* plants. This was explored using measurements obtained from plants growing in Lake Balaton (Hungary). The aim of this work was to seek a calibration between indices derived from spectral reflectance measurements and the assayed pigment content of *Phragmites australis* leaves. The calibration was performed using plants growing in Lake Balaton because, here, laboratory facilities were immediately available for the analysis of plant pigments; it was not possible to measure the concentration of chlorophyll-a in the apical leaves of plants examined later in the Norfolk Broads.

The apical leaves of *Phragmites australis* plants growing in Lake Balaton were systematically harvested from 25 stands in July 2004. The plants sampled exhibited perceivable variations in

performance. This enabled spectral reflectance measurements to be acquired from leaves in various states of physiological stress and, importantly, facilitated the collation of a suitable dataset for calibration purposes. The leaves harvested in the field were stored in the dark, in cool boxes, and were transported back to the laboratories of the Balaton Limnological Research Institute (BLRI). The apical leaves, upon arrival at the BLRI, were immediately transferred to a darkroom laboratory to enable spectral reflectance measurements to be acquired. Three replicate spectral reflectance measurements were acquired from each leaf using the methods described in Section 7.4.1.2. The exact position on each leaf from which the replicate spectral measurements were made was marked; this was subsequently used to inform the determination of the chlorophyll-a, enabling the spectral and pigment data to be accurately paired to optimise the calibration of the spectral reflectance indices. The concentration of chlorophyll-a was determined, in triplicate, from samples of leaf tissue (0.283 cm^2) removed from each position marked during the laboratory darkroom spectrometry. Chlorophyll-a was extracted from the leaf material in a tissue homogeniser for 4 h with 80% acetone (v/v) in distilled water. Glass beads were added to aid the maceration of the fibrous plant tissue. The concentration of chlorophyll-a in the extract was subsequently determined spectrophotometrically, following clarification by centrifugation (10 min at 5000 *g*), using the equations of Wellburn (1994).

The spectral reflectance data were used to derive a range of indices (see Section 7.4.1.2) previously shown to be sensitive to variations in the plant pigmentation. Pearson's Product-Moment correlation and least-squares regression analysis were then used to calibrate the spectral reflectance indices to the measured concentration of chlorophyll-a in the leaf tissues.

7.4.2.2 Norfolk Broads (UK)

In total, 55 stands of *Phragmites australis* were sampled in Hickling Broad over a 2-year period. This sampling was conducted during three intensive field campaigns in August 2004, June 2005 and August 2005. The sampling was strictly limited to littoral stands – i.e. plants rooting in the lake sediment and subject to permanent inundation – samples were not obtained from the surrounding terrestrial fenland reedswamp as it was perceived these plants would not be

exposed to the same pressures as those growing in the lake. The field sampling was conducted in a systematic manner to ensure that the resulting dataset described the full spatial variation in reedswamp performance across the lake (see Figure 7.1).

The geographical location of each stand was recorded using a handheld GPS. Initial observations on the condition of the plants were recorded and, in particular, any visual evidence of recent plant dieback (e.g. stand fragmentation, clumped habit, leaf yellowing) was catalogued. Reed dieback was often readily identifiable from the presence of relict rhizomes protruding into the open water. Prior to destructive sampling, *in-situ* spectral reflectance measurements ($R_{(\lambda)}$) of the plant canopy were acquired using a handheld ASD FieldSpec® spectroradiometer according to the methods detailed in Section 7.4.2.1. Immediately following the acquisition of the *in-situ* $R_{(\lambda)}$ measurements, 25 apical leaves were subsequently harvested from the plants and retained for further $R_{(\lambda)}$ measurements under laboratory darkroom conditions. The culms of the *Phragmites australis* plants were then harvested above the rhizome mass from a 0.5 x 0.5 m quadrat and the material was retained for subsequent biometic measurements (data not considered further here). The depth of the overlying water column to the vertical rhizome was also recorded.

Sediment samples for chemical analysis were obtained from the *Phragmites australis* stands using a large diameter lake corer. The corer was deployed from a boat and used to extract a sediment sample from the rhizosphere of the *Phragmites australis* plants. The upper 0.10 m of the sediment core was carefully removed and retained for further analysis. To examine for differences in the redox conditions between stands of *Phragmites australis* in Hickling Broad, limited measurements of the sediment redox potential (mV) were made *in-situ* during sampling in August 2005. Where possible, the redox potential was measured, in triplicate, by inserting a portable Platinum redox electrode (attached to a millivoltmeter) into the centre of the sediment cores removed for chemical analysis. The redox potential was measured against an Ag/AgCl reference electrode. No correction was applied for differences in pH. Unfortunately in many instances, it proved difficult to extract a sufficiently intact sediment core to allow the redox potential to be measured before oxidation occurred. As a result, measurements of the redox

potential were only acquired for a limited number of stands and were, therefore, not used for statistical analyses.

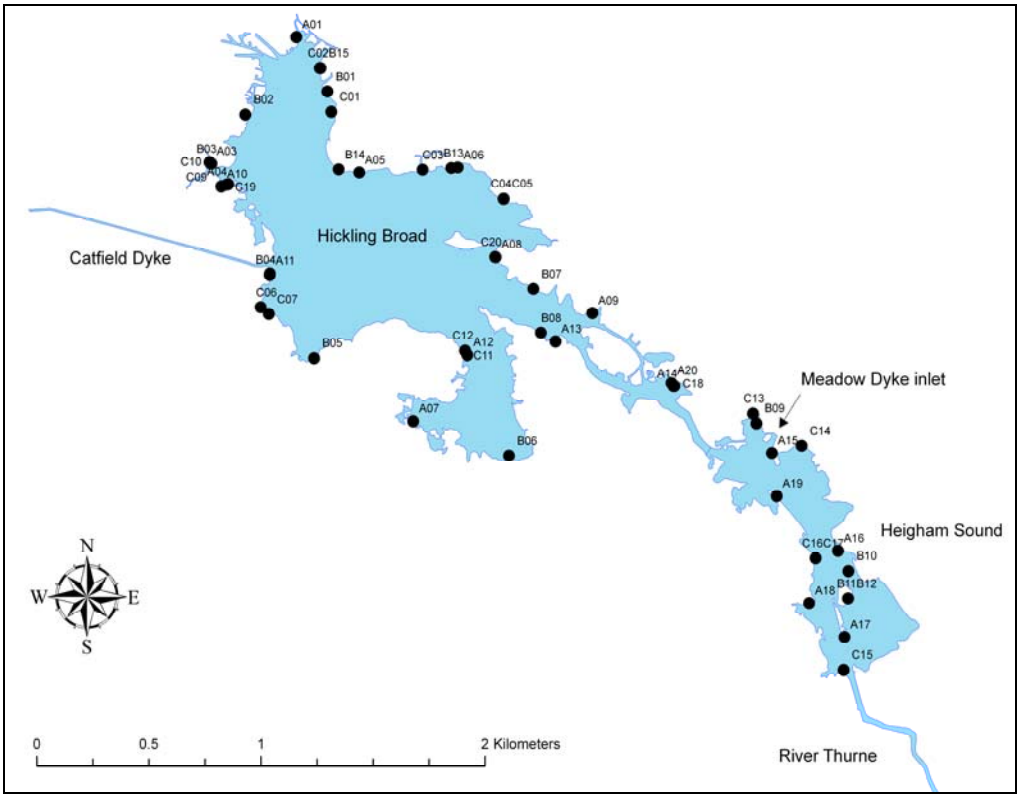

Figure 7.1 Map detailing the stands of *Phragmites australis* sampled in Hickling Broad and Heigham Sound during August 2004 (sites A01-A20), June 2005 (sites B01-B15) and August 2005 (sites C01-C20).

7.4.3 In-Situ and Laboratory Spectrometry

7.4.3.1 In-Situ Field-Based Spectrometry: Canopy-Scale

Spectral reflectance measurements of the *Phragmites australis* stands were made in the field using a handheld ASD FieldSpec® spectroradiometer. The technical specifications of the ASD FieldSpec instrument are detailed in Section 3.4.1. The spectrometer was attached to a telescopic pole which enabled the instrument to be raised and maintained at constant height of 1 m above the reedswamp canopy at nadir. Where possible, a constant geometry was maintained between the spectroradiometer and the sun. The instrument was calibrated to reflectance ($R_{(\lambda)}$) using a white Spectralon® reference panel. Reference panel calibrations and dark current measurements were performed prior to the acquisition of reflectance spectra at each sampling location. The spectral reflectance measurements were acquired as a mean of

25 replicate spectral scans from each stand; each scan itself was calculated from the mean of 10 instantaneous scans automatically averaged by the ASD FieldSpec's dedicated software. *In-situ* spectral reflectance measurements were only collected between 10.00 and 15.00 h GMT to minimise the effect of solar zenith variation (solar zenith angles ranged between 45-50°) and measurements were only made under clear skies.

7.4.3.2 Laboratory Darkroom Spectrometry: Leaf Scale

In addition to the *in-situ* (canopy-scale) spectrometry, spectral reflectance measurements were acquired in a laboratory darkroom environment from the 25 apical leaves harvested in the field from each *Phragmites australis* stand. Spectral reflectance ($R_{(\lambda)}$) measurements were made using a tripod-mounted ASD FieldSpec® spectroradiometer equipped with a 3.5° FOV (field-of-view) limiter. The instrument was calibrated to reflectance ($R_{(\lambda)}$) using a white Spectralon® reference panel. Two 300 W tripod-mounted halogen video lamps were used to provide the source of illumination; reference panel calibrations and dark current measurements were performed regularly to account for changes in the intensity of the illumination source. The spectral reflectance measurements were taken against a background composed of black cloth (< 5% $R_{(\lambda)}$ between 400 and 1000 nm) draped over all adjacent surfaces to exclude background spectral noise. Three spectral scans were acquired from each apical leaf; each of these scans was, itself, calculated as the mean of 10 instantaneous scans automatically averaged by the ASD FieldSpec's dedicated software.

7.4.3.3 Processing and Analysis of Spectral Data

The *in-situ* and laboratory darkroom spectra were interpolated to a final spectral resolution of 0.5 nm and truncated between 400-1000 nm to remove noise at the extremes of the instruments dynamic range. The spectral data was then smoothed to further reduce the influence of noise prior to analysis by passing a 5 nm running mean filter over the entire spectrum. The spectral reflectance measurements were then used to calculate a range of vegetation indices previously published in the literature and shown to be sensitive to variations in the chlorophyll-a content of plants at either the leaf- or canopy-scale. The various vegetation

indices calculated are detailed in Table 7.1. It should be noted, however, that only a selection of these indices were calculated from the Lake Balaton dataset.

Table 7.1 The various spectral reflectance and spectral derivative reflectance indices calculated from the *in-situ* and laboratory darkroom spectroradiometry (*c.f.* le Maire *et al*. (2004)).

Vegetation Index	Formula	Intended Scale	Reference
[$NDVI_{broad}$] [$NDVI_{hyper}$]	$(R_{NIR}-R_{red})/(R_{NIR}+R_{red})$ $(R_{800}-R_{680})/(R_{800}+R_{680})$	Canopy	Rouse *et al*. (1973)
[Green $NDVI_{broad}$] [Green $NDVI_{hyper}$]	$(R_{NIR}-R_{green})/(R_{NIR}+R_{green})$ $(R_{780}-R_{550})/(R_{780}+R_{550})$	Canopy	Gitelson *et al*. (1996)
[SIPI]	$(R_{800}-R_{445})/(R_{800}-R_{680})$	Leaf	Peñuelas *et al*. (1995)
[TCHVI]	$((R_{red}-R_{green})+(R_{NIR}-R_{red}))/$ $((\lvert R_{red}-R_{green}\rvert)+(\lvert R_{NIR}-R_{red}\rvert))$	Canopy	Yefremenko *et al*. (1998)
[NPQI]	$(R_{415}-R_{435})/(R_{415}-R_{435})$	Leaf	Barnes *et al*. (1992)
[DVI]	$R_{800}-R_{680}$	Canopy	Jordan (1969)
[SRPI]	$R_{430}-R_{680}$	Leaf	Peñuelas *et al*. (1994)
[NPCI]	$(R_{680}-R_{430})/(R_{680}+R_{430})$		
[PSSRb]	$R_{800}-R_{635}$	Leaf	Blackburn (1998)
[PSNDb]	$(R_{800}-R_{635})/(R_{800}-R_{635})$		
[$R_{shoulder}$]	mean $R_{(750-850)}$	Canopy	Strachan *et al*., (2002)
[PRI]	$(R_{531}-R_{570})/(R_{531}+R_{571})$	Leaf	Gamon *et al*. (1992)
[C420]	R_{420}/R_{695}	Leaf	Carter (1994)
[NDI]	$R_{800}-R_{680}$	Canopy	Jordan (1969)
[SR]	R_{NIR}/R_{red}	Leaf	Birth & McVey (1968)
[SR_{hyper}]	R_{800}/R_{680}		
[$R_{800}-R_{550}$]		Leaf	Buschmann & Nagel (Buschmann & Nagel, 1993)
[R_{800}/R_{550}]			
[R_{695}/R_{760}] [R_{605}/R_{760}] [R_{710}/R_{760}] [R_{695}/R_{670}] [R_{550}]		Leaf	Carter (1994)
[R_{675}/R_{700}] [$R_{675}/(R_{700}xR_{650})$]		Leaf	Chappelle *et al*. (1992)
[$R_{672}/(R_{550}xR_{708})$] [$R_{672}/R_{550}$] [$R_{860}/(R_{550}xR_{708})$]		Leaf	Datt (1998)
[R_{750}/R_{550}] [R_{750}/R_{700}] [R_{725}/R_{675}]		Leaf	Gitelson & Merzlyak (1994)
[$(R_{850}-R_{710})/(R_{850}-R_{680})$]		Leaf	Datt (1999)
[$(R_{780}-R_{710})/(R_{780}-R_{680})$]		Leaf	Maccioni *et al*. (2001)
[$(R_{700}-R_{670})$]		Leaf	McMurtrey *et al*. (1994)
[Red Edge]	Value of dR at red edge inflection point	Canopy	Miller *et al*. (1990)
[Red $Edge_{\lambda}$]	Wavelength of dR red edge inflection point		
[Green Edge]	Value of dR at green edge inflection point		Based on Peñuelas *et al*. (1994)
[Green $Edge_{\lambda}$]	Wavelength of dR green edge inflection point		Index developed in this thesis

7.4.4 Airborne Remote Sensing

Airborne remote sensing imagery (CASI-2) of the *Phragmites australis* reedswamp vegetation in the Upper Thurne region of the Norfolk Broads (including Hickling Broad and Heigham

Sound) was acquired by the NERC ARSF at 13:00 h GMT on 22 June 2005 and 29 August 2005. Further details of the NERC ARSF data acquisition campaigns in the Norfolk Broads are provided in Section 5.3.2. The CASI-2 instrument was operated using the default [Vegetation] bandset configuration which is designed to optimise the CASI-2 instrument for vegetation-based applications (see Table 6.1). The CASI-2 [Vegetation] data was geo-corrected, geo-registered and atmospherically corrected (to absolute radiance [w sr^{-1} m^{-2}] ($L_{(\lambda)}$) according to the methods outlined in Section 5.3.4.

The CASI-2 [Vegetation] imagery was initially processed using a Support Vector Machine (SVM) non-linear radial basis function learning algorithm in order to classify the extent of *Phragmites australis* reedswamp in Hickling Broad (see Section 6.4.4). The stands sampled in the field were identified in the image and used to create training data for the SVM algorithm. The conservative specification of a 0.95 probability threshold in SVM algorithm ensured that non-reedswamp areas were excluded from the classification. The subsequent image analysis procedures were only applied to the areas classified as reedswamp.

The results obtained from the laboratory darkroom and *in-situ* field-based spectrometry were used to inform the selection of candidate spectral indices (i.e. those shown to be optimally sensitive to variations in the physiological status of *Phragmites australis*) for application to the CASI-2 [Vegetation] imagery. The candidate spectral indices chosen also had to be harmonious to the [Vegetation] bandset configuration of the CASI-2 instrument. The CASI-2 [Vegetation] imagery was subsequently transformed using the formulations of the selected indices. The locations of the *Phragmites australis* stands sampled in the field were identified in the transformed CASI-2 [Vegetation] imagery and the spectral index information was extracted and used in the statistical analysis.

7.4.5 Sediment Chemistry

7.4.5.1 Organic Matter Content

The organic matter content (%) of the sediment samples obtained from the *Phragmites australis* stands in the Norfolk Broads was determined on an air-dried 3 g sediment sub-sample by the loss-on-ignition incurred following combustion at 500°C for 24 h in a muffle furnace.

7.4.5.2 Nitrogen and Phosphorus

The total-acid-extractable concentration of N and P in the sediment samples was determined following extraction using an adaptation of the sulphuric acid-hydrogen peroxide digestion procedure of Allen (1989). The sediment samples were prepared for digestion by air-drying for 7 d, grinding for 5 min in a steel Gy-ro mill and sieving < 2 mm. Subsequently, 200 mg of the < 2 mm sediment fraction was weighed into glass digestion tubes and 4.4 ml of the sulphuric acid-hydrogen peroxide reagent was added. The samples were kept on ice for 24 h to control foaming. The samples were then digested at 330°C in an aluminium heating block for 2.5 h.

The digested extract was clarified by filtration through a Whatman GF No. 540 filter paper (pre-washed with 0.5 M HNO_3). The concentration of total-extractable-N (TN) in the digest extracts was determined colourimetrically as ammonium (NH_4^+) against analytical standards using the Phenolhypochlorite method of Solórzan (1969).

The concentration of total-extractable-P (TP) in the digest extracts was determined colourimetrically as orthophosphate (PO_4^-) against analytical standards using the ammonium molybdate reduction method of Murphy & Riley (1962).

7.4.5.3 Total-Extractable Metals.

The total-aqua-regia-extractable concentrations of several metallic macronutrients (K, Ca, Na, Fe) in the sediment samples was determined following extraction using the Aqua Regia digestion method (e.g. Sastre *et al.,* 2002). The sediment samples were prepared for digestion by air-drying for 7 d, grinding for 5 min in a steel Gy-ro mill and sieving < 2 mm. Subsequently, 3 g of the < 2 mm sediment fraction was weighed into glass digestion tubes; 3.5 ml HNO_2 (65%)

and 10 ml HCl (30%) was added to the samples and they were kept on ice for 24 h to control foaming.

The samples were then digested at 140°C in an aluminium heating block for 2 h. The extract was clarified by filtration through a Whatman GF No. 540 filter paper (pre-washed with 0.5 M HNO_3). The total-extractable concentrations of Ca, Fe, K, Na, and Mg were determined against analytical standards using flame of acetylene atomic absorption spectrometry (AAS).

7.4.6 Statistical Analysis

The relationships between the indices formulated from the darkroom laboratory spectral reflectance measurements performed on the Lake Balaton apical leaves and the measured concentration of foliar chlorophyll-a was explored using correlation and regression analysis. Datasets were checked for normality in Minitab v.14 using the Anderson-Darling method (95% confidence level). Pearson's Product-Moment and Spearman Rank correlation analysis was, where appropriate, then used to assess the relationship between the spectral indices and the measured concentration of chlorophyll-a in the plant leaves. Where statistically significant correlations were observed, least-squares regression analysis was used to calibrate the spectral indices to the foliar chlorophyll-a concentration.

The spectral index that demonstrated the optimum relationship with the measured concentration of chlorophyll-a in the leaves of *Phragmites australis* from Lake Balaton was subsequently calculated, along with all the remaining indices detailed in Table 7.1, from the laboratory darkroom spectral reflectance measurements made from *Phragmites australis* leaves obtained from Hickling Broad. The algorithm for the optimum index was then used to calibrate the Hickling Broad darkroom spectrometry measurements, thus providing predicted values for the chlorophyll-a concentration; the estimated chlorophyll-a concentrations predicted by the optimum regression model were then used to assess the sensitivity of the remaining spectral indices (i.e. those not calculated from the Lake Balaton apical leaf spectra) to apical leaf chlorophyll-a.

These statistical analyses were used to confirm the sensitivity of the various spectral indices to changes in the physiological status of *Phragmites australis* plants. Once this sensitivity had been established, the full suite of spectral indices obtained from the *in-situ* and darkroom spectrometry, and the CASI-2 [SeaWiFS] imagery, were correlated against the sediment chemistry data. Where significant associations were found (at the 95% confidence level), least-squares regression analysis was used to derive quantitative relationships between the spectral response of the plants (i.e. physiological status) and sediment nutrient status.

The data were also partitioned into two further subsets, (i) samples from "non-dieback" stands and, (ii) samples from "dieback" stands (i.e. recent visible evidence of dieback), based upon the observations made during lake sampling. The non-parametric Mann Whitney test was subsequently used, in this case because of the limited number of observations for the "dieback" class (n = 11), to test for statistically significant differences in sediment chemistry and plant performance between healthy and dieback sites (at the 95 % confidence level). The resulting data were used to develop an understanding of the potential mechanism(s) of *Phragmites australis* dieback in the Norfolk Broads.

7.5 RESULTS AND DISCUSSION

7.5.1 Relations between Reflectance Spectra and Leaf Pigmentation

The spectral characteristics of *Phragmites australis* apical leaves in varying physiological states are depicted in Figure 7.2 (for clarity only a selection of the spectral reflectance measurements are shown). The spectral signature of *Phragmites australis* (at the leaf-scale) is typical of that often observed from vegetation. The spectra obtained from healthy *Phragmites australis* leaves demonstrate low spectral reflectance in the blue region (400-520 nm) due to strong absorption by chlorophyll and carotenoid pigments (xanthophylls and carotenes). The apical leaf spectra also exhibit a characteristic local reflectance maximum in the green region ("green peak") (*c*. 530-610 nm) due to decreased pigment absorption and the dissipation of light from the xanthophyll cycle. Spectral reflectance then decreases in the region immediately following the green peak, largely due to increasing absorption by chlorophyll pigments (chlorophyll-a and chlorophyll-b), culminating in a pronounced reflectance minimum at *c*. 680 nm caused by the

absorption maximum of chlorophyll-a. Spectral reflectance can then be observed to increase rapidly in the VNIR forming the characteristic red edge shoulder (*c.* 680-730 nm) and VNIR plateaux (> 730 nm) features.

It is notable that the spectral response from the apical leaves showed marked changes due, at least in part, to the variations in the measured concentration of chlorophyll-a. The most notable systematic change observed (for apical leaves with chlorophyll-a concentrations > 20 μg cm^{-2}) in response to increased plant vigour (i.e. higher concentrations of chlorophyll-a) was decreased spectral reflectance in the vicinity of the "green peak". This decrease in spectral reflectance probably reflects the effect of increased pigment absorption.

In comparison, the spectral response from heavily stressed leaves, i.e. those with chlorophyll-a concentrations < 20 μg cm^{-2}, demonstrated a significant increase in reflectance across the entire spectrum. This is likely to reflect the effect of decreased pigment absorption. Indeed, similar spectral responses to stress were observed by Davids & Tyler (2003) in the spectra of Silver Birch leaves exposed to radionuclide contamination. It is further evident that, for the heavily stressed leaves (chlorophyll-a concentrations < 20 μg cm^{-2}), the shape of the spectral signature also changes markedly and, in particular, the "green peak" and the reflectance minimum located at *c*. 690 nm (associated with chlorophyll-a absorption) are visibly less pronounced than in the equivalent features in the spectra of more healthy leaves (chlorophyll-a concentrations > 20 μg cm^{-2}).

Variation in apical leaf vigour also precipitated systematic change in the spectral response in the vicinity of the red edge (the transition from low to high spectral reflectance in the *c*. 690-720 nm region); it is notable that the position of the red edge shifts in the reflectance spectra to progressively longer wavelengths with increasing chlorophyll-a concentration. The pronounced variation in VNIR spectral reflectance appears to be unrelated to change in the concentration of chlorophyll-a. Spectral reflectance in the VNIR is not strongly influenced by leaf pigmentation; rather, it is dominated by backscattering processes associated with the cellular structure of the leaf tissue. It may be that the observed variation in the VNIR, particular in the spectra acquired

from stressed leaves, reflects the breakdown in the integrity of the palisade cells contained with the spongy mesophyll tissue in response to stress..

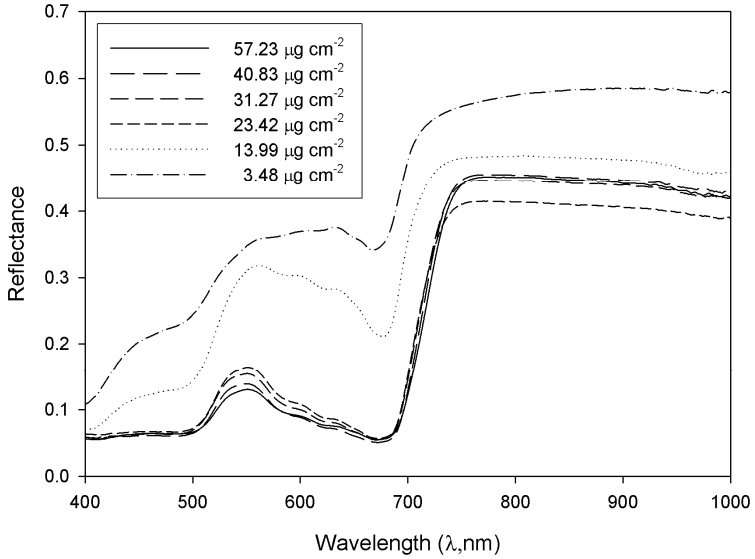

Figure 7.2 The effect of changes in the concentration of chlorophyll-a (3.48-57.23 µg cm^{-2}) on the spectral reflectance characteristics of *Phragmites australis* apical leaves obtained from Lake Balaton, Hungary.

The least-squares regression relationship between the measured concentration of chlorophyll-a in the *Phragmites australis* leaves obtained from Lake Balaton, and the spectral indices ([TCHVI], [Green $NDVI_{hyper}$], [R_{750}/R_{550}] and the [Red $Edge_{\lambda}$]) obtained from the darkroom spectrometry measurements is depicted in Figure 7.3. The spectral indices derived from the reflectance measurements typically demonstrated strong relationships with the measured concentration of chlorophyll-a in the apical leaves of the *Phragmites australis* plants from Lake Balaton. The [Red $Edge_{\lambda}$] demonstrated the strongest relationship with the measured concentration of chlorophyll-a, returning a coefficient of determination of R^2 = 0.95. Strong regression relationships were also derived with the band-ratio [R_{750}/R_{550}] and the [Green $NDVI_{hyper}$] (R^2 = 0.91 and 0.83 respectively). In the case of the [TCHVI], the regression model was only valid for chlorophyll-a concentrations > 20 µg cm^{-2}; the lack of a valid fit for concentrations < 20 µg cm^{-2} suggests that the formulation of the [TCHVI] was not suitable for quantifying pigment concentrations in highly stressed leaves. Increased scatter in the regression relationship between [Green $NDVI_{hyper}$] and [R_{750}/R_{550}] and the measured

concentration of chlorophyll-a was also observed for measurements from leaves with chlorophyll-a concentrations < 20 μg cm^{-2}.

These results suggest that the chlorophyll [Red $Edge_{\lambda}$] provides a highly sensitive index of plant physiological status as a function of variation in pigment content. This observation is substantiated in several foregoing studies which have also found that the [Red $Edge_{\lambda}$] is a sensitive predictor of chlorophyll-a (and, importantly, is also relatively insensitive to non-pigment-related effects) (Blackburn, 2002; Le Maire *et al.,* 2004; Smith *et al.,* 2005).

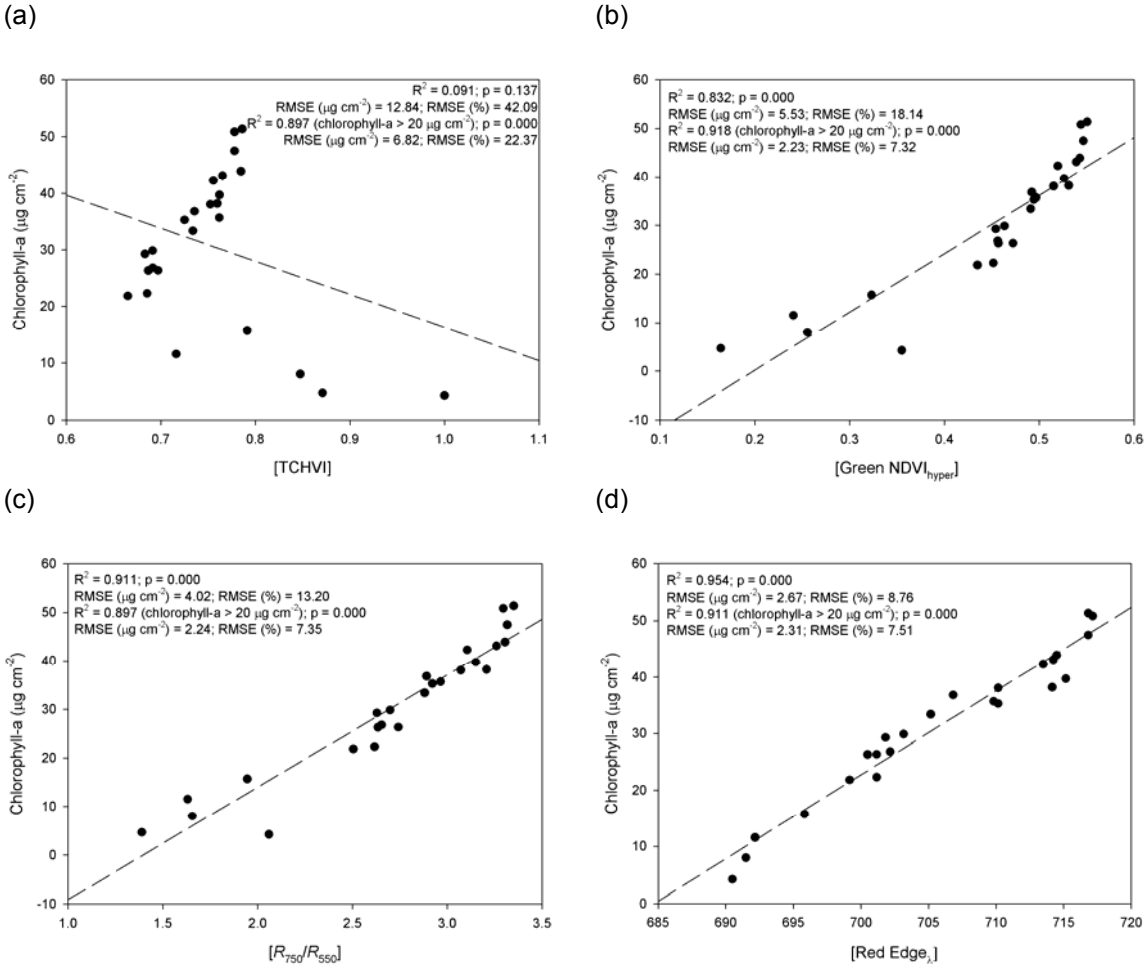

Figure 7.3 The relationship between (a) [TCHVI], (b) [Green $NDVI_{hyper}$], (c) [R_{750}/R_{550}] and (d) [Red $Edge_{\lambda}$] derived from laboratory darkroom spectrometry and the measured concentration of chlorophyll-a in the apical leaves of *Phragmites australis* in Lake Balaton, Hungary.

The regression model derived to equate the [Red $Edge_{\lambda}$] index to the measured concentration of chlorophyll-a was subsequently used to calibrate the [Red $Edge_{\lambda}$] measurements made from

the *Phragmites australis* apical leaves obtained from Hickling Broad (N.B. this was necessary because chlorophyll-a was not measured in the apical leaves collected from Hickling Broad). This provided predicted values for the chlorophyll-a concentration for the Hickling Broad apical leaves; these values were then used to assess the sensitivity of the remaining spectral indices to apical leaf chlorophyll-a (i.e. those indices not calculated from the Lake Balaton spectral reflectance measurements). The derived correlation coefficients between the entire suite of spectral indices and the [Red Edge$_\lambda$]-predicted apical leaf chlorophyll-a concentration is shown in Table 7.2.

Table 7.2 Correlation coefficients (*r*) for the relationship between the estimated concentration of chlorophyll-a (µg cm^{-2}) (Chl-a) in the apical leaves of *Phragmites australis* from Hickling Broad (predicted from the Lake Balaton [Red Edge$_\lambda$] algorithm) and the remaining spectral indices derived from the laboratory darkroom spectrometry (*n* = 55). Statistically significant correlations at the 95% confidence level are highlighted.

	[$NDVI_{broad}$]	[$NDVI_{hyper}$]	[Green $NDVI_{broad}$]	[Green $NDVI_{hyper}$]	[PRI]	[SIPI]	[TCHVI]	[NPQI]	[DVI]	[SRPI]	[NPCI]
Chl-a	0.546	0.344	0.870	0.897	-0.133	0.158	0.855	-0.154	-0.011	0.150	-0.166
	[PSSRb]	**[PSNDb]**	**[$R_{shoulder}$]**	**[C420]**	**[NDI]**	**[SR]**	**[SR_{hyper}]**	**[R_{550}/R_{800}]**	**]R_{750}/R_{550}]**	**[R_{725}/R_{675}]**	**[R_{800}-R_{550}]**
	0.614	0.631	-0.116	0.218	0.848	0.542	0.357	-0.897	0.872	-0.056	0.498
	[R_{800}/R_{550}]	**[R_{695}/R_{420}]**	**[R_{695}/R_{760}]**	**[R_{605}/R_{670}]**	**[R_{710}/R_{760}]**	**[R_{695}/R_{670}]**	**[R_{675}/R_{700}]**	**[$R_{675}/(R_{700}XR_{650})$]**	**[$R_{672}/(R_{550}XR_{708})$]**	**[R_{675}/R_{550}]**	**[$R_{660}/(R_{550}XR_{708})$]**
	0.873	-0.326	-0.652	-0.716	-0.891	-0.678	0.749	0.779	0.761	0.471	0.865
	[$(R_{850}$-$R_{710})$ $/(R_{850}$-$R_{680})$]	**[R_{750}/R_{700}]**	**[$(R_{542}$-$R_{MINRED})$ $/(R_{750}$-$R_{MINRED})$]**	**[$(R_{780}$-$R_{710})$ $/(R_{780}$-$R_{680})$]**	**[R_{700}/R_{670}]**	**[Red Edge]**	**[Green Edge]**	**[Red Edge$_\lambda$]**	**[Green Edge$_\lambda$]**	**[EGFR]**	**[EGFN]**
	0.940	0775	-0.829	0.937	-0.649	-0.195	-0.354	1.000	-0.049	0.219	0.394

The vast majority of the 44 spectral reflectance indices derived from the Hickling Broad laboratory darkroom spectrometry showed statistically significant correlations with the [Red $Edge_{\lambda}$]-predicted chlorophyll-a concentration; only 12 of the derived indices were not significantly correlated at the 95% confidence level. The correlation coefficients ranged between r = -0.897 to 0.940 with the strongest correlations occurring with the narrow band normalised difference indices $[(R_{850}-R_{710})/(R_{850}-R_{680})]$ and $[(R_{780}-R_{710})/(R_{780}-R_{680})]$; the formulation of each index dictated whether the observed relationship with the Red $Edge_{\lambda}$-predicted chlorophyll-a concentration was positive or negative. In general, the narrow band-ratios (e.g. $[(R_{850}-R_{710})/(R_{850}-R_{680})]$) appeared to be better predictors of variation in apical leaf pigment content than the broad band-ratios (e.g. $[NDVI_{broad}]$).

These strong correlations provide clear evidence that many of the spectral reflectance indices examined retain sensitivity to changes in the physiological status of *Phragmites australis* leaves. These indices were therefore assumed to be a quantitative metric of plant physiological status and were subsequently used explore the relation between the performance of *Phragmites australis* plants in Hickling Broad and sediment nutrient enrichment. Those indices that did not demonstrate a significant correlation were, however, not discarded from further analysis as it was perceived that they might be sensitivite to changes in physiological status that are not necessarily manifest in the pigmentation of the plant leaves (e.g. canopy architecture).

7.5.2 Sediment Chemistry

The mineral nutrient content of the sediment samples obtained from stands of *Phragmites australis* in Hickling Broad is detailed in Table 7.3. The mineralogy of the bottom sediments of Hickling Broad varied markedly between deposits of calcareous marl and dark-coloured amorphous muds. The marl sediment is characteristic of the Norfolk Broads, being derived from the precipitation of calcium ions from the strongly alkaline groundwater (the precipitation of calcium ions is these lakes is facilitated by *Chara* spp. vegetation) (Moss, 2001). Marl-dominated clays and slits were the predominant sediment underlying stands of *Phragmites australis* sampled along the north eastern shore of Hickling Broad. This sediment was typically

low in organic matter (<10%) (compared to the deposits of fine mud) and relatively cohesive. In contrast, the stands of *Phragmites australis* sampled along the south western shore of Hickling Broad, and those in Heigham Sound, were often rooting in deep deposits of the dark-coloured and unconsolidated mud. This mud typically had very high organic matter content (*c*. 20-65%). Moss (2001) dates the earliest appearance of this organic rich mud in sediment profiles obtained from the Norfolk Broads to *c*. 1840 and suggests its formation is strongly linked with the progressive eutrophication of the Broads. The accumulation of deep mud in Hickling Broad was also noted by Boorman & Fuller (1981) during their survey of the reedswamp in the late 1970s to early 1980s.

Table 7.3 The mean (± 2 standard errors) and range of sediment nutrient and metal concentrations, organic matter content, and water depth, measured in Hickling Broad (values in mg kg^{-1} dry weight sediment, unless otherwise stated).

n	**TN**	**TP**	**K**	**Fe**
54	982.6 (±163.4)	384.8 (±67.4)	3828 (±680)	55280 (±13000)
	(184.0-2403.0)	(43.8-948.6)	(873-9700)	(8940-208600)
Ca	**Na**	**Mg**	**Organic Matter (%)**	**Water Depth (m)**
29825 (±6392)	3844 (±756)	2358 (±522)	22.35 (±5.06)	0.61 (±0.10)
(458-81231)	(828-22627)	(19.2-3095.3)	(0.8-65.5)	(0-1.40)

The organic nature of the mud found within Hickling Broad would suggest that that it is mainly derived from the accretion of detritus within the *Phragmites australis* stands. This detritus may, in part, be derived from the decay of the *Phragmites australis* plants themselves. However, the formation of this mud is likely to have been substantially facilitated by the decay of algal blooms that have been a persistent occurrence in the lake since it became eutrophic. The growth and decay of epiphytic filamentous algae (often associated with the basal stems of plants) may be a further source of organic matter supplying *Phragmites australis* stands. Spatial variability in the organic matter content of the sediment sampled in Hickling Broad is shown in Figure 7.4.

The pronounced spatial variation observed in the occurrence of the organic mud (and, also, the depth of the deposit) would seem to indicate that organic matter is subject to pronounced

remobilisation and redistribution within the lake system. The continual resuspension of bottom sediments is a characteristic feature of shallow lakes, especially those, like Hickling Broad, that are relatively wind-exposed. In these shallow waters, sediment focusing processes can create substantial spatial heterogeneity in the deposition of the suspended sediment within the lake system (Scheffer, 1998). Sediment focusing processes often led to the progressive accretion of material in areas of deep and/or stagnant water. It is notable that deposits of organic mud were largely absent from stands located along the north eastern shore line of Hickling Broad. It would seem that suspended organic material is readily resuspended in these regions and moved through the system in a south easterly direction. This would account for the substantial accretions of organic matter observed in Heigham Sound; this region of the lake also receives a flux of sediment from the inlet of Meadow Dyke that supplies water from Horsey Mere to the north east. The pronounced accretion of mud would also seem to occur in the more sheltered and stagnant waters along the south eastern shoreline. These stagnant waters are created by the complex near-shore morphometry of the lake.

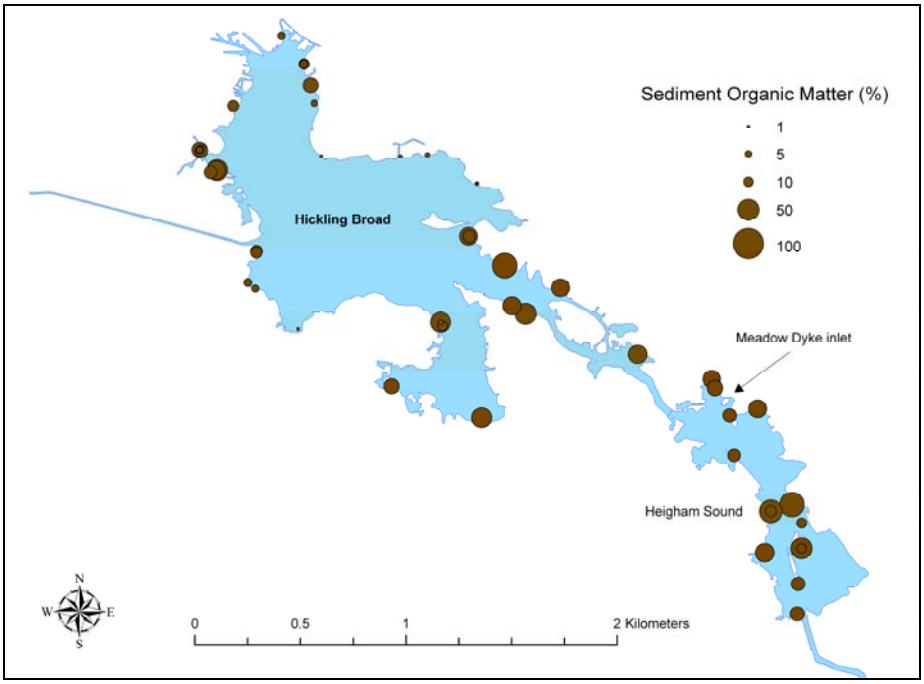

Figure 7.4 Spatial variability in the organic matter content (%) of the bottom sediment of Hickling Broad underlying the stands of *Phragmites australis* sampled during 2004 and 2005.

The influence of near-shore morphometry on sediment focussing processes is well documented (e.g. Blais & Kalff, 1995) and in Hickling Broad shore morphometry would seem to be a key

factor in regulating the sedimentation of particulate organic matter. Moreover, in these calm water zones, the sedimentation of organic matter is likely to be further enhanced by impedance of flow caused by the presence of reedswamp vegetation. Thus, the *Phragmites australis* stands in these regions may essentially function as foci for organic matter accretion.

The accretion of organic matter would also seem to influence the nutrient content of the sediment in the *Phragmites australis* stands. TP concentrations ranged between 43.8 and 948.6 mg kg^{-1} (mean = 348.8 mg kg^{-1}) and were typically higher in stands rooting in the organic mud. The mean TP concentration measured here is somewhat lower than the 2.92 mg g^{-1} (2920 mg kg^{-1}) and 1.38 mg g^{-1} (1380 mg kg^{-1}) TP previously measured by the Environment Agency in 1999 and 2000 respectively (Environment Agency, unpublished data) (although these TP concentrations are substantially higher that those measured in several other Broads by Pitt *et al*. (1997)). This difference may suggest a net loss of TP from the system since 1999 – perhaps due to decreased loading and subsequent equilibrium release and flushing loss. The differences may also reflect the fact that TP concentration of the lake sediment in this study was measured during mid-to-late summer when the sediment TP is often at its lowest in shallow lakes (Spears *et al.,* 2006) (the Environment Agency TP measurements were performed in December and September respectively). The sediment TP concentration is recognised to be highly dependent on the extent of plant colonisation; Rooney *et al*. (2003), for example, showed that plant colonisation can result in a ~70% loss of TP from littoral lake sediments compared to uncolonised profundal sediments. This also may account for the observed variation.

The organic matter content of the sediment was significantly positively correlated with the concentration of TP (r = 0.405; p = 0.004), Fe (r = 0.392; p = 0.005), Na (r = 0.782; p = 0.000) and Mg (r = 0.673; p = 0.000) (n = 54) which suggests, not unsurprisingly, that stands with higher organic matter content were more nutrient enriched than the stands rooting in the more inorganic marl-dominated sediments. TN in the sediment was not significantly correlated with organic matter content (r = 0.239; p = 0.098) (n = 54), but as N is highly labile in lake sediments and is not readily chelated by metal ions, the absence of a correlation here is not unexpected. Spatial variability in the concentration of TP, TN and K in Hickling Broad is shown in Figure 7.5.

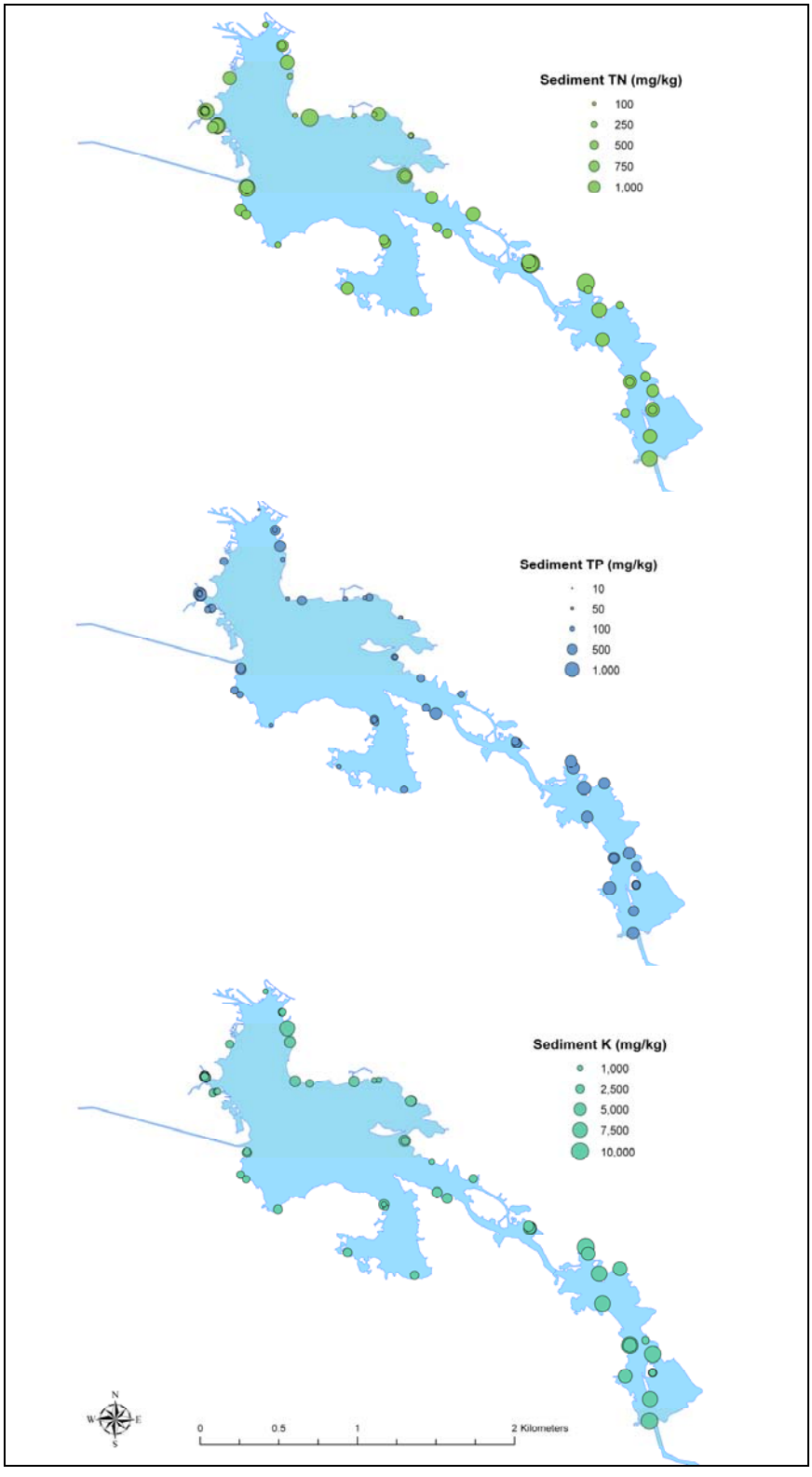

Figure 7.5 Spatial variability in the concentrations of TN, TP and K measured in the sediment of Hickling Broad underlying the stands of *Phragmites australis* sampled during 2004 and 2005.

The measured concentration of TP in the sediment of Hickling Broad was highest in a sheltered bay adjacent to Deep-Go Dyke that connects Hickling Broad in the north to Heigham Sound in the south. High TP concentrations were also measured throughout Heigham Sound (TP > 500 mg kg^{-1}). The lowest concentrations of TP were measured in the marl sediments along the north western shore (typically < 100 mg kg^{-}). Concentrations of TN were also somewhat spatially variable in the sediment, with high concentrations measured in samples obtained from the north eastern shore in the vicinity of Catfield dyke and near to the Meadow Dyke. These latter high concentrations probably reflect inputs of nitrate rich water received through the Meadow Dyke (via Horsey Mere) from the Waxham New Cut which drains agricultural land. The TN concentrations in the sediment did not however demonstrate the pronounced north-south gradient observed in TP. The high concentrations of K observed in the sediments of Heigham Sound probably reflects the effect of saltwater percolation into this region, either from localised upwelling of saline ground water or, probably more likely, the input of brackish water from Horsey Mere (which itself receives saline water from Waxham New Cut Dyke) via Meadow Dyke.

The discernible dark colouration of the mud in Hickling Broad suggests that this organic-rich sediment was highly anoxic. Sediment hypoxia is common in highly organic lake sediments because the supply of detritus fosters intense microbial decomposition which, in turn, increases the biological oxygen demand, leading to a pronounced oxygen deficit. The dark colouration is derived from the reduction of sulphate (SO_4^{2-}) in the sediment and its subsequent reaction with reduced iron (Fe(II)) to produce a black precipitate of ferrous sulphide (FeS). The limited measurements of the sediment redox potential made during lake sampling in August 2005 verified that the organic mud was typically more anoxic (-61 to -168 mV) compared to the more marl dominated sediment (-29 to -79 mV). Similarly, Crook *et al*. (Crook *et al*., 1983) found that redox potential of sediments in Hickling Broad varied considerably from relatively oxic conditions (+40 mV), to conditions of severe sediment hypoxia to (-250 mV).

7.5.3 Plant Physiological Status and Sediment Nutrition

The correlations between the spectral reflectance indices derived from the laboratory darkroom and *in-situ* field-based spectrometry (here assumed to be variously indicative of the physiological status of *Phragmites australis* plants) and the measured sediment chemistry parameters are detailed in Tables 7.4-7.10 for the respective sampling occasions. Many of the spectral indices derived from both the laboratory darkroom (and to a lesser extent, the *in-situ* field-based spectrometry) exhibited strong and significant correlations with the measures of sediment chemistry. The spectral indices derived from the laboratory darkroom spectrometry frequently demonstrated significant correlations with sediment TP, Na, Mg and organic matter. Significant correlations were also observed between several of the spectral indices and the measured concentration of Fe and TN; while only a few of the spectral indices demonstrated significant correlations with the concentration of Ca and water depth. The spectral indices derived from the *in-situ* field-based spectrometry, in contrast, consistently demonstrated significant correlations with the concentration of Ca; it is suggested that this may reflect the fact that sediment mineralogy had a direct effect on spectral reflectance measured in the field. The *in-situ* field-based spectral indices also consistently demonstrated significant correlations with organic matter and, in addition, some limited correlations with TP, Na and Mg were also observed. Water depth was also significantly correlated with several of the spectral indices from the *in-situ* field-based spectrometry when the three independent datasets were combined.

The strongest and greatest numbers of significant correlations were observed with the spectral data acquired from the measurements made during August 2004 and August 2005, with fewer and less strongly significant correlations being observed from the June 2005 dataset. This would seem to suggest the strongest association between plant physiological status and sediment chemistry occurs towards the end of the growing season prior to the onset of senescence. Correlations were also strongest when the datasets derived from the various sampling occasions were examined individually, rather than combined; this would also seem to suggest that the relationship between the physiological status of the plants and sediment chemistry is temporally dependent.

Table 7.4 Correlation coefficients (*r*) between the derived spectral reflectance indices from the laboratory darkroom spectrometry and the sediment chemistry parameters from stands of *Phragmites australis* sampled in Hickling Broad during August 2004.

	[$NDVI_{broad}$]	[$NDVI_{hyper}$]	[Green $NDVI_{broad}$]	[Green $NDVI_{hyper}$]	[PRI]	[SIPI]	[TCHVI]	[NPQI]	[DVI]	[SRPI]	[NPCI]	[PSSRb]	[PSNDb]	[$R_{shoulder}$]	[C420]	[NDI]	[SR]	[SR_{hyper}]	[R_{550}/R_{800}]	[R_{750}/R_{550}]	[R_{725}/R_{675}]	[R_{800}-R_{550}]
TN	0.123	0.100	0.039	0.011	-0.257	-0.171	-0.056	-0.028	0.013	0.346	-0.358	0.064	0.131	-0.014	0.256	0.161	0.068	0.049	-0.013	-0.013	0.044	-0.004
TP	0.178	-0.019	0.496	0.525	-0.178	-0.175	0.592	-0.530	-0.395	0.209	-0.219	0.293	0.258	-0.465	0.062	0.362	0.213	-0.027	-0.533	0.518	-0.222	-0.053
K	0.225	0.136	0.339	0.357	-0.126	-0.068	0.289	-0.399	-0.314	0.415	-0.423	0.214	0.253	-0.415	0.115	0.298	0.185	0.075	-0.359	0.343	-0.032	-0.124
Fe	0.264	0.114	0.413	0.417	-0.341	-0.125	0.367	-0.425	-0.057	0.336	-0.341	0.321	0.315	-0.110	0.084	0.386	0.267	0.078	-0.416	0.425	-0.049	0.175
Ca	-0.030	-0.098	0.126	0.161	-0.101	-0.398	0.241	-0.239	-0.353	0.517	-0.515	-0.037	0.031	-0.383	0.444	0.195	-0.091	-0.160	-0.177	0.096	-0.297	-0.207
Na	0.026	-0.108	0.267	0.293	0.031	-0.246	0.395	-0.384	-0.285	0.179	-0.182	0.088	0.085	-0.308	0.065	0.146	0.024	-0.140	-0.308	0.267	-0.258	-0.062
Mg	0.118	-0.049	0.390	0.422	-0.176	-0.304	0.488	-0.570	-0.374	0.344	-0.351	0.164	0.181	-0.433	0.054	0.295	0.099	-0.105	-0.438	0.391	-0.266	-0.087
Org. Matter	-0.118	-0.243	0.140	0.168	0.002	-0.345	0.334	-0.213	-0.144	0.133	-0.137	-0.051	-0.047	-0.106	0.115	0.050	-0.140	-0.297	-0.187	0.139	-0.364	0.011
Water Depth	0.020	-0.036	0.118	0.144	-0.293	-0.418	0.105	-0.328	-0.062	0.551	-0.542	0.038	0.059	-0.068	0.276	0.278	-0.010	-0.098	-0.137	0.151	-0.215	0.035

	[R_{800}/R_{550}]	[R_{698}/R_{420}]	[R_{698}/R_{760}]	[R_{608}/R_{670}]	[R_{710}/R_{760}]	[R_{698}/R_{670}]	[R_{678}/R_{700}]	[$R_{678}/(R_{700}XR_{860})$]	[$R_{672}/(R_{550}XR_{708})$]	[R_{678}/R_{550}]	[$R_{860}/(R_{550}XR_{708})$]	[$(R_{850}$-$R_{710})$ $/(R_{850}$-$R_{680})$]	[R_{750}/R_{700}]	[$(R_{542}$-$R_{MINRED})$ $/(R_{750}$-$R_{MINRED})$]	[$(R_{780}$-$R_{710})$ $/(R_{780}$-$R_{680})$]	[R_{700}/R_{670}]	[Red Edge]	[Green Edge]	[Red $Edge_N$]	[Green $Edge_N$]	[EGFR]	[EGFN]
TN	-0.037	-0.359	-0.174	-0.005	-0.158	-0.100	0.046	0.078	-0.038	-0.122	-0.010	0.108	0.110	0.059	0.143	-0.065	-0.026	-0.062	0.275	0.147	0.011	0.045
TP	0.537	-0.171	-0.212	-0.645	-0.382	-0.536	0.527	0.653	0.629	0.416	0.606	0.486	0.343	-0.571	0.453	-0.510	-0.413	-0.473	0.375	-0.211	-0.195	0.169
K	0.333	-0.203	-0.235	-0.259	-0.304	-0.129	0.220	0.449	0.337	0.116	0.384	0.295	0.244	-0.274	0.302	-0.173	-0.355	-0.340	0.399	0.107	-0.216	0.086
Fe	0.410	-0.172	-0.285	-0.411	-0.384	-0.304	0.341	0.485	0.333	0.161	0.404	0.390	0.361	-0.346	0.395	-0.300	-0.113	-0.234	0.423	-0.084	0.023	0.176
Ca	0.120	-0.519	-0.107	-0.296	-0.235	-0.494	0.451	0.271	0.377	0.273	0.222	0.331	0.105	-0.222	0.321	-0.474	-0.462	-0.505	0.370	0.030	-0.236	0.171
Na	0.292	-0.131	-0.053	-0.466	-0.165	-0.401	0.379	0.342	0.412	0.348	0.315	0.275	0.124	-0.376	0.234	-0.390	-0.311	-0.368	0.134	-0.171	-0.138	0.141
Mg	0.408	-0.174	-0.159	-0.545	-0.323	-0.436	0.478	0.522	0.544	0.371	0.467	0.422	0.238	-0.453	0.391	-0.460	-0.448	-0.413	0.373	-0.183	-0.285	0.057
Org. Matter	0.176	-0.179	0.071	-0.469	-0.094	-0.475	0.402	0.204	0.340	0.355	0.191	0.257	0.021	-0.306	0.199	-0.456	-0.191	-0.228	0.142	-0.446	-0.091	0.069
Water Depth	0.139	-0.342	-0.154	-0.241	-0.300	-0.349	0.322	0.299	0.195	0.098	0.207	0.294	0.213	-0.085	0.324	-0.351	-0.105	-0.190	0.382	-0.010	-0.006	0.115

Table 7.5 Correlation coefficients (*r*) between the derived spectral reflectance indices from the laboratory darkroom spectrometry and the sediment chemistry parameters from stands of *Phragmites australis* sampled in Hickling Broad during June 2005.

	[$NDVI_{broad}$]	[$NDVI_{hyper}$]	[Green $NDVI_{broad}$]	[Green $NDVI_{hyper}$]	[PRI]	[SIPI]	[TCHVI]	[NPQI]	[DVI]	[SRPI]	[NPCI]	[PSSRb]	[PSNDb]	[$R_{shoulder}$]	[C420]	[NDI]	[SR]	[SR_{hyper}]	[R_{550}/R_{800}]	[R_{750}/R_{550}]	[R_{725}/R_{675}]	[R_{800}-R_{550}]
TN	-0.002	-0.030	0.087	0.152	-0.033	-0.143	0.107	0.072	0.412	0.411	-0.408	0.058	0.046	0.441	0.065	0.311	0.016	-0.008	-0.135	0.181	-0.128	0.515
TP	0.422	0.366	0.421	0.427	0.048	0.152	0.277	0.457	0.336	0.148	-0.151	0.446	0.450	0.304	0.322	0.641	0.440	0.417	-0.429	0.430	0.199	0.477
K	0.431	0.340	0.285	0.220	0.008	0.469	0.091	0.601	0.132	-0.310	0.313	0.451	0.431	0.100	0.316	0.352	0.446	0.355	-0.219	0.275	0.305	0.174
Fe	0.608	0.531	0.480	0.417	-0.003	0.374	0.238	0.504	0.080	-0.137	0.132	0.595	0.595	0.013	0.340	0.557	0.629	0.581	-0.430	0.423	0.430	0.169
Ca	-0.112	0.003	-0.125	-0.096	0.005	-0.250	-0.088	0.408	0.238	0.278	-0.280	-0.126	-0.104	0.249	0.184	0.132	-0.115	0.024	0.087	-0.129	-0.097	0.233
Na	0.295	0.145	0.470	0.517	-0.395	-0.212	0.435	0.190	-0.111	0.345	-0.346	0.384	0.410	-0.140	0.061	0.588	0.308	0.200	-0.511	0.445	0.001	0.034
Mg	0.240	0.060	0.435	0.455	-0.337	-0.165	0.422	0.397	-0.203	0.131	-0.130	0.369	0.386	-0.224	0.214	0.531	0.253	0.106	-0.455	0.410	-0.069	-0.075
Org. Matter	-0.190	-0.405	0.265	0.392	-0.578	-0.692	0.474	-0.169	-0.337	0.557	-0.557	0.007	0.029	-0.304	-0.178	0.312	-0.182	-0.375	-0.370	0.303	-0.510	-0.190
Water Depth	-0.168	-0.101	-0.294	-0.254	-0.171	-0.215	-0.274	-0.192	0.109	0.074	-0.071	-0.343	-0.291	0.131	-0.470	-0.418	-0.253	-0.207	0.259	-0.317	0.028	0.021

	[R_{800}/R_{550}]	[R_{698}/R_{420}]	[R_{698}/R_{760}]	[R_{605}/R_{670}]	[R_{710}/R_{760}]	[R_{698}/R_{670}]	[R_{675}/R_{700}]	[$R_{679}/(R_{700}XR_{860})$]	[$R_{672}/(R_{550}XR_{708})$]	[R_{675}/R_{550}]	[$R_{860}/(R_{550}XR_{708})$]	[$(R_{850}-R_{710})$ $/(R_{850}-R_{680})$]	[R_{750}/R_{700}]	[$(R_{542}-R_{MINRED})$ $/(R_{750}-R_{MINRED})$]	[$(R_{780}-R_{710})$ $/(R_{780}-R_{680})$]	[R_{700}/R_{670}]	[Red Edge]	[Green Edge]	[Red $Edge_N$]	[Green $Edge_N$]	[EGFR]	[EGFN]
TN	0.170	-0.100	-0.168	-0.214	-0.305	-0.378	0.298	-0.114	-0.032	0.132	-0.043	0.283	0.363	-0.116	0.305	-0.395	0.349	0.306	0.322	-0.480	0.209	-0.108
TP	0.444	-0.335	-0.602	-0.115	-0.592	-0.345	0.195	0.073	-0.017	-0.056	0.197	0.507	0.676	-0.313	0.496	-0.236	0.191	-0.012	0.347	-0.197	0.306	0.254
K	0.253	-0.292	-0.421	0.046	-0.265	0.012	-0.044	0.136	-0.103	-0.251	0.131	0.168	0.399	-0.136	0.146	0.104	0.102	0.058	-0.033	0.220	0.094	0.036
Fe	0.435	-0.327	-0.655	0.059	-0.488	-0.049	-0.044	0.215	-0.022	-0.237	0.294	0.374	0.591	-0.279	0.344	0.107	-0.009	-0.194	0.127	0.030	0.193	0.337
Ca	-0.114	-0.236	-0.082	-0.030	-0.114	-0.371	0.166	-0.173	-0.098	-0.053	-0.143	0.125	0.124	0.068	0.119	-0.324	0.107	0.141	0.162	-0.037	0.013	-0.115
Na	0.480	-0.090	-0.454	-0.270	-0.630	-0.369	0.330	0.336	0.305	0.205	0.445	0.617	0.567	-0.431	0.624	-0.342	-0.281	-0.414	0.534	0.067	0.011	0.367
Mg	0.432	-0.229	-0.413	-0.321	-0.546	-0.387	0.368	0.397	0.311	0.200	0.442	0.551	0.499	-0.434	0.543	-0.327	-0.343	-0.410	0.450	0.241	-0.090	0.289
Org. Matter	0.340	0.134	-0.007	-0.587	-0.416	-0.549	0.620	0.378	0.515	0.607	0.429	0.535	0.258	-0.435	0.564	-0.649	-0.499	-0.426	0.659	0.184	-0.312	0.134
Water Depth	-0.303	0.476	0.371	0.277	0.352	0.398	-0.304	-0.316	-0.235	-0.099	-0.315	-0.330	-0.472	0.301	-0.293	0.233	0.091	0.010	-0.093	0.404	0.129	0.088

Table 7.6 Correlation coefficients (*r*) between the derived spectral reflectance indices from the laboratory darkroom spectrometry and the sediment chemistry parameters from stands of *Phragmites australis* sampled in Hickling Broad during August 2005.

	[$NDVI_{broad}$]	[$NDVI_{hyper}$]	[Green $NDVI_{broad}$]	[Green $NDVI_{hyper}$]	[PRI]	[SIPI]	[TCHVI]	[NPQI]	[DVI]	[SRPI]	[NPCI]	[PSSRb]	[PSNDb]	[$R_{shoulder}$]	[C420]	[NDI]	[SR]	[SR_{hyper}]	[R_{550}/R_{800}]	[R_{750}/R_{550}]	[R_{725}/R_{675}]	[R_{800}-R_{550}]
TN	0.362	0.272	0.352	0.317	-0.502	-0.270	0.306	-0.543	0.426	0.644	-0.639	0.366	0.399	0.367	0.656	0.461	0.330	0.256	-0.323	0.284	-0.055	0.515
TP	0.483	0.370	0.521	0.508	-0.475	0.176	0.481	-0.084	0.017	0.214	-0.220	0.484	0.517	-0.115	0.388	0.529	0.442	0.327	-0.510	0.491	0.029	0.365
K	0.422	0.476	0.337	0.319	-0.240	0.442	0.233	0.138	0.052	0.037	-0.044	0.348	0.375	-0.112	0.103	0.333	0.384	0.432	-0.319	0.308	0.320	0.202
Fe	0.659	0.639	0.581	0.552	-0.449	0.312	0.454	-0.060	0.002	0.473	-0.480	0.617	0.645	-0.223	0.466	0.631	0.625	0.611	-0.549	0.540	0.334	0.330
Ca	-0.084	-0.257	0.093	0.115	-0.120	-0.449	0.206	-0.283	0.250	0.122	-0.116	0.003	0.011	0.359	0.278	0.089	-0.092	-0.262	-0.124	0.101	-0.427	0.337
Na	0.603	0.473	0.658	0.650	-0.377	0.186	0.606	-0.206	-0.032	0.380	-0.395	0.621	0.643	-0.205	0.538	0.669	0.565	0.426	-0.645	0.655	0.061	0.422
Mg	0.644	0.489	0.692	0.678	-0.521	0.217	0.631	-0.234	0.114	0.317	-0.334	0.669	0.687	-0.051	0.543	0.700	0.608	0.437	-0.674	0.684	0.062	0.543
Org, Matter	0.663	0.524	0.641	0.604	-0.513	0.027	0.540	-0.434	0.131	0.661	-0.679	0.682	0.701	-0.039	0.716	0.711	0.629	0.484	-0.597	0.611	0.141	0.484
Water Depth	0.269	0.431	0.120	0.096	0.023	0.212	-0.006	-0.178	0.272	0.154	-0.172	0.155	0.198	0.147	0.124	0.179	0.207	0.357	-0.095	0.083	0.342	0.172

	[R_{800}/R_{550}]	[R_{695}/R_{420}]	[R_{695}/R_{760}]	[R_{605}/R_{670}]	[R_{710}/R_{760}]	[R_{695}/R_{670}]	[R_{675}/R_{700}]	[$R_{675}/(R_{700}XR_{650})$]	[$R_{672}/(R_{550}XR_{708})$]	[R_{675}/R_{550}]	[$R_{660}/(R_{550}XR_{708})$]	[$(R_{860}$-$R_{710})$ $/(R_{850}$-$R_{680})$]	[R_{750}/R_{700}]	[$(R_{542}$-$R_{MINRED})$ $/(R_{750}$-$R_{MINRED})$]	[$(R_{780}$-$R_{710})$ $/(R_{780}$-$R_{680})$]	[R_{700}/R_{670}]	[Red Edge]	[Green Edge]	[Red $Edge_\lambda$]	[Green $Edge_\lambda$]	[EGFR]	[EGFN]
TN	0.286	-0.618	-0.469	-0.370	-0.463	-0.553	0.489	0.352	0.246	0.149	0.263	0.451	0.446	-0.288	0.464	-0.488	-0.044	-0.399	0.495	0.055	0.359	0.476
TP	0.486	-0.405	-0.505	-0.454	-0.543	-0.417	0.414	0.516	0.477	0.274	0.497	0.533	0.493	-0.469	0.537	-0.410	-0.371	-0.611	0.609	-0.033	0.149	0.565
K	0.306	-0.116	-0.365	-0.074	-0.333	-0.044	0.039	0.285	0.208	-0.052	0.319	0.291	0.323	-0.222	0.295	-0.022	-0.188	-0.326	0.330	-0.053	0.093	0.312
Fe	0.531	-0.498	-0.664	-0.340	-0.625	-0.394	0.325	0.602	0.464	0.087	0.583	0.573	0.625	-0.446	0.586	-0.324	-0.306	-0.584	0.645	0.018	0.206	0.570
Ca	0.102	-0.233	-0.018	-0.355	-0.103	-0.366	0.392	0.066	0.153	0.385	0.023	0.154	0.063	-0.215	0.150	-0.396	0.042	-0.201	0.193	0.099	0.266	0.284
Na	0.645	-0.563	-0.653	-0.578	-0.668	-0.578	0.552	0.700	0.652	0.388	0.677	0.648	0.650	-0.618	0.657	-0.534	-0.304	-0.700	0.701	0.185	0.329	0.732
Mg	0.672	-0.562	-0.674	-0.603	-0.702	-0.559	0.567	0.710	0.632	0.380	0.678	0.681	0.677	-0.631	0.690	-0.531	-0.266	-0.697	0.737	0.123	0.377	0.748
Org, Matter	0.592	-0.730	-0.729	-0.564	-0.695	-0.637	0.579	0.721	0.560	0.261	0.625	0.651	0.709	-0.546	0.672	-0.549	-0.150	-0.615	0.717	0.240	0.444	0.710
Water Depth	0.074	-0.133	-0.272	0.143	-0.155	-0.006	-0.057	0.058	-0.056	-0.264	0.064	0.082	0.188	-0.012	0.103	0.065	0.127	-0.068	0.103	0.288	0.239	0.177

Table 7.7 Correlation coefficients (*r*) between the derived spectral reflectance indices from the laboratory darkroom spectrometry and the sediment chemistry parameters from stands of *Phragmites australis* sampled in Hickling Broad for combined datasets.

	[$NDVI_{broad}$]	[$NDVI_{hyper}$]	[Green $NDVI_{broad}$]	[Green $NDVI_{hyper}$]	[PRI]	[SIPI]	[TCHVI]	[NPQI]	[DVI]	[SRPI]	[NPCI]	[PSSRb]	[PSNDb]	[$R_{shoulder}$]	[C420]	[NDI]	[SR]	[SR_{hyper}]	[R_{550}/R_{800}]	[R_{750}/R_{550}]	[R_{725}/R_{675}]	[R_{800}-R_{550}]
TN	0.170	0.119	0.226	0.226	-0.045	-0.103	0.196	-0.121	0.199	0.213	-0.213	0.159	0.196	0.189	0.149	0.310	0.144	0.110	-0.230	0.197	-0.035	0.327
TP	0.308	0.165	0.513	0.516	-0.070	0.040	0.502	-0.280	-0.073	0.081	-0.085	0.364	0.356	-0.132	0.133	0.459	0.324	0.187	-0.519	0.513	-0.044	0.226
K	0.220	0.219	0.255	0.257	-0.057	0.179	0.183	-0.100	-0.078	0.032	-0.060	0.182	0.205	-0.142	0.114	0.273	0.192	0.181	-0.256	0.254	0.079	0.037
Fe	0.335	0.295	0.420	0.417	-0.112	0.137	0.336	-0.129	-0.021	0.109	-0.130	0.322	0.337	-0.102	0.181	0.462	0.324	0.289	-0.417	0.405	0.099	0.187
Ca	0.041	-0.059	0.148	0.150	-0.058	-0.304	0.195	-0.164	0.014	0.221	-0.222	0.080	0.106	0.025	0.222	0.174	0.025	-0.062	-0.159	0.122	-0.180	0.131
Na	0.259	0.114	0.461	0.471	-0.051	-0.065	0.471	-0.228	-0.159	0.168	-0.166	0.312	0.318	-0.215	0.119	0.406	0.260	0.125	-0.473	0.447	-0.080	0.123
Mg	0.294	0.132	0.523	0.535	-0.104	-0.047	0.528	-0.297	-0.191	0.129	-0.141	0.336	0.355	-0.255	0.151	0.486	0.279	0.118	-0.539	0.513	-0.114	0.130
Org, Matter	0.166	-0.029	0.415	0.436	-0.079	-0.229	0.461	-0.218	-0.159	0.248	-0.237	0.243	0.255	-0.178	0.078	0.381	0.159	-0.030	-0.434	0.413	-0.206	0.109
Water Depth	-0.203	-0.056	-0.138	-0.054	0.294	0.032	-0.033	0.058	-0.124	-0.086	0.058	-0.331	-0.258	-0.124	-0.214	-0.104	-0.281	-0.132	0.038	-0.120	-0.154	-0.134

	[R_{800}/R_{550}]	[R_{699}/R_{420}]	[R_{699}/R_{760}]	[R_{605}/R_{670}]	[R_{710}/R_{760}]	[R_{699}/R_{670}]	[R_{675}/R_{700}]	[$R_{679}/(R_{700}XR_{860})$]	[$R_{672}/(R_{550}XR_{708})$]	[R_{679}/R_{550}]	[$R_{860}/(R_{550}XR_{708})$]	[$(R_{850}-R_{710})$ $/(R_{850}-R_{680})$]	[R_{750}/R_{700}]	[$(R_{542}-R_{MINRED})$ $/(R_{750}-R_{MINRED})$]	[$(R_{780}-R_{710})$ $/(R_{780}-R_{680})$]	[R_{700}/R_{670}]	[Red Edge]	[Green Edge]	[Red $Edge_N$]	[Green $Edge_N$]	[EGFR]	[EGFN]
TN	0.194	-0.186	-0.252	-0.191	-0.318	-0.313	0.288	0.140	0.115	0.071	0.149	0.313	0.280	-0.193	0.328	-0.282	0.001	-0.055	0.401	-0.118	0.097	0.090
TP	0.516	-0.152	-0.344	-0.468	-0.469	-0.387	0.420	0.474	0.443	0.280	0.512	0.502	0.438	-0.475	0.489	-0.351	-0.147	-0.129	0.475	-0.111	-0.062	0.089
K	0.246	-0.154	-0.238	-0.089	-0.273	-0.095	0.095	0.238	0.168	0.007	0.265	0.250	0.240	-0.183	0.250	-0.095	-0.191	-0.217	0.253	0.084	0.006	0.215
Fe	0.400	-0.216	-0.393	-0.233	-0.466	-0.309	0.250	0.373	0.282	0.078	0.411	0.451	0.433	-0.334	0.452	-0.251	-0.192	-0.306	0.428	-0.009	0.156	0.354
Ca	0.128	-0.255	-0.118	-0.291	-0.184	-0.330	0.350	0.159	0.188	0.193	0.117	0.222	0.138	-0.174	0.224	-0.298	-0.003	0.061	0.292	0.043	-0.109	-0.106
Na	0.452	-0.139	-0.304	-0.452	-0.424	-0.403	0.419	0.458	0.451	0.299	0.468	0.465	0.380	-0.450	0.457	-0.365	-0.174	-0.176	0.417	0.047	-0.032	0.141
Mg	0.515	-0.183	-0.355	-0.501	-0.509	-0.443	0.488	0.532	0.514	0.323	0.543	0.551	0.435	-0.504	0.542	-0.422	-0.260	-0.255	0.536	0.099	-0.063	0.204
Org, Matter	0.421	-0.109	-0.234	-0.509	-0.414	-0.479	0.514	0.441	0.468	0.353	0.453	0.481	0.356	-0.434	0.477	-0.471	-0.173	-0.155	0.503	0.111	-0.067	0.103
Water Depth	-0.081	0.106	0.137	0.260	0.059	0.021	-0.045	-0.262	0.011	0.072	-0.066	0.007	-0.172	-0.012	-0.020	-0.097	-0.411	-0.470	-0.009	0.158	0.008	0.423

Table 7.8 Correlation coefficients (*r*) between the derived spectral reflectance indices from the field based spectrometry and the sediment chemistry parameters from stands of *Phragmites australis* sampled in Hickling Broad for August 2004.

	[$NDVI_{broad}$]	[$NDVI_{hyper}$]	[Green $NDVI_{broad}$]	[Green $NDVI_{hyper}$]	[PRI]	[SIPI]	[TCHVI]	[NPQI]	[DVI]	[SRPI]	[NPCI]	[PSSRb]	[PSNDb]	[$R_{shoulder}$]	[C420]	[NDI]	[SR]	[SR_{hyper}]	[R_{550}/R_{800}]	[R_{750}/R_{550}]	[R_{725}/R_{675}]	[R_{800}-R_{550}]
TN	0.132	0.159	-0.027	-0.010	0.124	0.051	-0.179	0.005	0.138	0.319	-0.320	0.188	0.124	0.122	0.194	0.173	0.194	0.228	0.015	0.007	0.238	0.111
TP	-0.208	-0.188	-0.312	-0.273	0.400	-0.263	-0.195	-0.199	-0.397	0.004	-0.007	-0.266	-0.199	-0.418	0.221	-0.177	-0.284	-0.274	0.267	-0.280	-0.275	-0.411
K	0.140	0.161	0.023	0.062	0.297	0.066	-0.146	0.004	-0.134	0.266	-0.267	0.016	0.129	-0.160	0.233	0.107	0.005	0.008	-0.074	0.012	0.039	-0.150
Fe	0.082	0.089	0.052	0.090	0.164	0.006	-0.027	0.035	-0.177	0.187	-0.195	-0.012	0.086	-0.198	0.238	0.066	-0.042	-0.055	-0.101	0.058	-0.044	-0.177
Ca	-0.229	-0.183	-0.442	-0.458	0.286	-0.396	-0.311	-0.561	-0.255	0.299	-0.288	-0.176	-0.245	-0.294	0.515	-0.160	-0.134	-0.057	0.454	-0.472	-0.037	-0.315
Na	-0.180	-0.156	-0.300	-0.277	0.258	-0.220	-0.226	-0.177	-0.330	-0.025	0.036	-0.209	-0.170	-0.355	0.180	-0.112	-0.220	-0.203	0.285	-0.253	-0.208	-0.349
Mg	-0.043	-0.021	-0.195	-0.149	0.408	-0.080	-0.254	-0.090	-0.310	0.073	-0.072	-0.101	-0.031	-0.348	0.191	-0.010	-0.127	-0.124	0.152	-0.136	-0.129	-0.331
Org, Matter	-0.094	-0.060	-0.357	-0.329	0.383	-0.026	-0.610	0.033	-0.090	-0.144	0.168	0.001	-0.063	-0.127	-0.029	0.045	-0.016	0.013	0.369	-0.203	-0.038	-0.128
Water Depth	0.233	0.238	0.010	0.022	0.261	0.247	-0.323	0.038	0.167	0.205	-0.193	0.296	0.245	0.141	0.097	0.272	0.292	0.304	-0.016	0.048	0.274	0.141

	[R_{800}/R_{550}]	[R_{698}/R_{420}]	[R_{698}/R_{760}]	[R_{605}/R_{670}]	[R_{710}/R_{760}]	[R_{698}/R_{670}]	[R_{675}/R_{700}]	[$R_{679}/(R_{700}XR_{680})$]	[$R_{672}/(R_{550}XR_{708})$]	[R_{679}/R_{550}]	[$R_{860}/(R_{550}XR_{708})$]	[$(R_{850}-R_{710})$ $/(R_{850}-R_{680})$]	[R_{750}/R_{700}]	[$(R_{542}-R_{MINRED})$ $/(R_{750}-R_{MINRED})$]	[$(R_{780}-R_{710})$ $/(R_{780}-R_{680})$]	[R_{700}/R_{670}]	[Red Edge]	[Green Edge]	[Red $Edge_N$]	[Green $Edge_N$]	[EGFR]	[EGFN]
TN	-0.039	-0.204	-0.144	0.353	-0.142	0.204	-0.232	-0.025	-0.235	-0.289	-0.098	-0.230	0.227	0.144	-0.039	0.212	0.172	0.239	0.147	0.263	0.141	-0.216
TP	-0.271	-0.239	0.133	0.085	0.156	-0.396	0.292	0.367	0.390	0.104	0.286	0.050	-0.217	0.075	-0.036	-0.342	-0.419	-0.480	-0.047	0.010	-0.379	0.015
K	-0.005	-0.200	-0.175	0.190	-0.130	0.024	-0.142	0.172	-0.010	-0.142	0.239	-0.227	0.047	0.118	-0.046	0.054	-0.149	-0.173	0.133	0.098	-0.133	0.119
Fe	0.055	-0.219	-0.112	0.031	-0.099	-0.073	-0.035	0.179	0.084	-0.002	0.276	-0.062	0.002	-0.010	0.056	-0.043	-0.221	-0.335	0.136	-0.104	-0.172	0.270
Ca	-0.516	-0.536	0.189	0.360	0.219	-0.127	0.125	0.345	0.279	-0.152	0.076	-0.312	-0.083	0.202	-0.268	-0.099	-0.166	-0.062	-0.083	0.129	-0.194	-0.377
Na	-0.259	-0.167	0.088	0.097	0.118	-0.342	0.275	0.356	0.349	0.036	0.227	0.043	-0.133	0.174	0.015	-0.293	-0.326	-0.353	-0.133	0.087	-0.302	-0.052
Mg	-0.137	-0.193	-0.036	0.180	-0.006	-0.251	0.139	0.365	0.280	-0.042	0.351	0.061	-0.050	0.180	0.071	-0.196	-0.330	-0.398	-0.056	0.033	-0.292	0.068
Org, Matter	-0.216	0.024	-0.033	0.447	-0.015	-0.293	0.267	0.379	0.231	-0.209	0.091	0.446	0.095	0.517	0.317	-0.221	-0.070	-0.074	-0.414	0.016	-0.064	-0.231
Water Depth	0.052	-0.090	-0.226	0.505	-0.261	0.232	-0.206	0.124	-0.153	-0.338	0.152	0.343	0.313	0.253	0.314	0.221	0.178	0.228	0.137	-0.316	0.152	-0.192

Table 7.9 Correlation coefficients (*r*) between the derived spectral reflectance indices from the field based spectrometry and the sediment chemistry parameters from stands of *Phragmites australis* sampled in Hickling Broad for June 2005.

	[$NDVI_{broad}$]	[$NDVI_{hyper}$]	[Green $NDVI_{broad}$]	[Green $NDVI_{hyper}$]	[PRI]	[SIPI]	[TCHVI]	[NPQI]	[DVI]	[SRPI]	[NPCI]	[PSSRb]	[PSNDb]	[$R_{shoulder}$]	[C420]	[NDI]	[SR]	[SR_{hyper}]	[R_{550}/R_{800}]	[R_{750}/R_{550}]	[R_{725}/R_{675}]	[R_{800}-R_{550}]
TN	0.182	0.131	0.163	0.209	0.113	0.209	0.127	-0.375	0.173	0.229	-0.191	0.333	0.229	0.169	0.160	0.244	0.305	0.297	-0.220	0.173	0.237	0.176
TP	0.209	0.154	0.115	0.166	0.223	0.218	0.044	-0.040	0.190	0.185	-0.172	0.252	0.260	0.190	0.314	0.318	0.209	0.178	-0.179	0.092	0.093	0.179
K	0.104	0.084	0.072	0.069	0.038	0.040	0.042	-0.062	0.123	0.239	-0.251	0.036	0.089	0.127	0.283	0.069	0.047	0.028	-0.073	0.018	0.002	0.109
Fe	0.008	-0.023	-0.063	-0.037	0.209	0.017	-0.080	0.134	0.006	-0.037	0.024	-0.035	0.038	0.013	0.185	0.098	-0.065	-0.097	0.028	-0.095	-0.154	-0.006
Ca	0.514	0.476	0.319	0.354	0.146	0.546	0.115	-0.003	0.332	0.273	-0.237	0.574	0.558	0.305	0.037	0.599	0.519	0.496	-0.363	0.312	0.409	0.314
Na	0.080	0.064	-0.097	-0.038	0.433	0.117	-0.172	0.191	-0.180	-0.220	0.223	0.090	0.187	-0.197	-0.001	0.359	-0.015	-0.039	0.019	-0.127	-0.166	-0.182
Mg	0.162	0.129	0.079	0.127	0.253	0.204	0.012	0.113	-0.052	-0.193	0.190	0.124	0.247	-0.064	-0.045	0.378	0.028	-0.016	-0.140	0.051	-0.134	-0.042
Org, Matter	0.090	0.063	0.021	0.095	0.361	0.154	-0.024	0.161	-0.190	-0.333	0.336	0.096	0.203	-0.209	-0.103	0.392	-0.021	-0.059	-0.110	0.021	-0.187	-0.167
Water Depth	-0.066	-0.003	-0.280	-0.319	0.193	-0.219	-0.327	0.385	-0.253	0.137	-0.143	-0.231	-0.100	-0.265	0.334	-0.112	-0.236	-0.207	0.317	-0.350	-0.170	-0.282

	[R_{800}/R_{550}]	[R_{695}/R_{420}]	[R_{695}/R_{760}]	[R_{605}/R_{670}]	[R_{710}/R_{760}]	[R_{695}/R_{670}]	[R_{675}/R_{700}]	[$R_{675}/(R_{700}XR_{650})$]	[$R_{672}/(R_{550}XR_{708})$]	[R_{675}/R_{550}]	[$R_{660}/(R_{550}XR_{708})$]	[$(R_{860}$-$R_{710})$ /$(R_{850}$-$R_{680})$]	[R_{750}/R_{700}]	[$(R_{542}$-$R_{MINRED})$ /$(R_{750}$-$R_{MINRED})$]	[$(R_{780}$-$R_{710})$ /$(R_{780}$-$R_{680})$]	[R_{700}/R_{670}]	[Red Edge]	[Green Edge]	[Red $Edge_\lambda$]	[Green $Edge_\lambda$]	[EGFR]	[EGFN]
TN	0.186	-0.147	-0.138	0.161	-0.211	0.166	-0.095	-0.049	-0.040	0.009	0.197	0.353	0.297	-0.244	0.328	0.191	0.158	-0.076	0.386	-0.248	0.159	0.203
TP	0.109	-0.322	-0.202	0.194	-0.307	0.021	-0.005	-0.043	-0.108	-0.052	0.097	0.474	0.286	-0.179	0.466	0.044	0.160	0.012	0.650	0.010	0.152	0.173
K	0.017	-0.306	-0.071	0.031	-0.037	0.043	-0.053	-0.183	-0.207	-0.032	-0.183	0.050	0.047	-0.051	0.046	0.043	0.082	0.102	0.262	0.367	0.064	0.035
Fe	-0.084	-0.207	-0.026	0.096	-0.107	-0.170	0.164	0.004	-0.047	-0.014	-0.086	0.274	0.022	-0.007	0.267	-0.167	-0.029	0.050	0.488	0.110	-0.038	-0.016
Ca	0.324	-0.002	-0.518	0.277	-0.582	0.297	-0.302	0.004	-0.234	-0.284	0.383	0.503	0.620	-0.195	0.524	0.325	0.348	0.113	0.456	0.016	0.330	0.266
Na	-0.099	-0.009	-0.181	0.239	-0.386	-0.331	0.309	0.545	0.314	-0.106	0.510	0.642	0.235	0.018	0.646	-0.292	-0.176	-0.267	0.642	0.051	-0.171	-0.041
Mg	0.074	0.039	-0.227	0.074	-0.390	-0.253	0.223	0.389	0.228	-0.014	0.496	0.591	0.253	-0.130	0.589	-0.230	-0.043	-0.231	0.649	0.213	-0.034	0.100
Org, Matter	0.047	0.103	-0.192	0.074	-0.418	-0.371	0.340	0.669	0.483	0.027	0.759	0.690	0.256	-0.148	0.696	-0.336	-0.209	-0.477	0.627	0.180	-0.193	-0.044
Water Depth	-0.359	-0.314	0.028	0.266	0.118	-0.093	-0.039	0.159	-0.049	-0.220	-0.145	-0.298	-0.153	0.409	-0.262	-0.110	-0.234	0.045	-0.253	0.306	-0.258	-0.325

Table 7.10 Correlation coefficients (*r*) between the derived spectral reflectance indices from the field based spectrometry and the sediment chemistry parameters from stands of *Phragmites australis* sampled in Hickling Broad for combined datasets.

	[$NDVI_{broad}$]	[$NDVI_{hyper}$]	[Green $NDVI_{broad}$]	[Green $NDVI_{hyper}$]	[PRI]	[SIPI]	[TCHVI]	[NPQI]	[DVI]	[SRPI]	[NPCI]	[PSSRb]	[PSNDb]	[$R_{shoulder}$]	[C420]	[NDI]	[SR]	[SR_{hyper}]	[R_{550}/R_{800}]	[R_{750}/R_{550}]	[R_{725}/R_{675}]	[R_{800}-R_{550}]
TN	-0.062	-0.058	-0.041	-0.032	0.132	-0.071	0.059	-0.234	0.059	0.035	-0.028	-0.009	-0.068	0.080	-0.020	-0.084	0.002	0.011	0.019	-0.039	0.021	0.067
TP	-0.167	-0.167	-0.201	-0.165	0.314	-0.189	-0.042	-0.183	-0.233	-0.035	0.042	-0.098	-0.152	-0.245	0.100	-0.133	-0.109	-0.111	0.160	-0.152	-0.143	-0.230
K	0.095	0.102	0.042	0.062	0.163	0.050	-0.071	-0.014	-0.032	0.186	-0.191	0.025	0.083	-0.052	0.191	0.060	0.026	0.021	-0.071	0.018	0.021	-0.043
Fe	0.004	0.002	-0.017	0.009	0.190	-0.027	-0.017	0.044	-0.115	0.020	-0.037	-0.056	0.006	-0.123	0.122	-0.005	-0.074	-0.090	-0.024	-0.049	-0.112	-0.115
Ca	-0.065	-0.054	-0.160	-0.154	0.215	-0.134	-0.112	-0.330	-0.056	0.168	-0.156	0.101	-0.058	-0.089	0.216	-0.015	0.109	0.129	0.163	-0.087	0.114	-0.083
Na	-0.135	-0.128	-0.234	-0.200	0.349	-0.146	-0.137	-0.066	-0.283	-0.141	0.138	-0.091	-0.109	-0.305	0.021	-0.060	-0.129	-0.131	0.201	-0.200	-0.189	-0.293
Mg	-0.077	-0.073	-0.128	-0.092	0.331	-0.077	-0.078	-0.063	-0.240	-0.114	0.102	-0.077	-0.060	-0.263	-0.004	-0.047	-0.111	-0.124	0.088	-0.096	-0.171	-0.240
Org, Matter	-0.134	-0.128	-0.217	-0.179	0.373	-0.074	-0.167	0.025	-0.191	-0.283	0.281	-0.084	-0.101	-0.202	-0.159	-0.050	-0.130	-0.140	0.192	-0.137	-0.206	-0.189
Water Depth	-0.292	-0.281	-0.287	-0.329	0.199	-0.287	0.025	-0.137	-0.187	-0.270	0.267	-0.412	-0.316	-0.135	-0.244	-0.370	-0.397	-0.388	0.300	-0.388	-0.343	-0.174

	[R_{800}/R_{550}]	[R_{698}/R_{420}]	[R_{698}/R_{760}]	[R_{605}/R_{670}]	[R_{710}/R_{760}]	[R_{698}/R_{670}]	[R_{675}/R_{700}]	[$R_{679}/(R_{700}XR_{680})$]	[$R_{672}/(R_{550}XR_{708})$]	[R_{679}/R_{550}]	[$R_{680}/(R_{550}XR_{708})$]	[$(R_{850}-R_{710})$ $/(R_{850}-R_{680})$]	[R_{750}/R_{700}]	[$(R_{542}-R_{MINRED})$ $/(R_{750}-R_{MINRED})$]	[$(R_{780}-R_{710})$ $/(R_{780}-R_{680})$]	[R_{700}/R_{670}]	[Red Edge]	[Green Edge]	[Red $Edge_N$]	[Green $Edge_N$]	[EGFR]	[EGFN]
TN	-0.035	0.017	0.082	0.038	0.092	0.116	-0.048	-0.123	-0.057	0.032	-0.117	-0.131	-0.059	-0.093	-0.136	0.082	0.071	0.142	-0.001	0.019	0.026	-0.167
TP	-0.137	-0.107	0.139	0.019	0.129	-0.246	0.227	0.174	0.295	0.132	0.079	0.039	-0.107	-0.052	-0.043	-0.202	-0.254	-0.363	0.009	0.044	-0.210	-0.029
K	0.011	-0.174	-0.101	0.085	-0.067	0.035	-0.101	0.061	-0.058	-0.082	0.056	-0.048	0.033	0.063	0.006	0.048	-0.054	-0.103	0.127	0.226	-0.038	0.071
Fe	-0.044	-0.117	-0.016	0.017	-0.012	-0.129	0.063	0.082	0.061	0.033	0.052	0.024	-0.039	-0.032	0.022	-0.118	-0.151	-0.216	0.135	0.037	-0.122	0.075
Ca	-0.097	-0.247	0.065	0.202	0.048	0.047	-0.006	0.193	0.148	-0.093	0.121	0.006	0.081	0.051	-0.021	0.073	0.004	-0.020	0.020	0.073	0.002	-0.122
Na	-0.191	-0.028	0.084	0.073	0.061	-0.346	0.292	0.324	0.327	0.059	0.203	0.133	-0.052	0.065	0.050	-0.297	-0.279	-0.307	0.014	0.085	-0.255	-0.092
Mg	-0.081	-0.013	0.043	0.015	0.037	-0.271	0.203	0.274	0.278	0.061	0.230	0.094	-0.054	0.018	0.026	-0.238	-0.247	-0.333	0.026	0.157	-0.213	-0.017
Org, Matter	-0.119	0.150	0.080	0.019	0.053	-0.363	0.333	0.341	0.332	0.057	0.227	0.206	-0.043	0.104	0.083	-0.327	-0.189	-0.180	-0.117	0.171	-0.197	-0.203
Water Depth	-0.363	0.257	0.315	-0.126	0.355	-0.084	0.154	-0.115	0.147	0.222	-0.309	-0.398	-0.420	-0.042	-0.426	-0.195	-0.167	0.168	-0.371	0.225	-0.266	-0.516

The strongest correlation derived from the August 2004 laboratory darkroom spectrometry was observed between the narrow band reflectance ratio [$R_{675}/(R_{700}xR_{650})$] and the concentration of TP in the sediment (r = 0.676; p = 0.002). The strongest correlation derived from the June 2005 laboratory darkroom spectrometry was also observed with the concentration of TP in the sediment but, in this instance, the optimum spectral index was [R_{750}/R_{700}] (r = 0.653; p = 0.006). The strongest correlation derived from the August 2005 laboratory darkroom spectrometry was observed between the [EGFN] index and the concentration of Mg in the sediment (r = 0.748; p = 0.000). In addition, several spectral indices (including the [Red Edge$_\lambda$]) demonstrated significant correlations (r > 0.700; P < 0.05) with the concentration of Na and organic matter content (see Figure 7.6). The strongest correlation derived from the combined datasets from August 2004, June 2005 and August 2005 was observed between [$(R_{850}/R_{710})/(R_{850}/R_{680})$] and the concentrations of Mg in the sediment (r = 0.551; p = 0.001).

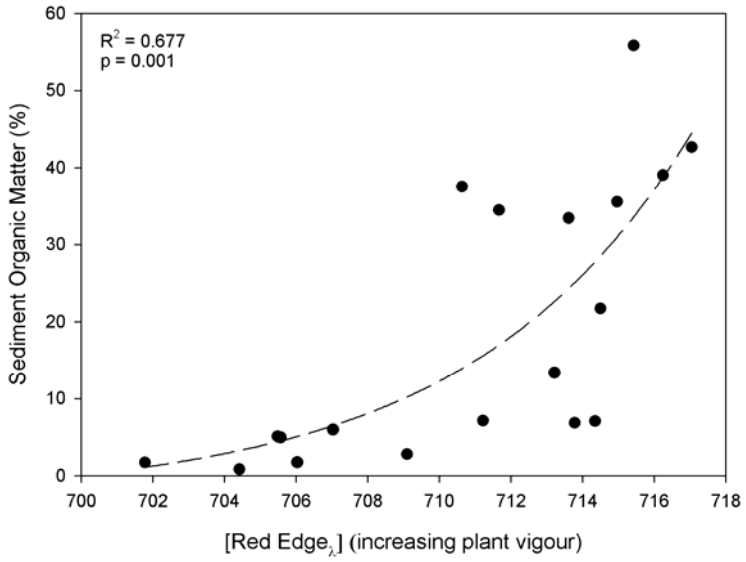

Figure 7.6 Non-linear exponential regression between sediment organic matter content and the physiological status of *Phragmites australis* as indicted by the [Red Edge$_\lambda$] spectral index derived from laboratory darkroom spectrometry of apical leaves harvested from stands in Hickling Broad during August 2005.

The strongest correlation derived from the August 2004 *in-situ* field-based spectrometry was observed between [TCHVI] and the organic matter content of the sediment (r = -0.610; p = 0.020). However, further inspection indicated that this atypical negative correlation between plant vigour and sediment organic matter was due to the effect of a single outlying data point.

The strongest correlation derived from the June 2005 *in-situ* field-based spectrometry was, again, also observed to occur between [$R_{860}/(R_{550}xR_{708})$] and the organic matter content of the sediment (r = 0.759; p = 0.001), but in this instance the correlation between the organic matter content of the sediment and plant vigour was positive (which also suggests the negative correlation observed from the August 2004 data was somewhat spurious). The relationship between [$R_{860}/(R_{550}xR_{708})$] and sediment organic matter is depicted in Figure 7.7. The strongest correlation derived from the combined *in-situ* field-based spectrometry datasets was observed between the [EGFN] index and water depth (r = -0.516; p = 0.008).

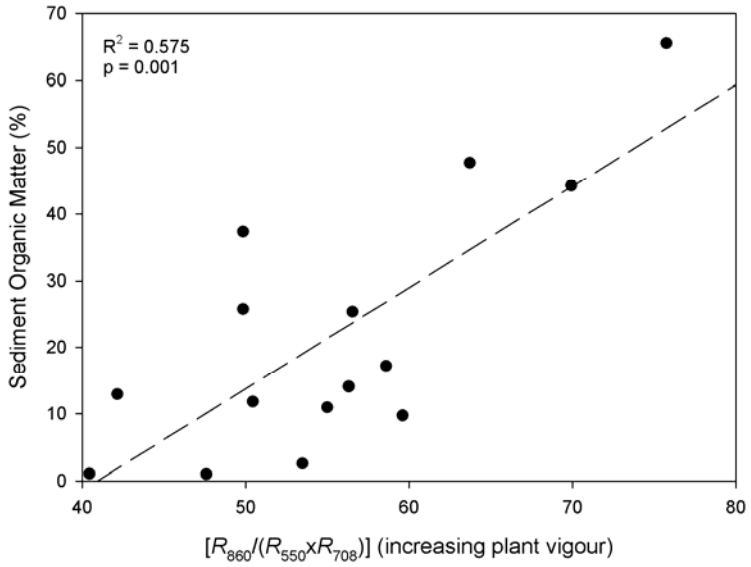

Figure 7.7 The linear regression relationship between sediment organic matter and the vigour of *Phragmites australis* as indicted by the [$R_{860}/(R_{550}xR_{708})$] spectral index derived from *in-situ* field-based spectrometry in Hickling Broad during June 2005.

The generally weaker correlations observed with the spectral indices derived from the *in-situ* field-based spectrometry were probably due to the fact that, at the stand scale, the spectral signature of *Phragmites australis* (and indeed most vegetation types) is greatly influenced by variation in plant morphology and, in particular, the architecture of the canopy (i.e. biomass, leaf-area-index, leaf orientation) and, thus, less so by leaf pigmentation. The relatively fine-scale spectra reflectance measurements attained in the field (i.e. instantaneous FOV = 0.45 m) may, therefore, be highly susceptible to random variations in the canopy structure that are essentially unrelated to the physiological status of the plants.

The correlation observed here between the various spectral indices (i.e. indicative of plant physiological status) and sediment chemistry implies that the stands of *Phragmites australis* growing on sediments enriched with organic matter were more vigorous than those growing on the more inorganic substrates. The higher concentrations of mineral nutrients (e.g. TP, Mg, Na, Fe) associated with those stands of *Phragmites australis* enriched with organic matter would seem to explain the notable differences in plant performance. Interestingly, no negative correlations were observed between plant physiological status and sediment nutrient enrichment (the only exceptions being the spurious correlations between some of the various spectral indices derived from the *in-situ* field-based spectrometry and sediment organic matter and water depth).

These explorative results would seem to suggest that remote sensing can be used to assess the physiological condition of aquatic plants at both the leaf- and canopy-scale. The Lake Balaton experiment demonstrated that relatively simple spectral-reflectance-based metrics can be derived to estimate the pigment content of *Phragmites australis* leaves. This provides, therefore, a clear route to the use of remote sensing for assessing the physiological status of emergent plants. The ability to quantify the physiological status of these plants subsequently allows process-based relationships between the phytophysiological response and ambient environmental conditions to be explored, as shown here through the derivation of significant correlations between plant physiological status and sediment nutrition. Similar work has also related plant physiological responses, quantified using remote sensing, to pressures such as heavy metal contamination (Kooistra *et al.,* 2004; Clevers *et al.,* 2004).

7.5.4 Airborne CASI-2 [Vegetation] Imagery

The radiance based [L_{710}/L_{760}] index was derived from the CASI-2 [Vegetation] imagery of the Upper Thurne system; this index was analogous to the spectral reflectance index [R_{710}/R_{760}] proposed by Carter (1994) and used above in the analysis of the *in-situ* and laboratory darkroom spectrometry (the [R_{710}/R_{760}] index could not be formulated from the CASI-2 [Vegetation] data as the image data was calibrated to radiance). This specific index was selected because it had previously demonstrated good relationships with both the chlorophyll-a

content of the *Phragmites australis* apical leaves (r = 0.891; p = 0.000) and several sediment chemistry parameters (e.g. organic matter, TP) and, further, the index was readily formulated using the [Vegetation] bandset configuration of the CASI-2 imagery. The multispectral CASI-2 [Vegetation] imagery (14 bands) is not ideally suited for the calculation of derivative spectral reflectance indices (e.g. [Red Edge$_\lambda$]) (such indices can only be adequately formulated from hyperspectral imagery products) and thus such indices were not considered for use with the CASI-2 [Vegetation] imagery.

The SVM algorithm used to classify the CASI-2 [Vegetation] imagery and delineate the extent of *Phragmites australis* reedswamp across Hickling Broad (and the wider Upper Thurne) yielded overall classification accuracies for the 22 June 2005 and 29 August 2005 CASI-2 [Vegetation] imagery of 79.3% and 81.1% respectively; the use of the 0.95 probability threshold in the classification algorithm effectively resulted in producer's accuracies of > 95% for the *Phragmites australis* reedswamp areas (the remaining pixels were unclassified). The *Phragmites australis* stands sampled concomitant to the CASI-2 [Vegetation] imagery were identified in the geo-registered CASI-2 [Vegetation] imagery and the corresponding values of [L_{710}/L_{760}] were extracted and correlated against the sediment chemistry measurements. The derived correlations are detailed in Table 7.11.

Table 7.11 Correlation coefficients (r) between the CASI-2 [Vegetation] derived [L_{710}/L_{760}] index and the various sediment mineral nutrients, organic matter (OM) and water depth (WD). Significant correlations at the 95% confidence level are highlighted.

		TN	TP	K	Fe	Ca	Na	Mg	OM	WD
	Jun 05†	-0.544	-0.705	-0.431	-0.586	-0.056	-0.544	-0.558	-0.665	0.301
[L_{710}/L_{760}]	Aug 05‡	0.163	-0.657	-0.542	-0.313	-0.050	-0.453	-0.548	-0.155	-0.035
	Combined	-0.180	-0.488	-0.352	-0.351	-0.072	-0.422	-0.502	-0.388	-0.025

†n = 15; ‡n = 20;

It is notable that the correlations between the CASI-2 [Vegetation] derived [L_{710}/L_{760}] index and the various sediment chemistry parameters are similar to those previously observed with the laboratory darkroom and *in-situ* field-based spectrometry data. Statistically significant

correlations were derived from the 22 June 2005 CASI-2 [Vegetation] image with the concentration of TN, TP, Fe Na and Mg and the organic matter content of the sediment.

Similar correlations were observed between [L_{710}/L_{760}] index extracted from the CASI-2 [Vegetation] image acquired on 29 August 2005 and sediment nutrient content. Statistically significant correlations were derived with the concentration of TP, K, Na, and Mg. However, rather unexpectedly, no significant correlation was observed between the CASI-2 [L_{710}/L_{760}] index derived from the 29 August 2005 and the sediment organic matter content. The lack of a correlation in this instance is more likely a facet of the dataset, rather than a mechanistic change in the relationship between the physiological status of the *Phragmites australis* plants and sediment organic matter, particularly as significant correlations between plant vigour and sediment organic matter were derived with both the laboratory darkroom and *in-situ* field-based spectrometry.

The correlation analysis performed on the amalgamated dataset again revealed further significant correlations between the CASI-2 [L_{710}/L_{760}] index and the concentration of TP, Na, Mg and the organic matter content of the sediment. The regression relationships between the CASI-2 [L_{710}/L_{760}] index and the sediment organic matter content and TP concentration are depicted in Figure 7.8; for the purposes of clarity, the counter-intuitive CASI-2 [L_{710}/L_{760}] index has been inverted (i.e. [L_{760}/I_{710}]) to yield positive relationships between index value and plant vigour.

The correlations obtained from the CASI-2 [L_{710}/L_{760}] index again suggests, as observed with the laboratory darkroom and *in-situ* field spectrometry, that the physiological status of the *Phragmites australis* in Hickling Broad was positively related to the organic and nutrient enrichment of the sediment (note that the [R_{710}/R_{760}] index was shown to be negatively related to increased plant vigour (i.e. chlorophyll-a) – see Table 7.2 for confirmation).

(a) (b)

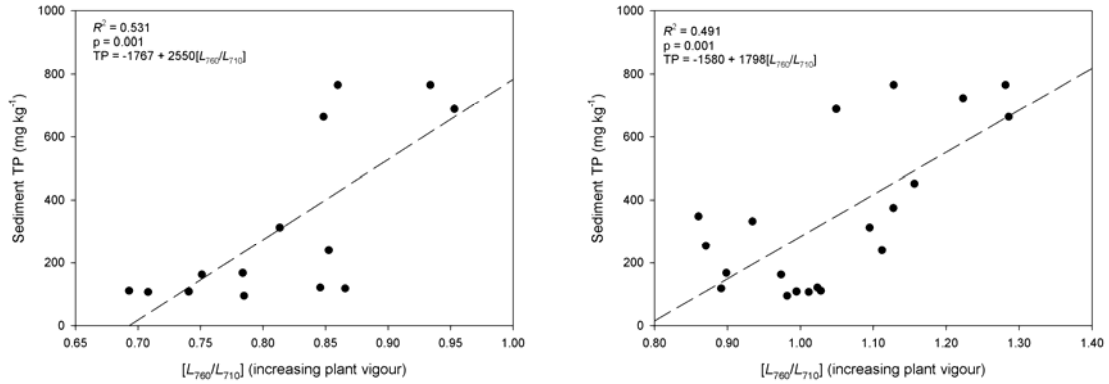

Figure 7.8 The regression relationships derived between the inverted [L_{710}/L_{760}] index derived from the (a) 22 June 2005 CASI-2 [Vegetation] imagery and (b) 29 August 2005 CASI-2 [Vegetation] and the TP concentration in the sediment of *Phragmites australis* stands.

In addition to the correlations detailed above, the [L_{710}/L_{760}] index derived from the 29 August 2005 CASI-2 [Vegetation] image was also noted to correlate strongly with the TN:TP (molar) ratio (n = 19; r = 0.800; p = 0.000). However, a similar correlation could not derived between [L_{710}/L_{760}] index and the TN:TP (molar) ratio from the June 2005 CASI-2 [Vegetation] image, which casts doubt on the robustness of this association. However, the lack of a significant correlation for the 22 June 2005 CASI-2 [Vegetation] image may simply reflect variability in the physiological response of the plants across the growing season. The regression relationship between the [L_{710}/L_{760}] index and the TN:TP (molar) ratio for the 29 August 2005 CASI-2 [Vegetation] image is depicted in Figure 7.9. In this instance, the TN:TP (molar) ratio was negatively related to plant vigour; the derived regression relationship explained over 64% of the observed variation in the physiological status (as quantified using the [L_{710}/L_{760}] index) of the *Phragmites australis* plants.

The CASI-2 [Vegetation] imagery [R_{710}/R_{760}] index images depicting spatial variability in the vigour of *Phragmites australis* reedswamp in Hickling Broad (and surrounding lakes and fens) on 22 June 2005 and 29 August 2005 are shown in Figure 7.10 and Figure 7.11 respectively. The 29 August 2005 CASI-2 [Vegetation] image was also subsequently calibrated using the regression relationships described above between the [L_{710}/L_{760}] band-ratio and the measured

concentration of TP and the TN:TP (molar) ratio to yield spatially-resolving maps depicting lake-scale heterogeneity in sediment nutrient enrichment (Figure 7.12 and Figure 7.13).

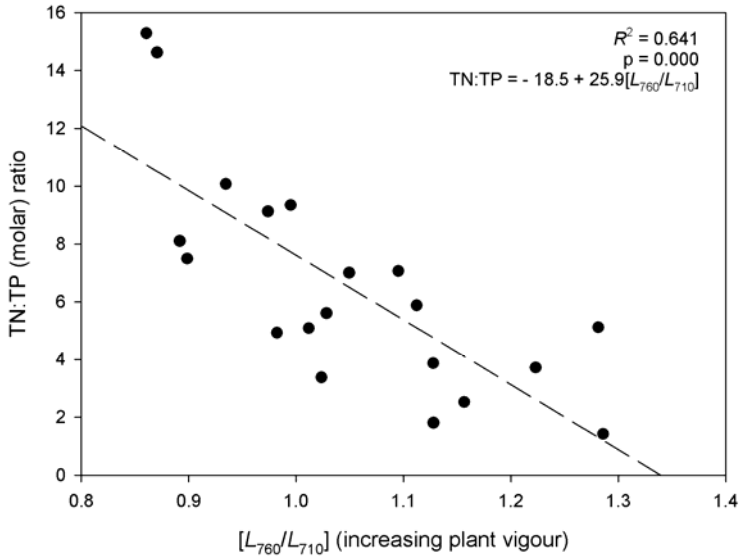

Figure 7.9 The regression relationship between the [R_{760}/R_{710}] index derived from the 29 August 2005 CASI-2 [Vegetation] image and the TN:TP (molar) ratio in the sediment of *Phragmites australis* stands.

The derived CASI-2 [Vegetation] images of *Phragmites australis* vigour show pronounced spatial and temporal variance in reed performance. The CASI-2 [Vegetation] images seem to show a general trend of the *Phragmites australis* reedswamp increasing in vigour through the growing season of 2005. This trend was also evidenced in the laboratory darkroom and *in-situ* field-based spectrometry datasets.

The CASI-2 [Vegetation] image acquired on 22 June 2005 reveals areas of stressed reed in the fenlands adjacent to the north eastern part of the lake. These stressed plants seem to show an association with the network of drainage ditches that bisect the fenland areas. The CASI-2 [Vegetation] image acquired 29 August 2005 also shows some evidence of stressed plants fringing these drainage ditches. It is also notable that the [L_{710}/L_{760}] CASI-2 [Vegetation] images indicate the existence of extensive areas of poorly performing reedswamp adjacent to Horsey Mere. However, the calibrated CASI-2 [Vegetation] images depicting the sediment TP concentration and the TN:TP (molar) ratio also exhibit some pronounced systematic features that would seem to be somewhat unnatural. In some instances, specifically in the TN:TP (molar

ratio) image, rapid transitions can be seen from areas of high TN:TP to areas of low TN:TP. The validity of these derived spatial patterns cannot be established without the need for further ground-truthing, which was beyond the remit of the expeditious work undertaken here. Given that the field-based sampling was conducted solely on littoral reedswamp, it would be unwise to over-extrapolate the relations derived with sediment nutrition in the lake to the surrounding, largely terrestrial, fenland. However, regardless of the strength of association with sediment nutrition, the CASI-2 [Vegetation] [L_{710}/L_{760}] band-ratio images do provide valuable insights into spatial variation in the physiological status of the vegetation in these fenland areas. This exemplifies the importance of the remote sensing approach as such information would be highly useful for informing future lake research and management activities.

The closer examination of the physiological status of the *Phragmites australis* plants growing in the littoral margins of Hickling Broad reveals a perceivable trend of increasing plant vigour from Hickling Broad southwards towards Heigham Sound. It is notable, this perceived gradient in plant vigour draws a parallel with the trends observed in the organic content and nutritional status of the sediment (as shown in Figure 7.4 and Figure 7.5). This gradient, interestingly, is also evident in the 29 August 2005 CASI-2 [Vegetation] image calibrated to the sediment TP concentration and, in particular, the TN:TP (molar) ratio. The spatial heterogeneity in the chemistry of the sediment in Hickling Broad is almost certainly a function of the hydraulic circulation patterns in the lake. Water enters Hickling Broad through Candle Dyke (north east shore of Hickling Broad) and Meadow Dyke (dyke connecting Horsey Mere to Hickling Broad) before flowing southwards, and thus transporting particulate material, into Heigham Sound. The “bottle neck” effect created by the outflow of water from Heigham Sound into the River Thurne slows the flow of water, which may be sufficient to promote the sedimentation of organic and nutrient rich particle matter in the southern part of Heigham Sound. This conjecture is supported in the spatial pattern of sediment organic matter content in Figure 7.3. This flow pattern is also likely to lead to the deposition of organic material in the shallow bays and backwater areas that are a prominent feature of Hickling Broad’s near-shore morphometry.

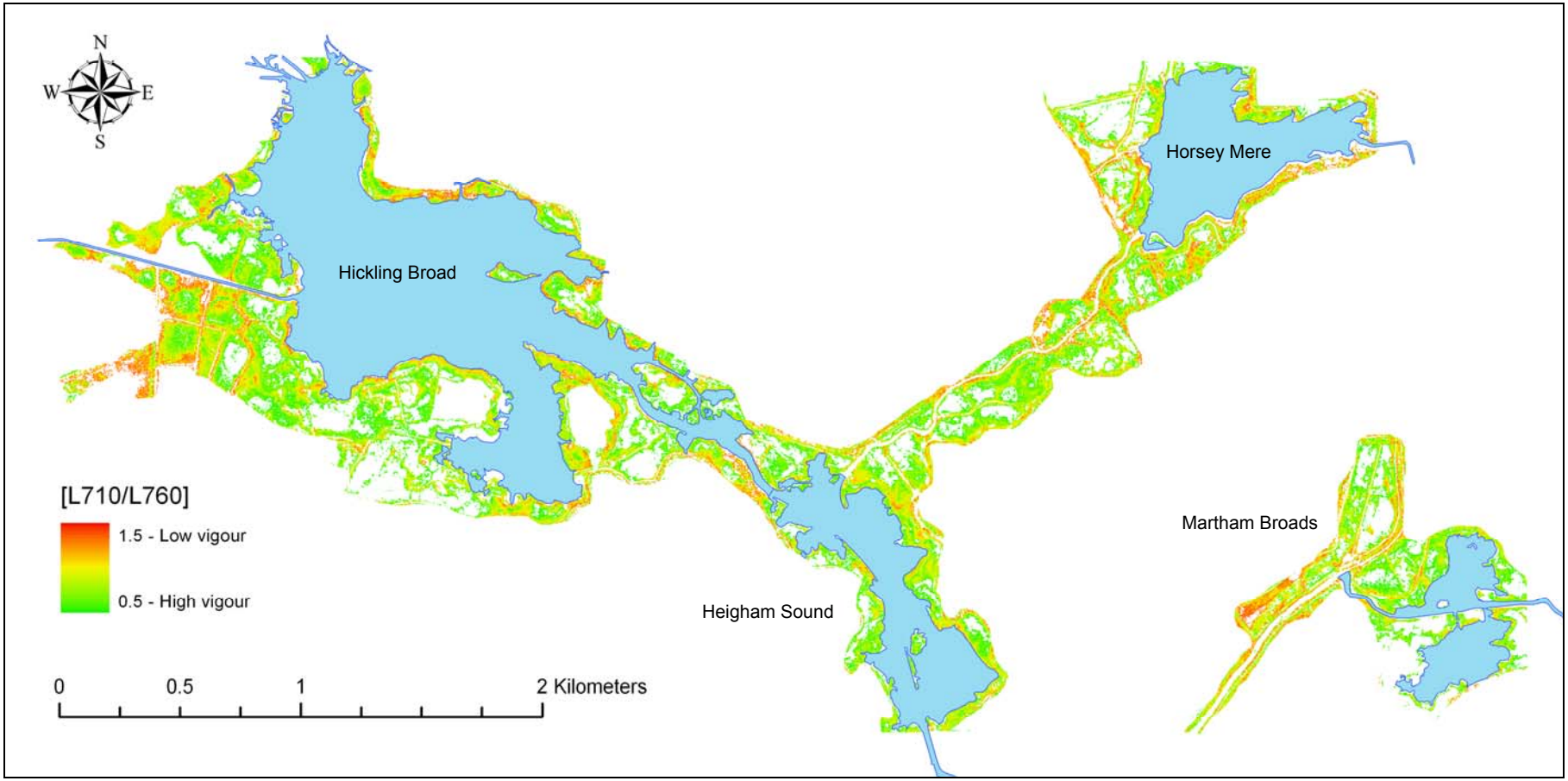

Figure 7.10 CASI-2 [Vegetation] image of *Phragmites australis* reedswamp vigour on 22 June 2005 as estimated by the [L_{710}/L_{760}] index.

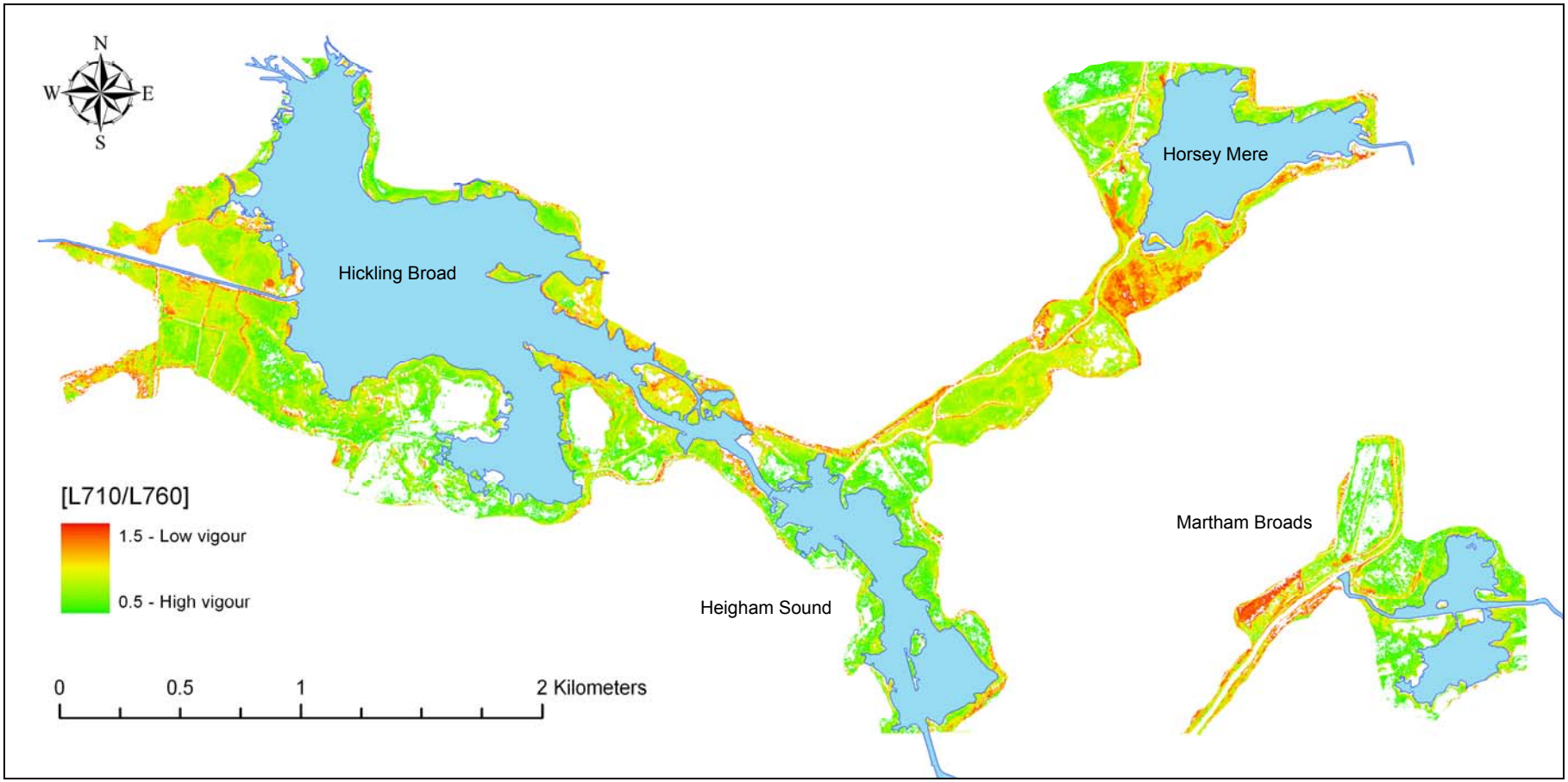

Figure 7.11 CASI-2 [Vegetation] image of *Phragmites australis* reedswamp vigour on 29 August 2005 as estimated by the [L_{710}/L_{760}] index.

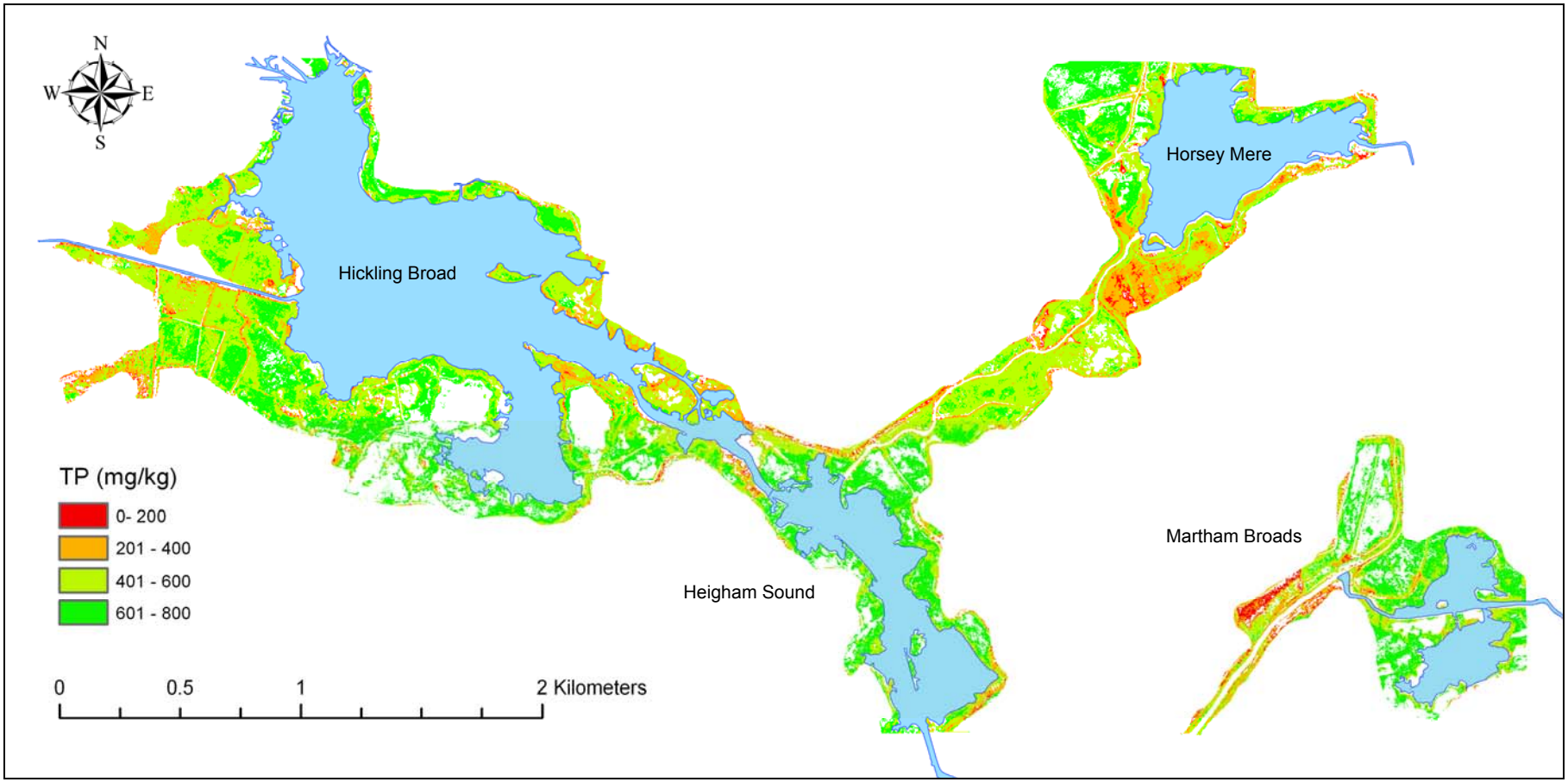

Figure 7.12 CASI-2 [Vegetation] image of sediment TP concentrations in Hickling Broad on 29 August 2005. The image was derived using the least-squares regression relationship derived between the vigour of *Phragmites australis* plants growing in the lake (quantified using the [L_{710}/L_{760}] band-ratio index) and the measured concentration of TP in the rooting sediment (R^2 = 0.491; p = 0.001).

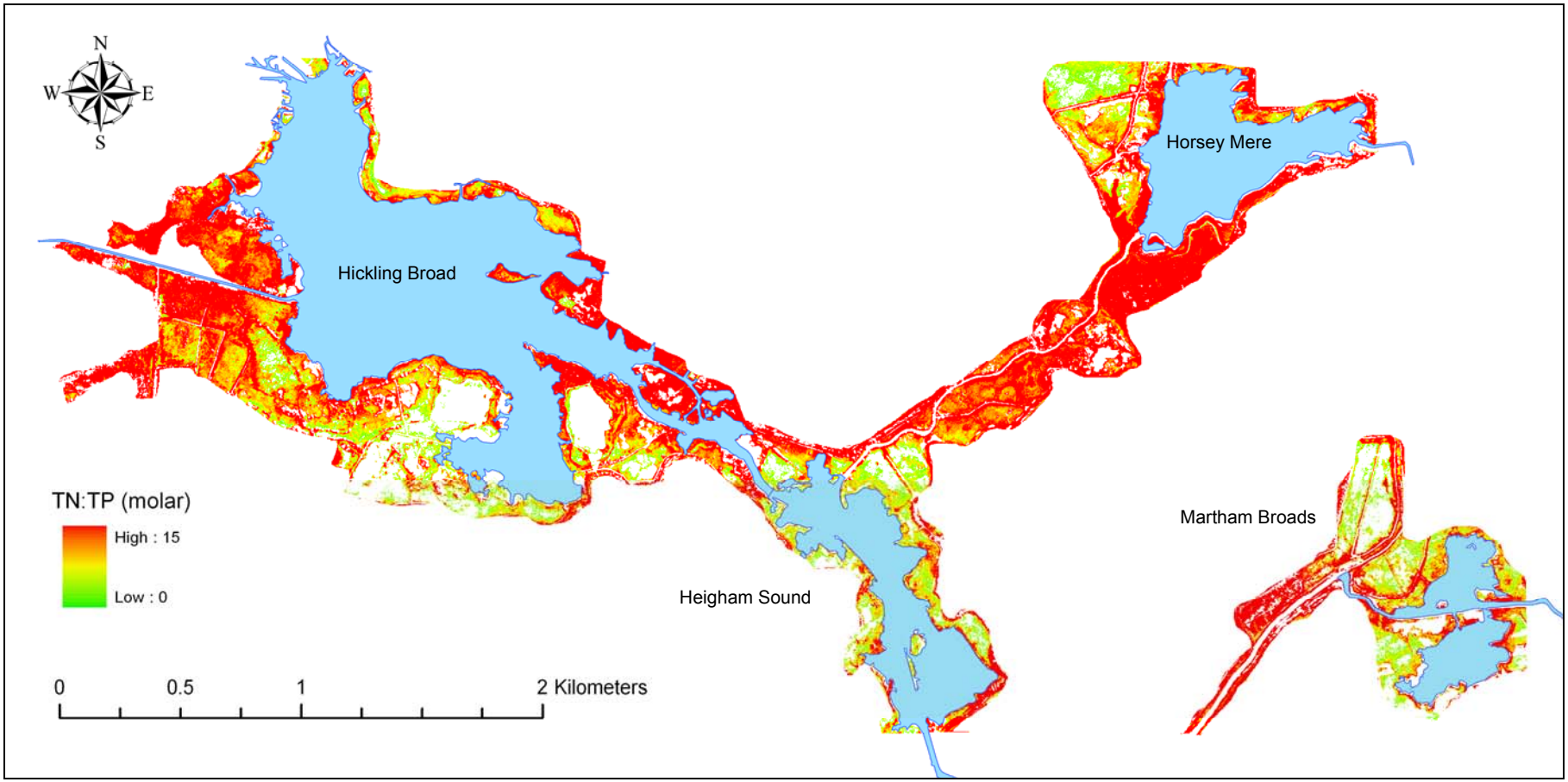

Figure 7.13 CASI-2 [Vegetation] image of sediment TN:TP (molar) ratio in Hickling Broad on 29 August 2005. The image was derived using the least-squares regression relationship derived between the vigour of *Phragmites australis* plants growing in the lake (quantified using the [L_{710}/L_{760}] band-ratio index) and the measured TN:TP (molar) ratio of the rooting sediment (R^2 = 0.641; p = 0.000).

The CASI-2 [Vegetation] images depicting spatial variability in the physiological status of *Phragmites australis* reedswamp in Hickling Broad demonstrate the potentially immense value that remote sensing technologies offer for the assessment of wetland plant ecophysiology. In this instance, remote sensing has been able to afford novel, lake-scale, insights into the physiological response of an aquatic plant community to nutrient enrichment. This could not have been achieved through conventional sampling approaches. It would seem that aquatic plant ecophysiology may provide a crucial route through which an improved understanding of process and function in shallow lakes may be attained. Remote sensing has an unrivalled ability to put such insights into a spatial context, thereby enabling process and function to be examined at an unprecedented whole lake-scale.

7.5.5 Reedswamp Dieback in Hickling Broad

The extent of fringing littoral reedswamp in Hickling Broad has declined over recent decades and now much of what remains is largely terrestrial in influence. It is apparent that very little, if any, recolonisation has occurred in the lake since the initial large-scale losses were documented by Boorman & Fuller (1981) and, later, Boar *et al*. (1989). However, somewhat paradoxically, it was generally observed, throughout the 2-year lake-sampling period, that the remaining littoral reedswamp in Hickling Broad appears to be in relatively good condition. Nevertheless, some evidence of recent dieback was observed at several, albeit somewhat isolated, locations throughout the lake. These dieback areas were readily identifiable by the presence of relict rhizome masses (see Figure 7.14).

The main areas of reed dieback observed in Hickling Broad during 2004 and 2005 are shown in Figure 7.15. In general, the most pronounced areas of reed dieback were found to occur within sheltered bays and backwaters. These dieback areas were typically characterised by shallow and stagnant water (perhaps due to locally high sedimentation rates) where the underlying sediment was commonly composed of the highly organic mud.

Figure 7.14 Photograph showing the presence of relict *Phragmites australis* rhizomes masses in Hickling Broad indicating a recent area of pronounced reedswamp dieback.

Rather surprisingly, notwithstanding evidence of recent regression, the remaining plants in the dieback areas typically appeared healthy and often no obvious evidence of declining plant performance, such as leaf chlorosis or, stand fragmentation, could be observed. These observations would seem to support the trends observed from the spectrometry and airborne CASI-2 imagery, which also showed a general positive association between organic matter accretion, nutrient enrichment and plant health.

In order to further explore the potential causes of reed dieback in Hickling Broad, differences in sediment chemistry between the dieback and non-dieback stands were assessed using the non-parametric Mann-Whitney test. The same statistical test was also applied to the values of two of the best performing spectral indices to examine for statistical differences in plant vigour between the dieback and non-dieback sites. The results of the Mann-Whitney tests are detailed in Table 7.12.

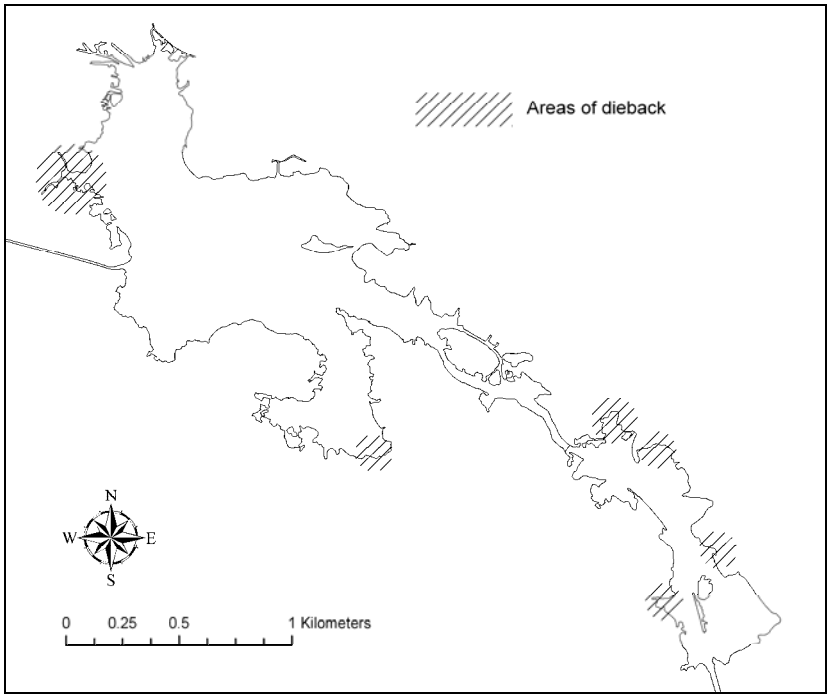

Figure 7.15 Map showing the main areas of *Phragmites australis* dieback recorded in Hickling Broad during 2004 and 2005.

Table 7.12 Mann-Whitney tests for the difference in sediment chemistry and selected spectral reflectance indices for non-dieback and dieback stands of *Phragmites australis* in Hickling Broad (significant *p* values in bold). Values in mg kg^{-1} unless otherwise stated.

	Median		95% CI	W	*p*
	Non-dieback (*n* = 43)	**Dieback** (*n* = 11)	**(Non-Dieback – Dieback)**		
TN	976	1010	(-262, 227)	-0.16	0.897
TP	312	688	(-245.3, -67.8)	1033.5	**0.001**
K	3048	3253	(-4166.1, 2080.3)	1162.0	0.668
Fe	1427	3457	(-6267.1, -841.7)	1062.0	**0.010**
Ca	28930	28342	(-29118, 42028)	1198.0	0.747
Na	2615	5685	(-9700, -2270)	1031.0	**0.001**
Mg	975	3033	(-5266.8, -1088.7)	1070.0	**0.016**
Org.Mat. (%)	13.40	36.50	(-30.40, -10.10)	852.0	**0.002**
Wat.Dep. (m)	0.70	0.30	(0.00, 0.57)	1329.5	**0.041**
[R_{710}/R_{760}]	0.490	0.465	(0.0018, 0.0474)	2.30	**0.036**
[Red Edge$_{\lambda}$]	711.36	714.13	(-5.17, -0.38)	-2.42	**0.026**

The results of the Mann-Whitney tests indicate the existence of notable statistical differences in the sediment chemistry between those stands of *Phragmites australis* exhibiting signs of recent dieback, and those where no evidence of dieback could be observed. The analysis shows that the dieback stands had a significantly higher organic matter content (non-dieback median = 13.4%; dieback median 36.5%). The dieback stands also exhibited significant higher concentrations of TP (non-dieback median = 155.8 mg kg^{-1}; dieback median = 344.1 mg kg^{-1}), Fe (non-dieback median = 2854.2 mg kg^{-1}; dieback median = 6915.4 mg kg^{-1}), Na (non-dieback median = 5230 mg kg^{-1}; dieback median = 11369 mg kg^{-1}), Mg (non-dieback median = 1949.4 mg kg^{-1}; dieback median = 6065.3 mg kg^{-1}) and were rooting in shallower water than the non-dieback sites (non-dieback median = 0.70 m; dieback median = 0.30 m). In addition, the application of the Mann Whitney tests to the values of the [R_{710}/R_{760}] and [Red Edge$_{\lambda}$] spectral reflectance indices confirmed that the remaining reedswamp vegetation in areas of recent dieback was marginally more vigourous than that growing in areas where no evidence of dieback could be observed. This probably reflects the increased nutrient status of the sediment in dieback stands.

The accumulation of organic matter may be a significant factor in the explanation of reed dieback in Hickling Broad. It was of note that, whilst evidence for dieback was observed for some (but certainly not all) stands rooting in the organic mud, no evidence of dieback was found in stands rooting on more inorganic substrates. Several previous authors have linked the dieback *Phragmites australis* in eutrophic lakes to the accumulation of organic matter in plant rhizospheres and the generation of a strong reducing hydrosoil environment (Denhartog *et al.,* 1989; Armstrong *et al.,* 1996; Armstrong *et al.,* 1996; Cizkova *et al.,* 1996; Van Der Putten, 1997; Fogli *et al.,* 2002). Indeed, Cizkova *et al* (1996) linked the occurrence of a surface layer of dark-coloured, heavily reducing, organic mud to the decline of *Phragmites australis* plants in fishponds in the Czech Republic. The organic mud described by Cizkova *et al* (1996) would seem similar to that observed in the Norfolk Broads, the formation of which is almost certainly linked to the growth and decay of phytoplankton blooms as a result of the eutrophication of the system.

The progressive accumulation of organic matter in *Phragmites australis* stands has been shown to accelerate the rate of microbial decomposition which, in turn, increases the biological oxygen demand in the sediment. The generation of anoxia in the rhizosphere can influence several important plant-sediment interactions including the inhibition of nutrient uptake, respiration and photosynthesis (Armstrong *et al.,* 1996). The switch to anaerobic microbial metabolism precipitated by oxygen stress can also lead to the production of a variable cocktail of potentially-toxic monocarboxylic organic acids as the end-product of anaerobic decomposition (Armstrong *et al.,* 1996; Armstrong & Armstrong, 1999; Armstrong & Armstrong, 2001). These phytotoxic volatile compounds include acetic, butyric, propionic, valeric and caproic acids. Cizkova *et al* (Cizkova *et al.,* 1999) measured total concentrations of monocarboxylic acids as high as 1.6 mM in eutrophic fishponds in the Czech Republic, sufficient to incite severe dieback. In addition to the production of monocarboxylic organic acids, the highly reducing conditions incurred by the decomposition of organic matter can also lead to the production of substantial concentrations of sulphide. Armstrong *et al*. (1996) associated the decline of *Phragmites australis* reedswamp in Lake Ferto (Hungary) with high concentrations of sulphide in the sediment (up to 4 mM).

Armstrong & Armstrong (1999) demonstrated that the toxicity of monocarboxylic organic acids is dependent on pH. The toxicity of the lower-volatile organic acids – such as acetic, propionic, n-butyric and n-caproic acid – is greatest when the acids occur in the undissociated lipid-soluble form. Armstrong & Armstrong (1999) show that, at pH 4.5, 63-70% of organic acids molecules occur in undissociated form whereas, at pH 6, >90% of organic acid molecules occur in the non-toxic ionised form; the exception being propionic acid which was found to have significant phytotoxic effects even at pH 6-7.

Cizkova *et al* (Cizkova *et al.,* 1996) suggest that calcium can have a favourable buffering effect in stands with high organic matter accumulations through the chelation and/or neutralisation of dissolved organic acids. The pH of the bottom sediments in the Norfolk Broads is typically neutral to slightly alkaline – due to high concentrations of calcium and magnesium. This would suggest the existence of a strong acid neutralisation capacity arguably sufficient to mediate any

toxic effects that might be incurred from the accrual of organic acids. The concentration of Ca in the sediment was found to be marginally lower (statistically not significant) in dieback stands than in the non-dieback stands, which would perhaps suggest a lower acid buffering capacity in dieback stands. However, given the very high concentrations of Ca in the sediments and waters of Hickling Broad, this small difference in the buffering capacity is arguably unlikely to have a major effect upon organic acid toxicity in dieback stands. Significantly, Nye (1986) showed that the pH of the rhizosphere of aquatic plants can be substantially lower than that often measured in the immediate hydrosoil. Unfortunately, no measurements of pH were obtained here. However, it is feasible that, even in the neutral/alkaline hydrosoils of Hickling Broad, conditions of low pH may develop in the rhizospheres. Thus, the manufacture of undissociated organic acids (sufficient to induce phytotoxic effects) may only occur in the most organic, mildly acidic, and oxygen starved, sediments. This may explain why dieback was such a highly localised phenomenon in the Broad despite chronic and system-wide eutrophication.

In addition to the potential effects of organic acid accumulation, the conversion of sulphate to various reduced sulphide species in the anoxic sediments of dieback stands may also have a significant phytotoxic effect on plants in Hickling Broad. Armstrong *et al*. (1996) demonstrated that, in *Phragmites australis*, concentrations of sulphide can reduce adventitious root and lateral growth, produce callous blockages and lignification of the vascular system and, in particular, inhibit bud and shoot development. Indeed, in the experiments of Armstrong *et al*. (1996), sulphide was found to have a greater effect on bud and shoot development than phytotoxic concentrations of undissociated acetic acid.

The production of sulphide may be a significant factor in the anoxic sediments of Hickling Broad. Dinka *et al*. (1995) suggested that the high levels of sulphate in brackish waters can lead to high concentrations of sulphide being produced, sufficient to have significant deleterious impacts on reed growth. Hickling Broad is brackish due to the percolation of salt water into the underlying groundwater aquifer. The concentration of SO_4^{2-} in Hickling Broad measured during lake sampling in 2004 was 295.9±8.6 mg l^{-1} – this concentration of sulphate equates to approximately 10% of that found in seawater. Sulphate-reducing bacteria require anaerobic

conditions and function optimally at pH 5.5-9; thus the alkaline hydrosoils of Hickling Broad may promote pronounced microbial reduction of sulphate. Hydrogen sulphide (H_2S) produced in the reduction of sulphate is readily soluble above pH 7 so, in Hickling Broad, it is likely to dissociate and form S^{2-} and HS^-; all three of these sulphide species are highly toxic to plants and it is thus possible that they may also be implicated in the dieback of *Phragmites australis* in Hickling Broad.

Crook *et al*. (1983) found no obvious relationship between the sediment redox potential, sulphide concentrations and regression of both floating and littoral-rooting stands of *Phragmites australis* in several of the Norfolk Broads. However, as the floating reedswamp growth-habit does not root in the sediment this is perhaps not unexpected. Sulphide toxicity in the sediment of Hickling Broad may be offset by the high concentrations of Fe in the sediment. In anoxic sediments, the Fe (III) is readily reduced to soluble Fe (II). Fe (II) can bind with sulphide and precipitates as FeS. FeS is significantly less toxic to plants than the soluble sulphide species. Phillips *et al*. (1999) suggest that Fe (II) is readily precipitated as FeS in the sediments of the Norfolk Broads and believe the formation of FeS over $FePO_4$ is one of the factors perpetrating the often high release of soluble reactive phosphorus from the bottom sediments of these lakes. Interestingly, van der Welle *et al*. (2006) found that sulphide immobilisation by Fe (II) was most effective at moderate Fe (II) concentrations but, significantly, at high Fe (II) concentrations, aquatic plants can be prone to Fe toxicity. Batty & Younger (2003) reported that a threshold concentration of 1 mg Fe (II) l^{-1} was sufficient to inhibit seedling growth in *Phragmites australis* – which may, in the context of Hickling Broad, explain the lack of regeneration. Thus, Fe (II) toxicity in anoxic sediments may also be a further factor associated with localised dieback of *Phragmites australis* in the Hickling Broad, particularly as the lake receives inputs of iron-rich ochre from the surrounding fen and marsh lands.

The dieback of *Phragmites australis* reedswamp in European lakes (including the Norfolk Broads) has also been linked to wildfowl grazing pressure. Prater (1995) suggested that the reedswamp decline observed in the Thurne Broads could be attributed to grazing wildfowl (including moulting Greylag geese (*Anser anser*)). However, as wildfowl generally flock in

sheltered bays where organic and anoxic sediments also occur, it is difficult to attribute cause and effect to these two competing hypotheses. It indeed may be the case that grazing by wildfowl exacerbates dieback of reed already exposed to phytotoxic stressors. However, interestingly, Van der Wyngaert *et al*. (2003) demonstrated that long-term grazing by moulting Greylag geese (*Anser anser*) on *Phragmites australis* in two Dutch marshes had a positive impact on plant performance, particularly on shoot emergence and regrowth. This would therefore seem to cast some doubt on the role of avian grazing in perpetuating the decline of reedswamp in the Norfolk Broads.

These expeditious results presented here suggest that eutrophication may be a significant, if indirect, cause of reed dieback in Hickling Broad. The localised accretion of organic matter in *Phragmites australis* stands, and the consequential generation of hypoxic conditions and the accumulation of organic acids, may be a key factor in the explanation of recent episodes of reed dieback. Sulphide and iron (II) toxicity may also be injurious to the plant health. However, little is known at present about the prevalence of these compounds in the lake (or any other of the Broads for that matter) and this is therefore a priority area for further research. Moreover, it would also seem pertinent to evaluate the effect of such phytotoxins on the growth and stability of other aquatic plants and, in particular, the submerged macrophyte community, as phytotoxin effects may, in part, also explain some of the current instabilities associated with these species in the lake. Vanwijck (1992) and Morris *et al* (2003), for example, have shown through laboratory experiments that organic matter accretion and sediment anoxia is severely detrimental to the growth of both *Vallisneria americana* and *Potamogenton pectinatus*.

7.5.6 Remote Sensing for Monitoring Reedswamp Dieback

The research presented here examined the novel and expeditious application of remote sensing for the assessment of wetland plant physiological status. This evaluation was conducted in the context of reedswamp dieback in the Norfolk Broads. It was clearly demonstrated that spectral reflectance (or radiance) based metrics could be constructed for the quantification of chlorophyll-a in plant leaves as a measure of physiological status. It would also seem possible to extrapolate these indices to the canopy scale, using either *in-situ* field-

based spectrometry or airborne CASI-2 imagery, in order to achieve a spatially synoptic understanding of plant ecophysiological responses to environmental conditions for example, in this instance, to spatial variability in nutrient enrichment and cycling.

The direct and pre-emptive identification of reed stress in relation to eutrophication pressures was not possible here, largely due to timing of the lake surveys (i.e. seemingly after dieback had occurred). The typically positive response of plants to the accretion of organic matter and nutrients is also likely to complicate the identification of stress in this situation, although the recognition of "overly" vigourous plants may provide a useful marker for delineating areas of reedswamp potentially at risk of collapse and could be used to inform further ground-based investigations.

7.6 CONCLUSIONS

The novel use of remote sensing for characterising spatial heterogeneity in aquatic plant ecophysiology was examined in the context of the response of *Phragmites australis* reedswamp to nutrient enrichment in Hickling Broad (UK). It was shown that the formulation of indices based on spectral reflectance band-ratios in the red and VNIR, or indices based upon the first-derivative transformation of reflectance data (i.e. [Red Edge$_\lambda$]), could be strongly related to the concentration of chlorophyll-a in plant leaves as a measure of plant physiological status (max. R^2 = 0.95). It was further shown that the extrapolation of these indices to the canopy scale, using *in-situ* and airborne remote sensing, enable the ecophysiological response of *Phragmites australis* plants to be linked to highly localised spatial variations in nutrient enrichment and cycling (i.e. sediment focusing). Variation in reedswamp vigour was typically positively correlated with the organic matter content and nutritional status of the lake sediment. The calibration of airborne CASI-2 remote sensing imagery enabled patterns in the ecophysiological response of *Phragmites australis* in Hickling Broad to this nutrient enrichment to be examined at an unprecedented lake-scale.

A statistical comparison of the sediment chemistry in reed stands exhibiting symptoms of recent dieback, and those where no evidence of dieback could be observed, revealed an association

between organic matter and nutrient enrichment and plant regression. In stagnant waters, the accumulation of organic matter in reed belts, may promote microbial activity and hence the generation of anoxic conditions in plant rhizospheres. It is hypothesised that in these hypoxic sediments, the accumulation of phytotoxic agents formed as by-products from anaerobic microbial decomposition, or the generation of reduced sulphate and iron species, may be the underlying cause of recent reed decline and non-regeneration in the lake.

It is clear that the remote sensing of plant ecophysiology is a novel and potential valuable approach for assessing the response of shallow lake systems to environmental change. These lake-scale vistas afforded by remote sensing technologies may, as here, be able to provide new and important spatial insights into ecosystem processes and, significantly, may be able to realise the timely diagnosis of stressors on ecosystem function.

8 GENERAL DISCUSSIONS AND CONCLUSIONS

8.1 INTRODUCTION

This chapter provides a synthesis of the research presented in this thesis. The rationale for the project is initially readdressed and the results obtained from the various proof-of-concept type studies presented herein are subsequently evaluated within this overarching conceptual framework. The implications of these results for the use of remote sensing in shallow lake ecology is discussed and, in particular, in the context of the European Union Water Framework Directive (2000/60/EC). The chapter, and thesis, then concludes with a more general deliberation with regards to the use of remote sensing in the study of lakes and other aquatic ecosystems and the identification of priorities for future research and development.

8.2 SHALLOW LAKES AND REMOTE SENSING

8.2.1 Shallow Lakes and the Monitoring of Ecological Status

Shallow lakes are an important ecological and socio-economic resource and provide many invaluable ecosystem services (Peterson *et al.,* 2003; Maler *et al.,* 2003). The impact of human activities, both at the lake and catchment scale, has precipitated fundamental changes in many shallow lake ecosystems, in the UK, Europe, and beyond and, as such, the ecological status of many shallow lakes has declined in response to these pressures. There is now an unprecedented interest in measuring and monitoring the ecological status of shallow lakes and, indeed, aquatic ecosystems in general, either in response to perturbation, or as a means of assessing the success of restoration activities.

Shallow lakes of good ecological status are often characterised by an abundance and diversity of aquatic plants, particularly submerged species, which fulfil important roles in sustaining key ecosystem processes (e.g. biogeochemical cycling) and functions (e.g. habitat provision). The ecological status of many shallows lakes has, however, been adversely affected by the impacts of eutrophication and, in many systems, nutrient enrichment has led to the development of nuisance phytoplankton blooms and the competitive exclusion of submerged aquatic plants.

The occurrence of potentially-toxic cyanobacterial blooms in shallow lakes is considered to be symptomatic of ecosystems suffering from the chronic effects of nutrient enrichment. The ecological status and trajectory of shallow lakes is thus largely conditioned by these dynamic shifts in the biotic regime (Scheffer *et al.,* 1993; Scheffer, 1998; Scheffer, 1998; Van Nes *et al.,* 2007; Scheffer & Jeppesen, 2007).

Shallow lakes are spatially complex and transient systems and the assessment and monitoring of ecological status in these environments is likely to be significantly hindered by the impracticalities – in terms of both time and resources – of obtaining accurate, but yet extensive, datasets in the face of considerable ecosystem heterogeneity. In this context, it has been suggested that remote sensing could make a significant contribution to the assessment, monitoring and policing of ecological status in lakes, rivers and transitional waters (Chen *et al.,* 2004; Gilvear *et al.,* 2004a; Gilvear *et al.,* 2004b; Valta-Hulkkonen *et al.,* 2005; Rowan *et al.,* 2006; Scanlan *et al.,* 2007; Gilvear *et al.,* 2007).

It has been shown that remote sensing can be used to monitor various (i) physical, (ii) bio-chemical and (iii) biotic elements in lakes that are of direct relevance to ecological investigations and the assessment of ecological status. However, many of these studies, for technological reasons or otherwise, have been conducted in large and/or deep lake systems. Little consideration, until now, has been given to the application of remote sensing in small and very shallow lakes and, furthermore, seldom has the derived data been used to address specific ecological questions. This thesis sought to further examine the application of remote sensing for the assessment of ecological status in shallow lakes through the development and application of techniques designed for measuring and monitoring important abiotic (e.g. tripton, CDOM, water transparency) and biotic (phytoplankton and aquatic plants) elements.

8.2.2 Abiotic Elements

The ecological status of shallow lakes, and the integrity of the ecosystem services which they provide, is dependent on many processes that operate at a variety of spatial and temporal scales. The capability of remote sensing to deliver information pertaining to some of these key

processes will, to a greater or lesser extent, determine its efficacy for the assessment of ecological status in shallow lakes and, moreover, will also determine the novelty and value of any derived insights into lake-scale processes and function.

The cycling of suspended sediment (tripton) in shallow lakes is a key process that has significant linkages to (i) the ambient light climate, (ii) the internal loading of nutrients, and (iii) the fate and behaviour of sediment-bound contaminants. Organic detritus also represents an important carbon source for heterotrophic organisms. The suspended sediment dynamics of shallow lakes can therefore have a profound influence on the biology of shallow lakes. It was shown in this thesis (**Chapter 3**) that remote sensing can be used to quantify the concentration of SPM in shallow lakes. Hyperspectral measurements of remote-sensing-reflectance were obtained from the Upper Thurne and Barton Broads (Norfolk, UK) and used to formulate empirical indices for the quantification of SPM and, further, to assess the relative contributions of inorganic and organic particulate matter to the total SPM load.

The accuracy to which remote sensing could be used to quantify SPM was somewhat dependent on the nature and concentration of the material in suspension. The quantification of (total) SPM and SPIM was readily achievable. Linear and non-linear least-squares regression analysis provided coefficients of determination of R^2 = 0.54-0.99 for the fit against measured concentrations. The most successful algorithms were generally constructed using the value of $R_{rs}(0+,\lambda)$ in wavelengths positioned on the VNIR plateaux (i.e. > 700 nm). The inorganic fraction is arguably the most optically-active component of tripton in lakes (high backscattering) and it is likely that it is this fraction that is responsible for the strong relationships observed with total SPM in the VNIR. Indeed, the sensitivity of the VNIR plateaux to variations in the SPIM load has been noted by previous authors (Curran & Novo, 1988; Pierson & Strombeck, 2001; Dekker *et al.,* 2001; Ammenberg *et al.,* 2002).

The quantification of SPOM would appear to be more problematic. In shallow lakes, where the concentration of SPOM and phytoplankton biomass does not necessarily co-vary, i.e. due to the pronounced resuspension of detritus, the estimation of SPOM may not always be readily

achievable. Good coefficients of determination were observed between the concentration of SPOM and $R_{rs}(0+,\lambda)$ (R^2 = 0.40-0.89) – but it is likely that the derived relationships were significantly dependent on the degree of covariance observed with other bio-optically active components. Indeed, in the absence of a strong correlation with chlorophyll-a or SPIM, the ability of remote sensing to estimate the concentration of suspended organic particulate matter was poor. Similar conclusions have been reached by previous authors (Pierson & Strombeck, 2001) and, as such, it is apparent that further work will be required to improve the estimation of SPOM from remotely sensed data.

Lakes are an important carbon store and make a significant contribution to the global cycling of carbon (Mulholland & Elwood, 1982; Biddanda & Cotner, 2002; Kortelainen *et al.,* 2004; Cole *et al.,* 2007) changes in the pool of dissolved organic carbon in lakes is therefore an important indicator of ecosystem function. This thesis examined that use of remote sensing for the quantification of coloured dissolved organic matter in shallow lakes (**Chapter 3**). It has been demonstrated by previous authors that remote sensing can be used to provide regional-scale determinations of coloured dissolved organic matter in lakes (Kutser *et al.,* 2005b; Menken & Brezonik, 2006). However, the estimation of CDOM in the shallow lakes of the Norfolk Broads proved problematic and an effective algorithm for estimating the CDOM absorption coefficient could not be formulated. It is suggested that is was due to the low and invariable concentrations of dissolved organic matter found in the Norfolk Broads. Interference from other optically-active components (algal pigments) is also likely to have been an additional complication. Remote sensing could contribute much to the regional-scale monitoring of dissolved organic carbon in lakes and thus the improved formulation of operational remote sensing algorithms for the quantification of CDOM should be made a future research priority.

The measurement of water transparency – in the form of the Secchi disc depth – is a simple but, nevertheless, important measure of the ambient light climate in lakes and is still used routinely for lake monitoring purposes. It was shown that the SDD can be readily estimation from remotely sensed data (**Chapter 3**). Algorithms formulated using the value of $R_{rs}(0+,\lambda)$ at 620.5 nm (R^2 = 0.93) and $dR/d\lambda$ at 640 nm (R^2 = 0.96) were found to effective for the estimation

of the SDD. Algorithms employing wavelengths positioned on the VNIR plateaux were also noted to be suitable for the estimation of the SDD.

The results outlined above clearly demonstrate that remote sensing has the potential to provide information on specific water quality elements that are of relevance to the understanding of shallow lake ecology and function. However, the derivation of such information at the regional scale (i.e. pan-European) will require the further develop of operation algorithms for the estimation of these parameters using current satellite technologies (e.g. MERIS, MODIS). The formulation of semi- or fully-analytical algorithms from bio-optical model simulations should be considered in future work (e.g. Dekker *et al.,* 2002).

8.2.3 Biotic Elements

8.2.3.1 Phytoplankton

Phytoplankton are an important component of the biological diversity of shallow lakes and fulfil an important role in carbon fixation and other key biogeochemical cycles. In many shallow lakes, particularly those with a legacy of nutrient enrichment, the development of mass populations of phytoplankton is a common problem. Moreover, for various reasons, highly eutrophic shallow lakes are often dominated by blooms of potentially-toxic cyanobacteria. The size and composition of the phytoplankton assemblage is therefore a key measure of ecological status in shallow lakes.

The use of remote sensing for estimating the concentration of chlorophyll-a in lakes has received considerable attention. However, in shallow, optically-complex, lakes results have often been disappointing (Liu *et al.,* 2003; Tyler *et al.,* 2006). In addition, the retrieval of chlorophyll-a concentrations from remotely sensed data can say little in regards to the floristic composition of phytoplankton assemblages.

Hyperspectral remote sensing measurements of $R_{rs}(0+,\lambda)$ were used to derive algorithms for the estimation of chlorophyll-a in the shallow lakes of the Norfolk Broads (**Chapter 3**). Various semi-empirical approaches to algorithm formulation were examined; these included green/blue

and NIR/red band-ratios and more novel indices derived from first-derivative and continuum-removal analysis. The multi-temporal robustness of the algorithms was assessed using independent validation data. Algorithms using multivariate subsets and partial least-squares regression models were also examined. The various algorithm formulations had a significant influence on the accuracy to which the concentration of chlorophyll-a could be estimated.

The green/blue band-ratios, often used in CASE I algorithms, were generally ineffectual for the estimation of chlorophyll-a. Improved results were observed using algorithms based upon NIR/red band-ratios. The performance of the NIR/red band-ratio algorithms varied considerably between the various multi-temporal datasets (R^2 = 0.46-0.80). The variability in the performance of the algorithms is difficult to explain, but it would seem possible that changes in the optical properties of the lakes (tripton backscattering, bottom reflectance) may have influenced algorithm performance. This observation was confirmed using sensitivity analyses based on simulations performed with the Hydrolight v.4.2 bio-optical model.

The algorithms formulated using first-derivative indices also demonstrated good relationships with the concentration of chlorophyll-a and, in comparison to the NIR/red band-ratio algorithms, would seem to retain greater multi-temporal transferability. The increased robustness of algorithms derived using first-derivative indices would seem to be due to a reduced sensitivity to changes in other non-co-varying bio-optically components (e.g. tripton). This observation was again substantiated using Hydrolight v.4.2. The algorithms formulated using indices derived from continuum-removal analysis also demonstrated reasonable relationships with the concentration of chlorophyll-a, but were typically not as effective as the NIR/red band-ratio or first-derivative algorithms. Multivariate regression models, utilising greater wavelength information, were shown to improve the accuracy of chlorophyll-a estimation from remotely sensed data. However, the empirical nature of these multivariate regression models means that the derived algorithms lack mechanistic clarity and, on this basis, may be unsuitable for more routine use.

The expeditious results derived from the shipboard-spectrometry surveys in the Norfolk Broads demonstrate that the determination of the chlorophyll-a concentration from remotely sensed data is possible in optically-complex shallow lakes. However, as chlorophyll-a is common to the vast majority of phytoplankton species, it cannot be used to derive information regarding the floristic composition of the phytoplankton community. The development of techniques for the detection and diagnosis of phytoplankton community composition has long been an objective for both limnological and, indeed, oceanographical remote sensing. The potential of remote sensing for the detection of phytoplankton community structure was examined through the use of novel mesocosm experiments and subsequent validation using data from the shallow lakes of the Norfolk Broads (**Chapter 4**).

The mesocosm experiments were used to simulate variable communities composed of four representative colour group taxa: brown (diatom spp.), green (*Scendesmus armatus*, *Selenastrum capricornatum*), blue-green (*Cylindrospermopsis raciborskii*, *Synechococcus* spp.) and red (*Synechococcus* spp.). Spectral reflectance measurements were acquired and PCA and MDA analyses were used to explore the spectral dissimilarities of the various pseudo-communities. It was shown that the respective colour group species differed significantly in terms of their spectral characteristics. These dissimilarities were attributed largely to variability in their absorption (a function of photopigment composition) and backscattering (a function of cell morphology) efficiencies. In particular, it was observed that cyanobacteria could be distinguished from other algal species, largely because of the diagnostic biomarker pigment C-phycocyanin. These dissimilarities were preserved in pseudo-communities composed of mixed species and it was shown that remote sensing could be potentially used to monitor succession between states of diatom, green and blue-green dominance in lakes. To the best of the author's knowledge, this is the first time that this capability has been demonstrated experimentally, or otherwise, in the context of lakes or coastal waters. The MDA analysis further evidenced that a simple ordination-based classification scheme could be developed to diagnose the dominant composition of algal blooms in lakes.

In addition to these qualitative approaches, algorithms were derived from the experimental mesocosm data using least-squares regression analysis for the quantification of specific biomarker pigments (fucoxanthin and C-phycocyanin). The concentration of these biomarker pigments was shown, albeit experimentally, to be quantifiable using remote-sensing-based algorithms formulated using simple band-ratio and first-derivative approaches (R^2 = 0.89-0.97). However, the robustness of the derived algorithms was shown to be greatly affected by the coincidental presence of other bio-optically active components (SPM and CDOM). These effects were particularly pronounced if variable concentrations of both SPIM and SPOM were introduced into the mesocosm experiments. These results reiterate some of the observations drawn from **Chapter 3**.

The capability to retrieve estimates of biomarker pigments from remotely sensed data was validated using shipboard measurements of $R_{rs}(0+,\lambda)$ in the Norfolk Broads. The formulation of an algorithm employing the [$R_{rs}(710)/R_{rs}(638.5)$] band-ratio was shown to be effective for the quantification of C-phycocyanin (R^2 = 0.96). The quantification of fucoxanthin was more problematic. However, an algorithm formulated using the [$R_{rs}(710)/R_{rs}(470)$] band-ratio was found to be sensitive to variations in fucoxanthin in waters where fucoxanthin:chlorophyll-a > 0.2 (R^2 = 0.94). However, due to the overlap in the absorption spectra of fucoxanthin and chlorophyll-a, the index was also highly correlated with the concentration of chlorophyll-a (R^2 = 0.90), and thus the sensitivity of this particular index to fucoxanthin should be interpreted with caution. These results substantiate that the detection of phytoplankton community composition from remotely sensed data, albeit at a broad level, can be achieved (Hunter *et al.,* 2007).

The detection and, indeed, quantification of cyanobacterial abundance in lakes would seem to be immediately achievable and substantial research is now being directed towards this goal (Simis *et al.,* 2005; Yang & Pan, 2006; Sridhar & Vincent, 2007; Simis *et al.,* 2007). The realisation of remote-sensing-based techniques for the detection of cyanobacterial blooms would represent a significant advancement for the assessment of ecological status and, further, the monitoring of cyanoHABs in lake and other inland waters. The spectral resolution of other taxonomic groups (e.g. diatoms, chlorophytes, red-tide species), through biomarker pigment

approaches, or otherwise, should be given further consideration in future studies. There is emerging evidence from ocean-colour research that phytoplankton functional types (e.g. microplankton, nanoflagellates) have characteristic bio-optical traits (photosynthetic quantum efficiencies, pigment ratios) that may be of use to the remotely-sensed detection of phytoplankton community structure (Fishwick *et al.,* 2006; Aiken *et al.,* 2007). Similar approaches should be pursued for the phytoplankton assemblages of lakes. The acquirement of long-term remote sensing datasets, paired with detailed floristic information (cell counts, pigments), would be of immense value to such work. In this context, opportunities for remote sensing campaigns to "piggy-back" existing long-term lake monitoring programmes should be explored.

The development of algorithms for the quantification of chlorophyll-a and other bio-optically active accessory pigments was pioneered in **Chapter 3** and **Chapter 4** using high spectral resolution *in-situ* measurements of $R_{rs}(0+,\lambda)$. The derived techniques were then examined in a more applied context using airborne remote sensing (CASI-2 [SeaWiFS]) imagery to explore spatial and temporal variations in the phytoplankton community of the Upper Thurne and Barton Broads (**Chapter 5**). Various contrasting approaches to the analysis of the multispectral CASI-2 [SeaWiFS] imagery were explored, including the derivation of algorithms employing band-ratio and continuum-removed indices and, further, novel approaches based upon complex solutions to linear spectral mixing models.

The algorithms formulated using water-leaving-radiance NIR/red CASI-2 [SeaWiFS] band-ratio approaches were shown to be effective for the quantification of both chlorophyll-a and C-phycocyanin. The optimum algorithm for the quantification of chlorophyll-a was derived from a CASI-2 [SeaWiFS] acquired on 29 August 2005 using the $[L_w(710)/L_w(670)]$ band-ratio. This algorithm yielded a coefficient of determination of $R^2 = 0.96$ for the fit against the measured concentration of chlorophyll-a. The RMSE obtained for the validation of the derived algorithm on further CASI-2 [SeaWiFS] imagery acquired on 28 February 2005, 21 April 2005 and 22 June 2005 were 11.08, 3.38 and 3.53 mg chlorophyll-a m^{-3} respectively. This multi-season

validation indicates that the performance of the chlorophyll-a NIR/red band-ratio algorithm was robust despite inherent variability in water quality.

The optimum algorithm derived for the quantification of C-phycocyanin was derived from a CASI-2 [SeaWiFS] image acquired on 29 August 2005 using the [$L_w(710)/L_w(620)$] band-ratio. This algorithm yielded a coefficient of determination of R^2 = 0.95 for the fit against the measured concentration of C-phycocyanin. The RMSEs obtained for the validation of the derived algorithm on further CASI-2 [SeaWiFS] imagery acquired on 21 April 2005 and 22 June 2005 were 6.63 and 9.03 mg C-phycocyanin m^{-3} respectively. This indicates that the algorithm was again robust. However, the errors observed for the validation of the C-phycocyanin algorithm were slightly higher than those for observed for chlorophyll-a. Other workers have suggested that the estimation of C-phycocyanin from remotely sensed data may be affected by the C-phycocyanin:chlorophyll-a or C-phycocyanin:chlorophyll-b ratio and variability in the C-phycocyanin specific-absorption coefficient (Simis *et al.,* 2005; Simis *et al.,* 2007). Changes in the relative contribution of cyanobacteria to total phytoplankton biomass, and physiological status, may have been responsible for the moderate variations observed in algorithm performance. In this context, further work is required to determine the limit of detection for C-phycocyanin in lakes. Moreover, the robustness of the concentration of C-phycocyanin as a quantitative biomarker for cyanobacteria is still somewhat unknown. This should be addressed in future studies, particularly in relation to variability in the ambient light climate and/or nutritional (particularly N) status.

Interestingly, these results somewhat contradict those observed using the algorithms derived from the *in-situ* $R_{rs}(0+,\lambda)$ measurements, which were far less robust than the algorithms derived from the CASI-2 [SeaWiFS] data (**Chapter 3)**. This may suggest the existence of scale effects. However, it should also be acknowledged that the algorithms were not derived from common datasets and any direct comparisons made between algorithms may be misleading.

The algorithms derived from spectral mixing, angle mapping and continuum-removal models (MTMF, LSMM, SAM) also demonstrated good relationships with the concentration of

chlorophyll-a and C-phycocyanin (R^2 = 0.68-0.83). Indeed, the spectral mixing and angle mapping models derived from the 21 April 2005 and 22 June 2005 CASI-2 [SeaWiFS] imagery outperformed the NIR/red band-ratio algorithms for the estimation of chlorophyll-a. However, it was noted that the model solutions used to parameterise the algorithms were essentially scene-dependent; this required the algorithms to be re-formulated for each independent dataset. This lack of robustness would seem to preclude the routine use of such algorithms. The resilience of the algorithms may have been improved with the use of a larger dataset for calibration purposes or, indeed, if the spectral mixing models had been populated using data derived from a suitable bio-optical model. This could be considered further in future studies.

The optimum NIR/red band-ratios algorithms for the estimation of chlorophyll-a and C-phycocyanin were applied to the seasonal time-series CASI-2 [SeaWiFS] imagery of the Upper Thurne and Barton Broads (**Chapter 5**). The calibrated images pertinently demonstrate the pronounced spatial variability that can occur in phytoplankton communities and, in this, instance, even within a series of small and well-mixed shallow lakes (Figure 5.17 and Figure 5.18). The calibrated CASI-2 [SeaWiFS] image of chlorophyll-a in the Upper Thurne Broads on 28 February 2005, for instance, shows marked inter-lake variability in phytoplankton biomass. It is particularly striking that the annual chlorophyll-a maximum can be seen occurring on Hickling Broad contemporaneous to the annual chlorophyll-a minimum on Horsey Mere; this is despite the fact the two lakes form part of the same hydrological system and are located less than 5 km apart.

The calibrated CASI-2 [SeaWiFS] chlorophyll-a and C-phycocyanin images captured on 29 August 2005, in contrast, show pronounced intra-lake variability in phytoplankton biomass. This variability was particularly apparent in Barton Broad due to the development of a bloom of the potentially-toxic cyanobacterium *Microcystis aeruginosa*. The characterisation of such spatial variability in phytoplankton biomass could not have been achieved using conventional lake-sampling approaches. The seasonal CASI-2 [SeaWiFS] images aptly demonstrate the merits of remote sensing as a tool for lake monitoring particularly, as is shown here, at the regional-scale.

Airborne remote sensing reconnaissance was subsequently used in a more applied context to explore the spatial ecology of the potentially-toxic and bloom-forming cyanobacterium *Microcystis aeruginosa*. High temporal resolution CASI-2 [SeaWiFS] imagery was captured and used to examine diurnal changes in the distribution of a *Microcystis aeruginosa* bloom on Barton Broad on 29 August 2005. Diurnal time-series CASI-2 [SeaWiFS] images acquired over Barton Broad at 09:30 h, 12:00 h and 16:00 h GMT on 29 August 2005 demonstrated that buoyant *Microcystis aeruginosa* colonies were passively evading the light-starved conditions encountered in the turbid waters through the formation of near-surface accumulations. The formation of these near-surface accumulations as evidence by the CASI-2 [SeaWiFS] imagery was shown to correlate with the wind speed; wind speeds > 4 m s^{-1} appeared to be sufficient to induce turbulent mixing and thus cause the dispersal of near-surface aggregations and entrain colonies in deeper waters. Moreover, the CASI-2 [SeaWiFS] imagery revealed that the formation of these near-surface aggregations was highly spatially variable across the lake. Indeed, in areas where the complexities of the near-shore morphometry created regions of more stagnant water, persistent near-surface accumulations were observed. It is suggested that these regions of near-stagnant water may have been important for the development and persistence of the *Microcystis aeruginosa* bloom. In this context, time-series remote sensing was able to provide new and novel insights into the spatial dynamics of cyanobacteria in shallow lakes that would have been otherwise unobtainable.

The capability of remote sensing as a tool for monitoring phytoplankton communities in shallow lakes was aptly demonstrated in the Norfolk Broads. It was shown that the concentration of chlorophyll-a and other, taxonomically-significant, pigments may be quantified using empirical or semi-empirical remote sensing algorithms. The extrapolation of these techniques to airborne CASI-2 imagery products yielded high resolution, spatially and temporally resolving, regional-scale panoramas of phytoplankton dynamics in the Upper Thurne and Barton Broads. Airborne surveillance is a pertinent tool for expeditious research and, as demonstrated in the context of potentially-toxic cyanobacterial blooms, in the provision of a rapid-reactionary monitoring response. However, the high operational costs of airborne surveillance would prohibit its use in

the routine monitoring of lakes. The further development of satellite-based algorithms for the estimation of chlorophyll-a (and other pigments) in lakes should be a priority for future studies. In this context, work is on-going to develop and refine operational chlorophyll-a algorithms for current satellite sensors such as ESA's MERIS and NASA's MODIS for applications in CASE II waters (Gons *et al.,* 2002; Pozdnyakov *et al.,* 2005; Giardino *et al.,* 2005; Doerffer & Schiller, 2007; Krawczyk *et al.,* 2007; Shutler *et al.,* 2007). Nonetheless, to maximise the potential of remote sensing for the monitoring of phytoplankton in lakes, satellite instruments with spectral capabilities equivalent to MERIS and SeaWiFS, but with greatly improved spatial resolving capabilities (i.e. < 30 m) will be needed to effect full operational remote-sensing-based monitoring of phytoplankton in lakes.

8.2.3.2 Aquatic Vegetation

The abundance and composition of aquatic vegetation is a major control on the ecological status of shallow lake ecosystems. Submerged, floating and emergent aquatic plants fulfil many important ecological functions in shallow lakes and, in particular, in the provision of a sink environment for excess nutrients, the immobilisation of aquatic-borne contaminants and in the creation of important habitat niches and refuges for other lake biota. In many shallow lakes, eutrophication has resulted in the loss of aquatic plant cover, particularly of submerged species. The reestablishment of submerged aquatic plants is considered to be a key objective for lake restoration strategies. The abundance and distribution of aquatic vegetation is therefore a key measure of the ecological status of shallow lakes.

The development of remote-sensing-based methodologies for the mapping of aquatic plants in shallow lakes would represent a significant development for the regional-scale assessment of shallow lake ecological status. However, to date, remote sensing has found only limited application in this context. The efficacy of remote sensing for mapping aquatic vegetation in shallow lakes was therefore explored further in this thesis. Hyperspectral *in-situ* reflectance measurements and airborne remote sensing data were used to examine the spectral characteristics of aquatic plant growth-habits and species in the Upper Thurne region of the

Norfolk Broads and determine the utility of remote sensing data for use in aquatic plant audits (**Chapter 6**).

The hyperspectral reflectance signatures of four freshwater macrophyte species (*Chara baltica*, *Nuphar lutea*, *Hippuris vulgaris* and *Phragmites australis*) with constrasting growth-habit characteristics were examined using *in-situ* spectrometry. These reflectance signatures were also compared to those of non-vegetated clear and turbid water. The reflectance signatures of the various macrophyte species were found to demonstrate some notable dissimilarities. These were most apparent in the "green-peak" (500-600 nm), red-edge (680-720 nm) and VNIR plateaux (> 720 nm) regions. This was further explored using PCA ordination analysis. The score-plots derived from the PCA analyses provided further evidence that the aquatic plants species examined were spectrally differentiable. The reflectance signatures of the emergent species *Phragmites australis* and the floating species *Nuphar Lutea* were notably different from those of the other macrophytes species and the spectra obtained from non-vegetated clear and turbid water. The spectral signatures of the partially-emergent species *Hippuris vulgaris* and the submerged *Chara baltica* species were also readily distinguished from those of the other macrophyte species. However, a degree of overlap could be perceived between the spectral signatures of the submerged and partially-emergent plants and the spectra obtained from areas of clear or turbid water where aquatic plants were absent.

The distribution of aquatic plant growth-habit associations and species was subsequently mapped in the shallow lakes of the Upper Thurne using airborne CASI-2 [Vegetation] data. Three contrasting classification models were compared. These included algorithms derived using Euclidean Minimum Distance (EMD), Maximum Likeihood (MLC) and Support Vector Machine (SVM) methodologies. The algorithms were initially used to classify the aquatic vegetation in the Upper Thurne system into four growth-habit categories: (i) emergent, (ii) partially-emergent, (iii) floating and (iv) submerged. The classifications accuracies for the EMD algorithm were poor (overall accuracy < 45%; $\kappa = 0.09$). Examination of the derived confusion matrix demonstrated indicated that the EMD algorithm frequently misclassified partially-emergent species (*Hippuris vulgaris*, *Potamogeton* spp.) and areas of turbid water without any

aquatic plant coverage. However, excellent classification accuracies were achieved with both the MLC and SVM algorithms (overall accuracy > 97%; κ > 0.73). These results clearly demonstrate that remote sensing could be used to map the distribution of aquatic plant growth-habits in shallow lakes. The high accuracies observed were no doubt fostered by the broad nature of the classification scheme. Nonetheless, changes in the distribution and cover of the various aquatic plant growth-habits would be of relevance as an indicator of ecological status in shallow lakes.

The CASI-2 [Vegetation] imagery was also used map the dominant species composition of aquatic plants beds in the clear water Martham Broads. The three contrasting classification models were again applied. The classification accuracy achieved with the EMD algorithm was again the poorest observed (72.2%; κ = 0.66). Higher classification accuracies were achieved with the MLC (78.0%; κ = 0.73) and, in particular, the SVM (87.1%; 0.84) algorithms. The classification accuracies achieved were probably slightly biased by the size of the training and validation sets used, particularly as these were more easily defined for *Chara* spp. beds, than for *Hippuris vulgaris* or *Nitellopsis obtusa*. However, it is notable that submerged *Chara* spp. beds could be easily delineated in the CASI-2 [Vegetation] imagery and, further, that the two dominant species encountered were spectrally distinguishable. This suggests that, in clear and shallow waters, it may be possible to diagnose the dominant species composition of submerged aquatic plants beds. Similar observations were made by Malthus & George (1997) and Williams *et al*., (2003). Variations in water depth and transparency are likely to be an important constraint on the detection of submerged aquatic plants in shallow lakes. This was evident in the examination of the CASI-2 [Vegetation] imagery of Hickling Broad where the detection of submerged *Chara* spp. beds was problematic in waters where the SDD was < 0.5 m.

The results achieved in the Norfolk Broads, albeit based on a limited number of aquatic plant species, suggests that remote sensing surveillance has much to offer for the survey of aquatic vegetation in lakes. However, significant further work will be required in this context before remote sensing can be used routinely for aquatic plant surveys in lakes. The development of a comprehensive spectral library for aquatic plants would be hugely beneficial for remote sensing

survey purposes; there is currently a dearth of information on the spectral characteristics of aquatic plant species. In addition, the effect of variations in water depth and transparency on the detection of submerged aquatic plants also needs to be more accurately established.

The potential capability of remote sensing as a tool for regional-scale survey of aquatic vegetation in lakes was developed further in **Chapter 7** through the novel use of laboratory darkroom and *in-situ* spectrometry data and airborne CASI-2 [Vegetation] imagery for the physiological assessment of emergent aquatic vegetation in shallow lakes. *Phragmites australis* reedswamp is an important functional component of shallow lake ecosystems. However, over recent decades, there has been a large-scale decline in the reedswamp habitat in many European shallow lakes. In many instances this decline has been linked to nutrient enrichment (Armstrong & Armstrong, 2001). In the Norfolk Broads, for example, the extent of reedswamp is known to have declined by > 75% between 1880 and 1977 (Boorman & Fuller, 1981). In this thesis, remote sensing technologies were employed to examine spatial variations in the performance of *Phragmites australis* and, subsequently, to attempt to relate observed variations in plant performance to underlying environmental factors.

Spectral reflectance measurements were acquired under darkroom conditions from *Phragmites australis* leaves harvested in Lake Balaton and used to examine the spectral response of plants to stress-related variations in leaf pigmentation. It was shown that changes in the pigmentation of the *Phragmites australis* leaves caused marked variations in the measured spectral response. A suite of spectral reflectance indices were subsequently calculated from the spectral reflectance measurements made in Lake Balaton and their sensitivity to variations in the chlorophyll-a content of the *Phragmites australis* leaves was examined using least-squares regression analysis. Many of the spectral indices examined demonstrated excellent relationships with the concentration of chlorophyll-a in the leaves. In particular, the chlorophyll red edge index, [Red-Edge$_\lambda$], exhibited a strong relationship with foliar chlorophyll-a (R^2 = 0.95). These results demonstrate that the assessment of physiological status in aquatic plants, albeit it at the leaf-scale, is achievable using hyperspectral remote sensing imaging.

The chlorophyll-a algorithm derived from the Lake Balaton dataset was used to subsequently calibrate Red-Edge$_\lambda$ index values obtained from darkroom spectral reflectance measurements made from *Phragmites australis* leaves harvested from plants in Hickling Broad. The calibrated dataset was also used to assess the sensitivity of a further series of spectral indices not previously calculated from the Lake Balaton dataset. The same spectra indices were also calculated from the canopy-scale spectral reflectance measurements made in Hickling Broad. The complete flotilla of spectral indices was correlated against various sediment chemistry parameters (e.g. TP, TN, K, organic matter) to explore the relationships between plant physiology (as evidence by the plant vigour related indices) and nutrient availability.

The correlation and least-squares regression analysis revealed a strong – but positive – association between sediment nutrient enrichment and plant vigour. The Red-Edge$_\lambda$ index derived from the laboratory darkroom measurements was, for example, found to be strongly related to sediment organic matter accumulation in the stands (R^2 = 0.68). Similar relationships were also observed for TP, Mg and Na. Statistical relationships between the spectral indices and sediment chemistry were more tenuous at the canopy-scale (likely due to canopy architecture effects), but some promising correlations were still observed. The [R(860)/R(550)xR(708)] index, for example, demonstrated a good relationship with sediment organic matter content (R^2 = 0.58). These explorative relationships demonstrate the value of remote sensing as a potential tool for assessing the physiological response of aquatic plants to variations in lake habitat quality.

The extrapolation of the derived techniques to airborne CASI-2 [Vegetation] imagery of littoral reedswamp in the shallow lakes of the Upper Thurne was used to assess variations in the performance of *Phragmites australis* plants at the lake-scale. Correlation and least-squares regression analysis again revealed strong associations between plant vigour and sediment nutrient enrichment. The CASI-2 [Vegetation] band-ratio index [L_w(710)L_w(760)] calculated from images acquired on 22 June 2005 and 29 August 2005 was correlated to sediment TP (R^2 = 0.49-0.53). In addition, the [L_w(710)L_w(760)] index derived from the 29 August 2005 CASI-2 [Vegetation] image was found to be strongly associated with the N:P (molar) ratio (R^2 = 0.64).

The subsequent calibration of the CASI-2 [Vegetation] imagery allowed the derivation of spatially-resolving maps depicting the physiological response of *Phragmites australis* plants to variation in sediment nutrition across the complete Upper Thurne system.

The remote-sensing-based characterisation of *Phragmites australis* physiological status in Hickling Broad revealed a positive association between plant performance and nutrient enrichment. However, somewhat paradoxically, the examination of sediment chemistry in healthy and dieback stands of *Phragmites australis* using 2-sample T-tests and Mann Whitney tests intimated towards a link between reed dieback and sediment nutrient enrichment. It was found that the sediment in dieback stands had higher concentrations of TP, Fe, Na, Mg and organic matter than the sediment of non-dieback stands. However, the remaining plants fringing recent dieback sites were shown to be typically more vigourous than those growing in the non-dieback areas.

It is suggested that the accretion of organic matter with the in dieback stands (derived from the decay of littoral plants and/or the decay of pelagic algal blooms) may be associated with reed dieback in the Norfolk Broads. Several previous authors have suggested that the copious flux of organic matter to lake sediments can accelerate decompositional processes, increasing the microbial demand for oxygen, and ultimately leading to the development of anoxic conditions (Cizkova *et al.,* 1996). The switch to anaerobic microbial metabolism in turn can lead to the production of numerous phytotoxic metabolites (e.g. organic acids). The accumulation phytotoxic organic acids is though to be a major cause of reed decline in European lakes (Armstrong *et al.,* 1996; Armstrong *et al.,* 1996; Vanderputten *et al.,* 1997; Cizkova *et al.,* 1999) and it would seem that a similar process may be affecting the performance of *Phargmites australis* in Hickling Broad. The production of S^{2-} and Fe (II) species in the reducing sediments may also be deleterious to plant growth. The prevalence of such phytotoxins in the Norfolk Broads is currently unknown and, as such, further work should be focussed on gaining an improved understanding of the production of these compounds in the sediments of these lakes and their effect on aquatic plant growth.

The results clearly demonstrate the merit of utilising remote sensing for assessing spatial variations in the physiological status of aquatic plant communities. The rapid surveys conducted using laboratory darkroom and *in-situ* spectrometry and airborne CASI-2 reconnaissance were able to provide novel spatial insights into the response of aquatic plant communities to eutrophication in shallow lakes. The synoptic "whole-lake" view obtained using airborne surveillance would have been unachievable using conventional methods. Work in floodplain wetlands has shown that the quantification of plant physiological status can also be used to examine heavy metal deposition in aquatic ecosystems (Kooistra *et al.,* 2004; Clevers *et al.,* 2004). It is apparent that similar approaches, using remote sensing to examine patterns in aquatic plant performance, could be employed to explore the fate and behaviour of other waterborne contaminants, such as trace metals or biocides, in lake ecosystems. This would be of value, not only for improving the current understanding of lake-scale responses to pollution events, but in the more general assessment of ecological status in lakes and other inland and transitional waters.

8.2.4 Remote Sensing and the Water Framework Directive (2000/60/EC)

8.2.4.1 The Assessment of Ecological Status in Lakes

The European Union Water Framework Directive (2000/66/EC) was implemented on 22 December 2000 with the aim of establishing a new, integrated, approach to the protection, improvement and sustainable use of Europe's rivers, lakes, estuaries, coastal- and groundwaters. The EU WFD requires Member States to achieve "good and non-deteriorating ecological status" in all rivers, lakes, estuaries, coastal- and groundwaters by 2015. In the context of lakes, the EU WFD requires the assessment of "ecological status" in all bodies of standing-water > 0.5 km^2. The assessment of ecological status is to be based an evaluation of (i) hydromorphological, (ii) physicochemical and, (iii) biological criteria against pre-determined reference conditions for specific-lake types. This approach allows site-specific reference conditions to be established for each lake and thus the definition of restoration targets (where applicable). Member States are also required to identify and link pressures to the ecological status of lakes. The assessment of ecological status will also include an appraisal of the

prevalence of specific priority substances (e.g. benzene, lead, mercury, tributyltin) that are considered to be hazardous to ecosystem (and human) health.

The definition of what, in practice, constitutes good ecological status in lakes, the construction of a workable typology, and the definition of suitable lake-specific reference conditions has, and continues to be, a major undertaking for the regulatory authorities concerned with the implementation of the WFD (Sondergaard *et al.,* 2005). However, once this framework is established, the continuous assessment, monitoring and policing of ecological status in lakes will be a massive challenge for regulatory authorities when the shear number and geographical distribution of lakes covered by the WFD legislation is taken into consideration. The timescales for surveillance/operational monitoring vary between 1 month and 6 years depending on the specific quality element to be assessed. This frequency of monitoring will be difficult, if not impossible, to achieve at a pan-European scale using current resources. It is therefore evident that the integration of remote sensing data, where appropriate, with more convention *in-situ* survey techniques may be crucial to the successful, and cost-effective, implementation of the WFD in Europe (Chen *et al.,* 2004; Gilvear *et al.,* 2004a; Gilvear *et al.,* 2007; Chen *et al.,* 2007)

8.2.4.2 Hydromorphological Elements

The hydromorphological elements of lakes to be assessed under the WFD include (i) the quanity and dynamics of water flow, (ii) residence time, (iii) connection to groundwater, (iv) lake depth variation, (v) quantity, structure and substrate of the lake bed and, (vi) structure of the lake shore.

The assessment of lake hydromorphology from remote sensing data has received little consideration in the literature, although comparable work has been conducted for river and estuarine environments (Gilvear *et al.,* 2004a; Gilvear *et al.,* 2007). Remote sensing has been shown to be a useful source of supplementary information for the conduction of the Lake Habitat Classification (Rowan *et al.,* 2006) and it is evident that a similar approach would be of value to the assessment of lake hydromorphology under the WFD.

Hydromorphological elements such as lakeshore structure (e.g. morphometry, composition) and the degree of anthropogenic modification (e.g. dams, piers, jetties, urban or industrial development) could be readily identified from remotely sensed data. It could also provide, in some circumstances, information pertaining to the quantity and dynamics of water flow and connectivity to groundwaters (see for example Tcherepanov *et al.,* 2005; Bohme *et al.,* 2006). In shallow waters, information could also be obtained regarding the quantity, structure and substrate of the bed. In this context, remote sensing has already been used to assess benthic habitat features in rivers and coastal waters (Kutser *et al.,* 2006; Gilvear *et al.,* 2007).

The detection of hydromorphological features using remote sensing data could be aided by the exploration of pattern recognition and feature extraction algorithms, to facilitate more conventional spectral-based classifiers (Hare *et al.,* 2001; Dillabaugh *et al.,* 2002; Gloaguen *et al.,* 2007). The further evaluation of such approaches would be merited in this context.

8.2.4.3 Physicochemical Elements

The physicochemical elements to be assessed under the water framework directive include (i) transparency, (ii) thermal conditions, (iii) oxygenation, (iv) salinity, (v) acidification status and, (vi) nutrient conditions. Of these various elements, the assessment of water transparency (as the SDD) is readily achievable in most, if not all, water types from remote sensing data. In this thesis, for example, it was shown that the SDD can be estimated to an accuracy of ±0.08-0.11 m (R^2 = 0.93-0.96) in clear water and turbid shallow lakes. The assessment of the thermal conditions in lakes could be obtained using thermal imaging which has been used in the past to assess lake surface temperatures (± 1°C) (although remote sensing cannot provide vertically-resolving temperature profiles) (Budd, 2004; Kay *et al.,* 2005). The acidification status of lakes would be more difficult to assess using remote sensing methodologies; although, the estimation of the CDOM absorption coefficient may be a useful proxy for assessing acidification from inputs of dissolved organic carbon (Brezonik *et al.,* 2005; Kutser *et al.,* 2005b).

8.2.4.4 Biological Elements

The biological elements used for the assessment of ecological status in lakes under the WFD directive include (i) the composition, abundance and biomass of phytoplankton, (ii) the composition and abundance of other aquatic flora, (iii) the composition and abundance of benthic invertebrate fauna and (iv) the composition and age structure of fish. This is an obvious area where remote sensing can contribute to the WFD. The biomass of the phytoplankton community in lakes can be quantified using remote sensing through the estimation of the chlorophyll-a concentration. This has been demonstrated on several occasions, for a variety of lakes types, and using a multitude of remote sensing instruments (Malthus & George, 1997; Ammenberg *et al.,* 2002; Tyler *et al.,* 2006; Giardino *et al.,* 2007). In this thesis, it was shown that, even in highly optically-complex shallow lakes, it was still possible to accurately quantify the concentration of chlorophyll-a (R^2 = 0.96). The expected development of operational algorithms for CASE II waters for platforms such as MERIS and MODIS will soon enable the routine monitoring of chlorophyll-a in the larger lakes covered by the EU WFD (10-100> km^2) at the pan-European scale.

The assessment of phytoplankton composition and abundance is more problematic. The taxonomic resolution achievable using conventional cell count methodologies, or even chemotaxonomic approaches, will never be achievable using remote sensing. Nevertheless, remote sensing could potentially be used to assess broad change in the dominant species composition of phytoplankton communities. The development of algorithms for the detection and quantify of cyanobacteria is being increasingly realised for lake waters (Sridhar & Vincent, 2007; Simis *et al.,* 2007). Indeed, it was shown in this thesis that the biomarker pigment C-phycocyanin could be estimated to a maximum accuracy of R^2 = 0.95. This is a highly pertinent development in the context of the WFD as the absolute and relative abundance of cyanobacteria is considered to be a good indictor of ecological status. It was also demonstrated in this thesis that broad changes in colour group composition (brown, green, blue-green) may be tracked from remote sensing platforms. The possible development of algorithms for the assessment of phytoplankton colour groups or, even, functional-types would be of direct value to the WFD (Fishwick *et al.,* 2006; Aiken *et al.,* 2007).

Information regarding the composition, abundance and biomass of aquatic plants could also be retrieved using remote sensing. The distribution of aquatic plant communities can be readily mapped using remote sensing platforms and, increasingly, information can be acquired on the dominant species composition (Malthus & George, 1997; Williams *et al.,* 2003; Pengra *et al.,* 2007). In this thesis it was shown that aquatic plant growth-habit types can be mapped from remotely sensed data and, in shallow clear water lakes, information relating to the composition of submerged communities can also be obtained. The estimation of submerged plant biomass has also been achieved using remote sensing (Yuan & Zhang, 2007). Similar approaches could also be developed for the assessment of microphytobenthos; promising results have already been attained from comparable work in river and estuarine ecosystems (Rainey *et al.,* 2003; Meleder *et al.,* 2003; Murphy *et al.,* 2005).

It has also been shown in this thesis, and elsewhere, that remote sensing can be used to assess the physiological status of aquatic plants (Penuelas *et al.,* 1993; Tilley *et al.,* 2003). Whilst there is no explicit requirement for such assessment in the EU WFD, such an approach could, nevertheless, be used to examine underlying changes in nutrient enrichment or, alternatively, contaminant discharges (e.g. priority substances). This type of proxy information would be highly relevant to the assessment of ecosystem pressures and impacts under the EU WFD

8.2.4.5 Future Development and Integration

The information provided by remote sensing platforms, as evidenced above, could make a substantial contribution to the appraisal of specific hydromorphological, physicochemical and biological elements for the assessment of ecological status in lakes as part of the EU WFD. However, remote sensing is no panacea for the regulatory authorities charged with the implementation of the WFD. There are many hydromorphological (depth, residence time), physicochemical (nutrients, oxygenation, salinity) and biological (benthic invertebrates, fish) elements that cannot be assessed using remote sensing. It is possible, in some circumstances, that reliable proxies could be constructed for these elements based upon empirical or

deterministic relationships using other, readily quantifiable, remote sensing metrics (e.g. transparency, chlorophyll-a, aquatic plant cover). However, proxy-based approaches are unlikely to be reliable and thus, on this basis, it is unlikely that remote sensing could operate as a stand-alone tool for the purposes of the EU WFD.

It is therefore clear that, in order to effectively implement the EU WFD, careful and considered integration of remote sensing surveillance alongside existing *in-situ* survey methodologies will be necessary. This will require improved collaboration between freshwater ecologists, remote sensing specialists and policy makers to ensure the data derived from remote sensing platforms is suitable for task and commands the necessary synergy with the data collated using *in-situ* surveys. Moreover, there are various levels at which remote sensing could be integrated into the EU WFD. It could be used, for example, to provide continuous near-real-time thematic information for every River Basin District, or, alternatively, it could be used in a more ad-hoc manner, to essentially "fill in the gaps" in *in-situ* datasets where data are missing because field-based surveys are impractical or disproportionately expensive to implement.

The construction of comprehensive remote sensing datasets for River Basin Districts should, however, be given serious considered as this would, importantly, ensure data continuity and would enact the establishment of long-term datasets for the purposes of change detection. Furthermore, as the EU WFD also requires the assessment of pressures, which may be difficult to identify and adequately characterise at the lake-scale, such datasets may be vital in deriving linkages between the ecological status of lakes and pressures at the catchment-scale. Remote sensing methodologies are also sympathetic to the issues associated with collation of data for transboundary systems and, in addition, could be readily harmonised or standardised across Member States.

There are some issues concerning the use of remote sensing for EU WFD purposes that will need to be further resolved. To effect the full integration of remote sensing into EU WFD monitoring strategies, operational algorithms will be required for all relevant hydromorphological, physicochemical and biological elements. This will require a considerable

amount of further research before such algorithms can be introduced into the existing processing chains for current satellites missions (e.g. MERIS, MODIS). Furthermore, as the observation of small to medium sized lakes (i.e. 0.5-10 km^2) is not possible from current satellite platforms, further technological advances will be necessary, although, in the short-term, the utility of data from existing high-spatial resolution terrestrial satellites (e.g. ALI, ASTER, IKONOS, Quickbird) should be further examined. The continuous data stream provided by satellite remote sensing platforms can be severely compromised by persistent cloud cover. To maintain a viable surveillance network, it may therefore be necessary to supplement remote-sensing-based monitoring programmes with data derived from sensors (optical, fluorescence, sonar) mounted on geostationary buoys, ships-of-opportunity or on remotely-operated-vehicles.

The ultimate objective of the WFD is to establish a new, integrated approach to the protection, improvement and sustainable use of Europe's rivers lakes, estuaries, coasts and groundwaters. This will require new and groundbreaking approaches to the assessment and monitoring of aquatic ecosystems. In this context, it is clear that remote sensing can provide a vital source of data for the assessment, monitoring and policing of ecological status at a pan-European scale.

8.2.5 Remote Sensing in Lake Ecology

It is has been argued that remote sensing technologies have much to offer the monitoring of ecological status in lakes. It is important to acknowledge, however, that the potential application of remote sensing technologies in lake ecology goes far beyond a simple monitoring capacity. Lakes are complex ecosystems and their responses to perturbations and pressures, be they natural, or anthropogenic, is rarely uniform at the lake-scale. Characterising heterogeneity at the "lakescape" level, or beyond, is problematic and typically requires some form of spatial inference to enable point-based measurements to be scaled to the wider ecosystem. Remote sensing offers a solution in this context. The spatially-resolving data afforded by remote sensing platforms allows point-based measurements to be evaluated within a geospatial framework. This readily enables bio-physical measurements to be extrapolated to the ecosystem scale and the elucidation of spatial variability in ecosystem responses to change (Turner *et al.,* 2003; Kerr & Ostrovsky, 2003).

In this thesis, this capability was demonstrated in two contexts, (i) the time-series remote sensing surveillance of spatial variability in vertical migration by *Microcystis aeruginosa* (**Chapter 5**) and, (ii) the characterisation of spatial variability in the physiological response of *Phragmites australis* reedswamp to eutrophication pressures (**Chapter 7**). In both instances, the use of remote sensing reconnaissance enabled the evaluation of ecosystem process and function at the lake-scale. This resolution could not have been achieved using point-based methodologies.

This illustrates what can be gained from the integration of remote sensing technologies into studies of lake ecology. Remote sensing has the ability to link pattern to process. In forming an improved understanding of how complex ecosystems function, and respond to pressures and perturbations, this is an increasingly important capability. It has long been recognised that spatial heterogeneity has ecological significance (Roff, 1974; Holt, 1984; Padisak, 1993; Pickett & Cadenasso, 1995). Remote sensing and associated geospatial disciplines, such as GIS and geostatistics, now afford a means by which spatial heterogeneity can be measured and understood in the context of ecosystem process and function. The increased application of remote sensing in the study of shallow lakes thus has the potential to yield new and meaningful insights into the ecology of these systems.

8.3 CONCLUSIONS

Shallow lakes are an important ecological and socio-economic resource. There is now an unprecedented interest in the ecological status and trajectory of shallow lakes and, indeed, all surface waters, in the face of the mounting pressures being exerted on these ecosystems and the services they provide. The European Union's Water Framework Directive (2000/60/EC) has placed increased emphasis on the development of new and cost-effective strategies for the assessment and surveillance of the ecological status of surface waters. In this context, it has been suggested that the spatially-resolving, regional-scale, panoramic data provided by remote sensing platforms may be pertinent for effecting the operational monitoring of lakes at the pan-European scale.

This thesis examined the use of remote sensing reconnaissance for the assessment and monitoring of ecological status in small and shallow lakes. In particular, emphasis was placed on the development of remote sensing approaches for assessing change in (i) phytoplankton assemblages and (ii) aquatic plant communities, as these biotic elements are key determinants of ecological status in lakes. The accurate estimation of chlorophyll-a concentrations, as a measure of total phytoplankton biomass, was shown to be readily achievable using remotely sensed data. It was further shown that, in addition to chlorophyll-a, the abundance of cyanobacteria could also be quantified through the estimation of the biomarker pigment C-phycocyanin. This represents some advancement for the remote sensing of lake phytoplankton assemblages. Novel mesocosm experiments also indicate that further broad-scale taxonomic differentiation may be possible for other algal groups.

The thesis also evidenced that remote sensing can be used to map the distribution of aquatic plants in shallow lakes, on the basis of growth-habit types, or broad species associations. Significantly, it was demonstrated that, in clear water lakes, remote sensing can be used to map the cover of submerged plants. The demonstration of this capability is vital if remote sensing is to be effectively used for the assessment of ecological status in shallow lakes. Furthermore, it was also established that the physiological status of emergent aquatic plants can be quantified using remote-sensing-based approaches. This enabled the response of aquatic plants to nutrient enrichment be assessed at a previously unparalleled lake-scale.

Remote sensing therefore has much to offer the assessment, monitoring and policing of ecological status in shallow lakes. This thesis has made a substantial contribution to furthering its application in this context. The relevance of remote sensing technologies to the European Union's Water Framework Directive has been clearly demonstrated and it has been also shown that remote sensing can also make an important contribution to furthering the understanding of lake-scale processes and function.

REFERENCES

Agbeti, M.D., Kingston, J.C., Smol, J.P. and Watters, C. (1997) Comparison of Phytoplankton Succession in Two Lakes of Different Mixing Regimes. *Archiv Fur Hydrobiologie* **140**, 37-69.

Aguirre-Gomez, R., Boxall, S.R. and Weeks, A.R. (2001a) Detecting Photosynthetic Algal Pigments in Natural Populations Using a High-Spectral-Resolution Spectroradiometer. *International Journal of Remote Sensing* **22**, 2867-2884.

Aguirre-Gomez, R., Weeks, A.R. and Boxall, S.R. (2001b) The Identification of Phytoplankton Pigments From Absorption Spectra. *International Journal of Remote Sensing* **22**, 315-338.

Ahn, Y.H., Bricaud, A. and Morel, A. (1992) Light Backscattering Efficiency and Related Properties of Some Phytoplankters. *Deep-Sea Research Part a-Oceanographic Research Papers* **39**, 1835-1855.

Aiken, J., Fishwick, J.R., Lavender, S., Barlow, R., Moore, G.F., Sessions, H., Bernard, S., Ras, J. and Hardman-Mountford, N.J. (2007) Validation of MERIS Reflectance and Chlorophyll During the Bencal Cruise October 2002: Preliminary Validation of New Demonstration Products for Phytoplankton Functional Types and Photosynthetic Parameters. *International Journal of Remote Sensing* **28**, 497-516.

Albert, A. and Mobley, C.D. (2003) An Analytical Model for Subsurface Irradiance and Remote Sensing Reflectance in Deep and Shallow Case-2 Waters. *Optics Express* **11**, 2873-2890.

Albright, T.P., Moorhouse, T.G. and Mcnabb, J. (2004) The Rise and Fall of Water Hyacinth in Lake Victoria and the Kagera River Basin, 1989-2001. *Journal of Aquatic Plant Management* **42**, 73-84.

Alexandridis, T.K., Takavakoglou, V., Crisman, T.L. and Zalidis, G.C. (2007) Remote Sensing and GIS Techniques for Selecting a Sustainable Scenario for Lake Koronia, Greece. *Environmental Management* **39**, 278-290.

Allee, R.J. and Johnson, J.E. (1999) Use of Satellite Imagery to Estimate Surface Chlorophyll a and Secchi Disc Depth of Bull Shoals Reservoir, Arkansas, Usa. *International Journal of Remote Sensing* **20**, 1057-1072.

Allen, S.E. (1989) Sulphuric Acid-Hydroxide Proceedure. In: Allen, S.E., Grimshaw, H.M., Parkinson, J.A. and Quarmby, C., (Eds.) *Chemical Analysis of Ecological Materials*, 2nd edn. New York: Blackwell Scientific Publishing.

Ammenberg, P., Flink, P., Lindell, T., Pierson, D. and Strombeck, N. (2002) Bio-Optical Modelling Combined with Remote Sensing to Assess Water Quality. *International Journal of Remote Sensing* **23**, 1621-1638.

Aplin, P. (2005) Remote Sensing: Ecology. *Progress in Physical Geography* **29**, 104-113.

Arenz, R.F., Lewis, W.M. and Saunders, J.F. (1996) Determination of Chlorophyll and Dissolved Organic Carbon From Reflectance Data for Colorado Reservoirs. *International Journal of Remote Sensing* **17**, 1547-1566.

Armstrong, J., Afreenzobayed, F. and Armstrong, W. (1996) Phragmites Die-Back: Sulphide- and Acetic Acid-Induced Bud and Root Death, Lignifications, and Blockages Within Aeration and Vascular Systems. *New Phytologist* **134**, 601-614.

Armstrong, J. and Armstrong, W. (1999) Phragmites Die-Back: Toxic Effects of Propionic, Butyric and Caproic Acids in Relation to Ph. *New Phytologist* **142**, 201-217.

Armstrong, J. and Armstrong, W. (2001) An Overview of the Effects of Phytotoxins on Phragmites Australis in Relation to Die-Back. *Aquatic Botany* **69**, 251-268.

Armstrong, J., Armstrong, W., Wu, Z.B. and Afreenzobayed, F. (1996) A Role for Phytotoxins in the Phragmites Die-Back Syndrome? *Folia Geobotanica & Phytotaxonomica* **31**, 127-&

Artigas, F.J. and Yang, J.S. (2005) Hyperspectral Remote Sensing of Marsh Species and Plant Vigour Gradient in the New Jersey Meadowlands. *International Journal of Remote Sensing* **26**, 5209-5220.

Artigas, F.J. and Yang, J.S. (2006) Spectral Discrimination of Marsh Vegetation Types in the New Jersey Meadowlands, Usa. *Wetlands* **26**, 271-277.

Arzandeh, S. and Wang, J.F. (2003) Monitoring the Change of Phragmites Distribution Using Satellite Data. *Canadian Journal of Remote Sensing* **29**, 24-35.

Auer, M.T. and Bub, L.A. (2004) Selected Features of the Distribution of Chlorophyll Along the Southern Shore of Lake Superior. *Journal of Great Lakes Research* **30**, 269-284.

Ayala-Silva, T. and Beyl, C.A. (2005) Changes in Spectral Reflectance of Wheat Leaves in Response to Specific Macronutrient Deficiency. **35**, 305-317.

Azimuth Systems (2005) *Airborne Remote Sensing Hyperspectral Direct Georeffering Package: AZGCORR. User's Manual*, UK: Azimuth Systems.

Baban, S.M.J. (1993) Detecting Water-Quality Parameters in the Norfolk Broads, Uk, Using Landsat Imagery. *International Journal of Remote Sensing* **14**, 1247-1267.

Baban, S.M.J. (1999) Use of Remote Sensing and Geographical Information Systems in Developing Lake Management Strategies. *Hydrobiologia* **396**, 211-226.

Bailey, M.C. and Hamilton, D.P. (1997) Wind Induced Sediment Resuspension: a Lake-Wide Model. *Ecological Modelling* **99**, 217-228.

Balayla, D.J. and Moss, B. (2003) Spatial Patterns and Population Dynamics of Plant-Associated Microcrustacea (Cladocera) in an English Shallow Lake (Little Mere, Cheshire). *Aquatic Ecology* **37**, 417-435.

Barko, J.W., Gunnison, D. and Carpenter, S.R. (1991) Sediment Interactions With Submersed Macrophyte Growth and Community Dynamics. *Aquatic Botany* **41**, 41-65.

Barlow, R.G., Cummings, D.G. and Gibb, S.W. (1997) Improved Resolution of Mono- and Divinyl Chlorophylls a and B and Zeaxanthin and Lutein in Phytoplankton Extracts Using Reverse Phase C-8 HPLC. *Marine Ecology-Progress Series* **161**, 303-307.

Barnes, J.D., Balaguer, L., Manrique, E., Elvira, S. and Davison, A.W. (1992) A Reappraisal of the Use of Dmso for the Extraction and Determination of Chlorophylls-a and Chlorophylls-b in Lichens and Higher-Plants. *Environmental and Experimental Botany* **32**, 85-100.

Batty, L.C. and Younger, P.L. (2003) Effects of External Iron Concentration Upon Seedling Growth and Uptake of Fe and Phosphate by the Common Reed, Phragmites Australis (Cav.) Trin Ex. Steudel. *Annals of Botany* **92**, 801-806.

Beeri, O. and Phillips, R.L. (2007) Tracking Palustrine Water Seasonal and Annual Variability in Agricultural Wetland Landscapes Using Landsat From 1997 to 2005. *Global Change Biology* **13**, 897-912.

Behrenfeld, M.J., Boss, E., Siegel, D.A. and Shea, D.M. (2005) Carbon-Based Ocean Productivity and Phytoplankton Physiology From Space. *Global Biogeochemical Cycles* **19**,

Belzile, C., Vincent, W.F., Howard-Williams, C., Hawes, I., James, M.R., Kumagai, M. and Roesler, C.S. (2004) Relationships Between Spectral Optical Properties and Optically Active Substances in a Clear Oligotrophic Lake. *Water Resources Research* **40**,

Bennett, A. and Bogorad, L. (1973) Complementary Chromatic Adaptation in a Filamentous Blue-Green-Alga. *Journal of Cell Biology* **58**, 419-435.

Bergamino, N., Loiselle, S.A., Cozar, A., Dattilo, A.M., Bracchini, L. and Rossi, C. (2007) Examining the Dynamics of Phytoplankton Biomass in Lake Tanganyika Using Empirical Orthogonal Functions. *Ecological Modelling* **204**, 156-162.

Bergmann, T., Fahnenstiel, G., Lohrenz, S., Millie, D. and Schofield, O. (2004) Impacts of a Recurrent Resuspension Event and Variable Phytoplankton Community Composition on Remote Sensing Reflectance. *Journal of Geophysical Research-Oceans* **109**,

Biddanda, B.A. and Cotner, J.B. (2002) Love Handles in Aquatic Ecosystems: the Role of Dissolved Organic Carbon Drawdown, Resuspended Sediments, and Terrigenous Inputs in the Carbon Balance of Lake Michigan. *Ecosystems* **5**, 431-445.

Birth, G.S. and Mcvey, G.R. (1968) Measuring Color of Growing Turf With a Reflectance Spectrophotometer. *Agronomy Journal* **60**, 640-&

Blackburn, G.A. (1998) Quantifying Chlorophylls and Caroteniods at Leaf and Canopy Scales: an Evaluation of Some Hyperspectral Approaches. *Remote Sensing of Environment* **66**, 273-285.

Blackburn, G.A. (1999) Relationships Between Spectral Reflectance and Pigment Concentrations in Stacks of Deciduous Broadleaves. *Remote Sensing of Environment* **70**, 224-237.

Blackburn, G.A. (2002) Remote Sensing of Forest Pigments Using Airborne Imaging Spectrometer and Lidar Imagery. *Remote Sensing of Environment* **82**, 311-321.

Blackburn, G.A. (2007) Hyperspectral Remote Sensing of Plant Pigments. *Journal of Experimental Botany* **58**, 855-867.

Blackburn, G.A. and Steele, C.M. (1999) Towards the Remote Sensing of Matorral Vegetation Physiology: Relationships Between Spectral Reflectance, Pigment, and Biophysical Characteristics of Semiarid Bushland Canopies. *Remote Sensing of Environment* **70**, 278-292.

Blais, J.M. and Kalff, J. (1995) The Influence of Lake Morphometry on Sediment Focusing. *Limnology and Oceanography* **40**, 582-588.

Blindow, I., Andersson, G., Hargeby, A. and Johansson, S. (1993) Long-Term Pattern of Alternative Stable States in 2 Shallow Eutrophic Lakes. *Freshwater Biology* **30**, 159-167.

Bloesch, J. (1995) Mechanisms, Measurement and Importance of Sediment Resuspension in Lakes. *Marine and Freshwater Research* **46**, 295-304.

Blom, G., Vanduin, E.H.S., Aalderink, R.H., Lijklema, L. and Toet, C. (1992) Modeling Sediment Transport in Shallow Lakes - Interactions Between Sediment Transport and Sediment Composition. *Hydrobiologia* **235**, 153-166.

Blomqvist, P., Jansson, M., Drakare, S., Bergstrom, A.K. and Brydsten, L. (2001) Effects of Additions of DOC on Pelagic Biota in a Clearwater System: Results From a Whole Lake Experiment in Northern Sweden. *Microbial Ecology* **42**, 383-394.

Blomqvist, P., Pettersson, A. and Hyenstrand, P. (1994) Ammonium-Nitrogen - a Key Regulatory Factor Causing Dominance of Non-Nitrogen-Fixing Cyanobacteria in Aquatic Systems. *Archiv Fur Hydrobiologie* **132**, 141-164.

Boar, R.R., Crook, C.E. and Moss, B. (1989) Regression of Phragmites-Australis Reedswamps and Recent Changes of Water Chemistry in the Norfolk Broadland, England. *Aquatic Botany* **35**, 41-55.

Bogdan, J.J., Budd, J.W., Eadie, B.J. and Hornbuckle, K.C. (2002) The Effect of a Large Resuspension Event in Southern Lake Michigan on the Short-Term Cycling of Organic Contaminants. *Journal of Great Lakes Research* **28**, 338-351.

Bohme, B., Steinbruch, F., Gloaguen, R., Heilmeier, H. and Merkel, B. (2006) Geomorphology, Hydrology, and Ecology of Lake Urema, Central Mozambique, With Focus on Lake Extent Changes. *Physics and Chemistry of the Earth* **31**, 745-752.

Boorman, L.A. and Fuller, R.M. (1981) The Changing Status of Reedswamp in the Norfolk Broads. *Journal of Applied Ecology* **18**, 241-269.

Boyd, D.S., Entwistle, J.A., Flowers, A.G., Armitage, R.P. and Goldsmith, P.C. (2006) Remote Sensing the Radionuclide Contaminated Belarusian Landscape: a Potential for Imaging Spectrometry? *International Journal of Remote Sensing* **27**, 1865-1874.

Brando, V.E. and Dekker, A.G. (2003) Satellite Hyperspectral Remote Sensing for Estimating Estuarine and Coastal Water Quality. *Ieee Transactions on Geoscience and Remote Sensing* **41**, 1378-1387.
Notes: Part Number: Part 1

Breukelaar, A.W., Lammens Ehrr, Breteler Jgpk and Tatrai, I. (1994) Effects of Benthivorous Bream (Abramis-Brama) and Carp (Cyprinus-Carpio) on Sediment Resuspension and Concentrations of Nutrients and Chlorophyll-a. *Freshwater Biology* **32**, 113-121.

Brezonik, P., Menken, K.D. and Bauer, M. (2005) Landsat-Based Remote Sensing of Lake Water Quality Characteristics, Including Chlorophyll and Colored Dissolved Organic Matter (CDOM). *Lake and Reservoir Management* **21**, 373-382.

Bricaud, A., Morel, A. and Prieur, L. (1981) Absorption by Dissolved Organic-Matter of the Sea (Yellow Substance) in the UV and Visible Domains. *Limnology and Oceanography* **26**, 43-53.

Bricaud, A., Morel, A. and Prieur, L. (1983) Optical-Efficiency Factors of Some Phytoplankters. *Limnology and Oceanography* **28**, 816-832.

Brivio, P.A., Giardino, C. and Zilioli, E. (2001) Validation of Satellite Data for Quality Assurance in Lake Monitoring Applications. *Science of the Total Environment* **268**, 3-18.

Broads Authority (2004) *Broads Plan 2004*, Norwich: Broads Authority.

Brown, C.W. and Podesta, G.P. (1997) Remote Sensing of Coccolithophore Blooms in the Western South Atlantic Ocean. *Remote Sensing of Environment* **60**, 83-91.

Brown, M., Gunn, S.R. and Lewis, H.G. (1999) Support Vector Machines for Optimal Classification and Spectral Unmixing. *Ecological Modelling* **120**, 167-179.

Bryant, R.G. and Gilvear, D.J. (1999) Quantifying Geomorphic and Riparian Land Cover Changes Either Side of a Large Flood Event Using Airborne Remote Sensing: River Tay, Scotland. *Geomorphology* **29**, 307-321.

Budd, J.W. (2004) Large-Scale Transport Phenomena in the Keweenaw Region of Lake Superior: the Ontonagon Plume and the Keweenaw Eddy. *Journal of Great Lakes Research* **30**, 467-480. Notes: Supplement: Suppl. 1

Budd, J.W., Drummer, T.D., Nalepa, T.F. and Fahnenstiel, G.L. (2001) Remote Sensing of Biotic Effects: Zebra Mussels (Dreissena Polymorpha) Influence on Water Clarity in Saginaw Bay, Lake Huron. *Limnology and Oceanography* **46**, 213-223.

Budd, J.W. and Warrington, D.S. (2004) Satellite-Based Sediment and Chlorophyll a Estimates for Lake Superior. *Journal of Great Lakes Research* **30**, 459-466.

Burgis, M.J. and Morris, P. (1987) *The Natural History of Lakes*, Cambridge: Cambridge University Press.

Buschmann, C. and Nagel, E. (1993) *In Vivo* Spectroscopy and Internal Optics of Leaves as Basis for Remote-Sensing of Vegetation. *International Journal of Remote Sensing* **14**, 711-722.

Campbell, J.B. (2002) *Introduction to Remote Sensing.*, 3rd edn. New York: The Guilford Press.

Campbell, P.K.E., Middleton, E.M., Mcmurtrey, J.E., Corp, L.A. and Chappelle, E.W. (2007) Assessment of Vegetation Stress Using Reflectance or Fluorescence Measurements. *Journal of Environmental Quality* **36**, 832-845.

Canfield, D.E., Langeland, K.A., Linda, S.B. and Haller, W.T. (1985) Relations Between Water Transparency and Maximum Depth of Macrophyte Colonization in Lakes. *Journal of Aquatic Plant Management* **23**, 25-28.

Cannizzaro, J.P. and Carder, K.L. (2006) Estimating Chlorophyll a Concentrations From Remote-Sensing Reflectance in Optically Shallow Waters. *Remote Sensing of Environment* **101**, 13-24.

Carpenter, S.R. and Lodge, D.M. (1986) Effects of Submersed Macrophytes on Ecosystem Processes. *Aquatic Botany* **26**, 341-370.

Carrick, H.J., Worth, D. and Marshall, M.L. (1994) The Influence of Water Circulation on Chlorophyll-Turbidity Relationships in Lake Okeechobee as Determined by Remote-Sensing. *Journal of Plankton Research* **16**, 1117-1135.

Carter, G.A. (1994) Ratios of Leaf Reflectances in Narrow Wavebands as Indicators of Plant Stress. *International Journal of Remote Sensing* **15**, 697-703.

Carvalho, L. and Kirika, A. (2003) Changes in Shallow Lake Functioning: Response to Climate Change and Nutrient Reduction. *Hydrobiologia* **506**, 789-796.

Celik, K. and Ongun, T. (2006) Seasonal Dynamics of Phytoplankton Assemblages Across Nutrient Gradients in Shallow Hypertrophic Lake Manyas, Turkey. *Lake and Reservoir Management* **22**, 250-260.

Chambers, P.A. and Kalff, J. (1985) Depth Distribution and Biomass of Submersed Aquatic Macrophyte Communities in Relation to Secchi Depth. *Canadian Journal of Fisheries and Aquatic Sciences* **42**, 701-709.

Chang, G.C., Dickey, T.D., Mobley, C.D., Boss, E. and Pegau, W.S. (2003) Toward Closure of Upwelling Radiance in Coastal Waters. *Applied Optics* **42**, 1574-1582.

Chappelle, E.W., Kim, M.S. and Mcmurtrey, J.E. (1992) Ratio Analysis of Reflectance Spectra (Rars) - an Algorithm for the Remote Estimation of the Concentrations of Chlorophyll-a, Chlorophyll-b, and Carotenoids in Soybean Leaves. *Remote Sensing of Environment* **39**, 239-247.

Chen, Q.L., Zhang, Y.Z., Ekroos, A. and Hallikainen, M. (2004) The Role of Remote Sensing Technology in the EU Water Framework Directive (WFD). *Environmental Science & Policy* **7**, 267-276.

Chen, Q.L., Zhang, Y.Z. and Hallikainen, M. (2007) Water Quality Monitoring Using Remote Sensing in Support of the EU Water Framework Directive (WFD): a Case Study in the Gulf of Finland. *Environmental Monitoring and Assessment* **124**, 157-166.

Chorus, I., Falconer, I.R., Salas, H.J. and Bartram, J. (2000) Health Risks Caused by Freshwater Cyanobacteria in Recreational Waters. *Journal of Toxicology and Environmental Health-Part B-Critical Reviews* **3**, 323-347.

Choubey, V.K. and Subramanian, V. (1992) Estimation of Suspended-Solids Using Indian Remote-Sensing Satellite-1a Data - a Case-Study From Central India. *International Journal of Remote Sensing* **13**, 1473-1486.

Cizkova, H., Brix, H., Kopecky, J. and Lukavska, J. (1999) Organic Acids in the Sediments of Wetlands Dominated by Phragmites Australis: Evidence of Phytotoxic Concentrations. *Aquatic Botany* **64**, 303-315.

Cizkova, H., Strand, J.A. and Lukavska, J. (1996) Factors Associated With Reed Decline in a Eutrophic Fishpond, Rozmberk (South Bohemia, Czech Republic). *Folia Geobotanica & Phytotaxonomica* **31**, 73-84.

Clevers, J.G.P.W., Kooistra, L. and Salas, E.A.L. (2004) Study of Heavy Metal Contamination in River Floodplains Using the Red-Edge Position in Spectroscopic Data. *International Journal of Remote Sensing* **25**, 3883-3895.

Codd, G.A., Morrison, L.F. and Metcalf, J.S. (2005) Cyanobacterial Toxins: Risk Management for Health Protection. *Toxicology and Applied Pharmacology* **203**, 264-272.

Cohen, W.B. and Goward, S.N. (2004) Landsat's Role in Ecological Applications of Remote Sensing. *Bioscience* **54**, 535-545.

Cole, J.J., Prairie, Y.T., Caraco, N.F., Mcdowell, W.H., Tranvik, L.J., Striegl, R.G., Duarte, C.M., Kortelainen, P., Downing, J.A., Middelburg, J.J. and Melack, J. (2007) Plumbing the Global Carbon Cycle: Integrating Inland Waters Into the Terrestrial Carbon Budget. *Ecosystems* **10**, 171-184.

Cortes, C. and Vapnik, V. (1995) Support-Vector Networks. *Machine Learning* **20**, 273-297.

Cozar, A., Galvez, J.A., Hull, V., Garcia, C.M. and Loiselle, S.A. (2005) Sediment Resuspension by Wind in a Shallow Lake of Esteros Del Ibera (Argentina): a Model Based on Turbidimetry. *Ecological Modelling* **186**, 63-76.

Crawford, S.A. (1979) Farm Pond Restoration Using *Chara vulgaris* Vegetation. *Hydrobiologia* **62**, 17-31.

Crook, C.E., Boar, R.R. and Moss, B. (1983) *The Decline of Reedswamp in the Norfolk Broads: Cuases Consequences and Solutions*, Norwich: Broads Authority.

Curran, P.J. and Novo, E.M.M. (1988) The Relationship Between Suspended Sediment Concentration and Remotely Sensed Spectral Radiance - a Review. *Journal of Coastal Research* **4**, 351-368.

Dale, H.M. and Gillespie, T.J. (1977) Influence of Submersed Aquatic Plants on Temperature-Gradients in Shallow-Water Bodies. *Canadian Journal of Botany-Revue Canadienne De Botanique* **55**, 2216-2225.

Dall'Olmo, G. and Gitelson, A.A. (2005) Effect of Bio-Optical Parameter Variability on the Remote Estimation of Chlorophyll-a Concentration in Turbid Productive Waters: Experimental Results. *Applied Optics* **44**, 412-422.

Dall'Olmo, G. and Gitelson, A.A. (2006) Effect of Bio-Optical Parameter Variability and Uncertainties in Reflectance Measurements on the Remote Estimation of Chlorophyll-a Concentration in Turbid Productive Waters: Modeling Results. *Applied Optics* **45**, 3577-3592.

Dall'Olmo, G., Gitelson, A.A. and Rundquist, D.C. (2003) Towards a Unified Approach for Remote Estimation of Chlorophyll-a in Both Terrestrial Vegetation and Turbid Productive Waters. *Geophysical Research Letters* **30**,

Dall'Olmo, G., Gitelson, A.A., Rundquist, D.C., Leavitt, B., Barrow, T. and Holz, J.C. (2005) Assessing the Potential of Seawifs and Modis for Estimating Chlorophyll Concentration in Turbid Productive Waters Using Red and Near-Infrared Bands. *Remote Sensing of Environment* **96**, 176-187.

Danson, F.M. and Plummer, S.E. (1995) Red-Edge Response to Forest Leaf-Area Index. *International Journal of Remote Sensing* **16**, 183-188.

Datt, B. (1998) Remote Sensing of Chlorophyll a, Chlorophyll B, Chlorophyll a+b, and Total Carotenoid Content in Eucalyptus Leaves. *Remote Sensing of Environment* **66**, 111-121.

Datt, B. (1999) Visible/Near Infrared Reflectance and Chlorophyll Content in Eucalyptus Leaves. *International Journal of Remote Sensing* **20**, 2741-2759.

Davids, C. and Tyler, A.N. (2003) Detecting Contamination-Induced Tree Stress Within the Chernobyl Exclusion Zone. *Remote Sensing of Environment* **85**, 30-38.

Davies, G.C. (1883) *Norfolk Broads and Rivers*, London: Blackwood.

Dekker A.G. (1993) *Detection of Optical Water Quality Parameters for Eutrophic Waters by High Resolution Remote Sensing. PhD Thesis.*, Amsterdam: Vrije Universiteit.

Dekker, A.G., Brando, V.E. and Anstee, J.M. (2005) Retrospective Seagrass Change Detection in a Shallow Coastal Tidal Australian Lake. *Remote Sensing of Environment* **97**, 415-433.

Dekker, A.G., Malthus, T.J. and Seyhan, E. (1991) Quantitative Modeling of Inland Water-Quality for High-Resolution MSS Systems. *IEEE Transactions on Geoscience and Remote Sensing* **29**, 89-95.

Dekker, A.G., Malthus, T.J., Wijnen, M.M. and Seyhan, E. (1992) The Effect of Spectral Bandwidth and Positioning on the Spectral Signature Analysis of Inland Waters. *Remote Sensing of Environment* **41**, 211-225.

Dekker, A.G. and Peters, S.W.M. (1993) The Use of the Thematic Mapper for the Analysis of Eutrophic Lakes - a Case-Study in the Netherlands. *International Journal of Remote Sensing* **14**, 799-821.

Dekker, A.G., Vos, R.J. and Peters, S.W.M. (2001) Comparison of Remote Sensing Data, Model Results and *In Situ* Data for Total Suspended Matter (TSM) in the Southern Frisian Lakes. *Science of the Total Environment* **268**, 197-214.

Dekker, A.G., Vos, R.J. and Peters, S.W.M. (2002) Analytical Algorithms for Lake Water TSM Estimation for Retrospective Analyses of TM and Spot Sensor Data. *International Journal of Remote Sensing* **23**, 15-35.

Delgado, M., Dejonge, V.N. and Peletier, H. (1991) Experiments on Resuspension of Natural Microphytobenthos Populations. *Marine Biology* **108**, 321-328.

Denhartog, C., Kvet, J. and Sukopp, H. (1989) Reed - a Common Species in Decline - Introduction. *Aquatic Botany* **35**, 1-4.

Dickey, T., Lewis, M. and Chang, G. (2006) Optical Oceanography: Recent Advances and Future Directions Using Global Remote Sensing and in Situ Observations. *Reviews of Geophysics* **44**,

Dieter, C.D. (1990) The Importance of Emergent Vegetation in Reducing Sediment Resuspension in Wetlands. *Journal of Freshwater Ecology* **5**, 467-473.

Dillabaugh, C.R., Niemann, K.O. and Richardson, D.E. (2002) Semi-Automated Extraction of Rivers From Digital Imagery. *Geoinformatica* **6**, 263-284.

Dimitriou, E. and Zacharias, L. (2007) Using State-of-the-Art Techniques to Develop Water Management Scenarios in a Lake Catchment. *Nordic Hydrology* **38**, 79-97.

Dinka, M., Szeglet, P.P. and Szabo, I. (1995) Hungarian Group Report. In: Van der Putten, W.H., (Ed.) *Reed News (Reports of the EC Project EUREED - EV5V-CT92-0083). Vol. 3*, pp. 96-107. Heteren, Netherlands: Institute of Ecology.

Doerffer, R. and Schiller, H. (2007) The Meris Case 2 Water Algorithm. *International Journal of Remote Sensing* **28**, 517-535.

Dokulil, M.T., Donabaum, K. and Teubner, K. (2007) Modifications in Phytoplankton Size Structure by Environmental Constraints Induced by Regime Shifts in an Urban Lake. *Hydrobiologia* **578**, 59-63.

Dokulil, M.T. and Teubner, K. (2000) Cyanobacterial Dominance in Lakes. *Hydrobiologia* **438**, 1-12.

Duan, H.T., Zhang, B., Liu, D.W., Zhang, Y.Z., Song, K.S. and Wang, Z.M. (2006) Relationship Between Fluorescence Peak Spectral Features and Chlorophyll-Alpha in Lake Chagan. *Journal of Infrared and Millimeter Waves* **25**, 355-359.

Duan, H.T., Zhang, Y.Z., Zhan, B., Song, K.S. and Wang, Z.M. (2007) Assessment of Chlorophyll-a Concentration and Trophic State for Lake Chagan Using Landsat TM and Field Spectral Data. *Environmental Monitoring and Assessment* **129**, 295-308.

Duda, K.A. and Abrams, M. (2005) ASTER and USGS Eros Disaster Response: Emergency Imaging After Hurricane Katrina. *Photogrammetric Engineering and Remote Sensing* **71**, 1346-1350.

Dworak, T., Gonzalez, C., Laaser, C. and Interwies, E. (2005) The Need for New Monitoring Tools to Implement the WFD. *Environmental Science & Policy* **8**, 301-306.

Eckerrot, A. and Pettersson, K. (1993) Pore Water Phosphorus and Iron Concentrations in a Shallow, Eutrophic Lake - Indications of Bacterial Regulation. *Hydrobiologia* **253**, 165-177.

Ekstrand, S. (1992) Landsat TM Based Quantification of Chlorophyll-a During Algae Blooms in Coastal Waters. *International Journal of Remote Sensing* **13**, 1913-1926.

Elliott, J.A., Thackeray, S.J., Huntingford, C. and Jones, R.G. (2005) Combining a Regional Climate Model With a Phytoplankton Community Model to Predict Future Changes in Phytoplankton in Lakes. *Freshwater Biology* **50**, 1404-1411.

Ellis, E.A. (1935) Wheatfen Broad, Surlingham. *Transactions of the Norfolk and Norwich Naturalists Society* **13**, 422-451.

ENVI (2003) *ENVI: A User's Guide*, Colorado, USA: RSI ENVI.

Evans, G.T. and Taylor, F.J.R. (1980) Phytoplankton Accumulation in Langmuir Cells. *Limnology and Oceanography* **25**, 840-845.

Fan, C.X., Zhang, L. and Qu, T.C. (2001) Lake Sediment Resuspension and Caused Phosphate Release - a Simulation Study. *Journal of Environmental Sciences-China* **13**, 406-410.

Finlayson, C.M. and Vandervalk, A.G. (1995) Classification and Inventory of the Worlds Wetlands. *Vegetatio* **118**, 1-2.

Fishwick, J.R., Aiken, J., Barlow, R., Sessions, H., Bernard, S. and Ras, J. (2006) Functional Relationships and Bio-Optical Properties Derived From Phytoplankton Pigments, Optical and Photosynthetic Parameters; a Case Study of the Benguela Ecosystem. *Journal of the Marine Biological Association of the United Kingdom* **86**, 1267-1280.

Fitzgerald, G.J., Rodriguez, D., Christensen, L.K., Belford, R., Sadras, V.O. and Clarke, T.R. (2006) Spectral and Thermal Sensing for Nitrogen and Water Status in Rainfed and Irrigated Wheat Environments. *Precision Agriculture* **7**, 233-248.

Flink, P., Lindell, T. and Ostlund, C. (2001) Statistical Analysis of Hyperspectral Data from Two Swedish Lakes. *Science of the Total Environment* **268**, 155-169.

Fogli, S., Marchesini, R. and Gerdol, R. (2002) Reed (*Phragmites australis*) Decline in a Brackish Wetland in Italy. *Marine Environmental Research* **53**, 465-479.

Frederiksen, M., Krause-Jensen, D., Holmer, M. and Laursen, J.S. (2004) Long-Term Changes in Area Distribution of Eelgrass (Zostera Marina) in Danish Coastal Waters. *Aquatic Botany* **78**, 167-181.

Frempong, E. (1981) Diel Variation in the Abundance, Vertical-Distribution, and Species Composition of Phytoplankton in a Eutrophic English Lake. *Journal of Ecology* **69**, 919-939.

Galat, D.L. and Verdin, J.P. (1988) Magnitude of Blue-Green-Algal Blooms in a Saline Desert Lake Evaluated by Remote-Sensing - Evidence for Nitrogen Control. *Canadian Journal of Fisheries and Aquatic Sciences* **45**, 1959-1967.

Gamon, J.A., Penuelas, J. and Field, C.B. (1992) A Narrow-Waveband Spectral Index That Tracks Diurnal Changes in Photosynthetic Efficiency. *Remote Sensing of Environment* **41**, 35-44.

Garrad, P.N. and Hey, R.D. (1987) Boat Traffic, Sediment Resuspension and Turbidity in a Broadland River. *Journal of Hydrology* **95**, 289-297.

George, D.G. (1993) Physical and Chemical-Scales of Pattern in Fresh-Water Lakes and Reservoirs. *Science of the Total Environment* **135**, 1-15.

George, D.G. (1997) The Airborne Remote Sensing of Phytoplankton Chlorophyll in the Lakes and Tarns of the English Lake District. *International Journal of Remote Sensing* **18**, 1961-1975.

George, D.G. (2000) Remote Sensing Evidence for the Episodic Transport of Phosphorus From the Littoral Zone of a Thermally Stratified Lake. *Freshwater Biology* **43**, 571-578.

George, D.G. and Edwards, R.W. (1976) Effect of Wind on Distribution of Chlorophyll a and Crustacean Plankton in a Shallow Eutrophic Reservoir. *Journal of Applied Ecology* **13**, 667-690.

George, D.G. and Heaney, S.I. (1978) Factors Influencing Spatial-Distribution of Phytoplankton in a Small Productive Lake. *Journal of Ecology* **66** , 133-155.

George, D.G. and Jones, D.H. (1987) Catchment Effects on the Horizontal Distribution of Phytoplankton in 5 of Scotland Largest Fresh-Water Lochs. *Journal of Ecology* **75**, 43-59.

George, D.G. and Malthus, T.J. (2001) Using a Compact Airborne Spectrographic Imager to Monitor Phytoplankton Biomass in a Series of Lakes in North Wales. *Science of the Total Environment* **268**, 215-226.

Ghezzi, P., Giardino, C., Pepe, M. and Zilioli, E. (1998) *Report on the 2nd SALMON Joint Meeting, Venice, CEC Progress Report*, Milano: CNR-IRRS Telerilevamento.

Giardino, C., Brando, V.E., Dekker, A.G., Strombeck, N. and Candiani, G. (2007) Assessment of Water Quality in Lake Garda (Italy) Using Hyperion. *Remote Sensing of Environment* **109**, 183-195.

Giardino, C., Candiani, G. and Zilioli, E. (2005) Detecting Chlorophyll-a in Lake Garda Using TOA Meris Radiances. *Photogrammetric Engineering and Remote Sensing* **71**, 1045-1051.

Gilvear, D., Tyler, A. and Davids, C. (2004a) Detection of Estuarine and Tidal River Hydromorphology Using Hyper-Spectral and Lidar Data: Forth Estuary, Scotland. *Estuarine Coastal and Shelf Science* **61**, 379-392.

Gilvear, D.J., Davids, C. and Tyler, A.N. (2004b) The Use of Remotely Sensed Data to Detect Channel Hydromorphology; River Tummel, Scotland. *River Research and Applications* **20**, 795-811.

Gilvear, D.J., Hunter, P.D. and Higgins, T. (2007) An Experimental Approach to the Measurement of the Effects of Water Depth and Substrate on Optical and Near Infra-Red Reflectance: a Field-Based Assessment of the Feasibility of Mapping Submerged Instream Habitat. *International Journal of Remote Sensing* **28**, 2241-2256.

Gilvear, D.J. and Mcinnes, R.J. (1994) Wetland Hydrological Vulnerability and the Use of Classification Procedures - a Scottish Case-Study. *Journal of Environmental Management* **42**, 403-414.

Gitelson, A. (1992) The Peak Near 700 Nm on Radiance Spectra of Algae and Water - Relationships of Its Magnitude and Position With Chlorophyll Concentration. *International Journal of Remote Sensing* **13**, 3367-3373.

Gitelson, A., Garbuzov, G., Szilagyi, F., Mittenzwey, K.H., Karnieli, A. and Kaiser, A. (1993) Quantitative Remote-Sensing Methods for Real-Time Monitoring of Inland Waters Quality. *International Journal of Remote Sensing* **14**, 1269-1295.

Gitelson, A. and Merzlyak, M.N. (1994) Spectral Reflectance Changes Associated With Autumn Senescence of Aesculus-Hippocastanum L. and Acer-Platanoides L. Leaves - Spectral Features and Relation to Chlorophyll Estimation. *Journal of Plant Physiology* **143**, 286-292.

Gitelson, A.A., Buschmann, C. and Lichtenthaler, H.K. (1999) The Chlorophyll Fluorescence Ratio F-735/F-700 as an Accurate Measure of the Chlorophyll Content in Plants. *Remote Sensing of Environment* **69**, 296-302.

Gitelson, A.A., Kaufman, Y.J. and Merzlyak, M.N. (1996) Use of a Green Channel in Remote Sensing of Global Vegetation From Eos-Modis. *Remote Sensing of Environment* **58**, 289-298.

Gitelson, A.A. and Merzlyak, M.N. (1997) Remote Estimation of Chlorophyll Content in Higher Plant Leaves. *International Journal of Remote Sensing* **18**, 2691-2697.

Gitelson, A.A., Nikanorov, A., Sabo, G. and Szilagyi, F. (1986) Etude de la qualite des eaux surface par teledetection. *IHAS Publications* **157**, 111-121.

Gitelson, A.A., Schalles, J.F., Rundquist, D.C., Schiebe, F.R. and Yacobi, Y.Z. (1999) Comparative Reflectance Properties of Algal Cultures With Manipulated Densities. *Journal of Applied Phycology* **11**, 345-354.

Gloaguen, R., Marpu, P.R. and Niemeyer, I. (2007) Automatic Extraction of Faults and Fractal Analysis From Remote Sensing Data. *Nonlinear Processes in Geophysics* **14**, 131-138.

Gons, H.J., Rijkeboer, M. and Ruddick, K.G. (2002) A Chlorophyll-Retrieval Algorithm for Satellite Imagery (Medium Resolution Imaging Spectrometer) of Inland and Coastal Waters. *Journal of Plankton Research* **24**, 947-951.

Goodin, D.G., Han, L.H., Fraser, R.N., Rundquist, D.C. and Stebbins, W.A. (1993) Analysis of Suspended-Solids in Water Using Remotely Sensed High-Resolution Derivative Spectra. *Photogrammetric Engineering and Remote Sensing* **59**, 505-510.

Gordon, H.R. (1988) Influence of Vertical Stratification on the Distribution of Irradiance at the Sea-Surface From a Point-Source in the Ocean. *Applied Optics* **27**, 2643-2645.

Gordon, H.R., Brown, O.B. and Jacobs, M.M. (1975) Computed Relationships Between Inherent and Apparent Optical-Properties of a Flat Homogeneous Ocean. *Applied Optics* **14**, 417-427.

Gould, R.W., Arnone, R.A. and Martinolich, P.M. (1999) Spectral Dependence of the Scattering Coefficient in Case 1 and Case 2 Waters. *Applied Optics* **38**, 2377-2383.

Hadjimitsis, D.G., Clayton, C.R.I. and Hope, V.S. (2004) An Assessment of the Effectiveness of Atmospheric Correction Algorithms Through the Remote Sensing of Some Reservoirs. *International Journal of Remote Sensing* **25**, 3651-3674.

Hamilton, M.K., Davis, C.O., Rhea, W.J., Pilorz, S.H. and Carder, K.L. (1993) Estimating Chlorophyll Content and Bathymetry of Lake Tahoe Using Aviris Data. *Remote Sensing of Environment* **44**, 217-230.

Han, L., Rundquist, D.C., Liu, L.L., Fraser, R.N. and Schalles, J.F. (1994) The Spectral Responses of Algal Chlorophyll in Water With Varying Levels of Suspended Sediment. *International Journal of Remote Sensing* **15**, 3707-3718.

Han, L.H. (2005) Estimating Chlorophyll-a Concentration Using First-Derivative Spectra in Coastal Water. *International Journal of Remote Sensing* **26**, 5235-5244.

Han, L.H. and Rundquist, D.C. (1997) Comparison of NIR/Red Ratio and First Derivative of Reflectance in Estimating Algal-Chlorophyll Concentration: a Case Study in a Turbid Reservoir. *Remote Sensing of Environment* **62**, 253-261.

Hare, J.L., Ferguson, J.F., Aiken, C.L.V. and Oldow, J.S. (2001) Quantitative Characterization and Elevation Estimation of Lake Lahontan Shoreline Terraces From High-Resolution Digital Elevation Models. *Journal of Geophysical Research-Solid Earth* **106**, 26761-26774.

Harma, P., Vepsalainen, J., Hannonen, T., Pyhalahti, T., Kamari, J., Kallio, K., Eloheimo, K. and Koponen, S. (2001) Detection of Water Quality Using Simulated Satellite Data and Semi-Empirical Algorithms in Finland. *Science of the Total Environment* **268**, 107-121.

Harrington, J.A., Schiebe, F.R. and Nix, J.F. (1992) Remote-Sensing of Lake Chicot, Arkansas - Monitoring Suspended Sediments, Turbidity, and Secchi Depth With Landsat Mss Data. *Remote Sensing of Environment* **39**, 15-27.

Harrison, A.W. and Coombes, C.A. (1988) An Opaque Cloud Cover Model of Sky Short Wavelength Radiance. *Solar Energy* **41**, 387-392.

Havens, K.E. (1991) Fish-Induced Sediment Resuspension - Effects on Phytoplankton Biomass and Community Structure in a Shallow Hypereutrophic Lake. *Journal of Plankton Research* **13**, 1163-1176.

Havens, K.E., Kukushima, T., Xie, P., Iwakuma, T., James, R.T., Takamura, N., Hanazato, T. and Yamamoto, T. (2001) Nutrient Dynamics and the Eutrophication of Shallow Lakes Kasumigaura (Japan), Donghu (PR China), and Okeechobee (USA). *Environmental Pollution* **111**, 263-272.

Hedger, R.D., Olsen, N.R.B., George, D.G., Malthus, T.J. and Atkinson, P.M. (2004) Modelling Spatial Distributions of *Ceratium Hirundnella* and *Microcystis* Spp. In a Small Productive British Lake. *Hydrobiologia* **528**, 217-227.

Hedger, R.D., Olsen, N.R.B., Malthus, T.J. and Atkinson, P.M. (2002) Coupling Remote Sensing With Computational Fluid Dynamics Modelling to Estimate Lake Chlorophyll-a Concentration. *Remote Sensing of Environment* **79**, 116-122.

Heim, B., Oberhaensli, H., Fietz, S. and Kaufmann, H. (2005) Variation in Lake Baikal's Phytoplankton Distribution and Fluvial Input Assessed by SeaWiFS Satellite Data. *Global and Planetary Change* **46**, 9-27.

Herodek, S.L.L.V.A. (1988) Lake Balaton: Research and Management. *Nexus Nyomda Budapest* 1-110.

Hirtle, H. and Rencz, A. (2003) The Relation Between Spectral Reflectance and Dissolved Organic Carbon in Lake Water: Kejimkujik National Park, Nova Scotia, Canada. *International Journal of Remote Sensing* **24**, 953-967.

Hoepffner, N. and Sathyendranath, S. (1992) Biooptical Characteristics of Coastal Waters - Absorption-Spectra of Phytoplankton and Pigment Distribution in the Western North-Atlantic. *Limnology and Oceanography* **37**, 1660-1679.

Hoepffner, N. and Sathyendranath, S. (1993) Determination of the Major Groups of Phytoplankton Pigments From the Absorption-Spectra of Total Particulate Matter. *Journal of Geophysical Research-Oceans* **98**, 22789-22803.

Holt, R.D. (1984) Spatial Heterogeneity, Indirect Interactions, and the Coexistence of Prey Species. *American Naturalist* **124**, 377-406.

Hoogenboom, H.J., Dekker, A.G. and Althuis, I.A. (1998) Simulation of AVIRIS Sensitivity for Detecting Chlorophyll Over Coastal and Inland Waters. *Remote Sensing of Environment* **65**, 333-340.

Hooker, S.B. and Mcclain, C.R. (2000) The Calibration and Validation of Seawifs Data. *Progress in Oceanography* **45**, 427-465.

Horppila, J. and Nurminen, L. (2001) The Effect of an Emergent Macrophyte (*Typha angustifolia*) on Sediment Resuspension in a Shallow North Temperate Lake. *Freshwater Biology* **46**, 1447-1455.

Humphries, S.E. and Lyne, V.D. (1988) Cyanophyte Blooms - the Role of Cell Buoyancy. *Limnology and Oceanography* **33**, 79-91.

Hunter, P.D., Tyler, A.N., Gilvear, D.J. and Willby, N.J. (submitted) The Spatial Dynamics of Vertical Migration by *Microcystis aeruginosa* in a Eutrophic Shallow Lake: A Case-Study using High Spatial Resolution Time-Series Airborne Remote Sensing. *Limnology & Oceanography.*

Hunter, P.D., Tyler, A.N., Presing, M., Kovacs, A.W. and Preston, T. (2007) Spectral Discrimination of Phytoplankton Colour Groups: The Effect of Particulate Suspended Matter and Sensor Spectral Resolution. *Remote Sensing of Environment,* in press.

Hysenstrand, P., Blonqvist, P. and Petterson, A. (1998) Factors determining cyanbacteria success in aquatic systems: a literature review. *Archive fur Hydrobiologie* **51**, 41-62.

Irfanullah, H.M. and Moss, B. (2005) A Filamentous Green Algae-Dominated Temperate Shallow Lake: Variations on the Theme of Clearwater Stable States? *Archiv Fur Hydrobiologie* **163**, 25-47.

Irvine, K., Moss, B., Bales, M. and Snook, D. (1993) The Changing Ecosystem of a Shallow, Brackish Lake, Hickling Broad, Norfolk, UK .1. Trophic Relationships With Special Reference to the Role of *Neomysis Integer*. *Freshwater Biology* **29**, 119-139.

Islam, A., Gao, J., Ahmad, W., Neil, D. and Bell, P. (2004) A Composite DOP Approach to Excluding Bottom Reflectance in Mapping Water Parameters of Shallow Coastal Zones From Tm Imagery. *Remote Sensing of Environment* **92**, 40-51.

Iwamura, T., Nagai, H. and Ishimura./S. (1970) Improved Methods for Determing the Contents of Chlorophyll, Protein, Ribonucleic and Deoxyribonucleic Acid. *Internationale Revue der gesamtam Hydrobiologie* **55**, 131-147.

Jacobsen, B.A. and Simonsen, P. (1993) Disturbance Events Affecting Phytoplankton Biomass, Composition and Species-Diversity in a Shallow, Eutrophic, Temperate Lake. *Hydrobiologia* **249**, 9-14.

Jago, R.A., Cutler, M.E.J. and Curran, P.J. (1999) Estimating Canopy Chlorophyll Concentration from Field and Airborne Spectra. *Remote Sensing of Environment* **68**, 217-224.

Jak, R.G., Maas, J.L. and Scholten, M.C.T. (1996) Evaluation of Laboratory Derived Toxic Effect Concentrations of a Mixture of Metals by Testing Fresh Water Plankton Communities in Enclosures. *Water Research* **30**, 1215-1227.

Jakubauskas, M., Kindscher, K., Fraser, A., Debinski, D. and Price, K.P. (2000) Close-Range Remote Sensing of Aquatic Macrophyte Vegetation Cover. *International Journal of Remote Sensing* **21**, 3533-3538.

Janauer, G.A. (1997) Macrophytes, Hydrology, and Aquatic Ecotones: a GIS-Supported Ecological Survey. *Aquatic Botany* **58**, 379-391.

Jaquet, J.M., Schanz, F., Bossard, P., Hanselmann, K. and Gendre, F. (1994) Measurements and Significance of Bio-optical Parameters for Remote-Sensing in 2 Sub-Alpine Lakes of Different Trophic State. *Aquatic Sciences* **56**, 263-305.

Jeffrey, S.W. and Vesk, M. (1997) Introduction to Marine Phytoplankton and their Pigment Signatures. In: Jeffrey, S.W., Mantoura, R.F.C. and Wright, S.W., (Eds.) *Phytoplankton Pigments in Oceanography: Guidelines to Modern Methods*, pp. 127-178. Paris: UNESCO.

Jensen, J.P., Jeppesen, E., Olrik, K. and Kristensen, P. (1994) Impact of Nutrients and Physical Factors on the Shift From Cyanobacterial to Chlorophyte Dominance in Shallow Danish Lakes. *Canadian Journal of Fisheries and Aquatic Sciences* **51**, 1692-1699.

Jeppesen, E., Jensen, J.P., Sondergaard, M., Lauridsen, T., Pedersen, L.J. and Jensen, L. (1997) Top-Down Control in Freshwater Lakes: the Role of Nutrient State, Submerged Macrophytes and Water Depth. *Hydrobiologia* **342**, 151-164.

Jernakoff, P., Hick, P., Ong, C., Hosja, W. and Grigo, S. (1996) Mapping Algal Blooms Using Airborne Digital Multi-Spectral Video and the Importance of Bloom Dynamics in the Collection of in-Water Data. *Marine Technology Society Journal* **30**, 36-45.

Jin, K.R., Ji, Z.G. and James, R.T. (2007) Three-Dimensional Water Quality and SAV Modeling of a Large Shallow Lake. *Journal of Great Lakes Research* **33**, 28-45.

Jones, J.I. and Sayer, C.D. (2003) Does the Fish-Invertebrate-Periphyton Cascade Precipitate Plant Loss in Shallow Lakes? *Ecology* **84**, 2155-2167.

Jordan, C.F. (1969) Derivation of Leaf-Area Index From Quality of Light on Forest Floor. *Ecology* **50**, 663-666.

Jurgens, K. and Stolpe, G. (1995) Seasonal Dynamics of Crustacean Zooplankton, Heterotrophic Nanoflagellates and Bacteria in a Shallow, Eutrophic Lake. *Freshwater Biology* **33**, 27-38.

Kallio, K., Kutser, T., Hannonen, T., Koponen, S., Pulliainen, J., Vepsalainen, J. and Pyhalahti, T. (2001) Retrieval of Water Quality From Airborne Imaging Spectrometry of Various Lake Types in Different Seasons. *Science of the Total Environment* **268**, 59-77.

Karl, D.M. (2002) Nutrient Dynamics in the Deep Blue Sea. *Trends in Microbiology* **10**, 410-418.

Kay, J.E., Kampf, S.K., Handcock, R.N., Cherkauer, K.A., Gillespie, A.R. and Burges, S.J. (2005) Accuracy of Lake and Stream Temperatures Estimated from Thermal Infrared Images. *Journal of the American Water Resources Association* **41**, 1161-1175.

Kelly, N.M., Fonseca, M. and Whitfield, P. (2001) Predictive Mapping for Management and Conservation of Seagrass Beds in North Carolina. *Aquatic Conservation-Marine and Freshwater Ecosystems* **11**, 437-451.

Kennison, G.C.B., Dunsford, D.S. and Schutten, J. (1998) Stable or Changing Lakes? A Classification of Aquatic Macrophyte Assemblages From a Eutrophic Shallow Lake System in the United Kingdom. *Aquatic Conservation-Marine and Freshwater Ecosystems* **8**, 669-684.

Kent, B.J. and Mast, J.N. (2005) Wetland Change Analysis of San Dieguito Lagoon, California, USA: 1928-1994. *Wetlands* **25**, 780-787.

Kent, M., Gill, W.J., Weaver, R.E. and Armitage, R.P. (1997) Landscape and Plant Community Boundaries in Biogeography. *Progress in Physical Geography* **21**, 315-353.

Kerr, J.T. and Ostrovsky, M. (2003) From Space to Species: Ecological Applications for Remote Sensing. *Trends in Ecology & Evolution* **18**, 299-305.

Kerrison, P.H., Annoni, D., Zarini, S., Ravera, O. and Moss, B. (1988) Effects of Low Concentrations of Heavy-Metals on Plankton Community Dynamics in a Small, Shallow, Fertile Lake. *Journal of Plankton Research* **10**, 779-812.

Kirk, J.T.O. (1994) *Light & Photosynthesis in Aquatic Ecosystems*, 2nd edn. London: Cambridge University Press.

Kokaly, R.F. and Clark, R.N. (1999) Spectroscopic Determination of Leaf Biochemistry Using Band-Depth Analysis of Absorption Features and Stepwise Multiple Linear Regression. *Remote Sensing of Environment* **67**, 267-287.

Kokaly, R.F., Despain, D.G., Clark, R.N. and Livo, K.E. (2003) Mapping Vegetation in Yellowstone National Park Using Spectral Feature Analysis of Aviris Data. *Remote Sensing of Environment* **84**, 437-456.

Kooistra, L., Leuven, R.S.E.W., Wehrens, R., Nienhuis, P.H. and Buydens, L.M.C. (2003) A Comparison of Methods to Relate Grass Reflectance to Soil Metal Contamination. *International Journal of Remote Sensing* **24**, 4995-5010.

Kooistra, L., Salas, E.A.L., Clevers, J.G.P.W., Wehrens, R., Leuven, R.S.E.W., Nienhuis, P.H. and Buydens, L.M.C. (2004) Exploring Field Vegetation Reflectance as an Indicator of Soil Contamination in River Floodplains. *Environmental Pollution* **127**, 281-290.

Koponen, S., Attila, J., Pulliainen, J., Kallio, K., Pyhalahti, T., Lindfors, A., Rasmus, K. and Hallikainen, M. (2007) A Case Study of Airborne and Satellite Remote Sensing of a Spring Bloom Event in the Gulf of Finland. *Continental Shelf Research* **27**, 228-244.

Koponen, S., Pulliainen, J., Kallio, K. and Hallikainen, M. (2002) Lake Water Quality Classification With Airborne Hyperspectral Spectrometer and Simulated Meris Data. *Remote Sensing of Environment* **79**, 51-59.

Kortelainen, P., Pajunen, H., Rantakari, M. and Saarnisto, M. (2004) A Large Carbon Pool and Small Sink in Boreal Holocene Lake Sediments. *Global Change Biology* **10**, 1648-1653.

Krawczyk, H., Neumann, A., Gerasch, B. and Walzel, T. (2007) Regional Products for the Baltic Sea Using Meris Data. *International Journal of Remote Sensing* **28**, 593-608.

Kromkamp, J., Konopka, A. and Mur, L.R. (1988) Buoyancy Regulation in Light-Limited Continuous Cultures of Microcystis-Aeruginosa. *Journal of Plankton Research* **10**, 171-183.

Kruse, F.A., Lefkoff, A.B., Boardman, J.W., Heidebrecht, K.B., Shapiro, A.T., Barloon, P.J. and Goetz, A.F.H. (1993) The Spectral Image-Processing System (SIPS) - Interactive Visualization and Analysis of Imaging Spectrometer Data. *Remote Sensing of Environment* **44**, 145-163.

Kufel, L. and Kufel, I. (2002) Chara Beds Acting as Nutrient Sinks in Shallow Lakes - a Review. *Aquatic Botany* **72**, 249-260.

Kullberg, A., Bishop, K.H., Hargeby, A., Jansson, M. and Petersen, R.C. (1993) The Ecological Significance of Dissolved Organic-Carbon in Acidified Waters. *Ambio* **22**, 331-337.

Kutser, T. (2004) Quantitative Detection of Chlorophyll in Cyanobacterial Blooms by Satellite Remote Sensing. *Limnology and Oceanography* **49**, 2179-2189.

Kutser, T., Metsamaa, L., Strombeck, N. and Vahtmae, E. (2006) Monitoring Cyanobacterial Blooms by Satellite Remote Sensing. *Estuarine Coastal and Shelf Science* **67**, 303-312.

Kutser, T., Pierson, D., Tranvik, L., Reinart, A., Sobek, S. and Kallio, K. (2005a) Using Satellite Remote Sensing to Estimate the Colored Dissolved Organic Matter Absorption Coefficient in Lakes. *Ecosystems* **8**, 709-720.

Kutser, T., Pierson, D.C., Kallio, K.Y., Reinart, A. and Sobek, S. (2005b) Mapping Lake CDOM by Satellite Remote Sensing. *Remote Sensing of Environment* **94**, 535-540.

Lacroix, G., Lescher-Moutoue, F. and Bertolo, A. (1999) Biomass and Production of Plankton in Shallow and Deep Lakes: Are There General Patterns? *Annales De Limnologie-International Journal of Limnology* **35**, 111-122.

Lambert, J.M. and Smith, C.T. (1961) The Norfolk Broads as man-made features. *New Scientist,* 775-777.

Lathrop, R.G., Lillesand, T.M. and Yandell, B.S. (1991) Testing the Utility of Simple Multi-Date Thematic Mapper Calibration Algorithms for Monitoring Turbid Inland Waters. *International Journal of Remote Sensing* **12**, 2045-2063.

Lathrop, R.G., Styles, R.M., Seitzinger, S.P. and Bognar, J.A. (2001) Use of GIS Mapping and Modeling Approaches to Examine the Spatial Distribution of Seagrasses in Barnegat Bay, New Jersey. *Estuaries* **24**, 904-916.

Le Maire, G., Francois, C. and Dufrene, E. (2004) Towards Universal Broad Leaf Chlorophyll Indices Using Prospect Simulated Database and Hyperspectral Reflectance Measurements. *Remote Sensing of Environment* **89**, 1-28.

Legleiter, C.J. (2003) Spectrally Driven Classification of High Spatial Resolution, Hyperspectral Imagery: a Tool for Mapping in-Stream Habitat. *Environmental Management* **32**, 399-411.

Legleiter, C.J. and Roberts, D.A. (2005) Effects of Channel Morphology and Sensor Spatial Resolution on Image-Derived Depth Estimates. *Remote Sensing of Environment* **95**, 231-247.

Leibovich, S. (1983) The Form and Dynamics of Langmuir Circulations. *Annual Review of Fluid Mechanics* **15**, 391-427.

Levin, S.A. (1992) The Problem of Pattern and Scale in Ecology. *Ecology* **73**, 1943-1967.

Li, H.Y., Budd, J.W. and Green, S. (2004) Evaluation and Regional Optimization of Bio-Optical Algorithms for Central Lake Superior. *Journal of Great Lakes Research* **30**, 443-458. Notes: Supplement: Suppl. 1

Li, J. and Narayanan, R.M. (2003) A Shape-Based Approach to Change Detection of Lakes Using Time Series Remote Sensing Images. *IEEE Transactions on Geoscience and Remote Sensing* **41**, 2466-2477.

Lichtenthaler, H.K. (1996) Vegetation Stress: an Introduction to the Stress Concept in Plants. *Journal of Plant Physiology* **148**, 4-14.

Lindell, T., Pierson, D., Premazzi, G. and Zilioli, E. (1999) *Manual for Monitoring European Lakes Using Remote Sensing Techniques*, Italy: European Commission Joint Research Centre.

Lindholm, T., Eriksson, J.E. and Meriluoto, J.A.O. (1989) Toxic Cyanobacteria and Water-Quality Problems - Examples From a Eutropic Lake on Aland, South West Finland. *Water Research* **23**, 481-486.

Linge, K.L. and Oldham, C.E. (2002) Arsenic Remobilization in a Shallow Lake: the Role of Sediment Resuspension. *Journal of Environmental Quality* **31**, 822-828.

Liu, D.S., Kelly, M. and Gong, P. (2006) A Spatial-Temporal Approach to Monitoring Forest Disease Spread Using Multi-Temporal High Spatial Resolution Imagery. *Remote Sensing of Environment* **101**, 167-180.

Liu, L.Y., Wang, J.H., Huang, W.J., Zhao, C.J., Zhang, B. and Tong, Q.X. (2004) Estimating Winter Wheat Plant Water Content Using Red Edge Parameters. *International Journal of Remote Sensing* **25**, 3331-3342.

Liu, X.H., Skidmore, A.K. and Van Oosten, H. (2002) Integration of Classification Methods for Improvement of Land-Cover Map Accuracy. *Isprs Journal of Photogrammetry and Remote Sensing* **56**, 257-268.

Liu, Y.S., Islam, M.A. and Gao, J. (2003) Quantification of Shallow Water Quality Parameters by Means of Remote Sensing. *Progress in Physical Geography* **27**, 24-43.

Lorenzen, C.J. and Jeffrey, S.W. (1980) Determination of Chlorophyll in Seawater. *UNESCO Technical Papers in Marine Science* **35**, 1-20.

Louchard, E.M., Reid, R.P., Stephens, F.C., Davis, C.O., Leathers, R.A. and Downes, T.V. (2003) Optical Remote Sensing of Benthic Habitats and Bathymetry in Coastal Environments at Lee Stocking Island, Bahamas: a Comparative Spectral Classification Approach. *Limnology and Oceanography* **48**, 511-521.
Notes: Part Number: Part 2

Luettich, R.A., Harleman, D.R.F. and Somlyody, L. (1990) Dynamic Behavior of Suspended Sediment Concentrations in a Shallow Lake Perturbed by Episodic Wind Events. *Limnology and Oceanography* **35**, 1050-1067.

Ma, R., Tang, J., Dai, J., Zhang, Y. and Song, Q. (2006) Absorption and Scattering Properties of Water Body in Taihu Lake, China: Absorption. *International Journal of Remote Sensing* **27**, 4277-4304.

Maccioni, A., Agati, G. and Mazzinghi, P. (2001) New Vegetation Indices for Remote Measurement of Chlorophylls Based on Leaf Directional Reflectance Spectra. *Journal of Photochemistry and Photobiology B-Biology* **61**, 52-61.

Madsen, J.D., Chambers, P.A., James, W.F., Koch, E.W. and Westlake, D.F. (2001) The Interaction Between Water Movement, Sediment Dynamics and Submersed Macrophytes. *Hydrobiologia* **444**, 71-84.

Maheu-Giroux, M. and De Blois, S. (2005) Mapping the Invasive Species Phragmites Australis in Linear Wetland Corridors. *Aquatic Botany* **83**, 310-320.

Maler, K.G., Xepapadeas, A. and De Zeeuw, A. (2003) The Economics of Shallow Lakes. *Environmental & Resource Economics* **26**, 603-624.

Malthus, T.J. and Dekker, A.G. (1995) First Derivative Indexes for the Remote-Sensing of Inland Water-Quality Using High-Spectral-Resolution Reflectance. *Environment International* **21**, 221-232.

Malthus, T.J. and George, D.G. (1997) Airborne Remote Sensing of Macrophytes in Cefni Reservoir, Anglesey, UK. *Aquatic Botany* **58**, 317-332.

Mantoura, R.F.C. and Llewellyn, C.A. (1983) The Rapid-Determination of Algal Chlorophyll and Carotenoid-Pigments and Their Breakdown Products in Natural-Waters by Reverse-Phase High-Performance Liquid-Chromatography. *Analytica Chimica Acta* **151**, 297-314.

Markensten, H. and Pierson, D.C. (2003) A Dynamic Model for Flow and Wind Driven Sediment Resuspension in a Shallow Basin. *Hydrobiologia* **494**, 305-311.

Mason, C.F. and Bryant, R.J. (1975) Changes in Ecology of Norfolk-Broads. *Freshwater Biology* **5**, 257-270.

Mason, R., Kim, E.H., Porter, E. and Soulen, H. (2003) The Impact of Sediment Resuspension on Mercury and Methylmercury Fate, Transport and Bioaccumulation Is Shallow Estuaries. *Geochimica Et Cosmochimica Acta* **67**, A274 Notes: Supplement: Suppl. 1

May, A.M.B., Pinder, J.E. and Kroh, G.C. (1997) A Comparison of Landsat Thematic Mapper and Spot Multi-Spectral Imagery for the Classification of Shrub and Meadow Vegetation in Northern California, Usa. *International Journal of Remote Sensing* **18**, 3719-3728.

McDermid, G.J., Franklin, S.E. and Ledrew, E.F. (2005) Remote Sensing for Large-Area Habitat Mapping. *Progress in Physical Geography* **29**, 449-474.

McKillop, R.J. and Clague, J.J. (2007) A Procedure for Making Objective Preliminary Assessments of Outburst Flood Hazard From Moraine-Dammed Lakes in Southwestern British Columbia. *Natural Hazards* **41**, 131-157.

Mcmurtrey, J.E., Chappelle, E.W., Kim, M.S., Meisinger, J.J. and Corp, L.A. (1994) Distinguishing Nitrogen-Fertilization Levels in-Field Corn (Zea-Mays L) With Actively Induced Fluorescence and Passive Reflectance Measurements. *Remote Sensing of Environment* **47**, 36-44.

McQueen, D.J. and Lean, D.R.S. (1987) Influence of Water Temperature and Nitrogen to Phosphorus Ratios on the Dominance of Blue-Green-Algae in Lake St-George, Ontario. *Canadian Journal of Fisheries and Aquatic Sciences* **44**, 598-604.

Melack, J.M. and Gastil, M. (2001) Airborne Remote Sensing of Chlorophyll Distributions in Mono Lake, California. *Hydrobiologia* **466**, 31-38.

Meleder, V., Barille, L., Launeau, P., Carrere, V. and Rince, Y. (2003) Spectrometric Constraint in Analysis of Benthic Diatom Biomass Using Monospecific Cultures. *Remote Sensing of Environment* **88**, 386-400.

Melgani, F. and Bruzzone, L. (2004) Classification of Hyperspectral Remote Sensing Images With Support Vector Machines. *Ieee Transactions on Geoscience and Remote Sensing* **42**, 1778-1790.

Menken, K.D. and Brezonik, P.L. (2006) Influence of Chlorophyll and Colored Dissolved Organic Matter (CDOM) on Lake Reflectance Spectra: Implications for Measuring Lake Properties by Remote Sensing. *Lake and Reservoir Management* **22**, 179-190.

Mertes, L.A.K. (2002) Remote Sensing of Riverine Landscapes. *Freshwater Biology* **47**, 799-816.

Metsamaa, L., Kutser, T. and Strombeck, N. (2006) Recognising Cyanobacterial Blooms Based on Their Optical Signature: a Modelling Study. *Boreal Environment Research* **11**, 493-506.

Miller, J.R., Hare, E.W. and Wu, J. (1990) Quantitative Characterization of the Vegetation Red Edge Reflectance .1. An Inverted-Gaussian Reflectance Model. *International Journal of Remote Sensing* **11**, 1755-1773.

Miller, P.I., Shutler, J.D., Moore, G.F. and Groom, S.B. (2006) Seawifs Discrimination of Harmful Algal Bloom Evolution. *International Journal of Remote Sensing* **27**, 2287-2301.

Miller, S.D., Haddock, S.H.D., Elvidge, C.D. and Lee, T.F. (2005) Detection of a Bioluminescent Milky Sea From Space. *Proceedings of the National Academy of Sciences of the United States of America* **102**, 14181-14184.

Millie, D.F., Fahnenstiel, G.L., Carrick, H.J., Lohrenz, S.E. and Schofield, O.M.E. (2002) Phytoplankton Pigments in Coastal Lake Michigan: Distributions During the Spring Isothermal Period and Relation With Episodic Sediment Resuspension. *Journal of Phycology* **38**, 639-648.

Mittenzwey, K.H., Breitwieser, S., Penig, J., Gitelson, A.A., Dubovitzkii, G., Garbusov, G., Ullrich, S., Vobach, V. and Muller, A. (1991) Fluorescence and Reflectance for the *In-situ* Determination of Some Quality Parameters of Surface Waters. *Acta Hydrochimica Et Hydrobiologica* **19**, 3-15.

Mittenzwey, K.H., Gitelson, A.A. and Kondratiev, K.Y. (1992) Determination of Chlorophyll-a of Inland Waters on the Basis of Spectral Reflectance. *Limnology and Oceanography* **37**, 147-149.

Mobley, C.D. (1994) *Light and Water: Radiative Transfer in Natural Waters*, San Diego: Academic Press.

Mobley, C.D. and Sundman, L.K. (2001) *Hydrolight 4.2 User's Guide*, 2nd edn. Redmond, USA: Sequoia.

Mooij, W.M., Hulsmann, S., Domis, L.N.D., Nolet, B.A., Bodelier, P.L.E., Boers, P.C.M., Pires, L.M.D., Gons, H.J., Ibelings, B.W., Noordhuis, R., Portielje, R., Wolfstein, K. and Lammens Ehrr (2005) The Impact of Climate Change on Lakes in the Netherlands: a Review. *Aquatic Ecology* **39**, 381-400.

Morel, A. and Gentili, B. (1991) Diffuse Reflectance of Oceanic Waters - Its Dependence on Sun Angle as Influenced by the Molecular-Scattering Contribution. *Applied Optics* **30**, 4427-4438.

Morris, K., Bailey, P.C., Boon, P.I. and Hughes, L. (2003) Alternative Stable States in the Aquatic Vegetation of Shallow Urban Lakes. Ii. Catastrophic Loss of Aquatic Plants Consequent to Nutrient Enrichment. *Marine and Freshwater Research* **54**, 201-215.

Moss, B. (1978) Ecological History of a Medieval Man-Made Lake - Hickling Broad, Norfolk, United-Kingdom. *Hydrobiologia* **60**, 23-32.

Moss, B. (1998) *The Ecology of Freshwaters: Man and Medium, Past to Future*, 3rd edn. London: Blackwell Science.

Moss, B. (2001) *The Broads*, London: Harper Collins.

Moss, B., Stephen, D., Alvarez, C., Becares, E., Van De Bund, W., Collings, S.E., Van Donk, E., De Eyto, E., Feldmann, T., Fernandez-Alaez, C., Fernandez-Alaez, M., Franken, R.J.M., Garcia-Criado, F., Gross, E.M., Gyllstrom, M., Hansson, L.A., Irvine, K., Jarvalt, A., Jensen, J.P., Jeppesen, E., Kairesalo, T., Kornijow, R., Krause, T., Kunnap, H., Laas, A., Lille, E., Lorens, B., Luup, H., Miracle, M.R., Noges, P., Noges, T., Nykanen, M., Ott, I., Peczula, W., Peeters Ethm, Phillips, G., Romo, S., Russell, V., Salujoe, J., Scheffer, M., Siewertsen, K., Smal, H., Tesch, C., Timm, H., Tuvikene, L., Tonno, I., Virro, T., Vicente, E. and Wilson, D. (2003) The Determination of Ecological Status in Shallow Lakes - a Tested System (Ecoframe) for Implementation of the European Water Framework Directive. *Aquatic Conservation-Marine and Freshwater Ecosystems* **13**, 507-549.

Mulholland, P.J. and Elwood, J.W. (1982) The Role of Lake and Reservoir Sediments as Sinks in the Perturbed Global Carbon-Cycle. *Tellus* **34**, 490-499.

Munyati, C. (2000) Wetland Change Detection on the Kafue Flats, Zambia, by Classification of a Multitemporal Remote Sensing Image Dataset. *International Journal of Remote Sensing* **21**, 1787-1806.

Murphy, J. and Riley, J.P. (1962) A Modified Single Solution Method for Determination of Phosphate in Natural Waters. *Analytica Chimica Acta* **26**, 31-&

Murphy, R.J., Tolhurst, T.J., Chapman, M.G. and Underwood, A.J. (2005) Remote-Sensing of Benthic Chlorophyll: Should Ground-Truth Data be Expressed in Units of Area or Mass? *Journal of Experimental Marine Biology and Ecology* **316**, 69-77.

Mutanga, O., Skidmore, A.K. and Prins, H.H.T. (2004) Predicting *In Situ* Pasture Quality in the Kruger National Park, South Africa, Using Continuum-Removed Absorption Features. *Remote Sensing of Environment* **89**, 393-408.

Nalewajko, C. and Murphy, T.P. (1998) A Bioassay to Assess the Potential Effects of Sediment Resuspension on Phytoplankton Community Composition. *Journal of Applied Phycology* **10**, 341-348.

Nellis, M.D., Harrington, J.A. and Wu, J.P. (1998) Remote Sensing of Temporal and Spatial Variations in Pool Size, Suspended Sediment, Turbidity, and Secchi Depth in Tuttle Creek Reservoir, Kansas: 1993. *Geomorphology* **21**, 281-293.

Nelson, S.A.C., Cheruvelil, K.S. and Soranno, P.A. (2006) Satellite Remote Sensing of Freshwater Macrophytes and the Influence of Water Clarity. *Aquatic Botany* **85**, 291-300.

Nixdorf, B. and Deneke, R. (1997) Why 'Very Shallow' Lakes Are More Successful Opposing Reduced Nutrient Loads. *Hydrobiologia* **342**, 269-284.

Novo, E.M.L.D., Barbosa, C.C.D., De Freitas, R.M., Shimabukuro, Y.E., Melack, J.M. and Pereira, W. (2006) Seasonal Changes in Chlorophyll Distributions in Amazon Floodplain Lakes Derived from MODIS Images. *Limnology* **7**, 153-161.

Nye, P.H. (1986) Tinker, P.B. and Lauchli, A., (Eds.) *Advances in Plant Nutrition Vol. 2*, pp. 129-153. New York: Praeger.

O'Reilly, J.E., Maritorena, S., Mitchell, B.G., Siegel, D.A., Carder, K.L., Garver, S.A., Kahru, M. and Mcclain, C. (1998) Ocean Color Chlorophyll Algorithms for Seawifs. *Journal of Geophysical Research-Oceans* **103**, 24937-24953.

O'Shea, C. (2005) *Using Remote Sensing to Explore the Spectral and Spatial Characteristics of Wetland Vegetation. Unpublished PhD Thesis*, University of Stirling.

Ogilvie, B.G. and Mitchell, S.F. (1998) Does Sediment Resuspension Have Persistent Effects on Phytoplankton? Experimental Studies in Three Shallow Lakes. *Freshwater Biology* **40**, 51-63.

Oliver, R.L. and Walsby, A.E. (1984) Direct Evidence for the Role of Light-Mediated Gas Vesicle Collapse in the Buoyancy Regulation of *Anabaena Flos-Aquae* (Cyanobacteria). *Limnology and Oceanography* **29**, 879-886.

Ostlund, C., Flink, P., Strombeck, N., Pierson, D. and Lindell, T. (2001) Mapping of the Water Quality of Lake Erken, Sweden, From Imaging Spectrometry and Landsat Thematic Mapper. *Science of the Total Environment* **268**, 139-154.

Oyama, Y., Matsushita, B., Fukushima, T., Nagai, T. and Imai, A. (2007) A New Algorithm for Estimating Chlorophyll-a Concentration From Multi-Spectral Satellite Data in Case II Waters: a Simulation Based on a Controlled Laboratory Experiment. *International Journal of Remote Sensing* **28**, 1437-1453.

Padisak, J. (1993) The Influence of Different Disturbance Frequencies on the Species Richness, Diversity and Equitability of Phytoplankton in Shallow Lakes. *Hydrobiologia* **249**, 135-156.

Padisak, J. and Reynolds, C.S. (2003) Shallow Lakes: the Absolute, the Relative, the Functional and the Pragmatic. *Hydrobiologia* **506**, 1-11.

Pal, M. and Mather, P.M. (2004) Assessment of the Effectiveness of Support Vector Machines for Hyperspectral Data. *Future Generation Computer Systems* **20**, 1215-1225.

Paterson, D.M., Wiltshire, K.H., Miles, A., Blackburn, J., Davidson, I., Yates, M.G., Mcgrorty, S. and Eastwood, J.A. (1998) Microbiological Mediation of Spectral Reflectance From Intertidal Cohesive Sediments. *Limnology and Oceanography* **43**, 1207-1221.

Patterson, A.H. (1920) *Through Broadland in a Breydon Punt*, Norwich: H.J. Vince.

Peckham, S.D., Chipman, J.W., Lillesand, T.M. and Dodson, S.I. (2006) Alternate Stable States and the Shape of the Lake Trophic Distribution. *Hydrobiologia* **571**, 401-407.

Pengra, B.W., Johnston, C.A. and Loveland, T.R. (2007) Mapping an Invasive Plant, Phragmites Australis, in Coastal Wetlands Using the EO-1 Hyperion Hyperspectral Sensor. *Remote Sensing of Environment* **108**, 74-81.

Penuelas, J., Baret, F. and Filella, I. (1995) Semiempirical Indexes to Assess Carotenoids Chlorophyll-a Ratio from Leaf Spectral Reflectance. *Photosynthetica* **31**, 221-230.

Penuelas, J., Gamon, J.A., Fredeen, A.L., Merino, J. and Field, C.B. (1994) Reflectance Indexes Associated With Physiological-Changes in Nitrogen-Limited and Water-Limited Sunflower Leaves. *Remote Sensing of Environment* **48**, 135-146.

Penuelas, J., Gamon, J.A., Griffin, K.L. and Field, C.B. (1993) Assessing Community Type, Plant Biomass, Pigment Composition, and Photosynthetic Efficiency of Aquatic Vegetation From Spectral Reflectance. *Remote Sensing of Environment* **46**, 110-118.

Peterson, G.D., Beard, T.D., Beisner, B.E., Bennet, E.M., Carpenter, S.R., Cumming, G.S., Dent, C.L. and Havlicek, T.D. (2003) Assessing Future Ecosystem Services: A Case Study of the Northern Highlands Lake District, Wisconsin. *Conservation Ecology* **7**,

Phillips, G., Bramwell, A., Pitt, J., Stansfield, J. and Perrow, M. (1999) Practical Application of 25 Years' Research Into the Management of Shallow Lakes. *Hydrobiologia* **396**, 61-76.

Phillips, G., Kelly, A., Pitt, J.A., Sanderson, R. and Taylor, E. (2005) The Recovery of a Very Shallow Eutrophic Lake, 20 Years After the Control of Effluent Derived Phosphorus. *Freshwater Biology* **50**, 1628-1638.

Phillips, G.L., Eminson, D. and Moss, B. (1978) Mechanism to Account for Macrophyte Decline in Progressively Eutrophicated Freshwaters. *Aquatic Botany* **4**, 103-126.

Pickett, S.T.A. and Cadenasso, M.L. (1995) Landscape Ecology - Spatial Heterogeneity in Ecological-Systems. *Science* **269**, 331-334.

Pierson, D.C. and Strombeck, N. (2001) Estimation of Radiance Reflectance and the Concentrations of Optically Active Substances in Lake Malaren, Sweden, Based on Direct and Inverse Solutions of a Simple Model. *Science of the Total Environment* **268**, 171-188.

Pitt, J.A., Kelly, A. and Phillips, G.L. (1997) Control of Nutrient Release from Sediments . In: Madgewick, F.J. and Phillips, G.L., (Eds.) *Restoration of the Norfolk Broads - Final Report*, UK: Broads Authority and Environment Agency.

Pokorny, J., Kvet, J., Ondok, J.P., Toul, Z. and Ostry, I. (1984) Production Ecological Analysis of a Plant Community Dominated by Elodea-Canadensis Michx. *Aquatic Botany* **19**, 263-292.

Pope, R.M. and Fry, E.S. (1997) Absorption Spectrum (380-700 nm) of Pure Water .2. Integrating Cavity Measurements. *Applied Optics* **36**, 8710-8723.

Pozdnyakov, D., Shuchman, R., Korosov, A. and Hatt, C. (2005) Operational Algorithm for the Retrieval of Water Quality in the Great Lakes. *Remote Sensing of Environment* **97**, 352-370.

Prater A.J. (1995) *Avian Grazers and their Impact on Reedswamps in Thurne Broads, Norfolk.* Unpublished Ph.D. Thesis. Norwich: UEA.

Presing, M., Herodek, S., Preston, T. and Voros, L. (2001) Nitrogen Uptake and the Importance of Internal Nitrogen Loading in Lake Balaton. *Freshwater Biology* **46**, 125-139.

Prieur, L. and Sathyendranath, S. (1981) An Optical Classification of Coastal and Oceanic Waters Based on the Specific Spectral Absorption Curves of Phytoplankton Pigments, Dissolved Organic-Matter, and Other Particulate Materials. *Limnology and Oceanography* **26**, 671-689.

Qin, B.Q., Hu, W.P., Gao, G., Luo, L.C. and Zhang, J.S. (2004) Dynamics of Sediment Resuspension and the Conceptual Schema of Nutrient Release in the Large Shallow Lake Taihu, China. *Chinese Science Bulletin* **49**, 54-64.

Quibell, G. (1991) The Effect of Suspended Sediment on Reflectance From Fresh-Water Algae. *International Journal of Remote Sensing* **12**, 177-182.

Quincey, D.J., Richardson, S.D., Luckman, A., Lucas, R.M., Reynolds, J.M., Hambrey, M.J. and Glasser, N.F. (2007) Early Recognition of Glacial Lake Hazards in the Himalaya Using Remote Sensing Datasets. *Global and Planetary Change* **56**, 137-152.

Rainey, M.P., Tyler, A.N., Gilvear, D.J., Bryant, R.G. and Mcdonald, P. (2003) Mapping Intertidal Estuarine Sediment Grain Size Distributions Through Airborne Remote Sensing. *Remote Sensing of Environment* **86**, 480-490.

Ramakrishnan, D., Ghosh, S.K., Raja, V.K.M., Chandran, R.V. and Jeyram, A. (2005) Trails of the Killer Tsunami: a Preliminary Assessment Using Satellite Remote Sensing Technique. *Current Science* **88**, 709-711.

Ramos, A.G., Martel, A., Codd, G.A., Soler, E., Coca, J., Redondo, A., Morrison, L.F., Metcalf, J.S., Ojeda, A., Suarez, S. and Petit, M. (2005) Bloom of the Marine Diazotrophic Cyanobacterium Trichodesmium Erythraeum in the Northwest African Upwelling. *Marine Ecology-Progress Series* **301**, 303-305.

Rantajarvi, E., Olsonen, R., Hallfors, S., Leppanen, J.M. and Raateoja, M. (1998) Effect of Sampling Frequency on Detection of Natural Variability in Phytoplankton: Unattended High-Frequency Measurements on Board Ferries in the Baltic Sea. *Ices Journal of Marine Science* **55**, 697-704.

Raychaudhuri, B. (2004) Study of Spectral Response of Plant Pigments for Remote Sensing Applications. *Indian Journal of Physics and Proceedings of the Indian Association for the Cultivation of Science* **78**, 677-680.

Reddy, K.R., Fisher, M.M. and Ivanoff, D. (1996) Resuspension and Diffusive Flux of Nitrogen and Phosphorus in a Hypereutrophic Lake. *Journal of Environmental Quality* **25**, 363-371.

Reynolds, C.S. (1973) Growth and Buoyancy of Microcystis-Aeruginosa Kutz-Emend-Elenkin in a Shallow Eutrophic Lake. *Proceedings of the Royal Society of London Series B-Biological Sciences* **184**, 29-50.

Reynolds, C.S. (2006) *Ecology of Phytoplankton*, London: Cambridge University Press.

Reynolds, C.S., Huszar, V., Kruk, C., Naselli-Flores, L. and Melo, S. (2002) Towards a Functional Classification of the Freshwater Phytoplankton. *Journal of Plankton Research* **24**, 417-428.

Reynolds, C.S., Oliver, R.L. and Walsby, A.E. (1987) Cyanobacterial Dominance - the Role of Buoyancy Regulation in Dynamic Lake Environments. *New Zealand Journal of Marine and Freshwater Research* **21**, 379-390.

Reynolds, C.S. and Rogers, D.A. (1976) Seasonal-Variations in Vertical Distribution and Buoyancy of Microcystis Aeruginosa Kutz Emend Elenkin in Rostherne-Mere, England. *Hydrobiologia* **48**, 17-23.

Reynolds, C.S. and Walsby, A.E. (1975) Water-Blooms. *Biological Reviews of the Cambridge Philosophical Society* **50**, 437-&

Richards, J.A. (1999) *Remote Sensing and Digital Analysis*, Berlin: Springer-Verlag.

Richardson, L.L. (1996) Remote Sensing of Algal Bloom Dynamics. *Bioscience* **46**, 492-501.

Rippka, R., Deruelles, J., Waterbury, J.B., Herdman, M. and Stanier, R.Y. (1979) Generic Assignments, Strain Histories and Properties of Pure Cultures of Cyanobacteria. *Journal of General Microbiology* **111**, 1-61.

Ritchie, J.C., Schiebe, F.R., Cooper, C.M. and Harrington, J.A. (1994) Chlorophyll Measurements in the Presence of Suspended Sediment Using Broad-Band Spectral Sensors Aboard Satellites. *Journal of Freshwater Ecology* **9**, 197-206.

Robarts, R.D. and Zohary, T. (1987) Temperature Effects on Photosynthetic Capacity, Respiration, and Growth-Rates of Bloom-Forming Cyanobacteria. *New Zealand Journal of Marine and Freshwater Research* **21**, 391-399.

Roff, D.A. (1974) Spatial Heterogeneity and Persistence of Populations. *Oecologia* **15**, 245-258.

Rooney, N., Kalff, J. and Habel, C. (2003) The Role of Submerged Macrophyte Beds in Phosphorus and Sediment Accumulation in Lake Memphremagog, Quebec, Canada. *Limnology and Oceanography* **48**, 1927-1937.

Rosso, P.H., Ustin, S.L. and Hastings, A. (2005) Mapping Marshland Vegetation of San Francisco Bay, California, Using Hyperspectral Data. *International Journal of Remote Sensing* **26**, 5169-5191.

Rouse, J.W., Haas, R.H., Schell, J.A. and Deering, D.W. (1973) Monitoring Vegetation Systens in the Great Plains with ERTS. In: *N. SP-351*, (Ed.) pp. 309-317. Washington: NASA.

Rowan, J.S., Carwardine, J., Duck, R.W., Bragg, O.M., Black, A.R., Cutler, M.E.J., Soutar, I. and Boon, P.J. (2006) Development of a Technique for Lake Habitat Survey (LHS) with Applications for the European Union Water Framework Directive. *Aquatic Conservation-Marine and Freshwater Ecosystems* **16**, 637-657.

Rowan, K.S. (1989) *Photosynthetic Pigments of Algae*, Cambridge: Cambridge University Press.

Rundquist, D.C., Han, L.H., Schalles, J.F. and Peake, J.S. (1996) Remote Measurement of Algal Chlorophyll in Surface Waters: the Case for the First Derivative of Reflectance Near 690 nm. *Photogrammetric Engineering and Remote Sensing* **62**, 195-200.

Salonen, K., Jones, R.I. and Arvola, L. (1984) Hypolimnetic Phosphorus Retrieval by Diel Vertical Migrations of Lake Phytoplankton. *Freshwater Biology* **14**, 431-438.

Salonen, K. and Rosenberg, M. (2000) Advantages From Diel Vertical Migration Can Explain the Dominance of Gonyostomum Semen (Raphidophyceae) in a Small, Steeply-Stratified Humic Lake. *Journal of Plankton Research* **22**, 1841-1853.

Sandjensen, K. and Borum, J. (1991) Interactions Among Phytoplankton, Periphyton, and Macrophytes in Temperate Fresh-Waters and Estuaries. *Aquatic Botany* **41**, 137-175.

Santruckova, H., Picek, T., Simek, M., Bauer, V., Kopecky, J., Pechar, L., Lukavska, J. and Cizkova, H. (2001) Decomposition Processes in Soil of a Healthy and a Declining Phragmites Australis Stand. *Aquatic Botany* **69**, 217-234.

Sarada, R., Pillai, M.G. and Ravishankar, G.A. (1999) Phycocyanin From Spirulina Sp: Influence of Processing of Biomass on Phycocyanin Yield, Analysis of Efficacy of Extraction Methods and Stability Studies on Phycocyanin. *Process Biochemistry* **34**, 795-801.

Sastre, J., Sahuquillo, A., Vidal, M. and Rauret, G. (2002) Determination of Cd, Cu, Pb and Zn in Environmental Samples: Microwave-Assisted Total Digestion Versus Aqua Regia and Nitric Acid Extraction. *Analytica Chimica Acta* **462**, 59-72.

Sathyendranath, S., Cota, G., Stuart, V., Maass, H. and Platt, T. (2001) Remote Sensing of Phytoplankton Pigments: a Comparison of Empirical and Theoretical Approaches. *International Journal of Remote Sensing* **22**, 249-273.

Sathyendranath, S., Prieur, L. and Morel, A. (1989) A 3-Component Model of Ocean Color and Its Application to Remote-Sensing of Phytoplankton Pigments in Coastal Waters. *International Journal of Remote Sensing* **10**, 1373-1394.

Sathyendranath, S., Stuart, V., Platt, T., Bouman, H., Ulloa, O. and Maass, H. (2005) Remote Sensing of Ocean Colour: Towards Algorithms for Retrieval of Pigment Composition. *Indian Journal of Marine Sciences* **34**, 333-340.

Sathyendranath, S., Watts, L., Devred, E., Platt, T., Caverhill, C. and Maass, H. (2004) Discrimination of Diatoms From Other Phytoplankton Using Ocean-Colour Data. *Marine Ecology-Progress Series* **272**, 59-68.

Scanlan, C.M., Foden, J., Wells, E. and Best, M.A. (2007) The Monitoring of Opportunistic Macroalgal Blooms for the Water Framework Directive. *Marine Pollution Bulletin* **55**, 162-171.

Schallenberg, M. and Burns, C.W. (2004) Effects of Sediment Resuspension on Phytoplankton Production: Teasing Apart the Influences of Light, Nutrients and Algal Entrainment. *Freshwater Biology* **49**, 143-159.

Schalles, J. and Yacobi, Y. (2000) Remote detection and seasonal patterns of phycocyanin, carotenoid and chlorophyll pigmentsin eutrophic waters. *Archiv fur Hydrobiologie: Special Issues, Advances in Limnology* **55**, 153-168.

Schalles, J.F., Gitelson, A.A., Yacobi, Y.Z. and Kroenke, A.E. (1998) Estimation of Chlorophyll a From Time Series Measurements of High Spectral Resolution Reflectance in an Eutrophic Lake. *Journal of Phycology* **34**, 383-390.

Scheffer, M. (1998) *The Ecology of Shallow Lakes*, London: Chapman & Hall.

Scheffer, M. (1999) The Effect of Aquatic Vegetation on Turbidity; How Important Are the Filter Feeders? *Hydrobiologia* **409**, 307-316.

Scheffer, M., Carpenter, S., Foley, J.A., Folke, C. and Walker, B. (2001) Catastrophic Shifts in Ecosystems. *Nature* **413**, 591-596.

Scheffer, M. and Carpenter, S.R. (2003) Catastrophic Regime Shifts in Ecosystems: Linking Theory to Observation. *Trends in Ecology & Evolution* **18** , 648-656.

Scheffer, M., Hosper, S.H., Meijer, M.L., Moss, B. and Jeppesen, E. (1993) Alternative Equilibria in Shallow Lakes. *Trends in Ecology & Evolution* **8**, 275-279.

Scheffer, M. and Jeppesen, E. (2007) Regime Shifts in Shallow Lakes. *Ecosystems* **10**, 1-3.

Scheffer, M., Rinaldi, S., Gragnani, A., Mur, L.R. and Vannes, E.H. (1997) On the Dominance of Filamentous Cyanobacteria in Shallow, Turbid Lakes. *Ecology* **78**, 272-282.

Scheffer, M., Szabo, S., Gragnani, A., Van Nes, E.H., Rinaldi, S., Kautsky, N., Norberg, J., Roijackers, R.M.M. and Franken, R.J.M. (2003) Floating Plant Dominance as a Stable State. *Proceedings of the National Academy of Sciences of the United States of America* **100**, 4040-4045.

Scheffer, M. and Van Nes, E.H. (2007) Shallow Lakes Theory Revisited: Various Alternative Regimes Driven by Climate, Nutrients, Depth and Lake Size. *Hydrobiologia* **584**, 455-466.

Schmid, H., Bauer, F. and Stich, H.B. (1998) Determination of Algal Biomass With Hplc Pigment Analysis From Lakes of Different Trophic State in Comparison to Microscopically Measured Biomass. *Journal of Plankton Research* **20**, 1651-1661.

Schmidt, K.S. and Skidmore, A.K. (2003) Spectral Discrimination of Vegetation Types in a Coastal Wetland. *Remote Sensing of Environment* **85**, 92-108.

Shanmugam, P., Ahn, Y.H. and Sanjeevi, S. (2006) A Comparison of the Classification of Wetland Characteristics by Linear Spectral Mixture Modelling and Traditional Hard Classifiers on Multispectral Remotely Sensed Imagery in Southern India. *Ecological Modelling* **194**, 379-394.

Shrivastava, R.J. and Gebelein, J.L. (2007) Land Cover Classification and Economic Assessment of Citrus Groves Using Remote Sensing. *ISPRS Journal of Photogrammetry and Remote Sensing* **61**, 341-353.

Shuchman, R., Korosov, A., Hatt, C., Pozdnyakov, D., Means, J. and Meadows, G. (2006) Verification and Application of a Bio-Optical Algorithm for Lake Michigan Using Seawifs: a 7-Year Inter-Annual Analysis. *Journal of Great Lakes Research* **32**, 258-279.

Shutler, J.D., Land, P.E., Smyth, T.J. and Groom, S.B. (2007) Extending the MODIS 1 km Ocean Colour Atmospheric Correction to the MODIS 500 M Bands and 500 M Chlorophyll-a Estimation Towards Coastal and Estuarine Monitoring. *Remote Sensing of Environment* **107**, 521-532.

Siegelman, H.W. and Kycia, J.H. (1978) Algal biliprotiens. In: Heleburst, J.A. and Craigie, J.S., (Eds.) *Handbook of Phycological Methods: Physiological and Biochemical Methods*, pp. 71-79. Cambridge: Cambridge University Press.

Simis, S.G.H., Peters, S.W.M. and Gons, H.J. (2005) Remote Sensing of the Cyanobacterial Pigment Phycocyanin in Turbid Inland Water. *Limnology and Oceanography* **50**, 237-245.

Simis, S.G.H., Ruiz-Verdu, A., Dominguez-Gomez, J.A., Pena-Martinez, R., Peters, S.W.M. and Gons, H.J. (2007) Influence of Phytoplankton Pigment Composition on Remote Sensing of Cyanobacterial Biomass. *Remote Sensing of Environment* **106**, 414-427.

Simis, S.G.H., Tijdens, M., Hoogveld, H.L. and Gons, H.J. (2005) Optical Changes Associated With Cyanobacterial Bloom Termination by Viral Lysis. *Journal of Plankton Research* **27**, 937-949.

Sims, D.A. and Gamon, J.A. (2002) Relationships Between Leaf Pigment Content and Spectral Reflectance Across a Wide Range of Species, Leaf Structures and Developmental Stages. *Remote Sensing of Environment* **81**, 337-354.

Skubinna, J.P., Coon, T.G. and Batterson, T.R. (1995) Increased Abundance and Depth of Submersed Macrophytes in Response to Decreased Turbidity in Saginaw Bay, Lake Huron. *Journal of Great Lakes Research* **21**, 476-488.

Smith, K.L., Steven, M.D. and Colls, J.J. (2004) Use of Hyperspectral Derivative Ratios in the Red-Edge Region to Identify Plant Stress Responses to Gas Leaks. *Remote Sensing of Environment* **92**, 207-217.

Smith, K.L., Steven, M.D. and Colls, J.J. (2005) Plant Spectral Responses to Gas Leaks and Other Stresses. *International Journal of Remote Sensing* **26**, 4067-4081.

Smith, V.H. (1983) Low Nitrogen to Phosphorus Ratios Favor Dominance by Blue-Green-Algae in Lake Phytoplankton. *Science* **221**, 669-671.

Solorzan.l (1969) Determination of Ammonia in Natural Waters by Phenolhypochlorite Method. *Limnology and Oceanography* **14**, 799-&

Sondergaard, M., Jensen, J.P. and Jeppesen, E. (2003) Role of Sediment and Internal Loading of Phosphorus in Shallow Lakes. *Hydrobiologia* **506**, 135-145.

Sondergaard, M., Jeppesen, E., Jensen, J.P. and Amsinck, S.L. (2005) Water Framework Directive: Ecological Classification of Danish Lakes. *Journal of Applied Ecology* **42**, 616-629.

Sondergaard, M., Kristensen, P. and Jeppesen, E. (1992) Phosphorus Release From Resuspended Sediment in the Shallow and Wind-Exposed Lake Arreso, Denmark. *Hydrobiologia* **228**, 91-99.

Spanglet, H.J., Ustin, S.L. and Rejmankova, E. (1998) Spectral Reflectance Characteristics of California Subalpine Marsh Plant Communities. *Wetlands* **18**, 307-319.

Spears, B.M., Carvalho, L., Perkins, R., Kirika, A. and Paterson, D.M. (2006) Spatial and Historical Variation in Sediment Phosphorus Fractions and Mobility in a Large Shallow Lake. *Water Research* **40**, 383-391.

Spears, B.M., Carvalho, L., Perkins, R., Kirika, A. and Paterson, D.M. (2007) Sediment Phosphorus Cycling in a Large Shallow Lake: Spatio-Temporal Variation in Phosphorus Pools and Release. *Hydrobiologia* **584**, 37-48.

Sridhar, B.B.M. and Vincent, R.K. (2007) Spectral Reflectance Measurements of a *Microcystis* Bloom in Upper Klamath Lake, Oregon. *Journal of Great Lakes Research* **33** , 279-284.

Stankelis, R.M., Naylor, M.D. and Boynton, W.R. (2003) Submerged Aquatic Vegetation in the Mesohaline Region of the Patuxent Estuary: Past, Present, and Future Status. *Estuaries* **26**, 186-195.

Stansfield, J., Moss, B. and Irvine, K. (1989) The Loss of Submerged Plants With Eutrophication .3. Potential Role of Organochlorine Pesticides - a Paleoecological Study. *Freshwater Biology* **22**, 109-132.

Stansfield, J.H., Perrow, M.R., Tench, L.D., Jowitt, A.J.D. and Taylor, A.A.L. (1995) Do Macrophytes Act as Refuges for Grazing Cladocera Against Fish Predation? *Water Science and Technology* **32**, 217-220.

Stansfield, J.H., Perrow, M.R., Tench, L.D., Jowitt, A.J.D. and Taylor, A.A.L. (1997) Submerged Macrophytes as Refuges for Grazing Cladocera Against Fish Predation: Observations on Seasonal Changes in Relation to Macrophyte Cover and Predation Pressure. *Hydrobiologia* **342**, 229-240.

Stcyr, L., Campbell, P.G.C. and Guertin, K. (1994) Evaluation of the Role of Submerged Plant Beds in the Metal Budget of a Fluvial Lake. *Hydrobiologia* **291**, 141-156.

Strachan, I.B., Pattey, E. and Boisvert, J.B. (2002) Impact of Nitrogen and Environmental Conditions on Corn as Detected by Hyperspectral Reflectance. *Remote Sensing of Environment* **80**, 213-224.

Strickland, J.D.H. and Parsons, T.R. (1972) A Practical Handbook of SeaWater Analysis. *Bulletin of Fisheries Research* **167**, 1-10.

Strombeck, N. and Pierson, D.C. (2001) The Effects of Variability in the Inherent Optical Properties on Estimations of Chlorophyll a by Remote Sensing in Swedish Freshwaters. *Science of the Total Environment* **268**, 123-137.

Su, L., Chopping, M.J., Rango, A., Martonchik, J.V. and Peters, D.P.C. (2007a) Differentiation of Semi-Arid Vegetation Types Based on Multi-Angular Observations From Misr and Modis. *International Journal of Remote Sensing* **28**, 1419-1424.

Su, L.H., Chopping, M.J., Rango, A., Martonchik, J.V. and Peters, D.P.C. (2007b) Support Vector Machines for Recognition of Semi-Arid Vegetation Types Using Misr Multi-Angle Imagery. *Remote Sensing of Environment* **107**, 299-311.

Sunshine, J.M., Pieters, C.M. and Pratt, S.F. (1990) Deconvolution of Mineral Absorption-Bands - An Improved Approach. *Journal of Geophysical Research-Solid Earth and Planets* **95**, 6955-6966.

Svab, E., Tyler, A.N., Preston, T., Presing, M. and Balogh, K.V. (2005) Characterizing the Spectral Reflectance of Algae in Lake Waters With High Suspended Sediment Concentrations. *International Journal of Remote Sensing* **26**, 919-928.

Takamura, N., Kadono, Y., Fukushima, M., Nakagawa, M. and Kim, B.H.O. (2003) Effects of Aquatic Macrophytes on Water Quality and Phytoplankton Communities in Shallow Lakes. *Ecological Research* **18**, 381-395.

Takamura, N. and Yasuno, M. (1984) Diurnal Changes in the Vertical-Distribution of Phytoplankton in Hypertrophic Lake Kasumigaura, Japan. *Hydrobiologia* **112**, 53-60.

Talling, J.F. and Parker, J.E. (2002) Seasonal Dynamics of Phytoplankton and Phytobenthos, and Associated Chemical Interactions, in a Shallow Upland Lake (Malham Tarn, Northern England). *Hydrobiologia* **487**, 167-181.

Tcherepanov, E.N., Zlotnik, V.A. and Henebry, G.M. (2005) Using Landsat Thermal Imagery and GIS for Identification of Groundwater Discharge Into Shallow Groundwater-Dominated Lakes. *International Journal of Remote Sensing* **26**, 3649-3661.

Teeter, A.M., Johnson, B.H., Berger, C., Stelling, G., Scheffner, N.W., Garcia, M.H. and Parchure, T.M. (2001) Hydrodynamic and Sediment Transport Modeling With Emphasis on Shallow-Water, Vegetated Areas (Lakes, Reservoirs, Estuaries and Lagoons). *Hydrobiologia* **444**, 1-24.

Thiemann, S. and Kaufmann, H. (2000) Determination of Chlorophyll Content and Trophic State of Lakes Using Field Spectrometer and IRS-1C Satellite Data in the Mecklenburg Lake District, Germany. *Remote Sensing of Environment* **73**, 227-235.

Thiemann, S. and Kaufmann, H. (2002) Lake Water Quality Monitoring Using Hyperspectral Airborne Data - a Semlempirical Multisensor and Multitemporal Approach for the Mecklenburg Lake District, Germany. *Remote Sensing of Environment* **81**, 228-237.

Tilley, D.R., Ahmed, M., Son, J.H. and Badrinarayanan, H. (2003) Hyperspectral Reflectance of Emergent Macrophytes as an Indicator of Water Column Ammonia in an Oligohaline, Subtropical Marsh. *Ecological Engineering* **21**, 153-163.

Titus, J.E. and Adams, M.S. (1979) Coexistence and the Comparative Light Relations of the Submersed Macrophytes *Myriophyllum-Spicatum* L and *Vallisneria-Americana* Michx. *Oecologia* **40**, 273-286.

Townsend, D.W., Cammen, L.M., Holloigan, P.M. and Campbell, D.E. (1994) Causes and Consequences of Variability in the Timing of Spring Phytoplankton Blooms. *Deep Sea Research Part I - Oceanographic Research Papers* **41**, 747-765.

Tranvik, L.J. (1990) Bacterioplankton Growth on Fractions of Dissolved Organic-Carbon of Different Molecular-Weights From Humic and Clear Waters. *Applied and Environmental Microbiology* **56**, 1672-1677.

Turner, W., Spector, S., Gardiner, N., Fladeland, M., Sterling, E. and Steininger, M. (2003) Remote Sensing for Biodiversity Science and Conservation. *Trends in Ecology & Evolution* **18**, 306-314.

Tyler, A.N., Svab, E., Preston, T., Presing, M. and Kovacs, W.A. (2006) Remote Sensing of the Water Quality of Shallow Lakes: a Mixture Modelling Approach to Quantifying Phytoplankton in Water Characterized by High-Suspended Sediment. *International Journal of Remote Sensing* **27**, 1521-1537.

Underwood, A.J., Chapman, M.G. and Connell, S.D. (2000) Observations in Ecology: You Can't Make Progress on Processes Without Understanding the Patterns. *Journal of Experimental Marine Biology and Ecology* **250**, 97-115.

Valta-Hulkkonen, K., Kanninen, A., Iivonen, R. and Leka, J. (2005) Assessment of Aerial Photography as a Method for Monitoring Aquatic Vegetation in Lakes of Varying Trophic Status. *Boreal Environment Research* **10**, 57-66.

Valta-Hulkkonen, K., Kanninen, A. and Pellikka, P. (2004) Remote Sensing and GIS for Detecting Changes in the Aquatic Vegetation of a Rehabilitated Lake. *International Journal of Remote Sensing* **25**, 5745-5758.

Van Den Wyngaert, I.J.J., Wienk, L.D., Sollie, S., Bobbink, R. and Verhoeven, J.T.A. (2003) Long-Term Effects of Yearly Grazing by Moulting Greylag Geese (Anser Anser) on Reed (Phragmites Australis) Growth and Nutrient Dynamics. *Aquatic Botany* **75**, 229-248.

Van Der Putten, W.H. (1997) Die-Back of Phragmites Australis in European Wetlands: an Overview of the European Research Programme on Reed Die-Back and Progression (1993-1994). *Aquatic Botany* **59**, 263-275.

Van Der Welle, M.E.W., Cuppens, M., Lamers, L.P.M. and Roelofs, T.G.M. (2006) Detoxifying Toxicants: Interactions Between Sulfide and Iron Toxicity in Freshwater Wetlands. *Environmental Toxicology and Chemistry* **25**, 1592-1597.

Van Luijn, F., Boers, P.C.M., Lijklema, L. and Sweerts Jpra (1999) Nitrogen Fluxes and Processes in Sandy and Muddy Sediments From a Shallow Eutrophic Lake. *Water Research* **33**, 33-42.

Van Nes, E.H., Rip, W.J. and Scheffer, M. (2007) A Theory for Cyclic Shifts Between Alternative States in Shallow Lakes. *Ecosystems* **10**, 17-27.

Van Nes, E.H. and Scheffer, M. (2003) Alternative Attractors May Boost Uncertainty and Sensitivity in Ecological Models. *Ecological Modelling* **159** , 117-124.

Van Nes, E.H. and Scheffer, M. (2005) Implications of Spatial Heterogeneity for Catastrophic Regime Shifts in Ecosystems. *Ecology* **86**, 1797-1807.

Vanderploeg, H.A., Johengen, T.H., Lavrentyev, P.J., Chen, C., Lang, G.A., Agy, M.A., Bundy, M.H., Cavaletto, J.F., Eadie, B.J., Liebig, J.R., Miller, G.S., Ruberg, S.A. and Mccormick, M.J. (2007) Anatomy of the Recurrent Coastal Sediment Plume in Lake Michigan and Its Impacts on Light Climate, Nutrients, and Plankton. *Journal of Geophysical Research-Oceans* **112**,

Vanderputten, W.H., Peters, B.A.M. and Vandenberg, R.S. (1997) Effects of Litter on Substrate Conditions and Growth of Emergent Macrophytes. *New Phytologist* **135**, 527-537.

Vanwijck, C., Degroot, C.J. and Grillas, P. (1992) The Effect of Anaerobic Sediment on the Growth of Potamogeton-Pectinatus L. - the Role of Organic-Matter, Sulfide and Ferrous Iron. *Aquatic Botany* **44**, 31-49.

Vanwijk, R.J. (1988) Ecological-Studies on *Potamogeton-Pectinatus* L .1. General-Characteristics, Biomass Production and Life-Cycles Under Field Conditions. *Aquatic Botany* **31**, 211-258.

Vincent, R.K., Qin, X.M., Mckay, R.M.L., Miner, J., Czajkowski, K., Savino, J. and Bridgeman, T. (2004) Phycocyanin Detection from Landsat TM Data for Mapping Cyanobacterial Blooms in Lake Erie. *Remote Sensing of Environment* **89**, 381-392.

Visser, P.M. (1995) *Growth and Movement of the Cyanobacterium Microcystis in Stable and Artifically Mixed Water Columns. PhD Thesis*, University of Amsterdam.

Visser, P.M., Ketelaars, H.A.M., Vanbreemen Lwca and Mur, L.R. (1996) Diurnal Buoyancy Changes of Microcystis in an Artificially Mixed Storage Reservoir. *Hydrobiologia* **331**, 131-141.

Visser, P.M., Passarge, J. and Mur, L.R. (1997) Modelling Vertical Migration of the Cyanobacterium Microcystis. *Hydrobiologia* **349**, 99-109.

Webster, I.T. (1990) Effect of Wind on the Distribution of Phytoplankton Cells in Lakes. *Limnology and Oceanography* **35**, 989-1001.

Weeks, S.J., Currie, B., Bakun, A. and Peard, K.R. (2004) Hydrogen Sulphide Eruptions in the Atlantic Ocean Off Southern Africa: Implications of a New View Based on Seawifs Satellite Imagery. *Deep-Sea Research Part I-Oceanographic Research Papers* **51**, 153-172.

Wellburn, A.R. (1994) The Spectral Determination of Chlorophyll-a and Chlorophhyll-b, as Well as Total Carotenoids, Using Various Solvents With Spectrophotometers of Different Resolution. *Journal of Plant Physiology* **144**, 307-313.

Williams, A.E.P. and Hunt, E.R. (2004) Accuracy Assessment for Detection of Leafy Spurge With Hyperspectral Imagery. *Journal of Range Management* **57**, 106-112.

Williams, A.P. and Hunt, E.R. (2002) Estimation of Leafy Spurge Cover From Hyperspectral Imagery Using Mixture Tuned Matched Filtering. *Remote Sensing of Environment* **82**, 446-456.

Williams, D.J., Rybicki, N.B., Lombana, A.V., O'brien, T.M. and Gomez, R.B. (2003) Preliminary Investigation of Submerged Aquatic Vegetation Mapping Using Hyperspectral Remote Sensing. *Environmental Monitoring and Assessment* **81**, 383-392.

Windham, L. and Lathrop, R.G. (1999) Effects of *Phragmites australis* (Common Reed) Invasion on Aboveground Biomass and Soil Properties in Brackish Tidal Marsh of the Mullica River, New Jersey. *Estuaries* **22**, 927-935.

Winterbottom, S.J. and Gilvear, D.J. (1997) Quantification of Channel Bed Morphology in Gravel-Bed Rivers Using Airborne Multispectral Imagery and Aerial Photography. *Regulated Rivers-Research & Management* **13**, 489-499.

Wright, C. and Gallant, A. (2007) Improved Wetland Remote Sensing in Yellowstone National Park Using Classification Trees to Combine Tm Imagery and Ancillary Environmental Data. *Remote Sensing of Environment* **107**, 582-605.

Wright, S.W., Jeffrey, S.W., Mantoura, R.F.C., Llewellyn, C.A., Bjornland, T., Repeta, D. and Welschmeyer, N. (1991) Improved Hplc Method for the Analysis of Chlorophylls and Carotenoids From Marine-Phytoplankton. *Marine Ecology-Progress Series* **77**, 183-196.

Yan, F.L., Wang, S.X., Zhou, Y., Xiao, Q., Zhu, L.Y., Wang, L.T. and Jiao, Y.Q. (2006) Monitoring the Water Quality of Taihu Lake by Using Hyperion Hyperspectral Data. *Journal of Infrared and Millimeter Waves* **25**, 460-464.

Yang, D.T. and Pan, D.L. (2006) Hyperspectral Retrieval Model of Phycocyanin in Case II Waters. *Chinese Science Bulletin* **51**, 149-153.

Yang, M.D., Sykes, R.M. and Merry, C.J. (2000) Estimation of Algal Biological Parameters Using Water Quality Modeling and Spot Satellite Data. *Ecological Modelling* **125**, 1-13.

Yang, X.J. (2005) Remote Sensing and GIS Applications for Estuarine Ecosystem Analysis: an Overview. *International Journal of Remote Sensing* **26**, 5347-5356.

Ye, S.W., Li, Z.J., Lek-Ang, S., Feng, G.P., Lek, S. and Cao, W.X. (2006) Community Structure of Small Fishes in a Shallow Macrophytic Lake (Niushan Lake) Along the Middle Reach of the Yangtze River, China. *Aquatic Living Resources* **19**, 349-359.

Ye, Z.H., Cheung, K.C. and Wong, M.H. (2001) Copper Uptake in *Typha Latifolia* as Affected by Iron and Manganese Plaque on the Root Surface. *Canadian Journal of Botany-Revue Canadienne De Botanique* **79**, 314-320.

Yefremenko, V.V., Moshkov, A.V., SemenovA.A. and Chimitdorzhiyez, T.N. (1998) Use of False Colour Scanner Imagery to Detect Vegetation Stress. *GIS Science and Remote Sensing* **35**, 218-226.

Yuan, L. and Zhang, L.Q. (2007) The Spectral Responses of a Submerged Plant *Vallisneria spiralis* With Varying Biomass Using Spectroradiometer. *Hydrobiologia* **579**, 291-299.

Zaneveld, J.R.V. and Boss, E. (2003) The Influence of Bottom Morphology on Reflectance: Theory and Two-Dimensional Geometry Model. *Limnology and Oceanography* **48**, 374-379. Notes: Part Number: Part 2

Zhang, Y.L., Qin, B.Q., Zhu, G.W., Zhang, L. and Yang, L.Y. (2007) Chromophoric Dissolved Organic Matter (CDOM) Absorption Characteristics in Relation to Fluorescence in Lake Taihu, China, a Large Shallow Subtropical Lake. *Hydrobiologia* **581**, 43-52.

Zhang, Y.Z., Pulliainen, J., Koponen, S. and Hallikainen, M. (2003) Empirical Algorithms for Secchi Disk Depth Using Optical and Microwave Remote Sensing Data From the Gulf of Finland and the Archipelago Sea. *Boreal Environment Research* **8**, 251-261.

Zhou, Y.Y., Li, J.Q. and Fu, Y.Q. (2000) Effects of Submerged Macrophytes on Kinetics of Alkaline Phosphatase in Lake Donghu - I. Unfiltered Water and Sediments. *Water Research* **34**, 3737-3742.

Zohary, T. and Breen, C.M. (1989) Environmental-Factors Favoring the Formation of Microcystis-Aeruginosa Hyperscums in a Hypertrophic Lake. *Hydrobiologia* **178**, 179-192.